frontiers | Research Topics

Integrated diagnostics and biomarker discovery in endocrinology and biomedical sciences

Edited by
Sijung Yun, Princy Francis and Stephen Wank

Published in
Frontiers in Endocrinology

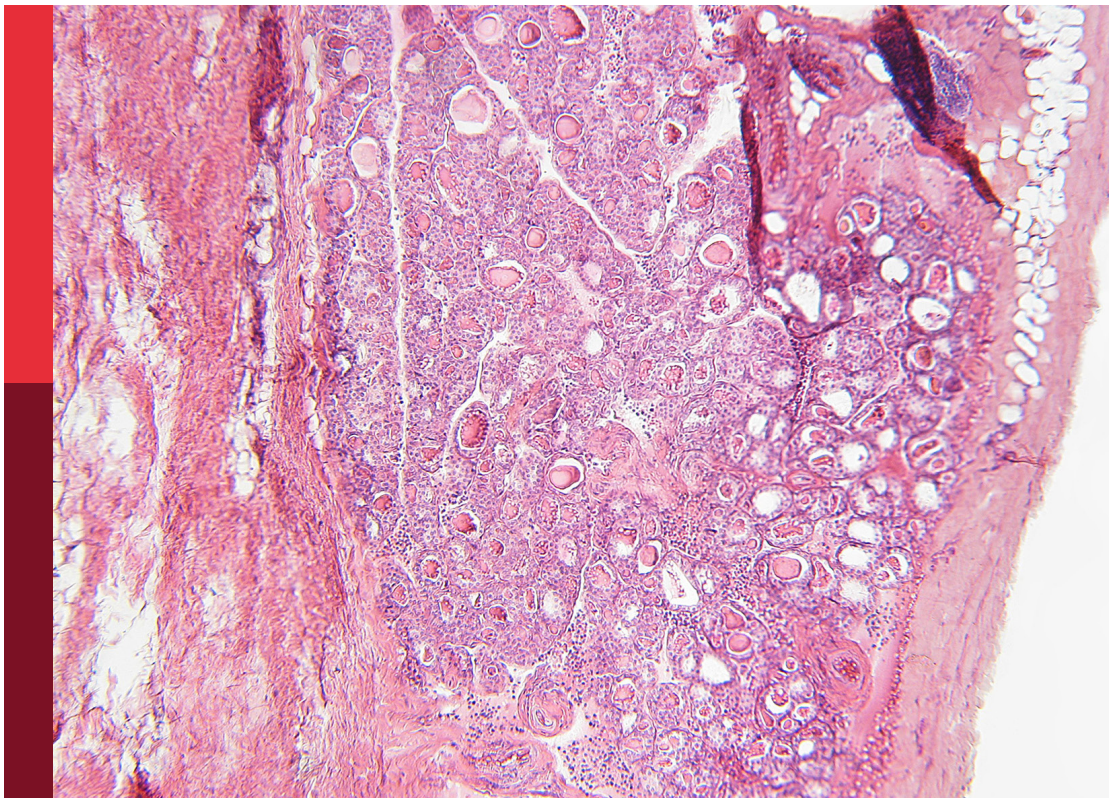

ISSN 1664-8714
ISBN 978-2-8325-5753-2
DOI 10.3389/978-2-8325-5753-2

About Frontiers

Frontiers is more than just an open access publisher of scholarly articles: it is a pioneering approach to the world of academia, radically improving the way scholarly research is managed. The grand vision of Frontiers is a world where all people have an equal opportunity to seek, share and generate knowledge. Frontiers provides immediate and permanent online open access to all its publications, but this alone is not enough to realize our grand goals.

Frontiers journal series

The Frontiers journal series is a multi-tier and interdisciplinary set of open-access, online journals, promising a paradigm shift from the current review, selection and dissemination processes in academic publishing. All Frontiers journals are driven by researchers for researchers; therefore, they constitute a service to the scholarly community. At the same time, the *Frontiers journal series* operates on a revolutionary invention, the tiered publishing system, initially addressing specific communities of scholars, and gradually climbing up to broader public understanding, thus serving the interests of the lay society, too.

Dedication to quality

Each Frontiers article is a landmark of the highest quality, thanks to genuinely collaborative interactions between authors and review editors, who include some of the world's best academicians. Research must be certified by peers before entering a stream of knowledge that may eventually reach the public - and shape society; therefore, Frontiers only applies the most rigorous and unbiased reviews. Frontiers revolutionizes research publishing by freely delivering the most outstanding research, evaluated with no bias from both the academic and social point of view. By applying the most advanced information technologies, Frontiers is catapulting scholarly publishing into a new generation.

What are Frontiers Research Topics?

Frontiers Research Topics are very popular trademarks of the *Frontiers journals series*: they are collections of at least ten articles, all centered on a particular subject. With their unique mix of varied contributions from Original Research to Review Articles, Frontiers Research Topics unify the most influential researchers, the latest key findings and historical advances in a hot research area.

Find out more on how to host your own Frontiers Research Topic or contribute to one as an author by contacting the Frontiers editorial office: frontiersin.org/about/contact

Integrated diagnostics and biomarker discovery in endocrinology and biomedical sciences

Topic editors

Sijung Yun — Predictiv Care, Inc., United States

Princy Francis — Mayo Clinic Arizona, United States

Stephen Wank — National Institutes of Health (NIH), United States

Citation

Yun, S., Francis, P., Wank, S., eds. (2024). *Integrated diagnostics and biomarker discovery in endocrinology and biomedical sciences*. Lausanne: Frontiers Media SA. doi: 10.3389/978-2-8325-5753-2

Table of contents

frontiers | Frontiers in Endocrinology

ORIGINAL RESEARCH
published: 27 June 2022
doi: 10.3389/fendo.2022.906310

Integrating Choline and Specific Intestinal Microbiota to Classify Type 2 Diabetes in Adults: A Machine Learning Based Metagenomics Study

Qiang Zeng[1†], Mingming Zhao[2,3†], Fei Wang[1†], Yanping Li[4], Huimin Li[5,6], Jianqiong Zheng[7], Xianyang Chen[8,9], Xiaolan Zhao[10], Liang Ji[3], Xiangyang Gao[1], Changjie Liu[3], Yu Wang[11], Si Cheng[2], Jie Xu[2], Bing Pan[3], Jing Sun[12], Yongli Li[13], Dongfang Li[14,15], Yuan He[5,6] and Lemin Zheng[2,3*]*

[1] Health Management Institute, the Second Medical Center & National Clinical Research Center for Geriatric Diseases, Chinese People's Liberation Army General Hospital, Beijing, China, [2] China National Clinical Research Center for Neurological Diseases, Tiantan Hospital, Advanced Innovation Center for Human Brain Protection, The Capital Medical University, Beijing, China, [3] The Institute of Cardiovascular Sciences and Institute of Systems Biomedicine, School of Basic Medical Sciences, Peking University Health Science Center, Key Laboratory of Molecular Cardiovascular Science of Ministry of Education, Key Laboratory of Cardiovascular Molecular Biology and Regulatory Peptides of Ministry of Health, Beijing Key Laboratory of Cardiovascular Receptors Research, Beijing, China, [4] Department of Nutrition, Harvard T.H. Chan School of Public Health, Boston, MA, China, [5] National Human Genetic Resources Center, Beijing, China, National Research Institute for Family Planning, Beijing, China, [6] Chinese Academy of Medical Sciences & Peking Union Medical College, Beijing, China, [7] Department of Obstetrics and Gynecology, The Third Clinical Institute Affiliated to Wenzhou Medical University, The Third Affiliated Hospital of Shanghai University, Wenzhou People's Hospital, Wenzhou Maternal and Child Health Care Hospital, Wenzhou, China, [8] Bao Feng Key Laboratory of Genetics and Metabolism, Zhongyuan Biotechnology Holdings Group, Beijing, China, [9] Zhong Guan Cun Biological and Medical Big Data Center, Zhong Guan Cun Medical Engineering & Health Industry Base, Beijing, China, [10] Southwest Hospital, Third Military Medical University, Chongqing, China, [11] Health Management Center, The 910th Hospital of People's Liberation Army, Quanzhou, China, [12] Health Management Center, The China-Japan Union Hospital of Jilin University, Changchun, China, [13] Department of Health Management, Henan Provincial People's Hospital, Zhengzhou, China, [14] Department of Microbial Research, WeHealthGene Institute, Shenzhen, Guangdong, China, [15] Institute of Statistics, NanKai University, Tianjin, China*

OPEN ACCESS

Edited by:
Katsumi Iizuka,
Fujita Health University, Japan

Reviewed by:
Kanishka Nilaweera,
Teagasc, Ireland
Yanyan Liu,
Gifu University, Japan

****Correspondence:***
Yuan He
heyuan8506@126.com
Lemin Zheng
zhengl@bjmu.edu.cn

†These authors have contributed equally to this work

Specialty section:
This article was submitted to Diabetes: Molecular Mechanisms, a section of the journal Frontiers in Endocrinology

Received: *28 March 2022*
Accepted: *13 May 2022*
Published: *27 June 2022*

Citation:
Zeng Q, Zhao M, Wang F, Li Y, Li H, Zheng J, Chen X, Zhao X, Ji L, Gao X, Liu C, Wang Y, Cheng S, Xu J, Pan B, Sun J, Li Y, Li D, He Y and Zheng L (2022) Integrating Choline and Specific Intestinal Microbiota to Classify Type 2 Diabetes in Adults: A Machine Learning Based Metagenomics Study. Front. Endocrinol. 13:906310. doi: 10.3389/fendo.2022.906310

Emerging evidence is examining the precise role of intestinal microbiota in the pathogenesis of type 2 diabetes. The aim of this study was to investigate the association of intestinal microbiota and microbiota-generated metabolites with glucose metabolism systematically in a large cross-sectional study in China. 1160 subjects were divided into three groups based on their glucose level: normal glucose group (n=504), prediabetes group (n=394), and diabetes group (n=262). Plasma concentrations of TMAO, choline, betaine, and carnitine were measured. Intestinal microbiota was measured in a subgroup of 161 controls, 144 prediabetes and 56 diabetes by using metagenomics sequencing. We identified that plasma choline [Per SD of log-transformed change: odds ratio 1.36 (95 confidence interval 1.16, 1.58)] was positively, while betaine [0.77 (0.66, 0.89)] was negatively associated with diabetes, independently of TMAO. Individuals with diabetes could be accurately distinguished from controls by integrating data on choline, and certain microbiota species, as well as traditional risk factors (AUC=0.971). KOs associated with the carbohydrate metabolism pathway were enhanced in individuals with high choline level. The functional shift in the carbohydrate metabolism pathway in high choline group was driven by

species *Ruminococcus lactaris*, *Coprococcus catus* and *Prevotella copri*. We demonstrated the potential ability for classifying diabetic population by choline and specific species, and provided a novel insight of choline metabolism linking the microbiota to impaired glucose metabolism and diabetes.

Keywords: choline, intestinal microbiota, TMAO, type 2 diabetes, machine learning

1 INTRODUCTION

Recently, emerging evidence is examining the precise role of intestinal microbiota in the pathogenesis of type 2 diabetes (diabetes) (1). Data are accumulating that patients with diabetes had a moderate intestinal dysbiosis. Metagenome-wide association studies have demonstrated a highly significant association between butyrate-producing bacteria such as *Roseburia intestinalis* and *Faecalibacterium prausnitzii* concentrations and diabetes (2). Fecal transplantation in humans further highlights the possibility of modulating human metabolism by directly altering the microbiota, showing that insulin sensitivity was improved along with the increase of butyrate-producing bacteria after fecal transferring from lean donors to male recipients with metabolic syndrome (3). Microbiota may directly modulate host metabolism by short-chain fatty acids especially butyrate, endotoxaemia, and specific intestinal bacteria (such as *Akkermansia muciniphila*) which plays a role in anti-inflammatory and beneficial metabolic functions (4).

Trimethylamine-N-oxide (TMAO) is a plasma metabolite and its generation is dependent on the intestinal microbiota from TMA, which primarily metabolizes from dietary choline, betaine and L-carnitine in the intestinal tract. Thereafter, TMA is metabolized to TMAO by enzymes of the flavin monooxygenase (FMO) family in liver (5). Numerous studies have demonstrated TMAO is a novel predictive risk factor of adverse cardiovascular outcomes (5–7). The mechanism appears to involve that TMAO interacting with platelets, altering stimulus-dependent calcium signaling, fostering platelet hyper-reactivity *in vivo*, and promoting vascular inflammation in animal models (8). Several studies further demonstrated that plasma TMAO was elevated in patients with diabetes compared to healthy controls, possibly due to TMAO converting enzyme FMO3 which exerted broad effects on glucose and lipid metabolism (9). Knockdown of hepatic FMO3 significant decreased circulating TMAO levels and atherosclerosis in mice, accompanying decreases in hepatic lipids and in levels of plasma lipids, glucose, and insulin (10). Also, recent study showed that elevated levels of circulating choline were significantly associated with diabetes (11). Intervention study has found the associations between change in choline and that in insulin sensitivity independently of concurrent changes in TMAO (12). However, advanced correlations of blood glucose, related phenotypes and microbial metabolites including plasma choline, betaine and TMAO, and whether these metabolites are related to human intestinal microbiota were unknown. Thus, the aim of this study was to investigate the associations of TMAO and its precursors (choline, betaine and carnitine) with glucose metabolism, and to explore the potential mechanism targeting intestinal microbiota and their effects on the human health.

Abbreviations: AUC, Area under the receiver operating curve; CAZy, Carbohydrate-Active EnZymes; CVD, Cardiovascular disease; FMO, Flavin monooxygenase; HDL, High-density lipoprotein; HOMA-IR, Homeostasis model assessment of insulin resistance; IQR, Interquartile range; KEGG, Kyoto Encyclopedia of Genes and Genomes; KO, KEGG orthologue group; LDL, Low-density lipoprotein; LEfSe Linear discriminant analysis (LDA) effect size; MRM, Multiple reaction monitoring; ROC, Receiver operating characteristic; TC, Total cholesterol; TG, Triglyceride; TMA, Trimethylamine; TMAO, Trimethylamine-N-oxide; UA, Uric acid.

2 METHODS

2.1 Population

We conducted a cross-sectional study at three health examination centers from Jan. 2016 to Sep. 2017, aiming to examine the association of intestinal microbiota, microbiota-generated metabolites with glucose metabolism in Chinese adults. The two-stage cluster sampling method was used to, first selected three cities according to geographical region and dietary/lifestyle habit (Northern region: Changchun; Southern region: Quanzhou; Western region: Chongqing), and then selected one local representative health examination center from each city (Changchun: The China-Japan Union Hospital; Quanzhou: The 910th Hospital of People's Liberation Army; Chongqing: Southwest Hospital). A total of 1160 subjects (aged 20-75 years) who participated in annual health examinations were randomly selected in each center with complete information on demographics, personal characteristics (including weight, height and waist circumference) and clinical characteristics (including blood pressure, blood glucose, lipid concentrations, uric acid and serum creatinine). Exclusion criteria for study participation included: i) younger than 20 years or older than 75 years; ii) exposed to antibiotic, probiotics, acid reducing medications or proton pump inhibitor one month before physical examination; iii) suffered from diarrhea, constipation, hematochezia or other gastrointestinal infectious diseases one month prior to physical examination; iv) experienced enema or other gastroenterology operations one month before physical examination; v) suffered from mental disorders, autoimmune diseases or psychological imbalance; vi) had drug abuse history, which resulted in 1160 subjects for current study. Detailed study flow is shown in **Figure 1**. This study was approved by the Ethical Committee of the Chinese People's Liberation Army General Hospital and was in accordance

with the Helsinki Declaration. Every subject provided written informed consent.

2.2 Outcomes

Type 2 Diabetes status was used as main outcomes. Prediabetes was defined as a fasting plasma glucose from 5.6 to 6.9mmol/L, and diabetes was defined as a fasting plasma glucose ≥7.0mmol/L. In addition, the following outcomes were used: hypertension was defined as having a systolic blood pressure ≥140mmHg and/or diastolic blood pressure ≥90mmHg; dyslipidemia was defined as having plasma total cholesterol ≥6.22mmol/L and/or fasting triglycerides ≥2.26mmol/L and/or LDL cholesterol ≥4.14mmol/L and/or HDL-cholesterol <1.04mmol/L; hyperuricemia was defined as having uric acid ≥420 mg/dL for men and ≥357mg/dL for women.

2.3 Covariates

All clinical data was collected according to standard procedures. Subjects underwent anthropometric measurements in barefoot and light clothing. Body weight (measured to the nearest 0.1kg) and height (measured to the nearest 0.1cm) were collected and BMI was calculated by dividing weight (kg) by height squared (m2). Blood pressure was recorded using a recently calibrated electronic sphygmomanometer in the supine position with the right arm after 5minutes rest. Blood samples were obtained after an overnight fast for measurement of blood glucose, total and high-density lipoprotein cholesterol, triglycerides, uric acid and serum creatinine. Low-density lipoprotein cholesterol was calculated using the Friedewald formula. Serum creatinine was measured using Jaffe's kinetic method. All blood samples were analyzed at a local laboratory in each city rather than a central laboratory. Because all the laboratories were affiliated with a top tertiary hospital and completed a standardized and certificated method for blood test, these results have been widely considered comparably across laboratories in China.

2.4 Microbiota-Generated Metabolites Measurements

Analytes (TMAO, betaine, choline, and carnitine) were measured in one center laboratory as described previously (13). Briefly, 20μl plasma were mixed with 80μl of 10μM d9-(trimethyl)-labelled internal standards in methanol. Protein was precipitated and the supernatant was recovered following centrifugation at 20,000g at 4°C for 10min. The precise concentration was measured by API 5500Q-TRAP mass spectrometer (AB SCIEX, Framingham, MA). Analytes were monitored using electrospray ionization in positive-ion mode with multiple reaction monitoring (MRM) of precursor and characteristic product-ion transitions of TMAO at m/z 76→58, d9-TMAO at m/z 85→66, choline at m/z 104→59.8, d9-choline at m/z 113.2→68.9, carnitine at m/z 162.1→103, d9-carnitine at m/z 171.1→102.8, betaine at m/z 118→59, d11-betaine at 129.1→65.9, respectively. Three quality control samples with different metabolites concentrations were measured every twenty samples and the CV% values were below 10%. The quartiles based on TMAO, choline, betaine, and carnitine, separately, TMAO levels for the quartile groups were as follows: Q1 <0.98, Q2: 0.98~1.58, Q3: 1.59~2.52, Q4 > 2.52mmol/L; Choline levels for the quartiles were as follows: Q1 <7.2, Q2: 7.2~8.5, Q3: 8.6~10.1, Q4 > 10.1mmol/L; Betaine levels for the quartiles were as follows: Q1 < 37.3, Q2: 37.3~43.3, Q3: 43.4~51.3, Q4 > 51.3mmol/L. Carnitine levels for the quartiles were as follows: Q1 < 48.2, Q2: 48.2~55.1, Q3: 55.2~61.9, Q4 > 61.9mmol/L.

2.5 Gut Microbiota Measurements

2.5.1 Stool Sample Collection and DNA Extraction

During physical examination, fresh stools were collected from the individuals using sterile stool containers. For each individual, approximately 5g of hard stools were obtained using the swab (Huachenyang Technology CO., LTD, Shenzhen, China). The stool samples were preserved using stool collection tubes (Axygen,

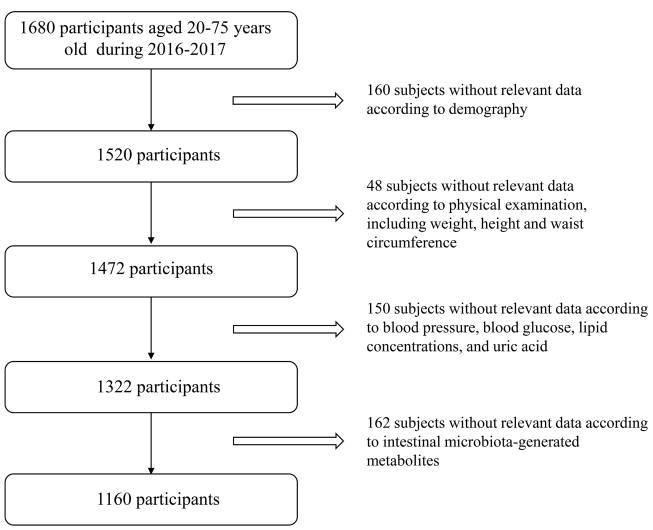

FIGURE 1 | Flow chart of the study participant.

California, USA) with Microlution (ML001-A, Dayun Ltd, Shenzhen, China), and then transferred to -80°C refrigerator (DW-86L626, Haier, China) within half an hour. Bacterial DNA was extracted from stool samples using Power Soil DNA Isolation kit (Mo Bio Laboratories, Carlsbad) at WeHealthGene Co., Ltd according to the manufacturer's instruction.

2.5.2 Library Construction and Metagenomics Sequencing

DNA library construction was performed with the following workflow as suggested by the manufacturer (Illumina, San Diego): cluster generation, template hybridization, isothermal amplification, linearization, blocking and denaturation, and hybridization of the sequencing primers. We constructed paired-end (PE) library with insert size of 350bp, and each sample contains around 20 million PE reads after high-throughput sequencing. For samples at stages I, their libraries were sequenced with 75 or 90 base pairs, while the libraries were sequenced with 90 base pairs for samples at stage II.

2.5.3 Quality Control and Host Genome Filtering

High quality reads were obtained with the following filtering criteria: If any one of paired-end reads i) contains10% ambiguous N bases; ii) or more than 50% low quality (Q<5) bases, the paired-end reads were thrown away. Then, the clean reads were subjected to human genomes (human genome reference hg19) from the National Center for Biotechnology Information GenBank with SOAPaligner (version 2.21,"-m 250 -x 450 -v 5 -r 1 -l 35 -M 4"), and the reads which mapped to human genome were abandoned (14). The filtered reads were retained for further analysis.

2.5.4 Gene Abundance, Functional Annotation and Taxonomic Profiling

The qualified reads from the samples were aligned to the upgraded non-redundant gene catalogue (15) with SOAPaligner (version 2.21, "-m 250 -x 450 -v 5 -r 1 -l 35 -M 4"), wand the mapped reads with less than 7 mismatches were kept. Based on the gene length and the number of mapped reads, the abundances of genes were obtained for each sample with previous published method (16).

To obtain the functional distributions of genes, we aligned them to the proteins/domains in KEGG databases (release 59.0) and CAZy database using BLASTP (e-value ≤1e-5). The KEGG orthologue group (KO) or CAZy families with the highest scoring annotated hit (s) which containing at least one HSP (high-scoring segment pair) scoring over 60 bits was selected. The abundance of KEGG orthology/module in each sample was calculated by summing the abundance of genes which annotated to the same functional item. With shotgun metagenomic data, the composition of microbial community on different taxonomic level was detected for each sample using MetaPhlAn2 pipeline with default parameters (17).

2.6 Statistical Analyses

Continuous variables are summarized as mean (SD) if normally distributed and median [interquartile range (IQR)] if nonnormally distributed. The unpaired Student t-test or Wilcoxon signed rank test for continuous variables and Chi-squared test for categorical variables were employed to examine between group differences. The associations between intestinal microbiota-generated metabolites and diabetes were examined by applying logistic regression models with adjustment for potential confounders including age, sex and BMI. The levels of TMAO, betaine, choline, carnitine were divided into quartiles and the lowest quartile was used as the reference group. Sensitivity analysis was conducted i) by including lifestyle factors, alcohol consumption, smoking habit, dietary habit, exercise habit, sleeping habit, stool shape, whether eating probiotics supplements, whether having conditions of regular defecation, diarrhea, or constipation, as covariates in a subgroup population; ii) by further adjusted other metabolites in the models. Statistical analysis was performed using STATA software version 13.0 (StataCorp., College Station, TX) or GraphPad Prism 6 software. Statistical tests were 2-sided and a P value<0.05 was considered statistically significant.

We pre-processed the intestinal microbiota abundant data and deleted the variables with 0 value greater than 20%. The Shannon index and principal coordinates analysis (PCoA) was calculated with the vegan package in R software (Version 3.4.3). PCoA was performed and displayed by ade4 package, cluster packages, fpc packages, and clusterSim package in R software. PLS-DA was performed using SIMCA-P software to cluster the sample plots across groups. The relative abundance of these features was subjected to statistical analyses. Linear discriminant analysis (LDA) effect size (LEfSe) analysis was used to detect the features (organisms, KOs, or CAZy genes) most likely to explain differences between the prediabetes, diabetes and control group, as well as high (top quartile) and low groups (lowest quartile) of choline and TMAO. Different features with an LDA score cut-off of 2.0 were identified. Taxa-based functional profiles was calculating by FishTaco software. Correlations between enriched species, metabolites and clinical indices were tested with MaAslin2. Dimension reduction analysis was based on the PLS-DA, where the variables were selected by variable importance projection (VIP)>1 and mean difference screening (P<0.05) as biomarkers 1; variables were selected by one-way ANOVA (P<0.05) as biomarkers 2; only microbiota indicators were selected by one-way ANOVA (P<0.05) as biomarkers 3; and traditional risk factors were selected as biomarkers 4. Classification machine learning algorithms using Support Vector Machines (SVM), Random Forests (RF), Decision Tree (DT) were performed to obtain the optimal diagnostic model using R. The OPLS-DA model analysis was based on muma and ropls package, and the SVM, RF and DT and was based on svm, random forest, and rpart package. Then, in order to evaluate the performance of the predictive model and get more precise curves, we used a 10-fold cross-validation for each model. ROC curve analysis was performed using the highest validated AUC values, and variable importance was measured by GINI coefficient. The ROC curves were conducted by pROC package.

3 RESULTS

3.1 Association of Intestinal Microbiota-Generated Metabolites With Prediabetes and Diabetes

We conducted a cross-sectional study including a total of 1160 subjects (aged 20-75 years) who participated in annual health examinations. The sample size varied according to the number of missing data, with missing data on metabolites outcome variables (n =1 for TMAO and choline, as well as n =5 for betaine), or other covariates (n =33). Baseline characteristics of the 1160 participants are shown in **Table 1**. The median (mean) plasma concentrations of TMAO, choline, betaine, and L-carnitine were 1.59 μmol/L (IQR: 0.98 to 2.52μmol/L), 8.58 μmol/L (IQR: 7.23 to 10.10μmol/L), 43.4 μmol/L (IQR: 37.30 to 51.32 μmol/L), and 55.2 ± 10.8 (mean ± SEM), respectively. Participants with higher levels of blood glucose were more likely to be older, had a higher proportion of males, and had higher levels of BMI, blood pressure, and were more likely to be dyslipidemia and hypeluricemia. In the three groups of diabetes, prediabetes and controls, TMAO was significantly higher in participants with diabetes compared with controls, and choline was higher in participants with hyperglycemia than controls. There was an inverse dose-response association between plasma betaine concentration and fasting glucose in the three groups. Cubic spline curves showed that TMAO associated with blood glucose as a J-shape. Choline linearly increased with increasing blood glucose, while betaine linearly decreased with increasing blood glucose (**Figure S1**)

Following multivariate logistic regression analyses adjusting for age, sex and BMI, each SD increment in log-transformed plasma concentration for TMAO and choline was associated with 16-36% increased odds of diabetes (P<0.05), while each SD increment of log-transformed plasma betaine was correlated with 23% decreased odds of diabetes (P<0.001) (**Table 2**). Participants in the top quartile of TMAO had 1.67 fold higher odds of diabetes compared with the lowest quartile. In general, the association of plasma TMAO, choline and betaine with diabetes was consistent across total group, and subgroups after stratification by sex and age groups (all *Ps* for interaction > 0.05). In the sensitivity analyses, the odds ratios for the metabolites did not change appreciably with additional adjustment for lifestyle factors in the subgroup; Findings were similar when per SD of all metabolites were included into the same adjusted model, that TMAO [odds ratio and 95%CI: 1.25 (1.01-1.54)], choline [1.74 (1.38-2.19)], betaine [0.58 (0.47-0.71)] and carnitine [0.72 (0.59-0.89)] remained significantly associated with diabetes. Parameter estimates were slightly attenuated after further adjustment for metabolic biomarkers including blood pressure, lipids and uric acid. Further, when we put four quartiles of all metabolites into one model, the association between the top quartile of TMAO and diabetes was also significant (1.57 [1.03-2.39]).

3.2 Prediabetes and Diabetes-Associated Intestinal Microbial Species and Metabolites

We further performed metagenomic sequencing of 361 fecal samples (56 samples from diabetes, 145 from prediabetes, and 160 healthy controls), and the baseline characteristics of individuals were presented in **Table S1**. The shannon index based on the species profile was calculated to estimate the within-sample (α) diversity. The α-diversity of the intestinal microbiome was similar at the species level in the three groups. Similarity, no significant differences were found in β-diversity based on PCoA between the three groups. Genes were aligned to the NR database and annotated to taxonomic groups, and a supervised comparison of the microbiota by utilizing the LEfSe analysis was performed. Our results identified 3 bacterial species consisting *Coprococcus catus*, *Eubacterium siraeum*, and *Fusobacterium ulcerans* were significantly enriched in the

TABLE 1 | Baseline characteristics according to controls, prediabetes and diabetes.

	Total n = 1160	Controls n = 504	Prediabetes n = 394	Diabetes n = 262	P value
Age, years	46.0 (38.0, 52.0)	42.0 (35.0, 51.0)	47.0 (40.0, 52.0)	48.0 (42.0, 53.0)	< 0.001
Male, %	65.2	57.9	68.0	74.8	< 0.001
BMI, kg/m^2	27.4 (25.4, 29.3)	27.5 (24.7, 29.4)	27.5 (26.0, 29.0)	28.2 (26.4, 30.9)	< 0.001
Systolic BP, mmHg	129 (118, 139)	125 (114, 135)	129 (119, 140)	135 (123, 146)	< 0.001
Diastolic BP, mmHg	82 ± 12	79.6 ± 11.4	83.0 ± 12.5	85.0 ± 12.6	< 0.001
Fasting glucose, mmol/L	5.7 (5.2, 6.6)	5.2 (4.9, 5.4)	5.9 (5.7, 6.1)	8.5 (7.3, 10.5)	< 0.001
Total cholesterol, mmol/L	5.3 (4.6, 5.9)	5.0 (4.4, 5.7)	5.4 (4.8, 5.9)	5.4 (4.9, 6.2)	< 0.001
Triglycerides, mmol/L	1.8 (1.2, 2.7)	1.5 (1.0, 2.3)	1.8 (1.3, 2.6)	2.4 (1.6, 3.7)	< 0.001
HDL cholesterol, mmol/L	1.2 (1.1, 1.4)	1.2 (1.1, 1.4)	1.2 (1.1, 1.4)	1.2 (1.0, 1.4)	0.082
LDL cholesterol, mmol/L	2.8 (2.4, 3.2)	2.7 (2.3, 3.2)	2.8 (2.4, 3.2)	2.9 (2.5, 3.5)	< 0.001
Uric acid, mg/dL	372.5 ± 98.0	360.5 ± 100.1	387.6 ± 97.4	373.2 ± 92.0	< 0.001
Hypertension, %	33.7	25.4	35.8	46.6	< 0.001
Dyslipidemia, %	52.2	42.3	52.0	71.4	< 0.001
Hypeluricemia, %	34.4	29.8	39.8	37.0	< 0.001
TMAO, μmol/L	1.59 (0.98, 2.52)	1.5 (0.9, 2.3)	1.6 (1.0, 2.5)	1.7 (1.1, 3.3)	0.040
Choline, μmol/L	8.58 (7.23, 10.10)	8.2 (6.9, 9.9)	8.3 (7.1, 9.8)	9.3 (7.9, 11.0)	< 0.001
Betaine, μmol/L	43.4 (37.30, 51.32)	44.4 (37.7, 52.9)	43.6 (37.7, 51.2)	41.0 (35.2, 48.6)	0.003
Carnitine, μmol/L	55.2 ± 10.8	55.5 ± 10.4	55.4 ± 10.8	54.5 ± 11.7	0.434

BMI, body mass index; BP, blood pressure; HDL, high-density lipoproterin; LDL, low-density lipoprotein; TMAO, trimethylamine N-oxide.

TABLE 2 | Relationship between plasma concentrations of TMAO, choline, betaine, carnitine and diabetes (μmol/L)[a].

	Per SD of log-transformed change*	P value	Quartiles*				P for trend
			1 (lowest)	2	3	4 (highest)	
Total							
TMAO	1.16 (1.00, 1.35)	0.049	1.00	1.14 (0.75, 1.73)	0.92 (0.60, 1.41)	1.67 (1.11, 2.51)*	0.035
Choline	1.36 (1.16, 1.58)	< 0.001	1.00	1.32 (0.86, 2.05)	1.68 (1.10, 2.57)*	1.93 (1.27, 2.92)**	0.001
Betaine	0.77 (0.66, 0.89)	< 0.001	1.00	0.77 (0.53, 1.12)	0.57 (0.38, 0.86)**	0.47 (0.31, 0.70)***	< 0.001
Carnitine	0.85 (0.73, 0.98)	0.026	1.00	0.79 (0.56, 1.17)	0.76 (0.52, 1.13)	0.68 (0.45, 1.02)	0.062
Males							
TMAO	1.28 (1.07, 1.53)	0.006	1.00	1.29 (0.79, 2.11)	1.03 (0.62, 1.69)	2.08 (1.29, 3.36)*	0.009
Choline	1.33 (1.11, 1.59)	0.002	1.00	1.29 (0.78, 2.14)	1.78 (1.09, 2.90)*	1.85 (1.14, 3.02)*	0.006
Betaine	0.79 (0.66, 0.94)	0.009	1.00	0.74 (0.47, 1.17)	0.56 (0.35, 0.90)*	0.53 (0.33, 0.85)**	0.004
Carnitine	0.86 (0.72, 1.03)	0.104	1.00	0.75 (0.48, 1.20)	0.81 (0.50, 1.27)	0.65 (0.40, 1.05)	0.107
Females							
TMAO	0.90 (0.69, 1.17)	0.429	1.00	0.77 (0.35, 1.71)	0.66 (0.29, 1.47)	0.84 (0.38, 1.86)	0.624
Choline	1.45 (1.07, 2.00)	0.017	1.00	1.37 (0.57, 3.31)	1.53 (0.66, 3.56)	2.07 (0.92, 4.66)	0.076
Betaine	0.73 (0.57, 0.95)	0.017	1.00	0.88 (0.43, 1.80)	0.63 (0.29, 1.38)	0.30 (0.13, 0.72)**	0.005
Carnitine	0.83 (0.63, 1.09)	0.174	1.00	0.89 (0.42, 1.89)	0.68 (0.31, 1.52)	0.79 (0.36, 1.73)	0.444
≤45 years old							
TMAO	1.12 (0.89, 1.41)	0.341	1.00	1.11 (0.59, 2.10)	0.92 (0.48, 1.76)	1.61 (0.85, 3.04)	0.256
Choline	1.50 (1.17, 1.94)	0.002	1.00	1.52 (0.76, 3.06)*	2.02 (1.01, 4.03)	2.32 (1.16, 4.64)**	0.011
Betaine	0.93 (0.73, 1.16)	0.470	1.00	1.62 (0.88, 2.97)	1.03 (0.53, 2.00)	0.88 (0.43, 1.80)	0.500
Carnitine	0.81 (0.64, 1.03)	0.080	1.00	0.86 (0.46, 1.59)	0.63 (0.33, 1.21)	0.61 (0.32, 1.19)	0.093
>45 years old							
TMAO	1.19 (0.97, 1.45)	0.092	1.00	1.14 (0.65, 2.01)	0.92 (0.52, 1.63)	1.70 (0.99, 2.92)	0.080
Choline	1.29 (1.06, 1.57)	0.012	1.00	1.22 (0.69, 2.16)	1.53 (0.89, 2.62)*	1.79 (1.05, 3.03)*	0.022
Betaine	0.68 (0.56, 0.83)	< 0.001	1.00	0.45 (0.27, 0.75)**	0.38 (0.23, 0.65)***	0.31 (0.19, 0.53)***	< 0.001
Carnitine	0.89 (0.74, 1.07)	0.220	1.00	0.75 (0.45, 1.26)	0.86 (0.52, 1.41)	0.76 (0.45, 1.28)	0.391

*For the definition of abbreviations, see **Table 1**.*

[a]In according to the quartiles based on TMAO, choline, betaine, and carnitine, separately, TMAO levels for the quartile groups were as follows: Q1 <0.98, Q2: 0.98~1.58, Q3: 1.59~2.52, Q4 > 2.52mmol/L; Choline levels for the quartiles were as follows: Q1 <7.2, Q2: 7.2~8.5, Q3: 8.6~10.1, Q4 > 10.1mmol/L; Betaine levels for the quartiles were as follows: Q1 < 37.3, Q2: 37.3~43.3, Q3: 43.4~51.3, Q4 > 51.3mmol/L. Carnitine levels for the quartiles were as follows: Q1 < 48.2, Q2: 48.2~55.1, Q3: 55.2~61.9, Q4 > 61.9mmol/L.

**Adjusted for traditional risk factors include age, sex, and body mass index; *P < 0.05, **P < 0.01, ***P < 0.001.*

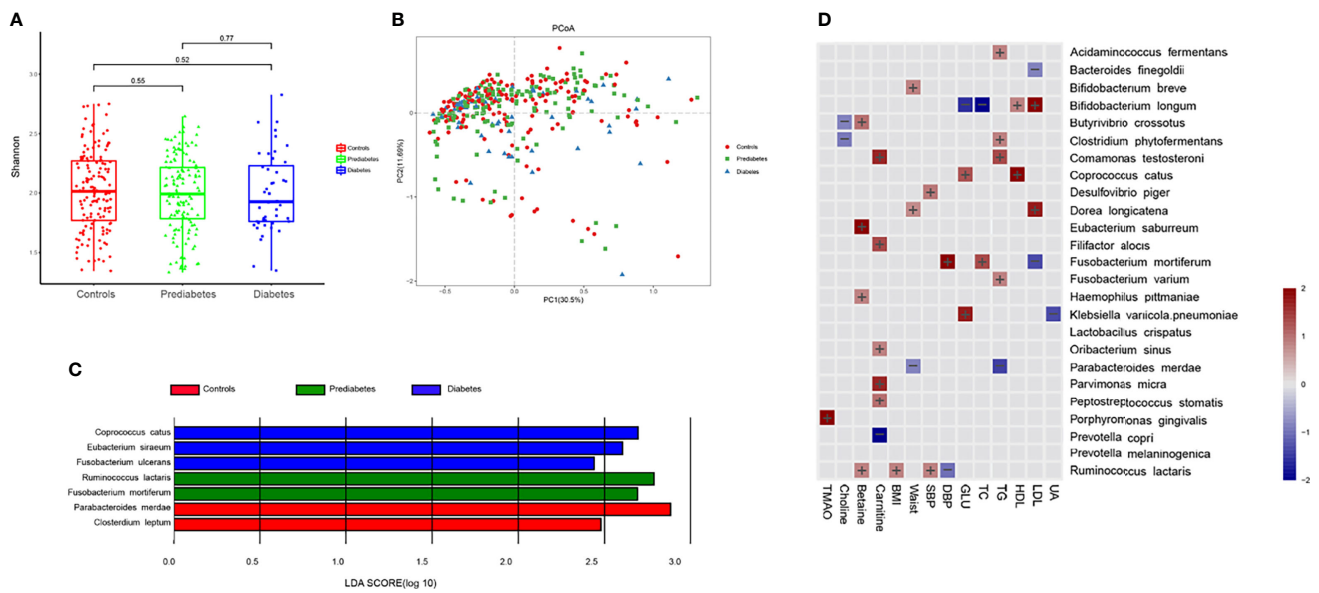

FIGURE 2 | Prediabetes and diabetes-associated intestinal microbiota. **(A)** Box plot showing the species-based α-diversity (Shanon index) in controls, prediabtes, and diabetes. **(B)** Species-based principal coordinates analysis (PCoA) of controls, prediabtes, and diabetes. **(C)** Linear discriminant analysis (LDA) effect size (LEfSe) analysis revealed significant bacterial differences in fecal microbiota in controls, prediabtes, and diabetes. **(D)** Associations between clinical parameters, intestinal microbiota-generated metabolites and microbial species were estimated by MaAsLin2.

diabetes group. Two species *Ruminococcus lactaris* and *Fusobacterium mortiferum*, were enriched in the prediabetes group. Other two bacterial species, including *Parabacteroides merdae* and *Clostridium leptum*, were enriched in the normal glucose control group (**Figures 2A–C**).

Results of multivariate association analysis with MaAsLin2 between microbiota-generated metabolites, clinical indices, and microbial species were presented in **Figure 2D**. Among the microbial species significantly correlated with blood glucose, *Klebsiella variicola.pneumoniae* and *Coprococcus catus* were positively associated, whereas *Bifidobacterium longum* were inversely associated with blood glucose. Physiological parameters of SBP, DBP, BMI, waistline, TC, TG, HDL-C and HDL-C were also included in the analysis. We observed that microbial species enriched in diabetes or prediabetes was generally positively with adverse metabolic parameters, whereas species enriched in controls was associated with improved metabolic parameters, such as *Parabacteroides merdae* was inversely associated with TG and waistline. For microbiota-generated metabolites, *Porphyromonas gingivalis* was positively correlated with TMAO. *Butyrivibrio crossotus* and *Clostridum phytofermentans* were inversely correlated with choline. Four species, including *Butyrivibrio crossotus*, *Eubacterium saburreum, Haemophilus pittmaniae* and *Ruminococcus lactaris* was posively associated with betaine.

3.3 Identification of Prediabetes and Diabetes Based on Machine Learning Algorithms

To illustrate the microbial and metabolic signature of prediabetes and diabetes, we exploit the potential of microbiome and metabolites for classifying prediabetes and diabetes from controls. The strategy of combining classical statistics and multivariate statistics were carried out, and we found the biomarkers distinguishing prediabetes from controls using traditional risk factors, and biomarkers that distinguished diabetes from controls using P value based on one-way ANOVA. Moreover, after 10-fold cross-validation, RF model showed highly promising performance for classifying prediabetes and diabetes from controls (prediabetes vs. controls, diabetes vs. control) (**Figure 3**). For diabetes, compared with models using traditional risk factors (AUC=0.938) or only using microbiome indicators (AUC=0.948), a RF algorithm integrating traditional risk factors with microbiome and metabolites performed better (AUC=0.971). The most informative microbiome features contributing to this classifier were *Coprococcus catus*, *Parabacteroides merdae*, *Ruminococcus lactaris*, *Bacteroides eggerthii*, *Prevotella copri*, and *Fusobacterium varium*, and choline was more effective than TMAO for classifying diabetes from controls (*P* value for Gini coefficient <0.05). To further elucidate whether sex has an effect on the microbial and metabolic signature, we also built models for classifying prediabetes and diabetes from controls by sex (**Figure S2**). For diabetes in males, the most informative microbiome features contributing to this classifier were *Coprococcus catus*, *Fusobacterium varium, Parabacteroides merdae, Ruminococcus lactaris, Prevotella copri* and *Bacteroides eggerthii*., For diabetes in females, the most informative microbiome were *Bacteroides eggerthii, Prevotella copri, Coprococcus catus, Parabacteroides merdae, Fusobacterium varium*, as well as *Ruminococcus lactaris*. The most informative microbiome features contributing to this classifier ranked somewhat differently in males and females. For prediabetes, we observed that the RF model using microbiome and selected traditional risk factors, such as waistline and age, did not display the better predictive performance (AUC=0.839) compared with that only using traditional risk factors (AUC=0.888). After sex stratified, the pattern was consistent, also, the risk factors ranked differently in males and females". Sensitivity analyses by further adjusted lifestyle risk factors were conducted to inspect the robustness of our findings, and the selected indicator to build the classification models were consistent.

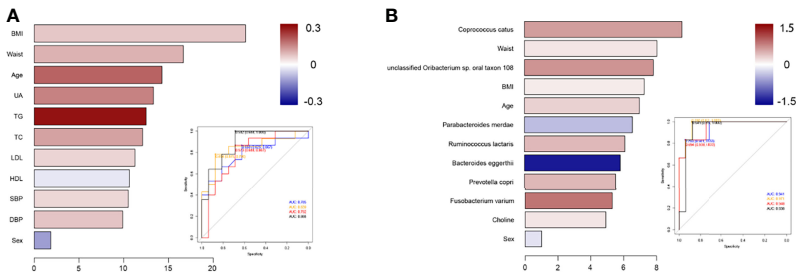

FIGURE 3 | Classification models using selected indicators to identify prediabetes or diabetes patients from controls. **(A)** The selected traditional risk indicators distinguished prediabetes from control based on the Random Forest model. The lengths of bar in the histogram represent Gini coefficient, which indicates the importance of the indicators for classification. The color denotes the enrichment of indicators in control (blue) and in prediabetes or diabetes (red). ROC of classifier models using four groups of biomarkers for prediabetes versus control. AUC = 0.785 for biomarkers 1 (blue curve), AUC = 0.839 for biomarkers 2 (yellow curve), AUC = 0.792 for biomarkers 3 (red curve), and AUC = 0.888 for biomarkers 4 (black curve). **(B)** The ANOVA-selected indicators distinguish diabetes from control based on the Random Forest model. ROC of classifier models using four groups of biomarkers for diabetes versus control. AUC = 0.941 for biomarkers 1 (blue curve), AUC = 0.971 for biomarkers 2 (yellow curve), AUC = 0.948 for biomarkers 3 (red curve), and AUC = 0.938 for biomarkers 4 (black curve).

3.4 Functional Characterization in Intestinal Microbiome of High or Low Choline Levels

All the genes were aligned to the KEGG database and CAZy database, and proteins were assigned to the KEGG orthology and CAZy families. Pathways involved in carbohydrate metabolism were enriched in high choline or low TMAO group. KEGG pathways including 'glycolysis gluconeogenesis', 'fructose and mannose metabolism', and 'galactose metabolism', were all highly enriched in the microbiome of high choline individuals. Conversely, KEGG pathways belonging to the 'pentose and glucoronate interconversions', 'starch and sucrose metabolism', and 'galactose metabolism', were significantly enriched in the microbiome of low TMAO individuals (**Figures 4A, B**). Among the CAZy genes for metabolizing different carbohydrate substrates, those contributing to insulin degradation were significantly enriched in high choline group, whereas those contributing to starch, insulin and pectin degradation were enriched in low TMAO group (**Figures 4C, D**). According to the TMA production potential, TMAO production potential was inversely correlated to glucose level, although the association did not reach statistical significance. Several KOs associated with the carbohydrate metabolism process were enhanced in individuals with low TMA production potential (**Figure 4E**).

We next examined FishTaco's calculated taxon-level contributions to functional differences, focusing on carbohydrate metabolism pathways, which were observed as choline-associated functional shifts. The specie *Ruminococcus lactaris*, as well as *Coprococcus catus* and *Prevotella copri*, were the main drivers of the enrichment of the carbohydrate metabolism pathway in the condition of high choline. The species *Parabacteroides merdae*, was the major driver of the enrichment in the carbohydrate metabolism pathway, while *Bacteroides eggerthii* attenuated that enrichment in the condition of low choline. At the module level, some species, for example *Prevotella copri*, drove the observed shift in one function while attenuating the shift in another (**Figure S3**).

4 DISCUSSION

Our study systematically investigated the associations of intestinal microbiota and microbiota-generated metabolites with glucose metabolism. In this study, we observed that plasma choline was positively, while betaine was negatively associated with diabetes, independently of TMAO in Chinese adults. Individuals with diabetes could be accurately distinguished from controls by integrating data on choline, and certain species abundance, as well as some traditional risk factors such as age, sex, BMI and waistline. Additionally, some species, for example diabetes-associated species *Prevotella copri* drove the observed shift in one function while attenuating the shift in another at the module level, which implies species often had complex impacts

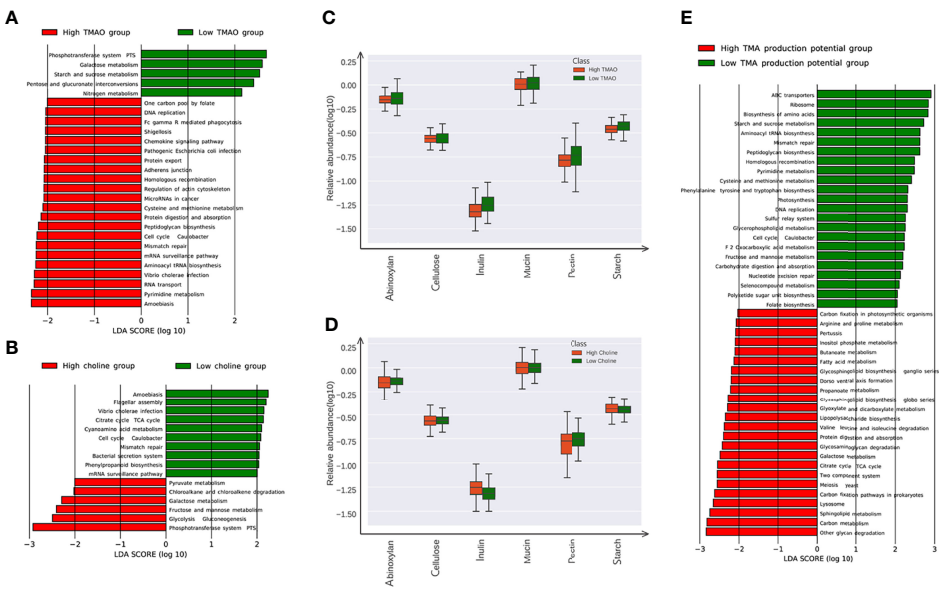

FIGURE 4 | Microbial gene functions annotation in the low (lower thirds) and high (higher thirds) TMAO/Choline groups. **(A)** The average abundance of KEGG modules differentially enriched in gut microbiome of the low and high TMAO groups. Five modules enriched in low TMAO group, and 22 modules overrepresented in high TMAO group are shown in green and red, respectively. **(B)** The average abundance of KEGG modules differentially enriched in gut microbiome of low and high choline groups. Five modules enriched in low choline group, and twenty twou modules overrepresented in high choline group are shown in green and red, respectively. **(C)** The average abundance of CAZy family involved in metabolism of inulin, pectin, and starch significantly altered in the low and high TMAO groups. **(D)** The average abundance of CAZy family involved in metabolism of inulin significantly altered in the low and high choline groups. **(E)** The average abundance of KEGG modules differentially enriched in gut microbiome of groups with the low and high TMA production potential. 23 modules enriched in low TMA production potential group, and 24 modules overrepresented in high TMAO group are shown in green and red, respectively.

on the observed shift in function. Greater attention should be paid to plasma choline because it is more stable, and links the microbiota to impaired glucose metabolism and diabetes.

According to recent series of researches, intestinal microbiota can metabolize trimethylamine (TMA)-containing nutrients to produce TMA in the intestine, which is subsequently converted into TMAO by host FMO3 in the liver (18). Manipulation of TMAO concentrations in mice through inhibiting host FMO3 can prevent the development of hyperglycemia, hyperlipidemia, and atherosclerosis in a diabetic mouse model (10). Plasma level of TMAO was found to be higher in diabetic individuals in observed studies (11, 19). The meta-analysis of continuous variable documented that levels of TMAO were 0.36μmol/L higher in patients with diabetes than in that without diabetes (20). However, in intervention studies, a reduction of choline rather than TMAO showed significant associated with losses of body fat, fasting insulin and HOMA-IR, as well as 2-year improvements in glucose and insulin resistance (12, 21). Similarly, circulating level of choline decreased in morbidly obese patients after bariatric surgery along with level of TMAO significantly increased after the weight loss. Mice fed a choline-deficient diet also observed to have improved insulin resistance and glucose metabolism (22). In our results, there was a positive relationship between plasma choline and adverse glucose metabolism independently of TMAO. We speculate the blood glucose modulated by choline was possibly through different diabetes-related mechanisms besides TMAO. Choline (or the choline metabolite betaine) is a methyl donor involved in one-carbon metabolism and play a critical role in methylation reactions, including DNA methylation, as well as DNA stability and repair. Disruption of epigenetic mechanisms may significantly impact the development of metabolic disease by increasing oxidative stress, reducing chromosome stability, and promoting the development of obesity, insulin resistance, and vascular dysfunction (23). Previous epidemiological study have demonstrated that DNA methylomic changes are associated with chronic health conditions such as glucose level alteration, and most DNA meta-methylome changes occurred 80-90 days before clinically detectable glucose elevation (24). Besides, data from KEGG pathways and Cazy enzymes showed microbial functions in the condition of high choline displayed higher capacity for carbohydrate utilization, by which we also speculated that microbiota might directly induce adverse glucose metabolism through other metabolites, rather than TMAO production. For example, intestinal microbiota was able to synthesize amino acids, such as aromatic amino acids (AAAs) and branched-chain amino acids (BCAAs), and choline was further positively connected to these diabetes-related amino acids (12, 25).

Plasma betaine, contrary to choline, was inversely associated with diabetes in our study. Previous study has showed that plasma choline and betaine were investigated in relation to cardiovascular disease risk with opposite directions, that choline was positively, conversely betaine was inversely associated with several components of cardiometabolic risk profiles in different populations (26, 27). Glycine betaine mainly from the food items could be transformed into a group of betainized compounds by the gut microbiota. In recent interventional and animal studies, betainized compounds correlated with improved glucose metabolism and the risk of diabetes (28). Among adults with the metabolic syndrome, PAB, one betainized compounds, was associated with favorable fasting insulin, lipid profiles and inflammation (29). Several bacterial taxa, including *Akkermansia*, *Bifidobacterium*, *Coriobacteriaceae*, *Lactobacillus*, *Parasutterella*, and *Ruminococcus*, may involve in betaine metabolism in animal study (30). Betaine is formed in kidney and liver by choline oxidation, or obtained from food of cereal grains, especially whole-grain rye and wheat. Betaine serves as a methyl donor in the betaine-homocysteine methyltransferase reaction, which is responsible for the betaine-dependent remethylation of homocysteine to methionine (31). There is an important crosstalk between choline/1-carbon metabolism (such as betaine) and the pathways of insulin sensitivity, fact deposition and energy metabolism through epigenetic modifications. This may explain why there is a paradox: increased plasma concentration of choline associated with hyperglycemia, but decreased plasma concentration of betaine also related to hyperglycemia. Given that most of the evidence is cross-sectional, it cannot be used to establish cause and effect between betaine deficiency and hyperglycemia. Diagnostic performance of betained compounds in blood is important for future research, which need further studies to elucidate mechanisms.

Two independent metagenome-wide association studies in European and Asian patients with diabetes, showed that the concentrations of butyrate-producing such as *Roseburia intestinalis* and *Faecalibacterium prausnitzii* decreased in diabetic subjects, and the proportion of opportunistically pathogenic *Clostridium* species increased (2, 32). Zhang et al. (33) focused on the analysis of the intestinal microbiota in prediabetes using 16S rDNA-based high-throughput sequencing. Patients with prediabetes already differed from normal glucose people, that prediabetes had lower proportions of butyrate-producing bacteria such as *Akkermansia muciniphila ATCCBAA-835*, and *Faecalibacterium prausnitzii L2-6*, whereas bacteria such as *Clostridiales* sp. *SS3/4*, and *Haemophilus parainfluenzae T3T1* were more abundant. In Danish adults, the intestinal microbiota differed the most between prediabetes and controls were genus *Clostridium* and *Akkermansia muciniphila*, which both displayed lower abundance in prediabetes group (34). Despite there was a similar trend in some universal butyrate-producing bacteria, the bacterial taxa were markedly different in diverse populations, demonstrating the microbiota is dramatically impacted by research method, diet, medication use, ethnicity and geographical locations. In our study, we found that *Coprococcus catus* belonged to *Firmicutes* was the common microbial characteristics of diabetes, and contributed a lot to distinguish individuals with diabetes from controls, which is consistent with previous studies that phyla *Firmicutes* (eg.*Coprococcus catus*) were more abundant in obese people those had worse glucose level (35, 36). *Ruminococcus* flora help gut epithelial cells to absorb sugars, which might contribute to weight gain in the host. Results from diabetic rats model demonstrated that blood glucose was positively correlated with *Ruminococcus* (37). In previous animal studies, two *Parabacteroides* species, including *Parabacteroides distasonis* and *Parabacteroides goldsteinii*, played roles in anti-obesity, hyperglycemia, and insulin

resistant (38, 39). *Parabacteroides merdae*, which is opportunistic pathogenic taxa, was reported frequently distributed in hypertensive gut microbiome, further investigations whether *Parabacteroides merdae* play preventive role in the progression of diabetes need be conducted. Since a number of *Ruminococcus* species are known to be associated with metabolic diseases, also *Bacteroides eggerthii* abundance was reported significantly higher in obese children and correlated positively with body fat percentage and negatively with insoluble fiber intake (40). Based on data from the MetaHIT, *Prevotella copri* was identified as the main species driving the positive association between biosynthesis of branched-chain amino acids (BCAAs) and insulin resistance, and mice fed with *Prevotella copri* had increased insulin resistance, aggravate glucose intolerance and elevated levels of BCAAs (41). Deficiency of gut short-chain fatty acid (SCFA) is associated with diabetes. We also observed that several *Bifidobacterium* species, including *Bifidobacterium bifidum*, *Bifidobacterium_longum*, *Bifidobacterium_breve*, and *Bifidobacterium adolescentis* were important for classification prediabets and control groups. Zhao et al. (42) found that adopting a high-fiber diet promoted the growth of SCFA-producing species including *Bifidobacterium longum* in diabetic humans, in company with the elevated levels of glucagon-like peptide-1, a decline in hemoglobin A1c levels, and improved blood glucose levels. Although the results yielded different species biomarkers, our findings indicated that choline may be more effective to classify diabetes group from control group, comparing to specific species.

Our study has several strengths and limitations. First, this study introduced data of metagenome and microbiota-generated metabolites in a population-based study, which is to date the largest in Asian allowing us to directly examine bacterial functional genes. Second, we enrolled relatively healthy study population, whereas many of the TMAO studies to date have been limited to participants with metabolic disease or undergoing various medical procedures. Third, we were also able to assess associations of disease biomarkers not only with TMAO, but also choline, carnitine, and betaine. Our study also had some limitations. The major limitation of this study was a cross-sectional study, and the statistically significant association between intestinal microbiota, microbiota-generated metabolites and host health do not establish causality. Longitudinal studies are needed to determine the stronger evidence of these associations. Second, we did not have postprandial blood sugar or HbA1c data available in this study, which may induce a misclassification bias. However, the misclassification of undiagnosed diabetic women into normal glycemic group was more likely to weaken the associations. Third, we did not adjust for potential confounders such as dietary factors. Diet may modify the associations of choline or its metabolites with disease risk. However, in the sensitive analyses, the results were somewhat consistent after further adjusted lifestyle factors including dietary habit.

In this study, we found that the integrating choline and microbiota species, as well as traditional risk factors specific was consistently more effective to classify diabetes from healthy controls. The blood glucose metabolism modulated by microbial metabolites, such as choline and TMAO, were possibly through different diabetes-related mechanisms. These results provide evidence that higher microbial choline was positively associated with glucose metabolism and type 2 diabetes, especially highlight great potential ability for classifying diabetes population by choline and specific intestinal species.

DATA AVAILABILITY STATEMENT

The datasets presented in this study can be found in online repositories. The names of the repository/repositories and accession number(s) can be found below: https://www.ncbi.nlm.nih.gov/, PRJNA511714.

ETHICS STATEMENT

The studies involving human participants were reviewed and approved by Ethical Committee of the Chinese People's Liberation Army General Hospital. The patients/participants provided their written informed consent to participate in this study.

AUTHOR CONTRIBUTIONS

Conceptualization: QZ, LZ, YH, and MZ. Data curation: QZ, YH, XZ, MZ. Formal analysis: All authors. Funding acquisition: QZ, XZ, YH. Investigation: All authors. Methodology: QZ, YH, XZ, MZ. Project administration: QZ, XZ. Resources: QZ, XZ. Software: YH, XC, DL. Supervision: QZ, YH. Validation: QZ, XZ. Writing - original draft: QZ, MZ, FW. Writing - review and editing: YH, HL, XZ, YPL. QZ, LZ and YH are the guarantors of this work and, as such, had full access to all of the data in the study and take responsibility for the integrity of the data and the accuracy of the data analysis. All authors contributed to the article and approved the submitted version.

FUNDING

This work was supported by Grants 81872920, 81602854, 81561128020, 91639108, 81370235 and 81970425 from the Natural Science Foundation of China. This project was also supported by Grant 2016YFC0903000 from Ministry of Science and Technology of China.

ACKNOWLEDGMENTS

The authors wish to thank the support of all the investigators and participants who contributed to this study.

SUPPLEMENTARY MATERIAL

The Supplementary Material for this article can be found online at: https://www.frontiersin.org/articles/10.3389/fendo.2022.906310/full#supplementary-material

REFERENCES

1. Khan MT, Nieuwdorp M, Backhed F. Microbial Modulation of Insulin Sensitivity. *Cell Metab* (2014) 20(5):753–60. doi: 10.1016/j.cmet.2014.07.006
2. Qin J, Li Y, Cai Z, Li S, Zhu J, Zhang F, et al. A Metagenome-Wide Association Study of Gut Microbiota in Type 2 Diabetes. *Nature* (2012) 490(7418):55–60. doi: 10.1038/nature11450
3. Vrieze A, Van Nood E, Holleman F, Salojarvi J, Kootte RS, Bartelsman JF, et al. Transfer of Intestinal Microbiota From Lean Donors Increases Insulin Sensitivity in Individuals With Metabolic Syndrome. *Gastroenterology* (2012) 143(4):913–6e7. doi: 10.1053/j.gastro.2012.06.031
4. Depommier C, Everard A, Druart C, Plovier H, Van Hul M, Vieira-Silva S, et al. Supplementation With Akkermansia Muciniphila in Overweight and Obese Human Volunteers: A Proof-Of-Concept Exploratory Study. *Nat Med* (2019) 25(7):1096–103. doi: 10.1038/s41591-019-0495-2
5. Wang Z, Klipfell E, Bennett BJ, Koeth R, Levison BS, Dugar B, et al. Gut Flora Metabolism of Phosphatidylcholine Promotes Cardiovascular Disease. *Nature* (2011) 472(7341):57–63. doi: 10.1038/nature09922
6. Li XS, Obeid S, Klingenberg R, Gencer B, Mach F, Raber L, et al. Gut Microbiota-Dependent Trimethylamine N-Oxide in Acute Coronary Syndromes: A Prognostic Marker for Incident Cardiovascular Events Beyond Traditional Risk Factors. *Eur Heart J* (2017) 38(11):814–24. doi: 10.1093/eurheartj/ehw582
7. Tang WH, Wang Z, Levison BS, Koeth RA, Britt EB, Fu X, et al. Intestinal Microbial Metabolism of Phosphatidylcholine and Cardiovascular Risk. *New Engl J Med* (2013) 368(17):1575–84. doi: 10.1056/NEJMoa1109400
8. Zhu W, Gregory JC, Org E, Buffa JA, Gupta N, Wang Z, et al. Gut Microbial Metabolite Tmao Enhances Platelet Hyperreactivity and Thrombosis Risk. *Cell* (2016) 165(1):111–24. doi: 10.1016/j.cell.2016.02.011
9. Li D, Kirsop J, Tang WH. Listening to Our Gut: Contribution of Gut Microbiota and Cardiovascular Risk in Diabetes Pathogenesis. *Curr Diabetes Rep* (2015) 15(9):63. doi: 10.1007/s11892-015-0634-1
10. Miao J, Ling AV, Manthena PV, Gearing ME, Graham MJ, Crooke RM, et al. Flavin-Containing Monooxygenase 3 as a Potential Player in Diabetes-Associated Atherosclerosis. *Nat Commun* (2015) 6:6498. doi: 10.1038/ncomms7498
11. Schugar RC, Shih DM, Warrier M, Helsley RN, Burrows A, Ferguson D, et al. The Tmao-Producing Enzyme Flavin-Containing Monooxygenase 3 Regulates Obesity and the Beiging of White Adipose Tissue. *Cell Rep* (2017) 19(12):2451–61. doi: 10.1016/j.celrep.2017.05.077
12. Heianza Y, Sun D, Li X, DiDonato JA, Bray GA, Sacks FM, et al. Gut Microbiota Metabolites, Amino Acid Metabolites and Improvements in Insulin Sensitivity and Glucose Metabolism: The Pounds Lost Trial. *Gut* (2018) 68(2):263–70. doi: 10.1136/gutjnl-2018-316155
13. Liu J, Zhao M, Zhou J, Liu C, Zheng L, Yin Y. Simultaneous Targeted Analysis of Trimethylamine-N-Oxide, Choline, Betaine, and Carnitine by High Performance Liquid Chromatography Tandem Mass Spectrometry. *J Chromatogr B Analyt Technol BioMed Life Sci* (2016) 1035:42–8. doi: 10.1016/j.jchromb.2016.09.026
14. Li R, Yu C, Li Y, Lam TW, Yiu SM, Kristiansen K, et al. Soap2: An Improved Ultrafast Tool for Short Read Alignment. *Bioinf (Oxford England)* (2009) 25 (15):1966–7. doi: 10.1093/bioinformatics/btp336
15. Xie H, Guo R, Zhong H, Feng Q, Lan Z, Qin B, et al. Shotgun Metagenomics of 250 Adult Twins Reveals Genetic and Environmental Impacts on the Gut Microbiome. *Cell Syst* (2016) 3(6):572–84e3. doi: 10.1016/j.cels.2016.10.004
16. Arumugam M, Raes J, Pelletier E, Le Paslier D, Yamada T, Mende DR, et al. Enterotypes of the Human Gut Microbiome. *Nature* (2011) 473(7346):174–80. doi: 10.1038/nature09944
17. Truong DT, Franzosa EA, Tickle TL, Scholz M, Weingart G, Pasolli E, et al. Metaphlan2 for Enhanced Metagenomic Taxonomic Profiling. *Nat Methods* (2015) 12(10):902–3. doi: 10.1038/nmeth.3589
18. Tang WH, Hazen SL. The Contributory Role of Gut Microbiota in Cardiovascular Disease. *J Clin Invest* (2014) 124(10):4204–11. doi: 10.1172/JCI72331
19. Tang WH, Wang Z, Li XS, Fan Y, Li DS, Wu Y, et al. Increased Trimethylamine N-Oxide Portends High Mortality Risk Independent of Glycemic Control in Patients With Type 2 Diabetes Mellitus. *Clin Chem* (2017) 63(1):297–306. doi: 10.1373/clinchem.2016.263640
20. Zhuang R, Ge X, Han L, Yu P, Gong X, Meng Q, et al. Gut Microbe–Generated Metabolite Trimethylamine N-Oxide and the Risk of Diabetes: A Systematic Review and Dose-Response Meta-Analysis. *Obes Rev* (2019) 20(6):883–94. doi: 10.1111/obr.12843
21. Heianza Y, Sun D, Smith SR, Bray GA, Sacks FM, Qi L. Changes in Gut Microbiota–Related Metabolites and Long-Term Successful Weight Loss in Response to Weight-Loss Diets: The Pounds Lost Trial. *Diabetes Care* (2018) 41(3):413–9. doi: 10.2337/dc17-2108
22. Raubenheimer PJ, Nyirenda MJ, Walker BR. A Choline-Deficient Diet Exacerbates Fatty Liver But Attenuates Insulin Resistance and Glucose Intolerance in Mice Fed a High-Fat Diet. *Diabetes* (2006) 55(7):2015–20. doi: 10.2337/db06-0097
23. Wang J, Wu Z, Li D, Li N, Dindot SV, Satterfield MC, et al. Nutrition, Epigenetics, and Metabolic Syndrome. *Antioxid Redox Signal* (2012) 17 (2):282–301. doi: 10.1089/ars.2011.4381
24. Chen R, Xia L, Tu K, Duan M, Kukurba K, Li-Pook-Than J, et al. Longitudinal Personal DNA Methylome Dynamics in a Human With a Chronic Condition. *Nat Med* (2018) 24(12):1930–9. doi: 10.1038/s41591-018-0237-x
25. Wang TJ, Larson MG, Vasan RS, Cheng S, Rhee EP, McCabe E, et al. Metabolite Profiles and the Risk of Developing Diabetes. *Nat Med* (2011) 17(4):448–53. doi: 10.1038/nm.2307
26. Konstantinova SV, Tell GS, Vollset SE, Nygard O, Bleie O, Ueland PM. Divergent Associations of Plasma Choline and Betaine With Components of Metabolic Syndrome in Middle Age and Elderly Men and Women. *J Nutr* (2008) 138(5):914–20. doi: 10.1093/jn/138.5.914
27. Fu BC, Hullar MAJ, Randolph TW, Franke AA, Monroe KR, Cheng I, et al. Associations of Plasma Trimethylamine N-Oxide, Choline, Carnitine, and Betaine With Inflammatory and Cardiometabolic Risk Biomarkers and the Fecal Microbiome in the Multiethnic Cohort Adiposity Phenotype Study. *Am J Clin Nutr* (2020) 111(6):1226–34. doi: 10.1093/ajcn/nqaa015
28. Karkkainen O, Lankinen MA, Vitale M, Jokkala J, Leppanen J, Koistinen V, et al. Diets Rich in Whole Grains Increase Betainized Compounds Associated With Glucose Metabolism. *Am J Clin Nutr* (2018) 108(5):971–9. doi: 10.1093/ajcn/nqy169
29. Tuomainen M, Kärkkäinen O, Leppänen J, Auriola S, Lehtonen M, Savolainen MJ, et al. Quantitative Assessment of Betainized Compounds and Associations With Dietary and Metabolic Biomarkers in the Randomized Study of the Healthy Nordic Diet (Sysdiet). *Am J Clin Nutr* (2019) 110 (5):1108–18. doi: 10.1093/ajcn/nqz179
30. Koistinen VM, Karkkainen O, Borewicz K, Zarei I, Jokkala J, Micard V, et al. Contribution of Gut Microbiota to Metabolism of Dietary Glycine Betaine in Mice and in Vitro Colonic Fermentation. *Microbiome* (2019) 7(1):103. doi: 10.1186/s40168-019-0718-2
31. Lever M, George PM, Slow S, Bellamy D, Young JM, Ho M, et al. Betaine and Trimethylamine-N-Oxide as Predictors of Cardiovascular Outcomes Show Different Patterns in Diabetes Mellitus: An Observational Study. *PloS One* (2014) 9(12):e114969. doi: 10.1371/journal.pone.0114969
32. Karlsson FH, Tremaroli V, Nookaew I, Bergstrom G, Behre CJ, Fagerberg B, et al. Gut Metagenome in European Women With Normal, Impaired and Diabetic Glucose Control. *Nature* (2013) 498(7452):99–103. doi: 10.1038/nature12198
33. Zhang X, Shen D, Fang Z, Jie Z, Qiu X, Zhang C, et al. Human Gut Microbiota Changes Reveal the Progression of Glucose Intolerance. *PloS One* (2013) 8(8): e71108. doi: 10.1371/journal.pone.0071108
34. Allin KH, Tremaroli V, Caesar R, Jensen BAH, Damgaard MTF, Bahl MI, et al. Aberrant Intestinal Microbiota in Individuals With Prediabetes. *Diabetologia* (2018) 61(4):810–20. doi: 10.1007/s00125-018-4550-1
35. Kasai C, Sugimoto K, Moritani I, Tanaka J, Oya Y, Inoue H, et al. Comparison of the Gut Microbiota Composition Between Obese and Non-Obese Individuals in a Japanese Population, as Analyzed by Terminal Restriction Fragment Length Polymorphism and Next-Generation Sequencing. *BMC Gastroenterol* (2015) 15:100–. doi: 10.1186/s12876-015-0330-2
36. Andoh A, Nishida A, Takahashi K, Inatomi O, Imaeda H, Bamba S, et al. Comparison of the Gut Microbial Community Between Obese and Lean Peoples Using 16s Gene Sequencing in a Japanese Population. *J Clin Biochem Nutr* (2016) 59(1):65–70. doi: 10.3164/jcbn.15-152
37. Zhou W, Xu H, Zhan L, Lu X, Zhang L. Dynamic Development of Fecal Microbiome During the Progression of Diabetes Mellitus in Zucker Diabetic

Fatty Rats. *Front Microbiol* (2019) 10:232(232). doi: 10.3389/fmicb.2019.00232
38. Wang K, Liao M, Zhou N, Bao L, Ma K, Zheng Z, et al. Parabacteroides Distasonis Alleviates Obesity and Metabolic Dysfunctions *Via* Production of Succinate and Secondary Bile Acids. *Cell Rep* (2019) 26(1):222–35e5. doi: 10.1016/j.celrep.2018.12.028
39. Wu TR, Lin CS, Chang CJ, Lin TL, Martel J, Ko YF, et al. Gut Commensal Parabacteroides Goldsteinii Plays a Predominant Role in the Anti-Obesity Effects of Polysaccharides Isolated From Hirsutella Sinensis. *Gut* (2019) 68 (2):248–62. doi: 10.1136/gutjnl-2017-315458
40. Lopez-Contreras BE, Moran-Ramos S, Villarruel-Vazquez R, Macias-Kauffer L, Villamil-Ramirez H, Leon-Mimila P, et al. Composition of Gut Microbiota in Obese and Normal-Weight Mexican School-Age Children and Its Association With Metabolic Traits. *Pediatr Obes* (2018) 13(6):381–8. doi: 10.1111/ijpo.12262
41. Pedersen HK, Gudmundsdottir V, Nielsen HB, Hyotylainen T, Nielsen T, Jensen BA, et al. Human Gut Microbes Impact Host Serum Metabolome and Insulin Sensitivity. *Nature* (2016) 535(7612):376–81. doi: 10.1038/nature18646
42. Zhao L, Zhang F, Ding X, Wu G, Lam YY, Wang X, et al. Gut Bacteria Selectively Promoted by Dietary Fibers Alleviate Type 2 Diabetes. *Science* (2018) 359(6380):1151–6. doi: 10.1126/science.aao5774

Conflict of Interest: Author XC was employed by the company Bao Feng Key Laboratory of Genetics and Metabolism in Beijing. Author DL was employed by the company WeHealthGene Institute in Shenzhen.

The remaining authors declare that the research was conducted in the absence of any commercial or financial relationships that could be construed as a potential conflict of interest.

frontiers | Frontiers in Endocrinology

ORIGINAL RESEARCH
published: 30 June 2022
doi: 10.3389/fendo.2022.882192

Integrated Digital Health Solutions in the Management of Growth Disorders in Pediatric Patients Receiving Growth Hormone Therapy: A Retrospective Analysis

Vincenzo Tornincasa[1], *David Dixon*[1], *Quentin Le Masne*[1], *Blaine Martin*[1], *Lilian Arnaud*[1], *Paula van Dommelen*[2] *and Ekaterina Koledova*[3*]

[1] Ares Trading S.A. (an affiliate of Merck KGaA), Eysins, Switzerland, [2] Department of Child Health, The Netherlands Organization for Applied Scientific Research TNO, Leiden, Netherlands, [3] Global Medical Affairs Cardiometabolic & Endocrinology, Merck Healthcare KGaA, Darmstadt, Germany

OPEN ACCESS

Edited by:
Eli Hershkovitz,
Soroka Medical Center, Israel

Reviewed by:
Giorgio Radetti,
Ospedale di Bolzano, Italy
Bradley Scott Miller,
University of Minnesota Children's Hospital, United States

***Correspondence:**
Ekaterina Koledova
ekaterina.koledova@merckgroup.com

Specialty section:
This article was submitted to Pediatric Endocrinology, a section of the journal Frontiers in Endocrinology

Received: *23 February 2022*
Accepted: *06 June 2022*
Published: *30 June 2022*

Citation:
Tornincasa V, Dixon D, Le Masne Q, Martin B, Arnaud L, van Dommelen P and Koledova E (2022) Integrated Digital Health Solutions in the Management of Growth Disorders in Pediatric Patients Receiving Growth Hormone Therapy: A Retrospective Analysis. Front. Endocrinol. 13:882192. doi: 10.3389/fendo.2022.882192

Digital health has seen rapid advancements over the last few years in helping patients and their healthcare professionals better manage treatment for a variety of illnesses, including growth hormone (GH) therapy for growth disorders in children and adolescents. For children and adolescents requiring such therapy, as well as for their parents, the treatment is longitudinal and often involves daily injections plus close progress monitoring; a sometimes daunting task when young children are involved. Here, we describe our experience in offering devices and digital health tools to support GH therapy across some 40 countries. We also discuss how this ecosystem of care has evolved over the years based on learnings and advances in technology. Finally, we offer a glimpse of future planned enhancements and directions for digital health to play a bigger role in better managing conditions treated with GH therapy, as well as model development for adherence prediction. The continued aim of these technologies is to improve clinical decision making and support for GH-treated patients, leading to better outcomes.

Keywords: digital health, growth hormone treatment, pediatric endocrinology, adherence monitoring, patient engagement

INTRODUCTION

Over the last decade, healthcare has experienced a digital revolution. Rapid advances in connected health, mobile technology, artificial intelligence (AI), and gamification, including through virtual and augmented reality (VR/AR) techniques, are making a difference in how patients are diagnosed, treated, and managed. At the same time, healthcare systems are facing a crossroads that is characterized by resource limitation and an increased demand for personalized patient care. Digitalization has changed these dynamics by improving patient access to information, facilitating monitoring, intervention, and communications with healthcare providers, and thus reducing traditional limitations associated with healthcare services (1–5). Indeed, digital health has played a key role in keeping systems operational during the COVID-19 pandemic, helping patients

to access care in more convenient ways without the burden of regular office visits and the unnecessary risk of exposure to infection (6, 7).

Digital health solutions are typically disease-specific and address certain conditions and patient populations. Healthcare system complexities and nuances unique to each country often mean that these solutions are tailored to a particular country and difficult to seamlessly transfer from one setting to another. Here, we share our perspectives and experience from over a decade of providing digital health solutions for managing growth hormone (GH) therapy in children and adolescents. These solutions represent one of the most broadly implemented digital health solutions in pediatrics. We will also discuss how we envision future directions and opportunities for improving the management of growth disorders using digital health, including findings on models for adherence prediction.

GH THERAPY

GH is important for physical growth and maintenance of healthy body composition and cardiovascular wellbeing (8). There are multiple genetic, environmental, metabolic, and nutritional causes of growth failure in children. In this respect, GH therapy is approved for a range of specific short stature conditions to increase growth and adult height, and improve metabolic and psychosocial health (9–11). When short stature is detected specialist evaluation and management is warranted (12, 13). Initial evaluation to accurately identify the cause is based on patient history, meticulous recording of height and height velocity (auxology), and endocrine tests (14). Approved indications for GH administration include GH deficiency and rare non-GH deficient disorders such as Turner syndrome (TS) and lack of catch-up growth after being born small for gestational age (SGA). GH deficiency has an estimated prevalence of 1:4,000 to 1:10,000 children (15, 16), and can become apparent at different ages. Severe cases can present within the first 6 months after birth, whereas milder cases manifest in later childhood (15). TS has a prevalence of approximately 1:2,000 females and may be diagnosed shortly after birth, but is frequently only diagnosed from short stature at around pubertal age (17). For children born SGA, approximately 90% show catch-up growth within 4 years, and prevalence for those remaining short and qualifying for GH therapy is 1:1,800 to 1:3,250 births (18, 19).

Once diagnosed and prescribed GH therapy, the child and their parents/caregivers are instructed on the administration of daily injections by nurses. While long-acting GH formulations requiring once-weekly injections have recently been approved, these therapies are new and their long-term safety and efficacy records are not yet as thoroughly established (20–22).

The patient's multi-year journey on GH therapy involves frequent injections and regular clinic visits (typically every 6 months) to assess growth and metabolic parameters. Along this journey and depending on the healthcare setting, they receive various levels of information, support, and encouragement to comply with the therapy regimen. HCPs may also be involved in dealing with clinical, emotional, and behavioral issues that arise both early in the treatment path and later during teenage years, including when transitioning from adolescence to adulthood (23, 24). In early childhood, parents or caregivers are often involved in administering injections, and supporting routine. In adolescents, continuation of GH therapy may be required into adulthood to optimize body composition maturation and metabolic factors that could adversely affect their cardiovascular health (25–27).

For all indications, optimal response requires early GH initiation and continuous treatment for several years through adolescence (11, 15, 28). Response is highest in the first year of therapy, declining over subsequent years (15, 16, 29). As a result, it is imperative to closely monitor children throughout treatment. Within the clinic, several important diagnostic and management tools are available to assess the cause and track the therapy response including catch-up growth, genetic analyses, GH stimulation tests, serum insulin-like growth factor-1 (IGF-1) concentration, bone age, and brain magnetic resonance imaging (3).

For optimal outcomes, two important considerations are: adherence to therapy (extent to which the patient's behavior matches agreed recommendations from their HCP); and persistence with therapy (*lack of discontinuation*). Non-adherence can be defined in various ways, from taking doses smaller than prescribed to skipping injections intermittently (30). Therapies for many chronic conditions are associated with suboptimal adherence (31–34). In the case of GH administration, this has negative effects on the catch-up growth response (34–37) and, and potentially, on achieving target adult height. While adherence to GH therapy is crucial, it is difficult to measure and is often reliant on patient testimony or proxy measurements such as prescription records or vial counting (38). In conjunction, detection of poor adherence to GH treatment can be problematic because patients or caregivers may be reluctant to admit to or recall missed doses and may therefore overestimate their adherence to treatment during discussions with their healthcare providers (39). These challenges most likely explain the wide range of estimated prevalence of non-adherence (from 5% to 82%), making it is difficult to compare adherence rates among studies (40, 41). Factors shown to be strongly associated with non-adherence and lack of persistence include misperceptions about the consequences of missed doses, lack of understanding of the disease and GH therapy, discomfort with injections, dissatisfaction with growth outcomes, and inadequate or problematic contact with HCPs (30, 42–44). Several strategies have been recommended to enhance adherence (42, 45–47); however, there is a need for standardized measures to accurate monitoring adherence and clinical outcomes, to support patient management (48).

DIGITAL HEALTH ECOSYSTEM FOR GH THERAPY

Released in 2006 by Merck Healthcare KGaA (Darmstadt, Germany), the easypod™ drug delivery solution was designed to

support children undergoing GH therapy for growth disorders (49, 50). It was specifically designed with the comfort of the children in mind as a friendly-to-use auto-injector for administration of recombinant human GH (r-hGH, somatropin, Saizen®, Merck Healthcare KGaA, Darmstadt, Germany) (51). It features a skin sensor, an automatic needle attachment that hides the needle, audible and visual signals, and customizable injection settings, such as needle speed and depth, to minimize pain on injection. The device, which is available in multiple languages, also includes a display that provides confirmation of dose injected, last injection date and time, and remaining dose in the cartridge, along with instructions and reminders. Clinics can further customize dose settings and allow for dose adjustments, as necessary (52).

While some level of historic data was available on the device display, it was recognized early on that this can be better tracked and visualized *via* computer software. The information on date, time, and dose allows adherence to be tracked, assisting HCPs in their therapy decisions. Initial digital health software, dubbed the easypod™ clinical kit, obtained the information from the device using a USB connection and a docking station in the clinic, which allowed for analysis on a connected computer with Microsoft Windows-based programs. Over the intervening years, with the prominence of the world wide web and cloud architecture, the easypod™ connect system was developed to centralize data for each clinic and enable monitoring of patients' progress. easypod™ connect version 1.0, released in 2011, was a web-based system that allowed data transmission by the patient/caregiver through a USB-connected docking station provided by the clinic. In subsequent years, the ability to transmit data directly from the docking station *via* a cellular network was added. easypod™ connect version 2.0, released in 2014, included software to analyze more than 90 reference charts for growth and advanced reporting tools to comprehensively monitor the patient's progress. It also provided the ability to interconnect with external electronic health record (EHR) platforms for simple enrolment and reporting (53). The easypod™ connect Next ecosystem, released in 2020, provided more seamless and intuitive programs to help HCPs better track the progress of each patient (**Figure 1**).

The ecosystem currently includes the easypod™ connect platform and reporting system, the growlink™ app that can be used by patients and their families to monitor progress and provide educational information, and the TuiTek™ patient support program (PSP). Based on the COM-B behavioral management framework, TuiTek is a combination of behavioral science (Tuition) and technologic innovation (Tek). It provides a foundation for the creation of personalized, behaviorally-driven, self-management support solutions for patients, caregivers, and HCPs living with and managing GH therapy (54).

AR and gaming have become valuable tools in engaging and educating patients, particularly young children, as part of their treatment journey (55). The easypod™ AR app has been developed to provide training and engagement using avatars and games to familiarize young patients and their families with the easypod™ device.

In recent years, other pharmaceutical companies have also offered digital health solutions to better support patients requiring GH therapy and their HCPs. The Growth Track Wizard™ (Novo Nordisk, Bagsværd, Denmark) is a web-based, patient-facing platform that allows parents and children to track their own growth, receive information about their treatment, and order supplies. Similarly, the GroAssist® (Pfizer, New York, NY, United States) patient support app provides medication and appointment reminders, tracks injection site rotations and reactions, tracks and graphically displays growth based on self-measured height and weight, and provides a rewards scheme to keep children and parents engaged. However, these apps do not currently connect to any injection device.

With connected health and digital health becoming more prevalent in today's clinical practice, Merck Healthcare KGaA's (Darmstadt, Germany) efforts to enhance this digital health ecosystem have focused on multiple fronts including empowering physicians and nurses in their treatment decisions (53). The aim is to make patients more central to the process by providing digital technologies that engage and support them throughout treatment (56). Another important consideration was to enable evidence generation through clinical studies to demonstrate the efficacy of these tools (34). Over the years, the company has collected data from more than 25,000 patients, in nearly 40 countries, allowing analysis of real-world data (38) to glean insights and identify new capabilities to support HCPs and patients along their journey.

Empowering HCPs

With digital platforms, clinicians and nurses often face difficulties in managing separate systems and login accounts, with possible requirement of double entry across systems and no clarity over patients that require the most attention. Greater use of electronic medical record (EMR) or EHR systems across healthcare, mitigates the problems to some extent. However, there remains a great deal of hesitation regarding double entry of data and availability of patient records. In the case of GH-treated patients, different approaches were utilized to empower HCPs.

Connectivity links with EMR/EHR systems have been added to allow data exchange and direct input, including patient demographics and data reporting, to avoid duplicate data entry (57, 58). While this is a beneficial feature in theory, these processes have not been utilized to their full potential due to the complexity of hospital information technology infrastructures and rules around implementing such EMR/EHR links. The variety of different systems makes it a requirement for one-off and customized interconnection for each hospital or clinic, which has made it impractical. As such, interoperability becomes the norm, bidirectional flow of information between the two systems will make things much smoother and avoid the need for duplicate data entry.

Based on user feedback and focus groups, comprising physicians and nurses with experience using the system, the company also revamped the easypod™ connect system to improve performance and make it more friendly and intuitive (**Figure 2**). Changes included providing actionable insights and making information more readily available in graphical and

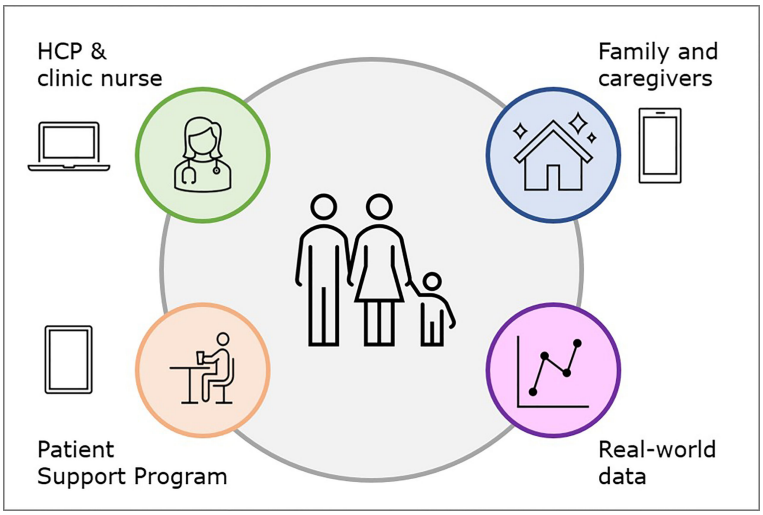

FIGURE 1 | Growth hormone digital health ecosystem.

report forms, and features have been added to allow simpler inputting of demographic and auxologic information, thus enabling easy recording of growth information within the ecosystem. Prediction models for growth, adult height, and risks of non-adherence and lack of persistence are being developed, and will be incorporated in the system in the future to assist HCPs in long-term management of patients (44, 59, 60).

Engaging and Educating Patients

With patient centricity as a fundamental principle, it was important to provide digital health tools and solutions that engage, educate, and complement the lives of patients and their parents/caregivers during their GH therapy journey. This resulted in the growlink™ patient app, which enables patients and their parents/caregivers to obtain information and resources related to their condition (**Figure 3**) (61). Along with injection reminders and an overview of overall adherence, it allows patients to self-report height and weight data (62) that is transmitted to the HCP *via* the platform. growlink™ also facilitates patients' interactions with their care team and patient support services to answer questions or provide supplies such as needles. The latest enhancements to the growlink™ patient app include personalized and relevant content to engage and educate patients and their families during their treatment journey.

Evidence Generation

Improving medical adherence requires estimation of its magnitude, but there is little guidance on tools for evaluating

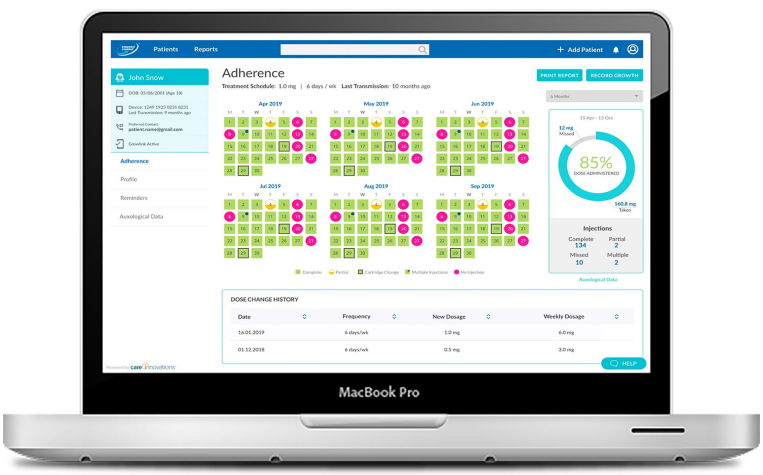

FIGURE 2 | Physician views of the easypod™ connect system.

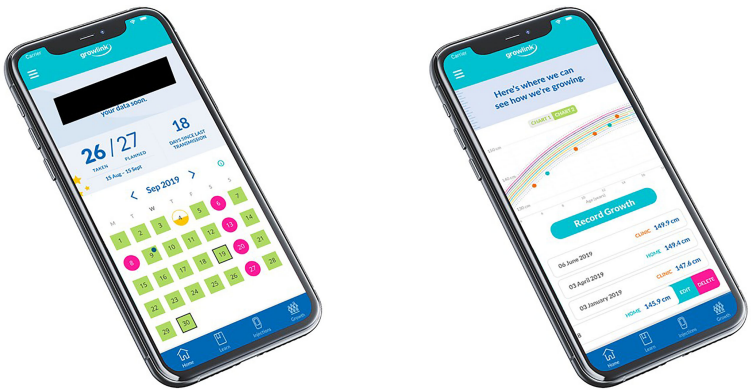

FIGURE 3 | Views of the growlink™ patient app.

adherence (40, 63, 64). Physicians and nurses need access to quick and actionable insights for treatment decisions, including the response to therapy, dose adjustments, customize injection settings, or the need to switch medications. The ecosystem enables objective measurement of adherence to GH therapy. However, early on it became evident that sound scientific evidence is important to support the clinical efficacy of digital solutions. Therefore, the company carried out the global, 5-year Easypod Connect Observational Study (ECOS), with almost 1,200 children with growth disorders, to assess adherence to therapy derived from the easypod™ connect system. The analysis showed high adherence to GH therapy delivered *via* the easypod™ device, which was maintained over time (65). Adherence rates were high throughout, with a median rate of 93.7% in the first year and 87.2% in the third year. Median adherence across the 5 years, based on the individual period of follow-up for each subject, was 89.3%, which equated to <1 missed injection per week on average, irrespective of whether 6 or 7 weekly injections were prescribed. Importantly, this high level of adherence was positively associated with growth outcomes, specifically change in height and height velocity evaluated at 1 and 2 years (34, 65).

The ECOS data also showed similar adherence rates for patients already receiving GH when starting to use the easypod™ connect device and patients naïve to GH therapy (38). Further analyses showed relatively lower adherence for boys than girls, and for young children (≤8 years old) who performed most injections themselves and children who started GH therapy at an older age (≥14 years old) (66). Such data can identify children at risk of low adherence who could be more carefully followed, with appropriate interventions to help avert any fall in adherence.

Harnessing Data

Much progress has been made over recent years concerning the power of data science and large datasets that can be assessed using AI and machine-learning. Information derived from the ecosystem is stored securely and pseudo-anonymized when analyzed for research, similar to other digital health solutions where patient data privacy is a core principle (67–69). Informed consent obtained upon enrolment, along with end-user license agreements, allow the use of pseudo-anonymized data, on the condition that no protected health information on specific patients is made available. The large amount of data from patients using the system over multiple years has the potential to provide insights into the GH therapy journey. Most of this work has focused on factors that influence adherence and persistence with GH therapy. Factors including age and height at the start of treatment, disease severity, sex of the child, level of parent/caregiver or nurse specialist involvement and personalization of the treatment (dose adjustments, customize injection speed/depth, etc.) are significant contributors (70). To have a more complete picture, it would be helpful to incorporate further data, such as growth and socio-economic factors. There are provisions within the system for HCPs to enter auxology information, but this is often not done. This is due to lack of resources and the fact that not all patients in a clinic would receive the same therapy. To address this challenge, work is ongoing with clinics in different countries to fund resources for manual completion of this task. While not ideal, given that each clinic must provide information for a handful of their patients every few months, it is a practical solution that will enable richer analysis of available data.

OUTCOMES ANALYSIS

Database Information

For analysis purposes, data were extracted for all patients from 2007 to the end of 2020 from the database on 18 February 2021, which is a longer timeframe than previously reported (38). Overall, this included 20,264 patients from 38 countries who had transmitted data from 11.5 million injections. **Figure 4** shows the increases over time in the number of patients (**Figure 4A**), number of injections transmitted (**Figure 4B**), number of countries (**Figure 4C**), and countries with active patients (**Figure 4D**).

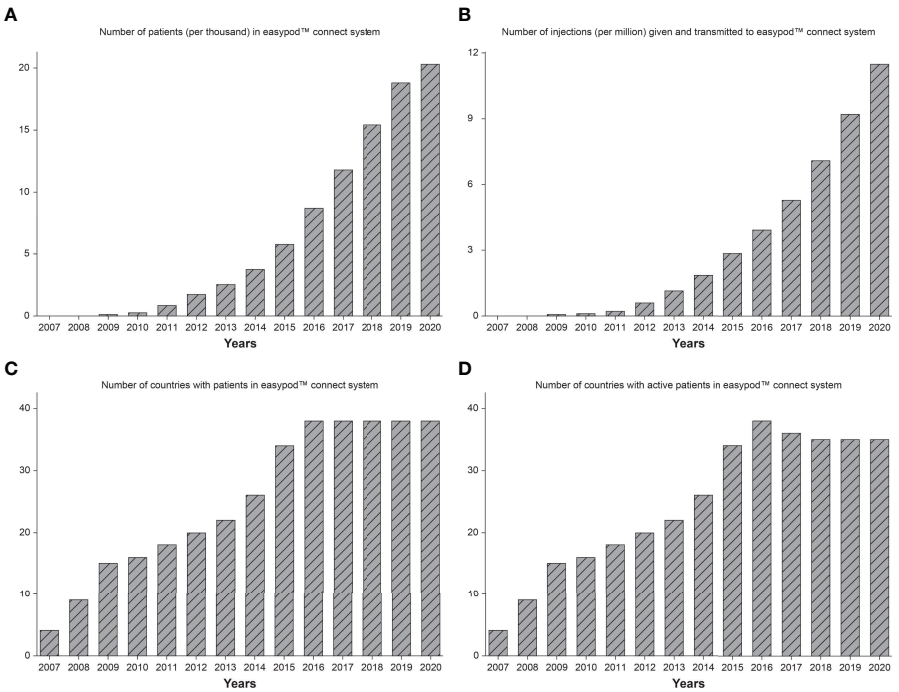

FIGURE 4 | Number of patients **(A)**, number of injections transmitted **(B)**, number of countries **(C)**, and number of countries with active patients **(D)**, in the easypod™ connect database from release in 2007 to end of 2020.

Country Localization

Beyond localizing the solution with language translations for each country, it requires ensuring compliance with local rules and regulations as well as local healthcare system operations. As part of a new country release, the platform is configured in consultation with local resources to adapt to local needs. For instance, strict patient privacy regulations preclude patient support nurses to view any information except patient names and the date of their last data transmission. In countries where Health Authority regulations allow more freedom to operate in the way of direct patient interactions, patient support nurses have access to patient information including adherence levels and even growth data, if available. This has resulted in the highest number of active users and active transmissions. These countries also include some of the highest levels of adherence to therapy. This is likely due to the fact that patient support nurses can intervene and provide training and assistance when necessary. Longer-term plans call for personalized content offered *via* the growlink™ patient app based on patients' age, lifestyle, and language preferences, as well as provision of personalized emotional support and adaptation of language used to the cultural nuances of each country.

Adherence Outcomes

The annual proportion of patients with high adherence (≥85% of prescribed doses administered) between 2010 and 2020 is shown in **Figure 5** according to global region and duration of GH therapy. The proportion with high adherence tended to increase over time, but differences were observed between regions (**Figure 5A**). The proportion of patients with high adherence increased over time in Europe, North America, and Asia, but no consistent change was found among Latin-American/Caribbean patients. **Figure 5B** shows the overall proportion with high adherence (≥85%) between 1–36 months of treatment, stratified by region. The proportion with high adherence decreased over time on treatment, with the strongest decrease in Latin-American/Caribbean and Asian countries. From 24 months onwards, the number of patients in North American and Asian countries was low, making these results less stable.

Catch-Up Growth Outcomes

Height data from 2007 to the end of 2020 were extracted from the database on 18 February 2021. Patients aged ≤18 years with ≥2 recorded growth measurements and adherence data available during treatment were included. Linear interpolation between height measurements was applied to calculate monthly catch-up growth [Change in Height Standard Deviation Score (ΔHSDS)] overall, and by high (≥85%), intermediate (>56%–84%) and low (≤56%) adherence. **Figure 6** shows the mean catch-up growth (ΔHSDS) between 0 and 48 months, stratified by adherence rate (consistently either a high, intermediate or low level at each month). Adherence level had a statistically significant effect on ΔHSDS ($p<0.001$) indicating that maintaining a high level of adherence supports catch-up growth (71).

An analysis of height gain in relation to the cost of GH therapy found that using the easypod™ device resulted in cost

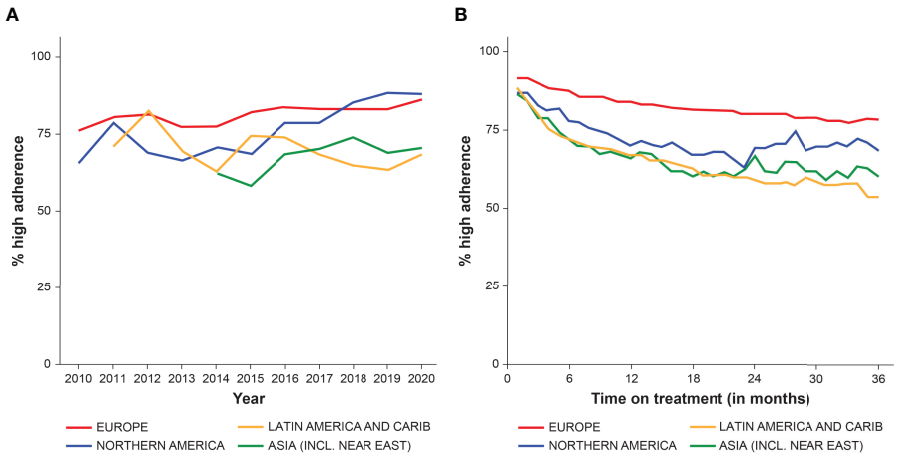

FIGURE 5 | The proportion of patients with high adherence (≥85%) from 2010 to end of 2020, stratified by region, by year **(A)**, and between 0–36 months of GH therapy **(B)**.

savings versus other GH therapy formulations (72). This was likely due to the ecosystem enabling improved adherence and earlier identification of poor responders. Wastage was also reduced compared with other GH formulations and delivery methods, adding to the cost savings.

PREDICTION MODELS

Adherence

Technological advancements help the HCP choose the most effective treatment regimen or intervention; predictions of future outcomes could enable improved treatment based on the individual patient's requirements. Machine-learning has been used in recent years to develop digital models to predict adherence to treatment for diseases such as diabetes (73), tuberculosis (74), Crohn's disease (75), and heart failure (76), based on real-world data. Therefore, similar tools for predicting patient adherence to GH therapy could help to identify appropriate times for intervention to try to alleviate any decrease and manage patient growth outcomes better.

A recurrent neural network was used to devise a prediction model for individual-level future therapy adherence, using a dataset of 2,500 patients on GH therapy with the platform randomly allocated into sets for training, validation, and testing (59). The mean sensitivity and specificity per patient for predicting suboptimal adherence (<85%) were 0.70 and 0.88, respectively. Sensitivity with the prediction model was better than that of the simple average, with very little cost of sensitivity, and the receiver operating curves (ROC) were better for the model than the simple average. It was concluded that the proposed model would be incorporated into the physician interface of the eco-system. A traffic lights presentation could be used to indicate when adherence is likely to be suboptimal, enabling personalized recommendations to address adherence issues, which should improve patient engagement and adherence (70).

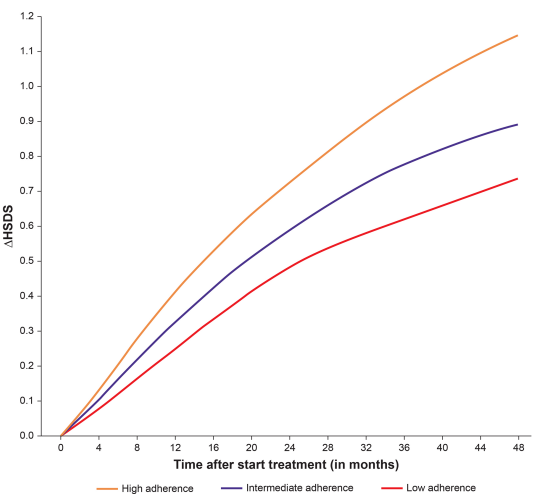

FIGURE 6 | Mean catch-up growth (ΔHSDS) between 0–48 months stratified by high, intermediate, and low adherence.

Growth

Growth response to GH treatment depends on several factors such as age, age at start of therapy, sex, indication, and GH dose. Since the 1990s, data from large cohorts of GH-treated children have been used in several different algorithms devised to predict the growth response from such factors (3, 29). Due to the requirement to input the necessary data, these prediction models have only been used to a limited extent. The easypod™ connect system already includes individual patient information on these factors and a growth prediction model has been developed using data from a trial cohort. When height at the start of use is entered, the predicted height over the subsequent years is shown in tabular format and graphically. In the future,

this may provide HCPs the opportunity to check if the observed growth starts to deviate from the predicted growth, with a traffic lights system similar to that for adherence that can alert the HCP to any problems in growth response. Such support would enable individualization and optimization of therapy.

NEW TECHNOLOGICAL FRONTIERS

In 2020, Merck Healthcare KGaA (Darmstadt, Germany) assembled a panel of scientific experts to consult on the future of and emerging opportunities for its digital health tools to support GH patients, their caregivers, and healthcare team. The resulting framework helped define a roadmap for the evolution of the easypod™ connect digital health ecosystem (12).

For patients, new technologies such as VR/AR and gamification provide the means to better engage the children involved. AR provides the opportunity to offer training, engagement, and support to patients. Complementary apps for this purpose have already been released in multiple countries. Monitoring and tracking height and weight information is also an important element of closing the data loop. Connected weight scales are readily available and there are plans to integrate these as part of the growlink™ patient app. Obtaining height measurements at home in an accurate and simple manner is more difficult. There are systems such as LiDAR (Light Detection and Ranging) that can calculate three-dimensional measurements but require either latest generation smartphones or expensive scanners (77, 78). Many mobile devices already have AR functionalities, and these are being developed within the platform for educational purposes. However, AR can also be adapted for measurement of vertical surfaces that are not flat (79, 80), and can be used to measure human height (81).

Such developments could support future capabilities of the growlink™ app which already provides opportunities to better assess patients' wellbeing and address their needs through questionnaires by their physician and behavior-changing techniques. In addition, it provides relevant and timely content to support social and emotional wellbeing. Digital therapeutics, generally based on cognitive behavioral training, are also seeing large adoption across digital health for various conditions such as anxiety, stress, and depression, and could potentially be considered to improve support for patients requiring GH therapy, with their unique conditions and issues (54, 82, 83). As the focus is broad, attention must be given to ensure that patients and families who have low digital literacy and access can adopt and best utilize these solutions.

To assist HCPs, the company's future efforts will focus on providing meaningful insights that allow them to make better informed clinical decisions and triage the workload towards improved management and support for patients across their journey. Data analysis efforts are expected to result in prediction tools that drive improved adherence and persistence to therapy. The aim is to help HCPs better monitor, track, and manage patients between office visits including appropriate interventions when applicable.

CONCLUSIONS

Supporting patients across their disease journey means more than just providing them and their physicians with a therapy. Beyond a drug, it means all stakeholders involved are provided with the tools, information, services, and support needed to achieve their goal of improving health outcomes. In the setting of GH therapy, this has meant a long-term commitment to providing innovative devices, digital health solutions, and patient support services. This has enabled thousands of patients to achieve their goal of reaching their full height potential.

While enthusiasm and support for digital health technologies was initially slow, these efforts have picked up rapidly over the last few years with broader awareness and acceptance amongst both patients and HCPs. The COVID-19 pandemic has revealed the power such digital health technologies have to better connect patients and HCPs (84). No solution is perfect, however, and to that end, it is necessary to continue the pursuit of introducing innovations and new technologies that address the needs of pediatric patients requiring GH therapy, and all involved in their care. While not intended to replace HCPs, but rather augment and support them in the care delivery process, such work should continue to focus on better understanding the needs of patients and HCPs, generating solutions that address their unique needs and personalizing them to their circumstances.

DATA AVAILABILITY STATEMENT

The original contributions presented in the study are included in the article/supplementary material. Further inquiries can be directed to the corresponding author.

ETHICS STATEMENT

Ethical review and approval was not required for the study on human participants in accordance with the local legislation and institutional requirements. Written informed consent to participate in this study was provided by the participants' legal guardian/next of kin.

AUTHOR CONTRIBUTIONS

VT contributed to the design and interpretation of data for the manuscript. DD and QM oversaw and provided expert review for the analytical plan and results. BM reviewed the manuscript in terms of specific contributions for content related to the use of augmented reality in digital health. LA was involved in data collection/analysis and revision of the manuscript. PvD was involved in data analysis, data interpretation, writing of the outcomes analysis, critical review of the manuscript, and read and approved the final version of the manuscript. EK contributed to the concept, data analysis for the section on real-world evidence, and content development and review. All authors provided their final approval to submit the manuscript.

FUNDING

Merck KGaA, Darmstadt, Germany (CrossRef Funder ID: 10.13039/100009945). The authors declare that this study received funding from Merck (CrossRef Funder ID: 10.13039/100009945). The funder had the following involvement in the study: study design, data collection and analysis, decision to publish, and preparation of the manuscript.

ACKNOWLEDGMENTS

Medical writing assistance was provided by Merat Bagha, Tiba Medical Inc., Beaverton, OR, USA, Dr Peter Bates, Cambridge Medical Writing Services, Cambridge, UK, and Sinéad Mutton of inScience Communications, Springer Healthcare Ltd, UK, and was funded by Merck KGaA, Darmstadt, Germany.

REFERENCES

1. Bhavnani SP, Narula J, Sengupta PP. Mobile Technology and the Digitization of Healthcare. *Eur Heart J* (2016) 37(18):1428–38. doi: 10.1093/eurheartj/ehv770
2. Braune K, Gajewska KA, Thieffry A, Lewis DM, Froment T, O'Donnell S, et al. Why #Wearenotwaiting-Motivations and Self-Reported Outcomes Among Users of Open-Source Automated Insulin Delivery Systems: Multinational Survey. *J Med Internet Res* (2021) 23(6):e25409. doi: 10.2196/25409
3. Labarta JI, Ranke MB, Maghnie M, Martin D, Guazzarotti L, Pfäffle R, et al. Important Tools for Use by Pediatric Endocrinologists in the Assessment of Short Stature. *J Clin Res Pediatr Endocrinol* (2021) 13(2):124–35. doi: 10.4274/jcrpe.galenos.2020.2020.0206
4. Rantala K. *Professionals in Value Co-Creation Through Digital Healthcare Services* Vol. 189). Jyväskylä Studies in Business and Economics (2018).
5. Yaron M, Sher B, Sorek D, Shomer M, Levek N, Schiller T, et al. A Randomized Controlled Trial Comparing a Telemedicine Therapeutic Intervention With Routine Care in Adults With Type 1 Diabetes Mellitus Treated by Insulin Pumps. *Acta Diabetol* (2019) 56(6):667–73. doi: 10.1007/s00592-019-01300-1
6. Alhasan M, Hasaneen M. Digital Imaging, Technologies and Artificial Intelligence Applications During Covid-19 Pandemic. *Comput Med Imaging Graph* (2021) 91:101933. doi: 10.1016/j.compmedimag.2021.101933
7. Choukou M-A, Taha A, Qadeer A, Monnin C. Digital Health Technology for Remote Care in Response to the Covid-19 Pandemic: A Scoping Review. *Eur Rev Med Pharmacol Sci* (2021) 25(8):3386–94. doi: 10.26355/eurrev_202104_25751
8. Dunger D, Darendeliler F, Kandemir N, Harris M, Rabbani A, Kappelgaard A-M. What Is the Evidence for Beneficial Effects of Growth Hormone Treatment Beyond Height in Short Children Born Small for Gestational Age? A Review of Published Literature. *J Pediatr Endocrinol* (2020) 33(1):53–70. doi: 10.1515/jpem-2019-0098
9. Argente J, Tatton-Brown K, Lehwalder D, Pfäffle R. Genetics of Growth Disorders-Which Patients Require Genetic Testing? *Front Endocrinol (Lausanne)* (2019) 10:602. doi: 10.3389/fendo.2019.00602
10. Collett-Solberg PF, Ambler G, Backeljauw PF, Bidlingmaier M, Biller BMK, Boguszewski MCS, et al. Diagnosis, Genetics, and Therapy of Short Stature in Children: A Growth Hormone Research Society International Perspective. *Horm Res Paediatr* (2019) 92(1):1–14. doi: 10.1159/000502231
11. Wit JM, Deeb A, Bin-Abbas B, Al Mutair A, Koledova E, Savage MO. Achieving Optimal Short- and Long-Term Responses to Paediatric Growth Hormone Therapy. *J Clin Res Pediatr Endocrinol* (2019) 11(4):329–40. doi: 10.4274/jcrpe.galenos.2019.2019.0088
12. Dimitri P, Fernandez-Luque L, Banerjee I, Bergadá I, Calliari LE, Dahlgren J, et al. An Ehealth Framework for Managing Pediatric Growth Disorders and Growth Hormone Therapy. *J Med Internet Res* (2021) 23(5):e27446. doi: 10.2196/27446
13. van Dommelen P, van Zoonen R, Vlasblom E, Wit JM, Beltman M. Expert Committee. Guideline for Referring Short or Tall Children in Preventive Child Health Care. *Acta Paediatr* (2021) 110(4):1231–8. doi: 10.1111/apa.15625
14. Savage MO, Backeljauw PF, Calzada R, Cianfarani S, Dunkel L, Koledova E, et al. Early Detection, Referral, Investigation, and Diagnosis of Children With Growth Disorders. *Horm Res Paediatr* (2016) 85(5):325–32. doi: 10.1159/000444525
15. Dattani MT, Malhotra N. A Review of Growth Hormone Deficiency. *Paediatr Child Health* (2019) 29(7):285–92. doi: 10.1016/j.paed.2019.04.001
16. Murray PG, Dattani MT, Clayton PE. Controversies in the Diagnosis and Management of Growth Hormone Deficiency in Childhood and Adolescence. *Arch Dis Child* (2016) 101(1):96–100. doi: 10.1136/archdischild-2014-307228
17. Berglund A, Stochholm K, Gravholt CH. The Epidemiology of Sex Chromosome Abnormalities. *Am J Med Genet C Semin Med Genet* (2020) 184(2):202–15. doi: 10.1002/ajmg.c.31805
18. Fujita K, Nagasaka M, Iwatani S, Koda T, Kurokawa D, Yamana K, et al. Prevalence of Small for Gestational Age (Sga) and Short Stature in Children Born Sga Who Qualify for Growth Hormone Treatment at 3 Years of Age: Population-Based Study. *Pediatr Int* (2016) 58(5):372–6. doi: 10.1111/ped.12859
19. Tamaro G, Pizzul M, Gaeta G, Servello R, Trevisan M, Böhm P, et al. Prevalence of Children Born Small for Gestational Age With Short Stature Who Qualify for Growth Hormone Treatment. *Ital J Pediatr* (2021) 47(1):82. doi: 10.1186/s13052-021-01026-3
20. Miller BS, Velazquez E, Yuen KCJ. Long-Acting Growth Hormone Preparations - Current Status and Future Considerations. *J Clin Endocrinol Metab* (2020) 105(6):dgz149. doi: 10.1210/clinem/dgz149
21. Yuen KCJ, Alter CA, Miller BS, Gannon AW, Tritos NA, Samson SL, et al. Adult Growth Hormone Deficiency: Optimizing Transition of Care From Pediatric to Adult Services. *Growth Hormone IGF Res* (2021) 56:101375. doi: 10.1016/j.ghir.2020.101375
22. Yuen KCJ, Miller BS, Biller BMK. The Current State of Long-Acting Growth Hormone Preparations for Growth Hormone Therapy. *Curr Opin Endocrinol Diabetes Obes* (2018) 25(4):267–73. doi: 10.1097/MED.0000000000000416
23. Attanasio AF, Shavrikova EP, Blum WF, Shalet SM. Quality of Life in Childhood Onset Growth Hormone-Deficient Patients in the Transition Phase From Childhood to Adulthood. *J Clin Endocrinol Metab* (2005) 90(8):4525–9. doi: 10.1210/jc.2005-0439
24. Hauffa BP, Touraine P, Urquhart-Kelly T, Koledova E. Managing Transition in Patients Treated With Growth Hormone. *Front Endocrinol (Lausanne)* (2017) 8:346. doi: 10.3389/fendo.2017.00346
25. Attanasio AF, Shavrikova E, Blum WF, Cromer M, Child CJ, Paskova M, et al. Continued Growth Hormone (Gh) Treatment After Final Height Is Necessary to Complete Somatic Development in Childhood-Onset Gh-Deficient Patients. *J Clin Endocrinol Metab* (2004) 89(10):4857–62. doi: 10.1210/jc.2004-0551
26. Johannsson G, Albertsson-Wikland K, Bengtsson BA. Discontinuation of Growth Hormone (Gh) Treatment: Metabolic Effects in Gh-Deficient and Gh-Sufficient Adolescent Patients Compared With Control Subjects. Swedish Study Group for Growth Hormone Treatment in Children. *J Clin Endocrinol Metab* (1999) 84(12):4516–24. doi: 10.1210/jcem.84.12.6176
27. van Pareren Y, Mulder P, Houdijk M, Jansen M, Reeser M, Hokken-Koelega A. Effect of Discontinuation of Growth Hormone Treatment on Risk Factors for Cardiovascular Disease in Adolescents Born Small for Gestational Age. *J Clin Endocrinol Metab* (2003) 88(1):347–53. doi: 10.1210/jc.2002-020458
28. Kum CD, Rho JG, Park HK, Lee HS, Hwang JS. Factors Influencing Growth Hormone Therapy Effect During the Prepubertal Period in Small for Gestational Age Children Without Catch-Up Growth. *Ann Pediatr Endocrinol Metab* (2021) 26(1):31–7. doi: 10.6065/apem.2040096.048
29. Wit JM, Ranke MB, Albertsson-Wikland K, Carrascosa A, Rosenfeld RG, Van Buuren S, et al. Personalized Approach to Growth Hormone Treatment: Clinical Use of Growth Prediction Models. *Horm Res Paediatr* (2013) 79(5):257–70. doi: 10.1159/000351025
30. Graham S, Weinman J, Auyeung V. Identifying Potentially Modifiable Factors Associated With Treatment Non-Adherence in Paediatric Growth Hormone

Deficiency: A Systematic Review. *Horm Res Paediatr* (2018) 90(4):221–7. doi: 10.1159/000493211
31. Calthorpe RJ, Smith SJ, Rowbotham NJ, Leighton PA, Davies G, Daniels T, et al. What Effective Ways of Motivation, Support and Technologies Help People With Cystic Fibrosis Improve and Sustain Adherence to Treatment? *BMJ Open Respir Res* (2020) 7(1):e000601. doi: 10.1136/bmjresp-2020-000601
32. Ferrante G, Licari A, Marseglia GL, La Grutta S. Digital Health Interventions in Children With Asthma. *Clin Exp Allergy* (2021) 51(2):212–20. doi: 10.1111/cea.13793
33. Steenkamp D, Eby EL, Gulati N, Liao B. Adherence and Persistence to Insulin Therapy in People With Diabetes: Impact of Connected Insulin Pen Delivery Ecosystem. *J Diabetes Sci Technol* (2021) 1932296821997923:1–8. doi: 10.1177/1932296821997923
34. van Dommelen P, Koledova E, Wit JM. Effect of Adherence to Growth Hormone Treatment on 0-2 Year Catch-Up Growth in Children With Growth Hormone Deficiency. *PLoS One* (2018) 13(10):e0206009. doi: 10.1371/journal.pone.0206009
35. Cutfield WS, Derraik JG, Gunn AJ, Reid K, Delany T, Robinson E, et al. Non-Compliance With Growth Hormone Treatment in Children Is Common and Impairs Linear Growth. *PLoS One* (2011) 6(1):e16223. doi: 10.1371/journal.pone.0016223
36. de Arriba Muñoz A, Muñiz VC, Saez JJA, Beisti A, Llovet E, Aizpún JIL. Impact of Adherence on Growth Response During the First 2 Years of Growth Hormone Treatment. *Endocrine* (2021) 72(2):513–23. doi: 10.1007/s12020-020-02560-6
37. De Pedro S, Murillo M, Salinas I, Granada ML, Martinez M, Puig-Domingo M, et al. Variability in Adherence to Rhgh Treatment: Socioeconomic Causes and Effect on Children's Growth. *Growth Hormone IGF Res* (2016) 26:32–5. doi: 10.1016/j.ghir.2015.12.002
38. Koledova E, Tornincasa V, van Dommelen P. Analysis of Real-World Data on Growth Hormone Therapy Adherence Using a Connected Injection Device. *BMC Med Inform Decis Mak* (2020) 20(1):176. doi: 10.1186/s12911-020-01183-1
39. Bozzola M, Colle M, Halldin-Stenlid M, Larroque S, Zignani M. Treatment Adherence With the Easypod™ Growth Hormone Electronic Auto-Injector and Patient Acceptance: Survey Results From 824 Children and Their Parents. *BMC Endocr Disord* (2011) 11:4. doi: 10.1186/1472-6823-11-4
40. Fisher BG, Acerini CL. Understanding the Growth Hormone Therapy Adherence Paradigm: A Systematic Review. *Horm Res Paediatr* (2013) 79(4):189–96. doi: 10.1159/000350251
41. Rodríguez Arnao MD, Rodríguez Sánchez A, Díez López I, Ramírez Fernández J, Bermúdez de la Vega JA, Yeste Fernández D, et al. Adherence and Long-Term Outcomes of Growth Hormone Therapy With Easypod™ in Pediatric Subjects: Spanish Ecos Study. *Endocr Connect* (2019) 8(9):1240–9. doi: 10.1530/ec-19-0325
42. Acerini CL, Wac K, Bang P, Lehwalder D. Optimizing Patient Management and Adherence for Children Receiving Growth Hormone. *Front Endocrinol (Lausanne)* (2017) 8:313. doi: 10.3389/fendo.2017.00313
43. Rosenfeld RG, Bakker B. Compliance and Persistence in Pediatric and Adult Patients Receiving Growth Hormone Therapy. *Endocr Pract* (2008) 14(2):143–54. doi: 10.4158/EP.14.2.143
44. Spataru A, van Dommelen P, Arnaud L, Masne QL, Quarteroni S, Koledova EB. Persistence of Use in Children Receiving Growth Hormone Therapy. *J Endocr Soc* (2021) 5(Supplement_1):A681–A2. doi: 10.1210/jendso/bvab048.1389
45. Bagnasco F, Di Iorgi N, Roveda A, Gallizia A, Haupt R, Maghnie M, et al. Prevalence and Correlates of Adherence in Children and Adolescents Treated With Growth Hormone: A Multicenter Italian Study. *Endocr Pract* (2017) 23(8):929–41. doi: 10.4158/EP171786.OR
46. Dunkel L, Fernandez-Luque L, Loche S, Savage MO. Digital Technologies to Improve the Precision of Paediatric Growth Disorder Diagnosis and Management. *Growth Hormone IGF Res* (2021) 59:101408. doi: 10.1016/j.ghir.2021.101408
47. Mohseni S, Heydari Z, Qorbani M, Radfar M. Adherence to Growth Hormone Therapy in Children and Its Potential Barriers. *J Pediatr Endocrinol Metab* (2018) 31(1):13–20. doi: 10.1515/jpem-2017-0157
48. Kardas P, Aguilar-Palacio I, Almada M, Cahir C, Costa E, Giardini A, et al. The Need to Develop Standard Measures of Patient Adherence for Big Data: Viewpoint. *J Med Internet Res* (2020) 22(8):e18150. doi: 10.2196/18150
49. Dahlgren J. Easypod: A New Electronic Injection Device for Growth Hormone. *Expert Rev Med Devices* (2008) 5(3):297–304. doi: 10.1586/17434440.5.3.297
50. Francois-Xavier L. Electronic Recording of Growth Hormone Dosing History: The Easypod™ Auto-Injector. *Curr Drug Ther* (2010) 5(4):271–6. doi: 10.2174/157488510792927474
51. Dahlgren J, Veimo D, Johansson L, Bech I. Patient Acceptance of a Novel Electronic Auto-Injector Device to Administer Recombinant Human Growth Hormone: Results From an Open-Label, User Survey of Everyday Use. *Curr Med Res Opin* (2007) 23(7):1649–55. doi: 10.1185/030079907x210589
52. Tauber M, Payen C, Cartault A, Jouret B, Edouard T, Roger D. User Trial of Easypod, an Electronic Autoinjector for Growth Hormone. *Ann Endocrinol (Paris)* (2008) 69(6):511–6. doi: 10.1016/j.ando.2008.04.003
53. ONdrugDelivery. *Innovative Solutions: Digital Devices, Drug Delivery and Services in Healthcare* (2018) (Accessed September 30, 2021).
54. Malik S, Moloney C, Koledova E, Reston J, Weinman J. Designing a Personalized Digital Patient Support Program for Patients Treated With Growth Hormone: Key Design Considerations. *J Med Internet Res* (2020) 22(7):e18157. doi: 10.2196/18157
55. Parsons D, MacCallum K. Current Perspectives on Augmented Reality in Medical Education: Applications, Affordances and Limitations. *Adv Med Educ Pract* (2021) 12:77–91. doi: 10.2147/amep.S249891
56. McNally M, Long F, Poskitt H, Cancela J, Koledova E, Castro JS, et al. Patients and Caregivers Perspectives on a Mobile App That Tracks Adherence and Outcomes in Children With Growth Disorders Treated With Recombinant Human Growth Hormone (R-Hgh). *Horm Res Pediatr* (2018) 90(Suppl 1):375. doi: 10.1159/000492307
57. *PAEDLOGIC. Softwarelösung Für Ärzte* (Accessed September 30, 2021).
58. *REPAR - Registries | Registry.Cz* (Accessed September 30, 2021).
59. Araujo M, van Dommelen P, Koledova E, Srivastava J. Using Deep Learning for Individual-Level Predictions of Adherence With Growth Hormone Therapy. *Stud Health Technol Inform* (2021) 281:133–7. doi: 10.3233/shti210135
60. Spataru A, van Dommelen P, Arnaud L, Masne QL, Quarteroni S, Koledova EB. A Machine Learning Approach for Identifying Children at Risk of Suboptimal Adherence to Growth Hormone Therapy. *J Endocr Soc* (2021) 5(Supplement_1):A672–A3. doi: 10.1210/jendso/bvab048.1371
61. *Growlink™ App – Apps on Google Play* (Accessed September 30, 2021).
62. Fernandez-Luque L, Al Herbish A, Al Shammari R, Argente J, Bin-Abbas B, Deeb A, et al. Digital Health for Supporting Precision Medicine in Pediatric Endocrine Disorders: Opportunities for Improved Patient Care. *Front Pediatr* (2021) 9:715705. doi: 10.3389/fped.2021.715705
63. Alfian SD, Pradipta IS, Hak E, Denig P. A Systematic Review Finds Inconsistency in the Measures Used to Estimate Adherence and Persistence to Multiple Cardiometabolic Medications. *J Clin Epidemiol* (2019) 108:44–53. doi: 10.1016/j.jclinepi.2018.12.003
64. Lam WY, Fresco P. Medication Adherence Measures: An Overview. *BioMed Res Int* (2015) 2015:217047. doi: 10.1155/2015/217047
65. Koledova E, Stoyanov G, Ovbude L, Davies PSW. Adherence and Long-Term Growth Outcomes: Results From the Easypod™ Connect Observational Study (Ecos) in Paediatric Patients With Growth Disorders. *Endocr Connect* (2018) 7(8):914–23. doi: 10.1530/EC-18-0172
66. Boman N, Fernandez-Luque L, Koledova E, Kause M, Lapatto R. Connected Health for Growth Hormone Treatment Research and Clinical Practice: Learnings From Different Sources of Real-World Evidence (Rwe)-Large Electronically Collected Datasets, Surveillance Studies and Individual Patients' Cases. *BMC Med Inform Decis Mak* (2021) 21(1):136. doi: 10.1186/s12911-021-01491-0
67. Arshad S, Arshad J, Khan MM, Parkinson S. Analysis of Security and Privacy Challenges for DNA-Genomics Applications and Databases. *J BioMed Inform* (2021) 119:103815. doi: 10.1016/j.jbi.2021.103815
68. Flors-Sidro JJ, Househ M, Abd-Alrazaq A, Vidal-Alaball J, Fernandez-Luque L, Sanchez-Bocanegra CL. Analysis of Diabetes Apps to Assess Privacy-Related Permissions: Systematic Search of Apps. *JMIR Diabetes* (2021) 6(1):e16146. doi: 10.2196/16146
69. Ozeran L, Solomonides A, Schreiber R. Privacy Versus Convenience: A Historical Perspective, Analysis of Risks, and an Informatics Call to Action. *Appl Clin Inform* (2021) 12(2):274–84. doi: 10.1055/s-0041-1727197

70. Spataru A, Quarteroni S, Arnaud L, van Dommelen P, Koledova E, Le Masne Q. High Engagement of Patients Monitored by a Digital Health Ecosystem Indicates Significant Improvements of Key R-Hgh Treatment Metrics. *Stud Health Technol Inform* (2021) 281:829–33. doi: 10.3233/shti210295
71. Koledova E, Bagha M, Arnaud L, Piras F, van Dommelen P. Optimising Adherence Using a Connected Injection Device Can Improve Growth Outcomes: Evidence From Real-World Data on 11 Million Injections in 20,000 Patients With Growth Disorders. *Horm Res Pediatr* (2021) 94(Suppl 1):58. doi: 10.1159/000518849
72. Foo J, Maghnie M, Colao A, Vlachaki I, Colombo G. Cost-Consequence Analysis for Human Recombinant Growth Hormone (R-Hgh) Treatment Administered *Via* Different Devices in Children With Growth Hormone Deficiency in Italy. *Clinicoecon Outcomes Res* (2019) 11:525–37. doi: 10.2147/CEOR.S195265
73. Wu XW, Yang HB, Yuan R, Long EW, Tong RS. Predictive Models of Medication Non-Adherence Risks of Patients With T2d Based on Multiple Machine Learning Algorithms. *BMJ Open Diabetes Res Care* (2020) 8(1): e001055. doi: 10.1136/bmjdrc-2019-001055
74. JA Killian, B Wilder, A Sharma, V Choudhary, B Dilkina and M Tambe eds. *Learning to Prescribe Interventions for Tuberculosis Patients Using Digital Adherence Data*. New York, NY, USA: Association for Computing Machinery (2019).
75. Wang L, Fan R, Zhang C, Hong L, Zhang T, Chen Y, et al. Applying Machine Learning Models to Predict Medication Nonadherence in Crohn's Disease Maintenance Therapy. *Patient Prefer Adherence* (2020) 14:917–26. doi: 10.2147/ppa.S253732
76. Karanasiou GS, Tripoliti EE, Papadopoulos TG, Kalatzis FG, Goletsis Y, Naka KK, et al. Predicting Adherence of Patients With Hf Through Machine Learning Techniques. *Healthc Technol Lett* (2016) 3(3):165–70. doi: 10.1049/htl.2016.0041
77. Huang L, Guo H, Rao Q, Hou Z, Li S, Qiu S, et al. Body Dimension Measurements of Qinchuan Cattle With Transfer Learning From Lidar Sensing. *Sensors (Basel)* (2019) 19(22):5046. doi: 10.3390/s19225046
78. Patil AK, Balasubramanyam A, Ryu JY, B N PK, Chakravarthi B, Chai YH. Fusion of Multiple Lidars and Inertial Sensors for the Real-Time Pose Tracking of Human Motion. *Sensors (Basel)* (2020) 20(18):E5342. doi: 10.3390/s20185342
79. Ballester A, Parrilla E, Piérola A, Uriel J, Pérez C, Piqueras P, et al. Data-Driven Three-Dimensional Reconstruction of Human Bodies Using a Mobile Phone App. *Int J Digital Hum* (2016) 1(4):361–88. doi: 10.1504/ijdh.2016.084581
80. Bergquist R, Stenbeck N. *Using Augmented Reality to Measure Vertical Surfaces* Linköping: Linköping University. (2018).
81. Ismail NA, Tan CW, Mohamed SE, Salam MS, Ghaleb FA. Mobile Based Augmented Reality for Flexible Human Height Estimation Using Touch and Motion Gesture Interaction. *IOP Conf Ser: Mater Sci Eng* (2020) 979:12017. doi: 10.1088/1757-899X/979/1/012017
82. Taylor CB, Fitzsimmons-Craft EE, Graham AK. Digital Technology Can Revolutionize Mental Health Services Delivery: The Covid-19 Crisis as a Catalyst for Change. *Int J Eat Disord* (2020) 53(7):1155–7. doi: 10.1002/eat.23300
83. Taylor CB, Graham AK, Flatt RE, Waldherr K, Fitzsimmons-Craft EE. Current State of Scientific Evidence on Internet-Based Interventions for the Treatment of Depression, Anxiety, Eating Disorders and Substance Abuse: An Overview of Systematic Reviews and Meta-Analyses. *Eur J Public Health* (2021) 31(31 Suppl 1):i3–i10. doi: 10.1093/eurpub/ckz208
84. van Dommelen P, Arnaud L, Le Masne Q, Koledova E. The Impact of Lockdown Regulations Caused by the Covid-19 Pandemic on Adherence to Recombinant Human Growth Hormone Therapy: Evidence From Real-World Data. *Horm Res Paediatr* (2021) 94(Suppl 1):137. doi: 10.1159/000518849

Conflict of Interest: VT, DD, QM, BM, and LA are employees of Ares Trading SA (an affiliate of Merck KGaA), Eysins, Switzerland. PD has a consultancy agreement with Merck KGaA, Darmstadt, Germany. EK is an employee of Merck KGaA, Darmstadt, Germany and holds shares in the company. The authors declare that this study received funding from Merck (CrossRef Funder ID: 10.13039/100009945). The funder had the following involvement in the study: study design, data collection and analysis, decision to publish, and preparation of the manuscript.

frontiers | Frontiers in Endocrinology

TYPE Review
PUBLISHED 10 January 2023
DOI 10.3389/fendo.2022.993081

OPEN ACCESS

EDITED BY
Lisa M. Butler,
University of Adelaide, Australia

REVIEWED BY
Elizabeth Neumann,
University of California, Davis, United States
Jose Luis Gomez-Ariza,
University of Huelva, Spain

*CORRESPONDENCE
Zhibin Zhang
Zhibin-zhang@nankai.edu.cn
Ruibing Chen
rbchen@tju.edu.cn
Xiangyang Zhang
xiangyang.zhang@tju.edu.cn

SPECIALTY SECTION
This article was submitted to Cancer Endocrinology, a section of the journal Frontiers in Endocrinology

RECEIVED 13 July 2022
ACCEPTED 15 December 2022
PUBLISHED 10 January 2023

CITATION
Hou Y, Gao Y, Guo S, Zhang Z, Chen R and Zhang X (2023) Applications of spatially resolved omics in the field of endocrine tumors.
Front. Endocrinol. 13:993081.
doi: 10.3389/fendo.2022.993081

Applications of spatially resolved omics in the field of endocrine tumors

Yinuo Hou[1], Yan Gao[1], Shudi Guo[1], Zhibin Zhang[2*], Ruibing Chen[1*] and Xiangyang Zhang[1*]

[1]School of Pharmaceutical Science and Technology, Tianjin University, Tianjin, China, [2]General Surgery, Tianjin First Center Hospital, Tianjin, China

Endocrine tumors derive from endocrine cells with high heterogeneity in function, structure and embryology, and are characteristic of a marked diversity and tissue heterogeneity. There are still challenges in analyzing the molecular alternations within the heterogeneous microenvironment for endocrine tumors. Recently, several proteomic, lipidomic and metabolomic platforms have been applied to the analysis of endocrine tumors to explore the cellular and molecular mechanisms of tumor genesis, progression and metastasis. In this review, we provide a comprehensive overview of spatially resolved proteomics, lipidomics and metabolomics guided by mass spectrometry imaging and spatially resolved microproteomics directed by microextraction and tandem mass spectrometry. In this regard, we will discuss different mass spectrometry imaging techniques, including secondary ion mass spectrometry, matrix-assisted laser desorption/ionization and desorption electrospray ionization. Additionally, we will highlight microextraction approaches such as laser capture microdissection and liquid microjunction extraction. With these methods, proteins can be extracted precisely from specific regions of the endocrine tumor. Finally, we compare applications of proteomic, lipidomic and metabolomic platforms in the field of endocrine tumors and outline their potentials in elucidating cellular and molecular processes involved in endocrine tumors.

KEYWORDS

endocrine tumors, liquid chromatography-mass spectrometry, mass spectrometry imaging, microextraction, multi-omics, spatially resolved microproteomics

1 Introduction

The endocrine system comprises thyroid gland, pituitary gland, parathyroid glands, adrenal glands, pancreas, gonads, pineal gland and thymus. The endocrine glands secrete hormones, which directly enter the bloodstream and come into effect until they reach their target organs. These hormones trigger complicated biological processes, including energy homeostasis, metabolism, reproduction, growth and motions (1).

Endocrine tumors derive from endocrine cells with high heterogeneity in function, structure and embryology, and are characteristic of a marked diversity and tissue heterogeneity (2). They occur in any of the major endocrine organs, including thyroid gland, pituitary gland, parathyroid glands, adrenal glands and the endocrine pancreas (3–6). According to the latest WHO classification, endocrine tumors include pituitary tumors, thyroid neoplasms, parathyroid tumors, paragangliomas and pheochromocytomas, neuroendocrine neoplasms, adrenal cortical tumors and familial endocrine tumor syndromes (7–13). Though most endocrine tumors are benign or low-grade cancers that grow and spread slowly, a few are malignant. For example, thyroid carcinoma is the most common endocrine malignancy (14–17). Based on the GLOBOCAN estimation on cancer incidence and mortality, provided by the International Agency for Research on Cancer, the global incidence of thyroid carcinoma ranked 7th in both sexes and 4th for women in 2020. The mortality of thyroid carcinoma is relatively lower compared to other cancers (0.5 per 100,000 in women and 0.3 per 100,000 in men) (18). The diagnosis of endocrine tumors can be performed by blood/urine tests, ultrasound, computed tomography, magnetic resonance imaging, biopsy and so on (19–22). Fine needle aspiration (FNA) biopsy is frequently recommended to diagnose thyroid neoplasms and parathyroid tumors, where a needle is inserted into the nodules or lumps of patients to collect cells. FNA is a simple diagnostic modality. But it is limited in discriminating ambiguous carcinoma subtypes and additional surgical procedures are required to obtain final diagnosis (23, 24).

The occurrence of endocrine tumors often brings about hyper- or hypo- hormone secretion and potentially causes a succession of disorders, such as hypercalcemia, hypertension and hyperthyroidism (25–28). The tumor tissues comprise of various cell types (such as neoplastic cells, endothelial cells, immune cells, etc.), subpopulations and substructures, which in turn lead to the formation of heterogeneous tissue microenvironment (29–31). Treatments should not only be directed at tumor cells but also should take molecular and cellular interactions within the tumor microenvironment into consideration. High heterogeneity of endocrine tumors is one challenge for the analyses at molecular level. To comprehensively clarify the molecule alternations, both chemical information and spatial distribution of molecules within the tumor microenvironment need to be taken into account. Spatial omics offers increasing insights into pathobiological processes of tumor microenvironment, which allows to understand the location of a cell within tissue, indicates where proteins, lipids or metabolites are expressed in a spatial context and facilitates the identification of unknown cellular regulation processes (32). Mass spectrometry (MS) has shown its advantages in analyzing biomolecules (proteins, peptides, lipids, metabolites, etc.) of complex biological samples at the spatially resolved level (33–35).

Mass spectrometry is an incredibly sensitive analytical technique (down to fmol) that measures the mass-to-charge ratio (m/z) of molecules and atoms to determine their molecular weight, enabling qualitative and quantitative analysis for the samples (36, 37). The ion source, mass analyzer and detector are essential components for a mass spectrometer. The sample is first ionized by the ion source to generate a mixture of ions. In the following, the mass analyzer takes the ions and separates them based on m/z value. Finally, the ions reach the detector and yield signals. Different ionization techniques include electron ionization, chemical ionization, secondary ion mass spectrometry (SIMS), desorption electrospray ionization (DESI), field ionization, fast atom bombardment, laser desorption/ionization (LDI), electrospray ionization (ESI), matrix-assisted laser desorption/ionization (MALDI) and so on (38). There are also multiple types of mass analyzers, such as time-of-flight (TOF), magnetic sector, linear quadrupole, linear quadrupole ion trap, quadrupole ion trap, Fourier transform-ion cyclotron resonance (FT-ICR) and Orbitrap (39). TOF mass analyzers separate ions according to their m/z values based on the length of time it takes them to travel through a flight tube. One advantage of TOF is that it can possess a wide range of m/z values. FT-ICR mass analyzers separate ions based on a magnetic field while Orbitrap mass analyzers use an electrostatic field. Both FT-ICR and Orbitrap mass analyzers have high mass resolution and mass accuracy (40, 41). Tandem mass spectrometer (MS/MS) is involved with more than one mass analyzer in a single instrument. In MS/MS, the precursor ions (generated by DESI, ESI, MALDI, etc.) with a specific m/z value are selected and fragmented in a collision cell or chamber to generate product ions for detection (42). Fragmentation techniques include collision induced dissociation, high-energy collision dissociation, electron-capture dissociation, electron transfer dissociation, ultraviolet photodissociation and so on (43–47). Mass spectrometry imaging (MSI) is an imaging technique for *in situ* analysis of tissues and cells by determining the relative abundance and distribution of biomolecules (e.g., peptides, proteins, lipids, and metabolites) based on MS (48). For MSI, the sample is ionized pixel by pixel and a mass spectrum is generated for each pixel. The mass spectra are collected at discrete x, y coordinates. For a given m/z value, a heat map image can be created by plotting its intensities in all pixels across the scanned area (49–51). MSI can detect and image thousands of biomolecules in a single run, serving as a promising technique in biological and clinical analysis (52–55). Liquid chromatography-mass spectrometry (LC-MS) and liquid chromatography with tandem mass spectrometry (LC-MS/MS) involve the chromatographic separation of analytes followed by the detection of their m/z value. With the help of high-performance liquid chromatography or ultra-performance liquid chromatography, the complexity of analytes extracted from the biological samples is effectively reduced and more analytes can be detected by MS (56). To provide a broad coverage of molecules with different chemical

and physical properties, different chromatographic platforms are developed, including reversed-phase chromatography, hydrophobic-interaction chromatography and ion exchange chromatography (57–59). LC-MS and LC-MS/MS are widely used in the biological and clinical research, including the field of endocrine tumors (60–65). Spatially resolved LC-MS can be achieved by coupling with laser microdissection (LMD) or liquid microjunction (LMJ), which are two microextraction methods used to extract analytes within the target area of the heterogeneous tumors (66, 67). The combination of microextraction and LC-MS allows the measurement of *m/z* value and spatial location of analytes in the samples.

With the development of MS techniques, chromatographic separation methods and microextraction methods, great progress has been made in clarifying the cellular and molecular mechanisms of endocrine tumorigenesis, progression and metagenesis (68–70). Many biomolecules, such as proteins, lipids and metabolites that present significantly different expression between the tumor tissue and the normal tissue have the potential to act as diagnostic and prognostic biomarkers and therapeutic targets for endocrine tumors (71–73). For example, Coelho et al. reviewed the capability of MS in the diagnosis of thyroid carcinoma from metabolomics. Rossi et al. summarized the potential of steroid profiling by MS in the management of adrenocortical carcinoma (ACC), and Li et al. reviewed the use of MS in proteome-centered multi-omics of human pituitary adenomas (74–76). In this review, we will focus on the application of MS in the field of spatial multi-omics (proteomics, lipidomics and metabolomics) of endocrine tumors, highlighting MSI, LC-MS and microextraction methods. In Supplementary Table 1, spatially resolved proteomics, lipidomics, and metabolomics on endocrine tumors are summarized.

2 Mass spectrometry imaging in proteomics, lipidomics and metabolomics of endocrine tumors

2.1 Mass spectrometry imaging

Mass spectrometry imaging is capable of mapping thousands of biomolecules *in situ* without labelling. Different ion sources and instrument configurations provide different MSI approaches. Secondary ion mass spectrometry-mass spectrometry imaging (SIMS-MSI), matrix-assisted laser desorption/ionization-mass spectrometry imaging (MALDI-MSI) and desorption electrospray ionization-mass spectrometry imaging (DESI-MSI) are the most widely used platforms. SIMS was the first technique employed for tissue imaging (77, 78). The spot size of primary ion beam can be focused to ~50 nm. SIMS is characteristic of high spatial resolution (79–81). In 1997, Caprioli et al. introduced MALDI-MS for tissue imaging (82). With the broad molecule detection coverage, MALDI-MSI is popularly used in the imaging of proteins, lipids and metabolites within biological tissues (83–85). DESI was presented in 2004 and the potential for spatial analysis of plant or animal tissues was demonstrated (86). In 2005, Wiseman et al. reported the first application of DESI-MSI in imaging mouse pancreas, rat brain and metastatic human liver adenocarcinoma tissues (87). These three MSI techniques give full play to their individual advantages in biological and clinical research involved with endocrine tumors (88–93). Their respective advantages and disadvantages are listed in Table 1.

2.1.1 Secondary ion mass spectrometry-mass spectrometry imaging

SIMS-MSI can reach micron and submicron spatial resolution, capable of imaging single cells or subcellular organelles (94–96). The highest spatial resolution of SIMS-MSI, down to tens of nanometers, outperforms the other two MSI techniques (97–99). The principle of SIMS-MSI is shown in Figure 1A. In SIMS-MSI, a high-energy primary ion beam strikes the sample surface, causing the interaction of sputtering, ion reflection and recoil sputtering between the ions and the surface. The interaction processes result in the emission of secondary ions (100).

There are various types of commercially available primary ion beams, including monatomic (Au^+, Cs^+ and O^-) and polyatomic ion beams (C_{60}^+), liquid metal ion guns (LMIGs) (Bi_3^+ and Au_3^+) and gas cluster ion beams (GCIBs) (Ar_{4000}^+, $(CO_2(CO_2)_{2000}^+$ and $(H_2O)_{2000}^+$) (101–106). The sensitivity and spatial resolution of SIMS-MSI are influenced by the type, the energy and the focusing spot size of the primary ion beams. The monatomic ion beams limit SIMS-MSI to the detection of elements or very small (e.g., diatomic) fragments of molecules (107). LMIGs produce increased sensitivity while still being readily focused to tens to hundreds of nanometers. The use of polyatomic ion beams and GCIBs further improves the sensitivity to higher mass species (102). Lipids and metabolites have been spatially resolved in different cell types of breast cancer (105). A primary ion beam with high energy tends to have high secondary ion yields. However, highly energetic primary ion beams induce strong fragmentation of the analytes and generate very small ion fragments (97). The spatial resolution of SIMS-MSI can reach a few hundred nanometers when the spot size of primary ion beam is focused ≤ 50 nm (108). For GCIBs, the typical optimal spot size is around 1-5 μm and the increased sensitivity is obtained at a loss of spatial resolution (107). For SIMS-MSI, it is essential to select a primary ion beam with appropriate energy (typically between 25 and 70 keV kinetic energy) and focusing spot size to obtain ideal sensitivity and spatial resolution. The selection depends on the types of target tissues and target analytes (109).

TABLE 1 Advantages and disadvantages of SIMS-MSI, MALDI-MSI and DESI-MSI.

MSI methods	SIMS-MSI	MALDI-MSI	DESI-MSI
Ionization method	SIMS	MALDI	DESI
Ionization condition	Vacuum	Vacuum/Ambient	Ambient
Spatial resolution	Down to 50-100 nm	Down to ~ 1 μm	Down to ~ 10 μm
Advantages	High spatial resolution	High applicability to biomolecules Fast acquisition with up to 40 pixel per second	Minimum sample preparation
Disadvantages	Abundant fragmentation Less reproducible Expensive	Require matrix application	Low spatial resolution

2.1.2 Matrix-assisted laser desorption/ionization-mass spectrometry imaging

MALDI-MSI can measure molecules with a wide mass coverage, ranging from 100 Da to beyond 100kDa; and it can measure molecules with different polarities, ranging polar lipids to ionic metabolites (110–112). The majority of MSI studies are performed by MALDI-MSI (113). In MALDI-MSI, the desorption/ionization of the analytes is performed with the assistance of matrices, as described in Figure 1B (114). The matrix is applied to the sample surface and form co-crystals with the analytes. The co-crystals can absorb energy upon laser irradiation. The energy uptake then causes evaporation and ionization of the analyte (82, 115).

The matrices do make a great difference to the ionization process and the selection mainly depends on chemical properties of the molecules of interest (116). The matrices are generally crystalline solids of low vapor pressure. Including 2,5-dihydroxybenzoic acid (2,5-DHB), alpha-cyano-4-hydroxycinnamic acid (CHCA), sinapinic acid (SA), 9-aminoacridine (9-AA) and 1,5-diaminonaphthalene, a diversity of common organic matrices that fit the ionization of different classes of molecular species are listed in Table 2 (129, 132–138). SA is frequently used to assist the ionization of intact proteins (139). 2,5-DHB can be used to image lipids, peptides, and amino acids in the positive ion mode (140–142). 9-AA is preferred to be performed under negative ion mode for the ionization of polar metabolites (143). The application of matrices is required to assist the ionization and subsequent detection of analytes. However, matrices sometimes bring about ion suppression effects and induce sensitivity loss for analytes (144). CHCA is commonly used as a MALDI matrix in the ionization of peptides. When the peptide sample is quite dilute and/or the sample contains salts, the CHCA matrix can form clusters with *m/z* value above 500 (145, 146). These intense CHCA clusters may interfere with peptide signals and complicate the spectra. To reduce the ion suppression effects of CHCA matrix, Ucal et al. used ammonium phosphate monobasic as the addictive of CHCA in the analysis of thyroid carcinoma tissue and found that the addition of ammonium phosphate monobasic could decrease CHCA cluster formation and improve the peptide signals (147). Schlosser et al. utilized different matrix components, additives and a cationizing agent to analyze the effects of matrix composition on signal suppression and found that the mixture of 2,5-DHB and CHCA yielded highly improved ion signals in peptide analysis, compared with using CHCA alone (148). Apart from the matrix clusters, matrices (such as CHCA and 2,5-DHB) could also form adducts with lipids, amines and amino acids. The metabolite-matrix adducts decrease the intensities of the metabolites and further complicate the MS spectra (149).

2.1.3 Desorption electrospray ionization-mass spectrometry imaging

DESI-MSI is carried out by applying pneumatically-assisted electrospray to produce charged solvent droplets directly at the sample surface (150, 151). The charged droplets impact the surface and produce gaseous ions, which are mainly multiply charged as in the case with ESI (Figure 1C) (86, 152–154). DESI-MSI is performed under ambient conditions and requires no matrix application or other advanced sample preparation, allowing biological tissues to be analyzed in their native state (155, 156). DESI-MSI is one of the MSI methods that have the least destructive effect on the biological tissues. The same tissue section is able to be analyzed repeatedly (77, 157, 158). The spatial resolution of DESI-MSI is typically 150-200 μm and the maximum is better than 10 μm (159).

Before a DESI-MSI analysis, it is essential to optimize the following parameters, including the spray solvent composition, the velocity of the spray gas, the spray-to-surface and sampling orifice-to-surface distance, sprayer-to-surface angle and surface-to-desolvation capillary angle (160–165). Failure of optimization of DESI-MSI parameters will lead to poor sensitivity and/or low spatial resolution.

2.2 Sample preparation for mass spectrometry imaging

Sample preparation protocols are of great importance for the MSI analysis, mainly encompassing sample collection, processing and post-sectioning treatments (166, 167).

10.3389/fendo.2022.993081

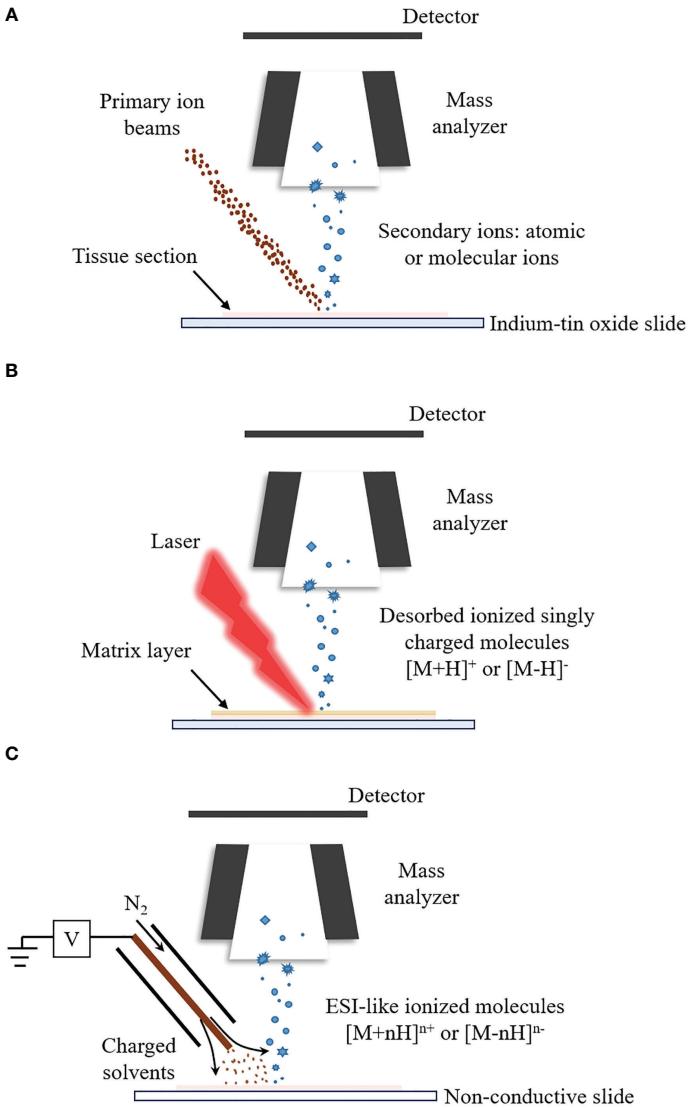

FIGURE 1
The ionization principles for SIMS-MSI, MALDI-MSI and DESI-MSI. A mass spectrometer is at least composed of ion source, mass analyzer and detector. Different ion sources determine different ionization process. **(A)** Ionization process of SIMS-MSI. A primary ion beam possessing energy strikes the sample surface, causing the interaction between the ions and the surface. The interaction processes bring about the emission of atoms and molecules from the sample surface. **(B)** Ionization process of MALDI-MSI. Before the analysis, the matrix is applied to the sample surface. The matrix forms co-crystals with the analytes. The co-crystals can absorb the laser's energy upon laser irradiation. The energy uptake then causes evaporation and desorption/ionization of the analytes. **(C)** Ionization process of DESI-MSI. It is carried out by applying pneumatically-assisted electrospray, which produces charged solvent droplets directly at the sample surface. The charged droplets impact the surface and produce gaseous ions.

Improper sample collection and storage may induce degradation of the analytes or introduce interferences, such as blood and chemical reagents (168–170). Non-standard operations may cause variations in sensitivity, spatial resolution and mass accuracy among technical replicates, leading to poor reproducibility (171). And the obtained MSI results cannot reflect the real nature of tissues under study (172). Therefore, it is essential to standardize each sample preparation protocol before MS data acquisition (173).

2.2.1 Fresh frozen tissues, formalin fixed paraffin embedded tissue blocks and cytologic samples

As distinguished from LC-MS, MSI maps biomolecules directly from the tissue surface *in situ*. Therefore, it is important to preserve the original nature and integrity of the tissue during the process of sample preparation and data acquisition (51, 116). Most samples of endocrine tumors used in MSI analysis are surgically resected suspicious nodules or

TABLE 2 Common organic matrixes applied in MALDI-MSI.

Common organic matrixes in MALDI-MSI	Target molecules
SA (117, 118)	Proteins
2,5-dihydroxyacetophenone (119)	Proteins
CHCA (112, 120)	Peptides and lipids
2,5-DHB (121–123)	Lipids, peptides and drugs
9-AA (124)	Lipids and metabolites
1,5-diaminonaphthalene (125, 126)	Lipids and metabolites
1,8-bis (dimethylamino) naphthalene (127)	Lipids and metabolites
Graphene oxide (128)	Lipids
Hydralazine (129)	Proteins, lipids and metabolites
N- (1-naphthyl) ethylenediamine dihydrochloride (130)	Lipids and metabolites
Norharman (131)	Lipids
Quercetin (132)	Lipids

lumps, e.g., fresh frozen tissues and formalin fixed paraffin embedded (FFPE) blocks of tissues. In some cases, cytological samples are obtained by FNA (117, 174, 175). For fresh frozen tissues or cytological samples, it is necessary to reduce the time spent in harvesting the sample and the acquired fresh sample needs to be snap-frozen in liquid nitrogen right away (176–178). At last, samples can be preserved below -80° until the analysis. Heat-stabilization and *in situ* focused microwave irradiation are two alternatives to snap freezing the freshly harvested tissues (179). Heat-stabilization inactivates the enzymes by quickly heating the tissues to 95°C while *in situ* focused microwave irradiation heats the tissues with focused microwaves to deactivate enzymes within 2 seconds (180, 181). The processed tissues can be preserved in the freezer extended periods.

For FFPE tissue blocks, the fixation can preserve the cellular architecture and the composition of cells in the tissue; however, it also results in cross-linking between nucleic acids, between proteins and between nucleic acids and proteins (182). The cross-linking between proteins inhibits the proteomic analysis by MS seriously (183). This challenge can be overcome by specific sample processing and post-sectioning treatments.

2.2.2 Sample processing

Figure 2A shows sample preparation protocols of fresh frozen tissues in MSI. The first step is to slice the tissue into thin sections by cryo-microtome (typically 3-20 μm) (184–186). The tissue sections are then mounted onto the glass slides, metal targets or indium-tin oxide (ITO) coated glass slides. Before sectioning fresh frozen tissues, various embedding media can be used to preserve the morphology of the tissues and assist with the tissue section, including optimal cutting temperature medium (OCT), carboxymethyl cellulose, gelatin, agarose or ice (121, 187–191). However, OCT could suppress analyte signals and is not recommended in MSI (189, 192). A universal embedding media composed of hydroxypropyl methylcellulose and polyvinylpyrrolidone has been demonstrated to be compatible with SIMS-MSI, MALDI-MSI and DESI-MSI (193). The section temperature significantly varies according to tissue types (172, 194). Tissues containing water are sectioned at higher temperature whereas tissue samples that contain more fat can be sectioned at a lower temperature (195). For FFPE tissue blocks, the tissue sections can be analyzed by MSI after a series of treatments including deparaffinization, rehydration and antigen retrieval, as presented in Figure 2A. In addition, the cytologic samples collected by FNA are smeared onto ITO slides or non-conductive slides for the following MSI analysis (Figure 2B) (118, 174).

Histology staining is frequently cooperated with MSI to connect the histology features of the tissue with the molecular profiles (196). It has been demonstrated the distribution of biomolecules obtained by MSI correlates well with the histology structure of the tissue (197–199).

2.2.3 Post-sectioning treatments

Post-sectioning treatments aim to enhance the sensitivity of analytes of interest. Biological tissues contain numerous molecular species, whose abundance varies widely. If the abundance of targeted analytes is relatively low, it is necessary to tailor post-sectioning treatments (200).

Washing is a common post-sectioning treatment, aiming to remove those interfering molecules and increase the signal intensity of target analytes within the samples (201). The washing strategy with ethanol solutions and water has been commonly applied in the proteomic analysis to remove

10.3389/fendo.2022.993081

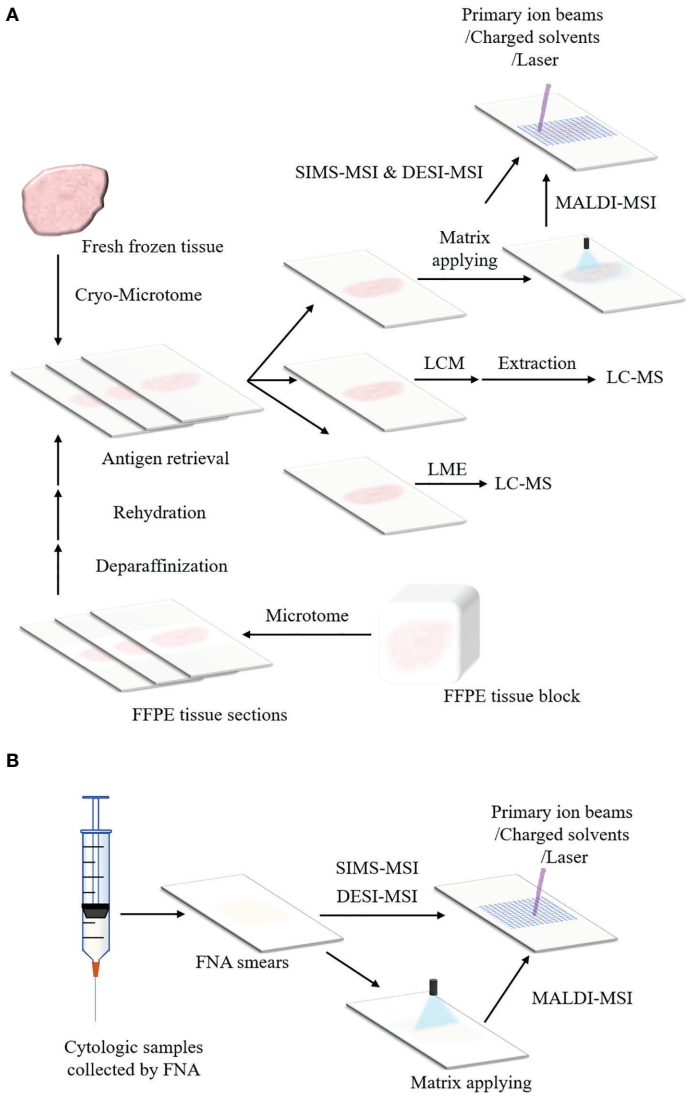

FIGURE 2
Schemes of sample preparation for MSI and microproteomics. **(A)** Preparation protocols of fresh frozen tissues and FFPE tissue blocks for MSI and LMD or LMJ guided microproteomics. The fresh frozen tissue is sliced into sections by cryo-microtome and the tissue sections are placed on ITO slides or non-conductive slides. Then the tissue sections can be processed with MSI (For MALDI-MSI, matrix applying before data acquisition is necessary). The tissue section can also be processed with LMD or LMJ. For LMD, the region of interest within the tissue section is cut off and extracted, followed by LC-MS. For LMJ, the extracts obtained from the target region within the tissue surface can be directly analyzed by LC-MS. After data acquisition, data analysis is performed. For the FFPE tissue block, it is sliced into tissue sections by microtome. These FFPE tissue sections can be analyzed by MSI or LC-MS until they are treated with deparaffinization, rehydration and antigen retrieval. **(B)** Preparation protocols of cytologic samples for MSI. The cytologic samples are collected by FNA. The cytologic samples are smeared onto the ITO slides or non-conductive slides for the analysis of MSI.

interfering salts or lipids (202, 203). The washing solution with ammonium formate or ammonium acetate was proved to enhance detection sensitivity of lipid species (204).

For bottom-up proteomics, on-tissue digestion is performed, involving proteolytic digestion of proteins before analysis by MS (205–207). It is especially advantageous for FFPE samples. On-tissue digestion applies trypsin solution to the sample surface after antigen retrieval. The trypsin facilitates the digestion of cross-linking proteins (136, 208). Abdelmoula et al. studied FFPE tissue blocks of oncocytic follicular thyroid cancer by MALDI-MSI (209). Before the matrix application, the tissue section was proceeded with deparaffinization, dehydration, antigen retrieval and trypsin digestion. The MSI results showed that hundreds of proteolytic peptide ions were detected and that many of them exhibited specific distributions in association with the histological structure of the tissues. FFPE tissues treated with on-tissue digestion is proved to be compatible with the following proteomic analysis (210).

Chemical derivation is another post-sectioning strategy to increase the detection sensitivity of specific lipids and metabolites, such as steroids, catecholamine, and phospholipids (PLs) (211–215). Ibrahim et al. performed an on-tissue chemical derivation of dopamine, epinephrine and norepinephrine with 4- (N-methyl) pyridinium boronic acid in SIMS-MSI and LDI-MSI of porcine adrenal gland tissue (216). They demonstrated that the derivation significantly improved the detection sensitivity of catecholamines in tissue sections for both MSI techniques. Wang et al. achieved simultaneous imaging of free fatty acids (FFAs) and phospholipids with a high sensitivity in thyroid cancer tissue by chemical derivation of FFAs with N,N-dimethylpiperazine iodide (127).

2.2.4 Data processing and analysis

The raw data of MSI is made of individual spectra with spatial and molecular information, so it is generally complex and high dimensional. The basic steps of MSI data processing consist of denoising, baseline subtraction, normalization, peak picking and peak alignment (217, 218). Due to variations in instruments, sample heterogeneity and sample preparation, noises and fluctuations in mass exist in the MSI raw data. Data processing helps reduce the technical and analytical variations, providing a more reliable elaboration of the MSI dataset (219). After data processing, the MSI dataset can be submitted to the statistical analysis. Huang et al. developed a data processing pipeline for spatially resolved metabolomics analysis (219). In the pipeline, 7 data pre-treatment methods (centering, normalization, automatic scaling, UV scaling, Pareto scaling, log transformation and square root transformation) were investigated before a partial least squares discriminant analysis. And the following score test and classification test revealed that log transformations can reveal more low-abundance biomarkers and produce better classification results.

The data analysis for MSI can be performed with MassImager, Biomap, Data Explorer, MALDI Imaging Team Imaging Computing System, FlexImaging, oMALDI Server 5.1 and SCiLS Lab (116, 220–225). Multivariate methods are applied, such as principal component analysis, clustering methods, factorization methods and classification methods (226). These statistical analyses may discriminate differential molecules between normal and tumor tissues and find potential biomarkers for the tumor. Different from the publicly available and commercial software tools, *Cardinal* is an open-source R package that implements data processing (normalization, baseline correction, peak detection and peak alignment), visualization of mass spectra, statistical segmentation (principal component analysis, Spatially-Aware and Spatially Aware Structurally Adaptive) and classification (partial least squares discriminant analysis and orthogonal projections) of ion images for MSI (227). *Cardinal* also introduced Spatial Shrunken Centroids, a novel method for model-based image segmentation and classification.

2.3 Mass spectrometry imaging in proteomics of endocrine tumors

Gene alternations play a fundamental role in endocrine tumors (228, 229). For example, BRAF (v-Raf murine sarcoma viral oncogene homolog B1) mutations, RAS (rapidly accelerated fibrosarcoma) mutations and RET (Proto-oncogene tyrosine-protein kinase receptor Ret) rearrangements are common genetic alternations in papillary thyroid carcinoma (PTC) and follicular thyroid carcinoma (FTC); GNAS (guanine nucleotide binding protein, alpha stimulating) gene mutations happens in sporadic pituitary adenomas while MEN1 (menin 1) and AIP (aryl hydrocarbon receptor interacting protein) mutations in family isolated pituitary adenoma (230, 231). Though great achievements have been made in elucidating the mechanism and pathology of endocrine tumors through genomic analysis, the gene expression and protein expression lack apparent correlation (4, 232–234). Proteins are gene products, the executors of cellular processes and more closely related to the phenotypes (235). Proteomics is complementary to genomics in revealing the alternations in structure, function and interactions of proteins in tumorigenesis and tumor progress. With MSI as the analysis tool, proteomics in endocrine tumors has showed the potential to discover different protein signatures between the tumor tissues and adjacent normal tissues and to discriminate among different subtypes of thyroid cancers. The spatially resolved proteomics of endocrine tumors can contributed to a better understanding of the overall mechanism involved in the tumorigenesis, progression, and metastasis.

The application of MSI in proteomics is capable of discriminating between the normal tissue and the cancer tissue as well as distinguishing between different subtypes of thyroid tumors (236–238). Mainini et al. analyzed the cytological smears obtained by *ex vivo* FNA from 7 patients with hyperplastic nodules or PTC using MALDI-MSI (239). The MSI data was processed with hierarchical cluster analysis and principal component analysis to evaluate the different proteomic expressions. And hyperplastic nodules and PTC were successfully discriminated by hierarchical cluster analysis and principal component analysis. Pagni et al. used MALDI-MSI to compare the protein profiles of cytologic samples obtained from patients diagnosed as hyperplastic nodules, Hürthle cell follicular adenoma, medullary thyroid carcinoma (MTC) and PTC (176). They evaluated 6 proteins whose expression in PTC were different from that of benign lesions, but similar to that of MTC. Different protein profiles that could distinguish between PTC and MCT were also detected. Calligaris et al. presented the application of MALDI-MSI in detecting and discriminating nonpathological human pituitary glands, hormone secreting and non-secreting human pituitary adenomas (240). They validated the capability of MALDI-MSI to image prolactin (PRL), growth hormone (GH), adrenocorticotropic hormone

(ACTH) and thyroid stimulating hormone (TSH) within normal glands and adenomas, but also submitted the MSI data to principal component analysis to evaluate the different protein signatures among nonpathological human pituitary glands, hormone secreting and non-secreting human pituitary adenomas. It was revealed that the sensitivity and specificity of MSI data distinguishing ACTH secreting adenomas from nonpathological pituitary were 100% and 93%, the sensitivity and specificity of MSI data distinguishing GH secreting adenomas from nonpathological pituitary were 82% and 100% and the sensitivity and specificity of MSI data distinguishing PRL secreting adenomas from nonpathological pituitary were 50% and 100%, respectively.

The application of MSI proteomics is also capable of finding potential protein biomarkers for the diagnosis of endocrine tumors (241). Nipp et al. performed MALDI-MSI and immunohistochemistry (IHC) on PTC tissues to find biomarkers for the metastasis of PTC (242). Using MALDI-MSI, they successfully found that thioredoxin, S100-A10 (p11, the ligand of Annexin-II) and S100-A6 (Calcyclin) could specially distinguish metastatic PTC from non-metastatic PTC. And IHC validated that these three overexpressed proteins were significantly associated with lymph node metastasis of PTC with p values < 0.005 (p value for thioredoxin: 0.00003; p value for S100A10: 0.00018; p value for S100-A6: 0.0013; Fisher's exact test).

The application of MSI in proteomics is capable of bringing insight into the endocrine tumor progression. Tissue necrosis is common in advanced and aggressive solid tumors (243). Scott et al. studied the N-linked glycosylation of proteins in human thyroid cancer tissue by MALDI-MSI (244). They demonstrated that proteins with high mannose or branched glycans were specially distributed in the cancer and stromal regions, whereas the glycans of proteins in necrotic regions presented limited branching, contained sialic acid modification and lacked fucose modification. Gawin et al. used MALDI-MSI to compare protein profiles between the primary PTC located in the thyroid gland and the PTC with synchronous metastases in regional lymph nodes (245). Thirty-six proteins were found remarkably different in abundance between primary PTC and metastatic PTC, which were then annotated as proteins involved in the organization of the cytoskeleton and chromatin, as well as proteins involved in immunity-related functions.

2.4 Mass spectrometry imaging in lipidomics of endocrine tumors

Lipids are hydrophobic or amphipathic compounds with great differences in their chemical composition and structure (246). Lipids are divided into 8 categories: fatty acyls, glycerolipids, glycerophospholipids, sphingolipids, sterol lipids, prenol lipids, saccharolipids and polyketides (247). Lipids involve in many essential cellular processes, including chemical-energy storage, composition of cell membrane bilayer, cell-cell interactions and cellular signal transduction. Lipidomics has been defined as a tool of full characterization of lipid molecular species and of their biological roles with respect to expression of proteins involved in lipid metabolism and function, including gene regulation (248). Abnormal lipid metabolism has been considered as a key feature of cancers (249–252). Stearoyl-CoA desaturase (SCD1) has been proved to be highly expressed in PTC, FTC and anaplastic thyroid carcinoma (ATC) (253, 254). SCD1, a fatty acyl desaturase encoded by stearoyl-CoA desaturase 1 gene, plays an important role in *de novo* lipid biosynthesis (255). It is a rate-limiting enzyme in the reaction of producing monounsaturated fatty acids (such as oleic acid and palmitoleic acid) from saturated fatty acids (such as stearic and palimitic acid). Monounsaturated fatty acids are the substrates for the synthesis of triglycerides, sphingolipids, glycolipids, (PLs), and other lipoproteins (256, 257). The elevated SCD1 promotes the proliferation, migration and invasion of cancer cells in PTC, FTC and ATC. Several research groups have focused on the lipidomics of endocrine tumors by MSI to analyze multiple lipid species and detect lipid alternations during the tumorigenesis (177, 258).

MSI showed the competency for detecting specific phosphatidylcholine (PC), sphingomyelin (SM) and phosphatidic acid (PA) species that may associate with the pathological behaviors of PTC. Ishikawa et al. investigated the distribution of lipids within cancerous and normal tissues from PTC patients using MALDI-MSI and MS/MS identification (259). The MSI analysis was performed by MALDI-TOF/TOF with 2,5-DHB as the matrix. And it was found that three species with m/z value 798.5, 796.5 and 741.5 were remarkably increased in the cancerous tissue compared to the normal tissue. A hybrid quadrupole/TOF mass spectrometer equipped with an orthogonal MALDI source was used to identify these three ions as $[PC\ (16:0/18:1)+K]^+$ and $[PC\ (16:0/18:2)+K]^+$ and $[SM\ (d18:0/16:1)+K]^+$, respectively. Wojakowska et al. employed MALDI-MSI to find lipids that could discriminate between PTC tissues and adjacent non-cancerous thyroid tissues (260). They found that intensities of PC (32:0), PC (32:1), PC (34:1), PC (36:3), SM (34:1), SM (36:1) and PA (36:2) and PA (36:3) of the cancerous tissue were significantly higher than that of the non-cancerous tissue.

MSI is also competent for imaging differential molecular signatures for oncocytic thyroid tumors, e.g., the abnormal expression of cardiolipins (CLs). CLs play an important role in the stability and integrity of mitochondrial structure and function. There is increasing evidence in the CL metabolism reprogramming of cancers. However, the exact mechanism by which CLs modulate cancer remains to be clarified (261). Zhang et al. conducted the DESI-MSI analysis to image and characterize the lipid composition for the oncocytic thyroid

tumors (Hurthle cell adenoma and Hurthle cell carcinoma) (262). They found that CL species were distributed in the oncocytic thyroid tumor with an abnormally high abundance and diversity, as compared with the non-oncocytic thyroid tumors (PTC, FTC and follicular adenoma) and normal thyroid samples. Feider et al. applied the integrated DESI-field asymmetric ion mobility spectrometry-MSI approach to measure CLs in oncocytic thyroid tumors (163). They validated the existence of abundant CL species in the entire thyroid tissue section and managed to identify *m/z* values of 723.479, 737.494 and 747.473 as CL (72:6), CL (74:8) and CL (76:9). The ion images of MSI demonstrated that oncocytic thyroid tumor was present throughout the tissue section, MSI images were consistent with histologic images. The spatial distribution of CLs among the entire tissue has the potential to indicate specific locations of oncocytic thyroid tumor.

Moreover, MSI is competent for the detection of FFAs and PLs of the cancer tissue and the para-cancer tissue to elucidate the relatives between changes of FFAs and PLs and the cancer development (263–265). FFAs are an essential constituent of PLs. It has been revealed that FFAs greatly influence the energy storge in the cancer microenvironment and act as second cellular messengers (266). The metabolism of FFAs is an essential step in *de novo* lipogenesis, which is more active in the cancer tissue compared with the normal tissue (267, 268). Wang et al. simultaneously imaged FFAs and PLs in the thyroid cancer tissue and the para-cancer tissue by MALDI-MSI (127). They found that the intensities of 7 FFAs (arachidic acid (C20:0), oleic acid (C18:1), linolenic acid (C18:3), palmitoleic acid (C16:1), arachidonic acid (C20:4), docosahexaenoic acid (C22:6) and linoleic acid (C18:2)) were significantly higher in the cancer tissue than that of the para-cancer tissue. The correlation between FFAs and PLs was analyzed by submitting the intensity of each detected PL and FFA derivative in each spot for the cancer tissue and the para-cancer tissue to Spearman correlation analysis. The heatmaps of the correlation between FFAs and PLs in thyroid cancer samples were created to reveal that the saturated FFAs (C16:0 and C18:0) were positively correlated with PLs. This is because palmitic acid (C16:0) is the main product of *de novo* fatty acid synthesis and a precursor for the synthesis of other fatty acids. Combined with the upregulation of palmitic acid in cancer tissue, this phenomenon is due to the more active *de novo* synthesis of fatty acids in cancer tissue to provide abundant precursors for other lipid metabolism.

2.5 Mass spectrometry imaging in metabolomics of endocrine tumors

Metabolites are intermediate end products generated by chemical reactions within cells, tissues and organs (269). Metabolomics, focusing on the altered metabolites and metabolic pathways within the biological sample, is a promising technique in shedding light on the molecular mechanisms of endocrine tumors (270–272). MSI has made great progress in the metabolomic analysis of endocrine tumors, involving detection of altered metabolites, elucidation of tumor metabolism reprogramming and identification of possible biomarkers (273).

MSI has the ability to present the histology heterogeneity but also can reveal the metabolic heterogeneity within the tumor. Huang et al. studied the metabolism of PTC by ambient pressure DESI-MSI (274). They built a spatially resolved metabolomic data processing pipeline that revealed the tumor microregion heterogeneity. A clear discrimination among the tumor, the stromal and the normal tissue was shown. The para-cancer region was further segmented into different microregions based on the differential metabolic profiles. Additionally, this study showed that the abundances of phenylalanine, leucine and tyrosine were the highest in the tumor region, followed by the stromal region, lowest in the normal tissue. It has been revealed that amino acids are involved in glycolysis and tricarboxylic acid cycles, reshaping the cellular metabolism (275). Cancers demand abundant amino acids to promote cancer cell proliferation, invasion and metastasis. Amino acids were usually present to be increasingly expressed in PTC (276–279).

MSI has the ability to help elucidate the molecular mechanism of the pheochromocytoma. The adrenal medulla, in the central part of the adrenal gland, is composed of chromaffin cells that synthesize catecholamines. The hormones exert their effects by acting on alpha- and beta- adrenoreceptors in the central nervous system and the periphery (280). The “fight or flight response” is a key mechanism and causes a number of physiological changes, such as increased blood pressure, increased cardiac output and increased glycogenolysis in liver and muscle tissue (281). Pheochromocytoma is formed in the adrenal medulla. This type of tumor produces and releases a large amount of circulating catecholamines and leads to a constant activation of the “fight or flight response” (282). Takeo et al. visualized the distribution of adrenaline and noradrenaline in the normal tissue and the pheochromocytoma tissue (213). They demonstrated that both catecholamines were distributed in the adrenal medulla of the normal tissue, whereas pheochromocytoma tissue showed a moderate adrenaline level and an elevated level of noradrenaline with a homogeneous distribution among the whole tumor region.

MSI has the potential to provide additional support for the hypothesis that aldosterone-producing cell cluster (APCC) is the origin of aldosterone-producing adenoma (APA) (283). It is reported that aldosterone or 18-oxocortisol is a potential serum marker of APA. Sugiura et al. visualized the distribution of aldosterone or 18-oxocortisol in APCC, possible APCC-to-APA transitional lesions and APA by MALDI-MSI (284). The ion images revealed that aldosterone and 18-oxocortisol congregated

within the tumor regions where aldosterone synthase was distributed. The imaging results of possible APCC-to-APA transitional lesions even suggested a path of cellular migration from APCC to form APA inside the adrenal glands. Sun et al. used MALDI-MSI to compare the metabolomic phenotypes between APCC and APA (285). They processed the MALDI spectra by component analysis. Depending on their respective metabolite distribution patterns, the APCC were divided into 2 subgroups. Metabolic profiles of APCC in subgroup 1 were distinct from APA, whereas subgroup 2 displayed metabolic profiles similar to the APA group. Compared to subgroup 1, subgroup 2 presented increased hexose monophosphate shunt, enhanced metabolism of tryptophan *via* the kynurenine pathway and the significant enhancement of N-acetylglucosamine, which may be related to cell proliferation and APCC to APA transition.

MALDI-MSI has the potential to discriminate endocrine tumors with different genotypes based on the metabolic profiles. By using MALDI-FT-ICR with 9-AA matrix, Murakami et al. analyzed the metabolism of APAs by MSI (286). The metabolic data was processed with ortho-PLSDA clustering between KCNJ5- (potassium voltage-gated channel subfamily J member 5) and CACNA1D- (calcium voltage-gated channel subunit alpha1 D) mutated APAs. One hundred and thirty-seven differential metabolites were screened out (adjusted p value < 0.05). In the following, the significantly altered metabolites were submitted to the pathway analysis and the activation of purine metabolism in KCNJ5-mutated APAs was demonstrated (pathway impact = 0.13, $p < 0.001$, and FDR < 0.001).

3 Spatially resolved microproteomics in endocrine tumors

3.1 Spatially resolved microproteomics and microextraction approaches

Conventional proteomics usually performs extraction by preparing the whole piece of tissue into homogenate. The final protein or peptide sample is injected into the LC-MS system in solution. The homogenization process leads to the loss of the histological structure of the tissue and the spatial localization of the analytes (287). Moreover, proteins with low abundance sometimes cannot be detected due to the interference of abundant proteins (288). These challenges can be overcome by spatially resolved microproteomics, which allows quantitative and comparative proteomic analysis within a relatively small surface area (μm) in the tumor microenvironment (61, 289–295). Spatially resolved microproteomics is achieved by the collaboration of LC-MS and microextraction approaches. Laser microdissection (LMD) and liquid microjunction (LMJ) are two general microextraction approaches that help extract proteins from a relatively limited area of the sample surface (296–298).

3.1.1 Laser microdissection

LMD can isolate and harvest subpopulations of tissue cells relying on either infrared (IR) laser or ultraviolet (UV) laser coupled with a microscope (34). The histology structure of the sample is present under the microscope and regions of interest are determined by direct microscopic visualization (299).

Figures 3A–C respectively introduce the principles of three LMD systems from different vendors. In the system of Arcturus laser capture microdissection, the tissue section is located on the glass slide. A thermolabile membrane on bottom face of the cap is placed on the tissue section. The IR laser activates the membrane and the melted membrane extends to the tissue. The adhesion force of the selected tissue area to the activated membrane exceeds that to the glass slide. The selected area is removed from the tissue (300). In Zeiss's PALM microdissection, the tissue section is mounted on a polyethylene napthalate (PEN) membrane glass slide. After selecting the region of interest, the UV laser ablates the surrounding cells and cuts away the selected area (301). The cut-off areas are transported into a collective tube by a defined laser pulse against gravity. In the Leica LMD microdissection, the tissue section is mounted on the PEN membrane glass slide and placed upside down on the stage. The target tissue is dissected by the UV laser and directly falls into a vessel underneath the tissue section by gravity (302).

3.1.2 Liquid microjunction

LMJ performs microextraction within a well-defined area of the tissue using the liquid microjunction interface (303–305). The principle of LMJ is present in Figure 3D. In brief, a probe aspirates a certain amount of extraction solvent and dispenses a portion onto the tissue surface to create a liquid microjunction between the probe and the tissue surface. Analytes that are soluble in the solvent will be extracted into the liquid microjunction. After a predefined extraction time, the probe is aspirated and the extraction solution can be directly dispensed to LC-MS system (163, 306). Alternatively, it is possible to perform several cycles of extraction and pool all the collected solution in the same vial to increase the quantity of samples for the further analysis (307).

For spatially resolved microproteomics, there are two LMJ strategies (308). Firstly, localized on-tissue digestion is performed and digested peptides are extracted by LMJ (293). Secondly, intact proteins are directly extracted from regions of interest within the tissue (309). In conclusion, LMJ has shown great capacities in extraction of proteins from specific cell subpopulation, contributing extensively to the proteomic analysis (310–312).

10.3389/fendo.2022.993081

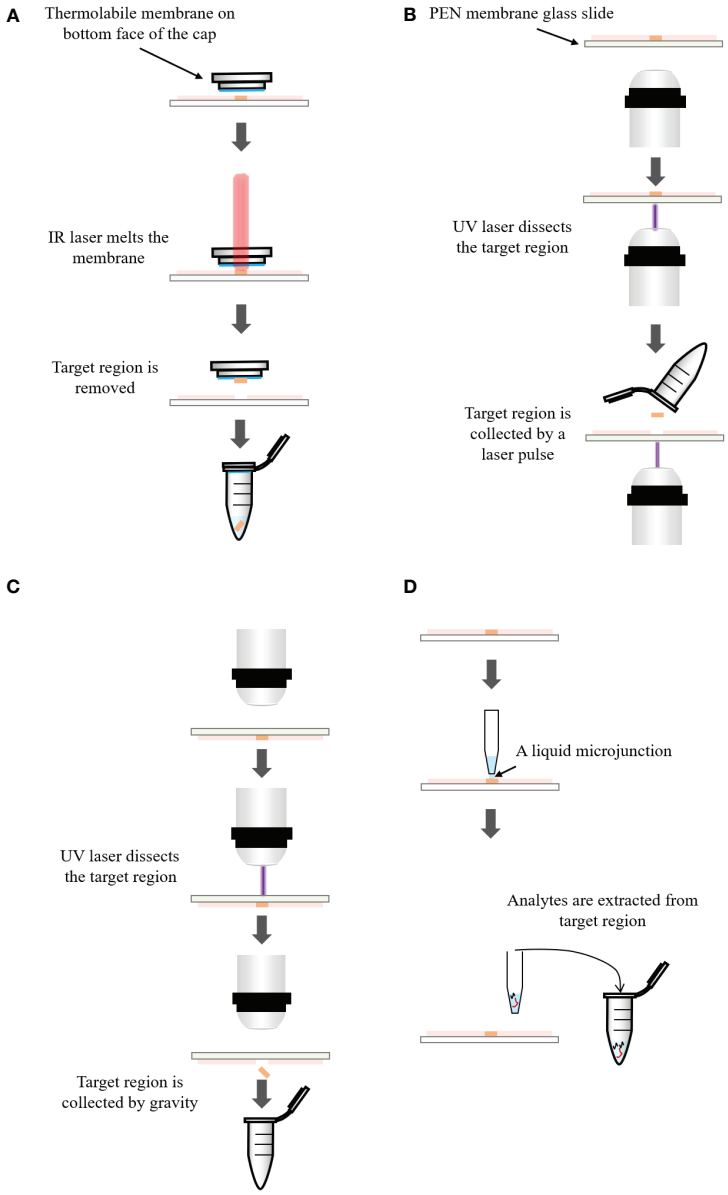

FIGURE 3
(A) Principle of the Arcturus laser capture microdissection. A thermolabile membrane on bottom face of the cap is placed on the tissue section. The infrared (IR) laser activates the membrane which extends to the tissue. The adhesion force of the tissue to the activated membrane exceeds that to the glass slide. The selected area is removed from the tissue. **(B)** Principle of the Zeiss's PALM microdissection. The tissue section is mounted on a polyethylene napthalate (PEN) membrane coated glass slide. After selecting the region of interest, ultraviolet (UV) laser ablates the surrounding cells and cuts away the selected area, which is then transported into a collection tube by a defined laser pulse against gravity. **(C)** Principle of the Leica LMD microdissection. The tissue section is mounted on the PEN membrane glass slide and placed upside down on the stage. The target tissue is dissected by the laser and directly falls into a collection tube underneath the tissue section. **(D)** Principle of liquid microjunction extraction. The probe aspirates the extraction solvent and dispenses a portion onto the tissue surface to create a liquid microjunction between the probe and the tissue surface. After a predefined extraction time, analytes that are soluble in the solvent are extracted into the liquid microjunction. The extracted solution can be analyzed by LC-MS directly.

3.1.3 Comparison of laser microdissection and liquid microjunction

There are some similarities between LMD and LMJ. Before being used, both of them need the histology structure of the samples, which can be obtained from histology staining, immunochemistry and MSI molecular histology images. Both of them are appliable to fresh frozen tissues, FFPE tissues and cytologic smears. There are also a few differences between them. For LMD, it can dissect regions of any size and any shape from the sample surface. It can cut off an area of tissue with a few

square milimeters. It can also allow to obtain a region with a few micrometers and even submicrometers in diameter. Therefore, LMD can isolate a large area of tissue, cell clusters, single cell and subcellular compartments. For LMJ, the droplet deposited on the sample surface is a circle 0.25 to 4 mm in diameter (313). LMJ is more appropriate to sample with the larger surface area (314). Besides, the dissected sample obtained by LMD needs to be extracted and it is always challenging to process the small volume of sample. LMJ can perform the extraction *in situ* from the target surface area of the sample and the extracts can be directly introduced into the LC-MS system. During the process, the sample consumption is largely reduced.

3.2 Application of spatially resolved microproteomics in endocrine tumors

LMD or LMJ coupled with MS/MS makes full use of their advantages in the analysis of heterogenous endocrine tumor tissues, allowing for in-depth proteomic analysis and capable of depicting the underlying protein alternations in the endocrine tumor microenvironment (315, 316).

Prolactinoma is a subtype of pituitary adenoma and encompasses various types of cells including prolactin cells, endothelial cells, fibroblasts and other stomal cells (317). To better explain the prolactinoma tumorigenesis from the proteomics level, Liu et al. dissected pure prolactin cells from prolactinomas using immune-LMD and performed bottom-up proteomic analysis on the extracted proteins (318). By searching the human International Protein Index database with MS/MS spectra, they successfully set up a specific prolactinoma spectral library of 2,243 proteins.

Amyloids are abnormal proteins, which deposit in the organs and tissues, such as brain, heart, bladder, skin, thyroid, parathyroid, muscles and nerves (319–321). As the amyloid deposition increases, the normal function of organs and tissues is disturbed (322). Some types of amyloidosis are associated with the occurrence and development of the diseases (323–325). Parathyroid hormone (PTH), a polypeptide hormone, has been shown to form amyloid and amyloid-like beta-sheet aggregation in parathyroid adenomas (326). Colombat et al. used LMD-LC-MS/MS to analyze the protein profiling for parathyroid adenomas whose histological analysis presented nodular typical amyloid deposits. And the LMD-LC-MS/MS spectra successfully identified the amyloid fibril protein in parathyroid adenomas as PTH (327). They speculated that the formation of amyloid in a subset of parathyroid adenomas resulted from inappropriate PTH production. The physiological hormone aggregation might escape the control of functional amyloid processes, leading to disease-amyloid aggregation of PTH.

The pituitary gland can be divided into two distinct regions both in anatomy and function: the anterior pituitary (adenohypophysis, AH) and the posterior pituitary (neurohypophysis, NH). The anterior pituitary comprises of five different types of epithelial endocrine cells, responsible for secreting GH, PRL, TSH, ACTH, follicle stimulating hormone and luteinizing hormone (328). The posterior secrets two hormones: oxytocin and vasopressin. Kertesz et al. used an automated LMJ system for profiling of arginine vasopressin and ACTH in normal human pituitary gland and pituitary adenomas (329). This spatially resolved sampling approach allowed selective protein extraction from the anterior and the posterior regions of the human pituitary gland as well as selective protein extraction from the tumor region and the normal posterior region of the ACTH secreting adenoma tissue. The separation and identification of the extracted proteins were processed with LC-MS/MS system. Heatmaps were created to show that arginine vasopressin was mostly distributed in NH regions and ACTH in AH regions. ACTH levels in secreting adenomas and normal AH regions were significantly higher than in non-secreting adenomas and NH regions. The results showed that the signature of arginine vasopressin and ACTH in a series of ACTH secreting and non-secreting pituitary adenomas was consistent with the histopathological evaluation.

4 Conclusion and perspective

Multi-omics analysis for endocrine tumors is gaining much attention in recent years (330–332). Endocrine tumors are characterized by a marked diversity and high heterogeneity. Most endocrine tumors are benign, evolving locally and slowly. However, a fraction of endocrine tumors are malignant, as evidenced by metastasis and fatal evolution (2). Biomarkers associated with tumorigenesis, progression and metastasis are intensively investigated, facilitating the development of novel diagnostic tools and promising treatments. MSI techniques show the strength in detection and identification of proteins, lipids and metabolites that altered significantly between the tumor tissue and the normal tissue. Compared with non-metastatic PTC, thioredoxin, S100-A10 and S100-A6 were significantly elevated in metastatic PTC (p values < 0.005). And the three proteins were identified as protein biomarkers for PTC with lymph node metastasis. Besides, CL species with an abnormal abundance and diversity are identified as candidate biomarkers for oncocytic thyroid tumor, such as CL (72:6), CL (72:8) and CL (76:9). Moreover, MSI result showed aldosterone and 18-oxocortisol congregated within the tumor regions where aldosterone synthase was distributed, serving as a complementary for the view that aldosterone or 18-oxocortisol has the potential to act as a biomarker for APA. With the advances in LC-MS and microextraction approaches, spatially resolved microproteomics in endocrine tumors has exhibited excellent performances in revealing the regional protein profiles within the heterogeneous tumor tissues.

The samples for endocrine tumors mainly comprise of fresh-frozen tissues, FFPE tissues and cytologic samples. Proteomics,

lipidomics and metabolomics guided by MSI and spatially resolved microproteomics can reflect the relative abundance and spatial distribution of analytes. The sample preparation protocols are crucial and need to be established based on the purpose of the study and the collected samples. It should be taken into account to protect the analytes from degradation and displacement within the tissue and preserve the integrity of the tissue during the preparation process.

MSI provides spatially resolved molecular analysis of biological samples without labelling. However, MSI is disadvantageous in molecule identification caused by local ion suppression and has limitations in the depth of molecule detection coverage compared with established proteomics, lipidomics and metabolomics based on LC-MS/MS analysis (333). The strategy that combines MSI, microextraction approaches and LC-MS has the potential to solve the above problem. In brief, the tissue is first analyzed with MSI to produce localization-registered mass spectra and ion images. The tissue is then segmented into different regions. And, the location information of the target region is passed to the LMD or LMJ. The microextraction is performed on the target regions. Lastly, the extracts are analyzed with LC-MS/MS. This strategy allows more comprehensive and deeper insights into the molecular heterogeneity uncovered by MSI and enables a better understanding of the molecular mechanism within the sample (289). It has shown the potential of improving the characterization and identification of proteins associated with endocrine tumors (329). One limitation for this strategy in lipidomcis and metabolomics is the small sample quantity obtained by microextraction, which poses challenges to the following LC-MS/MS analysis. Therefore, mass spectrometers and chromatographic methods with significantly enhanced sensitivity are required in this filed.

Advanced MSI techniques are remarkably promising in single cell metabolomics, where the analysis on metabolites is directly performed on single cells without any cell lysis, separation or label (334). The spatial resolution of SIMS-MSI with GCIBs as the primary ion beam can approach 1 μm, capable of imaging a single cell (335). A spatial resolution of around 1.4 μm has been achieved by the development of atmospheric pressure MALDI MSI platform (336). High spatial resolution MALDI-MSI (down to 0.5-5 μm) using both reflection and transmission geometries has been being developed by the Caprioli group (337, 338). MALDI-MSI is capable of mapping and visualizing lipids in a single cell of newly fertilized individual zebrafish embryos (339). MALDI-2 is a post post-ionization technique. After the initial MALDI ionization, a second laser that is parallel to the sample surface is applied to post-ionize neutral molecules. MALDI-2 reduces ion suppression effects and improves sensitivity by up to 3 orders of magnitude. And spatial resolution can reach 5 μm. By applying transmission-mode MALDI-2 ion source in MSI of the brain tissue, the subcellular resolution was achieved (340). MSI-based single cell metabolomics devotes to profiling metabolites spatially and/or temporally in a single cell level, providing insights into the intracellular and intercellular metabolic activities and revealing the intercellular heterogeneity.

With the development in mass spectrometry, chromatography, microextraction methods, sample preparation protocols and data analysis methods, analyses on the proteomics, lipidomics and metabolomics of endocrine tumors will provide new dimensional insights in molecular level, cellular even subcellular level and tissue level, aiding in overcoming the problems of pathophysiology, diagnosis, and treatment for endocrine tumors.

Author contributions

XZ and YH conceived of the concept and idea of this article. YH collected references, wrote and revised the manuscript, and was responsible for the corresponding work of the manuscript. SG collected partial references. YG, ZZ, RC and XZ participated in proofreading, editing and revision of the manuscript. All authors contributed to the article and approved the submitted version.

Acknowledgments

Thanks are given to ZZ for assistance with histopathologic information for endocrine tumors and to RC and XZ for valuable discussions.

Conflict of interest

The authors declare that the research was conducted in the absence of any commercial or financial relationships that could be construed as a potential conflict of interest.

Publisher's note

Supplementary material

The Supplementary Material for this article can be found online at: https://www.frontiersin.org/articles/10.3389/fendo.2022.993081/full#supplementary-material

References

1. Hiller-Sturmhofel S, Bartke A. The endocrine system: An overview. *Alcohol Health Res World* (1998) 22(3):153–64.

2. Scoazec JY. Endocrine tumors: biology and physiopathology. *Ann Pathol* (2005) 25(6):447–61. doi: 10.1016/S0242-6498(05)86160-7

3. Pang ALY, Chan W-Y. Molecular basis of diseases of the endocrine system. In: Coleman WB, editor. *Molecular pathology, 2nd ed.* (2018) London, United Kingdom: Academic Press. p. 477–505.

4. Xing M. Molecular pathogenesis and mechanisms of thyroid cancer. *Nat Rev Cancer* (2013) 13(3):184–99. doi: 10.1038/nrc3431

5. Lloyd RV, Osamura RY, Klöppel G, Rosai J eds. World health organization classification of endocrine tumours. In: *World health organization classification of tumours, 4*, vol. 10 . Lyon: IARC Press.

6. DeLellis RA, Lloyd RV, Heitz PU, Eng C eds. Pathology and genetics of tumours of endocrine organs. In: *World health organization classification of tumours*, vol. 8 . Lyon: IARC Press.

7. Mete O, Erickson LA, Juhlin CC, de Krijger RR, Sasano H, Volante M, et al. Overview of the 2022 WHO classification of adrenal cortical tumors. *Endocr Pathol* (2022) 33(1):155–96. doi: 10.1007/s12022-022-09710-8

8. Nose V, Gill A, Teijeiro JMC, Perren A, Erickson L. Overview of the 2022 WHO classification of familial endocrine tumor syndromes. *Endocr Pathol* (2022) 33(1):197–227. doi: 10.1007/s12022-022-09705-5

9. Rindi G, Mete O, Uccella S, Basturk O, La Rosa S, Brosens LAA, et al. Overview of the 2022 WHO classification of neuroendocrine neoplasms. *Endocr Pathol* (2022) 33(1):115–54. doi: 10.1007/s12022-022-09708-2

10. Mete O, Asa SL, Gill AJ, Kimura N, de Krijger RR, Tischler A. Overview of the 2022 WHO classification of paragangliomas and pheochromocytomas. *Endocr Pathol* (2022) 33(1):90–114. doi: 10.1007/s12022-022-09704-6

11. Erickson LA, Mete O, Juhlin CC, Perren A, Gill AJ. Overview of the 2022 WHO classification of parathyroid tumors. *Endocr Pathol* (2022) 33(1):64–89. doi: 10.1007/s12022-022-09709-1

12. Asa SL, Mete O, Perry A, Osamura RY. Overview of the 2022 WHO classification of pituitary tumors. *Endocr Pathol* (2022) 33(1):6–26. doi: 10.1007/s12022-022-09703-7

13. Baloch ZW, Asa SL, Barletta JA, Ghossein RA, Juhlin CC, Jung CK, et al. Overview of the 2022 WHO classification of thyroid neoplasms. *Endocr Pathol* (2022) 33(1):27–63. doi: 10.1007/s12022-022-09707-3

14. Luzon-Toro B, Fernandez RM, Villalba-Benito L, Torroglosa A, Antinolo G, Borrego S. Influencers on thyroid cancer onset: Molecular genetic basis. *Genes (Basel)* (2019) 10(11):913. doi: 10.3390/genes10110913

15. Olson E, Wintheiser G, Wolfe KM, Droessler J, Silberstein PT. Epidemiology of thyroid cancer: A review of the national cancer database, 2000-2013. *Cureus* (2019) 11(2):e4127. doi: 10.7759/cureus.4127

16. Wang J, Yu F, Shang Y, Ping Z, Liu L. Thyroid cancer: incidence and mortality trends in China, 2005-2015. *Endocrine* (2020) 68(1):163–73. doi: 10.1007/s12020-020-02207-6

17. Povoa AA, Teixeira E, Bella-Cueto MR, Batista R, Pestana A, Melo M, et al. Genetic determinants for prediction of outcome of patients with papillary thyroid carcinoma. *Cancers (Basel)* (2021) 13(9):2048. doi: 10.3390/cancers13092048

18. Sung H, Ferlay J, Siegel RL, Laversanne M, Soerjomataram I, Jemal A, et al. Global cancer statistics 2020: GLOBOCAN estimates of incidence and mortality worldwide for 36 cancers in 185 countries. *CA Cancer J Clin* (2021) 71(3):209–49. doi: 10.3322/caac.21660

19. Pemayun TG. Current diagnosis and management of thyroid nodules. *Acta Med Indones* (2016) 48(3):247–57.

20. Melmed S. Pituitary-tumor endocrinopathies. *N Engl J Med* (2020) 382 (10):937–50. doi: 10.1056/NEJMra1810772

21. Farrugia FA, Charalampopoulos A. Pheochromocytoma. *Endocr Regul* (2019) 53(3):191–212. doi: 10.2478/enr-2019-0020

22. Bourdeau I, El Ghorayeb N, Gagnon N, Lacroix A. Management of endocrine disease: Differential diagnosis, investigation and therapy of bilateral adrenal incidentalomas. *Eur J Endocrinol* (2018) 179(2):R57–67. doi: 10.1530/EJE-18-0296

23. Alshaikh S, Harb Z, Aljufairi E, Almahari SA. Classification of thyroid fine-needle aspiration cytology into Bethesda categories: An institutional experience and review of the literature. *Cytojournal* (2018) 15:4. doi: 10.4103/cytojournal.cytojournal_32_17

24. Bongiovanni M, Spitale A, Faquin WC, Mazzucchelli L, Baloch ZW. The Bethesda system for reporting thyroid cytopathology: A meta-analysis. *Acta Cytol* (2012) 56(4):333–9. doi: 10.1159/000339959

25. Rodrigo JP, Hernandez-Prera JC, Randolph GW, Zafereo ME, Hartl DM, Silver CE, et al. Parathyroid cancer: An update. *Cancer Treat Rev* (2020) 86:102012. doi: 10.1016/j.ctrv.2020.102012

26. Roman-Gonzalez A, Jimenez C. Malignant pheochromocytoma-paraganglioma: pathogenesis, TNM staging, and current clinical trials. *Curr Opin Endocrinol Diabetes Obes* (2017) 24(3):174–83. doi: 10.1097/MED.0000000000000330

27. Gervasoni JE, Cady B. Endocrine tumors. In: Bertino JR, editor. *Encyclopedia of cancer, 2nd ed.*, vol. p. Cambridge, Massachusetts: Academic Press (2002). p. 135–43.

28. Tevosian SG, Ghayee HK. Pheochromocytomas and paragangliomas. *Endocrinol Metab Clin North Am* (2019) 48(4):727–50. doi: 10.1016/j.ecl.2019.08.006

29. Fisher R, Pusztai L, Swanton C. Cancer heterogeneity: implications for targeted therapeutics. *Br J Cancer* (2013) 108(3):479–85. doi: 10.1038/bjc.2012.581

30. LeBleu VS. Imaging the tumor microenvironment. *Cancer J* (2015) 21 (3):174–8. doi: 10.1097/PPO.0000000000000118

31. Elkhattouti A, Hassan M, Gomez CR. Stromal fibroblast in age-related cancer: Role in tumorigenesis and potential as novel therapeutic target. *Front Oncol* (2015) 5:158. doi: 10.3389/fonc.2015.00158

32. Wu Y, Cheng Y, Wang X, Fan J, Gao Q. Spatial omics: Navigating to the golden era of cancer research. *Clin Transl Med* (2022) 12(1):e696. doi: 10.1002/ctm2.696

33. Holzlechner M, Eugenin E, Prideaux B. Mass spectrometry imaging to detect lipid biomarkers and disease signatures in cancer. *Cancer Rep (Hoboken)* (2019) 2(6):e1229. doi: 10.1002/cnr2.1229

34. von Eggeling F, Hoffmann F. Microdissection-an essential prerequisite for spatial cancer omics. *Proteomics* (2020) 20(17-18):e2000077. doi: 10.1002/pmic.202000077

35. Cilento EM, Jin L, Stewart T, Shi M, Sheng L, Zhang J. Mass spectrometry: A platform for biomarker discovery and validation for alzheimer's and parkinson's diseases. *J Neurochem* (2019) 151(4):397–416. doi: 10.1111/jnc.14635

36. Chubatyi ND, McEwen CN. Improving the sensitivity of matrix-assisted ionization (MAI) mass spectrometry using ammonium salts. *J Am Soc Mass Spectrom* (2015) 26(10):1649–56. doi: 10.1007/s13361-015-1205-z

37. Li C, Chu S, Tan S, Yin X, Jiang Y, Dai X, et al. Towards higher sensitivity of mass spectrometry: A perspective from the mass analyzers. *Front Chem* (2021) 9:813359. doi: 10.3389/fchem.2021.813359

38. Medhe S. Ionization techniques in mass spectrometry: A review. *Mass Spectrom Purif Tech* (2018) 04(01):1000126. doi: 10.4172/2469-9861.1000126

39. Haag AM. Mass analyzers and mass spectrometers. *Adv Exp Med Biol* (2016) 919:157–69. doi: 10.1007/978-3-319-41448-5_7

40. Hofmann AE, Chimiak L, Dallas B, Griep-Raming J, Juchelka D, Makarov A, et al. Using orbitrap mass spectrometry to assess the isotopic compositions of individual compounds in mixtures. *Int J Mass Spectrom* (2020) 457:116410. doi: 10.1016/j.ijms.2020.116410

41. Nikolaev EN, Kostyukevich YI, Vladimirov G. Fundamentals and simulations in FT-ICR-MS. In: *Fundamentals and applications of Fourier transform mass spectrometry* (2019) Amsterdam, Netherlands: Elsevier. p. 89–111.

42. Piraud M, Pettazzoni M, Lavoie P, Ruet S, Pagan C, Cheillan D, et al. Contribution of tandem mass spectrometry to the diagnosis of lysosomal storage disorders. *J Inherit Metab Dis* (2018) 41(3):457–77. doi: 10.1007/s10545-017-0126-3

43. Illiano A, Pinto G, Melchiorre C, Carpentieri A, Faraco V, Amoresano A. Protein glycosylation investigated by mass spectrometry: An overview. *Cells* (2020) 9(9):1986. doi: 10.3390/cells9091986

44. Zheng X, Smith RD, Baker ES. Recent advances in lipid separations and structural elucidation using mass spectrometry combined with ion mobility spectrometry, ion-molecule reactions and fragmentation approaches. *Curr Opin Chem Biol* (2018) 42:111–8. doi: 10.1016/j.cbpa.2017.11.009

45. Paine MRL, Poad BLJ, Eijkel GB, Marshall DL, Blanksby SJ, Heeren RMA, et al. Mass spectrometry imaging with isomeric resolution enabled by ozone-induced dissociation. *Angew Chem Int Ed Engl* (2018) 57(33):10530–4. doi: 10.1002/anie.201802937

46. Brodbelt JS, Morrison LJ, Santos I. Ultraviolet photodissociation mass spectrometry for analysis of biological molecules. *Chem Rev* (2020) 120(7):3328–80. doi: 10.1021/acs.chemrev.9b00440

47. Zhang J, Guo C, Huo X, Ma X, Li X, Abliz Z, et al. Unsaturated lipid isomeric imaging based on the paterno-buchi reaction in the solid phase in ambient conditions. *Talanta* (2021) 235:122816. doi: 10.1016/j.talanta.2021.122816

48. Cologna SM. Mass spectrometry imaging of cholesterol. *Adv Exp Med Biol* (2019) 1115:155–66. doi: 10.1007/978-3-030-04278-3_7

49. Pang X, Gao S, Ga M, Zhang J, Luo Z, Chen Y, et al. Mapping metabolic networks in the brain by ambient mass spectrometry imaging and metabolomics. *Anal Chem* (2021) 93(17):6746–54. doi: 10.1021/acs.analchem.1c00467

50. Castellanos A, Ramirez CE, Michalkova V, Nouzova M, Noriega FG, Francisco FL. Three dimensional secondary ion mass spectrometry imaging (3D-SIMS) of aedes aegypti ovarian follicles. *J Anal At Spectrom* (2019) 34(5):874–83. doi: 10.1039/C8JA00425K

51. Buchberger AR, DeLaney K, Johnson J, Li L. Mass spectrometry imaging: A review of emerging advancements and future insights. *Anal Chem* (2018) 90 (1):240–65. doi: 10.1021/acs.analchem.7b04733

52. Dilillo M, Heijs B, McDonnell LA. Mass spectrometry imaging: How will it affect clinical research in the future? *Expert Rev Proteomics* (2018) 15(9):709–16. doi: 10.1080/14789450.2018.1521278

53. Aichler M, Walch A. MALDI imaging mass spectrometry: current frontiers and perspectives in pathology research and practice. *Lab Invest* (2015) 95(4):422–31. doi: 10.1038/labinvest.2014.156

54. Bowman AP, Heeren RMA, Ellis SR. Advances in mass spectrometry imaging enabling observation of localised lipid biochemistry within tissues. *Trac-Trend Anal Chem* (2019) 120:115197. doi: 10.1016/j.trac.2018.07.012

55. Unsihuay D, Mesa Sanchez D, Laskin J. Quantitative mass spectrometry imaging of biological systems. *Annu Rev Phys Chem* (2021) 72:307–29. doi: 10.1146/annurev-physchem-061020-053416

56. John Lough W, Carlile M. Chromatography: Separation techniques in biology. In: Ramesh V, editor. *Biomolecular and bioanalytical techniques* (2019) Hoboken, New Jersey: Wiley. p. 123–52.

57. Tang H, Wang X, Xu L, Ran X, Li X, Chen L, et al. Establishment of local searching methods for orbitrap-based high throughput metabolomics analysis. *Talanta* (2016) 156-157:163–71. doi: 10.1016/j.talanta.2016.04.051

58. Triebl A, Trotzmuller M, Hartler J, Stojakovic T, Kofeler HC. Lipidomics by ultrahigh performance liquid chromatography-high resolution mass spectrometry and its application to complex biological samples. *J Chromatogr B Analyt Technol BioMed Life Sci* (2017) 1053:72–80. doi: 10.1016/j.jchromb.2017.03.027

59. Zullig T, Zandl-Lang M, Trotzmuller M, Hartler J, Plecko B, Kofeler HC. A metabolomics workflow for analyzing complex biological samples using a combined method of untargeted and target-list based approaches. *Metabolites* (2020) 10(9):342. doi: 10.3390/metabo10090342

60. Lee GB, Lee JC, Moon MH. Plasma lipid profile comparison of five different cancers by nanoflow ultrahigh performance liquid chromatography-tandem mass spectrometry. *Anal Chim Acta* (2019) 1063:117–26. doi: 10.1016/j.aca.2019.02.021

61. Zhu Y, Dou M, Piehowski PD, Liang Y, Wang F, Chu RK, et al. Spatially resolved proteome mapping of laser capture microdissected tissue with automated sample transfer to nanodroplets. *Mol Cell Proteomics* (2018) 17(9):1864–74. doi: 10.1074/mcp.TIR118.000686

62. Sun Q, Zhao H, Liu Z, Wang F, He Q, Xiu C, et al. Identifying potential metabolic tissue biomarkers for papillary thyroid cancer in different iodine nutrient regions. *Endocrine* (2021) 74(3):582–91. doi: 10.1007/s12020-021-02773-3

63. Burla B, Arita M, Arita M, Bendt AK, Cazenave-Gassiot A, Dennis EA, et al. MS-based lipidomics of human blood plasma: a community-initiated position paper to develop accepted guidelines. *J Lipid Res* (2018) 59(10):2001–17. doi: 10.1194/jlr.S087163

64. Geyer PE, Kulak NA, Pichler G, Holdt LM, Teupser D, Mann M. Plasma proteome profiling to assess human health and disease. *Cell Syst* (2016) 2(3):185–95. doi: 10.1016/j.cels.2016.02.015

65. Ehlhardt WJ, Woodland JM, Baughman TM, Vandenbranden M, Wrighton SA, Kroin JS, et al. Liquid chromatography/nuclear magnetic resonance spectroscopy and liquid chromatography/mass spectrometry identification of novel metabolites of the multidrug resistance modulator LY335979 in rat bile and human liver microsomal incubations. *Drug Metab Dispos* (1998) 26(1):42–51.

66. Kawata N, Kang D, Aiuchi T, Obama T, Yoshitake O, Shibata T, et al. Proteomics of human glomerulonephritis by laser microdissection and liquid chromatography-tandem mass spectrometry. *Nephrol (Carlton)* (2020) 25 (4):351–9. doi: 10.1111/nep.13676

67. Kertesz V, Cahill JF. Spatially resolved absolute quantitation in thin tissue by mass spectrometry. *Anal Bioanal Chem* (2021) 413(10):2619–36. doi: 10.1007/s00216-020-02964-3

68. Mosele N, Smith A, Galli M, Pagni F, Magni F. MALDI-MSI analysis of cytological smears: The study of thyroid cancer. *Methods Mol Biol* (2017) 1618:37–47. doi: 10.1007/978-1-4939-7051-3_5

69. Zhan X, Huang Y, Long Y. Two-dimensional gel electrophoresis coupled with mass spectrometry methods for an analysis of human pituitary adenoma tissue proteome. *Jove-J Vis Exp* (2018) 134):56739. doi: 10.3791/56739

70. Murakami M, Sun N, Greunke C, Feuchtinger A, Kircher S, Deutschbein T, et al. Mass spectrometry imaging identifies metabolic patterns associated with malignant potential in pheochromocytoma and paraganglioma. *Eur J Endocrinol* (2021) 185(1):179–91. doi: 10.1530/EJE-20-1407

71. Li D, Wu J, Liu Z, Qiu L, Zhang Y. Novel circulating protein biomarkers for thyroid cancer determined through data-independent acquisition mass spectrometry. *Peerj* (2020) 8:e9507. doi: 10.7717/peerj.9507

72. Velikanova LI, Shafigullina ZR, Vorokhobina NV, Malevanaya EV. Gas chromatography-mass spectrometry analysis of urinary steroid metabolomics for detection of early signs of adrenal neoplasm malignancy in patients with cushing's syndrome. *B Exp Biol Med+* (2019) 167(5):676–80. doi: 10.1007/s10517-019-04597-8

73. Ciregia F, Cetani F, Pardi E, Soggiu A, Piras C, Zallocco L, et al. Parathyroid carcinoma and adenoma Co-existing in one patient: Case report and comparative proteomic analysis. *Cancer Genom Proteom* (2021) 18(6):781–96. doi: 10.21873/cgp.20297

74. Coelho M, Raposo L, Goodfellow BJ, Atzori L, Jones J, Manadas B. The potential of metabolomics in the diagnosis of thyroid cancer. *Int J Mol Sci* (2020) 21 (15):5272. doi: 10.3390/ijms21155272

75. Rossi C, Cicalini I, Verrocchio S, Di Dalmazi G, Federici L, Bucci I. The potential of steroid profiling by mass spectrometry in the management of adrenocortical carcinoma. *Biomedicines* (2020) 8(9):314. doi: 10.3390/biomedicines8090314

76. Li N, Desiderio DM, Zhan XQ. The use of mass spectrometry in a proteome-centered multiomics study of human pituitary adenomas. *Mass Spectrom Rev* (2021) 41(6):964–1013. doi: 10.1002/mas.21710

77. Soudah T, Zoabi A, Margulis K. Desorption electrospray ionization mass spectrometry imaging in discovery and development of novel therapies. *Mass Spectrom Rev* (2021), 1-28. doi: 10.1002/mas.21736

78. Barnes K. The pixelation of mass spectrometry. *Nat Methods* (2015) 12 (S1):12. doi: 10.1038/nmeth.3532

79. He C, Fong LG, Young SG, Jiang H. NanoSIMS imaging: an approach for visualizing and quantifying lipids in cells and tissues. *J Invest Med* (2017) 65 (3):669–72. doi: 10.1136/jim-2016-000239

80. Noun M, Akoumeh R, Abbas I. Cell and tissue imaging by TOF-SIMS and MALDI-TOF: An overview for biological and pharmaceutical analysis. *Microsc Microanal* (2022) 28(1):1–26. doi: 10.1017/S1431927621013593

81. Lin Y, Wu K, Jia F, Chen L, Wang Z, Zhang Y, et al. Single cell imaging reveals cisplatin regulating interactions between transcription (co)factors and DNA. *Chem Sci* (2021) 12(15):5419–29. doi: 10.1039/D0SC06760A

82. Caprioli RM, Farmer TB, Gile J. Molecular imaging of biological samples: localization of peptides and proteins using MALDI-TOF MS. *Anal Chem* (1997) 69 (23):4751–60. doi: 10.1021/ac970888i

83. Neumann EK, Migas LG, Allen JL, Caprioli RM, Van de Plas R, Spraggins JM. Spatial metabolomics of the human kidney using MALDI trapped ion mobility imaging mass spectrometry. *Anal Chem* (2020) 92(19):13084–91. doi: 10.1021/acs.analchem.0c02051

84. Suckert T, Beyreuther E, Burger N, Muller J, Bodenstein E, Meinhardt M, et al. MALDI imaging detects lipid and peptide changes in a mouse model of radiation-induced brain injury. *Radiother Oncol* (2022) 170:S71–S2. doi: 10.1016/S0167-8140(22)02472-0

85. Erlmeier F, Sun N, Shen J, Feuchtinger A, Buck A, Prade VM, et al. MALDI mass spectrometry imaging-prognostic pathways and metabolites for renal cell carcinomas. *Cancers (Basel)* (2022) 14(7):1763. doi: 10.3390/cancers14071763

86. Takats Z, Wiseman JM, Gologan B, Cooks RG. Mass spectrometry sampling under ambient conditions with desorption electrospray ionization. *Science* (2004) 306(5695):471–3. doi: 10.1126/science.1104404

87. Wiseman JM, Puolitaival SM, Takats Z, Cooks RG, Caprioli RM. Mass spectrometric profiling of intact biological tissue by using desorption electrospray ionization. *Angew Chem Int Ed Engl* (2005) 44(43):7094–7. doi: 10.1002/anie.200502362

88. Kurczyk A, Gawin M, Chekan M, Wilk A, Lakomiec K, Mrukwa G, et al. Classification of thyroid tumors based on mass spectrometry imaging of tissue microarrays; a single-pixel approach. *Int J Mol Sci* (2020) 21(17):6289. doi: 10.3390/ijms21176289

89. Ucal Y, Tokat F, Duren M, Ince U, Ozpinar A. Investigating the peptide profile of noninvasive follicular thyroid neoplasm with papillary-like nuclear features (NIFTP): application of MALDI mass spectrometry imaging. *FEBS Open Bio* (2019) 9:402–3. doi: 10.1089/thy.2018.0392

90. Zhang M, He J, Li T, Hu H, Li X, Xing H, et al. Accurate classification of non-small cell lung cancer (NSCLC) pathology and mapping of EGFR mutation spatial distribution by ambient mass spectrometry imaging. *Front Oncol* (2019) 9:804. doi: 10.3389/fonc.2019.00804

91. Abbassi-Ghadi N, Antonowicz SS, McKenzie JS, Kumar S, Huang J, Jones EA, et al. *De novo* lipogenesis alters the phospholipidome of esophageal adenocarcinoma. *Cancer Res* (2020) 80(13):2764–74. doi: 10.1158/0008-5472.CAN-19-4035

92. Banerjee S, Manna SK. Assessment of metabolic signature for cancer diagnosis using desorption electrospray ionization mass spectrometric imaging. *Methods Mol Biol* (2019) 1928:275–97. doi: 10.1007/978-1-4939-9027-6_15

93. Desbenoit N, Walch A, Spengler B, Brunelle A, Rompp A. Correlative mass spectrometry imaging, applying time-of-flight secondary ion mass spectrometry and atmospheric pressure matrix-assisted laser desorption/ionization to a single tissue section. *Rapid Commun Mass Sp* (2018) 32(2):159–66. doi: 10.1002/rcm.8022

94. Passarelli MK, Pirkl A, Moellers R, Grinfeld D, Kollmer F, Havelund R, et al. The 3D OrbiSIMS-label-free metabolic imaging with subcellular lateral resolution and high mass-resolving power. *Nat Methods* (2017) 14(12):1175–83. doi: 10.1038/nmeth.4504

95. Pareek V, Tian H, Winograd N, Benkovic SJ. Metabolomics and mass spectrometry imaging reveal channeled *de novo* purine synthesis in cells. *Science* (2020) 368(6488):283–90. doi: 10.1126/science.aaz6465

96. Yuan ZY, Zhou QM, Cai LS, Pan L, Sun WL, Qumu SW, et al. SEAM is a spatial single nuclear metabolomics method for dissecting tissue microenvironment. *Nat Methods* (2021) 18(10):1223. doi: 10.1038/s41592-021-01276-3

97. Agüi-Gonzalez PJS, Phan NTN. SIMS imaging in neurobiology and cell biology. *J Anal At Spectrom* (2019) 34(7):1355–68. doi: 10.1039/C9JA00118B

98. Li B, Bhandari DR, Rompp A, Spengler B. High-resolution MALDI mass spectrometry imaging of gallotannins and monoterpene glucosides in the root of paeonia lactiflora. *Sci Rep* (2016) 6:36074. doi: 10.1038/srep36074

99. Dowsett D, Wirtz T. Co-Registered *In situ* secondary electron and mass spectral imaging on the helium ion microscope demonstrated using lithium titanate and magnesium oxide nanoparticles. *Anal Chem* (2017) 89(17):8957–65. doi: 10.1021/acs.analchem.7b01481

100. Benninghoven A. Developments in secondary ion mass spectroscopy and applications to surface studies. *Surface Sci* (1975) 53(1):596–625. doi: 10.1016/0039-6028(75)90158-2

101. Muramoto S, Graham D. Deep depth profiling using gas cluster secondary ion mass spectrometry: Micrometer topography development and effects on depth resolution. *Surf Interface Anal* (2021) 53(9):814–23. doi: 10.1002/sia.6983

102. Dimovska Nilsson K, Karagianni A, Kaya I, Henricsson M, Fletcher JS. (CO2)n(+), (H2O)n(+), and (H2O)n(+) (CO2) gas cluster ion beam secondary ion mass spectrometry: analysis of lipid extracts, cells, and alzheimer's model mouse brain tissue. *Anal Bioanal Chem* (2021) 413(16):4181–94. doi: 10.1007/s00216-021-03372-x

103. Mabrouk AB, Licitra C, Chateauminois A, Veillerot M. Effect of the molecular weight on the depth profiling of PMMA thin films using low-energy cs+ sputtering. *Surf Interface Anal* (2021) 53(10):884–92. doi: 10.1002/sia.6991

104. Jiang J, Hua L, Xie Y, Cao Y, Wen Y, Chen P, et al. High mass resolution multireflection time-of-Flight secondary ion mass spectrometer. *J Am Soc Mass Spectrom* (2021) 32(5):1196–204. doi: 10.1021/jasms.1c00016

105. Tian H, Sparvero LJ, Anthonymuthu TS, Sun WY, Amoscato AA, He RR, et al. Successive high-resolution (H2O)n-GCIB and C60-SIMS imaging integrates multi-omics in different cell types in breast cancer tissue. *Anal Chem* (2021) 93(23):8143–51. doi: 10.1021/acs.analchem.0c05311

106. Vanbellingen QP, Elie N, Eller MJ, Della-Negra S, Touboul D, Brunelle A. Time-of-flight secondary ion mass spectrometry imaging of biological samples with delayed extraction for high mass and high spatial resolutions. *Rapid Commun Mass Sp* (2015) 29(13):1187–95. doi: 10.1002/rcm.7210

107. Porta Siegel T, Hamm G, Bunch J, Cappell J, Fletcher JS, Schwamborn K. Mass spectrometry imaging and integration with other imaging modalities for greater molecular understanding of biological tissues. *Mol Imaging Biol* (2018) 20(6):888–901. doi: 10.1007/s11307-018-1267-y

108. Solon EG, Schweitzer A, Stoeckli M, Prideaux B. Autoradiography, MALDI-MS, and SIMS-MS imaging in pharmaceutical discovery and development. *AAPS J* (2010) 12(1):11–26. doi: 10.1208/s12248-009-9158-4

109. Popczun NJ, Breuer L, Wucher A, Winograd N. On the SIMS ionization probability of organic molecules. *J Am Soc Mass Spectrom* (2017) 28(6):1182–91. doi: 10.1007/s13361-017-1624-0

110. Berghmans E, Boonen K, Maes E, Mertens I, Pauwels P, Baggerman G. Implementation of MALDI mass spectrometry imaging in cancer proteomics research: Applications and challenges. *J Pers Med* (2020) 10(2):54. doi: 10.3390/jpm10020054

111. Sun C, Liu W, Mu Y, Wang X. 1,1'-binaphthyl-2,2'-diamine as a novel MALDI matrix to enhance the *in situ* imaging of metabolic heterogeneity in lung cancer. *Talanta* (2020) 209:120557. doi: 10.1016/j.talanta.2019.120557

112. Denti V, Piga I, Guarnerio S, Clerici F, Ivanova M, Chinello C, et al. Antigen retrieval and its effect on the MALDI-MSI of lipids in formalin-fixed paraffin-embedded tissue. *J Am Soc Mass Spectrom* (2020) 31(8):1619–24. doi: 10.1021/jasms.0c00208

113. Cobice DF, Goodwin RJ, Andren PE, Nilsson A, Mackay CL, Andrew R. Future technology insight: mass spectrometry imaging as a tool in drug research and development. *Br J Pharmacol* (2015) 172(13):3266–83. doi: 10.1111/bph.13135

114. Smolira A, Wessely-Szponder J. Importance of the matrix and the matrix/sample ratio in MALDI-TOF-MS analysis of cathelicidins obtained from porcine neutrophils. *Appl Biochem Biotechnol* (2015) 175(4):2050–65. doi: 10.1007/s12010-014-1405-1

115. Kailemia MJ, Ruhaak LR, Lebrilla CB, Amster IJ. Oligosaccharide analysis by mass spectrometry: A review of recent developments. *Anal Chem* (2014) 86(1):196–212. doi: 10.1021/ac403969n

116. Norris JL, Caprioli RM. Analysis of tissue specimens by matrix-assisted laser desorption/ionization imaging mass spectrometry in biological and clinical research. *Chem Rev* (2013) 113(4):2309–42. doi: 10.1021/cr3004295

117. Piga I, Capitoli G, Clerici F, Mahajneh A, Brambilla V, Smith A, et al. Ex vivo thyroid fine needle aspirations as an alternative for MALDI-MSI proteomic investigation: intra-patient comparison. *Anal Bioanal Chem* (2021) 413(5):1259–66. doi: 10.1007/s00216-020-03088-4

118. Piga I, Capitoli G, Denti V, Tettamanti S, Smith A, Stella M, et al. The management of haemoglobin interference for the MALDI-MSI proteomics analysis of thyroid fine needle aspiration biopsies. *Anal Bioanal Chem* (2019) 411(20):5007–12. doi: 10.1007/s00216-019-01908-w

119. Zhu X, Xu T, Peng C, Wu S. Advances in MALDI mass spectrometry imaging single cell and tissues. *Front Chem* (2021) 9:782432. doi: 10.3389/fchem.2021.782432

120. Mittal P, Condina MR, Klingler-Hoffmann M, Kaur G, Oehler MK, Sieber OM, et al. Cancer tissue classification using supervised machine learning applied to MALDI mass spectrometry imaging. *Cancers* (2021) 13(21):5388. doi: 10.3390/cancers13215388

121. Truong JXM, Spotbeen X, White J, Swinnen JV, Butler LM, Snel MF, et al. Removal of optimal cutting temperature (O.C.T.) compound from embedded tissue for MALDI imaging of lipids. *Anal Bioanal Chem* (2021) 413(10):2695–708. doi: 10.1007/s00216-020-03128-z

122. Bowman AP, Bogie JFJ, Hendriks JJA, Haidar M, Belov M, Heeren RMA, et al. Evaluation of lipid coverage and high spatial resolution MALDI-imaging capabilities of oversampling combined with laser post-ionisation. *Anal Bioanal Chem* (2020) 412(10):2277–89. doi: 10.1007/s00216-019-02290-3

123. Sezgin S, Hassan R, Zuhlke S, Kuepfer L, Hengstler JG, Spiteller M, et al. Spatio-temporal visualization of the distribution of acetaminophen as well as its metabolites and adducts in mouse livers by MALDI MSI. *Arch Toxicol* (2018) 92(9):2963–77. doi: 10.1007/s00204-018-2271-3

124. Wang J, Wang C, Han X. Enhanced coverage of lipid analysis and imaging by matrix-assisted laser desorption/ionization mass spectrometry *via* a strategy with an optimized mixture of matrices. *Anal Chim Acta* (2018) 1000:155–62. doi: 10.1016/j.aca.2017.09.046

125. Strnad S, Prazienkova V, Sykora D, Cvacka J, Maletinska L, Popelova A, et al. The use of 1,5-diaminonaphthalene for matrix-assisted laser desorption/ionization mass spectrometry imaging of brain in neurodegenerative disorders. *Talanta* (2019) 201:364–72. doi: 10.1016/j.talanta.2019.03.117

126. Liu H, Chen R, Wang J, Chen S, Xiong C, Wang J, et al. 1,5-diaminonaphthalene hydrochloride assisted laser desorption/ionization mass spectrometry imaging of small molecules in tissues following focal cerebral ischemia. *Anal Chem* (2014) 86(20):10114–21. doi: 10.1021/ac5034566

127. Wang SS, Wang YJ, Zhang J, Sun TQ, Guo YL. Derivatization strategy for simultaneous molecular imaging of phospholipids and low-abundance free fatty acids in thyroid cancer tissue sections. *Anal Chem* (2019) 91(6):4070–6. doi: 10.1021/acs.analchem.8b05680

128. Zhou D, Guo S, Zhang M, Liu Y, Chen T, Li Z. Mass spectrometry imaging of small molecules in biological tissues using graphene oxide as a matrix. *Anal Chim Acta* (2017) 962:52–9. doi: 10.1016/j.aca.2017.01.043

129. Tang W, Gordon A, Wang F, Chen Y, Li B. Hydralazine as a versatile and universal matrix for high-molecular coverage and dual-polarity matrix-assisted laser Desorption/Ionization mass spectrometry imaging. *Anal Chem* (2021) 93(26):9083–93. doi: 10.1021/acs.analchem.1c00498

130. Wang J, Qiu S, Chen S, Xiong C, Liu H, Wang J, et al. MALDI-TOF MS imaging of metabolites with a n-(1-naphthyl) ethylenediamine dihydrochloride matrix and its application to colorectal cancer liver metastasis. *Anal Chem* (2015) 87(1):422–30. doi: 10.1021/ac504294s

131. Groven RVM, Nauta SP, Gruisen J, Claes BSR, Greven J, van Griensven M, et al. Lipid analysis of fracture hematoma with MALDI-MSI: Specific lipids are associated to bone fracture healing over time. *Front Chem* (2021) 9:780626. doi: 10.3389/fchem.2021.780626

132. Wang XD, Han J, Pan JX, Borchers CH. Comprehensive imaging of porcine adrenal gland lipids by MALDI-FTMS using quercetin as a matrix. *Anal Chem* (2014) 86(1):638–46. doi: 10.1021/ac404044k

133. Guran R, Vanickova L, Horak V, Krizkova S, Michalek P, Heger Z, et al. MALDI MSI of MeLiM melanoma: Searching for differences in protein profiles. *PloS One* (2017) 12(12):e0189305. doi: 10.1371/journal.pone.0189305

134. Fernandez-Vega A, Chicano-Galvez E, Prentice BM, Anderson D, Priego-Capote F, Lopez-Bascon MA, et al. Optimization of a MALDI-imaging protocol for studying adipose tissue-associated disorders. *Talanta* (2020) 219:121184. doi: 10.1016/j.talanta.2020.121184

135. McMillen JC, Fincher JA, Klein DR, Spraggins JM, Caprioli RM. Effect of MALDI matrices on lipid analyses of biological tissues using MALDI-2 postionization mass spectrometry. *J Mass Spectrom* (2020) 55(12):e4663. doi: 10.1002/jms.4663

136. Ly A, Longuespee R, Casadonte R, Wandernoth P, Schwamborn K, Bollwein C, et al. Site-to-Site reproducibility and spatial resolution in MALDI-MSI of peptides from formalin-fixed paraffin-embedded samples. *Proteom Clin Appl* (2019) 13(1):e1800029. doi: 10.1002/prca.201800029

137. Calvano CD, Monopoli A, Cataldi TRI, Palmisano F. MALDI matrices for low molecular weight compounds: an endless story? *Anal Bioanal Chem* (2018) 410 (17):4015–38. doi: 10.1007/s00216-018-1014-x

138. Vermillion-Salsbury RL, Hercules DM. 9-aminoacridine as a matrix for negative mode matrix-assisted laser desorption/ionization. *Rapid Commun Mass Sp* (2002) 16(16):1575–81. doi: 10.1002/rcm.750

139. Pallua JD, Schaefer G, Seifarth C, Becker M, Meding S, Rauser S, et al. MALDI-MS tissue imaging identification of biliverdin reductase b overexpression in prostate cancer. *J Proteomics* (2013) 91:500–14. doi: 10.1016/j.jprot.2013.08.003

140. Neumann EK, Comi TJ, Spegazzini N, Mitchell JW, Rubakhin SS, Gillette MU, et al. Multimodal chemical analysis of the brain by high mass resolution mass spectrometry and infrared spectroscopic imaging. *Anal Chem* (2018) 90 (19):11572–80. doi: 10.1021/acs.analchem.8b02913

141. Dilillo M, Ait-Belkacem R, Esteve C, Pellegrini D, Nicolardi S, Costa M, et al. Ultra-high mass resolution MALDI imaging mass spectrometry of proteins and metabolites in a mouse model of glioblastoma. *Sci Rep* (2017) 7(1):603. doi: 10.1038/s41598-017-00703-w

142. Do T, Guran R, Jarosova R, Ondrackova P, Sladek Z, Faldyna M, et al. MALDI MSI reveals the spatial distribution of protein markers in tracheobronchial lymph nodes and lung of pigs after respiratory infection. *Molecules* (2020) 25 (23):5723. doi: 10.3390/molecules25235723

143. Sommella E, Salviati E, Caponigro V, Grimaldi M, Musella S, Bertamino A, et al. MALDI mass spectrometry imaging highlights specific metabolome and lipidome profiles in salivary gland tumor tissues. *Metabolites* (2022) 12(6):530. doi: 10.3390/metabo12060530

144. He H, Qin L, Zhang Y, Han M, Li J, Liu Y, et al. 3,4-dimethoxycinnamic acid as a novel matrix for enhanced *In situ* detection and imaging of low-Molecular-Weight compounds in biological tissues by MALDI-MSI. *Anal Chem* (2019) 91(4):2634–43. doi: 10.1021/acs.analchem.8b03522

145. Keller BO, Li L. Discerning matrix-cluster peaks in matrix-assisted laser desorption/ionization time-of-flight mass spectra of dilute peptide mixtures. *J Am Soc Mass Spectrom* (2000) 11(1):88–93. doi: 10.1016/S1044-0305(99)00126-9

146. Smirnov IP, Zhu X, Taylor T, Huang Y, Ross P, Papayanopoulos IA, et al. Suppression of alpha-cyano-4-hydroxycinnamic acid matrix clusters and reduction of chemical noise in MALDI-TOF mass spectrometry. *Anal Chem* (2004) 76 (10):2958–65. doi: 10.1021/ac035331j

147. Ucal Y, Ozpinar A. Improved spectra for MALDI MSI of peptides using ammonium phosphate monobasic in MALDI matrix. *J Mass Spectrom* (2018) 53 (8):635–48. doi: 10.1002/jms.4198

148. Schlosser G, Pocsfalvi G, Huszar E, Malorni A, Hudecz F. MALDI-TOF mass spectrometry of a combinatorial peptide library: effect of matrix composition on signal suppression. *J Mass Spectrom* (2005) 40(12):1590–4. doi: 10.1002/jms.937

149. Janda M, Seah BKB, Jakob D, Beckmann J, Geier B, Liebeke M. Determination of abundant metabolite matrix adducts illuminates the dark metabolome of MALDI-mass spectrometry imaging datasets. *Anal Chem* (2021) 93(24):8399–407. doi: 10.1021/acs.analchem.0c04720

150. Takats Z, Wiseman JM, Cooks RG. Ambient mass spectrometry using desorption electrospray ionization (DESI): instrumentation, mechanisms and applications in forensics, chemistry, and biology. *J Mass Spectrom* (2005) 40 (10):1261–75. doi: 10.1002/jms.922

151. Takáts Z, Wiseman JM, Gologan B, Cooks RG. Electrosonic spray ionization. a gentle technique for generating folded proteins and protein complexes in the gas phase and for studying ion-molecule reactions at atmospheric pressure. *Anal Chem* (2004) 76(14):4050–8. doi: 10.1021/ac049848m

152. Heck AJ, Van Den Heuvel RH. Investigation of intact protein complexes by mass spectrometry. *Mass Spectrom Rev* (2004) 23(5):368–89. doi: 10.1002/mas.10081

153. Felitsyn N, Peschke M, Kebarle P. Origin and number of charges observed on multiply-protonated native proteins produced by ESI. *Int J Mass Spectrom* (2002) 219(1):39–62. doi: 10.1016/S1387-3806(02)00588-2

154. Weston DJ. Ambient ionization mass spectrometry: current understanding of mechanistic theory; analytical performance and application areas. *Analyst* (2010) 135(4):661–8. doi: 10.1039/b925579f

155. Fernandes AM, Vendramini PH, Galaverna R, Schwab NV, Alberici LC, Augusti R, et al. Direct visualization of neurotransmitters in rat brain slices by desorption electrospray ionization mass spectrometry imaging (DESI - MS). *J Am Soc Mass Spectrom* (2016) 27(12):1944–51. doi: 10.1007/s13361-016-1475-0

156. Yang X, Song X, Zhang X, Shankar V, Wang S, Yang Y, et al. *In situ* DESI-MSI lipidomic profiles of mucosal margin of oral squamous cell carcinoma. *EBioMedicine* (2021) 70:103529. doi: 10.1016/j.ebiom.2021.103529

157. Bennet RV, Gamage CM, Fernandez FM. Imaging of biological tissues by desorption electrospray ionization mass spectrometry. *J Vis Exp* (2013) 77):e50575. doi: 10.3791/50575

158. Dexter A, Steven RT, Patel A, Dailey LA, Taylor AJ, Ball D, et al. Imaging drugs, metabolites and biomarkers in rodent lung: a DESI MS strategy for the evaluation of drug-induced lipidosis. *Anal Bioanal Chem* (2019) 411(30):8023–32. doi: 10.1007/s00216-019-02151-z

159. Yin R, Burnum-Johnson KE, Sun X, Dey SK, Laskin J. High spatial resolution imaging of biological tissues using nanospray desorption electrospray ionization mass spectrometry. *Nat Protoc* (2019) 14(12):3445–70. doi: 10.1038/s41596-019-0237-4

160. Gross JH. *Mass spectrometry. 3*. Cham, Switzerland: Springer (2017).

161. Claude E, Jones EA, Pringle SD. DESI mass spectrometry imaging (MSI). *Methods Mol Biol* (2017) 1618:65–75. doi: 10.1007/978-1-4939-7051-3_7

162. Towers MW, Karancsi T, Jones EA, Pringle SD, Claude E. Optimised desorption electrospray ionisation mass spectrometry imaging (DESI-MSI) for the analysis of Proteins/Peptides directly from tissue sections on a travelling wave ion mobility q-ToF. *J Am Soc Mass Spectrom* (2018) 29(12):2456–66. doi: 10.1007/s13361-018-2049-0

163. Feider CL, Elizondo N, Eberlin LS. Ambient ionization and FAIMS mass spectrometry for enhanced imaging of multiply charged molecular ions in biological tissues. *Anal Chem* (2016) 88(23):11533–41. doi: 10.1021/acs.analchem.6b02798

164. Guo R, Zhou L, Chen X. Desorption electrospray ionization (DESI) source coupling ion mobility mass spectrometry for imaging fluoropezil (DC20) distribution in rat brain. *Anal Bioanal Chem* (2021) 413(23):5835–47. doi: 10.1007/s00216-021-03563-6

165. Bodzon-Kulakowska A, Drabik A, Marszalek M, Kotlinska JH, Suder P. DESI analysis of mammalian cell cultures - sample preparation and method optimisation. *J Mass Spectrom* (2014) 49(7):613–21. doi: 10.1002/jms.3381

166. Goodwin RJA. Sample preparation for mass spectrometry imaging: small mistakes can lead to big consequences. *J Proteomics* (2012) 75(16):4893–911. doi: 10.1016/j.jprot.2012.04.012

167. Hermann J, Noels H, Theelen W, Lellig M, Orth-Alampour S, Boor P, et al. Sample preparation of formalin-fixed paraffin-embedded tissue sections for MALDI-mass spectrometry imaging. *Anal Bioanal Chem* (2020) 412(6):1263–75. doi: 10.1007/s00216-019-02296-x

168. Shah P, Zhang B, Choi C, Yang S, Zhou J, Harlan R, et al. Tissue proteomics using chemical immobilization and mass spectrometry. *Anal Biochem* (2015) 469:27–33. doi: 10.1016/j.ab.2014.09.017

169. Wangen R, Aasebo E, Trentani A, Doskeland SO, Bruserud O, Selheim F, et al. Preservation method and phosphate buffered saline washing affect the acute myeloid leukemia proteome. *Int J Mol Sci* (2018) 19(1):296. doi: 10.3390/ijms19010296

170. Hojat A, Wei B, Olson MG, Mao Q, Yong WH. Procurement and storage of surgical biospecimens. *Methods Mol Biol* (2019) 1897:65–76. doi: 10.1007/978-1-4939-8935-5_7

171. Diehl HC, Beine B, Elm J, Trede D, Ahrens M, Eisenacher M, et al. The challenge of on-tissue digestion for MALDI MSI- a comparison of different protocols to improve imaging experiments. *Anal Bioanal Chem* (2015) 407 (8):2223–43. doi: 10.1007/s00216-014-8345-z

172. Yoon S, Lee TG. Biological tissue sample preparation for time-of-flight secondary ion mass spectrometry (ToF-SIMS) imaging. *Nano Converg* (2018) 5 (1):24. doi: 10.1186/s40580-018-0157-y

173. Ucal Y, Coskun A, Ozpinar A. Quality will determine the future of mass spectrometry imaging in clinical laboratories: the need for standardization. *Expert Rev Proteomics* (2019) 16(6):521–32. doi: 10.1080/14789450.2019.1624165

174. Piga I, Capitoli G, Tettamanti S, Denti V, Smith A, Chinello C, et al. Feasibility study for the MALDI-MSI analysis of thyroid fine needle aspiration biopsies: Evaluating the morphological and proteomic stability over time. *Proteom Clin Appl* (2019) 13(1):e1700170. doi: 10.1002/prca.201700170

175. Pagni F, De Sio G, Garancini M, Scardilli M, Chinello C, Smith AJ, et al. Proteomics in thyroid cytopathology: Relevance of MALDI-imaging in distinguishing malignant from benign lesions. *Proteomics* (2016) 16(11-12):1775–84. doi: 10.1002/pmic.201500448

176. Pagni F, Mainini V, Garancini M, Bono F, Vanzati A, Giardini V, et al. Proteomics for the diagnosis of thyroid lesions: preliminary report. *Cytopathology* (2015) 26(5):318–24. doi: 10.1111/cyt.12166

177. Guo S, Wang Y, Zhou D, Li Z. Significantly increased monounsaturated lipids relative to polyunsaturated lipids in six types of cancer microenvironment are observed by mass spectrometry imaging. *Sci Rep* (2014) 4:5959. doi: 10.1038/srep05959

178. Guo S, Qiu L, Wang Y, Qin X, Liu H, He M, et al. Tissue imaging and serum lipidomic profiling for screening potential biomarkers of thyroid tumors by matrix-assisted laser desorption/ionization-Fourier transform ion cyclotron resonance mass spectrometry. *Anal Bioanal Chem* (2014) 406(18):4357–70. doi: 10.1007/s00216-014-7846-0

179. Mulder IA, Esteve C, Wermer MJ, Hoehn M, Tolner EA, van den Maagdenberg AM, et al. Funnel-freezing versus heat-stabilization for the visualization of metabolites by mass spectrometry imaging in a mouse stroke model. *Proteomics* (2016) 16(11-12):1652–9. doi: 10.1002/pmic.201500402

180. Cazares LH, Van Tongeren SA, Costantino J, Kenny T, Garza NL, Donnelly G, et al. Heat fixation inactivates viral and bacterial pathogens and is compatible with downstream MALDI mass spectrometry tissue imaging. *BMC Microbiol* (2015) 15:101. doi: 10.1186/s12866-015-0431-7

181. Sugiura Y, Honda K, Kajimura M, Suematsu M. Visualization and quantification of cerebral metabolic fluxes of glucose in awake mice. *Proteomics* (2014) 14(7-8):829–38. doi: 10.1002/pmic.201300047

182. Fox CH, Johnson FB, Whiting J, Roller PP. Formaldehyde fixation. *J Histochem Cytochem* (1985) 33(8):845–53. doi: 10.1177/33.8.3894502

183. Thavarajah R, Mudimbaimannar VK, Elizabeth J, Rao UK, Ranganathan K. Chemical and physical basics of routine formaldehyde fixation. *J Oral Maxillofac Pathol* (2012) 16(3):400–5. doi: 10.4103/0973-029X.102496

184. Shimma S, Sugiura Y. Effective sample preparations in imaging mass spectrometry. *Mass Spectrom (Tokyo)* (2014) 3(Spec Issue):S0029. doi: 10.5702/massspectrometry.S0029

185. Longuespee R, Kriegsmann K, Cremer M, Zgorzelski C, Casadonte R, Kazdal D, et al. In MALDI-mass spectrometry imaging on formalin-fixed paraffin-embedded tissue specimen section thickness significantly influences m/z peak intensity. *Proteomics Clin Appl* (2019) 13(1):e1800074. doi: 10.1002/prca.201800074

186. Dilmetz BA, Lee Y, Condina MR, Briggs M, Young C, Desire CT, et al. Novel technical developments in mass spectrometry imaging in 2020: A mini review. *Anal Sci Adv* (2021) 2(3-4):225–37. doi: 10.1002/ansa.202000176

187. Ma L, Xie Q, Du M, Huang Y, Chen Y, Chen D, et al. Sample preparation optimization of insects and zebrafish for whole-body mass spectrometry imaging. *Anal Bioanal Chem* (2022) 414(16):4777–90. doi: 10.1007/s00216-022-04102-7

188. Holm NB, Deryabina M, Knudsen CB, Janfelt C. Tissue distribution and metabolic profiling of cyclosporine (CsA) in mouse and rat investigated by DESI and MALDI mass spectrometry imaging (MSI) of whole-body and single organ cryo-sections. *Anal Bioanal Chem* (2022) 414(24):7167–77. doi: 10.1007/s00216-022-04269-z

189. Chen H, Li X, Chen F, Li L, Ye F, Bu H, et al. Performance comparison of two cryosection embedding agents used for desorption electrospray ionization mass spectrometry imaging. *J Sichuan Univ Med Sci ed* (2022) 53(2):303–9. doi: 10.12182/20220360106

190. Gill EL, Yost RA, Vedam-Mai V, Garrett TJ. Precast gelatin-based molds for tissue embedding compatible with mass spectrometry imaging. *Anal Chem* (2017) 89(1):576–80. doi: 10.1021/acs.analchem.6b04185

191. Neumann EK, Patterson NH, Allen JL, Migas LG, Yang H, Brewer M, et al. Protocol for multimodal analysis of human kidney tissue by imaging mass spectrometry and CODEX multiplexed immunofluorescence. *STAR Protoc* (2021) 2(3):100747. doi: 10.1016/j.xpro.2021.100747

192. Schwartz SA, Reyzer ML, Caprioli RM. Direct tissue analysis using matrix-assisted laser desorption/ionization mass spectrometry: practical aspects of sample preparation. *J Mass Spectrom* (2003) 38(7):699–708. doi: 10.1002/jms.505

193. Dannhorn A, Kazanc E, Ling S, Nikula C, Karali E, Serra MP, et al. Universal sample preparation unlocking multimodal molecular tissue imaging. *Anal Chem* (2020) 92(16):11080–8. doi: 10.1021/acs.analchem.0c00826

194. Zhang D, Huo G, Qu Z, Lv J, Yang Y, Li C, et al. Discussion on key points of freezing sectioning technology of experimental animals. *Drug Eval Res* (2019) 42(7):1359–61. doi: 10.7501/j.issn.1674-6376.2019.07.018

195. Dey P. Frozen section: Principle and procedure. In: *Basic and advanced laboratory techniques in histopathology and cytology* (2018) Singapore: Springer. p. 51–5.

196. Wang Z, Fu W, Huo M, He B, Liu Y, Tian L, et al. Spatial-resolved metabolomics reveals tissue-specific metabolic reprogramming in diabetic nephropathy by using mass spectrometry imaging. *Acta Pharm Sin B* (2021) 11(11):3665–77. doi: 10.1016/j.apsb.2021.05.013

197. Neumann EK, Djambazova KV, Caprioli RM, Spraggins JM. Multimodal imaging mass spectrometry: Next generation molecular mapping in biology and medicine. *J Am Soc Mass Spectrom* (2020) 31(12):2401–15. doi: 10.1021/jasms.0c00232

198. Kulbe H, Klein O, Wu Z, Taube ET, Kassuhn W, Horst D, et al. Discovery of prognostic markers for early-stage high-grade serous ovarian cancer by maldi-imaging. *Cancers (Basel)* (2020) 12(8):2000. doi: 10.1055/s-0040-1718157

199. Zang Q, Sun C, Chu X, Li L, Gan W, Zhao Z, et al. Spatially resolved metabolomics combined with multicellular tumor spheroids to discover cancer tissue relevant metabolic signatures. *Anal Chim Acta* (2021) 1155:338342. doi: 10.1016/j.aca.2021.338342

200. Sun C, Li Z, Ma C, Zang Q, Li J, Liu W, et al. Acetone immersion enhanced MALDI-MS imaging of small molecule metabolites in biological tissues. *J Pharm BioMed Anal* (2019) 176:112797. doi: 10.1016/j.jpba.2019.112797

201. Chen Y, Tang W, Gordon A, Li B. Development of an integrated tissue pretreatment protocol for enhanced MALDI MS imaging of drug distribution in the brain. *J Am Soc Mass Spectrom* (2020) 31(5):1066–73. doi: 10.1021/jasms.0c00003

202. Piga I, Heijs B, Nicolardi S, Giusti L, Marselli L, Marchetti P, et al. Ultra-high resolution MALDI-FTICR-MSI analysis of intact proteins in mouse and human pancreas tissue. *Int J Mass Spectrom* (2019) 437:10–6. doi: 10.1016/j.ijms.2017.11.001

203. Hoiem TS, Andersen MK, Martin-Lorenzo M, Longuespee R, Claes BSR, Nordborg A, et al. An optimized MALDI MSI protocol for spatial detection of tryptic peptides in fresh frozen prostate tissue. *Proteomics* (2022) 22(10):e2100223. doi: 10.1002/pmic.202100223

204. Angerer TB, Bour J, Biagi JL, Moskovets E, Frache G. Evaluation of 6 MALDI-matrices for 10 mum lipid imaging and on-tissue MSn with AP-MALDI-Orbitrap. *J Am Soc Mass Spectrom* (2022) 33(5):760–71. doi: 10.1021/jasms.1c00327

205. Phillips L, Gill AJ, Baxter RC. Novel prognostic markers in triple-negative breast cancer discovered by MALDI-mass spectrometry imaging. *Front Oncol* (2019) 9:379. doi: 10.3389/fonc.2019.00379

206. Gonzalez de San Roman E, Bidmon HJ, Malisic M, Susnea I, Kuppers A, Hubbers R, et al. Molecular composition of the human primary visual cortex profiled by multimodal mass spectrometry imaging. *Brain Struct Funct* (2018) 223(6):2767–83. doi: 10.1007/s00429-018-1660-y

207. Patel E. Fresh frozen versus formalin-fixed paraffin embedded for mass spectrometry imaging. *Methods Mol Biol* (2017) 1618:7–14. doi: 10.1007/978-1-4939-7051-3_2

208. De Sio G, Smith AJ, Galli M, Garancini M, Chinello C, Bono F, et al. A MALDI-mass spectrometry imaging method applicable to different formalin-fixed paraffin-embedded human tissues. *Mol Biosyst* (2015) 11(6):1507–14. doi: 10.1039/C4MB00716F

209. Abdelmoula WM, Skraskova K, Balluff B, Carreira RJ, Tolner EA, Lelieveldt BP, et al. Automatic generic registration of mass spectrometry imaging data to histology using nonlinear stochastic embedding. *Anal Chem* (2014) 86(18):9204–11. doi: 10.1021/ac502170f

210. Azimzadeh O, Atkinson MJ, Tapio S. Quantitative proteomic analysis using formalin-fixed, paraffin-embedded (FFPE) human cardiac tissue. *Methods Mol Biol* (2021) 2261:525–33. doi: 10.1007/978-1-0716-1186-9_33

211. Zhou Q, Fulop A, Hopf C. Recent developments of novel matrices and on-tissue chemical derivatization reagents for MALDI-MSI. *Anal Bioanal Chem* (2021) 413(10):2599–617. doi: 10.1007/s00216-020-03023-7

212. Manier ML, Spraggins JM, Reyzer ML, Norris JL, Caprioli RM. A derivatization and validation strategy for determining the spatial localization of endogenous amine metabolites in tissues using MALDI imaging mass spectrometry. *J Mass Spectrom* (2014) 49(8):665–73. doi: 10.1002/jms.3411

213. Takeo E, Sugiura Y, Uemura T, Nishimoto K, Yasuda M, Sugiyama E, et al. Tandem mass spectrometry imaging reveals distinct accumulation patterns of steroid structural isomers in human adrenal glands. *Anal Chem* (2019) 91(14):8918–25. doi: 10.1021/acs.analchem.9b00619

214. Cobice DF, Mackay CL, Goodwin RJ, McBride A, Langridge-Smith PR, Webster SP, et al. Mass spectrometry imaging for dissecting steroid intracrinology within target tissues. *Anal Chem* (2013) 85(23):11576–84. doi: 10.1021/ac402777k

215. Harkin C, Smith KW, Cruickshank FL, Logan Mackay C, Flinders B, Heeren RMA, et al. On-tissue chemical derivatization in mass spectrometry imaging. *Mass Spectrom Rev* (2022) 41(5):662–94. doi: 10.1002/mas.21680

216. Kaya I, Brulls SM, Dunevall J, Jennische E, Lange S, Martensson J, et al. On-tissue chemical derivatization of catecholamines using 4-(n-methyl)

pyridinium boronic acid for ToF-SIMS and LDI-ToF mass spectrometry imaging. *Anal Chem* (2018) 90(22):13580–90. doi: 10.1021/acs.analchem.8b03746

217. Jones EA, Deininger SO, Hogendoorn PCW, Deelder AM, McDonnell LA. Imaging mass spectrometry statistical analysis. *J Proteomics* (2012) 75(16):4962–89. doi: 10.1016/j.jprot.2012.06.014

218. Rafols P, Vilalta D, Brezmes J, Canellas N, Del Castillo E, Yanes O, et al. Signal preprocessing, multivariate analysis and software tools for MA(LDI)-TOF mass spectrometry imaging for biological applications. *Mass Spectrom Rev* (2018) 37(3):281–306. doi: 10.1002/mas.21527

219. Galli M, Zoppis I, Smith A, Magni F, Mauri G. Machine learning approaches in MALDI-MSI: clinical applications. *Expert Rev Proteomics* (2016) 13(7):685–96. doi: 10.1080/14789450.2016.1200470

220. Flinders B, Beasley E, Verlaan RM, Cuypers E, Francese S, Bassindale T, et al. Optimization of sample preparation and instrumental parameters for the rapid analysis of drugs of abuse in hair samples by MALDI-MS/MS imaging. *J Am Soc Mass Spectrom* (2017) 28(11):2462–8. doi: 10.1007/s13361-017-1766-0

221. Holzlechner M, Bonta M, Lohninger H, Limbeck A, Marchetti-Deschmann M. Multisensor imaging-from sample preparation to integrated multimodal interpretation of LA-ICPMS and MALDI MS imaging data. *Anal Chem* (2018) 90(15):8831–7. doi: 10.1021/acs.analchem.8b00816

222. Jardin-Mathe O, Bonnel D, Franck J, Wisztorski M, Macagno E, Fournier I, et al. MITICS (MALDI imaging team imaging computing system): a new open source mass spectrometry imaging software. *J Proteomics* (2008) 71(3):332–45. doi: 10.1016/j.jprot.2008.07.004

223. Kriegsmann J, Kriegsmann M, Kriegsmann K, Longuespee R, Deininger SO, Casadonte R. MALDI imaging for proteomic painting of heterogeneous tissue structures. *Proteom Clin Appl* (2019) 13(1):e1800045. doi: 10.1002/prca.201800045

224. Bradshaw R, Wilson G, Denison N, Francese S. Application of MALDI MS imaging after sequential processing of latent fingermarks. *Forensic Sci Int* (2021) 319:110643. doi: 10.1016/j.forsciint.2020.110643

225. He JM, Huang LJ, Tian RT, Li TG, Sun CL, Song XW, et al. MassImager: A software for interactive and in-depth analysis of mass spectrometry imaging data. *Anal Chim Acta* (2018) 1015:50–7. doi: 10.1016/j.aca.2018.02.030

226. Liu J, Xiong X, Ouyang Z. Data processing and analysis for mass spectrometry imaging. *Methods Mol Biol* (2015) 1203:195–209. doi: 10.1007/978-1-4939-1357-2_19

227. Bemis KD, Harry A, Eberlin LS, Ferreira C, van de Ven SM, Mallick P, et al. Cardinal: an r package for statistical analysis of mass spectrometry-based imaging experiments. *Bioinformatics* (2015) 31(14):2418–20. doi: 10.1093/bioinformatics/btv146

228. Lopes MBS. World health ozganization 2017 classification of pituitary tumors. *Endocrinol Metab Clin North Am* (2020) 49(3):375–86. doi: 10.1016/j.ecl.2020.05.001

229. Nanba K, Omata K, Gomez-Sanchez CE, Stratakis CA, Demidowich AP, Suzuki M, et al. Genetic characteristics of aldosterone-producing adenomas in blacks. *Hypertension* (2019) 73(4):885–92. doi: 10.1161/HYPERTENSIONAHA.118.12070

230. Vuong HG, Kondo T, Oishi N, Nakazawa T, Mochizuki K, Inoue T, et al. Genetic alterations of differentiated thyroid carcinoma in iodine-rich and iodine-deficient countries. *Cancer Med* (2016) 5(8):1883–9. doi: 10.1002/cam4.781

231. Gadelha MR, Trivellin G, Hernandez Ramirez LC, Korbonits M. Genetics of pituitary adenomas. *Front Horm Res* (2013) 41:111–40. doi: 10.1159/000345673

232. Hasin Y, Seldin M, Lusis A. Multi-omics approaches to disease. *Genome Biol* (2017) 18(1):83. doi: 10.1186/s13059-017-1215-1

233. Fortelny N, Overall CM, Pavlidis P, Freue GVC. Can we predict protein from mRNA levels? *Nature* (2017) 547(7664):E19–20. doi: 10.1038/nature22293

234. Kosti I, Jain N, Aran D, Butte AJ, Sirota M. Cross-tissue analysis of gene and protein expression in normal and cancer tissues. *Sci Rep* (2016) 6:24799. doi: 10.1038/srep24799

235. Pandey A, Mann M. Proteomics to study genes and genomes. *Nature* (2000) 405(6788):837–46. doi: 10.1038/35015709

236. Galli M, Zoppis I, De Sio G, Chinello C, Pagni F, Magni F, et al. A support vector machine classification of thyroid bioptic specimens using MALDI-MSI data. *Adv Bioinf* (2016) 2016:3791214. doi: 10.1155/2016/3791214

237. Galli M, Pagni F, De Sio G, Smith A, Chinello C, Stella M, et al. Proteomic profiles of thyroid tumors by mass spectrometry-imaging on tissue microarrays. *Biochim Biophys Acta Proteins Proteom* (2017) 1865(7):817–27. doi: 10.1016/j.bbapap.2016.11.020

238. Pietrowska M, Diehl HC, Mrukwa G, Kalinowska-Herok M, Gawin M, Chekan M, et al. Molecular profiles of thyroid cancer subtypes: Classification based on features of tissue revealed by mass spectrometry imaging. *Biochim Biophys Acta Proteins Proteom* (2017) 1865(7):837–45. doi: 10.1016/j.bbapap.2016.10.006

239. Mainini V, Pagni F, Garancini M, Giardini V, De Sio G, Cusi C, et al. An alternative approach in endocrine pathology research: MALDI-IMS in papillary thyroid carcinoma. *Endocr Pathol* (2013) 24(4):250–3. doi: 10.1007/s12022-013-9273-8

240. Calligaris D, Feldman DR, Norton I, Olubiyi O, Changelian AN, Machaidze R, et al. MALDI mass spectrometry imaging analysis of pituitary adenomas for near-real-time tumor delineation. *Proc Natl Acad Sci U S A.* (2015) 112(32):9978–83. doi: 10.1073/pnas.1423101112

241. Smith A, Galli M, Piga I, Denti V, Stella M, Chinello C, et al. Molecular signatures of medullary thyroid carcinoma by matrix-assisted laser desorption/ionisation mass spectrometry imaging. *J Proteomics* (2019) 191:114–23. doi: 10.1016/j.jprot.2018.03.021

242. Nipp M, Elsner M, Balluff B, Meding S, Sarioglu H, Ueffing M, et al. S100-A10, thioredoxin, and S100-A6 as biomarkers of papillary thyroid carcinoma with lymph node metastasis identified by MALDI imaging. *J Mol Med (Berl)* (2012) 90(2):163–74. doi: 10.1007/s00109-011-0815-6

243. Karsch-Bluman A, Feiglin A, Arbib E, Stern T, Shoval H, Schwob O, et al. Tissue necrosis and its role in cancer progression. *Oncogene* (2019) 38(11):1920–35. doi: 10.1038/s41388-018-0555-y

244. Scott DA, Norris-Caneda K, Spruill L, Bruner E, Kono Y, Angel PM, et al. Specific n-linked glycosylation patterns in areas of necrosis in tumor tissues. *Int J Mass Spectrom* (2019) 437:69–76. doi: 10.1016/j.ijms.2018.01.002

245. Gawin M, Kurczyk A, Stobiecka E, Fratczak K, Polanska J, Pietrowska M, et al. Molecular heterogeneity of papillary thyroid cancer: Comparison of primary tumors and synchronous metastases in regional lymph nodes by mass spectrometry imaging. *Endocr Pathol* (2019) 30(4):250–61. doi: 10.1007/s12022-019-09593-2

246. Zhao YY, Miao H, Cheng XL, Wei F. Lipidomics: Novel insight into the biochemical mechanism of lipid metabolism and dysregulation-associated disease. *Chem Biol Interact* (2015) 240:220–38. doi: 10.1016/j.cbi.2015.09.005

247. Fahy E, Subramaniam S, Murphy RC, Nishijima M, Raetz CR, Shimizu T, et al. Update of the LIPID MAPS comprehensive classification system for lipids. *J Lipid Res* (2009) 50 Suppl:S9–14. doi: 10.1194/jlr.R800095-JLR200

248. Spener F, Lagarde M, Géloên A, Record M. What is lipidoics? *Eur J Lipid Sci Tech* (2003) 105(9):481–2. doi: 10.1002/ejlt.200390101

249. Butler LM, Perone Y, Dehairs J, Lupien LE, de Laat V, Talebi A, et al. Lipids and cancer: Emerging roles in pathogenesis, diagnosis and therapeutic intervention. *Adv Drug Deliv Rev* (2020) 159:245–93. doi: 10.1016/j.addr.2020.07.013

250. Perrotti F, Rosa C, Cicalini I, Sacchetta P, Del Boccio P, Genovesi D, et al. Advances in lipidomics for cancer biomarkers discovery. *Int J Mol Sci* (2016) 17(12):1992. doi: 10.3390/ijms17121992

251. Zheng M, Wang W, Liu J, Zhang X, Zhang R. Lipid metabolism in cancer cells. *Adv Exp Med Biol* (2021) 1316:49–69. doi: 10.1007/978-981-33-6785-2_4

252. Pakiet A, Kobiela J, Stepnowski P, Sledzinski T, Mika A. Changes in lipids composition and metabolism in colorectal cancer: a review. *Lipids Health Dis* (2019) 18(1):29. doi: 10.1186/s12944-019-0977-8

253. von Roemeling CA, Marlow LA, Pinkerton AB, Crist A, Miller J, Tun HW, et al. Aberrant lipid metabolism in anaplastic thyroid carcinoma reveals stearoyl CoA desaturase 1 as a novel therapeutic target. *J Clin Endocrinol Metab* (2015) 100(5):E697–709. doi: 10.1210/jc.2014-2764

254. von Roemeling CA, Copland JA. Targeting lipid metabolism for the treatment of anaplastic thyroid carcinoma. *Expert Opin Ther Targets* (2016) 20(2):159–66. doi: 10.1517/14728222.2016.1086341

255. Ascenzi F, De Vitis C, Maugeri-Sacca M, Napoli C, Ciliberto G, Mancini R. SCD1, autophagy and cancer: implications for therapy. *J Exp Clin Cancer Res* (2021) 40(1):265. doi: 10.1186/s13046-021-02067-6

256. Guillou H, Zadravec D, Martin PG, Jacobsson A. The key roles of elongases and desaturases in mammalian fatty acid metabolism: Insights from transgenic mice. *Prog Lipid Res* (2010) 49(2):186–99. doi: 10.1016/j.plipres.2009.12.002

257. Miyazaki M, Ntambi JM. Role of stearoyl-coenzyme a desaturase in lipid metabolism. *Prostaglandins Leukot Essent Fatty Acids* (2003) 68(2):113–21. doi: 10.1016/S0952-3278(02)00261-2

258. DeHoog RJ, Zhang J, Alore E, Lin JQ, Yu W, Woody S, et al. Preoperative metabolic classification of thyroid nodules using mass spectrometry imaging of fine-needle aspiration biopsies. *Proc Natl Acad Sci U S A.* (2019) 116(43):21401–8. doi: 10.1073/pnas.1911333116

259. Ishikawa S, Tateya I, Hayasaka T, Masaki N, Takizawa Y, Ohno S, et al. Increased expression of phosphatidylcholine (16:0/18:1) and (16:0/18:2) in thyroid papillary cancer. *PloS One* (2012) 7(11):e48873. doi: 10.1371/journal.pone.0048873

260. Wojakowska A, Cole LM, Chekan M, Bednarczyk K, Maksymiak M, Oczko-Wojciechowska M, et al. Discrimination of papillary thyroid cancer from non-cancerous thyroid tissue based on lipid profiling by mass spectrometry imaging. *Endokrynol Pol* (2018) 69(1):2–8. doi: 10.5603/EP.a2018.0003

261. Ahmadpour ST, Maheo K, Servais S, Brisson L, Dumas JF. Cardiolipin, the mitochondrial signature lipid: Implication in cancer. *Int J Mol Sci* (2020) 21(21):8031. doi: 10.3390/ijms21218031

262. Zhang J, Yu W, Ryu SW, Lin J, Buentello G, Tibshirani R, et al. Cardiolipins are biomarkers of mitochondria-rich thyroid oncocytic tumors. *Cancer Res* (2016) 76(22):6588–97. doi: 10.1158/0008-5472.CAN-16-1545

263. Zhang J, Feider CL, Nagi C, Yu W, Carter SA, Suliburk J, et al. Detection of metastatic breast and thyroid cancer in lymph nodes by desorption electrospray ionization mass spectrometry imaging. *J Am Soc Mass Spectrom* (2017) 28(6):1166–74. doi: 10.1007/s13361-016-1570-2

264. Guo L, Lai Z, Wang Y, Li Z. *In situ* probing changes in fatty-acyl chain length and desaturation of lipids in cancerous areas using mass spectrometry imaging. *J Mass Spectrom* (2020) 56(4):e4621. doi: 10.1002/jms.4621

265. Mirnezami R, Veselkov K, Strittmatter N, Goldin RD, Kinross JM, Stebbing J, et al. Spatially resolved profiling of colorectal cancer lipid biochemistry *via* DESI imaging mass spectrometry to reveal morphology-dependent alterations in fatty acid metabolism. *J Clin Oncol* (2016) 34(15):e15104–e. doi: 10.1200/JCO.2016.34.15_suppl.e15104

266. Pavlova NN, Thompson CB. The emerging hallmarks of cancer metabolism. *Cell Metab* (2016) 23(1):27–47. doi: 10.1016/j.cmet.2015.12.006

267. Rohrig F, Schulze A. The multifaceted roles of fatty acid synthesis in cancer. *Nat Rev Cancer* (2016) 16(11):732–49. doi: 10.1038/nrc.2016.89

268. Yu XH, Ren XH, Liang XH, Tang YL. Roles of fatty acid metabolism in tumourigenesis: Beyond providing nutrition (Review). *Mol Med Rep* (2018) 18 (6):5307–16. doi: 10.3892/mmr.2018.9577

269. Rinschen MM, Ivanisevic J, Giera M, Siuzdak G. Identification of bioactive metabolites using activity metabolomics. *Nat Rev Mol Cell Biol* (2019) 20(6):353–67. doi: 10.1038/s41580-019-0108-4

270. Pinzariu O, Georgescu B, Georgescu CE. Metabolomics-a promising approach to pituitary adenomas. *Front Endocrinol (Lausanne)* (2018) 9:814. doi: 10.3389/fendo.2018.00814

271. Pei Z, Wang S. Recent advance in metabolomics of pituitary adenoma. *Chin J Neuromed* (2021) 20(5):536–9. doi: 10.3760/cma.j.cn115354-20200604-00445

272. Wishart DS. Metabolomics for investigating physiological and pathophysiological processes. *Physiol Rev* (2019) 99(4):1819–75. doi: 10.1152/physrev.00035.2018

273. Sun N, Kunzke T, Sbiera S, Kircher S, Feuchtinger A, Aichler M, et al. Prognostic relevance of steroid sulfation in adrenocortical carcinoma revealed by molecular phenotyping using high-resolution mass spectrometry imaging. *Clin Chem* (2019) 65(10):1276–86. doi: 10.1373/clinchem.2019.306043

274. Huang L, Mao X, Sun C, Luo Z, Song X, Li X, et al. A graphical data processing pipeline for mass spectrometry imaging-based spatially resolved metabolomics on tumor heterogeneity. *Anal Chim Acta* (2019) 1077:183–90. doi: 10.1016/j.aca.2019.05.068

275. Kelly B, Pearce EL. Amino assets: How amino acids support immunity. *Cell Metab* (2020) 32(2):154–75. doi: 10.1016/j.cmet.2020.06.010

276. Xu Y, Zheng X, Qiu Y, Jia W, Wang J, Yin S. Distinct metabolomic profiles of papillary thyroid carcinoma and benign thyroid adenoma. *J Proteome Res* (2015) 14(8):3315–21. doi: 10.1021/acs.jproteome.5b00351

277. Miccoli P, Torregrossa L, Shintu L, Magalhaes A, Chandran J, Tintaru A, et al. Metabolomics approach to thyroid nodules: a high-resolution magic-angle spinning nuclear magnetic resonance-based study. *Surgery* (2012) 152(6):1118–24. doi: 10.1016/j.surg.2012.08.037

278. Vettore L, Westbrook RL, Tennant DA. New aspects of amino acid metabolism in cancer. *Br J Cancer* (2020) 122(2):150–6. doi: 10.1038/s41416-019-0620-5

279. Enomoto K, Hotomi M. Amino acid transporters as potential therapeutic targets in thyroid cancer. *Endocrinol Metab (Seoul)* (2020) 35(2):227–36. doi: 10.3803/EnM.2020.35.2.227

280. McCarty R. Learning about stress: neural, endocrine and behavioral adaptations. *Stress* (2016) 19(5):449–75. doi: 10.1080/10253890.2016.1192120

281. Tank AW, Lee Wong D. Peripheral and central effects of circulating catecholamines. *Compr Physiol* (2015) 5(1):1–15. doi: 10.1002/cphy.c140007

282. Berends AMA, Eisenhofer G, Fishbein L, Horst-Schrivers A, Kema IP, Links TP, et al. Intricacies of the molecular machinery of catecholamine biosynthesis and secretion by chromaffin cells of the normal adrenal medulla and in pheochromocytoma and paraganglioma. *Cancers (Basel)* (2019) 11(8):1121. doi: 10.3390/cancers11081121

283. Nishimoto K, Tomlins SA, Kuick R, Cani AK, Giordano TJ, Hovelson DH, et al. Aldosterone-stimulating somatic gene mutations are common in normal adrenal glands. *Proc Natl Acad Sci U S A.* (2015) 112(33):E4591–9. doi: 10.1073/pnas.1505529112

284. Sugiura Y, Takeo E, Shimma S, Yokota M, Higashi T, Seki T, et al. Aldosterone and 18-oxocortisol coaccumulation in aldosterone-producing lesions. *Hypertension* (2018) 72(6):1345–54. doi: 10.1161/HYPERTENSIONAHA.118.11243

285. Sun N, Meyer LS, Feuchtinger A, Kunzke T, Knosel T, Reincke M, et al. Mass spectrometry imaging establishes 2 distinct metabolic phenotypes of aldosterone-producing cell clusters in primary aldosteronism. *Hypertension* (2020) 75(3):634–44. doi: 10.1161/HYPERTENSIONAHA.119.14041

286. Murakami M, Rhayem Y, Kunzke T, Sun N, Feuchtinger A, Ludwig P, et al. *In situ* metabolomics of aldosterone-producing adenomas. *JCI Insight* (2019) 4(17): e130356. doi: 10.1172/jci.insight.130356

287. Tang Y, Xie T, Wu S, Yang Q, Liu T, Li C, et al. Quantitative proteomics revealed the molecular characteristics of distinct types of granulated somatotroph adenomas. *Endocrine* (2021) 74(2):375–86. doi: 10.1007/s12020-021-02767-1

288. Ramadan N, Ghazale H, El-Sayyad M, El-Haress M, Kobeissy FH. Neuroproteomics studies: Challenges and updates. *Methods Mol Biol* (2017) 1598:3–19. doi: 10.1007/978-1-4939-6952-4_1

289. Dilillo M, Pellegrini D, Ait-Belkacem R, de Graaf EL, Caleo M, McDonnell LA. Mass spectrometry imaging, laser capture microdissection, and LC-MS/MS of the same tissue section. *J Proteome Res* (2017) 16(8):2993–3001. doi: 10.1021/acs.jproteome.7b00284

290. Mezger STP, Mingels AMA, Bekers O, Heeren RMA, Cillero-Pastor B. Mass spectrometry spatial-omics on a single conductive slide. *Anal Chem* (2021) 93 (4):2527–33. doi: 10.1021/acs.analchem.0c04572

291. Dewez F, Martin-Lorenzo M, Herfs M, Baiwir D, Mazzucchelli G, De Pauw E, et al. Precise co-registration of mass spectrometry imaging, histology, and laser microdissection-based omics. *Anal Bioanal Chem* (2019) 411(22):5647–53. doi: 10.1007/s00216-019-01983-z

292. Basu SS, Stopka SA, Abdelmoula WM, Randall EC, Gimenez-Cassina Lopez B, Regan MS, et al. Interim clinical trial analysis of intraoperative mass spectrometry for breast cancer surgery. *NPJ Breast Cancer* (2021) 7(1):116. doi: 10.1038/s41523-021-00318-5

293. Quanico J, Franck J, Cardon T, Leblanc E, Wisztorski M, Salzet M, et al. NanoLC-MS coupling of liquid microjunction microextraction for on-tissue proteomic analysis. *Biochim Biophys Acta Proteins Proteom* (2017) 1865(7):891–900. doi: 10.1016/j.bbapap.2016.11.002

294. Mallah K, Zibara K, Kerbaj C, Eid A, Khoshman N, Ousseily Z, et al. Neurotrauma investigation through spatial omics guided by mass spectrometry imaging: Target identification and clinical applications. *Mass Spectrom Rev* (2021) 42(1):189–205. doi: 10.1002/mas.21719

295. Huang P, Kong Q, Gao W, Chu B, Li H, Mao Y, et al. Spatial proteome profiling by immunohistochemistry-based laser capture microdissection and data-independent acquisition proteomics. *Anal Chim Acta* (2020) 1127:140–8. doi: 10.1016/j.aca.2020.06.049

296. Ezzoukhry Z, Henriet E, Cordelieres FP, Dupuy JW, Maitre M, Gay N, et al. Combining laser capture microdissection and proteomics reveals an active translation machinery controlling invadosome formation. *Nat Commun* (2018) 9 (1):2031. doi: 10.1038/s41467-018-04461-9

297. Tikka S, Monogioudi E, Gotsopoulos A, Soliymani R, Pezzini F, Scifo E, et al. Proteomic profiling in the brain of CLN1 disease model reveals affected functional modules. *Neuromol Med* (2016) 18(1):109–33. doi: 10.1007/s12017-015-8382-6

298. Cole LM, Clench MR, Francese S. Sample treatment for tissue proteomics in cancer, toxicology, and forensics. *Adv Exp Med Biol* (2019) 1073:77–123. doi: 10.1007/978-3-030-12298-0_4

299. Himmel LE, Hackett TA, Moore JL, Adams WR, Thomas G, Novitskaya T, et al. Beyond the H&E: Advanced technologies for *in situ* tissue biomarker imaging. *ILAR J* (2018) 59(1):51–65. doi: 10.1093/ilar/ily004

300. Espina V, Wulfkuhle JD, Calvert VS, VanMeter A, Zhou W, Coukos G, et al. Laser-capture microdissection. *Nat Protoc* (2006) 1(2):586–603. doi: 10.1038/nprot.2006.85

301. Gallagher RI, Blakely SR, Liotta LA, Espina V. Laser capture microdissection: Arcturus(XT) infrared capture and UV cutting methods. *Methods Mol Biol* (2012) 823:157–78. doi: 10.1007/978-1-60327-216-2_11

302. Chokechanachaisakul U, Kaneko T, Okiji T, Kaneko R, Suda H, Nor JE. Laser capture microdissection in dentistry. *Int J Dent* (2010) 2010:592694. doi: 10.1155/2010/592694

303. Quanico J, Franck J, Dauly C, Strupat K, Dupuy J, Day R, et al. Development of liquid microjunction extraction strategy for improving protein identification from tissue sections. *J Proteomics* (2013) 79:200–18. doi: 10.1016/j.jprot.2012.11.025

304. Comi TJ, Makurath MA, Philip MC, Rubakhin SS, Sweedler JV. MALDI MS guided liquid microjunction extraction for capillary electrophoresis-electrospray ionization MS analysis of single pancreatic islet cells. *Anal Chem* (2017) 89(14):7765–72. doi: 10.1021/acs.analchem.7b01782

305. Griffiths RL, Randall EC, Race AM, Bunch J, Cooper HJ. Raster-mode continuous-flow liquid microjunction mass spectrometry imaging of proteins in thin tissue sections. *Anal Chem* (2017) 89(11):5683–7. doi: 10.1021/acs.analchem.7b00977

306. Domenick TM, Vedam-Mai V, Yost RA. Design and implementation of a dual-probe microsampling apparatus for the direct analysis of adherent mammalian cells by ion mobility-mass spectrometry. *Anal Chem* (2020) 92 (17):12055–61. doi: 10.1021/acs.analchem.0c02714

307. Kertesz V, Van Berkel GJ. Sampling reliability, spatial resolution, spatial precision, and extraction efficiency in droplet-based liquid microjunction surface sampling. *Rapid Commun Mass Spectrom* (2014) 28(13):1553–60. doi: 10.1002/rcm.6931

308. Wisztorski M, Quanico J, Franck J, Fatou B, Salzet M, Fournier I. Droplet-based liquid extraction for spatially-resolved microproteomics analysis of tissue sections. *Methods Mol Biol* (2017) 1618:49–63. doi: 10.1007/978-1-4939-7051-3_6

309. Griffiths RL, Kocurek KI, Cooper HJ. Liquid extraction surface analysis (LESA) high-field asymmetric waveform ion mobility spectrometry (FAIMS) mass spectrometry for *In situ* analysis of intact proteins. *Methods Mol Biol* (2020) 2084:191–201. doi: 10.1007/978-1-0716-0030-6_12

310. Wisztorski M, Desmons A, Quanico J, Fatou B, Gimeno JP, Franck J, et al. Spatially-resolved protein surface microsampling from tissue sections using liquid extraction surface analysis. *Proteomics* (2016) 16(11-12):1622–32. doi: 10.1002/pmic.201500508

311. Ryan DJ, Nei D, Prentice BM, Rose KL, Caprioli RM, Spraggins JM. Protein identification in imaging mass spectrometry through spatially targeted liquid micro-extractions. *Rapid Commun Mass Sp* (2018) 32(5):442–50. doi: 10.1002/rcm.8042

312. Kertesz V, Vavrek M, Freddo C, Van Berkel GJ. Spatial profiling of stapled alpha-helical peptide ATSP-7041 in mouse whole-body thin tissue sections using droplet-based liquid microjunction surface sampling-HPLC-ESI-MS/MS. *Int J Mass Spectrom* (2019) 437:17–22. doi: 10.1016/j.ijms.2018.01.005

313. Kertesz V, Van Berkel GJ. Liquid microjunction surface sampling coupled with high-pressure liquid chromatography-electrospray ionization-mass spectrometry for analysis of drugs and metabolites in whole-body thin tissue sections. *Anal Chem* (2010) 82(14):5917–21. doi: 10.1021/ac100954p

314. Simon D, Oleschuk R. The liquid micro junction-surface sampling probe (LMJ-SSP); a versatile ambient mass spectrometry interface. *Analyst* (2021) 146 (21):6365–78. doi: 10.1039/D1AN00725D

315. Liu Y, Wu J, Liu S, Zhuang D, Wang Y, Shou X, et al. Immuno-laser capture microdissection of frozen prolactioma sections to prepare proteomic samples. *Colloids Surf B Biointerfaces* (2009) 71(2):187–93. doi: 10.1016/j.colsurfb.2009.02.005

316. Liu YC, Zhuang DX, Hou RP, Li JA, Xu GM, Song T, et al. Shotgun proteomic analysis of microdissected postmortem human pituitary using complementary two-dimensional liquid chromatography coupled with tandem mass spectrometer. *Anal Chim Acta* (2011) 688(2):183–90. doi: 10.1016/j.aca.2010.12.032

317. Zhan X, Wang X, Cheng T. Human pituitary adenoma proteomics: New progresses and perspectives. *Front Endocrinol (Lausanne)* (2016) 7:54. doi: 10.3389/fendo.2016.00054

318. Liu Y, Wu J, Yan G, Hou R, Zhuang D, Chen L, et al. Proteomic analysis of prolactinoma cells by immuno-laser capture microdissection combined with online two-dimensional nano-scale liquid chromatography/mass spectrometry. *Proteome Sci* (2010) 8:2. doi: 10.1186/1477-5956-8-2

319. Leonardi L AC, Beaudonnet G, Beauvais D, Cauquil C, Not A, Morassi O, et al. Skin amyloid deposits and nerve fiber loss as markers of neuropathy onset and progression in hereditary transthyretin amyloidosis. *Eur J Neurol* (2022) 29 (5):1477–87. doi: 10.1111/ene.15268

320. Siddiqi OK, Ruberg FL. Cardiac amyloidosis: An update on pathophysiology, diagnosis, and treatment. *Trends Cardiovasc Med* (2018) 28 (1):10–21. doi: 10.1016/j.tcm.2017.07.004

321. Sirohi D, Gandhi J, Amin MB, Luthringer DJ. Amyloidosis of the bladder and association with urothelial carcinoma: report of 29 cases. *Hum Pathol* (2019) 93:48–53. doi: 10.1016/j.humpath.2019.08.011

322. Thomas VE, Smith J, Benson MD, Dasgupta NR. Amyloidosis: diagnosis and new therapies for a misunderstood and misdiagnosed disease. *Neurodegener Dis Man* (2019) 9(6):289–99. doi: 10.2217/nmt-2019-0020

323. Benson MD, Buxbaum JN, Eisenberg DS, Merlini G, Saraiva MJM, Sekijima Y, et al. Amyloid nomenclature 2020: update and recommendations by the international society of amyloidosis (ISA) nomenclature committee. *Amyloid* (2020) 27(4):217–22. doi: 10.1080/13506129.2020.1835263

324. Martinez-Naharro A, Hawkins PN, Fontana M. Cardiac amyloidosis. *Clin Med* (2018) 18(Suppl 2):s30–s5. doi: 10.7861/clinmedicine.18-2-s30

325. Blank M, Hopf C. Spatially resolved mass spectrometry analysis of amyloid plaque-associated lipids. *J Neurochem* (2021) 159(2):330–42. doi: 10.1111/jnc.15216

326. Anderson TJ, Ewen SW. Amyloid in normal and pathological parathyroid glands. *J Clin Pathol* (1974) 27(8):656–63. doi: 10.1136/jcp.27.8.656

327. Colombat M, Barres B, Renaud C, Ribes D, Pericard S, Camus M, et al. Mass spectrometry-based proteomic analysis of parathyroid adenomas reveals PTH as a new human hormone-derived amyloid fibril protein. *Amyloid* (2021) 28 (3):153–7. doi: 10.1080/13506129.2021.1885023

328. El Sayed SA, Fahmy MW, Schwartz J. Physiology, pituitary gland. *StatPearls* (2022) Treasure Island, Florida: StatPearls Publishing.

329. Kertesz V, Calligaris D, Feldman DR, Changelian A, Laws ER, Santagata S, et al. Profiling of adrenocorticotropic hormone and arginine vasopressin in human pituitary gland and tumor thin tissue sections using droplet-based liquid-microjunction surface-sampling-HPLC-ESI-MS-MS. *Anal Bioanal Chem* (2015) 407(20):5989–98. doi: 10.1007/s00216-015-8803-2

330. Cui Y, Li C, Jiang Z, Zhang S, Li Q, Liu X, et al. Single-cell transcriptome and genome analyses of pituitary neuroendocrine tumors. *Neuro Oncol* (2021) 23 (11):1859–71. doi: 10.1093/neuonc/noab102

331. Boufraqech M, Nilubol N. Multi-omics signatures and translational potential to improve thyroid cancer patient outcome. *Cancers (Basel)* (2019) 11 (12):1988. doi: 10.3390/cancers11121988

332. Zhan X, Long Y. Exploration of molecular network variations in different subtypes of human non-functional pituitary adenomas. *Front Endocrinol (Lausanne)* (2016) 7:13. doi: 10.3389/fendo.2016.00013

333. Taylor AJ, Dexter A, Bunch J. Exploring ion suppression in mass spectrometry imaging of a heterogeneous tissue. *Anal Chem* (2018) 90(9):5637–45. doi: 10.1021/acs.analchem.7b05005

334. Minakshi P, Ghosh M, Kumar R, Patki HS, Saini HM, Ranjan K, et al. Single-cell metabolomics: Technology and applications. *Single-Cell Omics* (2019) London, United Kingdom: Academic Press, 319–53. doi: 10.1016/B978-0-12-814919-5.00015-4

335. Seydel C. Single-cell metabolomics hits its stride. *Nat Methods* (2021) 18 (12):1452–6. doi: 10.1038/s41592-021-01333-x

336. Kompauer M, Heiles S, Spengler B. Atmospheric pressure MALDI mass spectrometry imaging of tissues and cells at 1.4-mum lateral resolution. *Nat Methods* (2017) 14(1):90–6. doi: 10.1038/nmeth.4071

337. Zavalin A, Yang J, Haase A, Holle A, Caprioli R. Implementation of a Gaussian beam laser and aspheric optics for high spatial resolution MALDI imaging MS. *J Am Soc Mass Spectrom* (2014) 25(6):1079–82. doi: 10.1007/s13361-014-0872-5

338. Zavalin A, Yang J, Caprioli R. Laser beam filtration for high spatial resolution MALDI imaging mass spectrometry. *J Am Soc Mass Spectrom* (2013) 24(7):1153–6. doi: 10.1007/s13361-013-0638-5

339. Duenas ME, Essner JJ, Lee YJ. 3D MALDI mass spectrometry imaging of a single cell: Spatial mapping of lipids in the embryonic development of zebrafish. *Sci Rep* (2017) 7(1):14946. doi: 10.1038/s41598-017-14949-x

340. Niehaus M, Soltwisch J, Belov ME, Dreisewerd K. Transmission-mode MALDI-2 mass spectrometry imaging of cells and tissues at subcellular resolution. *Nat Methods* (2019) 16(9):925–31. doi: 10.1038/s41592-019-0536-2

10.3389/fendo.2022.993081

Glossary

ACTH	adrenocorticotropic hormone
AH	adenohypophysis
AIP	aryl hydrocarbon receptor interacting protein
APA	aldosterone-producing adenoma
APCC	aldosterone-producing cell cluster
ATC	anaplastic thyroid carcinoma
BRAF	v-Raf murine sarcoma viral oncogene homolog B1
CACNA1D	calcium voltage-gated channel subunit alpha1 D
CHCA	alpha-cyano-4-hydroxycinnamic acid
CLs	cardiolipins
DESI	desorption electrospray ionization
DESI-MSI	desorption electrospray ionization-mass spectrometry imaging
2,5-DHB	2,5-dihydroxybenzoic acid
ESI	electrospray ionization
FFAs	free fatty acids
FFPE	formalin fixed paraffin embedded
FNA	fine needle aspiration
GCIBs	gas cluster ion beams
GH	growth hormone
GNAS	guanine nucleotide binding protein, alpha stimulating
IHC	immunohistochemistry
IR	infrared
ITO	indium-tin oxide
KCNJ5	potassium voltage-gated channel subfamily J member 5
LMD	laser microdissection
LC-MS	liquid chromatography-mass spectrometry
LC-MS/MS	liquid chromatography with tandem mass spectrometry
LDI	laser desorption/ionization
LMJ	liquid microjunction
LMIGs	liquid metal ion guns
m/z	mass-to-charge ratio
MALDI	matrix-assisted laser desorption/ionization
MALDI-MSI	matrix-assisted laser desorption/ionization-mass spectrometry imaging
MEN1	menin 1
MS	mass spectrometry
MSI	mass spectrometry imaging
MTC	medullary thyroid carcinoma
NH	neurohypophysis
PA	phosphatidic acid
PC	phosphatidylcholine
PEN	polyethylene napthalate
PLs	phospholipids
PTC	papillary thyroid carcinoma
PTH	parathyroid hormone
PRL	prolactin
RAS	rapidly accelerated fibrosarcoma
RET	Proto-oncogene tyrosine-protein kinase receptor Ret
SA	sinapinic acid
SCD1	stearoyl-CoA desaturase
SIMS	secondary ion mass spectrometry
SIMS-MSI	secondary ion mass spectrometry-mass spectrometry imaging
SM	sphingomyelin
S100-A10 p11	the ligand of Annexin-II
S100-A6	Calcyclin
MS/MS	Tandem mass spectrometer
TOF	time-of-flight
TSH	thyroid stimulating hormone
UV	ultraviolet

frontiers | Frontiers in Endocrinology

TYPE Original Research
PUBLISHED 27 July 2023
DOI 10.3389/fendo.2023.1164679

OPEN ACCESS

EDITED BY
Princy Francis,
Mayo Clinic, United States

REVIEWED BY
Anastasia Filia,
University Hospital of Alexandroupolis, Greece
Ram Raj Singh,
University of California, Los Angeles, United States

*CORRESPONDENCE
Jia Zhou
zhoujia@zcmu.edu.cn

†These authors have contributed equally to this work

RECEIVED 13 February 2023
ACCEPTED 27 June 2023
PUBLISHED 27 July 2023

CITATION
Wu D, Ye L, Zhang X, Yin M, Guo Y and Zhou J (2023) Characteristics of steroid hormones in systemic lupus erythematosus revealed by GC/MS-based metabolic profiling.
Front. Endocrinol. 14:1164679.
doi: 10.3389/fendo.2023.1164679

Characteristics of steroid hormones in systemic lupus erythematosus revealed by GC/MS-based metabolic profiling

Dehong Wu[1†], Lingxia Ye[2†], Xiafeng Zhang[3], Mengdi Yin[3], Yixuan Guo[3] and Jia Zhou[3*]

[1]Department of Rheumatology, The Second Affiliated Hospital of Zhejiang Chinese Medical University, Hangzhou, Zhejiang, China, [2]Department of Endocrinology and Metabolism, The Second Affiliated Hospital, Zhejiang University School of Medicine, Hangzhou, Zhejiang, China, [3]Institute of Basic Research in Clinical Medicine, College of Basic Medical Sciences, Zhejiang Chinese Medical University, Hangzhou, Zhejiang, China

Background: Systemic lupus erythematosus (SLE) is a systemic autoimmune disease with a remarkable predominance in female, suggesting that steroid hormones may be involved in the pathogenesis. However, steroid signature of SLE patients has not been fully explored.

Methods: A metabolic profiling analysis based on gas chromatography/mass spectrometry (GC/MS) with high sensitivity and reproducibility was employed to comprehensively reveal SLE-specific steroid alterations.

Results: More than 70 kinds of steroids in urine were detected by gas chromatography/mass spectrometry (GC/MS) to reveal SLE-specific steroid alterations. Principle component analysis demonstrated that the steroid profile was obviously distinguished between patients with SLE and controls. A lower level of total androgens was observed in patients, and nine androgens [dehydroepiandrosterone (DHEA), testosterone, Etio, androsterone, βαβ-Diol, Epi-An, Epi-DHT, 16α-OH-DHEA, and A-Diol] underwent significant decrease. Moreover, patients with SLE exhibited a slightly higher level of total estrogens than controls, and three estrogens (17-Epi-E3, 17α-E2, and E3) were remarkably increased. Furthermore, we identified the elevation of two sterols (Lan and Chol), and the reduction of one corticoid (11-DeoxyF) and two progestins (5α-DHP and 11β-OH-Prog) in patients.

Discussion: In this study, metabolic signature of urinary steroids associated with SLE was comprehensively defined by GC/MS for the first time, and steroid metabolism disorders were found in patients with SLE, especially the conversion of androgens to estrogens. Our findings will provide new insights for a deeper understanding of the mechanism of steroid hormones in the pathogenesis of SLE and will help to unravel the reason of sexual disparity in SLE.

KEYWORDS

hormone, metabolic profiling, SLE, GC/MS, steroid

1 Introduction

Systemic lupus erythematosus (SLE) is a systemic autoimmune disease, characterized by T-cell dysfunction, abnormal B-cell activation, and autoantibody production. The clinical manifestations of SLE are complex and diverse, and most patients will gradually develop multiple-organ damage, among which renal damage is more prominent. The etiologies and mechanisms of the disease have not been fully understood. The incidence rate of SLE is about 70/100,000 in China and is increasing year by year. The occurrence of SLE has a remarkable predominance in women, with a 7–9:1 women-to-men ratio and is much more common in women of childbearing age (1), suggesting that, in addition to factors such as heredity, environment, and infection, hormones may also participate in the pathogenesis of SLE (2).

Some studies based on murine models or humans have suggested an association between steroid hormones and lupus. Recent clinical trials found that oral contraceptives containing estrogen activated the disease, but the use of contraceptives containing only progesterone can reduce the risk of SLE (3). Patients with SLE exacerbated with pregnancy, especially in terms of renal lupus (4). In female lupus-prone mice, estrogen supplementation can worsen the disease, whereas gonadectomy or androgens supplementation can ameliorate the disease; in addition, the removal of the gonads in male lupus-prone mice increases disease susceptibility (5, 6).

Numerous studies verified that hormones participate in the regulation of immune system, which might be one of the mechanisms behind. Estrogen, androgen, progestin, corticoid, and sterol are the main types of steroid hormones in the body. Different types of steroid hormones play different roles in the immune system, including the development, homeostasis, activation, and differentiation of lymphocytes and the production of cytokines, therefore impacting the immune responses differentially (7). Estrogen targeted a serious of immune cells, including T lymphocytes, B lymphocytes, mononuclear macrophages, and natural killer cells, which were all proven as important roles in the pathogenesis of SLE (8–10). Similarly, progesterone can also act on the above-mentioned various immune cells to exert an immunomodulatory effect (7). Androgens can reduce the proliferation and differentiation of lymphocytes and may inhibit the production of immunoglobulins (11), which is generally regarded as beneficial for autoimmune diseases.

Endogenous steroid hormones are usually generated in the adrenal cortex, ovaries, and testes, which are mainly produced by the metabolism of cholesterol through a series of enzymes. There are mutual transformations between various steroids in the body, which are constantly produced or consumed, maintaining in a dynamic equilibrium state. Disorders in steroid metabolism may influence the occurrence and development of SLE through immune dysfunction. Hence, exploring the expression characteristics of steroids in patients with SLE is of great value for the in-depth study of the pathological mechanism, diagnosis, and treatment of SLE. Previous studies have found abnormalities in hormones in patients with SLE, although these studies are mainly aimed at several common steroid hormones, such as estradiol (E2), testosterone, and dehydroepiandrosterone (DHEA) (12–14). However, there are dozens of steroids in the body, so it is necessary to perform a global analysis of the steroid profile in patients with SLE to better understand the correlation between SLE and hormones.

Major technologies for current monitoring hormone levels include radioimmunoassay, direct immunoassay, and mass spectrometry (MS)–based assay. Among these, radioimmunoassay and direct immunoassay are most widely used. Several studies comparing different assays indicated the discrepancies that the lack of precision and accuracy at low hormone concentrations makes immunoassays unreliable for monitoring patients with hypogonadism (15–18). Thus, MS-based assays become the gold standard for steroid hormones detection (19). Beyond that, MS-based assays can detect much more kinds of steroids than immunoassays. MS-based assays refer to gas chromatography (GC)/tandem MS and liquid chromatography (LC)/tandem MS. However, until now, there is no any paper reporting the steroid profile changes in patients with SLE with the method of MS-based assays.

To comprehensively characterize the SLE-specific metabolism of steroids, this study intends to employ a highly sensitive metabolic profiling analysis based on GC/MS to detect the changes in steroid hormones in the urine of SLE female patients, which might be helpful to deepen the understanding of the role of hormones in the pathogenesis of SLE and provide new ideas for the diagnosis and treatment of SLE.

2 Materials and methods

2.1 Subjects

This cross-sectional study enrolled 15 patients with SLE and 15 age-matched healthy volunteers at The Second Affiliated Hospital of Zhejiang Chinese Medical University between 1 January 2018 and 31 December 2019. All participants were women, 26 to 55 years old, not pregnant at the time. They all completed a screening evaluation that included a detailed medical history. These patients with SLE were diagnosed according to the 1997 American College of Rheumatology (ACR) Classification criteria and are under anti-SLE treatment, whereas the healthy volunteers were absent of any clinical manifestations of SLE or any inflammatory or autoimmune diseases. This study was approved by the ethics committee of The Second Affiliated Hospital of Zhejiang Chinese Medical University (No. AF-BG-006-1.0), and every subject has given an informed consent.

2.2 Reagents

The internal standards (d3-testosterone, d4-cortisol, d9-progesterone, d7-cholesterol, 13c3-androstene-3,17-dione, and 13c3-estrone) were purchased from Cerilliant (Round Rock, TX, USA). L-ascorbic acid, sodium acetate, acetic acid, β-glucosaldosidase/

arylsulfatase, ammonium iodide (NH4I), dithioerythritol (DTE), and N-methyl-n-(trimethylsilyl)trifluoroacetamide (MSTFA) were purchased from Sigma-Aldrich (St. Louis, MO, USA). Commercial standards of steroids (dehydroepiandrosterone, testosterone, 11-deoxycorticosterone, cortisone, cortisol, 16α-hydroxyestrone, pregnenolone, 17α-hydroxypregnenolone, epipregnanolone, dihydrotestosterone, 21-hydroxyprogesterone, androsterone, epiandrosterone, corticosterone, estrone, 17β-estradiol, estriol, 16-epiestriol, progesterone, 17α-hydroxyprogesterone, desmosterol, cholesterol, etc.) were purchased from Sigma-Aldrich, J&K Chemical Ltd. (Beijing, China), or Santa Cruz Biotechnology, Inc. (Santa Cruz, CA). Chromatographic pure hexane, methanol, and ethyl acetate were purchased from Merck (Fairfield, OH, USA). The Oasis HLB SPE cartridge was obtained from Waters (1.5 ml, 60 mg; Waters, Milford, MA, USA).

2.3 Sample collection and preparation for steroid profiling analysis

The analysis of urinary steroid profile was based on the protocol of Moon (20). Urine (10 ml) was collected from subjects between 6:00 and 8:00 in the morning, after fasting for 12 h. A total of 2 ml of urine was added into a microcentrifuge tube containing 20 µl of internal standard solution (d3-testosterone, 10 µg/ml; d4-cortisol, 35 µg/ml; d9-progesterone, 35 µg/ml; d7-cholesterol, 35 µg/ml; 13c3-androstene-3,17-dione, 10 µg/ml; and 13c3-estrone, 10 µg/ml). Before extraction and purification of steroids by SPE, the SPE cartridges were activated and balanced with 2 ml of methanol and 2 ml of pure water. Subsequently, the sample was loaded and washed with high pure water twice. Then, the steroids were eluted twice with 2 ml of methanol. The collected eluents were dried with a small stream of nitrogen. Acetate buffer (1 ml; 0.2 M, pH 5.2), 0.2% L-ascorbic acid (100 µl), and glucosaldehydase/arylsulfatase (50 µl) were added and then incubate at 55°C for 3 h. The solution was extracted twice with ethyl acetate/n-hexane (2:3, v/v). The upper layer were merged and concentrated to dry under nitrogen at 40°C and further dried in a vacuum dryer for 60 min. Before GC/MS analysis, 40 µl of MSTFA/NH4I/DTE mixture (500:4:2, v/w/w) was added for derivation and reacted for 20 min at 60°C in water bath. Equal amounts of urine samples were mixed as quality control (QC) samples and then subjected to the same treatment as described above and analyzed together with the actual samples.

2.4 Standard solution preparation

A series of reference standards were selected to generate steroid mass spectral library to explore the mass fragmentation characteristics of different kinds of steroids and support the structural identification of steroids in urine. Commercial steroid standards were prepared as stock solutions at a concentration of 100 µg/ml in methanol and stored at −20°C. Prior to analysis, the standard solutions were diluted to 0.1–10 µg/ml and lyophilized in a centrifugal concentrator. After derivatization using the method mentioned in Section 2.3, the mass spectra of each steroid standard were obtained by GC/MS.

2.5 GC/MS analysis

GC/MS analysis was performed on an Agilent 7890/5975C GC/MS (Agilent Technologies, Santa Clara, CA, USA). Steroids were separated using a 25 mm × 0.2 mm × 0.33 µm Ultra-1 column (J&W Scientific, Folsom, CA, USA). The sample injection volume was 2 µl with a split ratio of 5:1. Helium (99.9996%) was used as the carrier gas, and the flow rate was 1.0 ml/min. The oven temperature program was as follows: the initial temperature was 215°C, ramped to 260°C at 1°C/min and then ramped to 320°C at 15°C/min, and held for 5 min. The injector and transfer line temperatures were both 280°C. Full scan mode and selective ion scan were used for qualitative and quantitative analysis of urinary steroids, respectively. During the analysis process, different groups of samples were interspersed, and one QC sample was added to the analysis sequence for every five samples.

2.6 Data processing and statistical analysis

The structure of urinary steroid was identified by comparing the acquired mass spectra and retention indices with our self-constructed steroid mass spectral library, commercial National Institute of Standards and Technology (Boulder, CO, USA) library, and mass spectra published in previous references (20, 21). The peak area of each steroid was integrated by Agilent GC/MS workstation (Agilent Technologies, Santa Clara, CA, USA), and the quantitative ion was determined according to the standards or reference (21). After normalized to the internal standard of corresponding steroid species, the data were subjected to a principal component analysis (PCA) using the SIMCA-P 11.0 version (Umetrics AB, Umea, Sweden). PCA, as an unsupervised learning technique, is employed to reduce the dimensionality of complex datasets and identify the most significant variations within the data. By applying PCA, we can gain an overview of the disparities in steroid profiles between the SLE and control groups. Furthermore, orthogonal signal correction (OSC) partial least-squares discriminant analysis (PLS-DA) was performed to distinguish patients with SLE and controls and to screen the different steroids between groups. OSC PLS-DA is a supervised multivariate statistical analysis method that filters out irrelevant variations to classification and can more effectively capture the difference information between groups as compared to PCA. Analysis of variance testing of the cross-validated residuals (CV-ANOVA) was used to measure the reliability of the OSC PLS-DA model. VIP (variable importance in projection) values indicate the contribution of each variable to the distinction between groups in the OSC PLS-DA model. A high VIP value suggests that the corresponding variable is important in distinguishing between groups, whereas a low VIP value indicates a low correlation. Here, variables with VIP > 1.0 were selected as potential discriminant steroids. SPSS 18.0 (International Business Machines Corp., Armonk, USA) was employed to conduct T-test for each steroid. OSC PLS-DA (VIP > 1) and T-test ($P < 0.05$) were combined to find out the differential steroids between two groups. On the basis of the screened steroids, the pathway analysis was performed in the MetaboAnalyst website (http://www.metaboanalyst.ca), and the involved metabolic pathways were visualized by using Metscape

3.1.3. Furthermore, Pearson analysis was carried out to measure the correlation between the discriminant steroids and SLE disease activity index (SLEDAI).

3 Results

3.1 Clinical characteristics of participants

All subjects were women, and participants in both groups were matched in age ($p > 0.05$). Patients with SLE participating in the study fulfilled the ACR revised criteria for the classification of SLE and received anti-SLE treatment. The clinical characteristics of participants are listed in Supplementary Materials (Table S1). All patients with SLE showed positive antinuclear antibodies, and seven of them had kidney damage. None of the recruited subjects were taking any contraceptives, sex hormones, or related medicine.

3.2 Metabolic profiles of steroids in patients with SLE

Seventy-five kinds of steroids were detected in urine samples, including 23 kinds of androgens, 15 kinds of corticoids, 19 kinds of estrogens, 14 kinds of progestins, and four kinds of sterols (Figure 1). The full names and abbreviations of steroids are listed in Supplementary Materials (Table S2). Circular bar charts were used to display the composition of each steroid species, and the proportion of individual steroids in the corresponding steroid species was calculated and averaged over all samples (Figure 1B). As shown in Figure 1, the most abundant androgens was 16α-OH-DHEA, followed by Etio and androsterone; THE (tetrahydrocortisone), Allo THF (allotetrahydrocortisol), and THF were the three most abundant corticoids; among all estrogen, E3 and 17β-E2 had the highest abundance; in addition, P-tiol (Pregnanetriol) and 24S-OH-Chol (24S-Hydroxycholesterol) depicted a higher abundance.

3.3 Overall differences in steroids between patients with SLE and controls

To assess the general differences of steroid profiles between patients with SLE and controls, unsupervised PCA analysis was performed on steroid data after UV scaling. As shown in Figure 2, PCA score plot based on the first three principle components (R2X = 51.8%) demonstrated a tendency of separation between the SLE group and the control group, indicating an alteration in steroid hormone metabolism in patients with SLE.

3.4 Alterations in the total amount of steroids

The levels of total steroids, total androgens, total estrogens, total corticoids, total progestins, and total sterols in urea samples were measured for each participant. Compared with the control group, there were no significant changes in the levels of total steroids, total corticoids, total progestins, and total sterols in the SLE group. Significantly, there was a giant decrease in the level of total androgens in patients with SLE ($P < 0.05$), and there was a slight trend of elevation in total estrogens ($P < 0.1$, Figure 3).

3.5 Screening of altered steroid species in patients with SLE

To reveal the specific alterations of steroids in patients with SLE, PLS-DA was conducted to compare the steroid profiles between two groups after OSC filtration. The model matched well [R2Y(cum) = 0.932 and Q2Y(cum) = 0.799]. CV-ANOVA test was carried out for significance testing of OSC PLS-DA model, and the P-value of CV-ANOVA was less than 0.05, suggesting that the model was significant. The score plot showed that the steroid profiles of patients with SLE were obviously distinguished from that of the control group (Figure 4A). More interestingly, the biplot displaying co-chart scores and loadings showed that some kinds of androgens, corticoids, and progestins tended to be decreased; meanwhile, some kinds of sterols and estrogens seemed more enriched in patients with SLE (Figure 4B). The steroids with VIP>1 were listed in Figure 4C based on the OSC PLS-DA model.

Differential steroids between patients with SLE and healthy controls were screened according to the VIP values (VIP>1) of the OSC PLS-DA model and P-values of univariate analysis ($P < 0.05$). A total of 17 kinds of differential steroids were screened, of which none kinds of androgens (Etio, βαβ-Diol, testosterone, Epi-An, Epi-DHT, DHEA, 16α-OH-DHEA, A-Diol, and androsterone), one kind of corticoid (11-DeoxyF), and two kinds of progestins (5α-DHP and 11β-OH-Prog) were significantly decreased in patients with SLE, whereas three kinds of estrogens (17-Epi-E3, 17α-E2, and E3) and two kinds of sterols (Lan and Chol) showed significant increases in patients with SLE (Figure 5A).

Through metabolic pathway analysis, we found that the different steroids found in urine samples from patients with SLE and healthy controls were mainly enriched in biological processes such as steroidogenesis, androstenedione metabolism, and steroid biosynthesis (Figure 5B), suggesting the presence of steroid metabolism disorders in patients with SLE. In particular, the conversion of androgens to estrogens was promoted, which led to abnormal levels of androgens and estrogens.

3.6 Correlation between the differential steroids and SLEDAI

SLEDAI is an important indicator to assess the severity and activity of SLE clinically; the higher the score, the greater the activity and the more severe the disease. The relationship between the discriminant steroids and SLEDAI was evaluated using Pearson correlation analysis. Among them, three kinds of androgens (Etio, βαβ-Diol, and testosterone), one kind of corticoid (11-DeoxyF), and two kinds of progestins (5α-DHP and 11β-OH-Prog) were negatively correlated with SLEDAI, indicating that, as the levels of these steroids increase, the SLEDAI tends to decrease (Figure 6).

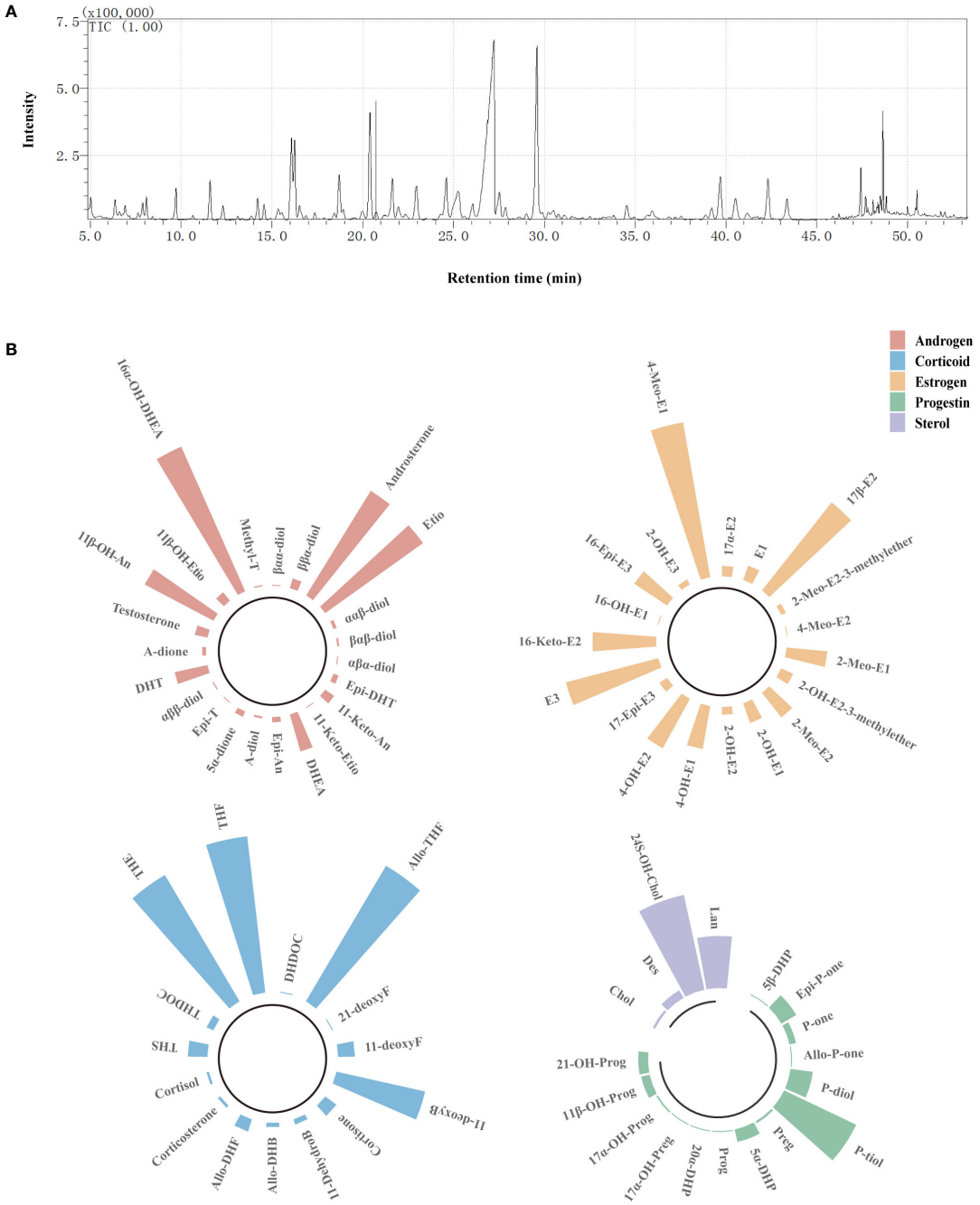

FIGURE 1
Detection of urinary steroids using GC/MS. **(A)** Steroid profile of QC sample. **(B)** Circular bar charts showing the composition of each steroid species. Bar represents the proportion of individual steroids in the corresponding steroid species, and the length of bar was determined on the basis of the average proportion of that steroid in all samples. Red bars refer to androgens, blue bars refer to corticoids, orange bars refer to estrogens, green bars refer to progestins, and purple bars refer to sterols.

The changes in these steroids may reflect aggravation or remission of SLE and may be closely related to the development or pathological process of SLE.

4 Discussion

SLE is a prototypical chronic autoimmune disease characterized by massive autoantibody production and systemic inflammatory responses involving multiple organs (22). The interaction of genetic and environmental factors and hormones lead to the imbalance of immune function, which lead to the destruction of target organs by circulating autoantibodies and inflammatory immune cells (23). The prominent gender and age bias in the pathogenesis of SLE suggested that hormones may play a pivotal role in this disease. However, the comprehensive changes of steroid hormones in patients with SLE have not been explored. Herein, a GC/MS-

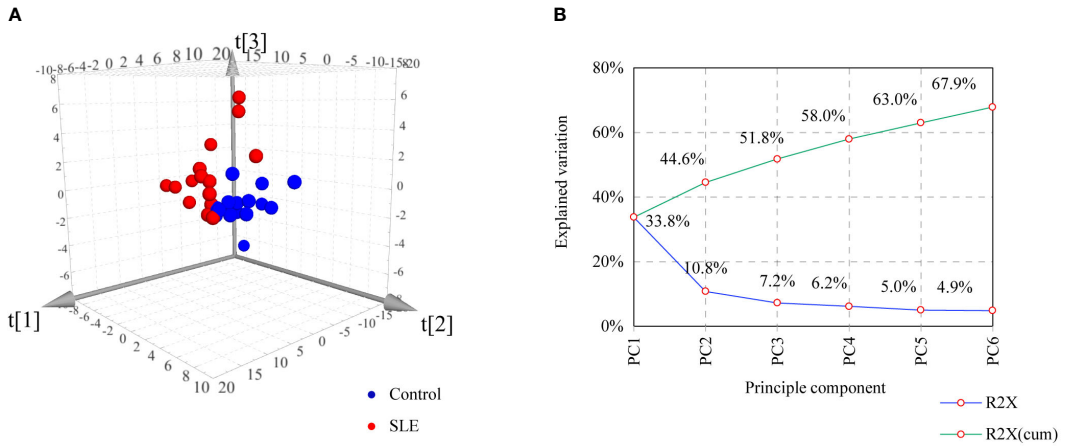

FIGURE 2
PCA of controls and patients with SLE based on urinary steroid profiles. **(A)** Score plot. **(B)** Scree plot showing the percentage of variance explained by individual principal component.

based metabolic profiling analysis was performed to reveal the specific steroid changes related to SLE.

Consistent with previous studies, the total amount of estrogens in patients with SLE had a slight trend of increment in this study. Further species analysis identified the upregulation of three estrogens in SLE: 17-Epi-E3, 17α-E2, and E3. It is generally assumed that estrogen can enhance humoral immune response and accelerate autoimmune disease, such as SLE (24, 25). Clinical studies have reported SLE activity flared up after taking female sex hormones (3). In addition, E2 has been shown to accelerate the immune hyperactivity by enhancing B-cell activity and promoting IL-10 production and to increase the production of immunoglobulin G (IgG) anti-double stranded DNA (dsDNA) antibodies in peripheral blood monocytes of patients with SLE (8). Moreover, the role of estrogen receptor (ER) has been investigated in various models of SLE. Ovariectomized New

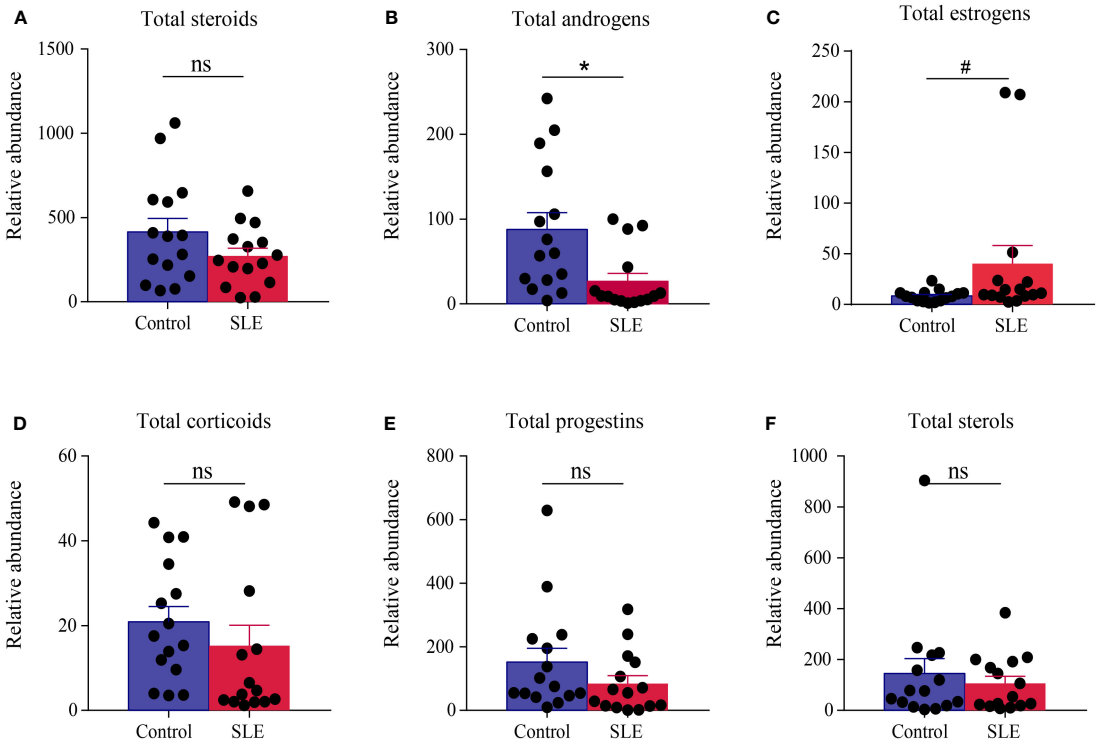

FIGURE 3
Comparison of the total amount of various steroids in the urine of the control group and patients with SLE. **(A)** Total steroids, **(B)** total androgens, **(C)** total estrogens, **(D)** total corticoids, **(E)** total progestins, and **(F)** total sterols. * indicates a significant difference ($P < 0.05$), # indicates a slight difference ($P < 0.1$), and ns indicates no statistical significance ($P > 0.1$).

10.3389/fendo.2023.1164679

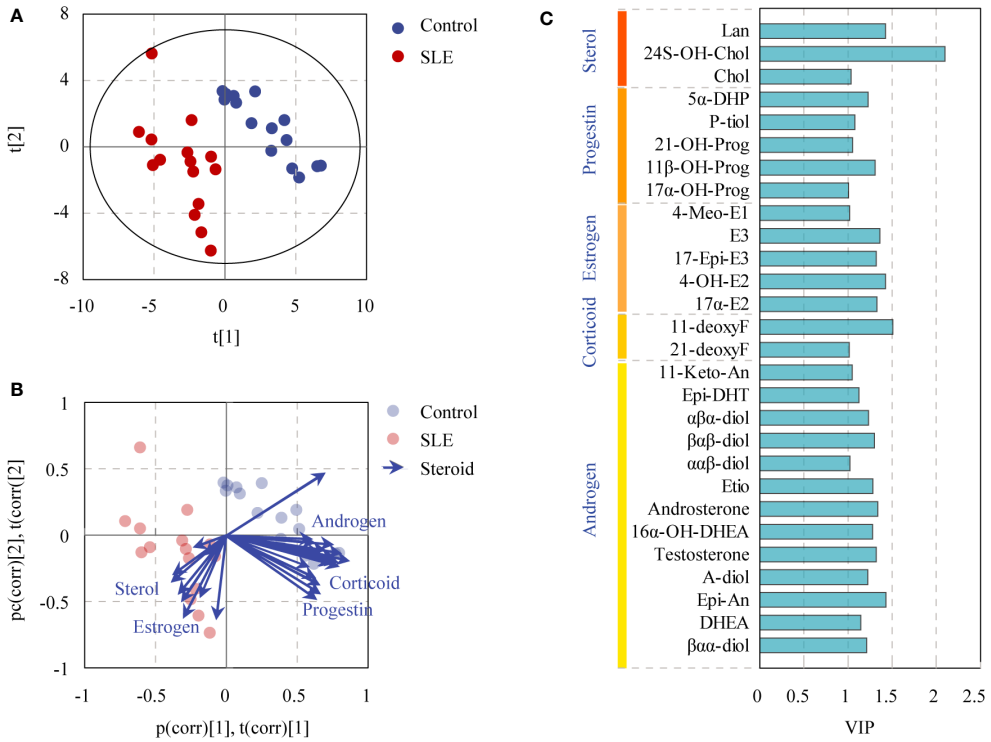

FIGURE 4
OSC PLS-DA of controls and patients with SLE based on urinary steroid profiles. **(A)** OSC PLS-DA score plot, **(B)** biplot displaying co-chart scores and loadings, and **(C)** steroids with VIP > 1.

Zealand Black/White (NZB/W) mice treatment with ERα agonist presented with increased levels of autoantibodies and led to worse mortality than the controls. Inversely, ERα deficiency reduced autoantibodies and glomerulonephritis and improved the survival in spontaneous murine model of lupus (NZB/W F1 mice) (26). Estrogen and ER signaling contribute to the activation of a number of cytokines, contributing to disease pathogenesis and organ pathology in lupus (27). Moreover, estrogen influences T-cell signaling and activation in T cells from patients with SLE. *In vivo* experiments have shown that estrogen downregulated FasL expression in an ER-dependent manner, which is a key molecule in inducing T-cell apoptosis, thereby inhibiting autoreactive T-cell apoptosis, suggesting that estrogen-mediated persistence of autoreactive T cells contributed to autoimmune activity of SLE (28).

Androgens are the precursors of estrogens. This study demonstrated the downregulation of androgens in SLE, not only in the total amount of androgens but also in the levels of nine individual androgens: Etio, βαβ-Diol, testosterone, Epi-An, Epi-DHT, DHEA, 16α-OH-DHEA, A-Diol, and androsterone. Previous studies have also found that women with lupus have lower androgen levels, including testosterone, DHT, DHEA, and DHEA-S (13, 29, 30). Historically, a number of studies have suggested that androgens are protective in SLE. Clinical research studies found that men with hypogonadism are at increased risk of developing SLE (31–33). Whereas in NZB/W mice, the female F1 mice develop severe disease in the first year, but only less than half of male mice developed severely within the same period (5, 34). Mechanisms are complex. Androgens can inhibit B lymphopoiesis and suppress the inflammatory responses of peripheral lymphoid cells through effects on T cells and indirect effects on B cells (35). In addition, androgens can also enhance immune complex clearance (36), a process generally associated with the development of SLE. In addition, low plasma testosterone levels in women may lead to decreased ability of the regulatory T cells to express FoxP3 (37). Treatment of lupus-prone mice with testosterone-like anabolic steroids or DHEA significantly reduced IgG anti-dsDNA antibody and improved survival (38–40). However, effort made on patients with SLE with androgenic compounds got totally inconsistent outcomes (41–45). Hence, much more efforts are still needed.

Then, progestins are also differential hormones in this study. Although the total amount of progestins did not change in lupus, two kinds of progestins (5α-DHP and 11β-OH-Prog) did decease in patients with SLE. Historically, SLE was usually characterized by low progesterone levels, just consistent with this study. In fact, progestins also play roles in the immune system but counteract the pathways affected by estrogen (46). Progesterone can impact $CD4^{+}$T and regulatory T cell differentiation and reduce T-cell proliferation and T-cell–dependent responses and cytokine production. Whereas on B cells, progesterone can reduce antibody production (47). Treatment of female NZB/W mice before onset with continuous progesterone can significantly reduce kidney damage, death, and selective inhibition of pathogenic anti-dsDNA IgG in the kidneys and serum (48). Thus, the immunosuppressive effects of progestins suggested its potential protective role on SLE.

10.3389/fendo.2023.1164679

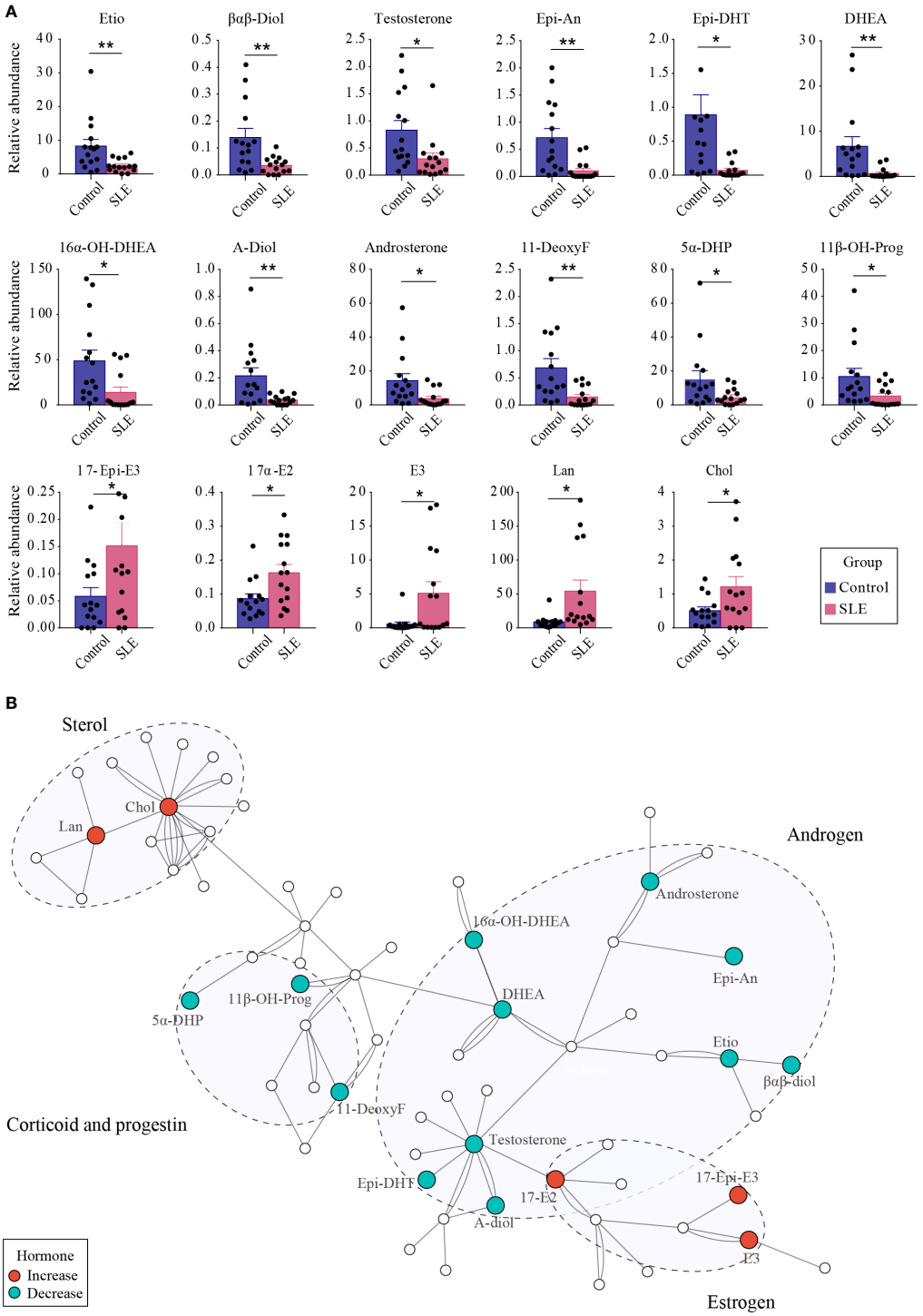

FIGURE 5
The difference of urinary steroids between the control group and patients with SLE. **(A)** Bar plot showing the changing trend of 17 different steroids between the two groups. ** indicates P < 0.01 between groups, and * indicates P < 0.05 between groups. **(B)** Pathway analysis of steroids that were altered in SLE patients. Red dots indicate significantly increased steroids in patients with SLE, whereas green dots indicate significantly reduced steroids.

Some strengths and weaknesses in this study should be noted. First of all, we adopted a latest but also most accurate metabolomics approach to detect the steroid hormone species. In addition, this study used urine sample instead of serum sample as a non-invasive measurement improvement. Unavoidably, the small sample size and the study design being a cross-sectional study were all disadvantages. Furthermore, although our study identified steroids that are significantly different in the urine of patients with SLE and control populations, it does not provide an in-depth study of the causal relationship between the steroid metabolism disorders and SLE.

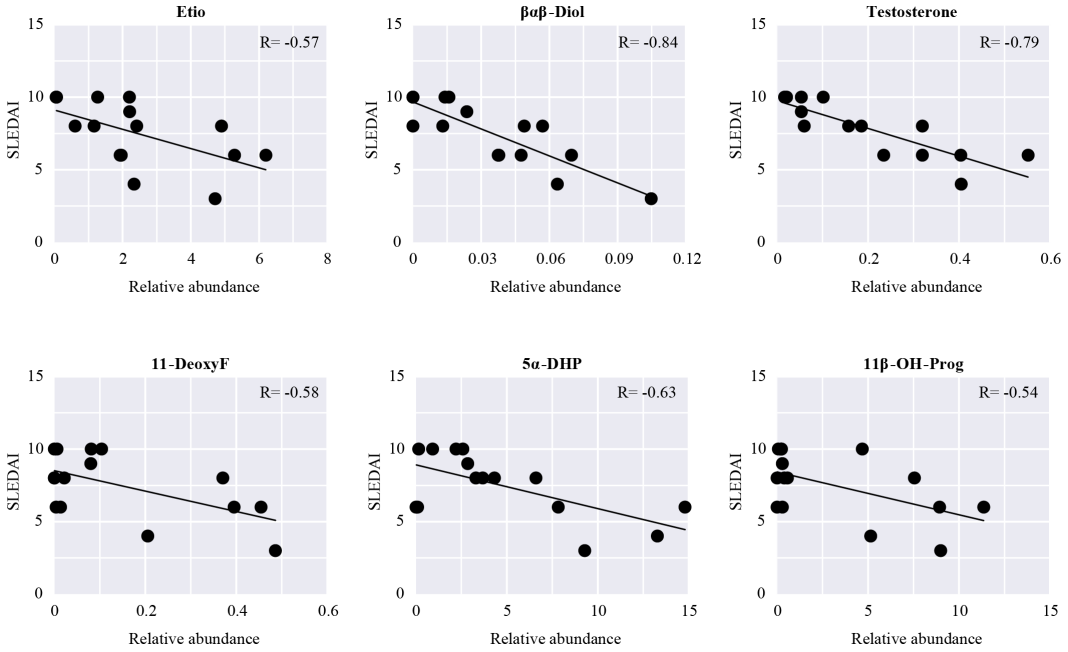

FIGURE 6
Pearson correlation analysis between SLEDAI and the differential steroids in patients with SLE. Scatter plots show steroids significantly related to SLEDAI ($P < 0.05$).

In this study, a GC/MS-based metabolic profiling analysis was performed to reveal the specific changes of steroids in the urine of patients with SLE. Up to 75 kinds of steroids were detected and compared between the controls and patients with SLE. The steroid profile was significantly distinguished in patients with SLE, characterized as the increase of three estrogens and two sterols as well as the decrease of nine androgens, one corticoid, and two progestins. In particular, the changes in androgens were the most significant. In addition to the reported DHEA and testosterone, other androgens such as Etio, androsterone, βαβ-Diol, Epi-An, Epi-DHT, 16α-OH-DHEA, and A-Diol also underwent significant changes. Our study revealed the presence of steroid metabolic disorders in patients with SLE, especially the conversion process of androgens to estrogens. These results may be valuable for further exploration of the pathogenesis of SLE and its potential new treatments.

Data availability statement

The datasets presented in this study can be found in online repositories. The names of the repository/repositories and accession number(s) can be found below: MTBLS7766 (Metabolights).

Ethics statement

The studies involving human participants were reviewed and approved by the Second Affiliated Hospital of Zhejiang Chinese Medical University (No. AF-BG-006-1.0). The patients/participants provided their written informed consent to participate in this study.

Author contributions

JZ designed the project. DW, XZ, and YG performed the experiments. JZ and MY conducted data analysis. LY and DW wrote the manuscript. JZ revised the manuscript. All coauthors have read and agreed to the published version of the manuscript.

Funding

The work was partially supported by the National Natural Science Foundation of China (nos. 81873102 and 81703966), the Zhejiang Provincial Natural Science Foundation of China (no. LY22H290006), the Joint Funds of the Zhejiang Provincial Natural Science Foundation of China (no. LBY22H270003), and the Research Project of Zhejiang Traditional Chinese Medicine Administration (no. 2022ZB171).

Acknowledgments

We appreciate the technical support from the Public Platform of Medical Research Center, Academy of Chinese Medical Science, Zhejiang Chinese Medical University.

Conflict of interest

The authors declare that the research was conducted in the absence of any commercial or financial relationships that could be construed as a potential conflict of interest.

Publisher's note

All claims expressed in this article are solely those of the authors and do not necessarily represent those of their affiliated organizations, or those of the publisher, the editors and the reviewers. Any product that may be evaluated in this article, or claim that may be made by its manufacturer, is not guaranteed or endorsed by the publisher.

Supplementary material

The Supplementary Material for this article can be found online at: https://www.frontiersin.org/articles/10.3389/fendo.2023.1164679/full#supplementary-material

References

1. Lisnevskaia L, Murphy G, Isenberg D. Systemic lupus erythematosus. *Lancet (London England)* (2014) 384(9957):1878–88. doi: 10.1016/s0140-6736(14)60128-8

2. Tsokos GC, Lo MS, Reis PC, Sullivan KE. New insights into the immunopathogenesis of systemic lupus erythematosus. *Nat Rev Rheumatol* (2016) 12 (12):716–30. doi: 10.1038/nrrheum.2016.186

3. Culwell K, Curtis K, del Carmen Cravioto M. Safety of contraceptive method use among women with systemic lupus erythematosus: a systematic review. *Obstet Gynecol* (2009) 114:341–53. doi: 10.1097/AOG.0b013e3181ae9c64

4. Petri M, Howard D, Repke J. Frequency of lupus flare in pregnancy. the Hopkins lupus pregnancy center experience. *Arthritis Rheum* (1991) 34(12):1538–45. doi: 10.1002/art.1780341210

5. Gubbels Bupp MR, Jorgensen TN, Kotzin BL. Identification of candidate genes that influence sex hormone-dependent disease phenotypes in mouse lupus. *Genes Immun* (2008) 9(1):47–56. doi: 10.1038/sj.gene.6364447

6. Markle JG, Frank DN, Mortin-Toth S, Robertson CE, Feazel LM, Rolle-Kampczyk U, et al. Sex differences in the gut microbiome drive hormone-dependent regulation of autoimmunity. *Science* (2013) 339(6123):1084–8. doi: 10.1126/science.1233521

7. Ngo S, Steyn F, McCombe P. Gender differences in autoimmune disease. *Front Neuroendocrinol* (2014) 35(3):347–69. doi: 10.1016/j.yfrne.2014.04.004

8. Kanda N, Tsuchida T, Tamaki K. Estrogen enhancement of anti–double-stranded DNA antibody and immunoglobulin G production in peripheral blood mononuclear cells from patients with systemic lupus erythematosus. *Arthritis Rheum* (1999) 42 (2):328–37. doi: 10.1002/1529-0131(199902)42:2<328::AID-ANR16>3.0.CO;2-#

9. Mor G, Muñoz A, Redlinger R, Silva I, Song J, Lim C, et al. The role of the Fas/Fas ligand system in estrogen-induced thymic alteration. *Am J Reprod Immunol* (2001) 46 (4):298–307. doi: 10.1034/j.1600-0897.2001.d01-16.x

10. Svenson J, EuDaly J, Ruiz P, Korach K, Gilkeson G. Impact of estrogen receptor deficiency on disease expression in the NZM2410 lupus prone mouse. *Clin Immunol (Orlando Fla)* (2008) 128(2):259–68. doi: 10.1016/j.clim.2008.03.508

11. Sakiani S, Olsen NJ, Kovacs WJ. Gonadal steroids and humoral immunity. *Nat Rev Endocrinol* (2013) 9(1):56–62. doi: 10.1038/nrendo.2012.206

12. Mok CC, Lau CS. Profile of sex hormones in male patients with systemic lupus erythematosus. *Lupus* (2000) 9(4):252–7. doi: 10.1191/096120300680198926

13. Treadwell E, Wiley K, Word B, Melchior W, Tolleson W, Gopee N, et al. Prolactin and dehydroepiandrosterone levels in women with systemic lupus erythematosus: the role of the extrapituitary prolactin promoter polymorphism at -1149G/T. *J Immunol Res* (2015) 2015:435658. doi: 10.1155/2015/435658

14. Klein SL, Flanagan KL. Sex differences in immune responses. *Nat Rev Immunol* (2016) 16(10):626–38. doi: 10.1038/nri.2016.90

15. Stanczyk FZ, Cho MM, Endres DB, Morrison JL, Patel S, Paulson RJ. Limitations of direct estradiol and testosterone immunoassay kits. *Steroids* (2003) 68(14):1173–8. doi: 10.1016/j.steroids.2003.08.012

16. Santen RJ, Demers L, Ohorodnik S, Settlage J, Langecker P, Blanchett D, et al. Superiority of gas chromatography/tandem mass spectrometry assay (GC/MS/MS) for estradiol for monitoring of aromatase inhibitor therapy. *Steroids* (2007) 72(8):666–71. doi: 10.1016/j.steroids.2007.05.003

17. Kushnir MM, Rockwood AL, Bergquist J, Varshavsky M, Roberts WL, Yue B, et al. High-sensitivity tandem mass spectrometry assay for serum estrone and estradiol. *Am J Clin Pathol* (2008) 129(4):530–9. doi: 10.1309/LC03BHQ5XJPJYEKG

18. Taylor AE, Keevil B, Huhtaniemi IT. Mass spectrometry and immunoassay: how to measure steroid hormones today and tomorrow. *Eur J Endocrinol* (2015) 173(2):D1–12. doi: 10.1530/EJE-15-0338

19. Conklin SE, Knezevic CE. Advancements in the gold standard: measuring steroid sex hormones by mass spectrometry. *Clin Biochem* (2020) 82:21–32. doi: 10.1016/j.clinbiochem.2020.03.008

20. Moon JY, Jung HJ, Moon MH, Chung BC, Choi MH. Heat-map visualization of gas chromatography-mass spectrometry based quantitative signatures on steroid metabolism. *J Am Soc Mass Spectrometry* (2009) 20(9):1626–37. doi: 10.1016/j.jasms.2009.04.020

21. Moon J-Y, Ha YW, Moon MH, Chung BC, Choi MH. Systematic error in gas chromatography-mass spectrometry–based quantification of hydrolyzed urinary steroids. *Cancer Epidemiol Biomarkers Prev* (2010) 19(2):388–97. doi: 10.1158/1055-9965.epi-09-0581

22. Guidelines for referral and management of systemic lupus erythematosus in adults. American college of rheumatology *Ad hoc* committee on systemic lupus erythematosus guidelines. *Arthritis Rheum* (1999) 42(9):1785–96. doi: 10.1002/1529-0131(199909)42:9<1785::aid-anr1>3.0.co;2

23. Mohan C, Putterman C. Genetics and pathogenesis of systemic lupus erythematosus and lupus nephritis. *Nat Rev Nephrol* (2015) 11(6):329–41. doi: 10.1038/nrneph.2015.33

24. Mcmurray RW. Estrogen, prolactin, and autoimmunity: actions and interactions. *Int Immunopharmacol* (2001) 1(6):995–1008. doi: 10.1016/S1567-5769(01)00045-5

25. Moulton VR. Sex hormones in acquired immunity and autoimmune disease. *Front Immunol* (2018) 9:2279. doi: 10.3389/fimmu.2018.02279

26. Li J, McMurray R. Effects of estrogen receptor subtype-selective agonists on autoimmune disease in lupus-prone NZB/NZW F1 mouse model. *Clin Immunol (Orlando Fla)* (2007) 123(2):219–26. doi: 10.1016/j.clim.2007.01.008

27. Kassi E, Moutsatsou P. Estrogen receptor signaling and its relationship to cytokines in systemic lupus erythematosus. *J Biomed Biotechnol* (2010) 2010:317452. doi: 10.1155/2010/317452

28. Kim WU, Min SY, Hwang SH, Yoo SA, Kim KJ, Cho CS. Effect of oestrogen on T cell apoptosis in patients with systemic lupus erythematosus. *Clin Exp Immunol* (2010) 161(3):453–8. doi: 10.1111/j.1365-2249.2010.04194.x

29. Jungers P, Nahoul K, Pelissier C, Dougados M, Tron F, Bach JF. Low plasma androgens in women with active or quiescent systemic lupus erythematosus. *Arthritis Rheum* (1982) 25(4):454–7. doi: 10.1002/art.1780250415

30. Lahita RG, Bradlow HL, Ginzler E, Pang S, New M. Low plasma androgens in women with systemic lupus erythematosus. *Arthritis Rheum* (1987) 30(3):241–8. doi: 10.1002/art.1780300301

31. Jimenez-Balderas FJ, Tapia-Serrano R, Fonseca ME, Arellano J, Beltran A, Yanez P, et al. High frequency of association of rheumatic/autoimmune diseases and untreated male hypogonadism with severe testicular dysfunction. *Arthritis Res* (2001) 3(6):362–7. doi: 10.1186/ar328

32. Seminog OO, Seminog AB, Yeates D, Goldacre MJ. Associations between klinefelter's syndrome and autoimmune diseases: English national record linkage studies. *Autoimmunity* (2015) 48(2):125–8. doi: 10.3109/08916934.2014.968918

33. Baillargeon J, Al Snih S, Raji MA, Urban RJ, Sharma G, Sheffield-Moore M, et al. Hypogonadism and the risk of rheumatic autoimmune disease. *Clin Rheumatol* (2016) 35(12):2983–7. doi: 10.1007/s10067-016-3330-x

34. Roubinian JR, Talal N, Greenspan JS, Goodman JR, Siiteri PK. Delayed androgen treatment prolongs survival in murine lupus. *J Clin Invest* (1979) 63 (5):902–11. doi: 10.1172/JCI109390

35. Gubbels Bupp MR, Jorgensen TN. Androgen-induced immunosuppression. *Front Immunol* (2018) 9:794. doi: 10.3389/fimmu.2018.00794

36. Shear HL, Roubinian JR, Gil P, Talal N. Clearance of sensitized erythrocytes in NZB/NZW mice. effects of castration and sex hormone treatment. *Eur J Immunol* (1981) 11(10):776–80. doi: 10.1002/eji.1830111008

37. Singh RP, Bischoff DS. Sex hormones and gender influence the expression of markers of regulatory T cells in SLE patients. *Front Immunol* (2021) 12:619268. doi: 10.3389/fimmu.2021.619268

38. Verheul HA, Stimson WH, den Hollander FC, Schuurs AH. The effects of nandrolone, testosterone and their decanoate esters on murine lupus. *Clin Exp Immunol* (1981) 44(1):11–7. Available at: https://pubmed.ncbi.nlm.nih.gov/6973425/.

39. Lucas JA, Ahmed SA, Casey ML, MacDonald PC. Prevention of autoantibody formation and prolonged survival in new Zealand black/New Zealand white F1 mice fed dehydroisoandrosterone. *J Clin Invest* (1985) 75(6):2091–3. doi: 10.1172/JCI111929

40. Verheul HA, Deckers GH, Schuurs AH. Effects of nandrolone decanoate or testosterone decanoate on murine lupus: further evidence for a dissociation of autoimmunosuppressive and endocrine effects. *Immunopharmacology* (1986) 11 (2):93–9. doi: 10.1016/0162-3109(86)90029-9

41. Lahita RG, Cheng CY, Monder C, Bardin CW. Experience with 19-nortestosterone in the therapy of systemic lupus erythematosus: worsened disease after treatment with 19-nortestosterone in men and lack of improvement in women. *J Rheumatol* (1992) 19(4):547–55. Available at: https://pubmed.ncbi.nlm.nih.gov/1593576/.

42. Chang DM, Lan JL, Lin HY, Luo SF. Dehydroepiandrosterone treatment of women with mild-to-moderate systemic lupus erythematosus: a multicenter randomized, double-blind, placebo-controlled trial. *Arthritis Rheum* (2002) 46 (11):2924–7. doi: 10.1002/art.10615

43. Petri MA, Mease PJ, Merrill JT, Lahita RG, Iannini MJ, Yocum DE, et al. Effects of prasterone on disease activity and symptoms in women with active systemic lupus erythematosus. *Arthritis Rheum* (2004) 50(9):2858–68. doi: 10.1002/art.20427

44. Marder W, Somers EC, Kaplan MJ, Anderson MR, Lewis EE, McCune WJ. Effects of prasterone (dehydroepiandrosterone) on markers of cardiovascular risk and bone turnover in premenopausal women with systemic lupus erythematosus: a pilot study. *Lupus* (2010) 19(10):1229–36. doi: 10.1177/0961203310371156

45. Letchumanan P, Thumboo J. Danazol in the treatment of systemic lupus erythematosus: a qualitative systematic review. *Semin Arthritis Rheum* (2011) 40 (4):298–306. doi: 10.1016/j.semarthrit.2010.03.005

46. Hughes G. Progesterone and autoimmune disease. *Autoimmun Rev* (2012) 11: A502–514. doi: 10.1016/j.autrev.2011.12.003

47. Tan IJ, Peeva E, Zandman-Goddard G. Hormonal modulation of the immune system - a spotlight on the role of progestogens. *Autoimmun Rev* (2015) 14(6):536–42. doi: 10.1016/j.autrev.2015.02.004

48. Hughes GC, Martin D, Zhang K, Hudkins KL, Alpers CE, Clark EA, et al. Decrease in glomerulonephritis and Th1-associated autoantibody production after progesterone treatment in NZB/NZW mice. *Arthritis Rheum* (2010) 60(6):1775–84. doi: 10.1002/art.24548

frontiers | Frontiers in Endocrinology

TYPE Mini Review
PUBLISHED 04 October 2023
DOI 10.3389/fendo.2023.1230045

OPEN ACCESS

EDITED BY
Sijung Yun,
Predictiv Care, Inc., United States

REVIEWED BY
Leandro Kasuki,
Instituto Estadual do Cérebro Paulo Niemeyer (IECPN), Brazil

*CORRESPONDENCE
Nareshni Moodley
nareshni.moodley@gmail.com

RECEIVED 27 May 2023
ACCEPTED 21 August 2023
PUBLISHED 04 October 2023

CITATION
Moodley N (2023) Copeptin analysis in endocrine disorders.
Front. Endocrinol. 14:1230045.
doi: 10.3389/fendo.2023.1230045

Copeptin analysis in endocrine disorders

Nareshni Moodley[1,2]*

[1]Department of Chemical Pathology, Inkosi Albert Luthuli Central Hospital, National Health Laboratory Services, Durban, South Africa, [2]Department of Laboratory Medicine (Chemical Pathology), University of Kwa-Zulu Natal, Durban, South Africa

Copeptin is cleaved from the same precursor as arginine vasopressin and is released in equimolar amounts with arginine vasopressin from the posterior pituitary in response to the same stimuli. Its level of stability in the blood, quick and simple analysis, and ease of automation make it much easier to analyze than arginine vasopressin, thereby offering a suitable alternative to measuring arginine vasopressin in endocrine disorders. Research has demonstrated the suitability of copeptin in adults for the differentiation of arginine vasopressin resistance and arginine vasopressin deficiency from primary polydipsia, in addition to the early identification of arginine vasopressin deficiency following pituitary surgery; however, further research is still required in the Syndrome of Inappropriate Antidiuretic Hormone (SIADH) and the pediatric population.

KEYWORDS

copeptin, diabetes insipidus, arginine vasopressin, endocrine, biomarker

1 Introduction

Copeptin is the 39-amino acid glycopeptide C-terminal portion of the precursor peptides preprovasopressin and provasopressin, from which arginine vasopressin (AVP) is also cleaved for release. AVP plays a pivotal role in the endocrine stress response by stimulating adrenocorticotrophic hormone release and in osmotic and cardiovascular homeostasis by promoting water conservation in the body *via* the kidney. It is predominantly produced in the hypothalamus but also in other tissues like the sympathetic ganglia, adrenal glands, and testes. The short plasma half-life of AVP of 5-20 min, high instability in plasma even when frozen, and high degree of platelet binding (over 90%) requiring complete pre-analytical removal of platelets make AVP difficult to measure. Copeptin is stable in plasma, needs no special pre-analytical treatment, and can be easily measured using many assays with small sample volumes and results in as little as 0.5-2.5 hours (1–3). Studies have found that blood copeptin levels are similar to blood AVP levels, making copeptin a suitable alternative to AVP (4, 5). Balanescu et al. reported that copeptin concentrations correlated more closely with plasma osmolality than AVP (5). Copeptin has also been shown to be stable for at least 7 days at room temperature and 14 days at 4°C (3, 6).

2 What we know about copeptin, the molecule

2.1 Formation

The precursor peptides preprovasopressin and provasopressin are mainly produced in the magnocellular neurons of the hypothalamus and are enzymatically separated into the nine-amino acid peptide arginine vasopressin (AVP), 39 amino acid copeptin (CTproAVP), and neurophysin II, all of which are released into the blood in equimolar concentrations from the posterior lobe of the pituitary gland primarily in response to decreased blood volume, high blood osmolality, stress, and/or low blood pressure (Figure 1) (1, 2).

2.2 Physiological function

The physiological role of copeptin is not fully defined; however, studies have shown that it is a chaperone-like molecule for pro-AVP formation and that it monitors protein folding and interacts with many glycosylated proteins through interaction with the calnexin/calreticulin system, thus increasing the formation of active hormone and decreasing the production of inactive hormone (2).

2.3 Elimination

The elimination of copeptin is also not fully understood; however, it is eliminated at least in part by the kidneys, with an inverse relationship between copeptin blood levels and glomerular filtration rate in patients with chronic kidney disease (2).

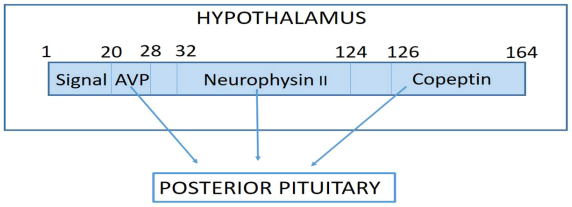

FIGURE 1
Pre-provasopressin is the precursor hormone of arginine Vasopressin (AVP) which is formed in the magnocellular nuclei of the hypothalamus, where the signal peptide is cleaved to form pro-AVP. Pro-AVP folds to place AVP in the binding pocket neurophysin II, so that it is protected from proteolysis. During transport to the posterior pituitary, AVP is cleaved off pro-AVP and finally another cleavage step seperates neurophysin II from copeptin with complete processing of the precursor hormones at the level of the posterior pituitary where all three molecules are stored and released into the blood in response to stimuli such as increased Osmolality, decreased blood pressure, decreased blood volume and/or stress.

2.4 Measurement

Numerous copeptin immunoassays and enzyme-linked immunosorbent (ELISA) assays have been developed. The two most studied immunoassays are an original sandwich immunoluminometric assay (LIA) and an automated immunofluorescent immunoassay (on the KRYPTOR platform), which show good correlation with very low and high levels of copeptin. However, the ELISA assay correlates poorly with both immunoassay methods, and therefore cut-offs developed on the immunoassay systems cannot be used for the ELISA assay results (2, 3).

3 Clinical applications in endocrinology

3.1 Diabetes insipidus

Diabetes insipidus (DI) is a condition characterized by disordered arginine vasopressin (AVP) secretion or action, resulting in the production of hypotonic urine (<300 mOsm/kg H2O) >50 ml/kg/day, with concurrent polydipsia (>3 L/day). It results from either decreased secretion of AVP (AVP deficiency) or resistance to AVP action (7).

AVP deficiency has various etiologies, such as pituitary or hypothalamic median eminence lesions, trauma, pituitary surgery, neoplastic, vascular, autoimmune, infectious, granulomatous, or hereditary forms (2, 7). Complete AVP resistance is due to a lack of aquaporin 2-mediated water reabsorption in the renal collecting duct, which may be due to electrolyte disturbances (hypercalcemia or hypokalemia, renal pathologies, gene mutations in the key proteins vasopressin V2 receptor or aquaporin 2) or secondary to adverse drug effects (e.g., lithium) (2, 3).

Patients with primary polydipsia have chronic excessive fluid intake (which can occur in health-conscious people who want to drink large amounts of water, who have dependency disorders or reduced thirst thresholds, and in psychiatric patients) with subsequent excretion of hypotonic urine, hence presenting similarly to DI. It is important to differentiate between AVP resistance, AVP deficiency, and primary polydipsia as their treatment differs and incorrect management could have dire consequences (2, 3).

The water deprivation test is the diagnostic gold standard for differentiating DI from its main differential diagnosis, primary polydipsia. During this test, patients are not allowed to ingest any water for a maximum period of 17 hours or until blood sodium concentrations exceed 150 mmol/l or 3-5% of the patient's initial body weight is lost, with measurements of urine excretion, urine osmolality, blood sodium, and blood osmolality during the water deprivation period. At the end of the water deprivation period, exogenous AVP is administered, and changes in urine osmolality are assessed for a period of time according to institutional protocols. Complete AVP deficiency is diagnosed based on the

recommendations of Miller et al. for a urine osmolality that does not rise to >300 mOsm/kg during the water deprivation period with a >50% increase post-exogenous AVP administration. AVP-resistant patients have no increase in urine osmolality after exogenous AVP administration, and partially AVP-deficient patients have a urine osmolality between 300 and 800 mOsm/kg during water deprivation with a >9% increase after AVP injection; however, this test has only 70% diagnostic accuracy and was developed in a small cohort of 29 patients. Current methods utilized to assess post-operative DI (serum and urine sodium, and osmolality and fluid balance determination) have low sensitivity and specificity (<50%) (3, 8). Studies have reported that copeptin is useful in various clinical conditions, especially in the differential diagnosis of polyuria-polydipsia syndrome (2, 9, 10).

Research has shown that an unstimulated, random copeptin cut-off of >21.4 pmol/L can diagnose AVP resistance with 100% sensitivity and specificity for diagnosis. Differentiating AVP deficiency from primary polydipsia does require stimulation testing due to the similar baseline copeptin values in these two conditions. The copeptin-based hypertonic saline stimulation test and the arginine stimulation test have been shown to have high diagnostic accuracy of 97% and 93%, respectively, for DI. The copeptin-based hypertonic saline infusion test has a diagnostic accuracy of 95-96.5% for partial DI and is safe and better tolerated than the water deprivation test (2, 10). Arginine is a less effective stimulus than copeptin, and therefore has a lower diagnostic accuracy but requires less blood sodium monitoring and is better tolerated (2). Atila et al. also assessed the copeptin-based glucagon stimulation test and found that glucagon-stimulated copeptin in healthy participants, using a copeptin cut-off level of 4.6 pmol/l, had a sensitivity of 100% and a specificity of 90% to discriminate between AVP deficiency and primary polydipsia (11). It has also been shown that post-operative copeptin results in patients after pituitary surgery are much lower in those who develop AVP deficiency than in those who do not (2, 8, 12–14); therefore, it could greatly assist in the prompt diagnosis of AVP deficiency in these subjects.

3.2 Syndrome of inappropriate antidiuretic hormone

SIADH is characterized by inappropriately elevated plasma AVP levels, decreased blood osmolality, inappropriately high urine osmolality, and normal or increased blood volume. It is a common cause of euvolemic hyponatremia in hospitalized patients. Causes of SIADH include brain pathology (such as surgery, tumors, infection, prolonged seizures, psychiatric disease, and stress), non-CNS tumors, lung disease, and certain medications (anticonvulsants, antiparkinsonian drugs, antipsychotics, antipyretics, antidepressants, angiotensin-converting enzyme inhibitors, antineoplastic drugs, and first-generation sulfonylureas) (15).

SIADH is diagnosed when blood osmolality is <275 mOsm/kg, blood sodium is ≤130 mmol/l, urine osmolality is greater than blood osmolality, urine sodium is high (usually >40 to 60 mmol/l), and cardiac, hepatic, renal, thyroid or adrenal failure, effects of pituitary surgery, diuretic therapy, or medications known to stimulate AVP have been excluded (15).

One study found persistently high copeptin values (>38 pmol/l) in patients with lung cancer and SIADH; however, cancer patients have many other reasons for increased AVP secretion, such as comorbidities, medications, vomiting, nausea, dehydration, or stress, and there is still insufficient evidence to support this (2). Nevertheless, this is an area of interest for future studies involving copeptin.

There has been one study that showed that the ratio of copeptin to urinary sodium could help differentiate SIADH from conditions with decreased blood volume; however, copeptin alone was insufficient (3). More research is required in this area to confirm this.

4 Physiologic range and pathologic cut-offs

Plasma concentrations of copeptin show a wide range between 1 and 13.8 pmol/l, with a median concentration of 4.2 pmol/l in healthy, normal-osmotic volunteers. Men have slightly but significantly higher copeptin levels than women. Copeptin has not been shown to be influenced by age, circadian rhythm, food intake or phases of the menstrual cycle, but copeptin levels decrease with oral fluid intake as low as 200 to 300ml (2, 3). There were no gender differences in copeptin levels during hypertonic saline infusion tests (3).

A random copeptin value of 21.4 pmol/l was found to have a diagnostic accuracy of 100% for AVP resistance (9). Another study also found random copeptin levels >20 pmol/l as good cut-offs for AVP resistance, with post-overnight water deprivation levels of <2.6 pmol/l indicating AVP deficiency (diagnostic accuracy of 78%), and a ratio of Δplasma copeptin levels before and after water deprivation to plasma sodium post water deprivation had a high diagnostic accuracy of 94% for AVP deficiency (3).

Stimulated copeptin values for differentiating AVP deficiency from primary polydipsia depend on the type of stimulation test performed. A cut-off of ≤4.9 pmol/l post-hypertonic saline infusion test has been suggested to diagnose AVP deficiency with high diagnostic accuracy of 96% (3, 9, 10). An arginine infusion test cut-off of ≤3.8 pmol/l has been used to diagnose AVP deficiency (2), and the possible cut-off for the glucagon stimulation test was found to be 4.6 pmol/l (11).

Initially, an insulin tolerance test was used to induce hypoglycemia in patients 3 months after transsphenoidal pituitary surgery, which showed low copeptin levels in patients with AVP deficiency of 3.7 ± 0.7 pmol/l, with hypoglycemic copeptin levels of <4.75 pmol/l having the best diagnostic accuracy of 100%. The surgery itself is a stressful event that can trigger AVP release; therefore, unstimulated post-surgery cut-offs were assessed. Suggested post-pituitary surgery cut-offs on day 1 post-op are <2.5 pmol/l for AVP deficiency and >30 pmol/l indicate no AVP deficiency (3, 8) or <3.6 pmol/l for AVP deficiency (14), whereas one study by Jang et al. found that day 2 copeptin values <3.1 pmol/l showed the best performance in predicting permanent AVP

TABLE 1 Published copeptin cut-off values.

Clinical Scenario	Cut-off (pmol/l)
AVP resistance	>21,4 (9)
Post-overnight water deprivation test	<2,6 indicative of AVP deficiency (3)
Hypertonic saline infusion test	≤4,9 (3, 9, 10)
Arginine infusion test	≤3,8 (2)
Glucagon stimulation test	<4,6 (11)
Post-pituitary surgery - Day 1 - Day 2 - 3 months - 3 months + insulin tolerance test	- <2,5= AVP deficiency; >30= no AVP deficiency (3, 8) - <3,1= AVP deficiency (13) - <1,9+normal serum sodium= AVP deficiency; ≥3,5= no AVP deficiency (16) - <4,75 (3)

deficiency (13). Kim et al. found that 3 months after transsphenoidal pituitary surgery, copeptin values of <1.9 pmol/l with normal serum sodium results were the best cut-off value for permanent AVP deficiency with a diagnostic accuracy of 81.8%; however, a copeptin value of ≥3.5 pmol/l excluded AVP deficiency with a negative predictive value of 100% (16). The cut-off values are summarized in Table 1.

5 Discussion

In the field of endocrinology, copeptin has been shown to play an important role in differentiating DI from primary polydipsia (2, 9, 10) and there are promising results regarding its utility in the diagnosis of post-pituitary surgery DI (2, 8, 12–14). The determination of appropriate cut-offs in a larger cohort and different populations is still needed. Another area that requires more research is the utility of copeptin in SIADH with other biomarkers. There are very few studies in the pediatric population, which is an important area to highlight in future studies on the utility of copeptin in endocrinology.

Author contributions

The author confirms being the sole contributor of this work and has approved it for publication.

Conflict of interest

The author declares that the research was conducted in the absence of any commercial or financial relationships that could be construed as a potential conflict of interest.

Publisher's note

References

1. Bolignano D, Cabassi A, Fiaccadori E, Ghigo E, Pasquali R, Peracino A, et al. Copeptin (CTproAVP), a new tool for understanding the role of vasopressin in pathophysiology. *Clin Chem Lab Med (CCLM)* (2014) 52(10):1447–56. doi: 10.1515/cclm-2014-0379

2. Christ-Crain M, Refardt J, Winzeler B. Approach to the patient:"Utility of the copeptin assay". *J Clin Endocrinol Metab* (2022) 107(6):1727–38. doi: 10.1210/clinem/dgac070

3. Refardt J, Winzeler B, Christ-Crain M. Copeptin and its role in the diagnosis of diabetes insipidus and the syndrome of inappropriate antidiuresis. *Clin Endocrinol* (2019) 91(1):22–32. doi: 10.1111/cen.13991

4. Jochberger S, Luckner G, Mayr VD, Wenzel V, Morgenthaler NG, Friesenecker BE, et al. Course of vasopressin and copeptin plasma concentrations in a patient with severe septic shock. *Anaesthesia Intensive Care* (2006) 34(4):498–500. doi: 10.1177/0310057X0603400415

5. Balanescu S, Kopp P, Gaskill MB, Morgenthaler NG, Schindler C, Rutishauser J. Correlation of plasma copeptin and vasopressin concentrations in hypo-, iso-, and hyperosmolar States. *J Clin Endocrinol Metab* (2011) 96(4):1046–52. doi: 10.1210/jc.2010-2499

6. Morgenthaler NG, Struck J, Alonso C, Bergmann A. Assay for the measurement of copeptin, a stable peptide derived from the precursor of vasopressin. *Clin Chem* (2006) 52(1):112–9. doi: 10.1373/clinchem.2005.060038

7. Christ-Crain M. Diabetes insipidus: new concepts for diagnosis. *Neuroendocrinology* (2020) 110(9-10):859–67. doi: 10.1159/000505548

8. Winzeler B, Zweifel C, Nigro N, Arici B, Bally M, Schuetz P, et al. Postoperative copeptin concentration predicts diabetes insipidus after pituitary surgery. *J Clin Endocrinol Metab* (2015) 100(6):2275–82. doi: 10.1210/jc.2014-4527

9. Timper K, Fenske W, Kühn F, Frech N, Arici B, Rutishauser J, et al. Diagnostic accuracy of copeptin in the differential diagnosis of the polyuria-polydipsia syndrome: a prospective multicenter study. *J Clin Endocrinol Metab* (2015) 100(6):2268–74. doi: 10.1210/jc.2014-4507

10. Fenske W, Refardt J, Chifu I, Schnyder I, Winzeler B, Drummond J, et al. A copeptin-based approach in the diagnosis of diabetes insipidus. *New Engl J Med* (2018) 379(5):428–39. doi: 10.1056/NEJMoa1803760

11. Atila C, Christ-Crain M, Gaisl O, Szinnai G, Vogt D, Werlen L. ODP313 glucagon-stimulated copeptin measurements in the differential diagnosis of diabetes insipidus: A double-blind randomized placebo-controlled study. *J Endocr Soc* (2022) 6 (Suppl 1):A492. doi: 10.1210/jendso/bvac150.1022

12. de Vries F, Lobatto DJ, Verstegen MJ, van Furth WR, Pereira AM, Biermasz NR. Postoperative diabetes insipidus: how to define and grade this complication? *Pituitary* (2021) 24(2):284–91. doi: 10.1007/s11102-020-01083-7

13. Jang HN, Kang H, Kim YH, Lim HS, Lee MK, Lee KR, et al. Serum copeptin levels at day two after pituitary surgery and ratio to baseline predict postoperative central diabetes insipidus. *Pituitary* (2022) 2:1–1. doi: 10.1007/s11102-022-01278-0

14. Rostom H, Noronha S, Jafar-Mohammadi B, May C, Borg A, Halliday J, et al. Post-pituitary surgery copeptin analysis as a 'rule-out'test for post-operative diabetes insipidus. *Endocrine* (2023) 79(2):358–64. doi: 10.1007/s12020-022-03220-7

15. Rifai N. *Tietz textbook of clinical chemistry and molecular diagnostics-e-book*. St. Louis, Missouri: Elsevier Health Sciences (2017).

16. Kim YH, Kim YH, Je YS, Lee KR, Lim HS, Kim JH. Changes in copeptin levels before and 3 months after transsphenoidal surgery according to the presence of postoperative central diabetes insipidus. *Sci Rep* (2021) 11(1):17240. doi: 10.1038/s41598-021-95500-x

frontiers | Frontiers in Endocrinology

TYPE Original Research
PUBLISHED 25 October 2023
DOI 10.3389/fendo.2023.1270772

OPEN ACCESS

EDITED BY
Sijung Yun,
Predictiv Care, Inc., United States

REVIEWED BY
Binhua Liang,
Public Health Agency of Canada (PHAC), Canada
Hye Kyung Lee,
National Institute of Diabetes and Digestive and Kidney Diseases (NIH), United States

*CORRESPONDENCE
Xinyan Wang
602055@hrbmu.edu.cn
Lina Chen
chenlina@ems.hrbmu.edu.cn

†These authors have contributed equally to this work

RECEIVED 01 August 2023
ACCEPTED 03 October 2023
PUBLISHED 25 October 2023

CITATION
Fu L, Li M, Lv J, Yang C, Zhang Z, Qin S, Li W, Wang X and Chen L (2023) Deep neural network for discovering metabolism-related biomarkers for lung adenocarcinoma. *Front. Endocrinol.* 14:1270772. doi: 10.3389/fendo.2023.1270772

Deep neural network for discovering metabolism-related biomarkers for lung adenocarcinoma

Lei Fu[1†], Manshi Li[2†], Junjie Lv[1†], Chengcheng Yang[3†], Zihan Zhang[1], Shimei Qin[1], Wan Li[1], Xinyan Wang[3*] and Lina Chen[1*]

[1]College of Bioinformatics Science and Technology, Harbin Medical University, Harbin, China, [2]Department of Radiation Oncology, The Fourth Affiliated Hospital of China Medical University, Shenyang, China, [3]Department of Respiratory, Second Affiliated Hospital of Harbin Medical University, Harbin, China

Introduction: Lung cancer is a major cause of illness and death worldwide. Lung adenocarcinoma (LUAD) is its most common subtype. Metabolite-mRNA interactions play a crucial role in cancer metabolism. Thus, metabolism-related mRNAs are potential targets for cancer therapy.

Methods: This study constructed a network of metabolite-mRNA interactions (MMIs) using four databases. We retrieved mRNAs from the Tumor Genome Atlas (TCGA)-LUAD cohort showing significant expressional changes between tumor and non-tumor tissues and identified metabolism-related differential expression (DE) mRNAs among the MMIs. Candidate mRNAs showing significant contributions to the deep neural network (DNN) model were mined. Using MMIs and the results of function analysis, we created a subnetwork comprising candidate mRNAs and metabolites.

Results: Finally, 10 biomarkers were obtained after survival analysis and validation. Their good prognostic value in LUAD was validated in independent datasets. Their effectiveness was confirmed in the TCGA and an independent Clinical Proteomic Tumor Analysis Consortium (CPTAC) dataset by comparison with traditional machine-learning models.

Conclusion: To summarize, 10 metabolism-related biomarkers were identified, and their prognostic value was confirmed successfully through the MMI network and the DNN model. Our strategy bears implications to pave the way for investigating metabolic biomarkers in other cancers.

KEYWORDS

lung adenocarcinoma, deep neural network, metabolite-mRNA interactions network, biomarkers, risk model

1 Introduction

Lung cancer is a significant public health concern as evidenced by its high morbidity and mortality rates (1). Among its various subtypes, lung adenocarcinoma (LUAD) is the most prevalent, accounting for approximately 40% of all cases (2). Metabolic alterations in LUAD are crucial for its diagnosis, prognosis, and treatment response (3). Despite advancements in our understanding of LUAD's pathogenesis and development of therapeutic strategies, it remains an aggressive and deadly tumor type. Therefore, the identification and development of prognostic metabolism-related biomarkers for predicting outcomes in LUAD bear clinical significance (4).

Biomarkers have emerged as valuable indicators for the timely diagnosis, prognosis, and prediction of treatment responses in LUAD. These biomarkers reflect a diverse range of molecular alterations, including genetic expression patterns (5). Several studies have attempted to investigate the relationship between biomarker expression and LUAD. For instance, elevated expression levels of PD-L1 have been associated with worse prognosis and reduced survival in lung adenocarcinoma patients (6). PD-L1 expression may serve as a potential predictive biomarker for response to immunotherapy and can help guide treatment decisions. High expression of certain receptor tyrosine kinases, such as the epidermal growth factor receptor (EGFR) has been identified in subsets of patients with LUAD and has been proven effective as targets for specific TKIs (7, 8). Altered expression of microRNAs (miRNAs) has been implicated in the development and progression of LUAD (9, 10). Assessment of expressions of these biomarker levels is important in selecting the most appropriate targeted therapy approach (11, 12).

Cancer, a metabolic disease, arises from alterations in metabolism triggered by genetic or non-genetic signals (13). Tumor cells exhibit distinct metabolic characteristics, including increased proliferation and resistance to apoptosis. As tumors actively manipulate metabolic systems to sustain their growth, targeting their metabolism is a promising approach for personalized cancer therapy (14, 15). Tumor cells often switch their metabolism from mitochondrial oxidative phosphorylation to glycolysis, a phenomenon known as the "Warburg effect." This provides energy and building blocks for tumor cell division, growth, and adaptation to oxidative stress (16). As tumor cells need to adapt their metabolic pathways to support their rapid growth and energy demands, they undergo metabolic reprogramming, a hallmark of cancer (17). Metabolic abnormalities contribute to the development and progression of cancer through the interactions between specific mRNAs and metabolites, referred to as metabolite-mRNA interactions. Metabolic pathways are crucial for tumor progression and survival; therefore, they have garnered significant research attention in the study of LUAD (18). Cao MDT, L.J., Boulanger J, et al., found that altered metabolic processes, such as increased glucose consumption, dysregulated lipid metabolism, and abnormal amino acid utilization occur commonly in LUAD cells. Understanding the intricacies underlying these metabolic alterations can provide valuable insights into the development of effective therapeutic strategies (19). Recently, Ksenia M. Shestakova et al., showed that the combination of metabolomics and cutting-edge bioinformatics is a practical tool for the accurate diagnosis of patients with non-small cell lung cancer (NSCLC) (20, 21). The study examined the relationship between metabolites and NSCLC and its original conceptualization offers a novel perspective on studying the connection between NSCLC and metabolites.

In the biomedical field, with the introduction of high-throughput technology, the amount of biomedical data, including genomic, metabolomic, and proteomic has massively accumulated (22). By storing, analyzing, and interpreting these impressive amounts of biomedical big data, it is possible to better understand human health and illness (23, 24). A type of deep learning and artificial intelligence, deep neural network (DNN) models have emerged as a potent tool for research in several fields of biology (25–27). Compared to classical machine learning techniques, deep learning has many advantages, such as strong self-learning capabilities and excellent generalization ability (28). Algorithms based on deep learning created from artificial neural networks are promising for identifying patterns and extracting features from large amounts of complex data to obtain biomarkers with clinical prognostic value (29).

Despite significant advances in biomarker identification, elucidation of metabolic pathways, and utilization of bioinformatics and machine learning techniques, several challenges remain. One of these is the identification of reliable biomarkers with high sensitivity and specificity (30). Integrating multi-omics data and utilizing DNN models is necessary to find reliable biomarkers for improving the accuracy of cancer diagnosis and prognosis prediction (31, 32). Hence, at the genomic level, the goal of our study was to identify metabolism-related biomarkers for LUAD by integrating data on gene expression, metabolite profiling, and protein interactions to construct a network of metabolites-mRNAs and mRNA interactions. We then introduced a DNN model to identify metabolism-related biomarkers for LUAD. Our findings could contribute to the advancement of metabolism-based research.

2 Materials and methods

The workflow of our investigation is shown in Figure 1, and the details are described in the subsequent sections.

2.1 Data sources

In this study, eight LUAD cohorts (Table 1) were obtained from The Tumor Genome Atlas (TCGA, https://portal.gdc.cancer.gov/), Gene Expression Omnibus (GEO, https://www.ncbi.nlm.nih.gov/geo/) (GSE36471, GSE42127, GSE68465, GSE72094, and GSE87340), and Clinical Proteomic Tumor Analysis Consortium data portal (CPTAC, https://cptac-data-portal.georgetown.edu/).

RNA-Sequence (Seq) and clinical data from 594 samples of LUAD (containing 535 tumor tissues and 59 non-tumor tissues) were acquired from the corresponding TCGA cohort. Table 2 lists

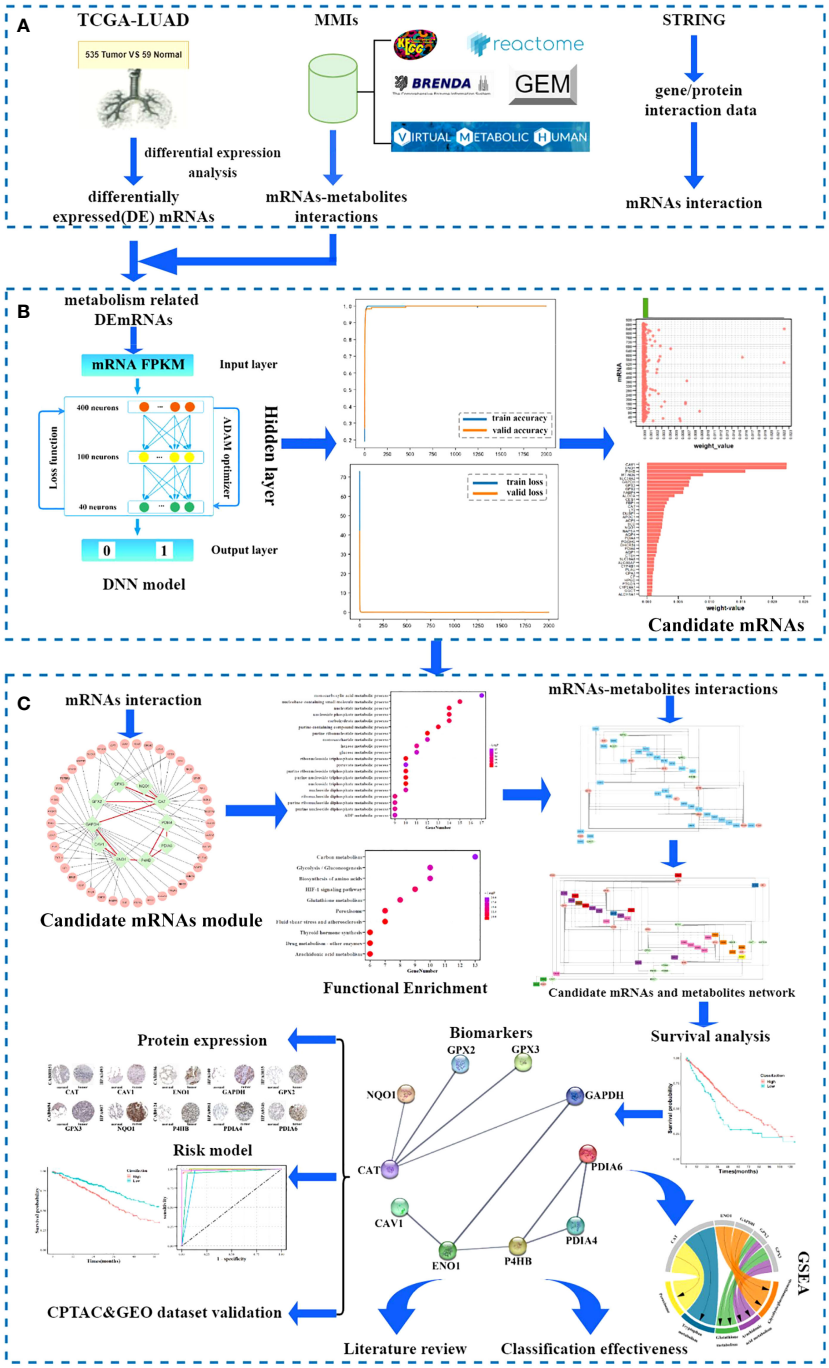

FIGURE 1
Workflow of the study. **(A)** Data sources. **(B)** Screening candidate mRNA. **(C)** Identification and validation of biomarkers.

the patients' clinical characteristics. Symbol and gene type attributes of RNA-Seq data were annotated using the Ensemble database. According to the gene type attribute, mRNAs were extracted.

For the microarray datasets (GSE36471, GSE42127, GSE68465, GSE72094, and GSE87340) generated by the Illumina and Agilent platforms, originally processed data (series matrix files) were used (33). Probe IDs were mapped to corresponding gene IDs using the platform files.

Using four different data sources, namely the Kyoto Encyclopedia of Genes and Genomes (KEGG) (34), Reactome (35), Human-GEM (36), and BRENDA (37), we retrieved metabolite-mRNAs interactions (MMIs) (38). The Virtual Metabolic Human database's metabolite abbreviations were utilized to standardize metabolite names to the universal nomenclature. A directed MMI network was constructed (the whole network was detailed in Supplementary Table S1),

TABLE 1 Datasets for lung adenocarcinoma used in this study.

Data source	Platform	Follow-up information	Sample count
TCGA	Illumina HiSeq 2000	OS	594
GSE36471	GPL9053	OS	115
GSE42127	GPL6884	OS	176
GSE68465	GPL96	OS	442
GSE72094	GPL15048	OS	442
GSE87340	GPL11154	OS	54
CPTAC (mRNA)	Illumina Hiseq 4000	–	204
CPTAC (protein)	Tandem mass tags	–	214

OS, Overall survival; -, No Overall Survival.

including 31227 unique MMIs covering 1869 metabolites and 4134 mRNAs.

2.2 Metabolism-related DEmRNA interaction network

Fragments per kilobase of exon per million read mapped (FPKM) values were chosen as the representative measure of mRNA expression from RNA-Seq data. Using the FPKM values, "Limma" (39) was employed to identify statistically significant and differentially expressed (DE) mRNAs between LUAD and non-tumor tissues. Specifically, a t-test was utilized for evaluating differential expression. A threshold of $|\log2(\text{fold-change})| \geq 1$ and a false discovery rate (FDR) adjusted p-value < 0.05 were adopted as criteria for determining statistical significance. The collection of metabolism-related DEmRNAs was determined by combining DEmRNAs with 4134 mRNAs obtained from the MMI network. Using the tool, STRING (Search Tool for the Retrieval of Interacting Genes) (https://string-db.org/) (40) with a confidence level >= 700, a metabolism-related DEmRNA interaction network was constructed.

TABLE 2 Clinical characteristics of the patients with lung adenocarcinoma.

Clinical characteristics	TCGA
Patient (n)	**594**
Age, years	
median	65
range	33–88
Sex (%)	
female	270 (45.4%)
male	317 (53.4%)
Absent	7 (1.2%)
Stage (%)	
Stage I	317 (53.4%)
Stage II	136 (22.9%)
Stage III	97 (16.3%)
Stage IV	28 (4.7%)
Absent	16 (2.7%)

2.3 Candidate mRNAs

2.3.1 Metabolism-related mRNA DNN model construction

The Google TensorFlow 2.0 architecture was used to generate a fully connected DNN model with numerous hidden layers, an output layer, and an input layer. Hence, we built a metabolism-related mRNA DNN model using the Google TensorFlow 2.0 architecture, comprising an input layer, three hidden layers, and an output layer, following a previously described workflow (41). The features of the DNN model were the FPKM values of the metabolism-related DEmRNAs. The output layer with a label of 1/0 indicated if the sample was cancerous or not. Given the small sample size, the Adaptive Moment Estimation (ADAM) optimizer with default Ker as parameters was selected. The loss function of binary cross-entropy was applied. The DNN model's performance was influenced by three parameters related to model training, including batch size, number of epochs, and learning rate. Model training requires multiple rounds of learning. The learning rate was considered when randomly selecting a batch of training sets in each round. A larger batch size results in faster model convergence but has weaker generalization ability. Therefore, the initial values for batch size and epoch were set to 16 and >= 1000, respectively, according to the sample size and number of features. When using a large batch size, a high learning rate was required to prevent underfitting, while a low learning rate was needed for a small batch size to avoid overfitting. To achieve optimal results, a learning rate of 0.0001 was set for subsequent learning cycles, and the parameters for batch size, epoch, and learning rate were continuously adjusted based on the validation accuracy curve and results of loss curve fitting.

2.3.2 Candidate mRNAs screening

In the DNN model, the larger the weight, the greater the corresponding feature's contribution. Features that contributed significantly to the DNN model were more biologically significant. Therefore, features were screened as candidate mRNAs based on the weight of the features. The arithmetic average of absolute Shapley Additive exPlanations (SHAP) values for the impact representing the importance of the feature to all samples was denoted as the weight and it was calculated using summary_plot. SHAP (42) is an approach in game theory to explain the output of a machine learning model. The SHAP values were obtained first. Assuming that the ith sample was x_i, the jth feature of the ith sample was x_{ij}, the predicted value of the model for that sample was $f(x_i)$, and the baseline of the entire model (usually the

mean of the target variables for all samples) was y_{base}, then the SHAP value obeyed the following equation:

$$f(x_i) = y_{base} + f(x_{i1}) + f(x_{i2}) + f(x_{i3}) + \cdots + f(x_{ik})$$

Where $f(x_{ij})$ was the SHAP value of x_{ij}. Intuitively, $f(x_{i1})$ was the contribution value of the 1st feature in the ith sample to the final prediction value $f(x_i)$. When $f(x_{i1}) > 0$, the feature improved the prediction value and had a positive effect; conversely, it meant that the feature lowered the prediction value and had a negative effect. The impact of a feature on the machine learning model was thus represented by the SHAP value. To determine an approximation of the SHAP values for the DNN models in this study, DeepExplainer from the Python SHAP module was employed. The SHAP value of each feature on each sample was obtained using force_plot. Finally, the weight value was calculated by summary_plot based on the arithmetic average of absolute SHAP values. Candidate mRNAs were screened by generating a scatter plot for a single variable with different histograms at the upper border of the plot using the weight values of the feature mRNAs in the DNN model.

2.4 Biomarkers

2.4.1 Biomarker identification

From the metabolism-related DEmRNA interaction network, the module of interacting candidate mRNAs and their one-step neighbors were collected. Gene ontology (GO) functional analysis (43) was conducted to identify the unique biological properties, including biological processes (BP), cellular components (CC), and molecular functions (MF). All mRNAs in the module were extracted for GO and KEGG pathway enrichment analyses, and analyzed on the metascape platform (https://metascape.org/) (44). Categories with the minimum overlap number of 3 and the hypergeometric test Benjamini-Hochberg adjusted p-value < 0.05 were selected.

Metabolism-related pathways and functional classes were chosen based on the results of enrichment analysis and the enriched mRNAs (including candidate mRNAs and one-step neighbors) were added to the MMI network to create a module of enriched mRNAs and metabolites, which was combined with the module of interacting candidate mRNAs to create a subnetwork comprising candidate mRNAs and metabolites.

Kaplan-Meier survival analyses (45) for candidate mRNAs in the subnetwork were conducted using the "survival" package in R to confirm the prognostic effect. Overall survival (OS) was defined as the time from the date of initial surgical resection to the date of death or last contact (censored), truncated at 120 months. Survival curves were drawn using Kaplan-Meier analysis and were compared using the log-rank test for assessing statistical significance. Based on the results of the survival analysis, candidate mRNAs were identified as biomarkers.

2.4.2 Biomarkers' classification effectiveness assessment

To assess the effectiveness of identified biomarkers for LUAD, 594 samples from the cohort of TCGA-LUAD were used. Traditional machine learning methods, including K-nearest neighbor (KNN) (46), Support Vector Machine (SVM) (47), Decision Tree (48), Naive Bayes (49), and Logistic regression (50) were applied for sample classification using identified biomarkers. Their performance was visualized as the area under (AUC) the receiver operating characteristic (ROC) curves.

2.4.3 Protein levels of biomarkers

Images depicting protein expression in normal tissue and pathology of tumor tissue sections were downloaded from the Human Protein Atlas (HPA, https://www.proteinatlas.org/) database to determine differential expression at the protein level.

2.5 Validation of biomarkers

Furthermore, Kaplan-Meier survival analysis was conducted in five independent GEO- LUAD datasets (GSE36465, GSE42127, GSE68465, GSE72094, and GSE87340) to further validate the prognostic value of biomarkers. A total of 204 samples of LUAD from CPTAC comprised an independent dataset and were used to validate the effectiveness of the identified biomarkers.

A literature review was conducted by searching the PubMed database for all articles published in the English Language on the relevant topics of identification of biomarkers for LUAD and the relationship between biomarkers and metabolites.

3 Results

3.1 Candidate mRNAs

First, in the TCGA dataset, using Student's t-test with a false-discovery rate (FDR) < 0.05 and | log2(fold-change) | >= 1, 4376 DEmRNAs between the 535 LUAD samples and 59 non-tumor samples were extracted; among them, 2448 and 1928 DEmRNAs were upregulated and downregulated, respectively (Figure 2A). A total of 887 metabolism-related DEmRNAs (Table S2) were obtained from the overlap of 4376 DEmRNAs and 4134 mRNAs from the MMI network. Using the STRING database, a metabolism-related DEmRNA interaction network was constructed with 887 nodes and 1852 edges (the entire network was detailed in Supplementary Table S3).

For the metabolism-related DEmRNA DNN model, the initial input layer was set with the FPKM values of 887 DEmRNAs, three hidden layers of 400, 100, and 40 neurons, and the 1/0 label as the output layer (Figure 2B). The 594 samples were split randomly with 80% in the training set and 20% in the testing set. Through the output label and after setting batch size = 16, epoch = 2000, and learning rate = 0.00001, the validation accuracy curve and loss curve both conformed to the general law of deep learning. The accuracy reached 99.7% (Figure 2C). Thus, the regularization optimization was effective.

Python's DeepExplainer SHAP module was applied to interpret the contribution of each mRNA to each sample in the DNN model;

10.3389/fendo.2023.1270772

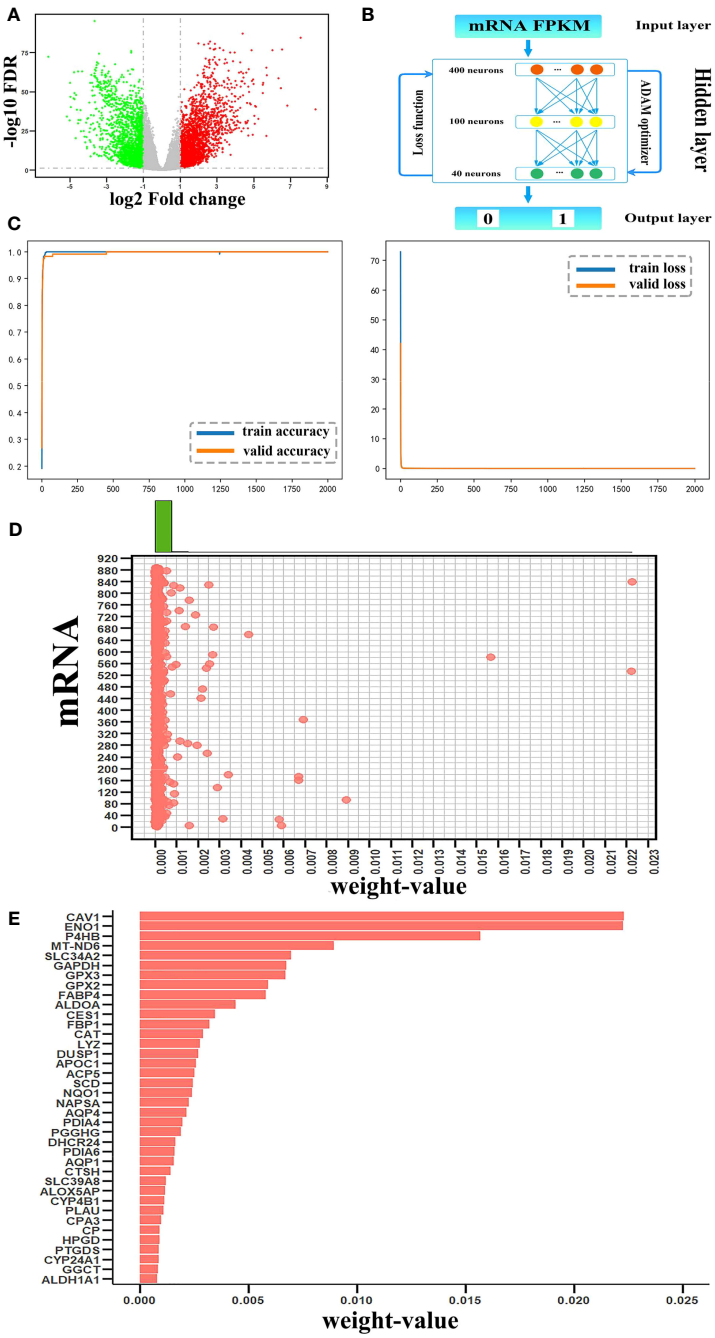

FIGURE 2
Candidate mRNAs. **(A)** Volcano plot of differentially expressed (DE)mRNAs between tumor and non-tumor samples. Red and green represented upregulated and downregulated DEmRNAs, respectively. **(B)** The structure of the DNN model. **(C)** The accuracy curve and the loss curve of the mRNA DNN model. **(D)** The joint distribution of weight values. The x-axis represents the weight-value of each mRNA and the y-axis represents 887 mRNAs, as 1–887 to indicate each mRNA. **(E)** The weight values of the top 38 candidate mRNAs.

SHAP values were obtained using force_plot. It demonstrated that each feature contributes differently to the prediction of the model from the base value (y_{base}) to the final fetch $f(x_i)$. Based on the definition of the weight of the mRNA in the DNN model, the arithmetic mean of the absolute SHAP values representing the influence of the feature on the importance of all samples were calculated by summary_plot and expressed as the corresponding weight values. To select candidate mRNAs with high contributions to DNN models, a scatterplot was generated for a single variable, and different histograms were plotted on the upper boundary of the scatterplot (Figure 2D). According to the distribution of mRNAs in the scatterplot, mRNAs arranged according to the weight values were mainly concentrated on two sides of the weight value of 0.00075; therefore, we chose these 38 mRNAs with weight value >

0.00075 as candidate mRNAs (Figure 2E). Statistical analysis showed that the top 38 mRNAs contributed 0.1558 to the total, while the remaining 849 mRNAs contributed 0.1109.

3.2 Analysis of the candidate mRNA module

A total of 38 candidate mRNAs were identified by differential expression analysis and DNN model screening. From the STRING database's protein interaction data, the metabolism-related DEmRNA network of LUAD was built. From this network, 10 candidate mRNAs (CAT, CAV1, ENO1, GAPDH, GPX2, GPX3, NQO1, P4HB, PDIA4, and PDIA6) showed interactions. The metabolism-related DEmRNAs network was segmented into an interacting candidate mRNA module (Figure 3A) that included these 10 candidate mRNAs for interaction and the 42 one-step neighbor mRNAs that they were connected with.

The metascape platform was used to conduct functional enrichment analysis based on GO and KEGG databases for candidate mRNAs of LUAD. Categories with the minimum overlap number of 3 and the hypergeometric test Benjamini-Hochberg adjusted p-value < 0.05 were selected. Fifty-two mRNAs were identified as considerably enriched in functional classes relevant to metabolic processes by GO enrichment analysis (Figure 3B), and arachidonic acid and glutathione metabolic pathways were included among the top 10 of the KEGG enrichment results (Figure 3C).

The KEGG database showed two metabolic pathways, namely glutathione metabolism (51) and arachidonic acid metabolism (52), which were chosen for subsequent analyses (Figure 4). First, in the glutathione metabolism pathway, reduced glutathione (GSH) is converted to oxidized glutathione by the enzymes GPX2 and GPX3 in glutathione metabolism (GSSG). Several prevalent human diseases, including lung cancer, are partially caused by impaired glutathione metabolism. Nevertheless, GPX2 and GPX3 are engaged in the body's metabolic mechanism for maintaining glutathione levels, which can successfully prevent lung cancer (53). In addition to being crucial for lowering inflammatory reactions, improving immunological function, and ensuring normal gene and protein expression, stabilizing glutathione metabolism also controls the proliferation and death of human cells.

In the metabolism of arachidonic acid, arachidonic acid functions through GPX2 and GPX3 to form 15(S)-HPETE (54). One of the six monohydroperoxy fatty acids generated by the non-enzymatic oxidation of arachidonic acid is 15(S)-HPETE (leukotrienes). Hydroxy fatty acid (+/-)15-HETE, which is more stable, is produced by reducing hydroperoxides. Arachidonic acid belongs to a group of bioactive substances produced by the 5-lipoxygenase pathway in oxidative metabolism, implicated in pathophysiological roles such as inflammation (55), acute hypersensitivity (56), and host defensive reactions. The lung is an

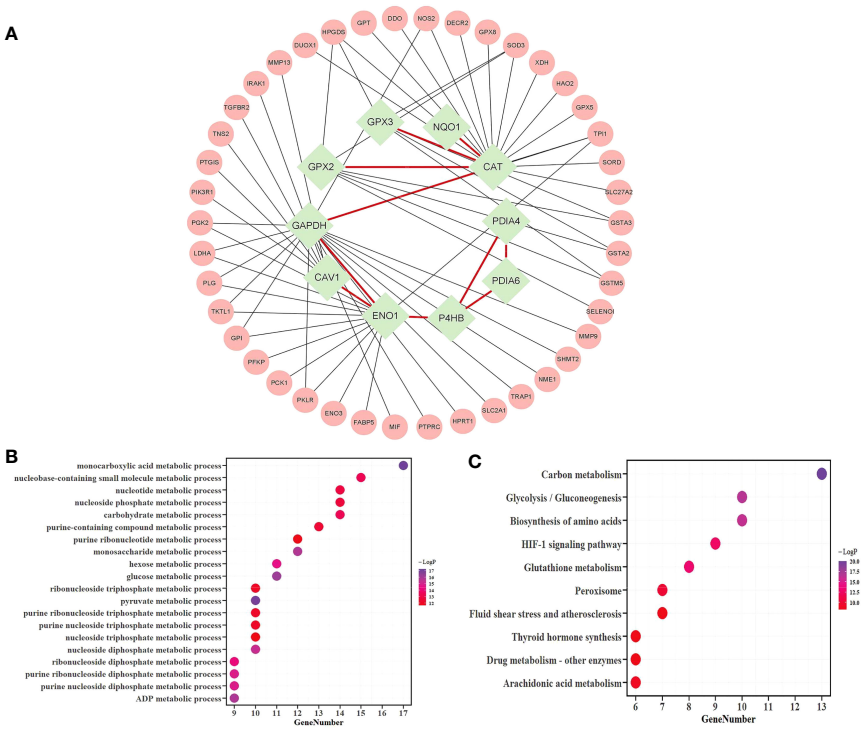

FIGURE 3
Analysis of the candidate mRNAs module. **(A)** The candidate mRNAs module. Results of the enrichment analyses of 52 mRNAs were represented in a bubble diagram; **(B)** The findings of the GO enrichment analysis for functions linked to metabolic processes, with -$\log_{10}$ P >= 10; **(C)** The results of the KEGG enrichment analysis, assuming -$\log_{10}$P >= 8.

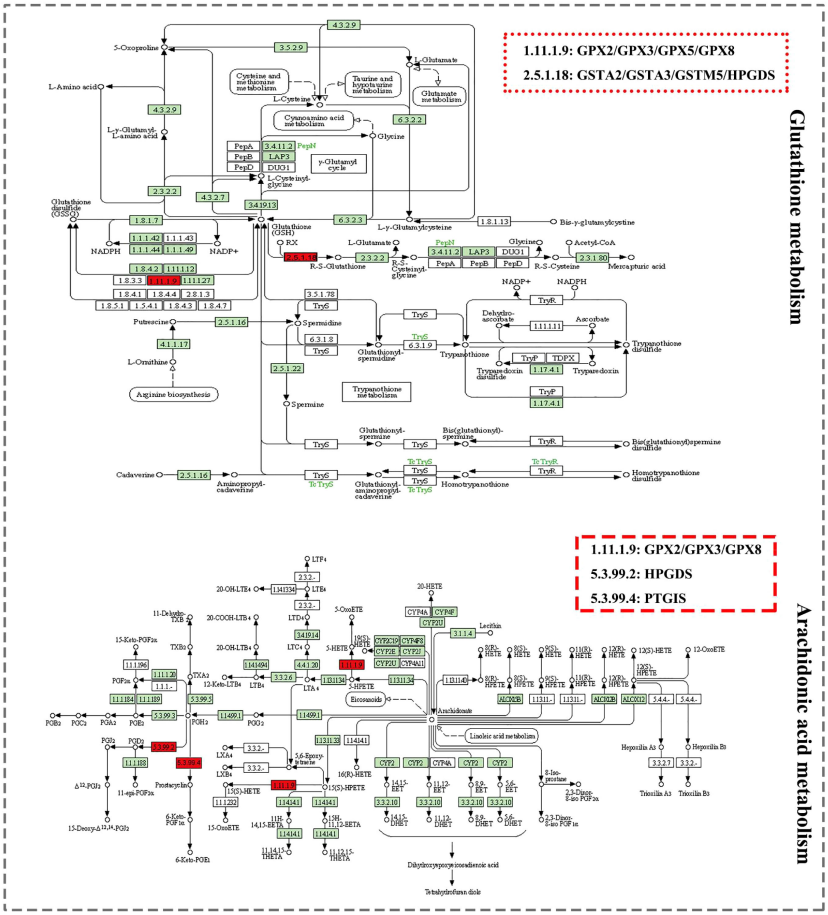

FIGURE 4
Glutathione and arachidonic acid metabolic pathways: Red tags showed enriched mRNAs.

important organ that is significantly affected (57). Additionally, there are three ways that arachidonic acid metabolites can influence the development and metastasis of lung cancer as follows: prostacyclin inhibits platelet-tumor cell contact; thromboxane increases platelet-tumor cell contact and thus encourages tumor cell invasion; prostaglandins' cytoprotective activity maintains the integrity of epithelial cells and affects tissues' responses to pro-tumorigenic substances, and through lipoxygenases (58).

3.3 Biomarkers

3.3.1 Biomarkers' identification

Twenty mRNAs, including six candidate mRNAs (CAV1, ENO1, GPX2, GPX3, NQO1, and P4HB) and 14 one-step neighbor mRNAs (GPI, GPX5, GPX8, GSTA2, GSTA3, GSTM5, HPGDS, MIF, MMP9, PIK3R1, PTGIS, PTPRC, TRAP1, and XDH) were enriched in the functional classes of glutathione and arachidonic acid metabolic pathways and metabolism-related biological processes.

A module of enriched mRNAs-metabolites was extracted from MMIs, including 20 mRNAs and 71 metabolites (Table S4). It was further refined to eliminate unimportant metabolites such as water, oxygen, H+, etc., and metabolites with a degree of 1, such as phosphate, xanthine, hypoxanthine, etc. Thus the refined module (Figure 5A) consisted of 15 mRNAs and 29 metabolites, including 5 candidate mRNAs (Table S5). This refined module was then combined with the module of interacting candidate mRNAs to create the subnetwork comprising candidate mRNAs and metabolites. Irrelevant mRNAs with a degree of 1 that did not contribute to the mRNA-metabolite association were removed (Figure 5B). Thus, the final subnetwork was constructed, including 10 candidate mRNAs together with 11 one-step neighbor mRNAs and 29 metabolites. Eight primary categories—energy, coenzymes, hydrogen peroxide, glutathione, prostaglandins, ketones, acids, and dopamine pigments—were utilized to classify the metabolites to conveniently display the types of mRNAs-linked metabolites.

Using the univariate Kaplan-Meier survival analysis, the predictive significance of candidate mRNAs in LUAD was assessed. The "ggsurvplot" package was used to plot survival curves, and log-rank tests were used to compare results (Figures 6A–J). Except for NQO1, the remaining nine candidate mRNAs had a substantial predictive ability. Next, we conducted a literature-based validation of NQO1's prognostic outcome in LUAD (59). We found that NQO1 is a potential therapeutic

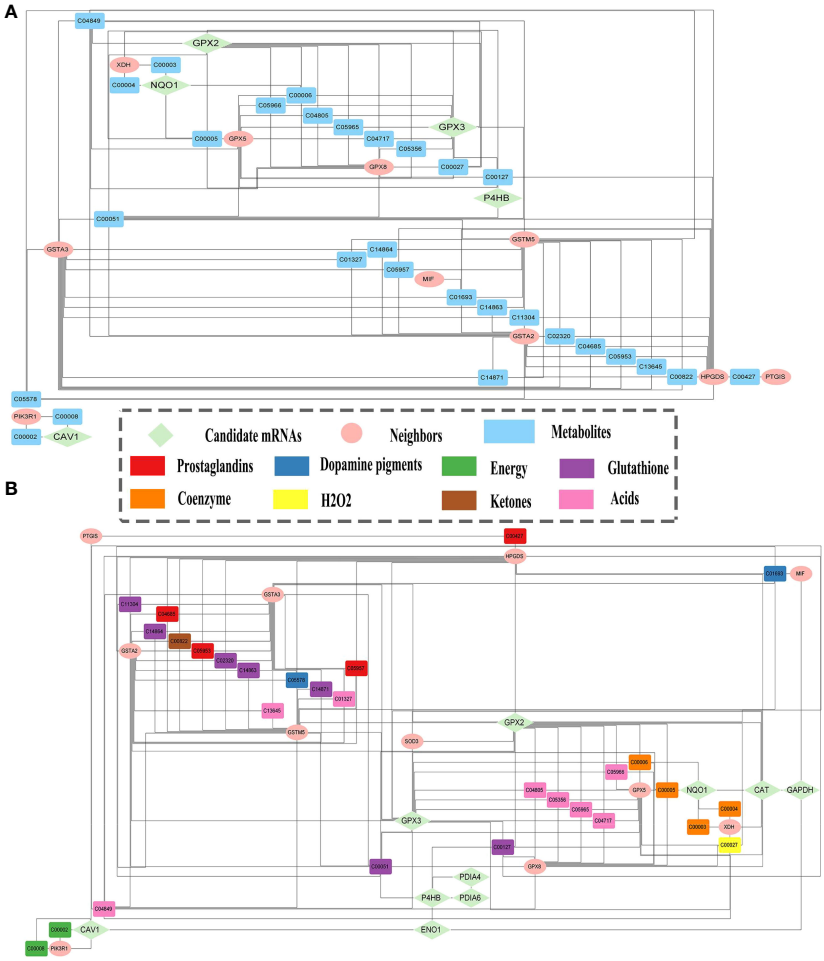

FIGURE 5
Candidate mRNAs and metabolites relationships. **(A)** The module of enriched mRNAs-metabolites. **(B)** Subnetwork of the relationships between metabolites and candidate mRNAs, and their one-step neighbor mRNAs.

target and predictive biomarker for LUAD. All the ten candidate mRNAs were identified as biomarkers.

To investigate biomarkers' function and correlations with the cancer phenotype, GSEA (https://www.gsea-msigdb.org/gsea/) (60) was performed using the expression data. The KEGG gene set was selected and biomarkers were ranked. In cancer, biomarkers were significantly enriched for glycolysis/gluconeogenesis, while arachidonic acid metabolism, glutathione metabolism, tryptophan metabolism, and peroxisome were enriched in the normal setting (Figure 6K). These findings shed light on the intricate relationship between biomarker expression and metabolic processes, thereby affirming the relevance and credibility of the identified metabolism-related biomarkers.

3.3.2 Biomarkers' classification effectiveness assessment

We assessed the effectiveness of biomarker-based classification in LUAD using traditional machine learning techniques (SVM, KNN, Decision Trees, Naive Bayes, and logistic regression). The classification effectiveness of each biomarker is shown in Figure 7. *A* total of 594 samples were split into a training set and a test set in a ratio of 8:2. TPR (sensitivity) was used as the vertical coordinate and FPR (1-specificity) as the horizontal coordinate to plot the ROC curves against different critical values. Most machine learning methods had good classification performance (AUC > 0.700), demonstrating the classification effectiveness and diagnostic values of all biomarkers for LUAD samples.

3.3.3 Differential expression analysis

Differential expression of the 10 biomarkers was analyzed between cancer and normal samples at the mRNA and protein level (Figure 8). In the CPTAC, all 10 biomarkers' coding proteins showed differential expression, and their expressions matched their mRNA levels in TCGA. The HPA database was searched for the expression profiles of the proteins corresponding to each of the 10 biomarkers in normal tissue and tumor tissue sections. The

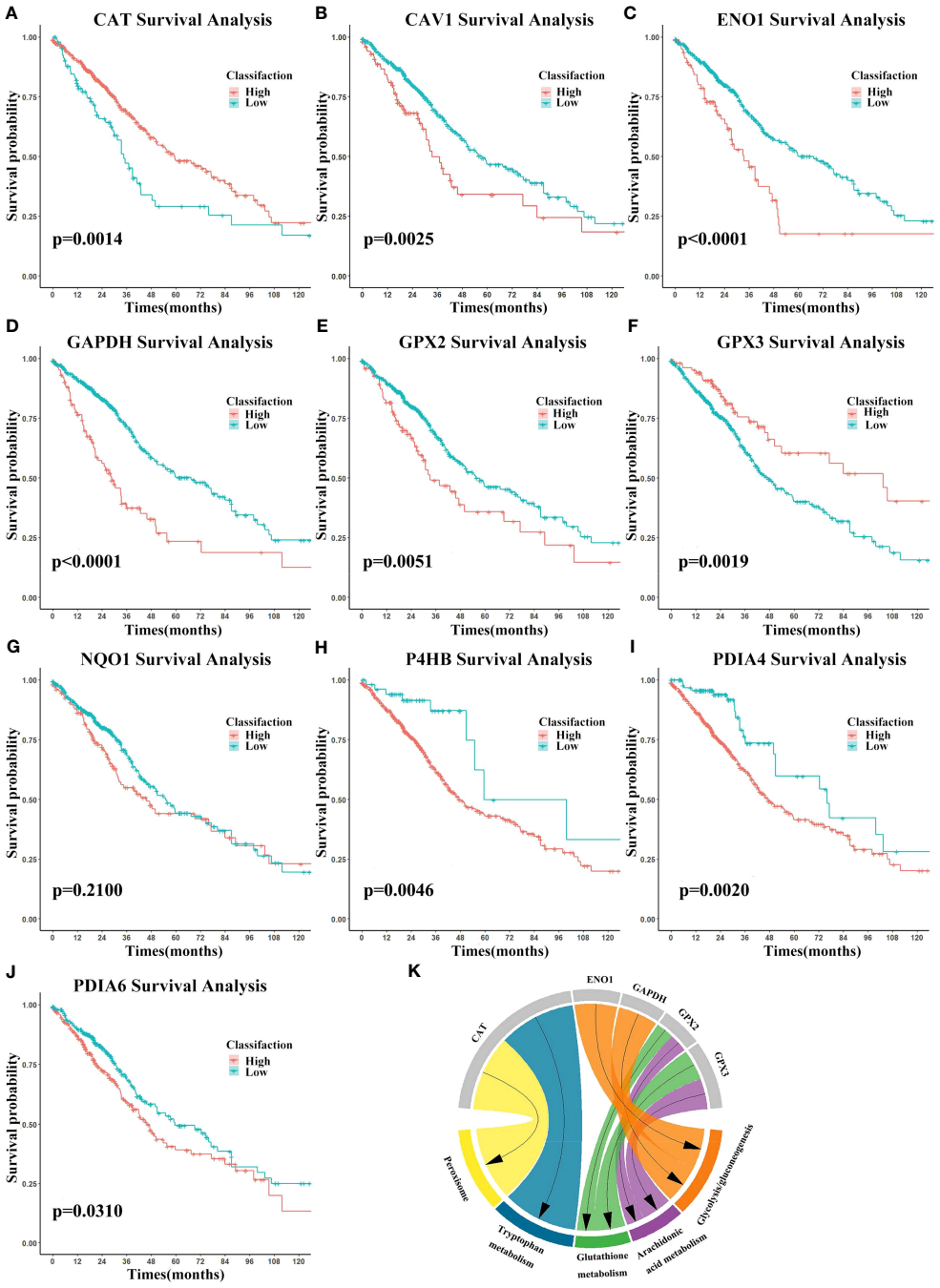

FIGURE 6
Biomarkers' survival analysis and gene set enrichment analysis (GSEA). **(A–J)** Survival curves using biomarker expression. Survival time is on the x-axis and survival probability is on the y-axis. **(K)** GSEA results were shown on the chart.

detection of homologous antibodies demonstrated that the differential protein expression in the samples was compatible with the information in the CPTAC database.

3.4 Validation of biomarkers

Prognostic values for biomarkers in LUAD were validated in five independent datasets obtained from GEO (Table 3). The percentage of validated significant prognosis for biomarkers was more than 70% and reached up to 90% in the GSE87340 dataset. Each biomarker was validated in more than three datasets. Combining the results of the TCGA and independent GEO datasets suggested that these biomarkers were stable predictors for survival in LUAD.

An independent CPTAC dataset was used to validate biomarkers' classification effectiveness for tumor and normal samples (Figure 9). Eight biomarkers (AUC > 0.900), NQO1

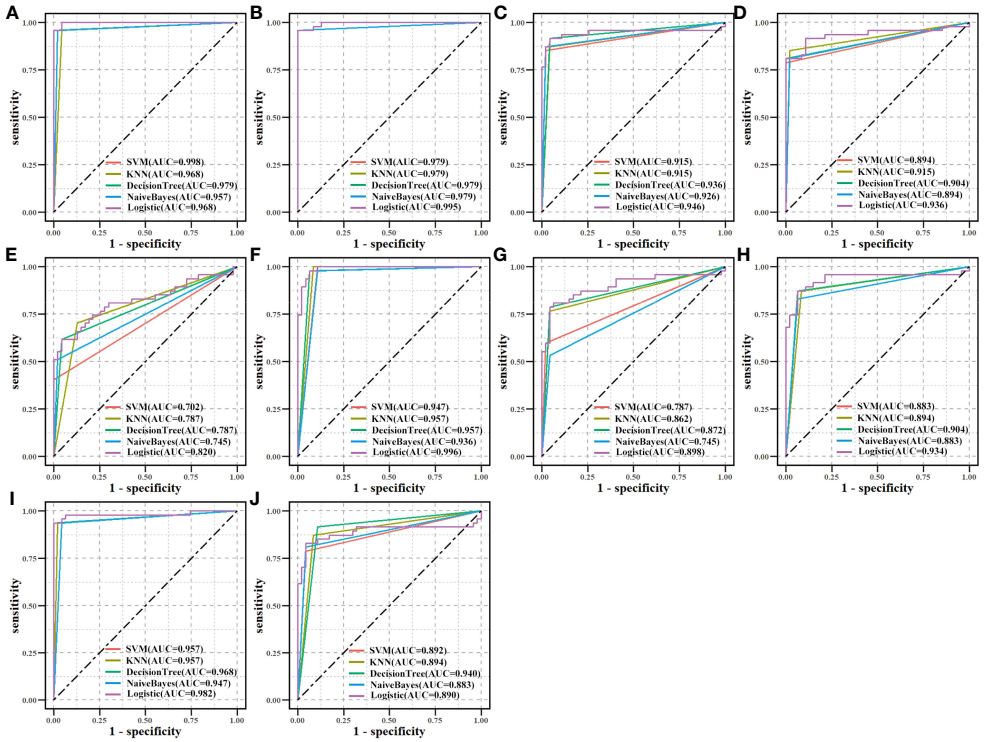

FIGURE 7
Biomarkers' classification effectiveness assessment under using different classifier models in TCGA. **(A)** CAT, **(B)** CAV1, **(C)** ENO1, **(D)** GAPDH, **(E)** GPX2, **(F)** GPX3, **(G)** NQO1, **(H)** P4HB, **(I)** PDIA4, and **(J)** PDIA6.

(AUC > 0.750), and GPX2 (AUC > 0.600) in all machine learning methods showed good classification performance, both on TCGA and CPTAC datasets. The results demonstrated the potential diagnostic values of all biomarkers for LUAD.

Finally, a literature review was carried out by searching the PubMed database for all publications published in English for the relevant biomarkers for LUAD. All 10 biomarkers had been validated in the literature as potential prognostic markers for LUAD (61–69). Four metabolites were directly connected to biomarkers in the subnetwork (Figure 5B). Cancer development may be linked to alterations in GPX2 and GPX3 activities, which were associated with glutathione (C00051), oxidized glutathione (C00127), and hydrogen peroxide (C00027). Glutathione is a specific tripeptide and engages in numerous intercellular activities. Cancer cells with high glutathione levels are resistant to chemotherapy (70). Oxidized glutathione (GSSG) is formed by glutathione peroxidases (GPXs). The GSSG content rises due to GPX3 overexpression, in turn, increasing glutathione levels (71). Hydrogen peroxide accelerates cell proliferation and decreases rapamycin-induced autophagy along with increasing intracellular reactive oxygen species (ROS) levels. Elevated intracellular levels of hydrogen peroxide and ROS lead to PTEN inactivation and AKT/mTOR pathway activation, which prevents autophagy and promotes LUAD cell growth (72). NQO1 is intimately connected to NADPH (C00005) and reduces the malignant characteristics of LUAD (73). miR-485-5p targets NADPH to oxidize NQO1 and inhibit PI3K/Akt, thus counteracting the inhibitory effect of NQO1 on the malignant phenotype of LUAD cells, thereby preventing LUAD cell proliferation and migration.

4 Discussion

LUAD is the most widely occurring subtype of lung cancer and among the major causes of death due to cancers. Cancer is a metabolic disease, and metabolic reprogramming is a result of certain oncogenic changes that promote cancer development and progression through complex interactions with the tumor ecosystem (74). Given this background, we constructed an MMI network to understand cancer metabolism comprehensively. As a result, 10 metabolism-related biomarkers were identified from a metabolic perspective using the DNN model in the MMI network. The survival prognosis and classification effectiveness of biomarkers were confirmed by the literature and data from TCGA, CPTAC, and GEO. ENO1, GAPDH, NQO1, PDIA4, and PDIA6 may serve as potential targets for cancer therapy (69, 75–77).

To strengthen our findings of the 10 metabolism-related biomarkers, we conducted differential expression analysis and survival analysis in the datasets derived from eight different cancer cohorts (including LUSC, BRCA, CESC, KICH, LIHC, PAAD, PRAD, and STAD) from TCGA (Table S6). The results of the differential expression analysis revealed that the expression patterns of the 10 biomarkers differed among seven cancers (including BRCA, CESC, KICH, LIHC, PAAD, PRAD, and

10.3389/fendo.2023.1270772

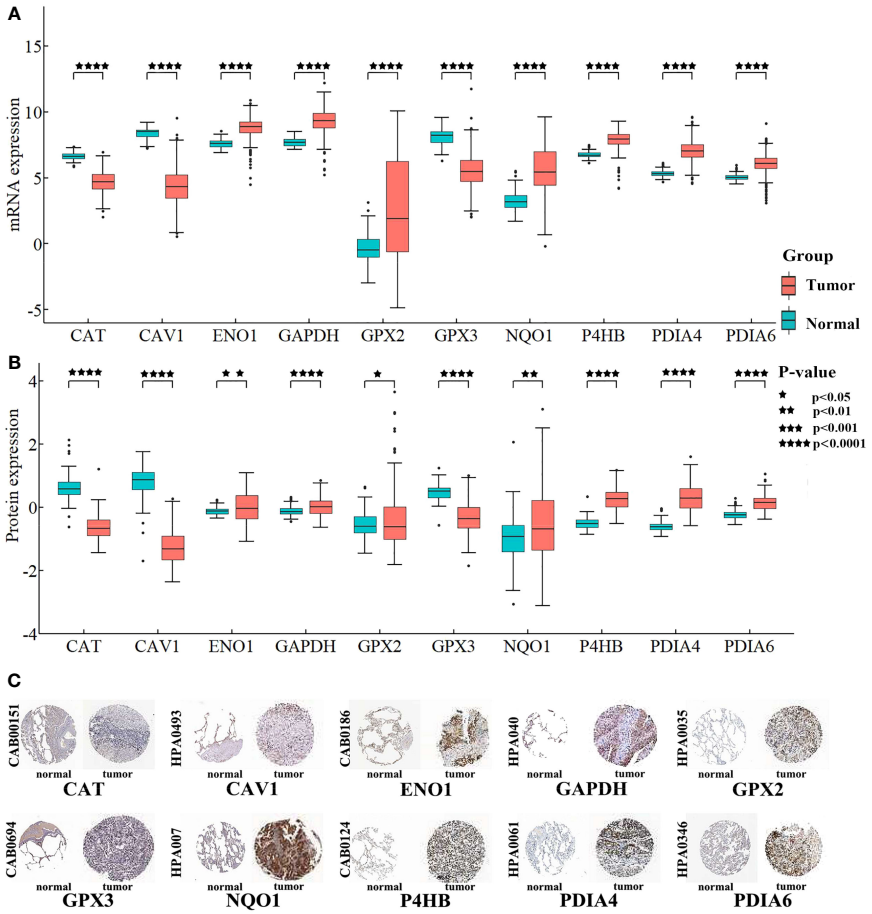

FIGURE 8
Differentially expression analysis for biomarkers. **(A)** Box plot shows the differential expression of mRNAs. The Y-axis is the biomarkers' expression after log2 transformation. **(B)** Box plot shows the differential expression of proteins. The Y-axis is the proteins' expression value after log2 transformation. **(C)** Proteins' differential expression in the HPA database. The left side of the panel shows the antibody numbers.

TABLE 3 Survival prognosis.

	GSE68465	GSE36471	GSE42127	GSE72094	GSE87340
CAT	0.0023	0.0030	0.0157	<0.0001	0.0002
CAV1	0.0180	0.1739	0.0433	0.0022	<0.0001
ENO1	0.1045	0.0027	0.0092	0.1032	0.0023
GAPDH	0.0019	0.0023	0.0084	<0.0001	0.0001
GPX2	0.0151	0.0007	0.0031	0.0003	0.1247
GPX3	0.0423	0.0447	0.0075	0.0002	0.0053
NQO1	0.0062	0.1604	0.0793	0.0151	0.0414
P4HB	0.0902	0.0190	0.0585	0.0216	0.0122
PDIA4	0.1178	0.0368	0.0038	0.0611	<0.0001
PDIA6	0.0223	0.0400	0.0028	0.0107	0.0001
Ratio	70%	80%	80%	80%	90%

Ratio: Ratio of biomarkers with prognostic survival (p less than 0.05).

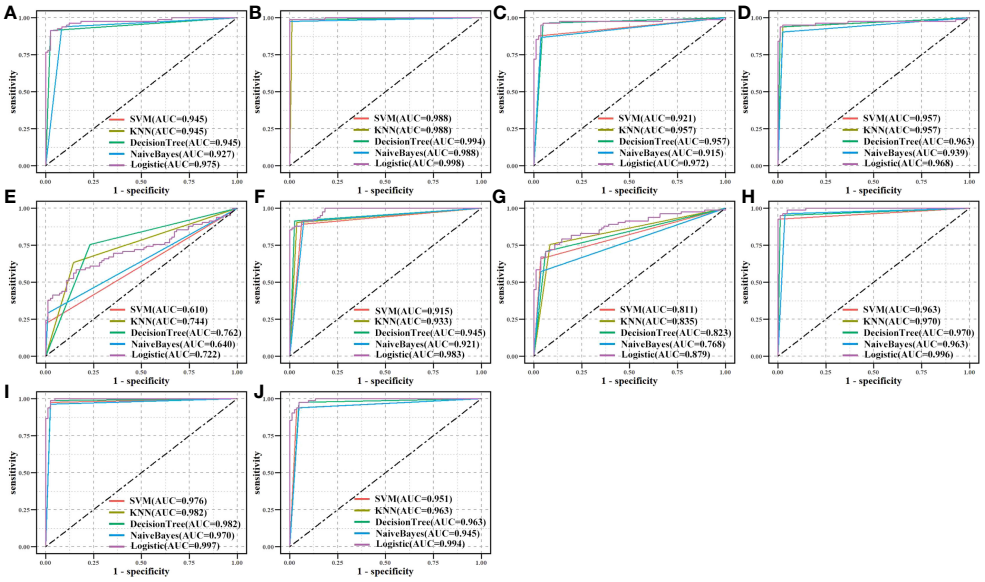

FIGURE 9
Validation of biomarkers' classification effectiveness assessment using different classifier models in the CPTAC independent dataset. **(A)** CAT, **(B)** CAV1, **(C)** ENO1, **(D)** GAPDH, **(E)** GPX2, **(F)** GPX3, **(G)** NQO1, **(H)** P4HB, **(I)** PDIA4, and **(J)** PDIA6.

STAD) compared to LUAD. Additionally, survival analysis indicated that the prognostic significance of the 10 biomarkers was statistically insignificant ($p > 0.05$) for the majority of these seven cancers. These observations suggested that the identified biomarkers in LUAD were not biomarkers for these seven cancers and were not consistently regulated in these seven cancers. LUAD and lung squamous cell cancer are the two predominant subtypes of NSCLC, and so, a comparison of the 10 biomarkers was performed in these two subtypes (Tables S6, S7). CAT, ENO1, NQO1, P4HB, and PDIA6 were unique to LUAD, while CAV1, GAPDH, GPX2, GPX3, and PDIA4 exhibited consistent trends in differential expression in both LUAD and lung squamous cell cancer, significant prognostic survival prediction ($p<0.05$), and excellent classification effectiveness. These mRNAs may serve as potential biomarkers for NSCLC. Furthermore, we conducted a differential analysis for biomarker expression in different stages of LUAD samples from TCGA (Table S8). GAPDH and P4HB were significantly different ($p<0.05$) between stages I and II, while ENO1, GAPDH, and PDIA6 were significantly different ($p<0.05$) between stages I and III and CAT, ENO1, GAPDH, P4HB, and PDIA6 were significantly different ($p<0.05$) between stages I and II+III. These are potential biomarkers for staging patients with LUAD.

Using four public databases (KEGG, Reactome, Human-GEM, BRENDA), we constructed an MMI network and it was found to be comprehensive and reliable. In the network, we established a metabolism-related mRNA DNN model, and candidate mRNAs were identified more precisely using the DNN model along with weight values. This was due to the inherent advantage of the DNN model to change the multidimensional weights of each feature during learning and describe intricate relationships between mRNAs. Therefore, it was more accurate at filtering features than conventional machine learning techniques. Moreover, when using the DNN model, the learning state of the model is usually assessed based on the decrease in the validation loss rate and the training loss rate during the learning process. In this situation, two phenomena are commonly encountered during deep learning: overfitting and underfitting. When the model was overfitting (Figure S1A), model regularization and reducing the learning rate are common optimization techniques; whereas, when the model was underfitting (Figure S1B), it is necessary to reduce both the learning rate and the batch size to improve the generalization ability. If both the validation loss rate and training loss rate converge to 0 (Figure S1C), no further training is required and the model is more suitable for generalization. Based on these considerations and the sample size of the TCGA dataset used in this study, batch size = 16, epoch = 2000, and learning rate = 0.00001 were chosen.

The identified biomarkers in this study were enriched in metabolic function classes and pathways in LUAD, and can potentially characterize a patient's dysfunction. Hence, the classification effectiveness of ten biomarkers which was assessed overall was based on GPX2 and GPX3 as factors from the enriched pathways and CAV1, ENO1, NQO1, and P4HB as factors from functional classes to determine whether a patient had cancer. The 594 samples (including 535 tumor samples and 59 normal samples) from TCGA were split into a training set and a testing set in a ratio of 8:2. The independent CPTAC dataset was used for validation in the same way (Figure 10). Both in the TCGA dataset and the CPTAC independent dataset, the majority of machine learning approaches showed good classification effectiveness (AUC > 0.800), highlighting the potential diagnostic values of biomarker combinations for LUAD samples.

10.3389/fendo.2023.1270772

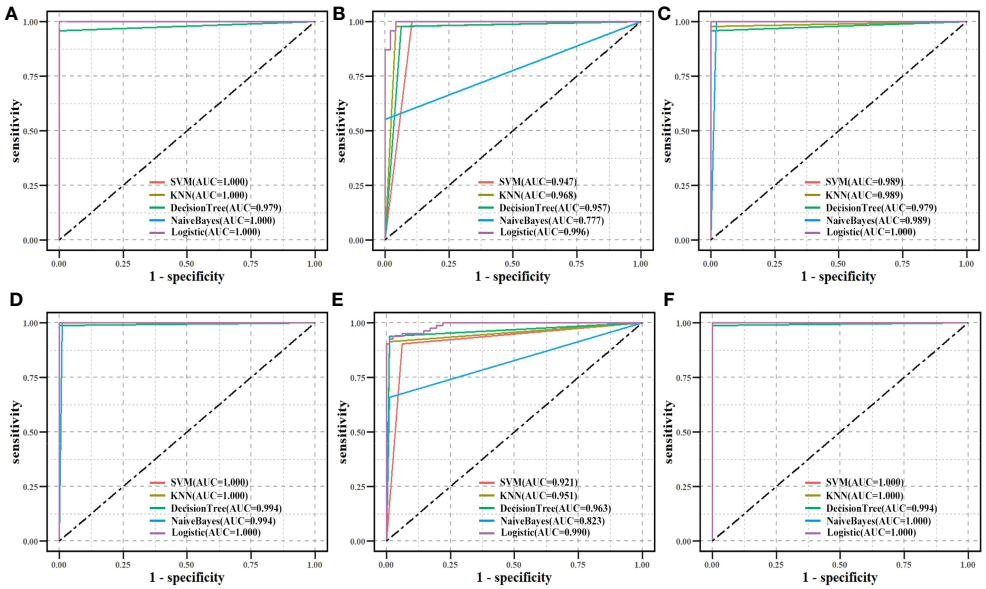

FIGURE 10
Biomarkers' classification effectiveness assessment using different classifier models in TCGA. **(A)** Ten biomarkers were assessed as an overall factor. **(B)** GPX2, GPX3 as a factor. **(C)** CAV1, ENO1, NQO1, and P4HB as a factor. Biomarkers' classification effectiveness assessment using different classifier models in CPTAC. **(D)** Ten biomarkers were assessed as an overall factor. **(E)** GPX2, GPX3 as a factor. **(F)** CAV1, ENO1, NQO1, and P4HB as a factor.

To examine the synergistic effect of the 10 markers on the prediction of patient prognosis, Lasso-penalized Cox regression (78) was conducted to screen biomarkers for building a risk model. The optimal value of the Lasso penalty parameter, λ, was determined as 0.0078 through 10-fold cross-validation (Figure S2). Then, to select the best model as the risk model (79), the outcomes of the Lasso analysis were evaluated using multifactorial Cox regression analysis. CAV1, ENO1, and GAPDH (which were defined as risk mRNAs) were used with a p-value threshold of 0.05 (Table 4), and the final risk model was constructed as follows:

$$RiskScore = (0.0024 \times EXP_{CAV1}) + (0.0009 \times EXP_{ENO1}) + (0.0005 \times EXP_{GAPDH}).$$

For all tumor samples in TCGA, risk scores were computed and divided into high- and low-risk groups using the median risk score as the cutoff. Distributions of risk scores, survival statuses, and survival curves (Figure S3A) are shown. To validate the risk model, GSE36471, GSE42127, GSE68465, and GSE72094 were used as the validation datasets. Risk scores were computed and high- and low-risk groups were obtained (Figures S3B–E). Patients in the risk-score-high group died more and had slightly shorter survival than those in the risk-score-low group. Kaplan-Meier curves illustrated patients with LUAD in the risk-score-high group had a worse overall survival rate than those in the risk-score-low group in all five datasets. DEmRNAs between high- and low-risk groups were identified and highly expressed DEmRNAs in the high-risk group were enriched in the cell cycle, including the mitochondrial cell cycle process, cell division, and regulation of the cell cycle process. Mounting evidence shows that cancer metabolism is intertwined with cell cycle regulatory mechanisms. Therapy aimed at cell cycle machinery thereby inhibits cancer cell division while also reversing malignant cell metabolism (80). Hence, the outcomes of the enrichment analysis supported the risk model which was based on metabolism-related biomarkers and confirmed the above-mentioned mRNAs' distinct roles in metabolism. The classification effectiveness of the risk model for high- and low-risk score groups in the samples from TCGA (Figure S4A) and GSE36471, GSE42127, GSE68465, and GSE72094 (Figures S4B–E) was good (AUC > 0.750). Consequently, the risk model had a good prognostic predictive value and classification effectiveness for LUAD, which also proved the reliability of these biomarkers.

TABLE 4 Multivariate Cox regression analyses.

	HR	95% CI	p-value
ENO1	1.0008	1.0001-1.0015	0.031
CAV1	1.0023	1.0003-1.0043	0.022
GAPDH	1.0006	1.0003-1.0008	<0.001

5 Conclusions

In conclusion, from the metabolism perspective, we constructed the MMI network and the DNN model and successfully applied them to predictions for LUAD. The importance of the 10 identified metabolism-related biomarkers was confirmed for prediction of survival and classification effectiveness. This integrated method and approach may offer a novel perspective to identify biomarkers for other malignancies.

Data availability statement

The original contributions presented in the study are included in the article/Supplementary Material, further inquiries can be directed to the corresponding authors.

Author contributions

LF: Formal Analysis, Investigation, Methodology, Software, Visualization, Writing – original draft, Writing – review & editing. JL: Data curation, Writing – review & editing. CY: Data curation, Writing – review & editing. ML: Validation, Writing – review & editing. ZZ: Writing – review & editing. SQ: Writing – review & editing. WL: Funding acquisition, Writing – review & editing. XW: Conceptualization, Data curation, Writing – review & editing. LC: Conceptualization, Funding acquisition, Supervision, Writing – review & editing.

Funding

The author(s) declare financial support was received for the research, authorship, and/or publication of this article. This research was funded by the National Natural Science Foundation of China (61702141; 81627901), the Natural Science Foundation of Heilongjiang Province (LH2021F043) and the Heilongjiang Postdoctoral Funds for Scientific Research Initiation (LBH-Q17132).

Acknowledgments

We thank Bullet Edits Limited for the linguistic editing and proofreading of the manuscript.

Conflict of interest

The authors declare that the research was conducted in the absence of any commercial or financial relationships that could be construed as a potential conflict of interest.

Publisher's note

Supplementary material

The Supplementary Material for this article can be found online at: https://www.frontiersin.org/articles/10.3389/fendo.2023.1270772/full#supplementary-material

References

1. Hutchinson BD, Shroff GS, Truong MT, Ko JP. Spectrum of lung adenocarcinoma - scienceDirect. *Semin Ultrasound CT MRI* (2019) 40(3):255–64. doi: 10.1053/j.sult.2018.11.009

2. Denisenko TV, Budkevich I, Zhivotovsky B. Cell death-based treatment of lung adenocarcinoma. *Cell Death Dis* (2018) 9(2):117. doi: 10.1038/s41419-017-0063-y

3. Yan L, Tan Y, Chen G, Fan J, Zhang J. Harnessing metabolic reprogramming to improve cancer immunotherapy. *Int J Mol Sci* (2021) 22(19):10268. doi: 10.3390/ijms221910268

4. He L, Chen J, Xu F, Li J, Li J. Prognostic implication of a metabolism-associated gene signature in lung adenocarcinoma. *Mol Ther Oncolytics.* (2020). doi: 10.1016/j.omto.2020.09.011

5. Sun YF, Yang XR, Zhou J, Qiu SJ, Fan J, Xu Y. Circulating tumor cells: advances in detection methods, biological issues, and clinical relevance. *J Cancer Res Clin Oncol* (2011) 137(8):1151–73. doi: 10.1007/s00432-011-0988-y

6. Sequist LV, Martins RG, Spigel D, Grunberg SM, Spira A, Jänne PA, et al. First-line gefitinib in patients with advanced non-small-cell lung cancer harboring somatic EGFR mutations. *J Clin Oncol Off J Am Soc Clin Oncol* (2008) 26(15):2442–9. doi: 10.1200/JCO.2007.14.8494

7. Shaw AT, Kim DW, Nakagawa K, Seto T, Crinó L, Ahn MJ, et al. Crizotinib versus chemotherapy in advanced ALK-positive lung cancer. *New Engl J Med* (2013) 368 (25):2385–94. doi: 10.1056/NEJMoa1214886

8. Belinsky SA, Palmisano WA, Gilliland FD, Crooks LA, Divine KK, Winters SA, et al. Aberrant promoter methylation in bronchial epithelium and sputum from current and former smokers. *Cancer Res* (2002) 62(8):2370–7.

9. Selamat SA, Chung BS, Girard L, Zhang W, Zhang Y, Campan M, et al. Genome-scale analysis of DNA methylation in lung adenocarcinoma and integration with mRNA expression. *Genome Res* (2012) 22(7):1197–211. doi: 10.1101/gr.132662.111

10. Garon EB, Rizvi NA, Hui R, Leighl N, Balmanoukian AS, Eder JP, et al. Pembrolizumab for the treatment of non-small-cell lung cancer. *New Engl J Med* (2015) 372(21):2018–28. doi: 10.1056/NEJMoa1501824

11. Passaro A, Palazzo A, Trenta P, Mancini ML, Morano F, Cortesi E. Molecular and clinical analysis of predictive biomarkers in non-small-cell lung cancer. *Curr Med Chem* (2012) 19(22):3689–700. doi: 10.2174/092986712801661149

12. Mueller T, Stucklin ASG, Postlmayr A, Metzger S, Gerber N, Kline C, et al. Advances in targeted therapies for pediatric brain tumors. *Curr Treat Options Neurol* (2020) 22(12). doi: 10.1007/s11940-020-00651-3

13. Seth Nanda C, Venkateswaran S, Patani N, Yuneva M. Defining a metabolic landscape of tumours: genome meets metabolism. *Br J Cancer* (2020) 122(2):136–49. doi: 10.1038/s41416-019-0663-7

14. Pavlova NN, Thompson CB. The emerging hallmarks of cancer metabolism. *Cell Metab* (2016) 23(1):27–47. doi: 10.1016/j.cmet.2015.12.006

15. Thompson CB, Ward PS. Metabolic reprogramming: a cancer hallmark even warburg did not anticipate. *Cancer Cell* (2012) 21(3):297–308. doi: 10.1016/j.ccr.2012.02.014

16. Roda N, Gambino V, Giorgio M. Metabolic constrains rule metastasis progression. *Cells* (2020) 9(9):2081. doi: 10.3390/cells9092081

17. Li X, Tang L, Deng J, Qi X, Zhang J, Qi H, et al. Identifying metabolic reprogramming phenotypes with glycolysis-lipid metabolism discoordination and intercellular communication for lung adenocarcinoma metastasis. *Commun Biol* (2022) 5(1):198. doi: 10.1038/s42003-022-03135-z

18. Schulze A, Harris AL. How cancer metabolism is tuned for proliferation and vulnerable to disruption. *Nature* (2012) 491(7424):364–73. doi: 10.1038/nature11706

19. Pavlova NN, Thompson CB. Metabolic plasticity in cancers-principles and clinical implications. *Nat Rev Clin Oncol* (2020). doi: 10.1126/science.aad8866

20. Shestakova KM, Moskaleva N, Boldin AA, Rezvanov PM, Shestopalov AV, Rumyantsev SA, et al. Targeted metabolomic profiling as a tool for diagnostics of patients with non-small-cell lung cancer. *Sci Rep* (2023) 13(1):11072. doi: 10.21203/rs.3.rs-2948248/v1

21. Carter DM. Announcement of the national epidermolysis bullosa registry. *J Am Acad Dermatol* (1987). doi: 10.1001/archderm.1987.01660280023003

22. Srivastava AK, Wang Y, Huang R, Skinner C, Thompson T, Pollard L, et al. Human genome meeting 2016: Houston, TX, USA. 28 February - 2 March 2016. *Hum Genomics* (2016) 10(Suppl 1):12. doi: 10.1186/s40246-016-0063-5

23. Cios. KJ, Mamitsuka H, Nagashima T, Tadeusiewicz R. Computational intelligence in solving bioinformatics problems - ScienceDirect. *Artif Intell Med* (2005) 35(1–2):1–8. doi: 10.1016/j.artmed.2005.07.001

24. Asgari E, Mofrad MRK. ProtVec: A continuous distributed representation of biological sequences. *Comput Sci* (2015) 10(11):e0141287. doi: 10.1371/journal.pone.0141287

25. Huys QJ, Maia T, Frank MJ. Computational psychiatry as a bridge from neuroscience to clinical applications. *Nat Neurosci* (2016) 19(3):404–13. doi: 10.1038/nn.4238

26. Esteva A, Kuprel B, Novoa RA, Ko J, Swetter SM, Blau HM, et al. Dermatologist-level classification of skin cancer with deep neural networks. *Nature* (2017) 546 (7660):686. doi: 10.3410/f.727237185.793554281

27. Hirasawa T, Aoyama K, Tanimoto T, Ishihara S, Shichijo S, Ozawa T, et al. Application of artificial intelligence using a convolutional neural network for detecting gastric cancer in endoscopic images. *Gastric Cancer* (2018) 21(4):653–60. doi: 10.1007/s10120-018-0793-2

28. Kather JN, Pearson AT, Halama N, Jäger D, Krause J, Loosen SH, et al. Deep learning can predict microsatellite instability directly from histology in gastrointestinal cancer. *Nat Med* (2019) 25(7):1054–6. doi: 10.1038/s41591-019-0462-y

29. Cao C, Liu F, Tan H, Song D, Shu W, Li W, et al. Deep learning and its applications in biomedicine. *Genomics Proteomics Bioinf* (2018) 16(1):17–32. doi: 10.1016/j.gpb.2017.07.003

30. Srivastava S. *Biomarkers in cancer screening and early detection*. Center for Prostate Disease Research, Department of Surgery, Uniformed Services University of the Health Sciences, Rockville, MD, USA (2017). pp. 16–26. doi: 10.1002/9781118468869.

31. Pécuchet N, Zonta E, Didelot A, Combe P, Thibault C, Gibault L, et al. Base-position error rate analysis of next-generation sequencing applied to circulating tumor DNA in non-small cell lung cancer: a prospective study. *PloS Med* (2016) 13(12): e1002199. doi: 10.1371/journal.pmed.1002199

32. He W, Xu D, Wang Z , et al. Detecting ALK-rearrangement of CTC enriched by nanovelcro chip in advanced NSCLC patients. *Oncotarget* (2016). doi: 10.18632/oncotarget.8305

33. Irizarry RA, Hobbs B, Collin F, Beazer-Barclay YD, Antonellis KJ, Scherf U, et al. Exploration, normalization, and summaries of high density oligonucleotide array probe level data. *Biostatistics* (2003) 4(2):249–64. doi: 10.1093/biostatistics/4.2.249

34. Kanehisa M, Sato Y, Kawashima M, Furumichi M, Tanabe M. KEGG as a reference resource for gene and protein annotation. *Nucleic Acids Res* (2016) 44(D1): D457–62. doi: 10.1093/nar/gkv1070

35. Croft D, O'Kelly G, Wu G, Haw R, Gillespie M, Matthews L, et al. Reactome: a database of reactions, pathways and biological processes. *Nucleic Acids Res* (2011) 39 (Database issue):D691. doi: 10.1093/nar/gkq1018

36. Robinson JL, Kocabaş P, Wang H, Cholley PE, Cook D, Nilsson A, et al. An atlas of human metabolism. *Sci Signal* (2020) 13(624):eaaz1482. doi: 10.1126/scisignal.aaz1482

37. Placzek S, Schomburg I, Chang A, Jeske L, Ulbrich M, Tillack J, et al. BRENDA in 2017: new perspectives and new tools in BRENDA. *Nucleic Acids Res* (2017) 45(D1): D380–8. doi: 10.1093/nar/gkw952

38. Chen D, Zhang Y, Wang W, Chen H, Ling T, Yang R, et al. Identification and characterization of robust hepatocellular carcinoma prognostic subtypes based on an integrative metabolite-protein interaction network. *Advanced Sci* (2021) (17):e2100311. doi: 10.1002/advs.202100311

39. Ritchie ME, Phipson B, Wu D, Hu Y, Law CW, Shi W, et al. limma powers differential expression analyses for RNA-sequencing and microarray studies. *Nucleic Acids Res* (2015) 43(7):e47. doi: 10.1093/nar/gkv007

40. Szklarczyk D, Gable AL, Nastou KC, Lyon D, Kirsch R, Pyysalo S, et al. The STRING database in 2021: customizable protein–protein networks, and functional characterization of user-uploaded gene/measurement sets. *Nucleic Acids Res* (2021) 49 (18):10800.

41. Fu L, Luo K, Lv J, Wang X, Qin S, Zhang Z, et al. Integrating expression data-based deep neural network models with biological networks to identify regulatory modules for lung adenocarcinoma. *Biol (Basel)* (2022) 11(9):1291. doi: 10.3390/biology11091291

42. Anjum M KK, Ahmad W, Ahmad A, Amin MN, Nafees A. New SHapley additive exPlanations (SHAP) approach to evaluate the raw materials interactions of steel-fiber-reinforced concrete. *Materials (Basel)* (2022) 15(18):6261. doi: 10.3390/ma15186261

43. Huang da W, Sherman BT, Lempicki RA. Bioinformatics enrichment tools: paths toward the comprehensive functional analysis of large gene lists. *Nucleic Acids Res* (2009) 37(1):1–13. doi: 10.1093/nar/gkn923

44. Zhou Y, Zhou B, Pache L, Chang M, Khodabakhshi AH, Tanaseichuk O, et al. Metascape provides a biologist-oriented resource for the analysis of systems-level datasets. *Nat Commun* (2019) 10(1):1523. doi: 10.1038/s41467-019-09234-6

45. Breslow N, Cox DR, Oakes DO. Analysis of survival data[J]. *New York N* (1984) 41(2):593. doi: 10.2307/253088

46. Singh S, Póczos B. Analysis of k-nearest neighbor distances with application to entropy estimation. *arXiv* (2016). doi: 10.48550/arXiv.1603.08578

47. Tong S, Koller D. Support vector machine active learning with applications to text classification. *J Mach Learn Res* (2002) 2(1):999–1006.

48. Wu D. Supplier selection: A hybrid model using DEA, decision tree and neural network. *Expert Syst Appl* (2009) 36(5):9105–12.

49. Mccallum A, Nigam K. A comparison of event models for Naive Bayes text classification. IN *AAAI-98 WORKSHOP ON LEARNING FOR TEXT CATEGORIZATION*. (1998), 41–8.

50. Allison PD. *Logistic regression using the SAS system: theory and application*. North Carolina: SAS Institute (2001).

51. Wang L, Ahn Y, Asmis R. Sexual dimorphism in glutathione metabolism and glutathione-dependent responses. *Redox Biol* (2020) 31:101410. doi: 10.1016/j.redox.2019.101410

52. Sonnweber T, Pizzini A, Nairz M, Weiss G, Tancevski I. Arachidonic acid metabolites in cardiovascular and metabolic diseases. *Int J Mol Sci* (2018) 19(11):3285. doi: 10.3390/ijms19113285

53. Jagust P, Alcalá S, Sainz J, Heeschen C, Sancho P. Glutathione metabolism is essential for self-renewal and chemoresistance of pancreatic cancer stem cells. *World J Stem Cells* (2020) 12(11):1410–28. doi: 10.4252/wjsc.v12.i11.1410

54. Soumya SJ, Binu S, Helen A, Anil Kumar K, Reddanna P, Sudhakaran PR. Effect of 15-lipoxygenase metabolites on angiogenesis: 15(S)-HPETE is angiostatic and 15(S)-HETE is angiogenic. *Inflammation Res* (2012) 61(7):707–18. doi: 10.1007/s00011-012-0463-5

55. Mori TA, Beilin LJ. Omega-3 fatty acids and inflammation. *Curr Atheroscl Rep* (2004) 6(6):461–7. doi: 10.1007/s11883-004-0087-5

56. Chen JP, Hou D, Pendyala L, Goudevenos JA, Kounis NG. Drug-eluting stent thrombosis: the Kounis hypersensitivity-associated acute coronary syndrome revisited. *JACC Cardiovasc Interventions* (2009) 2(7):583–93. doi: 10.1016/j.jcin.2009.04.017

57. Bell E, Ponthan F, Whitworth C, Westermann F, Thomas H, Redfern CP, et al. Cell survival signalling through PPARδ and arachidonic acid metabolites in neuroblastoma. *PloS One* (2013) 8(7):e68859. doi: 10.1371/journal.pone.0068859

58. Honn KV, Busse WD, Sloane BF. Prostacyclin and thromboxanes. Implications for their role in tumor cell metastasis. *Biochem Pharmacol* (1983) 32(1):1–11. doi: 10.1016/0006-2952(83)90644-5

59. Zhao Y, Feng HM, Yan WJ, Qin Y. Identification of the signature genes and network of reactive oxygen species related genes and DNA repair genes in lung adenocarcinoma. *Front Med (Lausanne)* (2021) 9:833829. doi: 10.3389/fmed.2022.833829

60. Subramanian A, Tamayo P, Mootha VK, Mukherjee S, Ebert BL, Gillette MA, et al. Gene set enrichment analysis: a knowledge-based approach for interpreting genome-wide expression profiles. *Proc Natl Acad Sci United States America* (2005) 102 (43):15545–50. doi: 10.1073/pnas.0506580102

61. Liu JS, Liu J, Xiao Q, Li XP, Chen J, Liu ZQ. Association of variations in the CAT and prognosis in lung cancer patients with platinum-based chemotherapy. *Front Pharmacol* (2023) 14:1119837. doi: 10.3389/fphar.2023.1119837

62. Li YP, Lin R, Chang MZ, Ai YJ, Ye SP, Han HM, et al. The effect of GPX2 on the prognosis of lung adenocarcinoma diagnosis and proliferation, migration, and epithelial mesenchymal transition. *J Oncol* (2022) 2022:7379157. doi: 10.1155/2022/7379157

63. Liu Z, Sun D, Zhu Q, Liu X. The screening of immune-related biomarkers for prognosis of lung adenocarcinoma. *Bioengineered* (2021) 12(1):1273–85. doi: 10.1080/21655979.2021.1911211

64. Liu XS, Zhou LM, Yuan LL, Gao Y, Kui XY, Liu XY, et al. NPM1 is a prognostic biomarker involved in immune infiltration of lung adenocarcinoma and associated with m6A modification and glycolysis. *Front Immunol* (2021) 12:751004. doi: 10.3389/fimmu.2021.751004

65. Yang L, Zhang R, Guo G, Wang G, Wen Y, Lin Y, et al. Development and validation of a prediction model for lung adenocarcinoma based on RNA-binding protein. *Ann Trans Med* (2021) 9(6):474. doi: 10.21037/atm-21-452

66. Tian Q, Zhou Y, Zhu L, Gao H, Yang J. Development and validation of a ferroptosis-related gene signature for overall survival prediction in lung adenocarcinoma. *Front Cell Dev Biol* (2021) 9:684259. doi: 10.3389/fcell.2021.684259

67. Tu Z, He X, Zeng L, Meng D, Zhuang R, Zhao J, et al. Exploration of prognostic biomarkers for lung adenocarcinoma through bioinformatics analysis. *Front Genet* (2021) 2:647521. doi: 10.3389/fgene.2021.647521

68. Liu X, Li L, Xie X, Zhuang D, Hu C. Integrated bioinformatics analysis of microarray data from the GEO database to identify the candidate genes linked to poor prognosis in lung adenocarcinoma. *Technol Health Care* (2023) 31(2):579–92. doi: 10.3233/THC-220165

69. Tufo G, Jones AW, Wang Z, Hamelin J, Tajeddine N, Esposti DD, et al. The protein disulfide isomerases PDIA4 and PDIA6 mediate resistance to cisplatin-induced cell death in lung adenocarcinoma. *Cell Death Differ* (2014) 21(5):685–95. doi: 10.1038/cdd.2013.193

70. Zmorzyński S, Świderska-Kołacz G, Koczkodaj D, Filip AA. Significance of polymorphisms and expression of enzyme-encoding genes related to glutathione in hematopoietic cancers and solid tumors. *Biomed Res Int* (2015) 2015:853573. doi: 10.1155/2015/853573

71. Kiriyama K, Hara K, Kondo A. Oxidized glutathione fermentation using Saccharomyces cerevisiae engineered for glutathione metabolism. *Appl Microbiol Biotechnol* (2013) 97(16):7399–404. doi: 10.1007/s00253-013-5074-8

72. Wang Y, Chen D, Liu Y, Zhang Y, Duan C, Otkur W, et al. AQP3-mediated H2O2 uptake inhibits LUAD autophagy by inactivating PTEN. *Cancer Sci* 112 (8):3278–92. doi: 10.1111/cas.15008

73. Chen Y, Wu L, Bao M. MiR-485-5p suppress the Malignant characteristics of the lung adenocarcinoma via targeting NADPH quinone oxidoreductase-1 to inhibit the PI3K/Akt. *Mol Biotechnol* (2023) 65(5):794–806. doi: 10.1007/s12033-022-00577-y

74. Sullivan LB, Gui DY, Vander Heiden MG. Altered metabolite levels in cancer: implications for tumour biology and cancer therapy. *Nat Rev Cancer* (2016) 16 (11):680–93. doi: 10.1038/nrc.2016.85

75. Yang M, Sun Y, Sun J, Wang Z, Zhou Y, Yao G, et al. Differentially expressed and survival-related proteins of lung adenocarcinoma with bone metastasis. *Cancer Med* (2018) 7(4):1081–92. doi: 10.1002/cam4.1363

76. Song SY, Jeong SY, Park HJ, Park SI, Kim DK, Kim YH, et al. Clinical significance of NQO1 C609T polymorphisms after postoperative radiation therapy in completely resected non-small cell lung cancer. *Lung Cancer* (2010) 68(2):278–82. doi: 10.1016/j.lungcan.2009.06.009

77. Ouyang X, Zhu R, Lin L, Wang X, Zhuang Q, Hu D. GAPDH is a novel ferroptosis-related marker and correlates with immune microenvironment in lung adenocarcinoma. *Metabolites* (2023) 13(2):142. doi: 10.3390/metabo13020142

78. Li Y, Lu F, Yin Y. Applying logistic LASSO regression for the diagnosis of atypical Crohn's disease. *Sci Rep* (2022) 12(1):11340. doi: 10.1038/s41598-022-15609-5

79. Jones GD, Brandt WS, Shen R, Sanchez-Vega F, Tan KS, Martin A, et al. A genomic-pathologic annotated risk model to predict recurrence in early-stage lung adenocarcinoma. *JAMA Surg* (2021) 156(2):e205601. doi: 10.1001/jamasurg.2020.5601

80. Liu J, Peng Y, Wei W. Cell cycle on the crossroad of tumorigenesis and cancer therapy. *Trends Cell Biol* (2022) 32(1):30–44. doi: 10.1016/j.tcb.2021.07.001

frontiers | Frontiers in Endocrinology

TYPE Case Report
PUBLISHED 14 November 2023
DOI 10.3389/fendo.2023.1205431

OPEN ACCESS

EDITED BY
Princy Francis
Mayo Clinic, United States

REVIEWED BY
Badr Kiaf,
Harvard Medical School, United States
Enrique Medina-Acosta,
State University of Northern Rio de Janeiro, Brazil
Sarah Alam,
Canadian Specialist Hospital, United Arab Emirates

*CORRESPONDENCE
Xiaomei Zhang
z.x.mei@163.com

RECEIVED 13 April 2023
ACCEPTED 19 September 2023
PUBLISHED 14 November 2023

CITATION
Xin S and Zhang X (2023) Case Report: Diabetes mellitus type MODY5 as a feature of 17q12 deletion syndrome with diabetic gastroparesis.
Front. Endocrinol. 14:1205431.
doi: 10.3389/fendo.2023.1205431

Case Report: Diabetes mellitus type MODY5 as a feature of 17q12 deletion syndrome with diabetic gastroparesis

Sixu Xin and Xiaomei Zhang*

Department of Endocrinology, Peking University International Hospital, Beijing, China

Background: Maturity-onset diabetes of the young type 5 (MODY5) is an uncommon, underrecognized condition that can be encountered in several clinical contexts. It is challenging to diagnose because it is considered rare and therefore overlooked in the differential diagnosis. Moreover, no typical clinical features or routine laboratory tests can immediately inform the diagnosis.

Case presentation: We report a 28-year-old man who was once misdiagnosed with type 1 diabetes due to decreased islet function and recurrent diabetic ketosis or ketoacidosis. However, he had intermittent nausea, vomiting, abdominal distension, and abdominal pain 6 months prior. Further examinations revealed agenesis of the dorsal pancreas, complex renal cyst, kidney stone, prostate cyst, hypomagnesaemia, and delayed gastric emptying. Accordingly, whole-exon gene detection was performed, and a heterozygous deletion mutation was identified at [GRCh37 (hg19)] chr17:34842526-36347106 (1.5 Mb, including *HNF1B* gene). The patient was eventually diagnosed with 17q12 deletion syndrome with gastroparesis.

Conclusion: We report a novel case of diabetes mellitus type MODY5 as a feature of 17q12 deletion syndrome caused by a new 17q12 deletion mutation, which will further broaden the genetic mutation spectrum of this condition. With the help of gene detection technology, these findings can assist endocrinologists in making the correct diagnosis of MODY5 or 17q12 deletion syndrome. Additionally, they can formulate an appropriate therapy and conduct genetic screening counseling for their family members to guide and optimize fertility.

KEYWORDS

maturity-onset diabetes of the young type 5, MODY 5, chromosome 17q12 deletion syndrome, *HNF1B*, diabetic gastroparesis

Introduction

Maturity-onset diabetes of the young (MODY) is a monogenic form of diabetes that is inherited in an autosomal dominant manner, and it accounts for approximately 1% –2% of diabetes cases (1). The typical clinical manifestations of MODY are often a family history of three or more generations, disease onset at a young age (before 25 years old), no type 1 diabetes mellitus (T1DM)-related autoantibodies, no need for insulin treatment, and no ketosis tendency. At present, 14 different MODY subtypes that are caused by 14 different pathogenic gene mutations have been identified; MODY5 is due to a mutation in the hepatocyte nuclear factor 1β (*HNF1B*) gene. The incidence of MODY5 is low, accounting for less than 5% of MODY cases (2). The genotype and clinical phenotype of MODY5 are very complex and easily cause misdiagnosis. Almost half of patients diagnosed with MODY5 (*HNF1B* mutation) have a mutation in the form of a whole gene deletion (3). In addition, 17q12 microdeletion syndrome, known as 17q12 deletion syndrome, is a rare chromosomal anomaly caused by the deletion of a small amount of material from a region in the long arm of chromosome 17. It is typified by the deletion of more than 15 genes, including *HNF1B*, resulting in kidney abnormalities, renal cysts, diabetes syndrome [renal cysts and diabetes (RCAD)], and neurodevelopmental or neuropsychiatric disorders (4).

Here, we report a patient who presented with diabetes mellitus (DM)-type MODY5 as a feature of 17q12 deletion syndrome with diabetic gastroparesis (DGP).

Case presentation

The patient, a 28-year-old man, was admitted to the Endocrinology Department of Peking University International Hospital on November 15, 2022, due to "six years of excessive drinking and urination, 6 months of paroxysmal nausea and vomiting". The patient had symptoms of thirst, polydipsia, and polyuria without inducement 6 years ago and was not diagnosed or treated. The fasting plasma glucose was 8.5 mmol/L (normal reference range is 3.9–6.1 mmol/L) in the posterior examination. Then, he was diagnosed with T1DM after examinations in an external hospital. The patient was given short-acting insulin for three meals and long-acting insulin before bed for anti-hyperglycaemic treatment. He was hospitalized many times for diabetic ketoacidosis (DKA) because of irregular insulin injections. When discharged from the hospital, the patient was given a preprandial subcutaneous injection of insulin lispro and a presleep subcutaneous injection of insulin glargine. The daily insulin consumption was approximately 47–64 units adjusted according to the blood glucose level. Six months prior, he had intermittent nausea and vomiting with no obvious inducement without abdominal pain and diarrhoea. He was diagnosed with diabetic ketosis (DK) by random intravenous plasma glucose with 21.4 mmol/L, arterial blood gas with pH 7.37, and urine ketone body with 3+. The symptoms were alleviated, and ketone bodies were negative after rehydration and insulin supplementation in the emergency department and then our endocrine department. After discharge, he still had intermittent nausea, vomiting, abdominal distension, and abdominal pain, especially after meals. He was given itopride hydrochloride tablets to promote gastrointestinal motility, pancreatin enteric-coated capsules to supplement digestive enzymes, and pinaverium bromide tablets to relieve symptomatic pain. Additionally, psychologists evaluated the patient's anxiety state and gave duloxetine and oxazepam to relieve anxiety. Unfortunately, the above treatment was not effective. Therefore, the patient himself stopped insulin injections and occasionally measured random peripheral blood glucose > 20 mmol/L. He was then admitted to our department for further diagnosis and treatment. During the course of DM, the patient had no blurred vision, numbness of limbs, cold feeling, acupuncture feeling, sleeve-like feeling, or intermittent claudication. He lost approximately 5 kg of weight in 9 months. For his past history, the patient was diagnosed with a renal cyst, kidney stone, and prostate cyst 3.5 years ago, 8 months ago, and 6 months ago, respectively. He denied a history of pancreatitis or pancreatic surgery. He was born at full term with a birth weight of 2.5 kg without hypoglycaemia. His growth and development are comparable to those of his peers. His mother and other family members did not have a history of DM. Physical examination results were as follows: temperature, 36.2°C; pulse, 72 times/min; respiration, 20 times/min; blood pressure, 140/87 mmHg; height, 175 cm; weight, 50 kg; BMI, 16.33 kg/m^2; waistline, 65 cm; hip, 77 cm; and waist-to-hip ratio, 0.84. He did not have a Cushing appearance. He had clear breath sounds in both lungs, no obvious dry and wet rales, regular heart rhythm, no murmur, and additional heart sounds in the auscultation area of each valve. He had boat-shaped abdomen, soft whole abdomen, mild tenderness in the upper abdomen, no rebound pain and muscle tension, normal bowel sounds, no oedema in both lower limbs, normal pulsation of bilateral dorsalis pedis arteries, normal sense of pain, temperature, and vibration, and a negative 10 g elastic wire test on both sides. Laboratory examination revealed that the venous fasting plasma glucose was 26.3 mmol/L, urine glucose 3+, and urine ketone body +. The arterial blood gas analysis was as follows: pH 7.46 (7.35–7.45), PaO_2 81 mmHg (80–100 mmHg), $PaCO_2$ 48 mmHg (35–45 mmHg), $HCO3^-$ 35.0 mmol/L (22–27 mmol/L), BE-b 10.5 mmol/L (–3.0 to 3.0 mmol/L), venous serum potassium ion 3.5 mmol/L (3.5–5.5 mmol/L), sodium ion 134 mmol/L (137–147 mmol/L), chloride ion 93 mmol/L (99–110 mmol/L), glycosylated haemoglobin 11.2% (4.0%–6.0%), and fasting serum C-peptide level fluctuated between 0.34–1.15 ng/ml (1.1–4.4 ng/ml) and 0.39–2.02 ng/ml 2 hours after breakfast (Figure 1). The patient was negative for glutamic acid decarboxylase antibody (GADA), islet cell antibody (ICA), and insulin autoantibody (IAA). The serum magnesium level fluctuated between 0.39 and 0.71 mmol/L (0.75–1.02 mmol/L). His liver function, glomerular filtration rate, serum lipids, uric acid, calcium, phosphorus, parathyroid hormone, and thyroid function were all within the normal range. The complications of diabetes were examined. No diabetic retinopathy was found in fundus photography, but cataracts were found in the right eye. The successive urinary microalbumin/creatinine ratio (UACR) was

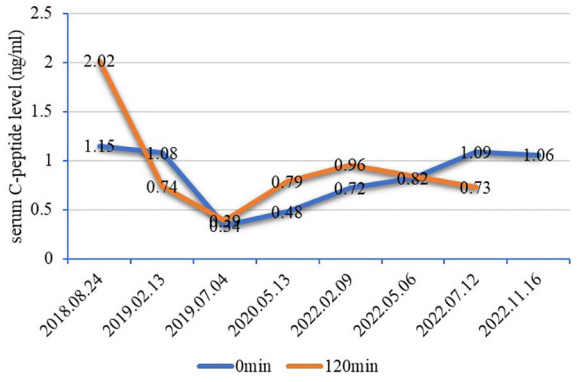

FIGURE 1
Line chart of serum C-peptide levels. The fasting serum C-peptide level fluctuated between 0.34–1.15 ng/ml (1.1–4.4 ng/ml) and 0.39–2.02 ng/ml for 2 hours after breakfast. There was islet β cell dysfunction but no absolute deficiency of serum C-peptide levels in this patient, which did not conform to the characteristics of T1DM. It is generally believed that C-peptide levels below 200 pmol/L (0.1 ng/ml) after stimulation indicate poor pancreatic function and that C-peptide levels below 600 pmol/L (0.2 ng/ml) after stimulation indicate that the islet function is damaged, which should alert to the possibility of T1DM or monogenic diabetes (5). T1DM, type 1 diabetes mellitus.

measured three times, and the values were 22.32 mg/g, 16.7 mg/g, and 15.85 mg/g (0–30 mg/g). Colour Doppler ultrasound of the carotid artery and lower limb artery showed no atherosclerotic plaque formation. Measurements of pulse wave velocity (PWV), ankle–brachial index (ABI), and quantitative sensory disturbance were normal. Digestive system diseases were evaluated. The enhanced CT scan of the abdomen showed agenesis of the dorsal pancreas (ADP) (considering pancreatic developmental variation), complex cysts of both kidneys, and small stones in the right kidney (Figure 2). An abdominal dynamic contrast-enhanced magnetic resonance scan did not show pancreatic duct dilation. Gastric emptying imaging showed that the gastric half-emptying time of semisolid food was approximately 80.53 min (37.25 ± 15.7 min). The tumor markers of the digestive tract, serum amylase, and lipase were normal. Gastroscopy showed chronic non-atrophic gastritis with bile reflux and a positive urease *Helicobacter pylori* (HP) test. Enteroscopy showed that the intestinal preparation was poor and that the mucosa below the sigmoid colon was normal. No abnormality was found in the upright abdominal plain film radiography and the ultrasound of the superior and inferior mesenteric arteries. The characteristics of this case are summarized as follows: 1) young onset of illness with a primary diagnosis of T1DM and therapy with long-term insulin replacement; 2) no family history of DM; 3) islet β cell dysfunction, but no absolute deficiency was observed; 4) negative for diabetes-related antibodies; and 5) abnormal development of multiple organs. Therefore, the diagnosis of T1DM was challenged. Specific types of DM could not be excluded. After informed consent of the patient was obtained, a peripheral blood sample was taken to Beijing Hope Group Biotechnology Co., Ltd., for examination. First, DNA interruption was performed, and a library was prepared. Then, DNA sample capture and PCR amplification were performed. Finally, the captured DNA samples were submitted for high-throughput sequencing. After the sequencing data were evaluated by Illumina Sequence Control Software (SCS) and qualified, data reading and bioinformatics analysis were performed. The results showed that the patient was suspected to have a heterozygous deletion mutation at [GRCh37 (hg19)] chr17:34842526-36347106 (1.5 Mb) that included 24 genes in total: *AATF*, *ACACA*, *C17orf78*, *DDX52*, *DHRS11*, *DUSP14*, *GGNBP2*, *HMGB1P24*, *HNF1B*, *LHX1*, *LHX1-DT*, *MIR2909*, *MIR378J*, *MRM1*, *MYO19*, *PIGW*, *RNA5SP439*, *RNU6-489P*, *SYNRG*, *TADA2A*, *TBC1D3K*, *TBC1D3L*, *YWHAEP7*, and *ZNHIT3* (Figure 3). This region contained the complete 17q12 recurrent region (including *HNF1B* gene), which is not enough to cause a disease with the confirmed single dose. According to the results of gene detection, the diagnosis was revised to 17q12 deletion syndrome. Considering the findings of poor long-term blood glucose control, significantly delayed gastric emptying time, and the digestive tract history, the patient was considered to have DGP. The treatment plan was as follows: 1) diet guidance of low-fat diabetes soft food or semiliquid food and multiple meals with small amounts for each, 2) insulin subcutaneous injection for glucose-lowering treatment, 3) mosapride citrate tablets for promoting total gastrointestinal motility, and 4) pancreatin enteric capsules for supplementing pancreatin. Treatment results and follow-up indicated that the

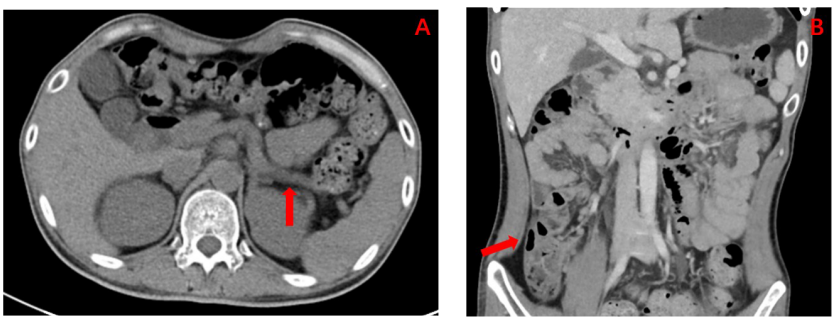

FIGURE 2
(A) Enhanced CT abdomen showing the result of dorsal pancreatic agenesis (as indicated by the red arrows; considering pancreatic developmental variation), an exceedingly rare congenital disease reported in the literature. **(B)** Enhanced CT abdomen showing the result of multiple complex renal cysts (as indicated by the red arrows).

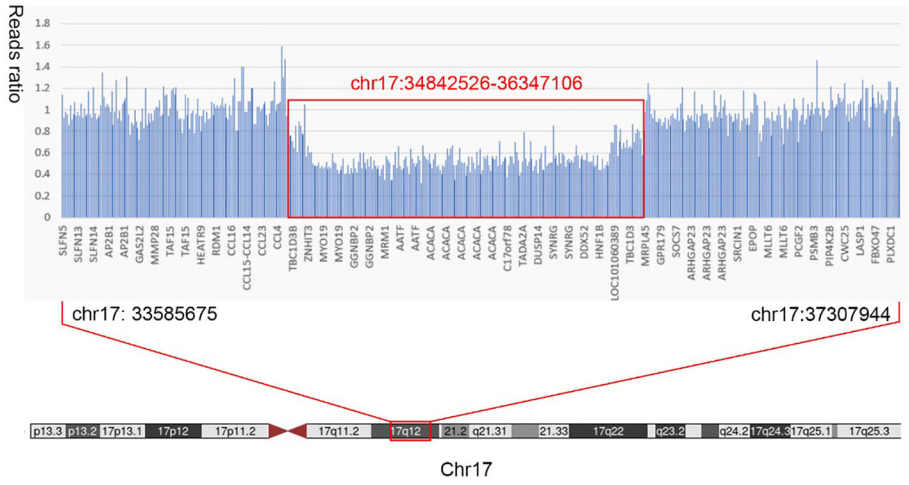

FIGURE 3
Results of whole-exon gene variation. The patient was suspected to have a heterozygous deletion mutation at chr17:34842526-36347106 (1.5 Mb) that included 24 genes in total: *AATF, ACACA, C17orf78, DDX52, DHRS11, DUSP14, GGNBP2, HMGB1P24, HNF1B, LHX1, LHX1-DT, MIR2909, MIR378J, MRM1, MYO19, PIGW, RNA5SP439, RNU6-489P, SYNRG, TADA2A, TBC1D3K, TBC1D3L, YWHAEP7,* and *ZNHIT3*.

patient's blood glucose fluctuation was reduced, with his fasting blood glucose fluctuating between 4 and 8 mmol/L and his 2-hour postprandial glucose fluctuating between 6 and 11 mmol/L. No symptomatic hypoglycaemia events occurred. His abdominal symptoms were significantly alleviated. Afterward, he did not seek medical attention due to unbearable abdominal pain (Table 1).

Discussion

Here, we report a novel case of diabetes mellitus type MODY5 as a feature of 17q12 deletion syndrome caused by a new 17q12 deletion mutation (including *HNF1B* gene) that has not been reported yet worldwide. 17q12 microdeletion syndrome, also known as 17q12 deletion syndrome, is a rare chromosomal anomaly caused by the deletion of a small amount of material from a region in the long arm of chromosome 17; this syndrome has an estimated prevalence of 1.6 per 100,000 citizens, with high penetrance and variable expressivity (6). Because the exogenic region on 17q12 is encompassed by segmental duplications, all patients with this syndrome exhibit the same unique genetic sequence of 1.4 Mb, including *HNF1B*, *ACACA*, and *LHX1* genes (7). It is typified by the deletion of more than 15 genes, including *HNF1B*, and results in kidney abnormalities, RCAD, and neurodevelopmental or neuropsychiatric disorders (4). This patient presented with kidney abnormalities and RCAD.

As described for intragenic *HNF1B* mutations, DM represents a frequent feature of 17q12 deletion syndrome and affects 63% of these patients (8). Although the association of DM and renal dysfunction in patients with *HNF1B* mutations is commonly known as RCAD, the frequent overlap of *HNF1B* mutations with 17q12 deletion syndrome is often underrecognized. Laffargue et al. (3) reported an association between *HNF1B* deletion and 17q12 deletion syndrome in virtually all cases. ADP is a very rare pancreatic developmental anomaly. During embryonic development, the dorsal pancreatic bud develops into the dorsal pancreas, which forms a small part of the pancreatic head, body, and tail. Less than 100 cases of ADP have been reported worldwide (9). There are two subtypes of ADP, complete and partial, in which the body or tail of the pancreas is underdeveloped or underdeveloped. In this case, the tail of the pancreas was missing, indicating partial dorsal pancreatic hypoplasia. The latest research has found that homeotic genes *GATA6* and *GATA4*, as well as human *HNF1B* gene, are involved in the regulation of pancreatic development. Human *HNF1B* gene belongs to the homeobox-containing family of transcription factors and is located on chromosome 17. It has regulatory effects on the morphological development of the pancreas and the differentiation of pancreatic endocrine cells (10–12). Because most islet cells are located in the tail of the pancreas, ADP usually causes insufficient islet cells, leading to the occurrence and development of diabetes. It also participates in the development of many important organs, including the kidney, liver, and reproductive system, and plays a central role in maintaining the normal function of organs (13). This gene is also the pathogenic gene of MODY5. The first *HNF1B* mutation with manifestation of MODY5 was described in 1997 (14). Since then, a great variety of clinical phenotypes have been described. The characteristic clinical manifestations of MODY5 include early-onset diabetes, kidney disease, pancreatic atrophy, pancreatic exocrine dysfunction, liver dysfunction, hypomagnesaemia, and urogenital abnormalities. Our patient presented with typical polycystic kidney manifestations, ADP, kidney stones, and prostate cysts, which were consistent with previous reports (15, 16). Although studies have shown that patients with mutations might have worse kidney damage than those with gene deletions (15), kidney damage was not present in this patient. These characteristics may exist without a family history because *de novo* mutations reportedly occur relatively frequently, as

TABLE 1 The timeline with relevant data from the episode of care.

Date		Symptoms	Examinations	Diagnosis	Treatments	Effects
2016 onset		thirst, polydipsia, polyuria	FPG: 8.5mmol/L, other results unavailable	T1DM	subcutaneous injection of short-acting insulin for three meals and long-acting insulin before bed (47-64 units per day)	repeated emergency or hospitalization treatment due to DK/DKA
2022.05.06		intermittent nausea, vomiting, abdominal distension and pain, diarrhea	FPG: 21.4mmol/L, HbA1c: 8.5%, fasting C-peptide: 0.82ng/ml, GADA: negative, ICA: negative, IAA: negative, urine glucose: 4+, urine ketone: 3+, arterial blood pH: 7.37, serum magnesium: 0.46mmol/L	DK	intravenous fluid infusion and insulin supplementation, itopride hydrochloride tablets, pancreatin enteric-coated capsules, pinaverium bromide tablets, duloxetine and oxazepam	peripheral blood sugar <10 mmol/L, urine glucose: 3+, urine ketone: +, no significant improvement in digestive system symptoms
2022.05.16-2022.08.22	2022.05.16	unresolved digestive symptoms including intermittent nausea, vomiting, abdominal distension and pain, diarrhea, aggravated after meals	gastroscopy: chronic non atrophic gastritis with bile reflux and a positive urease HP test	chronic non atrophic gastritis, Helicobacter pylori infection	Omeprazole Enteric-coated Capsules, Minocycline Hydrochloride Tablets, Colloidal Bismuth Pectin Capsules, Mosapride Citrate TabletsTrimebutine, Maleate Tablets, Berberine Hydrochloride Tablets, Montmorillonite Powder, Bacillus Licheniformis Capsule, Live Combined Bifidobacterium, Lactobacillus And Enterococcus Capsules, Pinaverium Bromide Tablets, Oryz-Aspergillus Enzyme and Pancreatin Tablet	poor response to treatment
	2022.07.09		enhanced CT scan of the abdomen: agenesis of the dorsal pancreas, complex cysts of both kidneys and small stones in the right kidney	ADP, complex renal cysts in both kidneys, right kidney stone		
	2022.07.22		ultrasound of the superior and inferior mesenteric arteries	Normal		
	2022.08.08		enteroscopy and upright abdominal plain film radiography	Normal		
	2022.08.10		MRCP	No dilation of pancreatic duct		
	2022.08.21		blood testing: liver function, CEA, CA19-9, CA72-4, AFP, amylase, lipase	Normal		
	2022.08.22		gastric emptying imaging: positive [a]	Gastroparesis	diet guidance of low-fat diabetes soft food or semiliquid food and multiple meals with small amounts for each	improved digestive system symptoms
2022.08.31			whole exon gene detection (plasma) [b]	17q12 Deletion Syndrome	insulin subcutaneous injection	FPG: 4-8 mmol/L, 2h-PPG: 6-11 mmol/L

FPG, fasting plasma glucose; T1DM, type 1 diabetes mellitus; DK, diabetic ketosis; DKA, diabetic ketoacidosis; GADA, glutamic acid decarboxylase antibody; IAA, insulin autoantibody; ICA, islet cell antibody; HbA1c, glycosylated haemoglobin; CT, computed tomography; ADP, genesis of the dorsal pancreas; MRCP, magnetic resonance cholangiopancreatography; CEA, carcinoembryonic antigen; CA19-9, cancer antigen 19-9; CA72-4, cancer antigen 72-4; AFP, alpha-fetoprotein; 2h-PPG, 2-hour postprandial glucose.

[a]Gastric emptying imaging showed that the gastric half-emptying time of semisolid food was approximately 80.53 min (37.25 ± 15.7 min).

[b]The results of plasma whole-exon gene detection showed that the patient was suspected to have a heterozygous deletion mutation at [GRCh37 (hg19)] chr17:34842526-36347106 (1.5 Mb). This region contained the complete 17q12 recurrent region (including HNF1B gene).

10.3389/fendo.2023.1205431

they are seen in 50%–60% of patients with *HNF1B* gene abnormalities (17, 18). This is believed to be the case. Currently, more than 230 *HNF1B* gene abnormalities have been identified, of which the incidence of gene deletions is higher than that of point mutations (19). However, most of them are heterozygous deletions. Large segment deletions or duplications of exons are extremely rare (15). Because almost half of patients diagnosed with MODY5 (*HNF1B* mutation) have a mutation in the form of a whole gene deletion, which is the most common cause of MODY5 (3), all patients with suspected MODY5 should be examined for common clinical features of 17q12 deletion syndrome to perform specific microarray testing of the deletion on chromosome 17q12. However, it should be noted that *de novo* mutations are responsible for 70% of 17q12 deletions (8). Thus, the absence of DM and other typical clinical features in their parents and other relatives could not exclude 17q12 deletion syndrome as a possible diagnosis. The risk for inheritance of this deletion in the offspring of affected patients is 50% (8). Consequently, all patients suspected or diagnosed with 17q12 deletion syndrome should be offered genetic counseling.

As mentioned earlier, ketoacidosis is rare at the time of diagnosis in patients with MODY5 (15). Studies have shown that there are differences in the function of islet cells in patients with MODY5 of different ethnic groups. Japanese individuals usually exhibit β cell dysfunction, while Caucasian individuals exhibit hyperinsulinaemia and insulin resistance (18). It is worth considering that the daily insulin dosage of this patient was 47–64 U, and the serum C-peptide level did not indicate an absolute lack of pancreatic islet function. However, he had recurring DK or DKA. Shenghui Ge et al. (20) reported possible reasons for this. First, there is obvious heterogeneity in MODY5 patients, and the clinical manifestations are different among different patients. Second, DK is a rare manifestation of MODY5 that might not have received much attention in previous studies (21). Finally, there might be a cumulative effect in the development of diabetes and DK, which occur when the disturbance of glucose metabolism caused by the mutation reaches a certain level. It has been reported that *HNF1B* mutations can also affect Na-Cl cotransporter function in the distal convoluted tube, leading to hypokalaemia, hypomagnesaemia, and metabolic alkalosis (22, 23). In the present case, hypomagnesaemia caused by Na-Cl cotransporter dysfunction seems to predominate over mild DKA caused by insulin deficiency in MODY5. In addition, DK typically manifests with acidaemia due to an accumulation of acidic ketone bodies. However, it can present as alkalaemia under certain but limited conditions, including vomiting and the use of diuretics. In this case, before the onset of nausea, vomiting, and abdominal pain, he had recurring DK and DKA. Thus, the above aetiological mechanisms are not suitable for this case. In addition, DKA resolved gradually after insulin therapy, but the abdominal pain, nausea, and vomiting continued. Although endocrine dysfunction constitutes one of the defining clinical manifestations of 17q12 deletion syndrome, impairment of exocrine pancreatic function is highly variable. Dubois-Laforgue et al. (15) reported exocrine pancreas dysfunction in 29 of 38 investigated patients (76%). Natascha Roehlen et al. (7) also revealed a frequency of 69% in all reported cases of *HNF1B* deletion. Tian Yang et al. (24) reviewed 22 cases of ADP with dorsal pancreatic hypoplasia. Although the majority of ADP patients were asymptomatic, abdominal pain was the most commonly reported symptom. Regrettably, the faecal elastase level could not be measured for our patient. After the experimental administration of pancreatin supplement, the patient's abdominal pain did not improve significantly. He also had digestive tract symptoms such as nausea, vomiting, and abdominal distension, which were significantly worse after eating meals. Considering the long-term poor control of blood glucose, the gastric emptying time was significantly delayed. There was reason to believe that DGP was also involved in the occurrence of abdominal pain. Therefore, a low-fat diet was recommended, and pancreatic enzyme supplements and mosapride citrate were given with meals to facilitate the digestive process. Abdominal pain and other gastrointestinal symptoms improved gradually.

Conclusion

In summary, we first reported a novel case of diabetes mellitus type MODY5 as a feature of 17q12 deletion syndrome with DGP. The deletion mutation at chr17: 34842526-36347106 has not yet been reported, which will further broaden the gene mutation spectrum of 17q12 deletion syndrome. It is worth noting that, as a manifestation of 17q12 deletion syndrome, MODY5 patients may have recurrent DK or DKA or no family history of DM. For patients with early-onset diabetes who are negative for insulin-related antibodies and have hypomagnesaemia and abnormalities of the kidney and pancreas, we should be alert to MODY5. Gene detection technology can assist endocrinologists in correctly diagnosing MODY5 or 17q12 deletion syndrome. However, it can also formulate appropriate therapy and conduct genetic screening counseling for their family members to guide and optimize fertility. However, this case report still has certain limitations. 1) Unfortunately, we were unable to obtain the patient's genetic pedigree. 2) As this is a case of 17q12 syndrome, it is regrettable that the patient's reproductive tract structure and function were not tested to comprehensively track the characteristics of their case. 3) The number of cases should be increased, and their clinical commonalities should be summarized to better understand the disease.

Data availability statement

The original contributions presented in the study are included in the article/supplementary material. Further inquiries can be directed to the corresponding author.

Ethics statement

The studies involving humans were approved by Biomedical Ethics Committee of Peking University International Hospital.

The studies were conducted in accordance with the local legislation and institutional requirements. The participants provided their written informed consent to participate in this study. Written informed consent was obtained from the individual(s) for the publication of any potentially identifiable images or data included in this article.

Author contributions

SX: Data extraction, data analysis, essay writing, and paper submission. XZ: Critical revision and paper submission. All authors contributed to the article and approved the submitted version.

Conflict of interest

The authors declare that the research was conducted in the absence of any commercial or financial relationships that could be construed as a potential conflict of interest.

Publisher's note

References

1. Fajans SS, Bell GI. MODY: history, genetics, pathophysiology, and clinical decision making. *Diabetes Care* (2011) 34:1878–84. doi: 10.2337/dc11-0035

2. Mateus JC, Rivera C, O'Meara M, Valenzuela A, Lizcano F. Maturity-onset diabetes of the young type 5 a MULTISYSTEMIC disease: a CASE report of a novel mutation in the HNF1B gene and literature review. *Clin Diabetes Endocrinol* (2020) 6:16. doi: 10.1186/s40842-020-00103-6

3. Laffargue F, Bourthoumieu S, Llanas B, Baudouin V, Lahoche A, Morin D, et al. Towards a new point of view on the phenotype of patients with a 17q12 microdeletion syndrome. *Arch Dis Childhood* (2015) 100:259–64. doi: 10.1136/archdischild-2014-306810

4. Nakamura M, Kanda S, Kajiho Y, Morisada N, Iijima K, Harita Y. A case of 17q12 deletion syndrome that presented antenatally with markedly enlarged kidneys and clinically mimicked autosomal recessive polycystic kidney disease. *CEN Case Rep* (2021) 10:543–8. doi: 10.1007/s13730-021-00604-y

5. Holt RIG, DeVries JH, Hess-Fischl A, Hirsch IB, Kirkman MS, Klupa T, et al. The management of type 1 diabetes in adults. A consensus report by the American Diabetes Association (ADA) and the European Association for the Study of Diabetes (EASD). *Diabetologia* (2021) 64:2609–52. doi: 10.1007/s00125-021-05568-3

6. Rasmussen M, Vestergaard EM, Graakjaer J, Petkov Y, Bache I, Fagerberg C, et al. 17q12 deletion and duplication syndrome in Denmark-A clinical cohort of 38 patients and review of the literature. *Am J Med Genet Part A* (2016) 170:2934–42. doi: 10.1002/ajmg.a.37848

7. Roehlen N, Hilger H, Stock F, Gläser B, Guhl J, Schmitt-Graeff A, et al. 17q12 deletion syndrome as a rare cause for diabetes mellitus type MODY5. *J Clin Endocrinol Metab* (2018) 103:3601–10. doi: 10.1210/jc.2018-00955

8. Mitchel MW, Moreno-De-Luca D, Myers SM, Levy RV, Turner S, Ledbetter DH, et al. 17q12 recurrent deletion syndrome. In: Adam MP, Everman DB, Mirzaa GM, Pagon RA, Wallace SE, Bean LJH, Gripp KW, Amemiya A, editors. *GeneReviews®*. Seattle: University of Washington (1993).

9. Cienfuegos JA, Rotellar F, Salguero J, Benito A, Solórzano JL, Sangro B. Agenesis of the dorsal pancreas: systematic review of a clinical challenge. *Rev Espanola Enfermedades Digestivas* (2016) 108:479–84. doi: 10.17235/reed.2016.4474/2016

10. Stanescu DE, Hughes N, Patel P, De León DD. A novel mutation in GATA6 causes pancreatic agenesis. *Pediatr Diabetes* (2015) 16:67–70. doi: 10.1111/pedi.12111

11. Shaw-Smith C, De Franco E, Lango Allen H, Batlle M, Flanagan SE, Borowiec M, et al. GATA4 mutations are a cause of neonatal and childhood-onset diabetes. *Diabetes* (2014) 63:2888–94. doi: 10.2337/db14-0061

12. De Vas MG, Kopp JL, Heliot C, Sander M, Cereghini S, Haumaitre C. Hnf1b controls pancreas morphogenesis and the generation of Ngn3+ endocrine progenitors. *Dev (Cambridge England)* (2015) 142:871–82. doi: 10.1242/dev.110759

13. El-Khairi R, Vallier L. The role of hepatocyte nuclear factor 1β in disease and development. *Diabetes Obes Metab* (2016) 18 Suppl 1:23–32. doi: 10.1111/dom.12715

14. Horikawa Y, Iwasaki N, Hara M, Furuta H, Hinokio Y, Cockburn BN, et al. Mutation in hepatocyte nuclear factor-1 beta gene (TCF2) associated with MODY. *Nat Genet* (1997) 17:384–5. doi: 10.1038/ng1297-384

15. Dubois-Laforgue D, Cornu E, Saint-Martin C, Coste J, Bellanné-Chantelot C, Timsit J, et al. Diabetes, associated clinical spectrum, long-term prognosis, and genotype/phenotype correlations in 201 adult patients with hepatocyte nuclear factor 1B (HNF1B) molecular defects. *Diabetes Care* (2017) 40:1436–43. doi: 10.2337/dc16-2462

16. Nagano C, Morisada N, Nozu K, Kamei K, Tanaka R, Kanda S, et al. Clinical characteristics of HNF1B-related disorders in a Japanese population. *Clin Exp Nephrol* (2019) 23:1119–29. doi: 10.1007/s10157-019-01747-0

17. Ulinski T, Lescure S, Beaufils S, Guigonis V, Decramer S, Morin D, et al. Renal phenotypes related to hepatocyte nuclear factor-1beta (TCF2) mutations in a pediatric cohort. *J Am Soc Nephrol JASN* (2006) 17:497–503. doi: 10.1681/ASN.2005101040

18. Carrillo E, Lomas A, Pinés PJ, Lamas C. Long-lasting response to oral therapy in a young male with monogenic diabetes as part of HNF1B-related disease. *Endocrinol Diabetes Metab Case Rep* (2017) 2017:17–0052. doi: 10.1530/EDM-17-0052

19. Stenson PD, Mort M, Ball EV, Evans K, Hayden M, Heywood S, et al. The Human Gene Mutation Database: towards a comprehensive repository of inherited mutation data for medical research, genetic diagnosis and next-generation sequencing studies. *Hum Genet* (2017) 136:665–77. doi: 10.1007/s00439-017-1779-6

20. Ge S, Yang M, Gong W, Chen W, Dong J, Liao L. Case Report: A case of HNF1B mutation patient with first presentation of diabetic ketosis. *Front Endocrinol* (2022) 13:917819. doi: 10.3389/fendo.2022.917819

21. Haaland WC, Scaduto DI, Maldonado MR, Mansouri DL, Nalini R, Iyer D, et al. A-beta-subtype of ketosis-prone diabetes is not predominantly a monogenic diabetic syndrome. *Diabetes Care* (2009) 32:873–7. doi: 10.2337/dc08-1529

22. Bech AP, Wetzels JF, Bongers EM, Nijenhuis T. Thiazide responsiveness testing in patients with renal magnesium wasting and correlation with genetic analysis: A diagnostic test study. *Am J Kidney Dis Off J Natl Kidney Foundation* (2016) 68:168–70. doi: 10.1053/j.ajkd.2015.12.023

23. Hayakawa-Iwamoto A, Aotani D, Shimizu Y, Kakoi S, Hasegawa C, Itoh S, et al. Maturity-onset diabetes of the young type 5, presenting as diabetic ketoacidosis with alkalemia: A report of a case. *J Diabetes Invest* (2022) 13:923–6. doi: 10.1111/jdi.13737

24. Yang T, Yang X, Wang L, Mo J. Agenesis of the dorsal pancreas presenting with diabetic ketoacidosis - a case report and literature review. *BMC Endocr Disord* (2019) 19:120. doi: 10.1186/s12902-019-0449-1

frontiers | Frontiers in Pediatrics

TYPE Review
PUBLISHED 16 November 2023
DOI 10.3389/fped.2023.1252035

OPEN ACCESS

EDITED BY
Sijung Yun,
Predictiv Care, Inc., United States

REVIEWED BY
Luis Rodrigo Macias Kauffer,
Universität zu Lübeck, Germany
Modupe Coker,
The State University of New Jersey, United States

*CORRESPONDENCE
Sheng Guo
guosheng@shchildren.com.cn

RECEIVED 03 July 2023
ACCEPTED 02 November 2023
PUBLISHED 16 November 2023

CITATION
He P, Shen X and Guo S (2023) Intestinal flora and linear growth in children.
Front. Pediatr. 11:1252035.
doi: 10.3389/fped.2023.1252035

Intestinal flora and linear growth in children

Pingsihua He, Xingyuan Shen and Sheng Guo*

Department of Endocrine, Genetics and Metabolism, Shanghai Children's Hospital, School of Medicine, Shanghai Jiao Tong University, Shanghai, China

The gut microbiota plays a critical role in human growth and development as well as the regulation of human pathophysiological processes. According to research, the gut microbiota controls the host's growth and development in areas such as nutrition, metabolism, endocrine hormones, and immune modulation. The human gut microbiota has an important role in child and adolescent growth, especially when nutritional conditions are poor. In this review, we focus on recent findings about the gut microbiota's influence on child growth, including the relationship between the gut microbiota and linear growth during pregnancy, infancy, childhood, and adolescence. Furthermore, we also review some mechanisms by which intestinal flora influence the host's linear growth. Although the data supports a link between intestinal flora and linear development in children, our review has limitations that prohibit us from fully verifying the causal relationship between gut flora and linear development in children. Improving the gut microbiota, in conjunction with renutrition techniques, has the potential to ameliorate the growth and development impairments currently associated with chronic illness and malnutrition in children.

KEYWORDS

intestinal flora, linear growth, IGF-1 (insulin-like growth factor-1), microbiota, SCFAs (short-chain fatty acids)

Introduction

Human development is divided into four distinct stages: fetal, infant, childhood, and adolescence. Each growth phase is governed by specific endocrine processes and is influenced by genetic, nutritional, and environmental factors (1). Growth retardation is defined as a problem in which individuals have significantly lower growth rates than healthy individuals, which is accompanied by metabolic disorders, systemic inflammation, or intestinal ecological dysregulation (2). After the age of two years, linear growth retardation caused by childhood malnutrition is largely irreversible (3). As a result, prevention or reversal of early interventions for factors contributing to growth retardation provides the best opportunity to improve outcomes (4). Growth retardation is the underlying cause of high morbidity and mortality in children under the age of five (5); it affects approximately 20% of children worldwide (2). Childhood malnutrition, which includes fetal growth restriction, growth retardation, wasting, vitamin A and zinc deficiency, and inadequate breastfeeding, has recently been estimated to cause 3.1 million child deaths per year, accounting for 45% of all child mortality (6). Infants with growth disorders are more likely to die from sepsis, pneumonia, diarrhea, and other infections, as well as from growth retardation (7). Long-term effects of infant malnutrition include short stature and low body weight, immune dysfunction and increased infection risk that persist into adulthood, cognitive impairment, poor academic performance, and decreased productivity in adulthood (8), and being less likely to reach their growth potential in adulthood (3).

Intestinal flora and human development

The gastrointestinal tract is home to trillions of microbes, known as the "gut microbiome". Bacteria, fungi, archaea, viruses, and protozoa make up the vast majority of the normal human gut microbiota. Firmicutes and Bacteroidetes were the most abundant in the intestinal flora, while Actinomycetes, Verrucomicrobia, and Proteobacteria were less abundant. The gut microbiota has the potential to influence our physiology in both health and disease (9). Because of the relationship between diet, different physiological states, and the microbiota's ability to produce metabolites from dietary consumption, these important features of the gut microbiota drive research into the functional aspects of microbial diversity (10). Dysbiosis, or disruption of the normal balance between gut microbiota and host, has been linked to the development and progression of obesity and other metabolic disorders, such as diabetes, insulin resistance, and early features of metabolic syndrome, in which the microbiota, the immune system, metabolic pathways, and inflammatory and allergic processes may be involved. Early in infancy, the fecal microbiota is dynamic and can be classified into three separate phases: developmental (3–14 months), transitional (15–30 months), and stable (31–46 months) (9). The first microbial occupancy has a significant impact on the overall health of life. Probiotic supplementation early in life reduces the incidence of neuropsychiatric issues in infancy, according to a study that investigates how the gut microbiota may influence nervous system function (11). Within the first 6 months of life, 75 infants were randomly assigned to either *Lactobacillus* rhamnosus GG or a placebo and were observed for 13 years. At the age of 13, 17.1% of children in the placebo group had attention deficit hyperactivity disorder (ADHD) or Asperger's syndrome, but no children in the probiotic group did (11). Any disruption in the colonization process of the gut microbiome could have long-term consequences for the host's growth, development, and later health. Infants' length, weight, and head and chest circumferences all increase dramatically during this phase of rapid growth. As the gut microbiota matures three years after birth, the prenatal period and the first three years of life are regarded as critical times for the formation of microbial colonization patterns (9). One of the most critical goals of postnatal development is to acquire a gut microbiota capable of benefiting from functions in the environment while also establishing a mucosal immune system capable of tolerating preferred community members and suppressing pathogens. Initially, it was thought that this colonization began during the birth process, but a study describing the identification of bacterial DNA in the placentas of healthy term infants and the discovery of bacteria in the amniotic fluid and meconium of preterm infants confirmed that the fetal gut bacteria groups may have appeared earlier (12).

Many factors influence the development and maturation of the gut microbiota, including placental inflammation, maternal infection during pregnancy, pregnancy course, duration, type of delivery, perinatal conditions, hospital environment and length of stay, feeding methods, antibiotic use, life methods, and geographic factors (13–16). Growth retardation has been linked to a variety of causes, including microbiome dysbiosis, neuroinflammation, endocrine disruptions, starvation, maternal influence, and stress (17). Immature microbiomes interact with risk factors for growth retardation in a two-way fashion, with gut infections, nutrition, birth weight, and other factors both impacting and being influenced by the "growth-restricted" microbiome (2). Overall, improper gut microbiota establishment, particularly in the first two years of life, can affect growth trajectories. Some of the theorized mechanisms of how the gut microbiota influences body weight include increased food energy acquisition, fat deposition promotion, altered exercise activity, satiety effects, and systemic inflammation activation (18).

Gut microbiota and linear growth

The influence of gut flora on prenatal linear growth

Fetal growth and development throughout pregnancy are significantly influenced by the fetal environment and the exchange of the fetal-maternal interface. Problems with fetal growth may result from changes in the intestinal flora of the pregnant mother brought on by the mother's genetic make-up, diet throughout pregnancy, delivery method, etc. The findings of genome-wide association studies indicate that there are 12,111 distinct single-nucleotide polymorphisms that are significantly linked with height and are predicted to explain 40%–50% of the phenotypic variance in human height (19). According to studies, the gut microbiota of preterm neonates' siblings in Actinobacteria, Bacilli, Bacteroidia, Clostridia, Erysipelotrichia, and Negativicutes bacteria share significant similarities, implying genetic or shared maternal and environmental effects on the preterm infant gut microbiota (20). Different genetic backgrounds also have an impact on microbial composition, immunological response, and host metabolism, all of which are critical for growth and development. It was shown that some genes associated with growth retardation in genetically defective mice have a dysbiosis of the gut flora. Nod2-deficient mice, for example, lack apoptotic and antifungal responses, have low bacterial populations in the gut, and are vulnerable to pathogenic infections; Card9 knockout mice show hindgut flora dysbiosis (21).

Maternal stunting is a risk factor for low birth weight and subsequent childhood stunting in low- and middle-income countries, sustaining a vicious intergenerational cycle of starvation. This cycle has a negative impact on the child's survival, growth, and neurodevelopment (4). Maternal gut inflammation is linked to poor fetal growth and poor delivery outcomes (4). According to a study of 19 longitudinal birth cohorts, small-for-gestational-age newborns contribute for 20% of childhood stunting and 30% of childhood wasting globally (22). Maternal height was found to be inversely related to child

stunting and overall child mortality in all low-income nations (23). This finding could be attributed to physical limits on fetal growth in smaller mothers, but other factors such as maternal inflammation, gut function, microbiota, and epigenetics could also play a role (4, 24). With an estimated 20% of stunting occurring *in utero*, intervention during the first few years of life may not be enough to prevent some of the most severe consequences of growth failure (25).

The diet of a mother during pregnancy and lactation influences the quantity of her microbiota, changing the bacterial repertoire that can be passed down to her kids during pregnancy and early life (26). The acquisition, composition, and microbial activity of the early newborn microbiota are influenced by maternal weight growth during pregnancy. Women who gained more weight during pregnancy had more bacterial diversity and richness than pregnant mothers who gained less weight. Infants born to moms more gestational weight were more likely to have a significant Bacteroidetes pattern and were less likely to have a Firmicutes dominant profile (27, 28). Several studies have confirmed the link between changes in maternal gut flora during childbirth and maternal gestational weight gain. Overweight moms' babies exhibited considerably higher amounts of fecal *Bacteroides* and *Staphylococcus* throughout the first 6 months. More *Bacteroides*, *Clostridium*, and *Staphylococcus* and fewer *Bifidobacterium* were related with higher maternal body weight and body mass index (BMI). Concentrations of *Akkermansia muciniphila*, *Staphylococcus*, and *Clostridium* were lower in infants born to normal-weight moms and mothers who reached normal gestational weight (29, 30).

In utero growth retardation is linked to maternal and placental inflammation and infection, as well as significant changes in host hormone levels, revealing a role for the microbiota-brain axis in fetal growth before birth (31). It is commonly acknowledged that vertical mother-to-infant microbiota transfer has a major impact on baby growth trajectories. Maintaining maternal microbial homeostasis is therefore crucial for preventing metabolic disruptions and growth deficits in children (32). Unfavorable factors, such as an unhealthy maternal diet during pregnancy, can have an effect on the mother's endocrine system and the acquisition of the infant's gut microbiota. One study revealed that a high-fat diet during pregnancy reduced bacterial colonization of the infant's gut and increased enterococci enrichment, with the impact lasting around a month after birth (33).

The manner of delivery, which transmits the neonatal gut microbiota and influences microbial composition, heredity, and function, is a fundamental driver of gut categorization in the first year of life. Vaginal birth has been demonstrated to enhance gut maturation and microbial variety, but cesarean surgery has been linked to gut microbiota acquired through maternal skin commensal bacteria. *Bacteroides* and *Bifidobacterium* were more abundant in infants born vaginally during the first three months of life, *Lactobacillus* and *Bacteroides* during the second three months of life, *Bacteroides* and *Bifidobacterium* during the second six months of life, and *Bacteroides*, *Enterobacter*, and *Streptococcus* after the first year of life. While infants born via cesarean section showed greater levels of *Clostridium* and *Lactobacillus* during the first three months of life, *Enterococcus* and *Clostridium* during the second three months of life, and *Lactobacillus* and *Staphylococcus* beyond the first year of life (34–36).

Preterm delivery, small-for-gestational age (SGA), or both cause approximately 20% of stunting (22). Preterm infants' initial gut microbiota differs from that of full-term newborns, and its microbiota composition is linked to changes in the composition of the mother's gut microbiota. A cross-sectional research of 55 preterm newborns discovered that preterm neonates had much lower gut microbiota alpha diversity and unique beta diversity clustering than term neonates. The contribution of maternal gut microbiota to first preterm gut colonization was greater after spontaneous delivery than after iatrogenic delivery and was not dependent on delivery mode (37). An Italian pilot study discovered that an increase α-diversity levels, and hence a decrease in *Lactobacillus* in the vaginal environment, may be connected with an increased risk of spontaneous preterm birth (38). When compared to full-term infants, the microbiota of preterm infants is determined by the date of gestation, with decreased variety and increased abundance of potentially pathogenic bacteria and decreased abundance of beneficial bacteria such as *Bifidobacterium* (39). SGA infants frequently have difficult pregnancies and deliveries, and prenatal events can alter gut and immune system maturation, as well as impair microbial balance and succession. Furthermore, stressors associated with neonatal life in the hospital, such as frequent antibiotic usage, invasive procedures, and maternal separation, can all lead to dysbiosis (40). A small cohort study discovered that SGA newborns had smaller abundances of *Klebsiella* and *Enterobacter* than AGA infants, and the Beta diversity of bacterial community structure began to segregate at postnatal day 30 (41). Transcriptome investigations of the SGA rat model revealed that IGF-2 expression was considerably reduced in CUG (catch-up growth)-SGA rats, which was associated with a decrease in lactic acid bacteria (42). The gut microbiome influences SGA infants' long-term prognosis in addition to regulating intrauterine growth. The incidence of Neisseriaceae, mucosal-hemolytic bacteria known to absorb iron-bound host proteins including hemoglobin, was considerably greater in the placental microbiota of intrauterine growth restriction (IUGR) patients. Furthermore, the rise of anaerobic bacteria like *Desulfovibrio* represents the development of a hypoxic environment in the IUGR placenta (43). In SGA newborns, certain pathogenic and conditional pathogenic bacteria, such as *Shigella*, *Ralstonia*, and *Clostridium*, increased or became the dominant microbiota. *Bacteroides fragilis* and *Clostridium saccharobutylicum* were detected in SGA newborns and may be linked to neurodevelopmental outcomes at 6 months (44).

In summary, the maternal microbiota is directly linked to the health of the baby, and its disruption can result in fetal growth and development abnormalities such as premature birth, SGA newborns, and macrosomia. Genetic variables (20), nutrition before and during pregnancy (30), manner of birth (36), and gestational age at birth (41) all influence baby microbiome colonization. *Lactobacillus* and *Bifidobacterium* have been shown to promote fetal growth, but pathogenic bacteria such as *Shigella*, *Ralstonia*, and *Clostridium* have been found to inhibit baby growth (29, 39). Furthermore, particular early-life microbes such as *Bacteroides*

fragilis and *Clostridium saccharobutylicum* are important for offspring brain development, which can affect baby health and long-term health (44). As a result, sensible treatments to change maternal or offspring microbiome from pregnancy to early childhood have significant implications for offspring health. However, current research on the gut microbiota of mothers and infants is primarily based on 16S RNA gene sequencing results. More research is needed to determine the actual mechanism of the effect on the microbiota and fetal growth, and there is still a long way to go before employing microbiota to interfere in fetal growth. There is still more to be discovered. The investigations on the effect of gut flora on prenatal linear development are summarized in **Table 1**.

Intestinal flora and early infant growth and development

Colonization of the newborn gut is thought to be vital for healthy growth because it influences gut maturation, metabolic, immunological, and brain development in early life. Microbiota interactions throughout infancy may be an important predictor of the host's long-term metabolic effects (45). Infants' early eating patterns and nutritional status are critical for the early molding of intestinal flora, and the interplay between intestinal flora and nutrition is critical for growth and development during infancy. In southern India, a longitudinal investigation of the gut microbiota of 10 infants with low birthweight and chronic stunting and 10 children with normal birthweight and no indications of stunting was done. From 3 months to 24 months of age, fecal samples were collected and examined every 3 months. The LEfSe algorithm was used to analyze differentially enriched taxa and found that the microbiota of stunted children was enriched in inflammatory bacteria from the Proteobacteria phylum, whereas the microbiota of normally developing children was enriched in probiotics, such as *Bifidobacteria longum* (12). A 6-year retrospective study of preterm children born at 35 weeks indicated that optimum postnatal nutrition enhanced early catch-up weight growth and improved linear development while having no influence on childhood BMI (46). According to a research of 108 healthy neonates in their first half year of life, breastfed

TABLE 1 Summarizes clinical studies on the effect of gut flora on prenatal linear growth.

Clinical situation	Author/year & geographic location	Study design	Growth features & influences	Features of gut microbial community	Identification strategy	PMID
Gestational weight gain	Collado et al., 2010, Finland	Case-control study	Maternal overweight and infant birth weight	The ratio of *Bifidobacterium* to *Clostridium coccoides* was considerably higher in infants born to normal-weight mothers than in infants born to overweight mothers.	FCM-FISH qPCR	20844065
	Stanislawski et al., 2017, Norway	Cohort study	Maternal weight gain, and the gut microbiota	Maternal pre-pregnancy OW/OB and excessive GWG were linked to the highly heritable family *Christensenellaceae*, the genera *Lachnospira*, *Parabacteroides*, *Bifidobacterium*, and *Blautia*.	16S rRNA sequencing	28870230
	Aatsinki et al., 2018, Finland	Cohort study	Gut microbiota and gestational weight gain	Firmicutes-dominated mid-pregnancy showed lower gestational weight growth than Bacteroidetes-dominated mid-pregnancy.	16S rRNA sequencing	29757063
Preterm birth	Prince et al., 2016, United States	Cross-sectional	Placental membrane microbiome and preterm birth	There was a considerable abundance of both urogenital and oral commensal bacteria in preterm patients with chorioamnionitis.	Whole-genome shotgun metagenomics.	26965447
	Jia et al., 2022, China	Cohort study	Preterm infants and gut microbes	The abundance of *Bifidobacterium* rose in the extremely preterm group until 120 days after birth, but it remained steady in the intermediate to late preterm and full term groups from day 14 after birth.	16S rRNA sequencing	35847070
	Chu et al., 2016, United States	Cohort study	Maternal high-fat diet and infant gut microbiome varies	*Bacteroides* levels were significantly lower in neonates exposed to a high-fat pregnancy diet.	16S rRNA sequencing	27503374
	Tirone et al., 2022, Italy	Pilot study	Maternal and neonatal microbiota and spontaneous preterm birth	Decrease in *Lactobacillus* in the vaginal environment, may be connected with an increased risk of spontaneous Preterm Birth	16S rRNA sequencing	35935374
	Hiltunen et al., 2022, Finland	Cross-sectional study	Maternal and neonatal microbiota and preterm birth	Preterm neonates had much lower gut microbiota alpha diversity and unique beta diversity clustering than term neonates.	16S rRNA sequencing	34349229
Small-for-gestational age	Chang et al., 2022, Taiwan	Cohort study	Gut microbiota and very low birth weight	SGA newborns had smaller abundances of *Klebsiella* and *Enterobacter* than AGA infants.	16S rRNA sequencing	36501188
	Chen et al., 2022, China	Cohort study	Gut microbiota in SGA infants and neurodevelopmental outcomes	Bacteroidota, *Bacteroides*, *Bacteroides fragilis*, and *Clostridium saccharobutylicum* may be linked to neurodevelopmental outcomes of SGA infants.	16S rRNA sequencing	36090083
	Hu et al., 2021, United States	Pilot study	Placental microbiota and SGA	The prevalence of *Neisseriaceae*, mucosal-hemolytic bacteria, was significantly higher in IUGR patients' placental microbiome.	16S rRNA sequencing	33107014

FCM-FISH, fluorescence *in situ* hybridization combined with flow cytometry; qPCRs, quantitative real-time PCRs; OW/OB, overweight/obese, GWG, gestational weight gain; SGA, small-for-gestational age.

newborns had more *Lactobacillus*, *Bacteroides*, and *Bifidobacterium* and less pathogens in their gut, which correlates to an accelerated rate of growth in infants (45). A significant decrease in the abundance of sialylated human milk oligosaccharides (HMOs) in human milk can result in severe growth failure in infants. Supplementation with sialylated HMOs promotes microbiota-dependent growth in stunted infants, possibly due to increased *Bifidobacteriaceae* abundance in infant gut (47). The amount of this oligosaccharide in the milk of malnourished mothers was reduced. The researchers discovered increased muscle mass, stronger bones, and significant changes in liver and brain metabolism when they administered oligosaccharides purified from whey to mice transplanted with stool from severely malnourished children. It implies that these findings have far-reaching implications and that controlling intestinal flora can affect children's nutritional status, but more clinical research is needed to back up these animal-based speculations (48). Microbial changes caused by weaning disruption delay intestinal barrier maturation and increase susceptibility to allergic inflammation, which may result in later growth retardation (49). Human breast milk contains a "different type of lactose" than cow's milk, which contains hundreds of oligosaccharides that promote Bifidobacteriales growth, according to research. Breastfeeding promotes the development of sensible and beneficial flora and assists babies in developing normally (50).

Poor infant hygiene and antibiotic-induced intestinal flora disruption are other key causes of linear growth disorder in newborns and early children. In Bangladeshi 2-years-old, small intestinal bacterial overgrowth (SIBO) was linked to poor hygiene, intestinal inflammation, and shorter length for age (51). Although no differences in intestinal permeability fecal markers were found in these SIBO-positive children, they did have elevated fecal calprotectin levels and were more likely to have growth retardation by the age of two (52). Evidence suggests that early-life antibiotic exposure is related to baby development and speed. One putative biological mechanism underpinning the effects of antibiotics on offspring development was structural and functional changes in the gut microbiota. A study from the Shanghai Mother-Child Pair Cohort examined 18 common antibiotics in meconium, including chlortetracycline, penicillin, and chloramphenicol, and used a multivariate linear regression model to examine antibiotic exposure, infant gut flora, and growth and development. Interdependence of indicators penicillin was discovered to have a negative relationship with gut microbiota Pielou and Simpson's index and a favorable relationship with growth velocity at 2–6 months (53). Another research investigating the long-term effects of neonatal and early childhood antibiotic exposure on child growth in an unselected birth cohort of 12,422 full-term infants discovered that males had significantly lower weight and height gains than girls during the first 6 years of life. Neonatal antibiotic exposure was linked to significant changes in the gut microbiome, notably a decrease in the number and diversity of fecal Bifidobacteriales before the age of two. Transplanting fecal microbiota from antibiotic-exposed children onto germ-free male mice resulted in substantial growth failure. Antibiotic exposure during pregnancy has been related to long-term changes in the gut microbiota, which may result in reduced growth in males during the first six years of life, according to this research (54). Another study revealed that early antibiotic exposure was not connected with enhanced growth velocity between delivery and discharge in neonates and infants in intensive care units inpatient antibiotics (55).

Linear growth disorder in infancy is connected with abnormal immunological inflammation and the disruption of gut flora. Prior to growth decrease, children with developmental delay had higher gut bacterial diversity and elevated inflammatory biomarkers, according to a longitudinal study of 78 Peruvian infants aged 5–12 months. Throughout the study, the fecal microbiota composition of stunted children was more diverse than that of healthy controls. *Ruminococcus 1* and *2*, *Clostridium sensu stricto*, and *Collinsella* abundance increased in stunted children but not in controls, but *Providencia* abundance dropped. The authors suggest that chronic, low levels of microbial translocation across the gastrointestinal mucosa may be the source of immune activation in children with developmental delays. However, because abnormalities in the gut microbiome exist prior to growth retardation, inflammatory chemicals derived by microbes may also contribute to chronic local irritation (56). Another study of 46 duodenal samples, 57 stomach samples, and 404 stool samples from stunted children aged 2–5 years in Africa found that the vast majority of stunted children exhibited gastrointestinal symptoms. In addition, *Escherichia coli/Shigella* sp. and *Campylobacter* sp. were shown to be more common in stunted children, although Clostridia, well-known butyrate makers, were reduced in comparison to nonstunted children. Oral bacteria were overrepresented in fecal samples from stunted children (57).

During infancy, there is a "critical window" for gut microbiota development, and disruptions in this process may be critical for children's growth and development (9, 16). Nutritional status (46), feeding techniques (47), hygienic conditions (51), antibiotic use (53), and intestinal inflammation (56) are major factors that induce intestinal flora alteration and impair children's growth and development, according to current clinical research. The majority of research support the identification of gut flora, such as *Bifidobacterium*, *Bacteroides*, and *Lactobacillus*, as being favorably associated with early baby growth. Actinomycetes, particularly Bifidobacteriales, are the most prevalent members of the gut microbiota in well-growing newborns (45, 47). However, research reports on the intestinal flora related with infant development retardation differ widely, owing to overgrowth of intestinal flora, overexpression of pathogenic bacteria, an abundance of *Ruminococcus*, *Clostridium sensu stricto*, and *Collinsella*, among other factors (51, 56). This may be related to the various research objects chosen by the researchers. In short, infancy is a vital stage for the creation of gut flora. Food influences the gut flora. The connection between nutritional status and gut flora is a significant area of interest in baby growth and development research. The clinical investigations on the effect of gut flora on early infant growth and development are summarized in **Table 2**.

TABLE 2 Summarizes clinical studies on the effect of gut flora on early infant growth and development.

Clinical situation	Author/year & geographic location	Study design	Growth features & influences	Features of gut microbial community	Identification strategy	PMID
Eating patterns and nutritional status	Tadros et al., 2022, United States.	Retrospective study	Nutritional support and microbiome acquisition.	Gammaproteobacteria postnatal abundance was inversely associated with early growth, but *Bacteroides* and *Lactobacillus* were favourably associated with childhood BMI.	16S RNA V4 sequencing	36016882
	Martin et al., 2016, Netherlands	Observational study	Nutritional supplementation and infant gut microbiome development	The presence of *Bifidobacterium animalis subsp. lactis* was discovered to be completely dependent on the method of feeding.	qPCR/RT qPCR	27362264
	Berger et al., 2020, Switzerland	Randomized controlled trial	Human milk oligosaccharides and infant fecal community	Supplementing newborns with sialylated HMOs enhances microbiota-dependent growth, presumably due to increased *Bifidobacteriaceae* abundance in the infant gut.	16S RNA V3–V4 sequencing	32184252
	Charbonneau et al., 2016, United States	Cohort and experiment study	Human milk oligosaccharides and infant fecal community	S-BMO promotes growth in gnotobiotic mice harboring the malawian infant culture collection and fed a prototypic malawian diet.	16S rRNA sequencing and COPRO-seq	26898329
Poor infant hygiene and antibiotic-induced intestinal flora disruption	Donowitz et al., 2016, United States	Cross-sectional study	Small intestinal bacterial overgrowth and shorter length	The markers of intestinal inflammation fecal Reg 1β and fecal calprotectin were elevated in SIBO-positive children.	Gas chromatograph	26758185
	Zhou et al., 2021, China	Cohort study	Antibiotic exposure, neonatal gut bacteria and infant growth speed	Penicillin exposure has a negative link with gut microbiota Pielou and Simpson's index and a positive relationship with growth velocity at 2–6 months.	16S RNA V3–V4 sequencing	34371267
	Uzan-Yulzari et al., 2021, Israel and Finland	Birth cohort study	Antibiotic exposure, neonatal gut bacteria and infant growth speed	Antibiotic therapy had the greatest impact on the genus *Bifidobacterium*.	16S RNA V4 sequencing and metagenomics	33500411
	Reid et al., 2019, United States	Retrospective study	Neonatal antibiotic exposure and infant growth	Antibiotic exposure was not connected with growth velocity between delivery and discharge in neonates and infants in ICU.	–	30500965
Gut inflamation and disruption of flora	Zambruni et al., 2019, United States	Pilot prospective study	Linear growth, intestinal damage, and systemic inflammation	*Ruminococcus* 1 and 2, *Clostridium sensu stricto*, and *Collinsella* abundance increased in stunted children but not in controls, but *Providencia* abundance dropped.	16S RNA V4 sequencing	31482782
	Vonaesch et al., 2018, France	Clinical trial	Microbiome "decompartmentalization" and linear growth delay	Oral bacteria were found to be overrepresented in fecal samples from stunted children, as were *Escherichia coli/Shigella* sp. and *Campylobacter* sp., while Clostridia, well-known butyrate makers, were reduced.	16S RNA sequencing and semiquantitative culture methods	30126990

BMI, body mass index; COPRO-Seq, COmmunity PROfiling by sequencing; HMOs, human milk oligosaccharides; S-BMO, sialylated bovine milk oligosaccharides; SIBO, small intestine bacterial overgrowth.

Adolescent linear growth and intestinal flora

Adolescence is a transitional period between childhood and maturity, a period of physical, neurological, psychological, and social changes, and a key time for growth and development. Some chronic mental illness states in childhood and adolescence, such as cognitive, emotional/social disturbances, sensory functional impairment, communication impairment, and so on, are intimately related to adolescents' growth and development. Although the pathophysiology of how psychiatric diseases such as anorexia nervosa (AN), ADHD, and autism spectrum disorder (ASD) affect growth and development in adolescents is not fully known, dysbiosis of the microbiota has been proposed as a possible explanation (18). AN is a severe psychiatric condition that primarily affects adolescents as a result of the severely detrimental consequences of caloric restriction on linear growth during puberty (58). A study of the composition and diversity of the gut microbiome in adolescents with anorexia before and after nutritional supplementation discovered that patients had greater individual differences in gut bacterial and metagenomic content, with fecal levels of serotonin, gamma-aminobutyric acid, dopamine, butyrate, and acetate decreasing in the samples (59). ADHD is one of the most frequent neurodevelopmental diseases in children. Numerous studies indicate that ADHD is linked to teenage growth and development (60). A Finnish study revealed

that adolescents with hyperactive-impulsive ADHD were taller, and elementary school kids with ADHD were shorter and smaller than a control group of children of the same age (61). A case-control research comparing Chinese children with ADHD to healthy controls discovered that those with ADHD had lower levels of *Faecalibacterium* and *Veillonellaceae*, whereas *Enterococcus* and *Odoribacter* were significantly higher (62). Despite the fact that autistic children's gut microbiota differs significantly from that of normal children, with a reduced proportion of *Coprococcus* and *Bifidobacterium*, the children's height does not alter (63). In adolescence, there has been minimal research on height in children with ASD, and some studies have found that the ASD group was significantly larger than the control group in terms of head circumference, weight, and BMI, but there was no difference in height (64).

Nutritional status can influence linear bone growth during adolescence and puberty by regulating growth plate chondrocytes, which are critical components of juvenile growth (65). Excess body weight early in childhood might have an impact on growth patterns. There is evidence that excess adiposity throughout childhood alters growth patterns and pubertal development. Several studies have found that obese children have a higher height velocity and a faster bone age during their prepubertal years (66). Several hormones released by adipose tissue may influence linear growth in the context of obesity, both through the growth hormone insulin-like growth factor-1 (IGF-1) axis and directly through the epiphyseal growth plate. In 11 of the 12 cohort studies that were the subject of a systematic review and meta-analysis, there was a positive connection between total protein intake and BMI. The meta-analysis suggested a favorable relationship between total protein intake and BMI. There may also be evidence showing a connection between a higher intake of animal protein in the diet and a higher BMI. However, there is no clear evidence linking total protein intake with an elevated risk of being overweight or obese. Only suggestive data partially support this association between total protein intake and an elevated risk of being overweight or obese (67). The effect of nutrition on the gut flora during adolescence is linked to linear growth in puberty. In respect to linear growth, a study of 350 girls aged 12–13 years that followed three major dietary patterns: healthy, heavy in sugar and salt, and a Western diet found that a healthy dietary pattern with enough intake of plant protein and white meat was connected with more favorable linear growth (65). Diet and dietary components have a significant impact on the composition of the gut microbiota and are among the most important contributors to bacterial flora changes. Existing research suggests that adopting a plant-based diet benefits the host microbiome, reduces inflammation, improves insulin sensitivity, and promotes optimal energy balance, which can lead to the prevention of chronic low-inflammation-related diseases (68).

In comparison to the high prevalence of malnutrition in newborns and early children, obesity or overweight in adolescents has a greater influence on children's growth and development. Obesity with developmental delay is more common in younger children and adolescents than obesity without developmental delay. A research in Vietnam found that 5% of overweight children were also stunted, whereas a study in Sao Paulo, Brazil found that 6% of children in low-income urban families were overweight and stunted, and that obesity with stunting was more common than obesity without stunting. Similarly, growth retardation and increased obesity were shown to coexist in a study of young children in urban areas of the Cape Peninsula, South Africa, and researchers believe that the community has transitioned from undernutrition to overnutrition without reaching optimal nutritional status (69). A bioinformatically re-analyzed study based on published amplicon sequencing data from the National Center for Biotechnology Information discovered that the impacts of obesity on the gut microbiota may be more severe in infancy than in adulthood and eventually endure throughout life. The study discovered significant changes in gut microbiota between children with and without obesity, while no similar differences were seen in the adult group. Using gut microbiota to predict pediatric obesity is more difficult, according to random forest models, than adult obesity. The data show that the gut microbiota is more vulnerable in childhood than in maturity (70). A cross-sectional study of taxonomic characteristics of the gut microbiota in 46 children and their association with obesity in diet-dependent children discovered that children with an abundance of *Holdemania* spp. and high protein and complex carbohydrate consumption had a lower z-BMI, waist circumference, and hip circumference. In contrast, they found a link between *Coprococcus catus* and a low intake of this dietary pattern and hip circumference (71). Decades of observational research have revealed differences in the composition of the gut microbial community between obese and healthy people, and seminal studies in which fecal microbes from obese adults were transplanted into gnotobiotic mice recapitulate weight gain and obesity-related metabolic signatures, demonstrating a direct causal link between disrupted gut microbiota and obesity. Correction of flora issues appears to help prevent or treat obesity-related growth and metabolic disorders (72). However, clinical trials of microbiota-targeting treatments have had conflicting outcomes. A recent systematic review and meta-analysis (73) identified 19 trials comparing probiotics or synbiotics to any strategy other than bariatric surgery or FMT. Individual trials show no significant improvement in body weight, while combined case analyses show no differences in body weight or body mass index between probiotics or synbiotics and controls (73). Obese children mature more quickly than lean children, which increases the risk of poor adult height and early puberty. Despite the fact that obese children have a quicker linear growth rate, body obesity may promote neuroendocrine events that contribute to the start of puberty (74).

Precocious puberty, which can disrupt the gut microbiome, is another concern associated with linear growth in teenagers. According to a Korean study that investigated the composition of the gut microbial community in obese teenagers, the abundance of *Bacteroides* and *Prevotella* is strongly associated with BMI, and the composition of *Bacteroides* is adversely associated with triglycerides and total cholesterol (75). Dong et al. (76).

discovered changes in the gut microbiota between individuals with idiopathic central precocious puberty (ICPP) and healthy girls. They discovered that the gastrointestinal genera found in ICPP are comparable to those linked to obesity, including *Ruminococcus*, *Gemmiger*, *Oscillibacter*, and *Clostridium XIVb*. In terms of microbial species, girls with ICPP had higher amounts of *Rumicoccus bromii*, *Ruminococcus gnavus*, and *Ruminococcus leptum*. The first two were discovered in obese people and were found to boost energy absorption and adipose tissue hyperplasia, whereas *Ruminococcus leptum* was found to influence human weight changes. These findings underscore the link between obesity, ICPP, and gut microbiome dysbiosis (32, 77). Another study discovered that the gut flora of central precocious puberty patients behaves similarly to that of other neurological illnesses, with an abundance of *Alistipes*, *Klebsiella*, and *Sutterella*. These microbes create neurotransmitter-like metabolites (serotonin and dopamine), which initiate early puberty and activate the hypothalamic-pituitary-gonadal axis (78). Although accurate estimates of height loss due to premature puberty are difficult to obtain, prior studies of untreated patients revealed an average height loss of 10 cm in girls and 20 cm in boys. Girls who receive gonadotropin-releasing hormone analog (GnRHa) treatment before the age of 6 years, on the other hand, can achieve a final height gain of 2–10 cm (79, 80). When compared to Tanner stage-matched controls, girls with true central precocious puberty show an adverse metabolic profile at diagnosis; even GnRHa treatment cannot correct this shortfall (81). The investigations on the effect of gut flora on adolescent linear growth are summarized in **Table 3**.

Key bacterial taxa associated with linear growth at different stages of childhood

Evidence suggests that certain aspects of the gut microbiota are linked to certain stages of growth and development in children (18). **Figure 1** depicts the characteristics of intestinal flora at various phases of children's growth and development, as well as the impact of intestinal flora on linear growth in children. The oral cavity (31, 82), vagina (36), and intestines (37) of the mother are major sources of neonatal intestinal flora. Hematogenous transfer of maternal oral bacteria during pregnancy may be an important factor in placental colonization (31, 83). Evidence suggests that patients who gave birth prematurely had a distinct gut microbiome dysbiosis compared to those who gave birth at term. *Porphyromonas*, *Streptococcus*, *Fusobacterium*, and *Veillonell* a were enriched in the preterm group, whereas *Coprococcus* and *Gemmiger* were significantly depleted. The majority of the enriched bacteria were oral bacteria that had been annotated (82). The mother's gut and the maternal vagina are the principal sources of microbiota for vaginally delivered newborns (84). The microbiome of newborns born via cesarean section is mostly derived from the mother's skin and the hospital environment (85). The most important factors influencing prenatal growth and development are prenatal weight gain (28–30), premature birth (31, 38, 39), and being small for gestational age (41, 44). According to research, these elements are linked to the creation and features of newborn gut flora. As illustrated in **Figure 1**, *Lactobacillus* and *Bifidobacterium* are advantageous to newborn growth throughout the perinatal period, however pathogenic bacteria such as *Shigella*, *Ralstonia*, and *Clostridium* may be detrimental. During infancy, nutritional status, feeding procedures, hygienic conditions, antibiotic usage, and intestinal inflammation are important factors that affect intestinal flora and impede children's growth and development. As illustrated in **Figure 1**, gut flora such as *Bifidobacterium*, *Bacteroides*, and *Lactobacillus* are favorably associated with infant growth. Pathogenic bacterial overexpression, as well as an abundance of *Ruminococcus*, *Clostridium sensu stricto*, and *Collinsella*, are all unfavorable factors. Infants' gut flora has stabilized between 31 and 46 months, hence children's growth rate tends to be constant and relatively slow from infancy until pre-adolescence (9). Adolescence is characterized by a succession of physical, neurological, psychological, and social changes, as well as the second growth spurt in life. Microbiota abnormalities associated with children's growth and development during this period are mostly associated with some particular diseases such as AN (59), ADHD (62), ASD (63), precocious puberty (76, 78), and obesity (71). *Alistipes*, Clostridiales, *Christensenellaceae*, and *Ruminococcaceae* abundance was linked to AN (59). ADHD was linked to an abundance of *Bacteroides caccae*, *Odoribacter splanchnicus*, *Paraprevotella xylaniphila*, and *Veillonella parvula* (62). *Bacteroides*, *Parabacteroides*, *Clostridium*, *Faecalibacterium*, and *Phascolarctobacterium* are more abundant in the gut of ASD children (63).

Possible mechanism of gut microbiota affecting linear growth

The anterior pituitary gland secretes growth hormone, which regulates insulin-like growth factor-1 (IGF-1) synthesis. One of the most fascinating theories that could explain the association between gut microbiota composition and linear and bulky growth in children is the involvement of gut microorganisms in boosting growth hormone. The gut microbiota can influence linear growth by influencing growth axis activity and changing hormone release. It could be one of the key methods by which the gut flora regulates linear development by modulating the action of the GH (growth hormone)/IGF-1 axis. Children who have chronic nutritional deficiencies develop growth hormone resistance and become stunted. The liver and peripheral tissues, including muscle, create IGF-1 which promotes growth throughout the body and organs. IGF-1 is a key mediator of bone growth that works in the endocrine, paracrine, and autocrine systems (86). In one mice investigation, researchers demonstrated that *Lactobacillus plantarum* strains in the gut microbiota maintain growth hormone action via signaling pathways in the liver, overcoming malnutrition-induced GH resistance. According to this research, certain beneficial bacteria can be employed to treat stunted growth and development caused by malnutrition (87). A study of Drosophila revealed that

TABLE 3 Summarizes studies on the effect of gut flora on adolescent linear growth.

Clinical situation	Author/year & geographic location	Study design	Growth features & influences	Features of gut microbial community	Identification strategy	PMID
Psychiatric diseases	Prochazkova et al., 2021, Czech Republic	Longitudinal study	Anorexia nervosa and intestinal microbiota	*Alistipes*, Clostridiales, *Christensenellaceae*, and *Ruminococcaceae* were the most common taxonomically distinctive flora in patients with AN.	16S rRNA sequencing and ITS7/ITS4 sequencing	33779487
	Wan et al., 2020, China	Case-control study	ADHD and intestinal microbiota	In the ADHD group, *Faecalibacterium prausnitzii*, *Lachnospiraceae bacterium*, and *Ruminococcus gnavus* were greatly reduced, but *Bacteroides caccae*, *Odoribacter splanchnicus*, *Paraprevotella xylaniphila*, and *Veillonella parvula* were significantly increased.	Shotgun metagenomic sequencing	32132899
	Iglesias-Vazquez et al., 2020, Spain	Systematic review and meta-analysis	ASD and intestinal microbiota	Children with ASD showed a significantly higher abundance of the genera *Bacteroides*, *Parabacteroides*, *Clostridium*, *Faecalibacterium*, and *Phascolarctobacterium* and a lower percentage of *Coprococcus* and *Bifidobacterium*.	16S rRNA sequencing, bacterial tag encoded FLX amplicon pyrosequencing, PCR or culture	32192218
Nutritional status	Yu et al., 2023, China	BioData mining	Obesity and gut microbiota	The gut microbiota was more vulnerable in childhood than in maturity	16S rRNA sequencing	36776907
	Orbe-Orihuela et al., 2022, México	Cross-sectional study	Diet-dependent childhood obesity and gut microbiota	Children with an abundance of *Holdemania* spp. and high protein and complex carbohydrate consumption had a lower z-BMI, waist circumference, and hip circumference.	Whole metagenome shotgun sequencing	35382951
	Suzumura et al., 2019, Brazil	Meta-analysis	probiotics or synbiotics and overweight	Although the quality of evidence is low to moderate, oral supplementation with probiotics or synbiotics has a slight effect on waist circumference but no effect on body weight or BMI.	Commercial probiotic powder, commercial probiotic yogurt, commercial synbiotic capsules or probiotic edam-type cheese	30924853
Precocious puberty	Dong et al., 2019, China	Cross-sectional study	Precocious puberty and gut microbiota	The ICPP group had higher GM diversity and was enriched for several GM species, including *Ruminococcus gnavus*, *Ruminococcus callidus*, *Ruminococcus bromii*, *Roseburia inulinivorans*, *Coprococcus eutactus*, *Clostridium leptum*, and *Clostridium lactatifermentans*, all of which are linked to obesity and the production of short-chain fatty acids.	16S rRNA sequencing	32038493
	Li et al., 2021, China	Cross-sectional study	Precocious puberty and gut microbiota	CPP patients have an abundance of *Alistipes*, *Klebsiella*, and *Sutterella*, which is comparable to other neurological disorders.	16S rRNA sequencing	33634977

ADHD, attention-deficit/hyperactivity disorder; AN, anorexia nervosa; ASD, autism spectrum disorder, CPP, central precocious puberty; GM, gut microbiota; ICPP, idiopathic central precocious puberty.

a common bacterium, *Acetobacter pomorum*, can modulate insulin/insulin-like growth factor signaling and hence influence Drosophila developmental speed, body size, and energy metabolism (88). On the one hand, excess short-chain fatty acids (SCFAs) produced by a specific benign bacteria provide an additional source of energy, resulting in an imbalance in energy regulation that promotes growth. SCFAs, on the other hand, have a role in glucose-stimulated insulin secretion from cells through interactions with the free fatty acid receptors FFA2 and FFA3, as well as the release of hunger-regulating peptide hormones. This seemingly contradictory finding demonstrates that, in addition to the SCFA levels produced by some gut microbiota members, some G-protein-coupled receptors (GPCRs) in the host can directly identify specific bacterial components, thereby controlling other metabolic processes that may contribute to body growth (10). In obese or overweight patients, a 12-week intervention with a low-carbohydrate diet (LCD) resulted in a considerable increase in the relative abundance of butyrate-producing bacteria, including *Parabacteroides* and *Oscillospira*. Furthermore, in the LCD group, participants with higher relative abundance of *Bacteroides* at baseline responded better to the LCD intervention and had greater weight loss outcomes. Some *Oscillospira* species may produce considerable levels of SCFAs, which aid in weight management as well as glucose and lipid homeostasis. Another notion is that *Oscillospira* can disrupt host glycans, allowing hosts to expend metabolic energy to restore destroyed glycoproteins. In this study, the increased abundance of *Parabacteroides* and *Oscillospira* could be a gut microbiota response to dietary intervention, assisting in LCD weight loss (89). Children who grow up in polluted surroundings are more likely to get intestinal infections and malnutrition, and they are more likely to develop overweight/obesity and accompanying comorbidities later in life. When

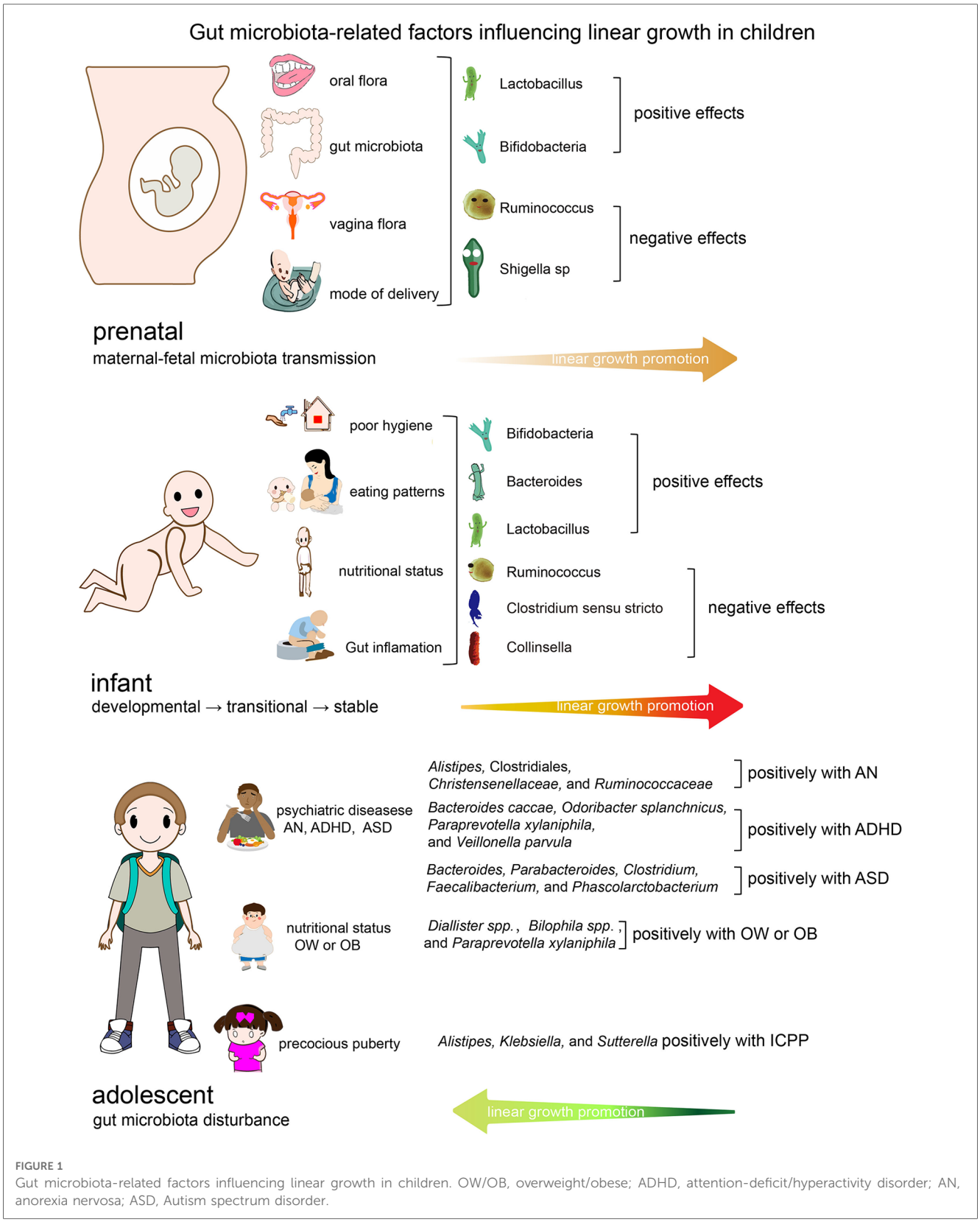

FIGURE 1
Gut microbiota-related factors influencing linear growth in children. OW/OB, overweight/obese; ADHD, attention-deficit/hyperactivity disorder; AN, anorexia nervosa; ASD, Autism spectrum disorder.

exposed to energy-rich meals, children who had height deficits in childhood were more likely to be overweight or obese as adults (90). To summarize, numerous studies have demonstrated that gut flora is closely associated to obesity, and that changing gut flora may be an essential factor in weight control. A randomized clinical trial of adolescent obesity patients discovered that fecal microbiota transplantation (FMT) had no effect on weight loss but did ameliorate metabolic abnormalities (91). The most important

link between and host IGF-1 levels appears to be SCFAs metabolized by gut bacteria from indigestible fiber-rich diets, but other mechanisms by which gut microbes influence bone growth may exist (92).

Another potentially growth-promoting mechanism for gut bacteria is the tryptophan (TRP)-kynurenine (KYN) -niacin pathway. In this process, indoleamine 2,3-dioxygenase (IDO) converts dietary tryptophan to kynurenine, which is then converted to niacin. Niacin is an important precursor of nicotinamide adenine dinucleotide (NAD+). Children with a greater kynurenine to tryptophan ratio (KT) had lower linear growth, according to studies, and experimental animal models have also indicated that a tryptophan deficit is associated with decreased growth velocity (93, 94). Undernutrition was found to affect various metabolic pathways, including choline and tryptophan metabolism, while also increasing the proteolytic activity of the gut flora. Additionally, metabolic adaptation to lower energy expenditure was observed in malnourished children, as demonstrated by increased N-methylnicotinamide and decreased -aminoisobutyric acid excretion. Undernourished children with stronger metabolic adaptability demonstrated quick catch-up growth many months early (95). The KYN: TRP/ KT ratios were shown to be strongly linked with children's growth in a study of stunted children in Bangladesh. This change in the TRP pathway could be due to environmental stresses such as chronic inflammation, environmental enteric dysfunction, inadequate protein consumption, or alterations in the gut microbiota, all of which can have a substantial impact on growth (96).

Furthermore, Gut microbiota may prompt immune cells to release certain cytokines, influencing the host's linear growth (56, 97, 98), and greater intestinal permeability produced by environmental intestinal dysfunction is hypothesized to cause higher bacterial product translocation, culminating in systemic inflammation and immunological activation (99). Chronic inflammatory illnesses, such as inflammatory bowel disease and juvenile idiopathic arthritis, are a major cause of stunted growth and development in children (100, 101). Systemic inflammation and immune activation may play a role in the development of linear growth disorders via cytokine-induced anorexia, nutrient utilization regulation, and/or interference with the growth hormone axis and bone metabolism (99). In a Zimbabwe birth cohort study, Prendergast et al. discovered that developmental delay was related to raised systemic inflammatory markers (C-reactive protein and 1-acid glycoprotein) and lower IGF-1 levels. The presence of intestinal injury in infants with developmental delays was demonstrated by higher plasma intestinal fatty acid-binding protein levels (102). Saari et al. discovered that children with *Helicobacter pylori* infection had low serum acylated ghrelin and growth retardation in a one-year longitudinal cohort study. *Helicobacter pylori* eradication successfully restores ghrelin levels and increases growth in children (103). Saari et al. found the same link between antibiotics and height in a large cohort of Finnish infants (104), and a meta-analysis of 10 randomized controlled trials found that antibiotic use increased height by 0.04 cm/month (105). However, in Niger, a large-scale study of azithromycin use and growth and development in children aged 6–60 months noticed no link between antibiotic use and improved human growth (106). Kosek et al. observed that kids with higher levels of fecal biomarkers of intestinal inflammation and intestinal barrier disruption were more likely to have linear growth retardation during the first 18 months of life in an international multicenter prospective study (107). Current studies (17, 104–107) on antibiotics and children's growth vary significantly, and there are many reasons for some of the differences, but the influence of environmental factors, which include the nutritional status of the children included in the studies, hygiene, feeding practices, drinking water, chronic inflammatory diseases, endocrine disorders, and so on, must all be considered.

In summary, the determinants of stunting operate at multiple causal levels, ranging from the most distal socioeconomic and political variables to the most proximal, such as food quantity and quality, as well as their biotransformation by the gut microbiota, host infection, immune dysfunction, and systemic physiology (108). **Figure 2** shows a schematic representation of the gut microbiota's contribution to children's linear growth. The potential mechanisms include: (1) alterations in food absorption (10, 47) (i.e., increased levels of health-promoting microbial metabolites such SCFAs and HMOs); and (2) endocrine hormones (86) (GH/IGF-1 axis). (3) Changes in immune regulation (56, 97) (including cytokines and gut inflammation); (4) Control of the gut-brain-bone axis (94, 96) (including neurotransmitters, appetite control, and Kyn/Trp).

Conclusion and future perspectives

Microbiome research is still in its early stages and has mostly concentrated on bacterial taxa, but the microbiome also contains the virome and fungiome. The convergence of the microbiome and metabolic window omics is an area with potential for optimization, particularly during important developmental phases. Potential modifications include taking probiotic supplements, reducing antibiotic exposure, and using the microbiome as a biomarker for precision treatment. These pathways need to be investigated further, and while there are many extensive multi-omics studies in the adult literature, pediatric data is limited. To examine the makeup and impact of changes in the gut microbiome, clinical trials, particularly in large cohorts of healthy children and children with various disorders, are required. Moreover, geography and food culture have an impact on the gut flora in children. Depending on the research subjects chosen and the research methodologies employed, various countries and regions may reach different findings. **Table 4** illustrates the clinical studies on intestinal microbiota and child growth in this review based on the cities/ countries where the research was conducted, as well as the research methodology used, characteristics of the included populations, and main conclusions. Currently, the countries and regions undertaking study on this topic are primarily centered in Europe (28–30, 37, 38, 45, 47, 54, 57), the

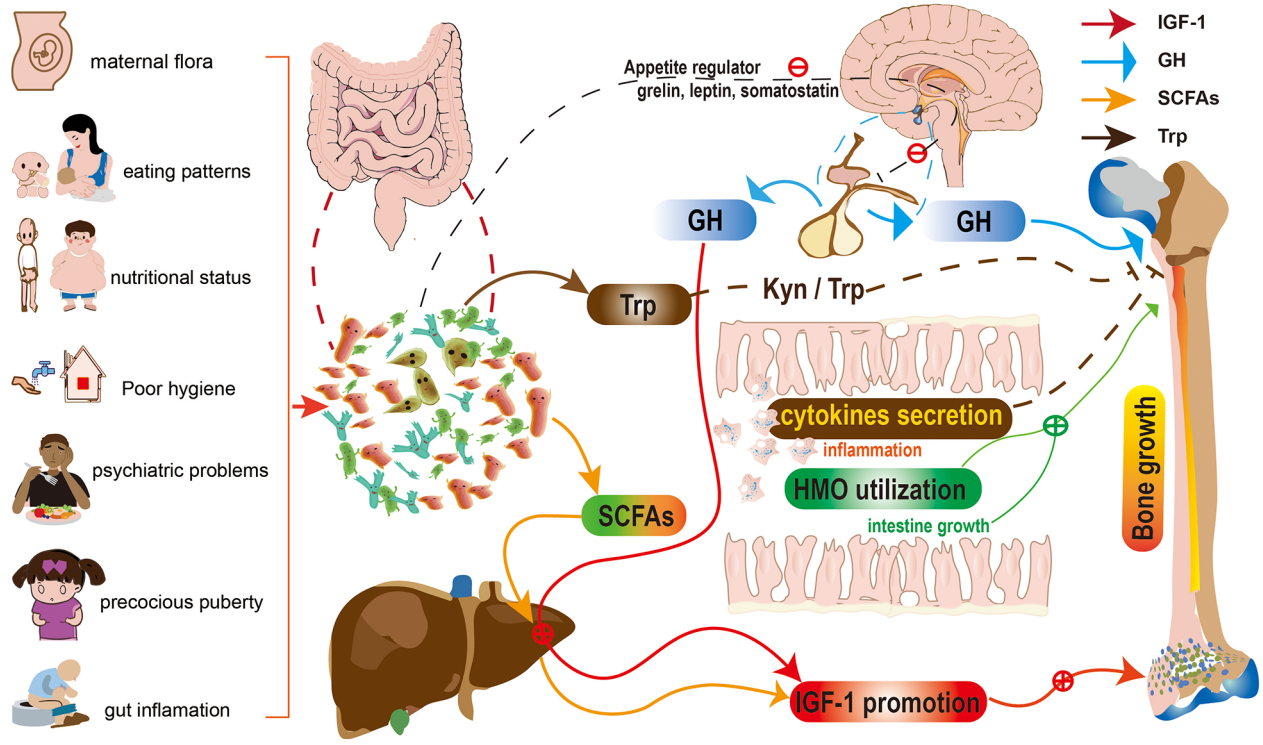

FIGURE 2
Schematic representation for the role of gut microbiota in children's linear growth. The potential mechanisms include: (1) alterations in food absorption (i.e., increased levels of health-promoting microbial metabolites such SCFAs and HMOs); and (2) endocrine hormones (GH/IGF-1 axis). (3) Changes in immune regulation (including cytokines and gut inflammation); (4) Control of the gut-brain-bone axis (including neurotransmitters, appetite control, and Kyn/Trp). HMOs, human milk oligosaccharides; SCFAs, Short-chain fatty acids; Kyn/Trp, kynurenine to tryptophan ratio; GH, growth hormone; IGF-1 insulin-like growth factor 1.

United States (33, 43, 46, 48, 51, 56), and China (39, 44, 53, 62, 76), with Africans, Bangladeshis, Europeans, and Chinese being the primary research subjects recruited. The primary areas of study are premature birth, intrauterine growth retardation, environmental sanitation, malnutrition, and so on. Chinese researchers are more interested in precocious puberty. According to the existing research literature, the association between gut microbiota and adolescent linear growth has received insufficient attention, and clinical research publications are limited. Furthermore, a better understanding of the relationships between the diverse microbiota and their components (bacteria, viruses, and fungi) is required (12). However, the mechanisms by which factors like maternal diet during pregnancy influence the microbiome of the offspring remain unknown. The vast majority of studies have been conducted in rodent models, with only a few mechanistic research studies conducted in humans. As a result, more validation is required before proceeding to clinical studies. Furthermore, there can be significant inter-individual variation in microbiota composition and drug responsiveness, meaning that conventional microbiota treatment may not be appropriate for every stunted patient. In phenotypically healthy populations, the use of multi-omics approaches such as metagenomics, metatranscriptomics, metaproteomics, and metabolomics aids in the discovery of microbial signals of growth retardation (2). Our present understanding of the gut microbiome is based on phylogenetic makeup (16S rRNA sequencing) or functional capacity (shotgun sequencing and identification of genes involved in metabolic pathways). Neither method fully captures trends in molecular crosstalk (caused by metabolites, antigens, signaling molecules, immunomodulators, and hormones) between the host and bacteria, resulting in systemic impacts on metabolism and the immune system. By including transcriptomics and metabolomics in the study of the dystrophic microbiota, researchers will gain a better understanding of how imbalances emerge. The majority of existing epidemiologic studies of malnutrition and gut microbiota are based on associations or correlations, making it impossible to determine the temporal order of these connections. To some extent, these problems can be addressed through longitudinal birth cohort studies of children or animal research. However, new and inventive ways are required to overcome these difficulties (12). With increased awareness and understanding comes the prospect of novel pharmaceutical targets and avenues for treating these diseases and promoting human health at all stages and ages (109).

TABLE 4 Clinacal studies that characterized gut microbiota associated with children's growth.

Regions and countries	Unfavorable conditions for children's growth	Study participants and age[a]	No.	Study's key findings	Methods	Ref.
EUROPE: Finland, Norway, Italy, Netherlands, Switzerland, France, Czech Republic, and Spain	Maternal overweight	Pregnant women 24 GW; m1 and m6; women 4 days after delivery and infants −y2	46; 42; 169	Bacteroidetes-dominated GMC in mid-pregnancy is associated with increased GWG and reduced alpha diversity (28). The composition and development of infant gut microbiota are influenced by BMI, weight, and weight gain of mothers during pregnancy (29). Maternal OW/OB was associated with lower maternal alpha diversity. Maternal pre-pregnancy OW/OB and excessive GWG were associated with taxonomic differences in the maternal gut microbiota (30).	16S rRNA sequencing	(28–30)
	Preterm birth	Preterm neonates (<35 GW), full-term neonates d3–d4; preterm neonates (≤30 GW)	80; 23	Preterm neonates exhibited significantly lower gut microbiota alpha diversity and distinct beta diversity clustering compared to term neonates (37). An increase in α-diversity values and a consequent fall in *Lactobacillus* in vaginal environment could be associated to a higher risk of spontaneous preterm birth (38).	16S rRNA sequencing	(37, 38)
	Poor infant hygiene	Infants −y6	12,422	Neonatal antibiotic exposure is linked to long-term gut microbiome disruption and may result in reduced growth in boys during the first 6 years of life, but antibiotic use later in childhood is linked to an increase in BMI (54).	16S rRNA sequencing	(54)
	Eating patterns and nutritional status	−m6; m3–m12	108; 98	After birth, colonization by *Bifidobacterium*, *Lactobacillus*, and *Bacteroides* species was modified by manner of delivery, type of feeding, and the presence of siblings, with differences observed at the species and temporal levels (45). Human milk oligosaccharides supplementation increased the number of newborns with fecal community types *Bifidobacteriaceae* in abundance (47).	16S rRNA sequencing	(45, 47)
	Gut inflamation	Stunted children y2–y5	57	The vast majority of the stunted children showed small intestinal bacterial overgrowth dominated by bacteria that normally reside in the oropharyngeal cavity (57).	16S rRNA sequencing; semiquantitative culture	(57)
United States	Preterm birth	Pregnant mothers in the early third trimester or intrapartum	163	Independent of maternal BMI, a high-fat maternal diet is associated with significant changes in the newborn gut microbiota at birth that last for 4–6 weeks (33).	16S rRNA sequencing	(33)
	SGA	Neonates with SGA, within 2 h after delivery	40	SGA patients had a considerably higher abundance of *Neisseriaceae* (43).	16S rRNA sequencing	(43)
	Eating patterns and nutritional status	Preterm infants −y5; stunted infant 6m	160; 25	Postnatal gut microbial colonization, a controllable factor, was linked to preterm infants' childhood growth (46). Sialylated milk oligosaccharides promote microbiota-dependent growth in models of infant undernutrition (48).	16S rRNA sequencing, Microbial RNA-Seq, Mass spectroscopy	(46, 48)
	Poor infant hygiene	Bangladeshi y2	90	SIBO is connected with linear growth failure and inadequate sanitation, regardless of recent or frequent diarrheal illness. SIBO has been linked to intestinal inflammation but not to increased permeability or systemic inflammation (51).	Enzyme-linked immunosorbent assay	(51)
	Gut inflamation	Peruvian infants m5–m12	78	Stunting in infants was preceded by an increase in indicators of enterocyte turnover and variations in fecal microbiota, and it was linked to higher levels of systemic inflammatory markers (56).	16S rRNA sequencing	(56)
China	Preterm birth	Preterm infants −y1	166	Determine the dynamic changing features of newborns' gut microbiomes at various gestational ages (39).	16S rRNA sequencing	(39)

(*Continued*)

TABLE 4 Continued

Regions and countries	Unfavorable conditions for children's growth	Study participants and age[a]	No.	Study's key findings	Methods	Ref.
	SGA	Term SGA and AGA neonates −7d	162	The gut microbial diversity of term SGA infants was significantly lower in the first week of life than that of term AGA infants (44).	16S rRNA sequencing	(44)
	Antibiotic exposure	Mother-child pairs m2–m6	295	Intrauterine antibiotic exposure can have an effect on newborn growth, and the neonatal gut flora may be involved (53).	16S rRNA sequencing	(53)
	Psychiatric diseases	Children with ADHD y6–y12	17	Differences in gut microbiota composition in ADHD participants may contribute to brain-gut axis abnormalities and impact neurotransmitter levels, which may contribute to ADHD symptoms (62).	Shotgun metagenomics sequencing	(62)
	Precocious puberty	Girls with ICPP y6–y8	48	The ICPP girls' intestinal flora is diversified, similar to that of obese children, and rich in short-chain fatty acid-producing intestinal flora (76).	16S rRNA sequencing	(76)
México	Obesity	OW/OB children y6–y12	46	The synergy between nutrition and the composition of children's gut microbiota may be a factor in the development of juvenile obesity and its complications (71).	Metagenome shotgun sequencing	(71)

GWG, gestational weight gain; GMC, gut microbiota composition; OW/OB, overweight/obese; SIBO, small intestine bacterial overgrowth; SGA, small for gestational age; AGA, appropriate for gestational age; BMI, body mass index; ASD, autism spectrum disorder; ICPP, idiopathic central precocious puberty.
[a]y, year of age; m, month of age; w, week of age; d, days of age.

Limitations

The purpose of this study is to review the establishment and alterations of the gut microbiota in children at various phases of development, as well as the impact on children's linear growth. We mainly talked about the association between growth and development disorders at various stages and changes in gut flora, but we also briefly discussed the connection between gut flora and nutrition, neurophysiology, endocrine, and immune inflammation in children at various growth and development stages. They have complicated interactions with each other. This review mostly includes cohort studies (26, 28, 30, 39, 41, 44, 45, 48, 53, 54, 56, 59), cross-sectional studies (31, 37, 46, 51, 71, 76, 78), case-control studies (29, 47, 55, 57, 62), and some animal studies focusing on particular mechanisms (48, 87, 88). Although the data supports a link between intestinal flora and linear development in children, our review has limitations that prohibit us from fully verifying the causal relationship between gut flora and linear development in children. First, there is a bidirectional association between changes in the gut microbiota and the risk/resilience of children to linear growth disorders, making it difficult to separate between cause and effect. The cohort and cross-sectional studies included in this review were limited to account for the complexities of gut microbiome affects on linear growth in humans due to sample size and study scope limitations. Second, to determine the causal link between the gut microbiota and linear growth, long-term clinical controlled trials with large sample sizes are required. However, due to the limits of currently available 16S RNA sequencing or metagenomics-based research methodologies, determining which species or groups of gut bacteria play a key role in addressing growth problems, even in animal studies, is difficult. As a result, the clinical research included in this review primarily used commercial probiotic or prebiotic supplements as treatment options, and the findings of these studies do not yet indicate which strains are relevant for resolving growth deficiency in which situations. Furthermore, the goal of this literature review is to provide readers with up-to-date and thorough research advances on the association between gut microbiota and linear growth in children. Although relevant studies are categorised and described, it is a general literature review with limits in how to evaluate a set of studies and make appropriate recommendations, which is inferior to the evaluation effect of a systematic review. In addition, we included research material on systematic reviews (63), meta-analyses (73), and biological data mining investigations (70) in this review. However, because of the scarcity of existing study data and a small number of research projects engaged, these studies have limited interpretation of the association between gut microbiota and linear development in children. In short, due to the limitations of current research, our review can only attempt to educate readers of the most recent findings in key subject areas. When the relevant research literature is substantial, a systematic review study on this topic can be done in the future to compensate for the deficiencies of this review.

Author contributions

PH and XS did the literature review and drafted the text. SG gathered the literature, wrote, and revised the manuscript.

All authors contributed to the article and approved the submitted version.

Funding

This work was financially supported by the Program of Science and Technology Commission of Shanghai Municipality (No. 20Y11905300).

Acknowledgments

The authors would like to thank Qixuan Guo (Shanghai Yichuan Senior High School) for her assistance in drawing the figures.

Conflict of interest

The authors declare that the research was conducted in the absence of any commercial or financial relationships that could be construed as a potential conflict of interest.

Publisher's note

References

1. Schei K, Simpson MR, Avershina E, Rudi K, Oien T, Juliusson PB, et al. Early gut fungal and bacterial microbiota and childhood growth. *Front Pediatr*. (2020) 8:572538. doi: 10.3389/fped.2020.572538

2. Qi M, Tan B, Wang J, Liao S, Deng Y, Ji P, et al. The microbiota-gut-brain axis: a novel nutritional therapeutic target for growth retardation. *Crit Rev Food Sci*. (2022) 62:4867–92. doi: 10.1080/10408398.2021.1879004

3. de Onis M, Branca F. Childhood stunting: a global perspective. *Matern Child Nutr*. (2016) 12(Suppl 1):12–26. doi: 10.1111/mcn.12231

4. Cowardin CA, Syed S, Iqbal N, Jamil Z, Sadiq K, Iqbal J, et al. Environmental enteric dysfunction: gut and microbiota adaptation in pregnancy and infancy. *Nat Rev Gastroenterol Hepatol*. (2023) 20(4):223–37. doi: 10.1038/s41575-022-00714-7

5. Muller O, Krawinkel M. Malnutrition and health in developing countries. *Can Med Assoc J*. (2005) 173:279–86. doi: 10.1503/cmaj.050342

6. Black RE, Victora CG, Walker SP, Bhutta ZA, Christian P, de Onis M, et al. Maternal and child undernutrition and overweight in low-income and middle-income countries. *Lancet*. (2013) 382:427–51. doi: 10.1016/S0140-6736(13)60937-X

7. McDonald CM, Olofin I, Flaxman S, Fawzi WW, Spiegelman D, Caulfield LE, et al. The effect of multiple anthropometric deficits on child mortality: meta-analysis of individual data in 10 prospective studies from developing countries. *Am J Clin Nutr*. (2013) 97:896–901. doi: 10.3945/ajcn.112.047639

8. Gwela A, Mupere E, Berkley JA, Lancioni C. Undernutrition, host immunity and vulnerability to infection among young children. *Pediatr Infect Dis J*. (2019) 38: e175–7. doi: 10.1097/INF.0000000000002363

9. Stewart CJ, Ajami NJ, O'Brien JL, Hutchinson DS, Smith DP, Wong MC, et al. Temporal development of the gut microbiome in early childhood from the TEDDY study. *Nature*. (2018) 562:583–8. doi: 10.1038/s41586-018-0617-x

10. Murugesan S, Nirmalkar K, Hoyo-Vadillo C, Garcia-Espitia M, Ramirez-Sanchez D, Garcia-Mena J. Gut microbiome production of short-chain fatty acids and obesity in children. *Eur J Clin Microbiol*. (2018) 37:621–5. doi: 10.1007/s10096-017-3143-0

11. Partty A, Kalliomaki M, Wacklin P, Salminen S, Isolauri E. A possible link between early probiotic intervention and the risk of neuropsychiatric disorders later in childhood: a randomized trial. *Pediatr Res*. (2015) 77:823–8. doi: 10.1038/pr.2015.51

12. Kane AV, Dinh DM, Ward HD. Childhood malnutrition and the intestinal microbiome. *Pediatr Res*. (2015) 77:256–62. doi: 10.1038/pr.2014.179

13. Dominguez-Bello MG, Costello EK, Contreras M, Magris M, Hidalgo G, Fierer N, et al. Delivery mode shapes the acquisition and structure of the initial microbiota across multiple body habitats in newborns. *Proc Natl Acad Sci U S A*. (2010) 107:11971–5. doi: 10.1073/pnas.1002601107

14. Brooks B, Olm MR, Firek BA, Baker R, Geller-McGrath D, Reimer SR, et al. The developing premature infant gut microbiome is a major factor shaping the microbiome of neonatal intensive care unit rooms. *Microbiome*. (2018) 6:112. doi: 10.1186/s40168-018-0493-5

15. Pabst O, Cerovic V, Hornef M. Secretory IgA in the coordination of establishment and maintenance of the microbiota. *Trends Immunol*. (2016) 37:287–96. doi: 10.1016/j.it.2016.03.002

16. Korpela K, de Vos WM. Early life colonization of the human gut: microbes matter everywhere. *Curr Opin Microbiol*. (2018) 44:70–8. doi: 10.1016/j.mib.2018.06.003

17. Wells JC, Sawaya AL, Wibaek R, Mwangome M, Poullas MS, Yajnik CS, et al. The double burden of malnutrition: aetiological pathways and consequences for health. *Lancet*. (2020) 395:75–88. doi: 10.1016/S0140-6736(19)32472-9

18. Ronan V, Yeasin R, Claud EC. Childhood development and the microbiome-the intestinal microbiota in maintenance of health and development of disease during childhood development. *Gastroenterology*. (2021) 160:495–506. doi: 10.1053/j.gastro.2020.08.065

19. Yengo L, Vedantam S, Marouli E, Sidorenko J, Bartell E, Sakaue S, et al. A saturated map of common genetic variants associated with human height. *Nature*. (2022) 610:704–12. doi: 10.1038/s41586-022-05275-y

20. Lim SJ, Aguilar-Lopez M, Wetzel C, Dutra S, Bray V, Groer MW, et al. The effects of genetic relatedness on the preterm infant gut microbiota. *Microorganisms*. (2021) 9(2):278. doi: 10.3390/microorganisms9020278

21. Rehman A, Sina C, Gavrilova O, Hasler R, Ott S, Baines JF, et al. Nod2 is essential for temporal development of intestinal microbial communities. *Gut*. (2011) 60:1354–62. doi: 10.1136/gut.2010.216259

22. Christian P, Lee SE, Donahue AM, Adair LS, Arifeen SE, Ashorn P, et al. Risk of childhood undernutrition related to small-for-gestational age and preterm birth in low- and middle-income countries. *Int J Epidemiol*. (2013) 42:1340–55. doi: 10.1093/ije/dyt109

23. Ozaltin E, Hill K, Subramanian SV. Association of maternal stature with offspring mortality, underweight, and stunting in low- to middle-income countries. *JAMA*. (2010) 303:1507–16. doi: 10.1001/jama.2010.450

24. Addo OY, Stein AD, Fall CH, Gigante DP, Guntupalli AM, Horta BL, et al. Maternal height and child growth patterns. *J Pediatr*. (2013) 163:549–54. doi: 10.1016/j.jpeds.2013.02.002

25. Prendergast AJ, Humphrey JH. The stunting syndrome in developing countries. *Paediatr Int Child Health*. (2014) 34:250–65. doi: 10.1179/2046905514Y.0000000158

26. Chu DM, Meyer KM, Prince AL, Aagaard KM. Impact of maternal nutrition in pregnancy and lactation on offspring gut microbial composition and function. *Gut Microbes*. (2016) 7:459–70. doi: 10.1080/19490976.2016.1241357

27. de Cuevillas B, Milagro FI, Tur JA, Gil-Campos M, de Miguel-Etayo P, Martinez JA, et al. Fecal microbiota relationships with childhood obesity: a scoping comprehensive review. *Obes Rev*. (2022) 23(Suppl 1):e13394. doi: 10.1111/obr.13394

28. Aatsinki AK, Uusitupa HM, Munukka E, Pesonen H, Rintala A, Pietila S, et al. Gut microbiota composition in mid-pregnancy is associated with gestational weight gain but not prepregnancy body mass Index. *J Womens Health*. (2018) 27:1293–301. doi: 10.1089/jwh.2017.6488

29. Collado MC, Isolauri E, Laitinen K, Salminen S. Effect of mother's weight on infant's microbiota acquisition, composition, and activity during early infancy: a prospective follow-up study initiated in early pregnancy. *Am J Clin Nutr*. (2010) 92:1023–30. doi: 10.3945/ajcn.2010.29877

30. Stanislawski MA, Dabelea D, Wagner BD, Sontag MK, Lozupone CA, Eggesbo M. Pre-pregnancy weight, gestational weight gain, and the gut microbiota of mothers and their infants. *Microbiome*. (2017) 5:113. doi: 10.1186/s40168-017-0332-0

31. Prince AL, Ma J, Kannan PS, Alvarez M, Gisslen T, Harris RA, et al. The placental membrane microbiome is altered among subjects with spontaneous preterm birth with and without chorioamnionitis. *Am J Obstet Gynecol*. (2016) 214:627.e1–e16. doi: 10.1016/j.ajog.2016.01.193

32. Neuman H, Debelius JW, Knight R, Koren O. Microbial endocrinology: the interplay between the microbiota and the endocrine system. *FEMS Microbiol Rev*. (2015) 39:509–21. doi: 10.1093/femsre/fuu010

33. Chu DM, Antony KM, Ma J, Prince AL, Showalter L, Moller M, et al. The early infant gut microbiome varies in association with a maternal high-fat diet. *Genome Med*. (2016) 8:77. doi: 10.1186/s13073-016-0330-z

34. Dedrick S, Sundaresh B, Huang Q, Brady C, Yoo T, Cronin C, et al. The role of gut microbiota and environmental factors in type 1 diabetes pathogenesis. *Front Endocrinol*. (2020) 11:78. doi: 10.3389/fendo.2020.00078

35. Lundgren SN, Madan JC, Emond JA, Morrison HG, Christensen BC, Karagas MR, et al. Maternal diet during pregnancy is related with the infant stool microbiome in a delivery mode-dependent manner. *Microbiome*. (2018) 6:109. doi: 10.1186/s40168-018-0490-8

36. Shaterian N, Abdi F, Ghavidel N, Alidost F. Role of cesarean section in the development of neonatal gut microbiota: a systematic review. *Open Med (Wars)*. (2021) 16:624–39. doi: 10.1515/med-2021-0270

37. Hiltunen H, Collado MC, Ollila H, Kolari T, Tolkko S, Isolauri E, et al. Spontaneous preterm delivery is reflected in both early neonatal and maternal gut microbiota. *Pediatr Res*. (2022) 91:1804–11. doi: 10.1038/s41390-021-01663-8

38. Tirone C, Paladini A, De Maio F, Tersigni C, D'Ippolito S, Di Simone N, et al. The relationship between maternal and neonatal microbiota in spontaneous preterm birth: a pilot study. *Front Pediatr*. (2022) 10:909962. doi: 10.3389/fped.2022.909962

39. Jia Q, Yu X, Chang Y, You Y, Chen Z, Wang Y, et al. Dynamic changes of the gut microbiota in preterm infants with different gestational age. *Front Microbiol*. (2022) 13:923273. doi: 10.3389/fmicb.2022.923273

40. Groer MW, Gregory KE, Louis-Jacques A, Thibeau S, Walker WA. The very low birth weight infant microbiome and childhood health. *Birth Defects Res C Embryo Today*. (2015) 105:252–64. doi: 10.1002/bdrc.21115

41. Chang HY, Chiang CJ, Chang JH, Hsu CH, Lin CY, Ko MH, et al. Characteristics of gut microbiota in small for gestational age infants with very low birth weight. *Nutrients*. (2022) 14(23):5158. doi: 10.3390/nu14235158

42. An J, Wang J, Guo L, Xiao Y, Lu W, Li L, et al. The impact of gut microbiome on metabolic disorders during catch-up growth in small-for-gestational-age. *Front Endocrinol*. (2021) 12:630526. doi: 10.3389/fendo.2021.630526

43. Hu J, Benny P, Wang M, Ma Y, Lambertini L, Peter I, et al. Intrauterine growth restriction is associated with unique features of the reproductive microbiome. *Reprod Sci*. (2021) 28:828–37. doi: 10.1007/s43032-020-00374-5

44. Chen X, Yan Z, Liu L, Zhang R, Zhang X, Peng C, et al. Characteristics of gut microbiota of term small gestational age infants within 1 week and their relationship with neurodevelopment at 6 months. *Front Microbiol*. (2022) 13:912968. doi: 10.3389/fmicb.2022.912968

45. Martin R, Makino H, Cetinyurek YA, Ben-Amor K, Roelofs M, Ishikawa E, et al. Early-life events, including mode of delivery and type of feeding, siblings and gender, shape the developing gut microbiota. *PLoS One*. (2016) 11:e0158498. doi: 10.1371/journal.pone.0158498

46. Tadros JS, Llerena A, Sarkar A, Johnson R, Miller EM, Gray HL, et al. Postnatal growth and gut microbiota development influenced early childhood growth in preterm infants. *Front Pediatr*. (2022) 10:850629. doi: 10.3389/fped.2022.850629

47. Berger B, Porta N, Foata F, Grathwohl D, Delley M, Moine D, et al. Linking human milk oligosaccharides, infant fecal community types, and later risk to require antibiotics. *mBio*. (2020) 11(2):e03196–19.. doi: 10.1128/mBio.03196-19

48. Charbonneau MR, O'Donnell D, Blanton LV, Totten SM, Davis JC, Barratt MJ, et al. Sialylated milk oligosaccharides promote microbiota-dependent growth in models of infant undernutrition. *Cell*. (2016) 164:859–71. doi: 10.1016/j.cell.2016.01.024

49. Al NZ, Dulauroy S, Marques R, Cousu C, Al BS, Dejardin F, et al. A weaning reaction to microbiota is required for resistance to immunopathologies in the adult. *Immunity*. (2019) 50:1276–88.e5. doi: 10.1016/j.immuni.2019.02.014

50. Gura T. Nature's first functional food. *Science*. (2014) 345:747–9. doi: 10.1126/science.345.6198.747

51. Donowitz JR, Haque R, Kirkpatrick BD, Alam M, Lu M, Kabir M, et al. Small intestine bacterial overgrowth and environmental enteropathy in Bangladeshi children. *mBio*. (2016) 7:e02102–15. doi: 10.1128/mBio.02102-15

52. McGrath CJ, Arndt MB, Walson JL. Biomarkers to stratify risk groups among children with malnutrition in resource-limited settings and to monitor response to intervention. *Horm Res Paediatr*. (2017) 88:111–7. doi: 10.1159/000471875

53. Zhou Y, Ma W, Zeng Y, Yan C, Zhao Y, Wang P, et al. Intrauterine antibiotic exposure affected neonatal gut bacteria and infant growth speed. *Environ Pollut*. (2021) 289:117901. doi: 10.1016/j.envpol.2021.117901

54. Uzan-Yulzari A, Turta O, Belogolovski A, Ziv O, Kunz C, Perschbacher S, et al. Neonatal antibiotic exposure impairs child growth during the first six years of life by perturbing intestinal microbial colonization. *Nat Commun*. (2021) 12:443. doi: 10.1038/s41467-020-20495-4

55. Reid BM, Eisenberg R, Forman K, LaTuga MS. Relationship between early antibiotic exposure and short-term growth velocity in premature neonates. *Am J Perinatol*. (2019) 36:1014–22. doi: 10.1055/s-0038-1675833

56. Zambruni M, Ochoa TJ, Somasunderam A, Cabada MM, Morales ML, Mitreva M, et al. Stunting is preceded by intestinal mucosal damage and microbiome changes and is associated with systemic inflammation in a cohort of Peruvian infants. *Am J Trop Med Hyg*. (2019) 101:1009–17. doi: 10.4269/ajtmh.18-0975

57. Vonaesch P, Morien E, Andrianonimiadana L, Sanke H, Mbecko JR, Huus KE, et al. Stunted childhood growth is associated with decompartmentalization of the gastrointestinal tract and overgrowth of oropharyngeal taxa. *Proc Natl Acad Sci U S A*. (2018) 115:E8489–98. doi: 10.1073/pnas.1806573115

58. Modan-Moses D, Yaroslavsky A, Pinhas-Hamiel O, Levy-Shraga Y, Kochavi B, Iron-Segev S, et al. Prospective longitudinal assessment of linear growth and adult height in female adolescents with anorexia Nervosa. *J Clin Endocrinol Metab*. (2021) 106:e1–10. doi: 10.1210/clinem/dgaa510

59. Prochazkova P, Roubalova R, Dvorak J, Kreisinger J, Hill M, Tlaskalova-Hogenova H, et al. The intestinal microbiota and metabolites in patients with anorexia nervosa. *Gut Microbes*. (2021) 13:1–25. doi: 10.1080/19490976.2021.1902771

60. Ptacek R, Kuzelova H, Stefano GB, Raboch J, Kream RM, Goetz M. ADHD and growth: questions still unanswered. *Neuroendocrinol Lett*. (2014) 35:1–6.

61. Rojo-Marticella M, Arija V, Morales-Hidalgo P, Esteban-Figuerola P, Voltas-Moreso N, Canals-Sans J. Anthropometric status of preschoolers and elementary school children with ADHD: preliminary results from the EPINED study. *Pediatr Res*. (2023) 94(4):1570–8. doi: 10.1038/s41390-023-02671-6

62. Wan L, Ge WR, Zhang S, Sun YL, Wang B, Yang G. Case-control study of the effects of gut microbiota composition on neurotransmitter metabolic pathways in children with attention deficit hyperactivity disorder. *Front Neurosci*. (2020) 14:127. doi: 10.3389/fnins.2020.00127

63. Iglesias-Vazquez L, Van Ginkel RG, Arija V, Canals J. Composition of gut microbiota in children with autism spectrum disorder: a systematic review and meta-analysis. *Nutrients*. (2020) 12(3):792. doi: 10.3390/nu12030792

64. Green C, Dissanayake C, Loesch D. A review of physical growth in children and adolescents with autism pectrum disorder. *Dev Rev*. (2015) 36:156–78. doi: 10.1016/j.dr.2015.02.001

65. Samadi M, Moradi S, Azadbakht L, Rezaei M, Hojati N. Adherence to healthy diet is related to better linear growth with open growth plate in adolescent girls. *Nutr Res*. (2020) 76:29–36. doi: 10.1016/j.nutres.2020.02.002

66. Marcovecchio ML, Chiarelli F. Obesity and growth during childhood and puberty. *World Rev Nutr Diet*. (2013) 106:135–41. doi: 10.1159/000342545

67. Arnesen EK, Thorisdottir B, Lamberg-Allardt C, Barebring L, Nwaru B, Dierkes J, et al. Protein intake in children and growth and risk of overweight or obesity: a systematic review and meta-analysis. *Food Nutr Res*. (2022) 66:10.29219/fnr.v66.8242. doi: 10.29219/fnr.v66.8242

68. Beam A, Clinger E, Hao L. Effect of diet and dietary components on the composition of the gut microbiota. *Nutrients*. (2021) 13(8):2795. doi: 10.3390/nu13082795

69. Lobstein T, Jackson-Leach R, Moodie ML, Hall KD, Gortmaker SL, Swinburn BA, et al. Child and adolescent obesity: part of a bigger picture. *Lancet*. (2015) 385:2510–20. doi: 10.1016/S0140-6736(14)61746-3

70. Yu Z, Yu XF, Zhao X, Su Z, Ren PG. Greater alteration of gut microbiota occurs in childhood obesity than in adulthood obesity. *Front Pediatr*. (2023) 11:1087401. doi: 10.3389/fped.2023.1087401

71. Orbe-Orihuela YC, Godoy-Lozano EE, Lagunas-Martinez A, Castaneda-Marquez AC, Murga-Garrido S, Diaz-Benitez CE, et al. Association of gut microbiota with dietary-dependent childhood obesity. *Arch Med Res*. (2022) 53:407–15. doi: 10.1016/j.arcmed.2022.03.007

72. Edwards PT, Kashyap PC, Preidis GA. Microbiota on biotics: probiotics, prebiotics, and synbiotics to optimize growth and metabolism. *Am J Physiol Gastrointest Liver Physiol*. (2020) 319:G382–90. doi: 10.1152/ajpgi.00028.2020

73. Suzumura EA, Bersch-Ferreira AC, Torreglosa CR, Da SJ, Coqueiro AY, Kuntz M, et al. Effects of oral supplementation with probiotics or synbiotics in overweight and obese adults: a systematic review and meta-analyses of randomized trials. *Nutr Rev*. (2019) 77:430–50. doi: 10.1093/nutrit/nuz001

74. Shalitin S, Gat-Yablonski G. Associations of obesity with linear growth and puberty. *Horm Res Paediatr*. (2022) 95:120–36. doi: 10.1159/000516171

75. Hu HJ, Park SG, Jang HB, Choi MK, Park KH, Kang JH, et al. Obesity alters the microbial community profile in Korean adolescents. *PLoS One*. (2015) 10:e0134333. doi: 10.1371/journal.pone.0134333

76. Dong G, Zhang J, Yang Z, Feng X, Li J, Li D, et al. The association of gut microbiota with idiopathic central precocious puberty in girls. *Front Endocrinol*. (2019) 10:941. doi: 10.3389/fendo.2019.00941

77. Calcaterra V, Rossi V, Massini G, Regalbuto C, Hruby C, Panelli S, et al. Precocious puberty and microbiota: the role of the sex hormone-gut microbiome axis. *Front Endocrinol*. (2022) 13:1000919. doi: 10.3389/fendo.2022.1000919

78. Li Y, Shen L, Huang C, Li X, Chen J, Li SC, et al. Altered nitric oxide induced by gut microbiota reveals the connection between central precocious puberty and obesity. *Clin Transl Med*. (2021) 11:e299. doi: 10.1002/ctm2.299

79. Carel JC, Lahlou N, Roger M, Chaussain JL. Precocious puberty and statural growth. *Hum Reprod Update*. (2004) 10:135–47. doi: 10.1093/humupd/dmh012

80. Cheuiche AV, Da SL, de Paula L, Lucena I, Silveiro SP. Diagnosis and management of precocious sexual maturation: an updated review. *Eur J Pediatr*. (2021) 180:3073–87. doi: 10.1007/s00431-021-04022-1

81. Sorensen K, Mouritsen A, Mogensen SS, Aksglaede L, Juul A. Insulin sensitivity and lipid profiles in girls with central precocious puberty before and during gonadal suppression. *J Clin Endocrinol Metab*. (2010) 95:3736–44. doi: 10.1210/jc.2010-0731

82. Yin C, Chen J, Wu X, Liu Y, He Q, Cao Y, et al. Preterm birth is correlated with increased oral originated microbiome in the gut. *Front Cell Infect Microbiol*. (2021) 11:579766. doi: 10.3389/fcimb.2021.579766

83. Fardini Y, Chung P, Dumm R, Joshi N, Han YW. Transmission of diverse oral bacteria to murine placenta: evidence for the oral microbiome as a potential source of intrauterine infection. *Infect Immun*. (2010) 78:1789–96. doi: 10.1128/IAI.01395-09

84. Chu DM, Ma J, Prince AL, Antony KM, Seferovic MD, Aagaard KM. Maturation of the infant microbiome community structure and function across multiple body sites and in relation to mode of delivery. *Nat Med*. (2017) 23:314–26. doi: 10.1038/nm.4272

85. Xiao L, Zhao F. Microbial transmission, colonisation and succession: from pregnancy to infancy. *Gut*. (2023) 72:772–86. doi: 10.1136/gutjnl-2022-328970

86. Yan J, Charles JF. Gut microbiota and IGF-1. *Calcif Tissue Int*. (2018) 102:406–14. doi: 10.1007/s00223-018-0395-3

87. Schwarzer M, Makki K, Storelli G, Machuca-Gayet I, Srutkova D, Hermanova P, et al. Lactobacillus plantarum strain maintains growth of infant mice during chronic undernutrition. *Science*. (2016) 351:854–7. doi: 10.1126/science.aad8588

88. Shin SC, Kim SH, You H, Kim B, Kim AC, Lee KA, et al. Drosophila microbiome modulates host developmental and metabolic homeostasis via insulin signaling. *Science*. (2011) 334:670–4. doi: 10.1126/science.1212782

89. Zhang S, Wu P, Tian Y, Liu B, Huang L, Liu Z, et al. Gut microbiota serves a predictable outcome of short-term low-carbohydrate diet (LCD) intervention for patients with obesity. *Microbiol Spectr*. (2021) 9:e0022321. doi: 10.1128/Spectrum.00223-21

90. Morais MB, Silva G. Environmental enteric dysfunction and growth. *J Pediatr (Rio J)*. (2019) 95(Suppl 1):85–94. doi: 10.1016/j.jped.2018.11.004

91. Leong K, Jayasinghe TN, Wilson BC, Derraik J, Albert BB, Chiavaroli V, et al. Effects of fecal microbiome transfer in adolescents with obesity: the gut bugs randomized controlled trial. *JAMA Netw Open*. (2020) 3:e2030415. doi: 10.1001/jamanetworkopen.2020.30415

92. Yan J, Herzog JW, Tsang K, Brennan CA, Bower MA, Garrett WS, et al. Gut microbiota induce IGF-1 and promote bone formation and growth. *Proc Natl Acad Sci U S A*. (2016) 113:E7554–63. doi: 10.1073/pnas.1607235113

93. Le Floc'H N, Otten W, Merlot E. Tryptophan metabolism, from nutrition to potential therapeutic applications. *Amino Acids*. (2011) 41:1195–205. doi: 10.1007/s00726-010-0752-7

94. Kosek MN, Mduma E, Kosek PS, Lee GO, Svensen E, Pan W, et al. Plasma tryptophan and the kynurenine-tryptophan ratio are associated with the acquisition of statural growth deficits and oral vaccine underperformance in populations with environmental enteropathy. *Am J Trop Med Hyg*. (2016) 95:928–37. doi: 10.4269/ajtmh.16-0037

95. Mayneris-Perxachs J, Lima AA, Guerrant RL, Leite AM, Moura AF, Lima NL, et al. Urinary N-methylnicotinamide and beta-aminoisobutyric acid predict catch-up growth in undernourished Brazilian children. *Sci Rep*. (2016) 6:19780. doi: 10.1038/srep19780

96. Gazi MA, Das S, Siddique MA, Alam MA, Fahim SM, Hasan MM, et al. Plasma kynurenine to tryptophan ratio is negatively associated with linear growth of children living in a slum of Bangladesh: results from a community-based intervention study. *Am J Trop Med Hyg*. (2020) 104:766–73. doi: 10.4269/ajtmh.20-0049

97. Wiggins JB, Trotman R, Perks PH, Swanson JR. Enteral nutrition: the intricacies of human milk from the immune system to the microbiome. *Clin Perinatol*. (2022) 49:427–45. doi: 10.1016/j.clp.2022.02.009

98. De Benedetti F, Alonzi T, Moretta A, Lazzaro D, Costa P, Poli V, et al. Interleukin 6 causes growth impairment in transgenic mice through a decrease in insulin-like growth factor-I. A model for stunted growth in children with chronic inflammation. *J Clin Invest*. (1997) 99:643–50. doi: 10.1172/JCI119207

99. Tigas S, Tsatsoulis A. Endocrine and metabolic manifestations in inflammatory bowel disease. *Ann Gastroenterol*. (2012) 25:37–44.

100. D'Angelo DM, Di Donato G, Breda L, Chiarelli F. Growth and puberty in children with juvenile idiopathic arthritis. *Pediatr Rheumatol Online J*. (2021) 19:28. doi: 10.1186/s12969-021-00521-5

101. Ferreira P, Cavalcanti AS, Silva G. Linear growth and bone metabolism in pediatric patients with inflammatory bowel disease. *J Pediatr (Rio J)*. (2019) 95 (Suppl 1):59–65. doi: 10.1016/j.jped.2018.11.002

102. Prendergast AJ, Rukobo S, Chasekwa B, Mutasa K, Ntozini R, Mbuya MN, et al. Stunting is characterized by chronic inflammation in Zimbabwean infants. *PLoS One*. (2014) 9:e86928. doi: 10.1371/journal.pone.0086928

103. Yang YJ, Sheu BS, Yang HB, Lu CC, Chuang CC. Eradication of Helicobacter pylori increases childhood growth and serum acylated ghrelin levels. *World J Gastroenterol*. (2012) 18:2674–81. doi: 10.3748/wjg.v18.i21.2674

104. Saari A, Virta LJ, Sankilampi U, Dunkel L, Saxen H. Antibiotic exposure in infancy and risk of being overweight in the first 24 months of life. *Pediatrics*. (2015) 135:617–26. doi: 10.1542/peds.2014-3407

105. Gough EK, Moodie EE, Prendergast AJ, Johnson SM, Humphrey JH, Stoltzfus RJ, et al. The impact of antibiotics on growth in children in low and middle income countries: systematic review and meta-analysis of randomised controlled trials. *BMJ*. (2014) 348:g2267. doi: 10.1136/bmj.g2267

106. Amza A, Kadri B, Nassirou B, Stoller NE, Yu SN, Zhou Z, et al. A cluster-randomized controlled trial evaluating the effects of mass azithromycin treatment on growth and nutrition in Niger. *Am J Trop Med Hyg*. (2013) 88:138–43. doi: 10.4269/ajtmh.2012.12-0284

107. Kosek M, Haque R, Lima A, Babji S, Shrestha S, Qureshi S, et al. Fecal markers of intestinal inflammation and permeability associated with the subsequent acquisition of linear growth deficits in infants. *Am J Trop Med Hyg*. (2013) 88:390–6. doi: 10.4269/ajtmh.2012.12-0549

108. Ahmed T, Auble D, Berkley JA, Black R, Ahern PP, Hossain M, et al. An evolving perspective about the origins of childhood undernutrition and nutritional interventions that includes the gut microbiome. *Ann N Y Acad Sci*. (2014) 1332:22–38. doi: 10.1111/nyas.12487

109. Ihekweazu FD, Versalovic J. Development of the pediatric gut microbiome: impact on health and disease. *Am J Med Sci*. (2018) 356:413–23. doi: 10.1016/j.amjms.2018.08.005

frontiers | Frontiers in Endocrinology

TYPE Original Research
PUBLISHED 16 November 2023
DOI 10.3389/fendo.2023.1171397

OPEN ACCESS

EDITED BY
Sijung Yun,
Predictiv Care, Inc., United States

REVIEWED BY
Stefano Ciardullo,
University of Milano Bicocca, Italy
Heekyong R. Bae,
Kyungpook National University,
Republic of Korea

*CORRESPONDENCE
Cheng Hu
hucheng10200@163.com
Guang Ji
jiliver@vip.sina.com

†These authors have contributed equally to this work and share first authorship

RECEIVED 22 February 2023
ACCEPTED 06 July 2023
PUBLISHED 16 November 2023

CITATION
Jiang Y, Zhuang X, Zhang J, Li M, Du S, Tian J, Yuan Y, Ji G and Hu C (2023) Clinical characterization and proteomic profiling of lean nonalcoholic fatty liver disease.
Front. Endocrinol. 14:1171397.
doi: 10.3389/fendo.2023.1171397

Clinical characterization and proteomic profiling of lean nonalcoholic fatty liver disease

Yuanye Jiang[1†], Xiaoyu Zhuang[2†], Jiaqi Zhang[3†], Meng Li[4], Shengnan Du[1], Jiyun Tian[1], Yifu Yuan[1], Guang Ji[4*] and Cheng Hu[2*]

[1]Department of Gastroenterology, Putuo Hospital, Shanghai University of Traditional Chinese Medicine, Shanghai, China, [2]Experiment Center for Science and Technology, Shanghai University of Traditional Chinese Medicine, Shanghai, China, [3]Department of Pharmacy, Shanghai Municipal Hospital of Traditional Chinese Medicine, Shanghai University of Traditional Chinese Medicine, Shanghai, China, [4]Institute of Digestive Diseases, Longhua Hospital, Shanghai University of Traditional Chinese Medicine, Shanghai, China

Introduction: Obesity has been historically associated with nonalcoholic fatty liver disease (NAFLD), but it can also occur in lean individuals. However, limited data is available on this special group. To investigate the clinical and proteomic characteristics of lean subjects with NAFLD, and to identify potential clinical variables and plasma proteins for diagnosing NAFLD in lean individuals, we collected clinical data from a large cohort of 2,236 subjects.

Methods: Diagnosis of NAFLD relied on detecting pronounced hepatic steatosis through abdominal ultrasonography. Participants were categorized into four groups based on body mass index: overweight NAFLD, overweight control, lean NAFLD, and lean control. Plasma proteomic profiling was performed on samples from 20 subjects in each group. The lean NAFLD group was compared to both lean healthy and obese NAFLD groups across all data.

Results and discussion: The results indicated that the lean NAFLD group exhibited intermediate metabolic profiles, falling between those of the lean healthy and overweight NAFLD groups. Proteomic profiling of plasma in lean subjects with or without NAFLD revealed 45 statistically significant changes in proteins, of which 37 showed high diagnostic value (AUC > 0.7) for lean NAFLD. These potential biomarkers primarily involved lipid metabolism, the immune and complement systems, and platelet degranulation. Furthermore, AFM, GSN, CFH, HGFAC, MMP2, and MMP9 have been previously associated with NAFLD or NAFLD-related factors such as liver damage, insulin resistance, metabolic syndromes, and extracellular homeostasis. Overall, lean individuals with NAFLD exhibit distinct clinical profiles compared to overweight individuals with NAFLD. Despite having worse metabolic profiles than their healthy counterparts, lean NAFLD patients generally experience milder systemic metabolic disturbances compared to obese NAFLD patients. Additionally, the plasma proteomic profile is significantly altered in lean NAFLD, highlighting the potential of differentially expressed proteins as valuable biomarkers or therapeutic targets for diagnosing and treating NAFLD in this population.

KEYWORDS

proteomic, biomarker, lipid metabolism, mass spectrometry, nonalcoholic fatty liver disease

1 Introduction

Nonalcoholic fatty liver disease (NAFLD) is a condition characterized by significant lipid deposition in the liver parenchyma without history of excessive alcohol consumption. The prevalence of NAFLD has reached high levels worldwide (~25%). Around 10-30% of people with NAFLD may develop a more serious condition called nonalcoholic steatohepatitis (NASH), which is characterized by hepatic inflammation and fibrosis. In some cases, patients with NASH may even progress to cirrhosis and develop various liver-related complications due to ongoing liver injury.

NAFLD is a pathogenically complex and clinically heterogeneous disease. It is strongly linked with metabolic syndrome (MetS) components such as obesity, diabetes, dyslipidemia, and hypertension (1). Although NAFLD is more common in the obese, a small but significant subset of patients are lean, which is defined as lean or non-obese NAFLD (2, 3). The definition of lean NAFLD commonly involves ethnic-specific BMI cut-offs, such as 25 kg/m^2 for Caucasians and 23 kg/m^2 for Asians (4).

Non-obese NAFLD is becoming increasingly prevalent worldwide. There is a strong ethnic difference in BMI and risk of NAFLD (5). It is noteworthy that Chinese populations have similar rates of NAFLD as western populations, even at much lower BMI levels (4). Lean NAFLD patients generally experience a less severe phenotype with better histologic and biochemical profile compared to those with a higher BMI. However, they may still exhibit full range of histopathological characteristics of NASH, including steatosis, lobular inflammation, hepatocyte ballooning, and/or fibrosis (6–8). Additionally, lean NAFLD subjects are prone to similar health issues and associated diseases as their obese counterparts, such as type 2 diabetes, cardiovascular disease, and hepatocellular carcinoma. Multiple studies have demonstrated that fibrosis progression is more rapid in this population, placing them at a higher risk for the development of severe liver disease in the future. Several studies have shown that fibrosis progression is faster in this group, putting them at higher risk for severe liver disease in the future (9, 10). In fact, there is accumulating evidence to suggest that lean NAFLD might be a distinct pathophysiological entity, with approximately 47%-65% cases resulting in NASH. The underlying pathophysiology is not well understood.

The early diagnosis and intervention of NAFLD is critical due to its progressive nature. The current gold standard for NAFLD diagnosis remains histological examination of liver biopsy specimen despite it is an invasive procedure with inevitable sampling bias and interobserver variability. It is also unlikely to be widely accepted in the real life. Instead, noninvasive methods, such as biomarker panels and imaging, are widely applied for diagnosing NAFLD in clinical practice. Radiologic modalities like ultrasonography are useful screening tools widely available and relatively accurate in diagnosing of fatty liver disease, although ultrasonography is operator dependent and cannot stage liver damage progression, such as hepatic fibrosis in NAFLD patients (11). Blood-based tests for liver diseases have gained attention in recent years (12), particularly the comparison of proteomes between disease and control blood samples to discover blood biomarkers of NAFLD. Blood indicators such as alanine aminotransferase (ALT) and aspartate aminotransferase (AST) may not elevate until histological liver injury occurs. Given that ALT levels may remain normal or only intermittently elevated in many patients with NAFLD, even those with advanced fibrosis, it is urgent to find better ways to evaluate NAFLD patients. This is particularly important for identifying individuals at risk for non-obese NAFLD, who lack the typical obesity phenotype and may not seek medical attention for NAFLD diagnosis. On the other hand, despite some progress in better understanding the disease, there has been little research on lean NAFLD due to the close relationship between obesity and NAFLD.

Mass spectrometry-based proteomics technology has revolutionized our ability to explore the complex and dynamic world of proteins. This cutting-edge technology holds great potential to provide new insights into disease mechanism and biomarker discovery (13–15). In this study, we aim to identify possible clinical variables and plasma proteins that offer potential application for diagnosing NAFLD in lean subjects. Additionally, we aim to discover novel biomarkers for lean NAFLD diagnosis. We hope to identify a panel of dependable protein biomarkers, instead of relying on a single marker, which could also improve the early detection of disease among at-risk group.

Abbreviations: WBC, white blood cells; RBC, red blood cells; HGB, haemoglobin; HCT, haematocrit; MCV, mean corpuscular volume; MCH, mean corpuscular haemoglobin; MCHC, mean corpuscular haemoglobin concentration; PLT, platelet; RDW, red blood cell distribution width; MPV, mean platelet volume; N, neutrophil; LY, lymphocyte; MO, monocyte; EO, eosinophil; BASO, basophils; TBA, total bile acid; CHE, cholinesterase; TB, total Bilirubin; DB, direct bilirubin; TP, total protein; ALB, albumin; γ-GT, γ-glutamyl transferase; AKP, alkaline phosphatase; AST, aspartate aminotransferase; ALT, alanine aminotransferase; GA, glycated albumin; HbA1c— hemoglobin A1c; HDL, high density lipoprotein; LDL, low density lipoprotein; TC, total cholesterol; TG, triglyceride; FBG —fasting blood glucose; Lp(a), lipoprotein a; BUN, blood urea nitrogen; Cr, creatinine; UA, uric acid; GFR, glomercular filtration rate; TgAb, thyroglobulin antibodies; TPOAb, thyroid peroxidase antibodies; TG-AB, thyroglobulin antibody; TR-Ab, thyrotropin receptor antibody; T3, 3,5,3'-L-triiodo-thyronine; T4, 3,5,3',5'-L-tetraiodo-thyronine; FT3, free T3; FT4, free T4; TSH, thyroid stimulating hormone.

2 Materials and methods

2.1 Participants

Participants were recruited from Putuo Hospital Affiliated to Shanghai University of Traditional Chinese Medicine, Shanghai, China, between March 2019 and November 2021. The **inclusion criteria** were 16-75 years of age, non-alcoholic people (alcohol intake < 210 g/week for men, <140 g/week for women), the availability of liver ultrasound data, and the availability of relevant demographic, clinical and examination information. **Exclusion criteria** were 1) laboratory or clinical evidence of

autoimmune, viral, inherited causes of liver disease or of drug induced liver injury; 2) in combination with extrahepatic fibrotic diseases including systemic lupus erythematosus, rheumatic diseases, renal failure, chronic obstructive pulmonary disease, and so on;3) malignant tumors, significant cardiovascular and cerebrovascular, urinary, kidney, hematopoietic system and other severe primary diseases or complications; 4) mental illness; 5) patients with type 1 diabetes or uncontrolled type 2 diabetes mellitus (defined as HbA1c≥ 9.5%), those who have adjusted hypoglycemic drugs 2 months before enrollment, or who have experienced severe hypoglycemic events; 6) thyroid dysfunction, including hyperthyroidism, hypothyroidism, subclinical hypothyroidism, Hashimoto's thyroiditis;

In total, 2,236 subjects meeting the criteria were recruited for this study. In line with the Guideline of prevention and treatment of nonalcoholic fatty liver disease (2018, China) formulated by the National Workshop on Fatty Liver and Alcoholic Liver Disease od Chinese Medical Association and Fatty Liver Disease Expert Committee of Chinese Medical Doctor Association (16), in the absence of other causes of fatty liver disease, NAFLD was diagnosed based on the detection of significant hepatic steatosis on abdominal ultrasonography. To minimize the subjective influence of different doctors on the results, each examination of included patients in this study was conducted by two ultrasound physicians. The protocol received approval from the Medical Ethics Committee. All participants have signed informed consent.

Ethnic-specific BMI cut-offs of 25 kg/m2 for Caucasians and 23 kg/m2 for Asians are typically used to define the "lean" population. For our study, only Chinese participants were included, and we used the Asian-specific BMI criteria to classify individuals as "lean" (BMI < 23) or "overweight" (BMI ≥ 23). Controls were healthy volunteers with no signs of liver disease or other chronic diseases. Participants were divided into two cohorts. The overweight cohort included overweight NAFLD group (n=1,100) and overweight control group (n=312), the lean cohort consisted of lean NAFLD group (n=403) and lean control group (n=421). Samples of 20 subjects in each group were used for plasma proteomic profiling.

2.2 Clinical and laboratory assessment

Venous blood was collected after overnight fasting for a minimum of 12 h. Participants underwent a standard physical examination that included blood pressure, height, weight, and waist circumference and hip circumference. Body mass index (BMI) was measured as the body weight in kilograms divided by the square of the height of the body in meters (kg/m^2). Detailed medical histories were obtained via questionnaire. Laboratory investigations included measurement of routine blood examination, fasting plasma glucose, lipid panel, liver biochemistry, and renal biochemistry, thyroid function tests were carried out on an automated chemistry analyzer (Hitachi 7600d-210, Japan).

The FIB-4 index was employed to assess the likelihood of significant liver fibrosis in participants. A higher FIB-4 score indicates a greater likelihood of fibrosis. FIB-4 scores are interpreted as below: scores below 1.30 indicate a low risk of significant fibrosis; scores between 1.30 and 2.67 indicate an indeterminate risk of significant fibrosis, requiring further evaluation; scores equal to or above 2.67 indicate a high risk of significant fibrosis (17–19)

2.3 Peptides preparation for MS analysis (high abundant protein depletion, protein extraction and digestion)

Removal of high abundant plasma proteins was performed using a High-Select^{TM} Top14 Abundant Protein Depletion Spin Column (Thermo Fisher Scientific) in accordance with the manufacturer's instructions. In brief, 10 µL of plasma sample was loaded onto the column and incubated at room temperature with gentle end-over-end mixing for 10 min. The filtrate was then collected by centrifuging at 1,000 g for 2 min. The resulting depleted protein sample was precipitated with acetone at -20°C for 2 h, followed by dissolution in 6 M guanidine hydrochloride and 50 mM ammonium bicarbonate (NH_4HCO_3, pH 8.0). The protein concentration was determined using BCA protein assay.

Dithiothreitol (final concentration of 20 mM) was added to the solution and incubate at 57°C for 30 min to reduce disulfide bonds, then iodoacetamide (final concentration of 80 mM) for alkylation of the free thiol group was added and incubated at room temperature for 30 min in the dark. To exchange the buffer and digest the protein, we employed filter-aided sample preparation (FASP) method developed by Wisniewski et al. (20) Briefly, proteins were loaded in 10 kDa centrifugal filter tubes (Merck) and washed with 50 mM NH_4HCO_3 for three times. Afterwards, samples were treated with sequence-level trypsin (Promega, Madison, MI) at an enzyme substrate ratio of 1:50 for 16 h at 37°C in 50 mM NH_4HCO_3. The peptides were eluted by centrifugation and desalted using a MonoSpin C18 column (GL Science, Tokyo, Japan).

2.4 LC-MS/MS proteomic analysis

Peptide samples were analyzed on an Easy-nLC 1000 system (Thermo Fisher Scientific) coupled with an Orbitrap Fusion Lumos mass spectrometer (Thermo Fisher Scientific). Separation of the peptide mixture was achieved using a PepMap C18 column (2µm, 75µm*250mm) at a flow rate of 300 nL/min over a 120 min gradient (mobile phase A was 0.1% formic acid in water; mobile phase B was 0.1% formic acid in acetonitrile). The analytical column temperature was set at 50°C during the experiments. The elution gradient was as follows: 0–2 min, 2 to 8% B; 2–82 min, 8 to 28% B; 82–102 min, 28 to 32% B; 102–120 min, 32 to 95% B.

Mass spectrometry was operated under a data-dependent acquisition (DDA) mode. The spray voltage was set at 2,200 V in positive ion mode and the ion transfer tube temperature was set to 275°C. For the MS1 full scan, ions with *m/z* ranging from 350 to 1,800 were acquired by Orbitrap mass analyzer at a resolution of

120,000. The automatic gain control (AGC) target was set as 1e6 and the maximum ion injection time was 50 ms. For the MS2 acquisition, a top-speed mode was employed with a duty cycle time of 3 s. Precursor ions were selected and fragmented with higher energy collision dissociation (HCD) of 30%. The resulting fragment ions were analyzed by Orbitrap mass analyzer, with the MS2 scan resolution set to 15,000 and an isolation window of 1.6 m/z. The AGC and maximal ion injection time for MS2 were set at 1e5 and 22 ms, respectively. A dynamic exclusion time of 60 s was applied.

2.5 MS database searching and differential protein analysis

MS raw data were processed using Proteome Discoverer 2.4 and searched against Swissprot human proteome database (released on June 20, 2021). Trypsin was set as the protease. The maximum number of missing cleavage site was set to 2 with a minimum peptide length of 7. The false discovery rates (FDR) of peptide, protein and site were all < 0.01. Carbamidomethyl (C) was considered as a fixed modification, and oxidized methionine, protein N-term acetylation, asparagine and glutamine deamidation were set as variable modifications.

A label-free quantification algorithm was used for protein quantitation. The protein abundance in each sample was determined as the sum of all normalized peptide areas for a given protein. For statistical analysis, proteins with valid values in at least 70% of the samples in one experimental group were further considered. Proteins with altered expression in NAFLD compared to healthy controls were identified by a two-sided t-test (P value < 0.05) and were defined as upregulated or downregulated if the N/H ratio was greater than 1.20 or less than 0.833, respectively. The top Gene Ontology (GO)/annotation terms were enriched using Cytoscape plug-in ClueGO and DAVID Bioinformatics Resource 6.8.

2.6 Statistical analysis

Statistical analysis was carried out using the statistical software SPSS 25.0 (SPSS Inc. Chicago, United States). Chicago, United States). The Pearson $\chi 2$ test was applied to categorical variables based on the sample size and theoretical frequency, the continuous correction formula of chi-square test or Fisher's exact probability method was used if necessary. Continuous normally distributed variables were compared between groups using Student's T test, expressed as mean ± standard deviation (SD), t-test for homogeneity of variance, and t' test for unequal variance. Continuous variables that were not normally distributed were compared between groups using the Mann-Whitney U test and reported as M (P25, P75). A p value less than 0.05 was considered statistically significant in all cases. To assess the diagnostic power of each potential biomarker in NAFLD, we used the area under the receiver operating characteristic (ROC) (AUC) curve.

3 Results

3.1 Clinical and biochemical characteristics

We collected clinical data from a large cohort of 2,236 subjects and used samples from 20 subjects in each group for plasma proteomic profiling. Figure 1 illustrates the overall study design. To exclude the influence of BMI, we initially compared the clinical characteristics and proteome profiles of subjects within each cohort, i.e., overweight NAFLD vs. overweight control, lean NAFLD vs. lean control. To better understand the differences in the pathogenesis of NAFLD between lean and overweight individuals, we then compared the data of lean NAFLD patients to that of overweight NAFLD patients. The demographic, clinical and biochemical characteristics are shown in Table 1.

The results show that middle-aged subjects have a higher prevalence of NAFLD. The overweight NAFLD group included 636 males (57.8%) and 464 females (42.2%), while the lean NAFLD group had a higher proportion of females (66.5%). Both the lean and overweight NAFLD groups had slightly higher BMIs than their respective healthy counterparts. Although the mean aminotransferase levels in lean NAFLD fall within the normal range, NAFLD patients in both lean and overweight cohorts exhibited elevated levels of ALT and AST, as well as AKP, γ-GT and CHE compared to their healthy counterparts.

Significant differences in almost all blood lipid indices, including HDL, LDL, TC, TG, APOB, and APOA1, were observed in both cohorts. While this study did not include subjects with hyperlipidemia or hypertriglyceridemia, both the overweight and lean NAFLD groups showed significantly higher levels of serum LDL, TC, TG, APOB, and lower levels of HDL and APOA1 than their healthy counterparts. These findings emphasize that a disorder of lipid metabolism can be present and may contribute to fatty liver disease in individuals with a normal weight.

As for the complete blood count test, significant higher levels of HGB, HCT, RBC and WBC were observed in both lean and overweight NAFLD groups when compared to their respective control groups. The overweight NAFLD patients exhibited the highest levels of HGB, HCT, RBC, and WBC. In addition, NAFLD patients also had significant raised fasting blood glucose, indicating a worse metabolic profile. According to research, an elevated platelet count might be linked to NASH (21), but this correlation was only found among overweight individuals with NAFLD compared to overweight controls. Lean NAFLD patients exhibited even significantly lower platelet count compared to their healthy counterparts.

The thyroid hormones are essential regulators of metabolism including lipid metabolism in the liver. Our findings in the overweight cohort were consistent with previous reports, showing a direct relationship between NAFLD and decreasing levels of FT4 (22). However, there was no significant difference in FT4 levels between the two lean groups. Both overweight and lean NAFLD patients showed increased levels of TSH, which is positively linearly associated with NAFLD risk, even within the euthyroid reference range (23). Notably, we found that lean NAFLD subjects had

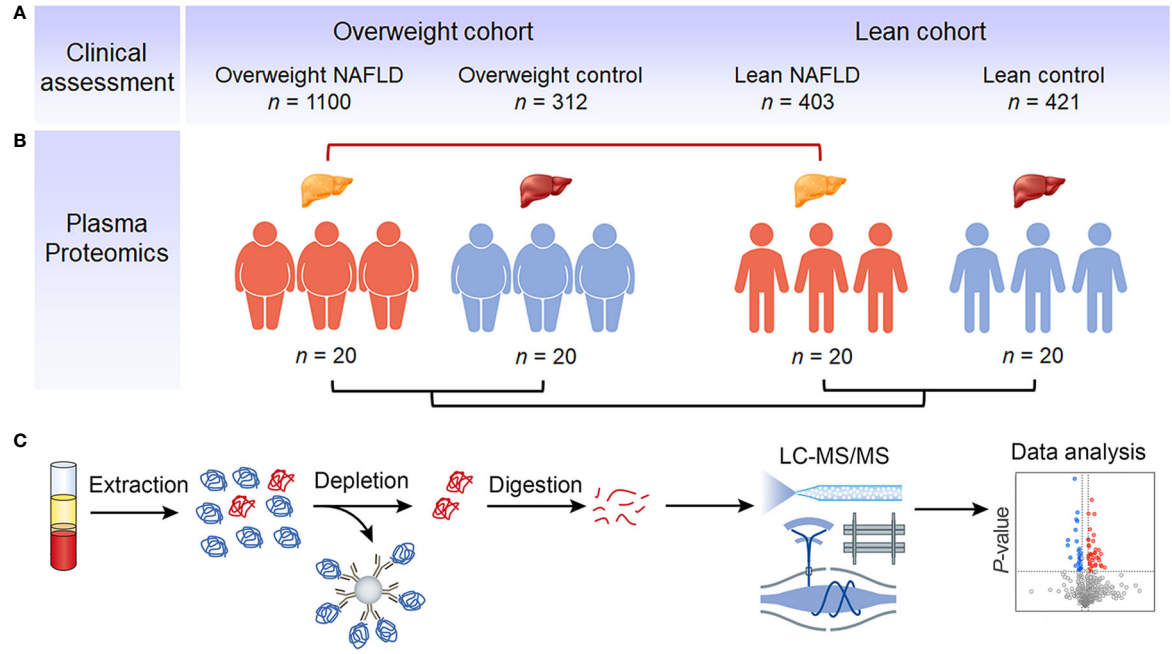

FIGURE 1
Study outline and proteomic workflow. Using BMI of 23 as the cut-off value, eligible NAFLD patients and healthy individuals were divided into overweight NAFLD group, overweight control group, lean NAFLD group and lean control group. The clinical data were collected from a large cohort of 2,236 subjects, with the number of subjects in each group indicated **(A)**. Samples of 20 subjects in each group were used for plasma proteomic profiling **(B)**. Fasting plasma was collected and analyzed using a MS-based proteomics strategy, including protein extraction, high abundant protein depletion, protein digestion, LC-MS/MS analysis, database search, and further computational analysis **(C)**.

significantly higher TSH levels than overweight NAFLD subjects (P<0.01).Numerous observational studies suggest that individuals with NAFLD have a significantly higher incidence of CKD compared to those without NAFLD (24–26). Uric acid (UA) and blood urea nitrogen (BUN) levels were notably elevated in both lean and overweight NAFLD patients compared to their matched healthy controls, with the highest levels of these indicators observed in overweight NAFLD. While creatinine has been reported as a factor associated with NAFLD in several studies (8) (27), we did not observe statistically significant differences in creatinine levels between NAFLD patients and controls in both overweight and lean cohorts.

3.2 Plasma proteome profiling

3.2.1 Overview

Label-free quantitative proteomics was conducted on plasma samples from 40 NAFLD patients and 40 healthy controls. The clinical characteristics of these subjects are shown in Table 1. After depletion of high-abundant blood proteins, a total of 959 proteins were identified, with 677 of these proteins being identified with ≥ 2 unique peptides. We quantified on average 621 proteins per individual. The dataset was filtered to ensure a 70% data completeness in at least one experimental group. Proteins that show a significant change >20% (with fold changes of > 1.20 or < 0.83) between any two groups (p<0.05) were considered as differentially expressed proteins (DEPs).

We first compared the proteome profiles of lean and overweight NAFLD patients and found that 54 proteins were significantly different between the two groups (Table S2). This suggests that lean NAFLD might be a distinct pathophysiological entity. Volcano plots were used to illustrate variations in the proteome profile, showing the ratio of mean protein concentrations of lean NAFLD to overweight NAFLD subjects (Figure 2A). In addition, a heat map was generated by hierarchically clustering the variables that effectively discriminating between the two groups with fold change > 1.20 or < 0.83 (Figure 2D).

When comparing the plasma proteome profiles of lean NAFLD to that of lean healthy controls, we identified 62 proteins that differ significantly between the two groups, with 34 proteins were upregulated and 28 were downregulated (Table 2 and Figures 2A, B). To validate the biological relevance of this dataset, pathway annotation was conducted using the ClueGO plug-in in Cytoscape and DAVID Bioinformatic Resource. The results suggest that these 62 candidate proteins are mainly involved in biological processes such as complement activation, platelet degranulation, neutrophil degranulation, cell adhesion, and immune and inflammatory response (Figure 2E).

In the comparison between overweight NAFLD and overweight healthy controls, significant changes were observed in the levels of 59 proteins, of which 30 and 29 were up- and down-regulated, respectively (Table S1 and Figures 2A, B). GO enrichment of DEPs associated with overweight NAFLD in term of biological process is shown in Figure S1. As shown in Venn diagram (Figure 2C), among the DEPs identified in the overweight cohort, 9 proteins also

10.3389/fendo.2023.1171397

TABLE 1 Demographic, clinical, anthropometrical and laboratory characteristics of the study population.

Variables	Lean NAFLD (n=403)	Lean control (n=421)	Overweight NAFLD (n=1100)	Overweight control (n=312)	P-value		
					LN-LC	ON-OC	LN-ON
Demographic data & physical characteristics							
Gender (M/F)	135/268	78/343	636/464	145/167	<0.001	<0.001	<0.001
Age (year)	48.00(37.00,58.00)	42.00(31.00,51.00)	53.00(44.00,65.00)	50.00(39.25,58.75)	<0.001	<0.001	<0.001
Height (cm)	163.00 (158.00,172.00)	162.00 (157.00,167.00)	167.00(160.00,173.00)	164.00(157.00,172.00)	<0.001	0.009	<0.001
Weight (kg)	58.00(54.00,64.00)	54.00(51.00,59.00)	74.00(66.00,82.00)	68.00(61.25,75.00)	<0.001	<0.001	<0.001
BMI (kg/m^2)	22.10(21.00,22.80)	20.90(19.80,21.90)	26.60(25.10,28.50)	24.71(23.84,26.23)	<0.001	<0.001	<0.001
FIB4 index	0.96(0.65,1.39)	0.90(0.57,1.31)	0.93(0.30,1.51)	0.99(0.55,1.44)	<0.05	0.370	0.189
Blood routine examination							
FBG (mmol/L)	4.90(4.60,5.40)	4.80(4.50,5.10)	5.30(4.80,5.90)	5.00(4.70,5.40)	<0.001	<0.001	<0.001
WBC (×109/L)	6.10(5.10,7.15)	5.70(4.80,6.70)	6.50(5.60,7.50)	6.00(5.20,7.00)	<0.001	<0.001	<0.001
RBC (%)	4.53(4.26,4.87)	4.34(4.10,4.64)	4.77(4.47,5.09)	4.61(4.33,4.89)	<0.001	<0.001	<0.001
Haemoglobin (g/L)	137.00 (126.00,148.00)	130.00 (123.00,140.00)	145.00(134.00,155.00)	140.00(128.25,150.00)	<0.001	<0.001	<0.001
Haematocrit (%)	40.80(38.00,43.70)	38.80(36.70,41.40)	42.90(40.20,45.50)	41.20(38.40,44.20)	<0.001	<0.001	<0.001
MCV (fL)	89.40(87.05,92.10)	89.60(87.30,92.30)	90.00(87.30,92.20)	89.70(87.20,92.60)	0.513	0.801	0.126
MCH (pg)	30.20(29.10,31.10)	30.30(29.20,31.10)	30.50(29.50,31.40)	30.50(29.60,31.40)	0.576	0.824	<0.001
MCHC (g/L)	336.00 (330.00,342.00)	335.00 (329.00,342.00)	337.00(331.00,344.00)	338.00(331.00,343.00)	0.294	0.533	0.008
Platelet (×109/L)	239.00 (206.00,285.00)	240.00 (206.00,281.00)	243.00(206.00,284.00)	228.00(195.00,270.00)	0.894	<0.001	0.629
RDW (×1012/L)	12.40(12.10,13.10)	12.50(12.00,13.10)	12.50(12.10,13.00)	12.50(12.10,13.00)	0.768	0.758	0.881
MPV (fL)	10.60(10.00,11.20)	10.60(10.10,11.20)	10.42(9.90,11.20)	10.60(10.00,11.20)	0.549	0.031	0.040
Neutrophil (%)	55.70(50.60,61.60)	54.40(49.10,60.40)	55.70(50.30,61.00)	55.90(50.00,60.70)	0.031	0.837	0.770
Lymphocyte (%)	34.30(28.65,39.60)	35.40(30.10,40.90)	33.80(28.60,38.80)	33.50(29.00,38.90)	0.025	0.901	0.315
Monocyte (%)	6.80(6.00,8.10)	6.90(6.00,7.80)	7.00(6.10,8.30)	7.30(6.20,8.50)	0.797	0.142	0.070
Eosinophil (%)	1.70(1.10,2.80)	1.70(1.00,2.80)	2.10(1.30,3.30)	1.80(1.20,3.30)	0.970	0.068	<0.001
Basophils (%)	0.50(0.30,0.70)	0.50(0.30,0.70)	0.50(0.40,0.70)	0.50(0.40,0.70)	0.044	0.838	<0.001
Renal function tests							
BUN (mmol/L)	5.10(4.30,5.95)	4.80(4.10,5.60)	5.30(4.50,6.20)	5.10(4.30,6.00)	0.004	0.008	<0.001
Creatinine (μmol/L)	62.00(55.00,73.00)	60.00(55.00,68.00)	70.00(59.00,81.00)	68.00(57.00,79.00)	0.111	0.079	<0.001
Uric acid (μmol/L)	317.00 (271.00,374.50)	288.00 (251.00,331.00)	380.00(322.00,447.00)	334.00(276.00,406.00)	<0.001	<0.001	<0.001
GFR (mL/min)	101.61(89.02,112.46)	100.39(87.20,117.95)	99.96(87.47,113.70)	93.17(76.56,109.40)	0.815	0.108	0.879
Liver function tests							
TB (μmol/L)	13.00(10.00,18.00)	13.00(10.25,16.75)	14.00(11.00,18.00)	14.00(10.00,18.00)	0.722	0.426	0.317
DB (μmol/L)	2.45(1.80,3.30)	2.60(1.90,3.20)	2.50(1.90,3.30)	2.50(1.78,3.20)	0.506	0.363	0.172
AKP (U/L)	68.00(57.00,86.00)	62.00(51.00,74.75)	78.00(65.00,92.00)	70.00(56.00,82.00)	<0.001	<0.001	<0.001

(Continued)

TABLE 1 Continued

Variables	Lean NAFLD (n=403)	Lean control (n=421)	Overweight NAFLD (n=1100)	Overweight control (n=312)	P-value		
					LN-LC	ON-OC	LN-ON
TP (g/L)	74.00(70.00,76.00)	74.00(71.00,76.00)	74.00(71.00,76.00)	72.00(70.00,75.00)	0.795	0.001	0.545
Albumin (g/L)	43.00(40.00,45.50)	45.00(43.00,46.00)	44.00(43.00,46.00)	44.00(42.00,45.00)	<0.001	0.042	<0.001
γ-GT (U/L)	21.00(14.00,32.00)	15.00(12.00,21.00)	31.00(20.75,47.00)	21.00(15.00,36.00)	<0.001	<0.001	<0.001
CHE (U/L)	8726.00 (7789.25,9824.00)	7802.00 (6935.00,8712.00)	9123.00(8311.00,10124.00)	8418.00 (7399.25,9296.00)	<0.001	<0.001	0.003
ALT (U/L)	13.00(9.00,19.00)	10.00(7.00,13.00)	18.00(13.00,26.00)	14.00(10.00,18.00)	<0.001	<0.001	<0.001
AST (U/L)	21.00(17.00,25.00)	20.00(17.00,23.00)	24.00(19.00,29.00)	21.00(17.75,26.00)	<0.001	<0.001	<0.001
TBA (μmol/L)	3.00(2.00,6.00)	3.00(2.00,4.00)	3.00(2.00,5.00)	3.00(2.00,5.00)	0.072	0.312	0.723
Lipid panel							
HDL-C (mmol/L)	1.27(1.08,1.47)	1.44(1.28,1.66)	1.13(1.00,1.30)	1.25(1.07,1.48)	<0.001	<0.001	<0.001
LDL-C (mmol/L)	3.34(2.75,3.87)	3.11(2.70,3.63)	3.50(2.99,3.97)	3.30(2.82, 3.89)	0.007	0.006	<0.001
TC (mmol/L)	5.11(4.47,5.91)	4.91(4.40,5.68)	5.23(4.63,5.93)	5.07(4.34,5.86)	0.008	0.004	0.102
TG (mmol/L)	1.35(0.90,1.99)	0.91(0.71,1.27)	1.70(1.24,2.43)	1.23(0.92,1.69)	<0.001	<0.001	<0.001
ApoA1 (g/L)	1.39(1.26,1.63)	1.52(1.34,1.75)	1.32(1.18,1.48)	1.38(1.23,1.60)	<0.001	<0.001	<0.001
ApoB (g/L)	0.91(0.76,1.09)	0.81(0.69,0.95)	1.00(0.84,1.16)	0.91(0.78,1.06)	<0.001	<0.001	<0.001
Lp(a) (mg/L)	60.00(35.00,124.00)	69.00(38.00,142.25)	59.50(34.00,132.75)	78.00(40.00,185.75)	0.362	0.010	0.910
Thyroid function tests							
TgAb (IU/mL)	1.74(1.00,15.30)	1.89(1.00,25.00)	1.32(1.00,4.48)	1.14(1.00,3.09)	0.242	0.349	0.052
TPOAb (IU/mL)	1.00(1.00,3.70)	1.00(1.00,3.99)	1.00(1.00,2.21)	1.30(1.00,5.70)	0.713	0.008	0.085
Tg (ng/mL)	5.41(3.39,8.24)	5.20(3.02,8.08)	5.16(3.14,8.46)	5.39(3.05,8.52)	0.166	0.976	0.328
TRAb (IU/L)	0.10(0.10,0.10)	0.10(0.10,0.35)	0.10(0.10,0.10)	0.34(0.10,0.66)	0.016	<0.001	0.220
T3(nmol/L)	1.90(1.69,2.10)	1.81(1.66,1.98)	1.95(1.75,2.20)	1.85(1.69,2.04)	0.019	0.006	0.063
T4(nmol/L)	101.00(92.70,113.00)	99.40(91.55,109.00)	101.00(91.70,114.00)	102.00(88.75,112.00)	0.280	0.517	0.629
FT3 (pmol/L)	5.05(4.68,5.41)	4.80(4.61,5.28)	5.04(4.71,5.43)	5.03(4.70,5.42)	0.041	0.875	0.788
FT4 (pmol/L)	11.10(10.20,12.00)	10.90(10.00,11.85)	10.70(10.00,11.70)	11.20(10.20,12.60)	0.274	0.003	0.035
TSH (μIU/L)	2.90(1.99,3.81)	2.64(1.86,3.81)	2.53(1.91,3.34)	2.11(1.64,3.12)	0.155	0.005	0.006

All variables are expressed as median (interquartile range) unless otherwise indicated. P -value assessed by Mann–Whitney U-test.
LN, lean NAFLD; LC, lean control; ON, overweight NAFLD; OH, overweight healthy; FBG, fasting blood glucose; WBC, white blood cells; RBC, red blood cells; MCV, mean corpuscular volume; MCH, mean corpuscular haemoglobin; MCHC, mean corpuscular haemoglobin concentration; RDW, red blood cell distribution width; MPV, mean platelet volume; BUN, blood urea nitrogen; GFR, glomercular filtration rate; TB, total Bilirubin; DB, direct bilirubin; AKP, alkaline phosphatase; TP, total protein; γ-GT, γ-glutamyl transferase; CHE, cholinesterase; ALT, alanine aminotransferase; AST, aspartate aminotransferase; TBA, total bile acid; HDL-C, high density lipoprotein cholesterol; LDL-C, low density lipoprotein cholesterol; TC, total cholesterol; TG, triglyceride; ApoA1, apolipoprotein A1; ApoB, apolipoprotein B; Lp(a), lipoprotein(a); TgAb, thyroglobulin antibody; TPOAb, thyroid peroxidase antibody; TgAb, thyroglobulin antibody; Tg, thyroglobulin; TRAb, thyrotropin receptor antibody; T3, triiodothyronine; T4, thyroxine; FT3, free T3; FT4, free T4; TSH, thyroid stimulating hormone.

differed significantly in abundance by NAFLD status within the lean cohort. Of note, these 9 overlapped DEPs displayed similar up-/down-regulated trend (APOF, GOLM1, IGHV3-7, MMP9, THBS1, S100A8, S100A12, TXN, LCN2) in both comparisons. Moreover, in the comparison of lean NAFLD and overweight NAFLD with their corresponding healthy controls, most of the DEPs were annotated as liver-specific or liver-enriched, indicating dysregulated hepatic protein synthesis and secretion in patients with NAFLD.

3.2.2 Potential biomarkers for diagnosing lean NAFLD

As mentioned above, 59 and 62 DEPs were identified in the overweight and lean cohorts, respectively. We then assessed the diagnostic power of each candidate biomarkers for NAFLD within each cohort by identifying classifiers/components with an area under the ROC curve (AUC) > 0.7. Tables 2, S1 shows a total of 39 and 43 proteins fulfill the criterion and could serve as biomarkers

10.3389/fendo.2023.1171397

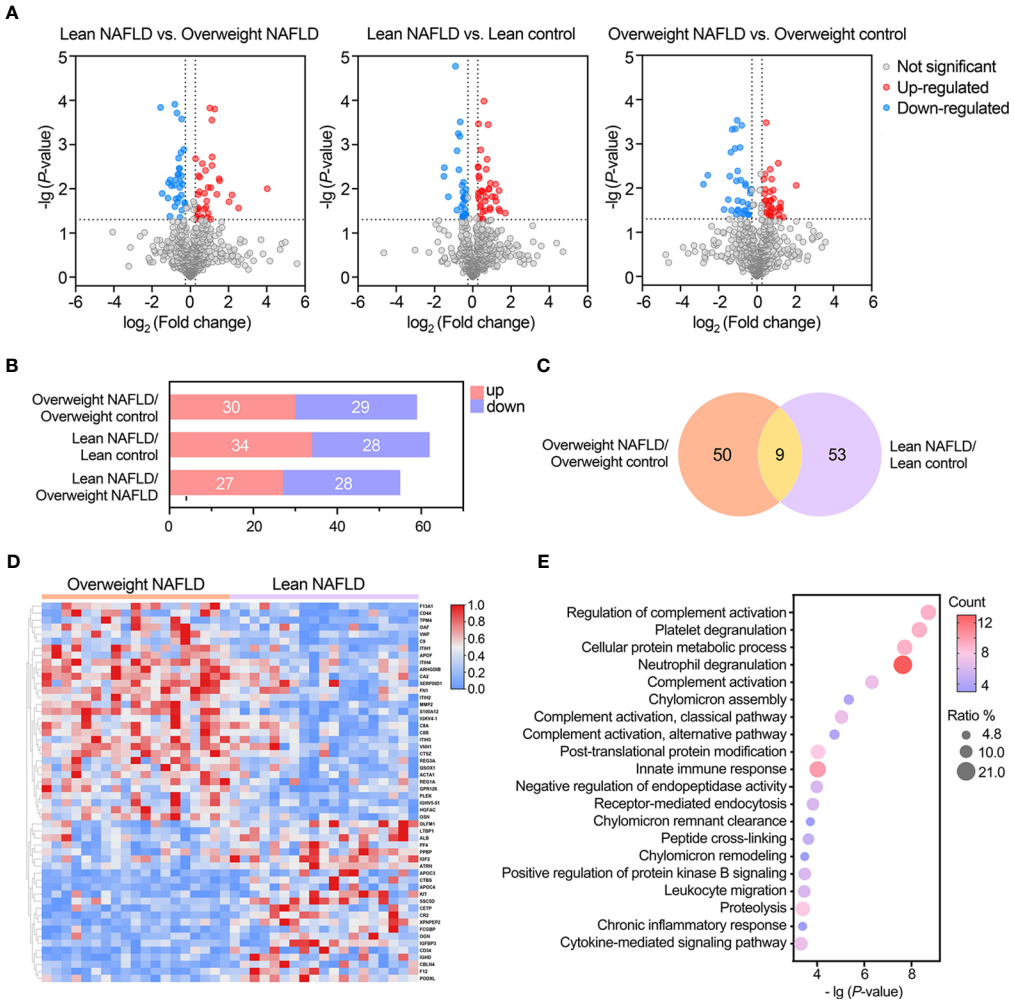

FIGURE 2
Statistical and bioinformatic analysis of the identified proteins reveled proteomic alterations associated with lean NAFLD and overweight NAFLD. **(A)** Volcano plots of identified proteins in the comparisons between lean NAFLD group vs. lean control group, overweight NAFLD group vs. overweight control group, and lean NAFLD group vs. overweight control group (cut-off value of fold-change >1.2; P-value (t-test) <0.05). **(B)** Bar chart shows the numbers of significantly up- and down-regulated proteins in the between- group comparisons. **(C)** Venn diagram shows the overlap of significantly differently expressed proteins found in lean and overweight cohort. **(D)** Hierarchical clustering heatmap of DEPs between lean NAFLD group and overweight control group. **(E)** GO enrichment of differentially expressed proteins associated with lean NAFLD in term of biological process.

for diagnosing NAFLD among lean and overweight cohorts, respectively. Among these, APOF, GOLM1, IGHV3-7 and THBS1 were found in both cohorts.

Table 2 provides a detailed summary of the AUCs, as well as the lower and upper limit of the 95% CI, sensitivities and specificities of the identified plasma proteins Hierarchical clustering was used to group all candidate biomarkers by similarities in their expression patterns (mean log2 intensities) among both cohorts (Figure 3A). ROC curves for proteins with high diagnostic power for NAFLD (AUC >0.8) in both lean and overweight individuals were also shown (Figures 3B, S2). After excluded the overlapped proteins which are statistically significantly different in both cohorts, a panel of 35 proteins that exclusively identified in lean cohort were considered as specific biomarkers for diagnosing lean NAFLD.

3.2.3 Plasma proteins highly associated with NAFLD observed in overweight cohort

Of the 55 proteins that exhibited significant changes in the comparison of overweight NAFLD with overweight healthy controls, 43 proteins reached an AUC > 0.7 (Table S1). As expected, some of these proteins have already been linked to NAFLD, such as RBP4, CETP, APCS, CD5L, and MMP9.

Retinol-binding protein 4 (RBP4) is synthesized in the liver that responsible for the transport of retinol to peripheral tissues. Available studies have described the correlation between RBP4 and NAFLD demonstrated that elevated RBP4 levels may contribute to the development of this condition (28–30). Our findings are consistent with these reports, as we observed significantly higher RBP4 levels in overweight NAFLD patients

10.3389/fendo.2023.1171397

TABLE 2 List of proteins found to be significantly differentially abundant between lean NAFLD patients and lean controls, with efficiency comparison of diagnostic indicators.

Gene Symbol	Protein	P value (LN vs. LC)	FC (LN/ LC)	AUC	CI (95%)	
					lower	upper
APOF	Apolipoprotein F	0.0000	0.47	0.959	0.903	1.000
C9	Complement component C9	0.0000	0.45	0.944	0.873	1.000
CA2	Carbonic anhydrase 2	0.0000	0.56	0.895	0.797	0.992
C8B	Complement component C8 beta chain	0.0001	0.67	0.880	0.765	0.995
GSN	Gelsolin	0.0000	0.59	0.871	0.759	0.983
APOH	Beta-2-glycoprotein 1	0.0003	1.31	0.863	0.744	0.981
VWF	von Willebrand factor	0.0001	0.68	0.857	0.736	0.978
ATRN	Attractin	0.0001	1.28	0.854	0.706	1.000
ITIH3	Inter-alpha-trypsin inhibitor heavy chain H3	0.0001	0.61	0.845	0.718	0.972
CD163	Scavenger receptor cysteine-rich type 1 protein M130	0.0001	1.53	0.842	0.712	0.972
CFH	Complement factor H	0.0003	1.26	0.836	0.711	0.962
PON3	Serum paraoxonase/lactonase 3	0.0001	0.53	0.836	0.706	0.967
ITIH1	Inter-alpha-trypsin inhibitor heavy chain H1	0.0003	0.78	0.827	0.692	0.963
MMP2	72 kDa type IV collagenase	0.0006	0.52	0.825	0.687	0.963
C4BPA	C4b-binding protein alpha chain	0.0005	1.23	0.822	0.689	0.955
ARHGDIB	Rho GDP-dissociation inhibitor 2	0.0003	0.61	0.819	0.684	0.954
LTF	Lactotransferrin	0.0010	1.71	0.810	0.660	0.959
VNN1	Pantetheinase	0.0012	0.64	0.810	0.666	0.954
QSOX1	Sulfhydryl oxidase 1	0.0016	0.62	0.804	0.657	0.952
CTSZ	Cathepsin Z	0.0036	0.59	0.789	0.643	0.936
ITIH2	Inter-alpha-trypsin inhibitor heavy chain H2	0.0018	0.68	0.787	0.640	0.933
PTPRJ	Receptor-type tyrosine-protein phosphatase eta	0.0066	1.28	0.787	0.637	0.936
F13A1	Coagulation factor XIII A chain	0.0075	0.73	0.781	0.629	0.933
SSC5D	Soluble scavenger receptor cysteine-rich domain-containing protein SSC5D	0.0009	1.64	0.781	0.630	0.931
THBS1	Thrombospondin-1	0.0011	0.69	0.781	0.627	0.935
ICAM2	Intercellular adhesion molecule 2	0.0064	1.53	0.769	0.610	0.928
APOB	Apolipoprotein B-100	0.0044	0.69	0.763	0.610	0.916
BTD	Biotinidase	0.0034	1.32	0.757	0.604	0.911
CAP1	Adenylyl cyclase-associated protein 1	0.0015	0.33	0.754	0.589	0.920
CNTN1	Contactin-1	0.0049	0.68	0.754	0.592	0.917
IGFBP3	Insulin-like growth factor-binding protein 3	0.0081	1.31	0.751	0.584	0.919
AFM	Afamin	0.0074	1.24	0.749	0.588	0.909
HGFAC	Hepatocyte growth factor activator	0.0185	0.77	0.746	0.586	0.905
OLFM1	Noelin	0.0056	1.41	0.743	0.582	0.904
SPP2	Secreted phosphoprotein 24	0.0306	0.67	0.725	0.552	0.898
SERPINA7	Thyroxine-binding globulin	0.0270	0.79	0.722	0.558	0.886

(Continued)

TABLE 2 Continued

Gene Symbol	Protein	P value (LN vs. LC)	FC (LN/ LC)	AUC	CI (95%)	
					lower	upper
GOLM1	Golgi membrane protein 1	0.0249	0.67	0.716	0.548	0.884
IGHV3-7	Immunoglobulin heavy variable 3-7	0.0121	0.72	0.716	0.551	0.882
SERPINF1	Pigment epithelium-derived facto	0.0065	1.43	0.711	0.544	0.877
S100A12	Protein S100-A12	0.0007	0.34			
TXN	Thioredoxin	0.0009	1.63			
FLNA	Filamin-A	0.0013	1.47			
LCN2	Neutrophil gelatinase-associated lipocalin	0.0027	1.71			
IGKV3D-20	Immunoglobulin kappa variable 3D-20	0.0036	1.56			
IGKV2-30	Immunoglobulin kappa variable 2-30	0.0039	0.51			
ANPEP	Aminopeptidase N	0.0067	1.41			
FAM3C	Protein FAM3C	0.0077	3.54			
APOC3	Apolipoprotein C-III	0.0101	1.83			
CFI	Complement factor I	0.0119	1.24			
ENO1	Alpha-enolase	0.0119	1.72			
P4HB	Protein disulfide-isomerase	0.0143	2.10			
IGFBP7	Insulin-like growth factor-binding protein 7	0.0180	2.17			
APOC2	Apolipoprotein C-II	0.0199	2.20			
KIT	Mast/stem cell growth factor receptor Kit	0.0202	1.79			
MMP9	Matrix metalloproteinase-9	0.0209	1.63			
ITGB1	Integrin beta-1	0.0226	0.68			
ENG	Endoglin	0.0267	1.89			
CFP	Properdin	0.0310	1.32			
FCGBP	IgGFc-binding protein	0.0335	1.47			
KRT5	Keratin, type II cytoskeletal 5	0.0363	1.52			
S100A8	Protein S100-A8	0.0444	2.59			
PODXL	Podocalyxin	0.0483	1.27			

LN, lean NAFLD; LC, lean control; ON, overweight NAFLD; OC, overweight control; FC, fold change; AUC, area under the receiver operating characteristic (ROC) curve.

compared to the healthy control group. By moving HDL-associated cholesterol to other lipoproteins, cholesteryl ester transfer protein (CETP) can affect the transport of peripheral tissue cholesterol, ultimately altering the levels of LDL and HDL cholesterol. We observed significantly decreased plasma CETP level in the overweight NAFLD group compared to healthy controls may support the reported finding that CETP plays a protective role in lipid and lipoprotein metabolism in obesity (31).Acute phase proteins, which play a crucial role in the innate defense of the liver, are immediately involved in hepatocyte injury. The differential expression of two acute phase proteins, serum amyloid P-component (APCS) and CD5 antigen-like protein (CD5L), between two overweight groups, suggests their potential as predictive markers for NAFLD in obese patients, as they regulate the innate and adaptive immune systems (15, 32).

3.2.4 Dysregulated lipid metabolism in lean NAFLD

Our proteomic data uncovered dysregulation of multiple apolipoproteins, including APOB, APOC2, APOC3, APOF, and APOH, in lean individuals with NAFLD compared to healthy lean individuals.

We found that apolipoprotein F (APOF) and apolipoprotein H (APOH) had significant diagnostic value for lean NAFLD, with AUC values of 0.959 and 0.863, respectively. Current data support that APOF preferentially blocks CETP activity when it is bound to LDL, thus reducing the flow of HDL-derived cholesteryl ester derived from HDL through this pathway (33). We found down-regulated plasma levels of APOF in both lean and overweight NAFLD groups compared to their matched healthy subjects, with the lowest level observed in lean NAFLD patients. Along this line, it

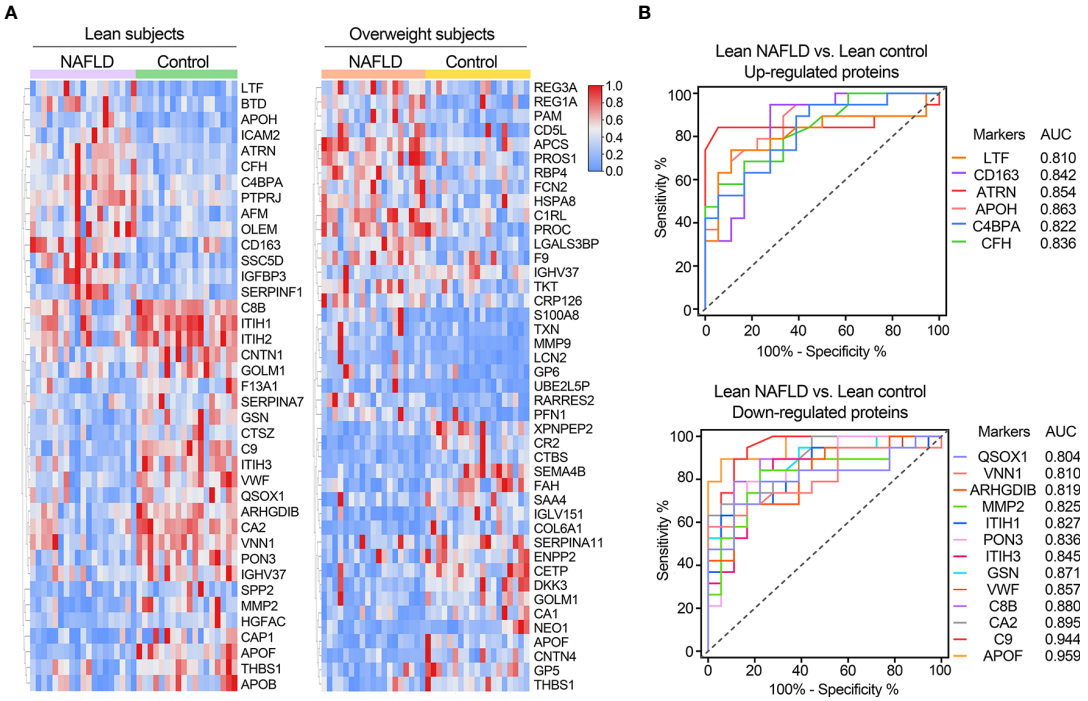

FIGURE 3
(A) Clustering heatmap of signature proteins that were differentially expressed in NAFLD and control groups (proteins with AUCs above 0.7 are shown). Clustering heatmap of proteins significantly differentially expressed in NAFLD and control groups in lean and obese cohorts, respectively (proteins with AUCs above 0.7 are shown). **(B)** Receiver operating characteristic (ROC) curves for potential diagnostic markers of lean NAFLD with AUC values above 0.8.

is not surprising that the lean NAFLD group exhibited significantly higher levels of CETP than the overweight NAFLD group. Additionally, elevated levels of APOH, APOC2, and APOC3 have been linked to clinically apparent arteriosclerosis and components of metabolic syndrome (MetS) (34–36). Our study also observed that plasma levels of APOH, APOC2 and APOC3 were significantly higher in lean individuals with NAFLD compared to those without, indicating a potential association between lean NAFLD with metabolic imbalance.

Along the same lines, when comparing lean NAFLD with overweight NALFD, increased levels of APOC2, APOC3, APOC4 and CETP were found in the former. This observation aligns with previous studies suggesting that lean NAFLD individuals tend to exhibit higher visceral adiposity index scores, which is an indicator of visceral fat function associated with cardio metabolic risk, than those who are overweight or obese.

3.2.5 Proteins involved in complement system and immune regulation in lean NAFLD

The complement system, a vital component of innate immunity, is predominantly produced in the liver, appears to be dysregulated in lean NAFLD patients. Specifically, the levels of C8B, C9, C4BPA, CFH, CFP, IGHV3-7, and THBS1, which are involved in complement system and immune regulation, were found to be significantly differently expressed in lean NAFLD group compared to lean healthy controls. C8B, C9, C4BPA and CFH were of high diagnosis value of lean NAFLD (AUC > 0.8). These results may indicate liver damage in lean NAFLD patients. Notably, the lean NAFLD group exhibited significantly elevated levels of plasma CFH, which has been implicated in insulin resistance and the pathophysiology of various inflammation-mediated diseases.

Other proteins related to immune and complement system, such as inter-α-trypsin inhibitor that has been identified as complement factors-interacting molecule and inhibit complement activation through the classical and alternative pathways, were also identified as potential biomarkers for lean NAFLD (37).

3.2.6 Plasma proteins highly associated with lean NAFLD

Platelet activation is known to increase in patients with MetS and obesity, likely reflecting the alterations in the platelet membrane component. The plasma proteomics data showed that 7 of 8 DEPs involved in platelet degranulation (APOH, CAP1, F13A1, ITIH3, QSOX1, SPP2, THBS1, and VWF) were downregulated in lean NAFLD patients. Among these, von Willebrand factor (VWF), which is known to mediate platelet adhesion and aggregation and is elevated in NAFLD patients, however, was significantly decreased in the lean NAFLD group.

A significant association was also found between lean NAFLD and several plasma proteins linked to liver injury and MetS, including afamin (AFM), insulin-like growth factor binding protein (IGFBP), gelsolin, and hepatocyte growth factor activator (HGFAC). In NAFLD, IGFBP3 levels are believed to be reduced, while elevated IGFBP3 levels correlate with atherosclerosis (38). In

this study, plasma level of IGFBP3 was significantly higher in lean NAFLD and performs well as a potential biomarker (AUC > 0.7). AFM has already been proposed as potential markers for NAFLD, with a closer association to hepatic lipid accumulation, liver damage, and insulin resistance than to obesity (39). This aligns with our observation, that the lean NAFLD group had notably higher levels of AFM. The plasma levels of gelsolin were found significantly decreased in lean NAFLD patients may suggest secondary inflammation and liver injury. On the other hand, lean NAFLD patients had obviously lower levels of HGFAC than lean healthy individuals, which should retard repair of damaged livers.

Matrix metalloproteinases (MMPs) involved in the turnover of fibrosis were also differently expressed in lean NAFLD patients. In comparison to the lean control group, we observed increased plasma levels of MMP9 but decreased levels of MMP2 in the lean NAFLD group. Coagulation factors would be expected to decrease when liver functions are impaired (40), even though in lean NAFLD patients, we only observed reductions in plasma coagulation factor XIII A chain (F13A1) levels.

4 Discussion

Within a metabolic continuum there is a normal weight classification of metabolically obese, defined as lean individuals who present with insulin resistance, hyperinsulinemia and atherogenic dyslipidaemia. Asians have been shown to develop significant metabolic disease outcomes at a lower BMI than other ethnic groups. The reason is not entirely clear. However, several factors have been proposed, including differences in body composition, genetics, and environmental factors such as diet and physical activity. As NAFLD is believed to be a hepatic manifestation of MetS, it is not surprising that the incidence of lean NAFLD in Chinese populations is significantly higher than in Western populations for a given BMI value. On the other, in a clinical retrospective study where the relationship between NAFLD and BMI as a risk factor was investigated, the study revealed that the occurrence of NAFLD is linked to lipid deposition, rather than BMI (41).

Despite the generally better histological and biochemical profile of lean NAFLD patients compared with NAFLD patients and higher BMI, clearly, lean NAFLD is a neglected and underappreciated subtype. In fact, compared with obese individuals, NAFLD in lean populations that do not have the readily recognizable phenotype of obesity are at increased risk for future severe liver disease. It is suggested that lean individuals with NAFLD can develop advanced liver disease, metabolic comorbidities, cardiovascular disease, and even mortality related to the liver. Despite lower fibrosis stages, the lean cohort had a higher risk of severe liver disease compared to overweight or obese NAFLD patients (10). In this context, early diagnosis of lean NAFLD is of great clinical significance. In this work, we aim to investigate the clinical and proteomic profiles of lean NAFLD. Our four study groups, namely lean NAFLD, lean control, overweight NAFLD, and overweight NAFLD, were defined based on BMI, as this is the most used tool for assessing normal and abnormal weight as part of the clinical routine.

We first cross-compared the clinical characteristics of the four groups. Both the lean and overweight NAFLD groups had slightly higher BMIs than their respective healthy counterparts. Despite all clinical parameters of the enrolled NAFLD patients being within normal ranges, we found that lean NAFLD patients were more likely to have components of the MetS and worse liver function tests compared to lean controls. Notably, lean NAFLD patients had significantly higher levels of liver enzymes, such as ALT and AST. Moreover, we observed that lean NAFLD patients had high LDL-C, hypertriglyceridemia, and higher levels of fasting blood glucose. Several blood indicators, including RBC, WBC, HGB, and HCT, were also higher in lean NAFLD patients. Although metabolic disorders may not directly affect blood cell counts, a complete blood cell count test can provide essential clinical information about the patient's overall health status and the presence of any underlying medical conditions. Research has shown that RBC and WBC counts are associated with MetS and insulin resistance. Furthermore, elevated levels of HGB and HCT values are often seen in overweight patients with predominant insulin resistance, and people with a raised HGB level are at a higher risk of developing abnormal liver function (42). Another study has suggested that WBC count is related to the occurrence of NAFLD (43).

Consistent with other reports, we also found that for the aforementioned clinical variables, lean NAFLD patients were in between overweight NAFLD and lean healthy controls, suggesting that lean NAFLD subjects may have favorable metabolic and pathological profiles than overweight NAFLD subjects. Of note, our lean NAFLD subjects had significant higher level of TSH than overweight NAFLD. TSH is an important hormone that regulates metabolism, including lipid metabolism in the liver. Higher levels of TSH within the normal range have also been linked to dyslipidemia. A large cross-sectional study involving 20,783 subjects in Spain demonstrated that TSH levels were positively associated with total cholesterol (TC) and low-density lipoprotein cholesterol (LDL-C) levels and negatively associated with high-density lipoprotein cholesterol (HDL-C) levels (23). Recent systematic reviews and meta-analyses suggested that, elevated TSH levels may be associated with the development and progression of NAFLD (44). Although previous studies on the relationship between thyroid function and NAFLD risk have been inconsistent and controversial, our clinical data poorer thyroid function may be closely related to dyslipidemia in lean individuals with NAFLD. Additional prospective research is needed to address these underlying mechanisms of thyroid function in lean NAFLD.

NAFLD has been consistently associated with a higher prevalence of chronic kidney disease (CKD) in numerous observational studies, indicating that individuals with NAFLD are at a significantly greater risk of developing CKD compared to those without the condition (24–26). Uric acid (UA), the end product of the breakdown of unwanted purines in humans, has been associated with a number of metabolic disorders. Consistent with our data, Zheng et al. demonstrated positive associations between high serum UA concentrations and the risk of lean NAFLD in Chinese adults, independent of the other metabolic factors (45). Based on these findings, serum UA could be considered as a simple and non-invasive marker for follow-up of patients with lean-NAFLD. In an

earlier study in which the diagnosis of NAFLD was based on blood tests, ultrasound imaging, and the liver/spleen ratio of computed tomography values, they showed that patients with NAFLD had significantly higher levels of BUN compared with control subjects. Creatinine has been reported as a factor associated with NAFLD in several studies (37), whereas we did not observe statistically significant differences between NAFLD patients and controls in both overweight and lean cohorts.

Platelets are well-known to play a role in the vascular complications of MetS and atherosclerosis, and emerging evidence suggests that they may also be involved in NAFLD. Many studies have investigated the relationship between platelets and NAFLD, with findings suggesting that NAFLD patients often have an elevated mean platelet volume (MPV), which is a reliable indicator of platelet activation (21). Some studies have reported lower platelet counts and higher MPV in NAFLD patients, nonetheless other researchers did not confirm these alterations (46, 47). In contrast to the above studies, our comparison of overweight NAFLD patients and overweight controls revealed that NAFLD patients had significantly higher platelet counts and significantly lower MPV. In the lean cohort, there was no significant difference in either MPV or platelet count between NAFLD patients and controls. In our large-scale samples, we observed significant lower platelet counts only in the comparison of lean NAFLD patients to lean controls. However, we found no statistical difference in MPV in both lean and obese NAFLD patients, despite previous reports that it is directly correlated with histological severity of hepatic inflammation and fibrosis.

These clinical findings underscore the importance of investigating NAFLD in lean subjects. On the other hand, currently established non-invasive methods in clinical practice for the diagnosis and NAFLD prognosis has some limitations; for example, it may not be sufficiently sensitive in the early stages of the disease, especially for lean subjects. To address this gap, mass spectrometry-based proteomics technology holds great potential in gain novel insights into disease mechanism and discovering new biomarkers. Therefore, we conducted a discovery proteomics analysis on 20 samples from each study group, with the aim of identifying novel proteins associated with lean NAFLD and understanding plasma protein changes in this condition among lean subjects. Based on pairwise comparisons of the proteomic data, we found that lean NAFLD and overweight NAFLD exhibit distinct proteomic profiles, and the two NAFLD entities may have different pathogenesis. We identified 62 DEPs that could predict the occurrence of NAFLD in lean subjects, which may provide a rich biomarker pool for lean NAFLD diagnosis. A considerable proportion of the DEPs are liver-specific or liver-enriched.

Apolipoproteins are structurally and functionally important lipid-transporting proteins in the blood circulation. As NAFLD bears strong associations with insulin resistance and dyslipidemia, we would expect plasma apolipoprotein concentrations to be altered in patients with chronic liver disease. APOF and APOH were found to have significant diagnostic value for lean NAFLD. APOF concentrations are considerably higher in individuals with high cholesterol levels but lower in those with high triglyceride levels. It has been notes that the response of APOF to plasma triglyceride levels is sex-varied. In male with high triglyceride levels, APOF levels are approximately half that of normolipidemic plasma, whereas in females, APOF levels have an upward trend. Despite The relationship between APOF and blood lipids remains controversial, nearly all of the reported data support the relationship between APOH and lipid metabolism, thrombosis, and inflammation. Increased levels of APOH were also associated with the presence of clinically evident components of arteriosclerosis and MetS (34). Previous studies have reported that serum levels of APOC2 and APOC3 were significantly higher in patients with MetS compared to those without (35, 36). We found only NAFLD patients within the lean cohort showed dysregulated apolipoproteins such as APOH, APOB, APOC2, and APOC3, implying that their lipid metabolism problems may differ from those of overweight or obese populations.

An important arm of the immune system is the complement cascade, which is controlled by a balance of activator and regulator proteins (48). Over-activation or dysregulation of the complement system can have far reaching clinical consequences. The complement system has been shown to be involved in NAFLD progression (49). The mechanisms of complement activation and regulation within the liver are incompletely understood. A considerable number of the significantly changed proteins in lean NAFLD patients are associated with complement and immune system. Among these, CFH has been implicated in insulin resistance, as well as pathophysiology of various inflammation-mediated diseases. It is reported that increased circulating CFH concentrations were observed in subjects with altered glucose tolerance, which could reflect the decreased insulin sensitivity and metabolic disturbances (50). Given that insulin resistance is an independent risk factor for NAFLD, it is not surprising that the lean NAFLD group exhibited significantly elevated levels of plasma CFH.

Platelets play a pivotal role in both hepatic homeostasis and the liver's response to injury. As mentioned above, in lean cohort, no significant differences in platelet count were observed between NAFLD patients and their healthy counterparts. However, the plasma proteomics data showed that 7 of 8 DEPs involved in platelet degranulation were downregulated in lean NAFLD patients. Of these, von Willebrand factor (VWF), a mediator of platelet adhesion and aggregation that has been shown to be elevated in patients with NAFLD, however, was found to be significantly decreased in the lean NAFLD group.

In addition to above proteins, we also observed a significant association between lean NAFLD and certain plasma proteins related to liver injury and MetS, represented by AFM, IGFBP, gelsolin, and HGFAC. The role of IGFBP3 in NAFLD is multifaceted. IGFBP3 is the major insulin binding protein such as growth factor 1 (IGF1) which is a stimulator of the production of IGFBP3. IGF1 is secreted by hepatocytes under growth hormone stimulation and has been shown to be protective in ischemic heart disease as well as in atherosclerosis. In NAFLD, IGFBP3 levels are believed to be reduced, while elevated IGFBP3 levels correlate with atherosclerosis (38). In this study, plasma level of IGFBP3 was significantly higher in lean NAFLD and performs well as a potential biomarker (AUC > 0.7). AFM is predominantly expressed in liver

and secreted into circulation. The Studies published to date demonstrate an increased AFM rate in patients with components of the MetS (51, 52), NAFLD (53), and alcoholic liver disease (ALD). It has previously been suggested that AFM may be a marker for NAFLD, since AFM was more closely linked to hepatic lipid accumulation, hepatic injury and insulin resistance than obesity (39). This is consistent with our observation that significantly higher AFM levels were found in the lean NAFLD group. Plasma gelsolin (GSN) has multiple physiological functions, such as being a substrate for extracellular matrix modulating enzymes, participating in the extracellular actin sensor system, and presenting inflammatory mediators to their receptors (54, 55). Consequently, gelsolin levels significantly may decrease after tissue injury in various conditions, including acute respiratory distress syndrome, acute injury to the lungs and liver, sepsis, major trauma, prolonged hyperoxia, and malaria (56, 57). Gelsolin could not be considered as a specific marker of lean NAFLD, however, the significantly decreased levels of plasma gelsolin in lean NAFLD patients may suggest secondary inflammation and liver injury. The growth factor activator Hepatocyte (HGFAC) is a primary activator of proHGF (the precursor form of hepatocyte growth factor) at the site of tissue damage, promoting accelerated healing of injured tissue, HGFAC deficiency can significantly disrupt subsequent tissue regeneration and repair (58). HGFAC is mainly synthesized by hepatocytes and circulates in the plasma. Lean NAFLD patients had obviously lower levels of HGFAC than lean healthy individuals, which should attenuated proHFG activation, thereby retarding repair of damaged livers.

5 Conclusions

Previous studies have shown several distinct proteins or patterns that differentiate end-stage liver diseases, particularly hepatocellular carcinoma. However, early-stage NAFLD may be overlooked. On the other hand, lean-type NAFLD, which lacks the typical obesity phenotype, is usually asymptomatic and may not seek medical advice. Due to the progressive nature of NAFLD, the early diagnosis and early intervention of lean NAFLD is of great clinical interest.

In this work, the large-scale clinical data revealed individuals with NAFLD who are lean have a distinct clinical profile from those who are overweight. Lean NAFLD patients exhibit worse metabolic profiles compared to their healthy counterparts, but generally experience fewer systemic metabolic issues than NAFLD subjects who are additionally obese.

By mass spectrometry-based proteomics technology, we were able to identify dozens of differentially expressed plasma proteins that could predict the occurrence of NAFLD in lean subjects, which may provide a novel biomarker pool for lean NAFLD diagnosis. The observed protein alterations in lean NAFLD indicate changes in lipid metabolism and inflammatory processes and complement activation, processes known to be associated with NAFLD. To the best of our knowledge, this study represents the first investigation into plasma proteomics of lean patients suffering from NAFLD.

Even though informative, our study also has limitations that need to be addressed. To validate the diagnostic biomarkers, a targeted mass spectrometry approach should be performed on a separate cohort for further refinement. While BMI is commonly used as a surrogate for body fat content, its utility in determining true body composition, especially in the lean population, may be insufficient. It is essential to investigate the importance of body fat distribution and specific genetic polymorphisms associated with a lean NAFLD, such as PNPLA3 and TM6SF2. Moreover, in this study, NAFLD diagnosis relied on ultrasonography, which can only estimate the prevalence of the disease, but not disease severity. Therefore, efforts should also made to explore effective biomarkers for assessing the progressive stages of lean NAFLD.

Data availability statement

The datasets presented in this study can be found in online repositories. The names of the repository/repositories and accession number(s) can be found in the article/Supplementary Material.

Ethics statement

The studies involving human participants were reviewed and approved by Clinical Ethics Committee of Putuo hospital affiliated to Shanghai University of Traditional Chinese Medicine. The patients/participants provided their written informed consent to participate in this study.

Author contributions

YJ and CH performed experiments. JZ analyzed data. ML, SD, JT and YY collected clinical serum sample. XZ prepared and wrote the manuscript. GJ reviewed the manuscript. All authors reviewed and approved the manuscript.

Funding

This work was financially supported by National Natural Science Foundation of China (82204686), Shanghai Natural Science Foundation (22ZR1455900); Shanghai Putuo District Health system Science and Technology Innovation Project key project (ptkwws202201); Reserve Outstanding TCM Talents Program of Shanghai University of Traditional Chinese Medicine (20D-RC-02); the Health Commission of Shanghai Municipality (ZY(2021-2023)-0203-04); Shanghai Putuo District Xinglin Excellent Youth Talent Training Program (ptxlyq2201); Shanghai Putuo District clinical characteristic disease construction project (2023tszb01)

Conflict of interest

The authors declare that the research was conducted in the absence of any commercial or financial relationships that could be construed as a potential conflict of interest.

Publisher's note

Supplementary material

The Supplementary Material for this article can be found online at: https://www.frontiersin.org/articles/10.3389/fendo.2023.1171397/full#supplementary-material

SUPPLEMENTARY FIGURE 1
GO enrichment of differentially expressed proteins associated with overweight NAFLD in term of biological process.

SUPPLEMENTARY FIGURE 2
Receiver operating characteristic (ROC) curves for potential diagnostic markers of overweight NAFLD with AUC values above 0.8.

SUPPLEMENTARY TABLE 1
Demographic, clinical, anthropometrical and laboratory characteristics of 80 subjects in proteomics study.

References

1. Lonardo A, Nascimbeni F, Maurantonio M, Marrazzo A, Rinaldi L, Adinolfi LE. Nonalcoholic fatty liver disease: Evolving paradigms. *World J Gastroenterol* (2017) 23 (36):6571–92. doi: 10.3748/wjg.v23.i36.6571

2. Ye Q, Zou B, Yeo YH, Li J, Huang DQ, Wu Y, et al. Global prevalence, incidence, and outcomes of non-obese or lean non-alcoholic fatty liver disease: a systematic review and meta-analysis. *Lancet Gastroenterol Hepatol* (2020) 5(8):739–52. doi: 10.1016/S2468-1253(20)30077-7

3. Kim D, Kim WR. Nonobese fatty liver disease. *Clin Gastroenterol Hepatol* (2017) 15(4):474–85. doi: 10.1016/j.cgh.2016.08.028

4. Younes R, Bugianesi E. NASH in lean individuals. *Semin Liver Dis* (2019) 39 (1):86–95. doi: 10.1055/s-0038-1677517

5. Petersen KF, Dufour S, Feng J, Befroy D, Dziura J, Dalla Man C, et al. Increased prevalence of insulin resistance and nonalcoholic fatty liver disease in Asian-Indian men. *Proc Natl Acad Sci USA* (2006) 103(48):18273–7. doi: 10.1073/pnas.0608537103

6. Kumar R, Mohan S. Non-alcoholic fatty liver disease in lean subjects: Characteristics and implications. *J Clin Transl Hepatol* (2017) 5(3):216–23. doi: 10.14218/JCTH.2016.00068

7. Ahadi M, Molooghi K, Masoudifar N, Namdar AB, Vossoughinia H, Farzanehfar M. A review of non-alcoholic fatty liver disease in non-obese and lean individuals. *J Gastroenterol Hepatol (Australia)* (2021) 36(6):1497–507. doi: 10.1111/jgh.15353

8. Leung JCF, Loong TCW, Wei JL, Wong GLH, Chan AWH, Choi PCL, et al. Histological severity and clinical outcomes of nonalcoholic fatty liver disease in nonobese patients. *Hepatology* (2017) 65(1):54–64. doi: 10.1002/hep.28697

9. Hae JK, Hyeong JK, Kwang EL, Dae JK, Soo KK, Chul WA, et al. Metabolic significance of nonalcoholic fatty liver disease in nonobese, nondiabetic adults. *Arch Intern Med* (2004) 164(19):2169–75. doi: 10.1001/archinte.164.19.2169

10. Hagström H, Nasr P, Ekstedt M, Hammar U, Stål P, Hultcrantz R, et al. Risk for development of severe liver disease in lean patients with nonalcoholic fatty liver disease: A long-term follow-up study. *Hepatol Commun* (2018) 2(1):48–57. doi: 10.1002/hep4.1124

11. Rinella ME. Nonalcoholic fatty liver disease a systematic review. *JAMA - J Am Med Assoc* (2015) 313(22):2263–73. doi: 10.1001/jama.2015.5370

12. Vilar-Gomez E, Chalasani N. Non-invasive assessment of non-alcoholic fatty liver disease: Clinical prediction rules and blood-based biomarkers. *J Hepatol* (2018) 68 (2):305–15. doi: 10.1016/j.jhep.2017.11.013

13. Geyer PE, Holdt LM, Teupser D, Mann M. Revisiting biomarker discovery by plasma proteomics. *Mol Syst Biol* (2017) 13(9):942. doi: 10.15252/msb.20156297

14. Keshishian H, Burgess MW, Specht H, Wallace L, Clauser KR, Gillette MA, et al. Quantitative, multiplexed workflow for deep analysis of human blood plasma and biomarker discovery by mass spectrometry. *Nat Protoc* (2017) 12(8):1683–701. doi: 10.1038/nprot.2017.054

15. Niu L, Geyer PE, Wewer Albrechtsen NJ, Gluud LL, Santos A, Doll S, et al. Plasma proteome profiling discovers novel proteins associated with non-alcoholic fatty liver disease. *Mol Syst Biol* (2019) 15(3):1–16. doi: 10.15252/msb.20188793

16. Fan JG, Wei L, Zhuang H, Cai W, Feng Chen D, Duan ZP, et al. Guidelines of prevention and treatment of nonalcoholic fatty liver disease (2018, China). *J Dig Dis* (2019) 20:163–73. doi: 10.1111/1751-2980.12685

17. Sugiyama A, Kurisu A, Bunthen E, Ouoba S, Ko K, Rakhimov A, et al. Distribution of FIB-4 index in the general population: analysis of 75,666 residents who underwent health checkups. *BMC Gastroenterol* (2022) 22(1):241. doi: 10.1186/s12876-022-02290-1

18. Shah AG, Lydecker A, Murray K, Tetri BN, Contos MJ, Sanyal AJ. Comparison of noninvasive markers of fibrosis in patients with nonalcoholic fatty liver disease. *Clin Gastroenterol Hepatol* (2009) 7(10):1104–12. doi: 10.1016/j.cgh.2009.05.033

19. Tokushige K, Ikejima K, Ono M, Eguchi Y, Kamada Y, Itoh Y, et al. Evidence-based clinical practice guidelines for nonalcoholic fatty liver disease/nonalcoholic steatohepatitis 2020. *J Gastroenterol* (2021) 56(11):951–63. doi: 10.1007/s00535-021-01796-x

20. Wiśniewski JR, Zougman A, Nagaraj N, Mann M. Universal sample preparation method for proteome analysis. *Nat Methods* (2009) 6(5):359–62. doi: 10.1038/nmeth.1322

21. Chauhan A, Adams DH, Watson SP, Lalor PF. Platelets: No longer bystanders in liver disease. *Hepatology* (2016) 64(5):1774–84. doi: 10.1002/hep.28526

22. Bano A, Chaker L, Plompen EPC, Hofman A, Dehghan A, Franco OH, et al. Thyroid function and the risk of nonalcoholic fatty liver disease: The Rotterdam study. *J Clin Endocrinol Metab* (2016) 101(8):3204–11. doi: 10.1210/jc.2016-1300

23. Santos-Palacios S, Brugos-Larumbe A, Guillén-Grima F, Galofré JC. A cross-sectional study of the association between circulating TSH level and lipid profile in a large Spanish population. *Clin Endocrinol (Oxf)* (2013) 79(6):874–81. doi: 10.1111/cen.12216

24. Marcuccilli M, Chonchol M. NAFLD and chronic kidney disease. *Int J Mol Sci* (2016) 17(4):562. doi: 10.3390/ijms17040562

25. Targher G, Chonchol MB, Byrne CD. CKD and nonalcoholic fatty liver disease. *Am J Kidney Dis* (2014) 64(4):638–52. doi: 10.1053/j.ajkd.2014.05.019

26. Sesti G, Fiorentino TV, Arturi F, Perticone M, Sciacqua A, Perticone F. Association between noninvasive fibrosis markers and chronic kidney disease among adults with nonalcoholic fatty liver disease. *PloS One* (2014) 9(2):e88569. doi: 10.1371/journal.pone.0088569

27. Becker J, Friedman E. Renal function status. *Am J Roentgenol* (2013) 200:827–9. doi: 10.2214/AJR.12.9872

28. Saki F, Karamizadeh Z, Honar N, Moravej H, Ashkani-Esfahani S, Namvar Shooshtarian MH. Association of plasma retinol binding protein-4 (RBP4) and sonographic grading of fatty liver in obese Iranian children. *Hepat Mon* (2012) 12 (12):e7103. doi: 10.5812/hepatmon.7103

29. Yang Q, Graham TE, Mody N, Preitner F, Peroni OD, Zabolotny JM, et al. Serum retinol binding protein 4 contributes to insulin resistance in obesity and type 2 diabetes. *Nature* (2005) 436(7049):356–62. doi: 10.1038/nature03711

30. Małecki P, Tracz J, Łuczak M, Figlerowicz M, Mazur-Melewska K, Służewski W, et al. Serum proteome assessment in nonalcoholic fatty liver disease in children: a preliminary study. *Expert Rev Proteomics* (2020) 17(7-8):623–32. doi: 10.1080/14789450.2020.1810020

31. Cole BK, Feaver RE, Wamhoff BR, Dash A. Non-alcoholic fatty liver disease (NAFLD) models in drug discovery. *Expert Opin Drug Discovery* (2018) 13(2):193–205. doi: 10.1080/17460441.2018.1410135

32. Lim JW, Dillon J, Miller M. Proteomic and genomic studies of non-alcoholic fatty liver disease - Clues in the pathogenesis. *World J Gastroenterol* (2014) 20 (26):8325–40. doi: 10.3748/wjg.v20.i26.8325

33. Liu Y, Morton RE. Apolipoprotein F: a natural inhibitor of cholesteryl ester transfer protein and a key regulator of lipoprotein metabolism. *Curr Opin Lipidol* (2020) 31(4):194–9. doi: 10.1097/MOL.0000000000000688

34. Castro A, Lázaro I, Selva DM, Céspedes E, Girona J, NúriaPlana, et al. APOH is increased in the plasma and liver of type 2 diabetic patients with metabolic syndrome. *Atherosclerosis* (2010) 209(1):201–5. doi: 10.1016/j.atherosclerosis.2009.09.072

35. Sumida Y, Nakajima A, Itoh Y. Limitations of liver biopsy and non-invasive diagnostic tests for the diagnosis of nonalcoholic fatty liver disease/nonalcoholic steatohepatitis. *World J Gastroenterol* (2014) 20(2):475–85. doi: 10.3748/wjg.v20.i2.475

36. Boiko AS, Mednova IA, Kornetova EG, Semke AV, Bokhan NA, Loonen AJM, et al. Apolipoprotein serum levels related to metabolic syndrome in patients with schizophrenia. *Heliyon* (2019) 5(7):e02033. doi: 10.1016/j.heliyon.2019.e02033

37. Garantziotis S, Hollingsworth JW, Ghanayem RB, Timberlake S, Zhuo L, Kimata K, et al. A. Inter-α-trypsin inhibitor attenuates complement activation and complement-induced lung injury. *J Immunol* (2007) 179(6):4187–92. doi: 10.4049/jimmunol.179.6.4187

38. Miller MH, Walsh SV, Atrih A, Huang JTJ, Ferguson MAJ, Dillon JF. The serum proteome of nonalcoholic fatty liver disease: A multimodal approach to discovery of biomarkers of nonalcoholic steatohepatitis. *J Gastroenterol Hepatol (Australia)* (2014) 29(10):1839–47. doi: 10.1111/jgh.12614

39. Kurdiova T, Balaz M, Kovanicova Z, Zemkova E, Kuzma M, Belan V, et al. Serum afamin a novel marker of increased hepatic lipid content. *Front Endocrinol (Lausanne)* (2021) 12:670425. doi: 10.3389/fendo.2021.670425

40. Dickneite G, Herwald H, Korte W, Allanore Y, Denton CP, Cerinic MM. Coagulation factor XIII: A multifunctional transglutaminase with clinical potential in a range of conditions. *Thromb Haemost* (2015) 113(4):686–97. doi: 10.1160/TH14-07-0625

41. Ciardullo S, Oltolini A, Cannistraci R, Muraca E, Perseghin G. Sex-related association of nonalcoholic fatty liver disease and liver fibrosis with body fat distribution in the general US population. *Am J Clin Nutr* (2022) 115(6):1528–34. doi: 10.1093/ajcn/nqac059

42. Bernhardt P, Kratzer W, Schmidberger J, Graeter T, Gruener B, Adler G, et al. Laboratory parameters in lean NAFLD: Comparison of subjects with lean NAFLD with obese subjects without hepatic steatosis. *BMC Res Notes* (2018) 11(1):1–8. doi: 10.1186/s13104-018-3212-1

43. Jiang Y, Zeng J, Chen B. Hemoglobin combined with triglyceride and ferritin in predicting non-alcoholic fatty liver. *J Gastroenterol Hepatol (Australia)* (2014) 29(7):1508–14. doi: 10.1111/jgh.12580

44. Guo Z, Li M, Han B, Qi X. Association of non-alcoholic fatty liver disease with thyroid function: A systematic review and meta-analysis. *Dig Liver Dis* (2018) 50(11):1153–62. doi: 10.1016/j.dld.2018.08.012

45. Zheng X, Gong L, Luo R, Chen H, Peng B, Ren W, et al. Serum uric acid and non-alcoholic fatty liver disease in non-obesity Chinese adults. *Lipids Health Dis* (2017) 16(1):1–7. doi: 10.1186/s12944-017-0531-5

46. Ozhan H, Aydin M, Yazici M, Yazgan O, Basar C, Gungor A, et al. Mean platelet volume in patients with non-alcoholic fatty liver disease. *Platelets* (2010) 21(1):29–32. doi: 10.3109/09537100903391023

47. Dalbeni A, Castelli M, Zoncapè M, Minuz P, Sacerdoti D. Platelets in non-alcoholic fatty liver disease. *Front Pharmacol* (2022) 13:842636. doi: 10.3389/fphar.2022.842636

48. Zipfel PF, Skerka C. Complement regulators and inhibitory proteins. *Nat Rev Immunol* (2009) 9(10):729–40. doi: 10.1038/nri2620

49. Laskowski J, Renner B, Pickering MC, Serkova NJ, Smith-Jones PM, Clambey ET, et al. Complement factor H–deficient mice develop spontaneous hepatic tumors. *J Clin Invest* (2020) 140(8):4039–54. doi: 10.1172/JCI135105

50. Moreno-Navarrete JM, Martínez-Barricarte R, Catalán V, Sabater M, Gómez-Ambrosi J, Ortega FJ, et al. Complement factor H is expressed in adipose tissue in association with insulin resistance. *Diabetes* (2010) 59(1):200–9. doi: 10.2337/db09-0700

51. Dieplinger H, Dieplinger B. Afamin–A pleiotropic glycoprotein involved in various disease states. *Clin Chim Acta* (2015) 446:105–10. doi: 10.1016/j.cca.2015.04.010

52. Kurdiova T, Balaz M, Kovanicova Z, Zemkova E, Kuzma M, Belan V, et al. Serum afamin a novel marker of increased hepatic lipid content. *Front Endocrinol (Lausanne)* (2021) 12:670425(September). doi: 10.3389/fendo.2021.670425

53. Bell LN, Theodorakis JL, Vuppalanchi R, Saxena R, Bemis KG, Wang M, et al. Serum proteomics and biomarker discovery across the spectrum of nonalcoholic fatty liver disease. *Hepatology* (2010) 51(1):111–20. doi: 10.1002/hep.23271

54. Bucki R, Levental I, Kulakowska A, Janmey P. Plasma gelsolin: function, prognostic value, and potential therapeutic use. *Curr Protein Pept Sci* (2008) 9(6):541–51. doi: 10.2174/138920308786733912

55. Marrocco C, Rinalducci S, Mohamadkhani A, D'Amici GM, Zolla L. Plasma gelsolin protein: A candidate biomarker for hepatitis B-associated liver cirrhosis identified by proteomic approach. *Blood Transfusion* (2010) 8(Suppl. 3):s105–112. doi: 10.2450/2010.017S

56. Piktel E, Levental I, Durnaś B, Janmey PA, Bucki R. Plasma gelsolin: Indicator of inflammation and its potential as a diagnostic tool and therapeutic target. *Int J Mol Sci* (2018) 19(9):2516. doi: 10.3390/ijms19092516

57. Bhosale SD, Moulder R, Venäläinen MS, Koskinen JS, Pitkänen N, Juonala MT, et al. Serum proteomic profiling to identify biomarkers of premature carotid atherosclerosis. *Sci Rep* (2018) 8(1):1–9. doi: 10.1038/s41598-018-27265-9

58. Fukushima T, Uchiyama S, Tanaka H, Kataoka H. Hepatocyte growth factor activator: A proteinase linking tissue injury with repair. *Int J Mol Sci* (2018) 19(11):1–11. doi: 10.3390/ijms19113435

frontiers | Frontiers in Endocrinology

TYPE Review
PUBLISHED 27 November 2023
DOI 10.3389/fendo.2023.1261860

OPEN ACCESS

EDITED BY
Princy Francis,
Mayo Clinic, United States

REVIEWED BY
Yong Zhang,
The Second Affiliated Hospital of Xi'an Jiaotong University, China
Labrini Papanastasiou,
General Hospital of Athens G. Genimatas, Greece

*CORRESPONDENCE
Angelika Buczyńska
angelika.buczynska@umb.edu.pl
Anna Popławska-Kita
annapoplawskakita@op.pl

†These authors have contributed equally to this work

RECEIVED 19 July 2023
ACCEPTED 10 November 2023
PUBLISHED 27 November 2023

CITATION
Buczyńska A, Kościuszko M, Krętowski AJ and Popławska-Kita A (2023) Exploring the clinical utility of angioinvasion markers in papillary thyroid cancer: a literature review. *Front. Endocrinol.* 14:1261860. doi: 10.3389/fendo.2023.1261860

Exploring the clinical utility of angioinvasion markers in papillary thyroid cancer: a literature review

Angelika Buczyńska[1*], Maria Kościuszko[2], Adam Jacek Krętowski[1,2†] and Anna Popławska-Kita[2*†]

[1]Clinical Research Centre, Medical University of Bialystok, Bialystok, Poland, [2]Department of Endocrinology, Diabetology and Internal Medicine, Medical University of Bialystok, Bialystok, Poland

Papillary thyroid cancer (PTC) is the most common type of thyroid cancer, and angioinvasion, the invasion of blood vessels by cancer cells, is a crucial pathological feature associated with disease progression and poor prognosis. Thus, a comprehensive search of scientific databases was conducted to identify relevant studies investigating angioinvasion markers in PTC. The selected studies were reviewed and analyzed to assess the clinical significance and potential utility of these markers in predicting angioinvasion and guiding treatment decisions. Numerous studies have investigated various markers associated with angioinvasion in PTC, including oxidative stress, vascular endothelial growth factor (VEGF), matrix metalloproteinases (MMPs), and other angiogenic factors. The results indicate that increased expression of these markers is correlated with the presence and extent of angioinvasion in PTC. Moreover, some studies suggest that these markers can serve as prognostic indicators and guide therapeutic strategies, such as selecting patients for more aggressive treatment approaches or targeted therapies. The findings from the reviewed literature highlight the potential clinical utility of angioinvasion markers in PTC. The identification and validation of reliable markers can aid in assessing the risk of angioinvasion, predicting disease progression, and optimizing treatment decisions for patients with PTC. However, further research and validation on larger patient cohorts are necessary to establish the robustness and generalizability of these markers in clinical practice.

KEYWORDS

papillary thyroid cancer, angioinvasion, VFGF, oxidative stress, integrins, sortilin, podoplanin

1 Introduction

Papillary thyroid cancer (PTC) is the most prevalent type of thyroid malignancy, accounting for approximately 80% of all thyroid cancer cases (1). Although generally associated with a favorable prognosis, PTC can exhibit varying degrees of aggressiveness, with certain cases demonstrating increased potential for invasion and metastasis (2). Angioinvasion, the invasion of cancer cells into blood or lymphatic vessels, is a critical determinant of tumor behavior and can significantly impact patient outcomes. Accurate assessment of angioinvasion in PTC is crucial for predicting disease progression, selecting appropriate treatment strategies, and optimizing patient management. While traditional histopathological techniques, such as lymphovascular invasion evaluation, have been utilized to assess angioinvasion, the identification of specific molecular markers has the potential to enhance diagnostic precision and prognostic accuracy (3).

Nowadays, various molecular markers have been investigated for their potential association with angioinvasion in PTC. Notably, vascular endothelial growth factor (VEGF), a well-known pro-angiogenic factor, has shown correlations with angioinvasion and tumor aggressiveness (4). Additionally, CD34, a cell surface glycoprotein used as a marker of microvessel density, and podoplanin, a protein involved in lymphatic vessel formation, have been implicated in angioinvasion in PTC (5, 6). Among others, oxidative stress markers, sortilin and integrins have been implicated in angiogenesis and may contribute to the angioinvasive phenotype of PTC (2). Understanding the molecular mechanisms underlying angioinvasion in PTC is crucial for improving diagnostic accuracy, prognostication, and therapeutic decision-making (7).

Through a comprehensive review of the existing literature, this study aims to consolidate the current knowledge on angioinvasion markers in PTC and explore promising novel markers. The study aimed to identify potential markers that can reliably indicate the presence of angioinvasion in PTC, which can improve risk stratification and facilitate personalized therapeutic interventions for patients with PTC.

2 Materials and methods

This literature review employed a systematic approach to identify and analyze studies investigating novel angioinvasion markers in PTC. The methodology ensured the inclusion of relevant studies and provided a rigorous evaluation of the available literature in this field (8). Thus, a systematic search was performed to identify relevant articles from various electronic databases, including PubMed, Scopus, and Web of Science (9). The search strategy utilized a combination of keywords and controlled vocabulary terms related to PTC, angioinvasion, and molecular markers. The search was conducted with no restrictions on language or publication date. Articles were included if they met the following criteria: PTC, investigated angioinvasion markers, provided relevant data or findings, and were published in peer-reviewed journals. Studies that were reviews, editorials, or conference abstracts were excluded. Full-text articles of the selected studies were then assessed for eligibility. Data from the included articles were extracted using a standardized form. The extracted data included study characteristics (e.g., author, year of publication), patient population, study design, angioinvasion markers investigated, methodology, and key findings. The extracted data were analyzed thematically to identify common trends, associations, and novel markers implicated in angioinvasion in PTC. The findings were summarized and presented descriptively. The quality and risk of bias of the included studies were evaluated using appropriate tools, such as the Newcastle-Ottawa Scale for observational studies (10) or the Cochrane Collaboration's tool for randomized controlled trials (11). As this study is a literature review, ethical approval was not required. The data were obtained from published studies, ensuring confidentiality and anonymity of the participants. The limitations of this study included the potential for publication bias, as only peer-reviewed articles were included, and the reliance on available literature. Additionally, the heterogeneity of the included studies may have affected the ability to perform quantitative analysis.

3 Papillary thyroid cancer epidemiology

PTC is the most common type of thyroid cancer, accounting for approximately 80-90% of all thyroid malignancies (12). The incidence of PTC has been steadily increasing over the past few decades in many countries worldwide (13, 14). This rise in incidence is partly attributed to increased detection due to advanced imaging techniques and improved diagnostic practices. Furthermore, PTC exhibits a strong female predominance. Women are approximately three times more likely to develop PTC than men (15). This gender disparity has been observed consistently across different populations and geographic regions. Several studies have investigated potential hormonal (estrogen receptors have been found in thyroid tissue, and estrogen can stimulate the growth and proliferation of thyroid cells) and genetic factors (such as BRAF mutation, other genetic alterations, such as RET/PTC rearrangements and RAS mutations) contributing to this gender difference (16). Moreover, PTC can affect individuals of all age groups, but it is most commonly diagnosed in adults aged 30-50 years. Thus, the incidence of PTC has been increasing among younger populations, particularly adolescents and young adults. The reasons for this age-specific trend are not fully understood, and further research is needed to explore potential risk factors (15). Nevertheless, PTC incidence rates vary significantly across different countries and regions. Higher incidence rates have been reported in regions with a higher iodine intake, such as areas of high goiter prevalence (17). The impact of environmental factors, genetic predisposition, and variations in healthcare practices on these geographical differences is a subject of ongoing research (17). Interestingly, exposure to ionizing radiation, especially during childhood, is a well-established risk factor for PTC (18). Individuals who have undergone radiation therapy for medical

conditions, such as Hodgkin's lymphoma or head and neck cancers, have an increased risk of developing PTC (19). Studies have consistently shown a dose-response relationship between radiation exposure and PTC risk.

The study conducted by Baloch et al. aimed to identify prognostic factors in well-differentiated follicular-derived carcinoma. It investigated various clinicopathological factors to determine their impact on patient prognosis. The results of the study revealed several significant prognostic factors associated with PTC prognosis, including age, tumor size, presence of lymph node metastasis, extrathyroidal extension, and distant metastasis. Older age, larger tumor size, presence of lymph node metastasis, and extrathyroidal extension were correlated with a poorer prognosis, while the presence of distant metastasis indicated a significantly worse outcome. The study provided valuable insights into prognostic factors, such as angioinvasion measurement, that can help predict the outcomes of patients with well-differentiated follicular-derived carcinoma, specifically PTC. These findings emphasize the importance of clinicians making informed decisions regarding treatment strategies and patient management based on angioinvasion detection and the presence of lymph node metastasis. Ultimately, angioinvasion detection could lead to improved patient care and outcomes (20).

4 Clinical management of PTC

The clinical management of PTC involves a multidisciplinary approach that includes surgery, radioactive iodine (RAI) therapy, thyroid hormone replacement, and long-term follow-up (21). The specific management strategy may vary depending on factors such as tumor characteristics, stage, patient age, and angioinvasion with lymph metastasis detection (22). The primary treatment for PTC is most frequently thyroidectomy. The extent of surgery may vary from a total thyroidectomy to a lobectomy (23). Lymph node dissection may be performed if there is evidence of lymph node involvement. The goal of surgery is to remove the primary tumor and any involved lymph nodes while minimizing the risk of recurrence. Following thyroidectomy, RAI therapy may be recommended for certain PTC patients, particularly those with high-risk features such as larger tumors, angioinvasion presents, lymph node involvement, or distant metastasis (24). RAI therapy involves the administration of a radioactive iodine isotope (iodine-131) that selectively targets and destroys any remaining thyroid tissue or cancer cells. This adjuvant therapy aims to eliminate residual disease and reduce the risk of recurrence (25). After thyroidectomy, lifelong thyroid hormone replacement therapy is essential to achieve suppression of thyroid-stimulating hormone (TSH) levels and to maintain normal thyroid hormone levels. This involves daily oral intake of synthetic thyroid hormone (levothyroxine) to replace the natural thyroid hormone produced by the thyroid gland (26). The goal is to suppress TSH levels, which helps prevent tumor growth and recurrence. Regular monitoring of thyroid hormone levels and adjustment of medication dosage is necessary to ensure optimal hormone replacement (27). Thus, PTC patients require long-term follow-up care to monitor for disease recurrence, assess treatment response, and manage any potential complications (28). In cases of locally advanced or metastatic PTC that does not respond to standard treatments, additional therapeutic options may be considered (29). These may include targeted therapies, such as tyrosine kinase inhibitors (e.g., lenvatinib, sorafenib), which block specific molecular pathways involved in cancer growth and angiogenesis. Clinical trials investigating novel therapies may also be an option for eligible patients (30, 31). From the other hand, in low-risk PTC less invasive techniques could be use. Thermal ablation refers to the use of heat-based techniques to treat thyroid nodules, including PTC. It is a minimally invasive procedure that aims to destroy or shrink the tumor without the need for surgery (32). Thermal ablation has shown promising results in the treatment of PTC, with studies demonstrating effective tumor control and minimal complications (33). However, it is important to note that surgery, such as thyroidectomy and lobectomy, remains the primary treatment approach for most cases of PTC (34). Therefore, identifying the presence or absence of angioinvasion would allow avoiding invasive procedures and the need for therapy for a large group of patients, as well as the requirement for lifelong observation. Furthermore, it would help identify a subgroup of patients at high risk for more aggressive progression of PTC, where the introduction of more radical therapy would be recommended as soon as possible.

5 Angioinvasion: markers and clinical implications

The evaluation of angioinvasion markers in PTC typically involves the assessment of specific molecular and cellular markers associated with tumor angiogenesis and invasiveness. These markers may include Vascular Endothelial Growth Factor (VEGF), CD34, podoplanin, integrins, and matrix metalloproteinases (MMPs) and oxidative stress markers. Through various techniques such as immunohistochemistry, gene expression analysis, and biomolecular assays, the expression levels and presence of these markers can be quantified and correlated with angioinvasion in PTC (3).

Accurate evaluation of angioinvasion markers holds significant clinical implications. It can provide valuable information regarding tumor behavior, likelihood of lymph node metastasis, risk of recurrence, and overall patient prognosis (35). This information can guide treatment decisions, such as the extent of surgery (total thyroidectomy vs. lobectomy), the need for lymph node dissection, and the consideration of adjuvant therapies. Furthermore, the identification and validation of novel angioinvasion markers in PTC have the potential to revolutionize clinical treatment options. Targeted therapies that specifically inhibit angiogenesis and tumor invasiveness could be developed, leading to improved patient outcomes (36). These therapies may include anti-angiogenic agents, tyrosine kinase inhibitors, or other molecular targeted therapies aimed at disrupting the signaling pathways involved in angiogenesis and tumor progression (37). However, it is important to note that while several markers have shown promise in preclinical and early clinical studies, further research is needed to validate their clinical utility, establish standardized diagnostic

criteria, and assess their effectiveness in larger patient populations (38). Rigorous clinical trials and translational research efforts are required to determine the efficacy, safety, and long-term outcomes of targeting angioinvasion markers in PTC treatment. Nevertheless, the evaluation of angioinvasion markers among PTC patients is essential for accurate prognosis determination and treatment decision-making (39). Continued research into novel markers and the development of targeted therapies hold great potential for improving clinical outcomes and personalized treatment options for PTC patients (40).

6 Oxidative stress involvement in PTC angioinvasion

Oxidative stress is known to play a role in the angioinvasion of PTC. Oxidative stress refers to an imbalance between the production of reactive oxygen species (ROS) and the body's antioxidant defense mechanisms, leading to cellular damage (41). Several studies have indicated that oxidative stress is involved in promoting angiogenesis, which is the process of new blood vessel formation that facilitates tumor growth and metastasis (42). In PTC, oxidative stress can arise from various sources, including increased ROS production by tumor cells, inflammation, and altered antioxidant capacity (43). The excessive production of ROS can induce the activation of signaling pathways that promote angiogenesis. These pathways involve factors such as VEGF, hypoxia-inducible factor 1-alpha (HIF-1α), and nuclear factor-kappa B (NF-κB), which contribute to the formation of new blood vessels in the tumor microenvironment (44). Furthermore, oxidative stress can lead to DNA damage and genetic alterations in tumor cells, promoting their invasive properties. It can also influence the expression of matrix metalloproteinases (MMPs), enzymes involved in extracellular matrix degradation and tumor invasion (45). MMPs play a crucial role in facilitating the breakdown of basement membranes and blood vessel walls, allowing tumor cells to invade surrounding tissues and enter the bloodstream (46).

The study performed by Azouzi et al. concerned on the role of nicotinamide adenine dinucleotide phosphate oxidase 4 (NOX4) as a critical mediator of BRAFV600E-induced downregulation of the sodium/iodide symporter (NIS) in PTC aimed to understand the mechanism underlying the loss of NIS expression in this disease. The results of the study demonstrated that activation of the BRAFV600E pathway led to upregulation of NOX4 expression, which in turn resulted in the overproduction of ROS in thyroid cancer cells. The increased ROS levels induced oxidative stress, leading to a decrease in NIS expression. It was found that NOX4 is directly involved in this process, and its inhibition restored NIS expression in thyroid cancer cells. Furthermore, it was observed that in tissue samples obtained from patients with papillary thyroid carcinoma, the presence of BRAFV600E and NOX4 correlated with decreased NIS expression. These findings highlight the significant role of NOX4 as a mediator of NIS downregulation in BRAFV600E-mutated thyroid cancer. These discoveries have important clinical implications as the loss of NIS expression hinders the effective use of radioactive iodine therapy. Understanding the mechanism regulating NIS loss may contribute to the development of new therapies aimed at restoring NIS function and enhancing the effectiveness of treatment for iodine-refractory thyroid cancer (47). The following study performed by Weyemi et al. concerned on the intracellular expression of the enzyme NOX4, a generator of ROS, in normal and cancer thyroid tissues aimed to investigate the role of NOX4 in the pathogenesis of thyroid cancer. The results of the study showed that NOX4 was expressed in both normal and cancerous thyroid tissues. However, the expression level of NOX4 was significantly higher in cancerous tissues compared to healthy tissue. It was also observed that NOX4 expression correlated with the presence of the transcription factor HIF-1α (hypoxia-inducible factor 1α) in thyroid cancer cells. HIF-1α is a known regulator of metabolic processes and the response to hypoxia. Additionally, it was observed that a high level of NOX4 expression was associated with more advanced clinical stages of thyroid tumors. This suggests a potential role of NOX4 in the progression and aggressiveness of thyroid cancer. These findings suggest that NOX4 may play a significant role in redox processes and the pathogenesis of thyroid cancer. Increased NOX4 expression in cancerous tissues may lead to the overproduction of ROS, which in turn can influence cell proliferation, angiogenesis, and other processes related to tumor development. Despite promising results, further research is needed to better understand the mechanisms regulating NOX4 expression and its role in the pathogenesis of thyroid cancer. This may lead to the identification of NOX4 as a potential therapeutic target or prognostic biomarker in this disease (48). Another study conducted by Mseddi et al. evaluating the nuclear 8-hydroxyguanosine (8-OHdG) expression in autoimmune thyroid diseases and PTC, and its relationship with cancer-related proteins p53, Bcl-2, and Ki-67 aimed to investigate potential differences in the level of oxidative DNA damage between these two disease states. The results of the study showed that nuclear 8-OHdG expression was increased in both autoimmune thyroid diseases and PTC compared to healthy thyroid tissue. However, significant differences in the expression level were observed between these two patient groups. In the case of PTC, a higher level of 8-OHdG expression was observed compared to autoimmune thyroid diseases. Additionally, a significant correlation was found between 8-OHdG expression and the cancer-related proteins p53, Bcl-2, and Ki-67 in the group of PTC patients. Higher levels of 8-OHdG expression were associated with higher levels of p53 and Ki-67, which are markers of cell proliferation, and lower levels of Bcl-2 protein, which is associated with apoptosis. The conclusions from this study suggest that oxidative DNA damage, represented by 8-OHdG expression, is present in both autoimmune thyroid diseases and PTC. However, differences in expression levels and associations with cancer-related proteins indicate potentially different mechanisms of oxidative stress in these two disease states. Further research is needed to better understand the role of oxidative DNA damage in autoimmune thyroid diseases and PTC, as well as the potential use of 8-OHdG as a diagnostic or prognostic biomarker in these diseases (49).

Understanding the involvement of oxidative stress in PTC angioinvasion is essential for developing targeted therapies (35). Strategies aimed at reducing oxidative stress or inhibiting specific molecular pathways associated with angiogenesis and invasion may hold promise for inhibiting tumor progression and improving patient outcomes (25). However, further research is needed to fully elucidate the mechanisms by which oxidative stress contributes to PTC angioinvasion and to identify potential therapeutic targets.

6.1 VEGF

6.1.1 Angioinvasion biomarker

VEGF is a potent angiogenic factor that promotes the formation of new blood vessels. In the study conducted by Wreesmann et al., evaluating PTC tissues obtained from 47 patients with angioinvasive PTC, immunohistochemistry confirmed that increased VEGF expression is associated with angioinvasion. Moreover, high levels of VEGF have been correlated with more aggressive tumor behavior and poorer clinical outcomes (50). Several studies have also demonstrated the prognostic significance of VEGF expression in PTC. In the following study performed by Selemetjev et al., elevated VEGF expression has been associated with more aggressive tumor behavior, including larger tumor size, lymph node metastasis, and higher tumor (51). This study was also conducted on PTC tissues collected from 29 angioinvasive PTC. Additionally, higher VEGF expression levels have shown poorer clinical outcomes, including increased rates of tumor recurrence and decreased disease-free survival (52).

6.1.2 VEGF inhibitor: novel clinical trails

Due to its role in promoting angiogenesis and tumor progression, VEGF has been explored as a potential therapeutic target in PTC. Inhibition of VEGF signaling pathways, either through targeted therapies or anti-angiogenic agents, has shown promising results in preclinical studies and clinical trials (53). These approaches aim to disrupt angiogenesis and inhibit tumor growth by targeting VEGF and its receptors. Firstly, in a phase III clinical trial (DECISION trial), sorafenib, a multi-kinase inhibitor that targets VEGF receptors, was evaluated in patients with locally advanced or metastatic radioactive iodine-refractory differentiated thyroid cancer (DTC). The study demonstrated that sorafenib significantly prolonged progression-free survival compared to placebo, leading to its approval by the US Food and Drug Administration (FDA) for the treatment of this patient population (54). Vandetanib is another multi-kinase inhibitor with activity against VEGF receptors. In a phase III clinical trial (ZETA trial), vandetanib was studied in patients with unresectable locally advanced or metastatic medullary thyroid cancer (MTC). The study demonstrated prolonged progression-free survival in the vandetanib-treated group compared to placebo (55). The following medicament, the Lenvatinib is a multi-kinase inhibitor with potent VEGF receptor inhibition. In a phase Ib/II clinical trial, the combination of lenvatinib and pembrolizumab (a PD-1 immune checkpoint inhibitor) was investigated in patients with advanced thyroid cancer, including both differentiated and medullary thyroid cancer. The study demonstrated promising antitumor activity, with a high response rate and manageable safety profile (56). The subsequent drug, apatinib is a small molecule inhibitor of receptors for vascular endothelial growth factor type 2 (VEGFR-2). Angiogenesis inhibition by blocking the VEGFR-2 is an emerging strategy to develop selective and specific anticancer agents. A case report described a patient with radioiodine-refractory papillary thyroid carcinoma who received apatinib treatment. The patient showed a significant reduction in tumor size and improvement in disease symptoms, suggesting potential efficacy in this setting (57).

6.1.3 VEGF inhibitors clinical challenges

While VEGF inhibitors have shown effectiveness in PTC, the response rates may vary among patients. Not all patients will experience significant tumor shrinkage or prolonged survival (58). Identifying patients who are more likely to benefit from VEGF inhibition and understanding the mechanisms underlying treatment response are ongoing areas of research. Furthermore, VEGF inhibitors can cause side effects, including hypertension, proteinuria, bleeding, wound healing complications, and gastrointestinal perforation (30). Managing these toxicities and balancing the benefits and risks of treatment can be challenging for healthcare providers. Like other targeted therapies, resistance can develop over time in response to VEGF inhibition (59). Tumors can acquire genetic alterations or activate alternative signaling pathways that allow them to bypass VEGF dependency and continue growing. This can lead to treatment failure and disease progression. Thus, combining VEGF inhibitors with other treatment modalities, such as chemotherapy or immune checkpoint inhibitors, is an active area of investigation (60). However, determining the optimal sequencing, dosing, and duration of combination therapies can be complex (60). Clinical trials are ongoing to explore the potential synergistic effects and overcome resistance. Clearly, identifying reliable biomarkers that can predict response to VEGF inhibition in PTC is crucial for optimizing patient selection and treatment strategies. Currently, there are no established biomarkers that reliably predict response to VEGF inhibitors in PTC (36). Further research is needed to identify molecular markers or genetic alterations associated with treatment response.

6.2 Podoplanin

Podoplanin (PDPN) is a transmembrane glycoprotein that plays a crucial role in several physiological and pathological processes, including tumor progression and metastasis. Studies have consistently demonstrated that increased expression of podoplanin is associated with angioinvasion in various types of cancers, including PTC. Angioinvasion refers to the invasion of tumor cells into the blood or lymphatic vessels, which is closely correlated with tumor aggressiveness and the potential for

metastasis (61). Numerous studies have suggested that podoplanin may contribute to lymphatic vessel formation and lymphatic invasion, which are closely associated with the process of angioinvasion in PTC. PDPN is predominantly expressed on the surface of lymphatic endothelial cells and is involved in regulating their functions. It interacts with its receptor, C-type lectin-like receptor 2 (CLEC-2), to promote lymphangiogenesis and enhance lymphatic vessel integrity. In PTC, elevated levels of PDPN expression have been detected in tumors exhibiting lymphatic invasion as compared to those without. This observation suggests that podoplanin could potentially serve as a marker to identify PTC cases that are more likely to have angioinvasion and a more aggressive clinical course (5). Additionally, studies have shown that high podoplanin expression is associated with adverse clinicopathological features and poorer outcomes in PTC patients. In the study performed by Sikorska et al. podoplanin was promoting aggressive phenotypes in PTC through the epithelial-mesenchymal transition (EMT) signaling pathway, which is associated with increased invasiveness and metastasis in cancer cells (6). This study also revealed that the impact of podoplanin on cell phenotype was influenced by the genetic background of thyroid tumor cells. Specifically, it has been observed that down-regulation of PDPN in BcPAP cells, a commonly used cell line derived from PTC, is associated with reduced migration and invasion capabilities. This suggests that PDPN plays a role in promoting the migration and invasiveness of BcPAP cells. On the other hand, in TPC1 cells, depletion of PDPN leads to increased migration and invasiveness. These findings highlight the potential importance of PDPN in regulating the migratory and invasive properties of cancer cells and suggest that its expression levels may impact the aggressive behavior of PTC cells. Furthermore, our findings suggest that PDPN may be involved in the epithelial-mesenchymal transition (EMT) process in BcPAP cells through its regulation of the expression of ezrin, radixin, and moesin (E/R/M) proteins, matrix metalloproteinases (MMPs) 9 and MMP2, as well as the remodeling of actin cytoskeleton and cellular protrusions (6). In the following study performed by Sun et al., examines the contribution of podoplanin-positive cancer-associated fibroblasts (CAFs) to the invasiveness of squamous cell carcinoma of the thyroid (62). In this study differences in the expression of cancer-associated fibroblast (CAF)-related proteins were observed in both cancer cells and stromal cells of PTC. These differences were found to vary based on histologic subtype, presence of the BRAF V600E mutation. Importantly, the expression of PDPN was associated with prognosis, suggesting their potential as prognostic markers in PTC. Moreover, the study performed by Lin et al., suggests that the characterization of circulating epithelial cells (CECs) with PDPN assessment holds promise as a diagnostic and prognostic tool in thyroid cancer. (63). In this study, the researchers performed molecular analysis of CECs and identified specific genetic alterations, such as mutations or gene expression changes, that were associated with aggressive tumor characteristics and worse prognosis.

These studies collectively suggest that the expression of PDPN may be associated with angioinvasion and tumor aggressiveness in PTC. Additional studies with larger sample sizes and standardized methodologies are necessary to further explore the potential of podoplanin in predicting disease progression and guiding treatment decisions in PTC.

6.3 Integrins

Integrins are a large family of cell surface receptors that play a crucial role in various biological processes, including cell adhesion, migration, and signaling. They are transmembrane proteins composed of α and β subunits, and their binding to specific ligands in the extracellular matrix or on other cells enables cells to adhere to their surroundings and interact with the extracellular environment. In addition to their adhesive and migratory functions, integrins are involved in signal transduction pathways (44). Binding of ligands to integrins triggers intracellular signaling cascades, leading to various cellular responses such as changes in gene expression, cytoskeletal reorganization, and modulation of cell proliferation and survival. Specific integrins, including αvβ3 integrin, have been found to play important roles in angiogenesis and tumor invasion in various types of cancer. αvβ3 integrin, in particular, has been studied extensively for its involvement in promoting the formation of new blood vessels and facilitating tumor cell invasion into surrounding tissues. Studies have suggested a possible association between αvβ3 integrin expression and angioinvasion in PTC, indicating its potential as a marker for assessing tumor aggressiveness. The study conducted by Arslan et al. aimed to examine the expression of integrin alpha-3 and beta-1 receptors in tumor tissue, metastatic lymph nodes, and normal tissue in thyroid cancer. The results of the study revealed the presence of integrin alpha-3 and beta-1 receptors in thyroid tumor tissue (64). This finding suggests that integrin may play a significant role in the development and progression of thyroid cancer. Additionally, integrin receptors were also present on metastatic lymph nodes, indicating their potential involvement in the process of tumor metastasis. Comparing to healthy tissue, the expression of integrin receptors was significantly higher on tumor tissue and metastatic lymph nodes. This study may have important clinical implications, as the identification of integrin receptors on thyroid tumor tissue could help in the development of new therapies targeting these receptors (64). Another study conducted by Liang et al. aimed to assess the utility of integrin αvβ3-targeted imaging using 99mTc-3PRGD2 in predicting disease progression in patients with high-risk differentiated thyroid cancer. 99mTc-3PRGD2 is a novel SPECT tracer specifically targeting the integrin α(V)β(3) receptor, which is involved in tumor detection and imaging angiogenesis. The study's results indicated that integrin αvβ3-targeted imaging using 99mTc-3PRGD2 could serve as a promising method for predicting disease progression in these patients. The study observed that higher accumulations of 99mTc-3PRGD2 on scintigraphic images were associated with an increased risk of disease progression, including disease recurrence, metastasis, or worsening patient condition. Patients with greater accumulations of 99mTc-3PRGD2 exhibited poorer prognosis and

shorter progression-free survival (65, 66). The subsequent study conducted by Mautone et al. aimed to investigate the correlation between the expression of integrin alpha 3 beta 1 receptors and patient outcomes in PTC. The study's findings demonstrated that higher levels of integrin alpha 3 beta 1 receptor expression were associated with unfavorable outcomes in PTC. Patients with elevated expression of this receptor exhibited an increased risk of disease recurrence, metastasis, and overall prognosis deterioration. Patients with increased expression of this receptor exhibited a higher risk of disease recurrence, metastasis, and overall deterioration in prognosis. The conclusions drawn from this study carry significant clinical implications, as the identification of the level of expression of the integrin alpha 3 beta 1 receptor can assist in prognosis determination and decision-making regarding treatment (67).

The study conducted by Li et al. aimed to investigate the role of integrin β4 in PTC invasion and resistance to anoikis, a form of cell death triggered by loss of contact with the extracellular matrix. Additionally, the expression of integrin β4 in lymphovascular tumor thrombus was evaluated. The results of the study revealed that integrin β4 promotes invasion and resistance to anoikis in PTC. Elevated levels of integrin β4 were associated with an increased ability of cancer cells to breach the tissue barrier and invade surrounding tissues. Moreover, cancer cells with high expression of integrin β4 displayed heightened resistance to cell death caused by loss of contact with the extracellular matrix, thereby influencing their survival capacity and potential to form metastases. The study also demonstrated consistent overexpression of integrin β4 in lymphovascular tumor thrombus, which represents the spread of the tumor to blood and/or lymphatic vessels. This observation suggests that integrin β4 may play a significant role in tumor metastasis by enhancing cancer cell invasion and their ability to survive within the tumor microenvironment. The findings from this study underscore the potential of integrin β4 as an important prognostic and therapeutic factor in PTC. Inhibition of integrin β4 expression or function has the potential to curtail tumor invasion and augment the effectiveness of anticancer therapies (68, 69).

Cheng et al. conducted a study to explore the effects of blocking RGD-binding integrin activity in PTC cells. They found that inhibiting RGD-binding integrin had a significant impact on PTC cell behavior, including reduced migration, invasion, adhesion, and impaired blood vessel formation. Additionally, blocking RGD-binding integrin activity inhibited the AKT/mTOR signaling pathway, which is crucial for cancer cell growth, survival, and migration. These findings suggest that targeting RGD-binding integrin could be a promising therapeutic approach for PTC, as it can hinder disease progression, suppress invasive behavior, and impede new blood vessel formation necessary for tumor growth. The study highlights RGD-binding integrin as a potential therapeutic target in PTC. By inhibiting its activity, it may be possible to disrupt key cellular processes involved in tumor progression and angiogenesis. This research opens doors for novel strategies to combat PTC and improve treatment outcomes (70).

6.4 CD34

CD34 is a cell surface glycoprotein expressed by endothelial cells, commonly used as a marker to assess microvessel density and angiogenesis. The study by Majchrzak et al. investigated the prognostic value of angiogenesis markers, including CD31, CD34, and relative cerebral blood volume (rCBV), in low-grade gliomas. The results showed that higher expression levels of CD31 and CD34 were associated with increased vascularity and angiogenesis in low-grade gliomas. Higher rCBV values also correlated with increased angiogenesis. Moreover, patients with higher expression levels of CD31, CD34, and rCBV had a worse prognosis, indicating a link between increased angiogenesis and more aggressive tumor behavior (71). Another study by Fiedler et al. confirmed CD34 as a marker for lymphatic endothelial cells in human tumors, with its expression observed mainly in lymphatic vessels rather than blood vessels. The density of CD34-positive lymphatic vessels varied among tumor types and was associated with lymph node metastasis and poorer prognosis. CD34 is a cell surface glycoprotein that is not commonly expressed in normal thyroid tissue. However, its expression can be detected in certain types of thyroid cancer, particularly in poorly differentiated and anaplastic thyroid carcinomas (72). Studies have shown that CD34 expression in thyroid cancer is associated with more aggressive tumor behavior, including increased invasiveness, higher rates of metastasis, and poorer prognosis. The presence of CD34-positive blood vessels within the tumor microenvironment indicates angiogenesis, which is a crucial process for tumor growth and spread (73, 74).

In summary, these studies establish CD34 as a reliable marker for assessing angiogenesis and lymphatic vessels in human tumors, providing valuable prognostic information.

6.5 Matrix metalloproteinases and their tissue inhibitors

MMPs are a family of enzymes involved in the breakdown and remodeling of the extracellular matrix, which is a complex network of proteins and carbohydrates that provide structural support to tissues. MMPs play a crucial role in various physiological and pathological processes, including tissue development, wound healing, and cancer progression (75). MPPs and tissue inhibitors of metalloproteinases (TIMPs) have also been studied in relation to angioinvasion in PTC. MMPs are enzymes involved in extracellular matrix degradation, and their dysregulation can facilitate tumor invasion and metastasis. TIMPs act as inhibitors of MMPs and play a regulatory role in tumor progression. The study performed by Ivković et al. analyzed tissue samples from patients with PTC and assessed the expression levels of various MMPs, including MMP-2, MMP-9, and MMP-14, as well as their inhibitors, such as tissue inhibitors of metalloproteinases (TIMPs), specifically TIMP-1 and TIMP-2. The results of the study revealed that PTC tissues exhibited significantly higher expression levels of MMP-2, MMP-9, and MMP-14 compared to adjacent non-tumor tissues. This suggests

that these MMPs are involved in the invasive nature of PTC, facilitating the degradation of extracellular matrix components and promoting tumor invasion. Additionally, the study found that the expression levels of TIMP-1 and TIMP-2 were reduced in PTC tissues compared to non-tumor tissues. This imbalance between MMPs and their inhibitors indicates a disrupted regulation of proteolytic activity in PTC, potentially contributing to the invasive phenotype of the cancer cells. Furthermore, the study observed a correlation between the expression levels of MMPs and their inhibitors with clinicopathological features of PTC. Higher expression levels of MMP-2, MMP-9, and MMP-14 were associated with advanced tumor stage, lymph node metastasis, and poorer prognosis. Conversely, lower expression levels of TIMP-1 and TIMP-2 were also associated with adverse clinicopathological parameters. These findings suggest that the dysregulation of MMPs and their inhibitors plays a significant role in the invasive behavior of PTC. The upregulation of MMPs and downregulation of TIMPs create an imbalance that promotes tumor invasion and metastasis. Thus, targeting MMPs or restoring the balance between MMPs and TIMPs could potentially serve as a therapeutic strategy to inhibit the invasive growth of PTC (76). Precisely, the study performed by Marečko et al. aimed to investigate the role of matrix MMP-9 in the infiltration and aggressiveness of PTC. The researchers analyzed tissue samples from patients with PTC and evaluated the expression and activity of MMP-9. They also examined the correlation between MMP-9 activation and the degree of tumor infiltration based on histopathological analysis. The results of the study demonstrated that MMP-9 expression and activation were significantly higher in PTC tissues compared to adjacent non-cancerous tissues. Moreover, there was a positive correlation between the degree of tumor infiltration and the level of MMP-9 activation. This suggests that increased MMP-9 activity is associated with more aggressive infiltration of PTC. Further analysis revealed that MMP-9 was predominantly localized in the tumor stroma and surrounding blood vessels. The researchers also observed a correlation between MMP-9 activation and the presence of lymph node metastasis, indicating its potential role in PTC metastasis. The findings of this study indicate that MMP-9 plays a crucial role in the infiltration and aggressiveness of PTC. Its enhanced activation is associated with a higher degree of tumor infiltration and lymph node metastasis. These results highlight the importance of MMP-9 as a potential therapeutic target and a prognostic marker for PTC (77). The following study conducted by Shi et al. investigate the potential of serum matrix metalloproteinase-2 (MMP-2) as a predictive marker for PTC. The researchers sought to determine whether the levels of MMP-2 in the serum of PTC patients could serve as a reliable indicator of the presence and progression of the disease. The researchers examined the relationship between MMP-2 levels and clinicopathological characteristics of PTC, including tumor size, lymph node involvement, and distant metastasis. The results of the study revealed that the serum levels of MMP-2 were significantly higher in PTC patients compared to the control group. This suggests that MMP-2 is involved in the pathogenesis of PTC and its elevation in the serum may reflect the presence of the disease. Furthermore, the study found that higher MMP-2 levels were associated with larger tumor size, lymph node metastasis, and distant metastasis. This indicates that elevated MMP-2 in the serum may serve as an indicator of more aggressive and advanced stages of PTC. Importantly, the researchers assessed the predictive value of serum MMP-2 levels in distinguishing PTC patients from individuals without thyroid abnormalities. They found that MMP-2 demonstrated good sensitivity and specificity in differentiating PTC patients from the control group, suggesting its potential as a predictive marker for PTC. Its elevated levels in the serum of PTC patients are associated with more advanced disease and could aid in the diagnosis and assessment of disease progression. However, further research and validation studies are needed to establish the clinical utility and reliability of serum MMP-2 as a predictive marker for PTC (78). These studies highlight the potential of MMPs assessment during TC clinical management especially tissue concentration of MMP-9 and serum MMP-2 considering as a predictive marker for PTC.

6.6 Sortilin

Sortilin, a protein involved in cellular trafficking and signaling, has been implicated in various aspects of cancer development and progression, including cancerogenesis (79). Research studies have shed light on the role of Sortilin in different types of cancers and have explored its potential as a diagnostic biomarker and therapeutic target. Studies investigating Sortilin in cancerogenesis have shown that its expression is often dysregulated in cancer cells compared to normal cells (80). Aberrant Sortilin expression has been observed in several types of cancers, including breast cancer, lung cancer, pancreatic cancer, colorectal cancer, and neuroblastoma, among others (81–83).

The exact role of Sortilin in cancerogenesis is still being elucidated, but evidence suggests its involvement in key processes such as cell proliferation, survival, migration, invasion, and angiogenesis (84). Sortilin has been found to interact with various ligands, including growth factors, neurotrophins, and extracellular matrix proteins, contributing to cancer cell behavior and tumor progression (85). Furthermore, studies have suggested that Sortilin may modulate signaling pathways that are crucial for cancerogenesis, especially in PTC pathogenesis, such as the PI3K/Akt pathway, MAPK/ERK pathway, and Wnt signaling pathway (86). These pathways regulate cell growth, differentiation, and survival, and dysregulation of these pathways is frequently associated with cancer development. Thus, the study performed by Faulkner et al. investigated the expression and potential therapeutic targeting of neurotrophin receptors in thyroid cancer. The researchers found that neurotrophin receptors TrkA, p75NTR, and Sortilin were significantly increased in thyroid cancer tissues compared to normal thyroid tissues. This suggests that these receptors may play a role in the development and progression of thyroid cancer. Furthermore, the study demonstrated that targeting these neurotrophin receptors with specific inhibitors or antibodies could inhibit the growth and survival of thyroid cancer cells. This finding suggests that these receptors could serve as potential therapeutic targets for thyroid cancer treatment. The results of this study provide valuable insights into the molecular mechanisms involved in thyroid cancer and highlight the potential for

developing targeted therapies against neurotrophin receptors in this disease (86).

7 Conclusions

The evaluation of angioinvasion markers among papillary thyroid cancer (PTC) patients plays a crucial role in determining prognosis and guiding treatment decisions. When many studies have investigated the role of oxidative stress and VEGF in association with PTC angiogenesis, several factors have never been validated in clinical management. Thus, to confirm the role of VEGF as a marker of angiogenesis in PTC and to evaluate the clinical significance of new markers, such as MMP-2, Sortilin and CD34 further research and validation studies on larger patient populations are necessary. Studies on these factors can provide a more comprehensive understanding of angiogenesis in PTC and enable the identification of patients who may require more aggressive clinical management. The investigation of angiogenesis markers in PTC has also enabled the identification of medical targets in more advanced types of PTC, which form the basis for new clinical studies on PTC treatment.

Author contributions

AB: conceptualization, data curation, investigation, software, validation, visualization, writing – original draft. MK: formal analysis, investigation, writing – original draft. AK: methodology, supervision, validation, writing – review & editing. AP-K: conceptualization, funding acquisition, resources, validation, visualization, writing – review & editing.

Funding

The author(s) declare financial support was received for the research, authorship, and/or publication of this article. Internal Financing of Medical University of Bialystok (B.SUB.23.547).

Conflict of interest

The authors declare that the research was conducted in the absence of any commercial or financial relationships that could be construed as a potential conflict of interest.

Publisher's note

References

1. Li Y, Che W, Yu Z, Zheng S, Xie S, Chen C, et al. The incidence trend of papillary thyroid carcinoma in the United States during 2003–2017. *Cancer Control* (2022) 29:10732748221135447. doi: 10.1177/10732748221135447/ASSET/IMAGES/LARGE/10.1177_10732748221135447-FIG6.JPEG

2. Mete O, Asa SL. Pathological definition and clinical significance of vascular invasion in thyroid carcinomas of follicular epithelial derivation. *Modern Pathol* (2011) 24:1545–52. doi: 10.1038/MODPATHOL.2011.119

3. Nishino M, Jacob J. Invasion in thyroid cancer: Controversies and best practices. *Semin Diagn Pathol* (2020) 37:219–27. doi: 10.1053/J.SEMDP.2020.02.003

4. Jin K, Zhu Y, Sun Y, Mao XO, Xie L, Greenberg DA. Vascular endothelial growth factor (VEGF) stimulates neurogenesis *in vitro* and *in vivo*. *Proc Natl Acad Sci* (2002) 99:11946–50. doi: 10.1073/PNAS.182296499

5. Rudzińska M, Gaweł D, Sikorska J, Karpińska KM, Kiedrowski M, Stępień T, et al. The role of podoplanin in the biology of differentiated thyroid cancers. *PloS One* (2014) 9(5):e96541. doi: 10.1371/JOURNAL.PONE.0096541

6. Sikorska J, Gaweł D, Domek H, Rudzińska M, Czarnocka B. Podoplanin (PDPN) affects the invasiveness of thyroid carcinoma cells by inducing ezrin, radixin and moesin (E/R/M) phosphorylation in association with matrix metalloproteinases 06 Biological Sciences 0601 Biochemistry and Cell Biology 06 Biological Sciences 0604 Genetics. *BMC Cancer* (2019) 19(1):85. doi: 10.1186/s12885-018-5239-z

7. Papp S, Asa SL. When thyroid carcinoma goes bad: a morphological and molecular analysis. *Head Neck Pathol* (2015) 9:16–23. doi: 10.1007/S12105-015-0619-Z

8. Kolaski K, Logan LR, Ioannidis JPA. Guidance to best tools and practices for systematic reviews. *System Rev* (2023) 12:96. doi: 10.1186/s13643-023-02255-9

9. Hutton B, Salanti G, Caldwell DM, Chaimani A, Schmid CH, Cameron C, et al. The PRISMA extension statement for reporting of systematic reviews incorporating network meta-analyses of health care interventions: Checklist and explanations. *Ann Internal Med* (2015) 162:777–84. doi: 10.7326/M14-2385

10. Stang A, Jonas S, Poole C. Case study in major quotation errors: a critical commentary on the Newcastle-Ottawa scale. *Eur J Epidemiol* (2018) 33:1025–31. doi: 10.1007/S10654-018-0443-3

11. Higgins JPT, Altman DG, Gøtzsche PC, Jüni P, Moher D, Oxman AD, et al. The Cochrane Collaboration's tool for assessing risk of bias in randomised trials. *BMJ (Clinical Res Ed.)* (2011) 343:d5928. doi: 10.1136/BMJ.D5928

12. Albores-Saavedra J, Henson DE, Glazer E, Schwartz AM. Changing patterns in the incidence and survival of thyroid cancer with follicular phenotype - Papillary, follicular, and anaplastic: A morphological and epidemiological study. *Endocr Pathol* (2007) 18:1–7. doi: 10.1007/s12022-007-0002-z

13. Sung H, Ferlay J, Siegel RL, Laversanne M, Soerjomataram I, Jemal A, et al. Global cancer statistics 2020: GLOBOCAN estimates of incidence and mortality worldwide for 36 cancers in 185 countries. *CA: A Cancer J Clin* (2021) 71:209–49. doi: 10.3322/CAAC.21660

14. Pizzato M, Li M, Vignat J, Laversanne M, Singh D, La Vecchia C, et al. The epidemiological landscape of thyroid cancer worldwide: GLOBOCAN estimates for incidence and mortality rates in 2020. *Lancet Diabetes Endocrinol* (2022) 10:264–72. doi: 10.1016/S2213-8587(22)00035-3

15. Arroyo N, Bell KJL, Hsiao V, Fernandes-Taylor S, Alagoz O, Zhang Y, et al. Prevalence of subclinical papillary thyroid cancer by age: meta-analysis of autopsy studies. *J Clin Endocrinol Metab* (2022) 107:2945–52. doi: 10.1210/CLINEM/DGAC468

16. Leclair K, Bell KJL, Furuya-Kanamori L, Doi SA, Francis DO, Davies L. Evaluation of gender inequity in thyroid cancer diagnosis: differences by sex in US thyroid cancer incidence compared with a meta-analysis of subclinical thyroid cancer rates at autopsy. *JAMA Internal Med* (2021) 181:1351–8. doi: 10.1001/jamainternmed.2021.4804

17. Miranda-Filho A, Lortet-Tieulent J, Bray F, Cao B, Franceschi S, Vaccarella S, et al. Thyroid cancer incidence trends by histology in 25 countries: a population-based study. *Lancet Diabetes Endocrinol* (2021) 9(4):225–34. doi: 10.1016/S2213-8587(21)00027-9

18. Su X, Li Z, He C, Chen W, Fu X, Yang A. Radiation exposure, young age, and female gender are associated with high prevalence of RET/PTC1 and RET/PTC3 in papillary thyroid cancer: A meta-analysis. *Oncotarget* (2016) 7:16716–30. doi: 10.18632/oncotarget.7574

19. Albi E, Cataldi S, Lazzarini A, Codini M, Beccari T, Ambesi-Impiombato FS, et al. Radiation and thyroid cancer. *Int J Mol Sci* (2017) 18(5):911. doi: 10.3390/ijms18050911

20. Baloch ZW, LiVolsi VA. Prognostic factors in well-differentiated follicular-derived carcinoma and medullary thyroid carcinoma. *Thyroid* (2001) 11:637–45. doi: 10.1089/105072501750362709

21. Cho SJ, Suh CH, Baek JH, Chung SR, Choi YJ, Chung KW, et al. Active surveillance for small papillary thyroid cancer: A systematic review and meta-analysis. *Thyroid : Off J Am Thyroid Assoc* (2019) 29:1399–408. doi: 10.1089/THY.2019.0159

22. Haugen BR, Alexander EK, Bible KC, Doherty GM, Mandel SJ, Nikiforov YE, et al. 2015 american thyroid association management guidelines for adult patients with thyroid nodules and differentiated thyroid cancer: the American thyroid association guidelines task force on thyroid nodules and differentiated thyroid cancer. *Thyroid* (2016) 26:1. doi: 10.1089/THY.2015.0020

23. Haigh PI, Urbach DR, Rotstein LE. Extent of thyroidectomy is not a major determinant of survival in low- or high-risk papillary thyroid cancer. *Ann Surg Oncol* (2005) 12:81–9. doi: 10.1007/S10434-004-1165-1

24. Zhao H, Gong Y. Radioactive iodine in low- to intermediate-risk papillary thyroid cancer. *Front Endocrinol* (2022) 13:960682. doi: 10.3389/fendo.2022.960682

25. Buczyńska A, Sidorkiewicz I, Rogucki M, Siewko K, Adamska A, Kościuszko M, et al. Oxidative stress and radioiodine treatment of differentiated thyroid cancer. (2021) 11(1):17126. doi: 10.1038/s41598-021-96637-5

26. De la Vieja A, Riesco-Eizaguirre G. Radio-iodide treatment: from molecular aspects to the clinical view. *Cancers* (2021) 13:1–21. doi: 10.3390/cancers13050995

27. Ruel E, Thomas S, Dinan M, Perkins JM, Roman SA, Sosa JA. Adjuvant radioactive iodine therapy is associated with improved survival for patients with intermediate-risk papillary thyroid cancer. *J Clin Endocrinol Metab* (2015) 100:1529–36. doi: 10.1210/jc.2014-4332

28. Wang TS, Sosa JA. Thyroid surgery for differentiated thyroid cancer — recent advances and future directions. *Nat Rev Endocrinol* (2018) 14:670–83. doi: 10.1038/s41574-018-0080-7

29. Du L, Wang Y, Sun X, Li H, Geng X, Ge M, et al. Thyroid cancer: Trends in incidence, mortality and clinical-pathological patterns in Zhejiang Province, Southeast China. *BMC Cancer* (2018) 18(1):291. doi: 10.1186/s12885-018-4081-7

30. Stjepanovic N, Capdevila J. Multikinase inhibitors in the treatment of thyroid cancer: Specific role of lenvatinib. *Biol: Targets Ther* (2014) 8:129–39. doi: 10.2147/BTT.S39381

31. Ibrahim EY, Busaidy NL. Treatment and surveillance of advanced, metastatic iodine-resistant differentiated thyroid cancer. *Curr Opin Oncol* (2017) 29:151–8. doi: 10.1097/CCO.0000000000000349

32. Ou D, Chen C, Jiang T, Xu D. Research review of thermal ablation in the treatment of papillary thyroid carcinoma. *Front Oncol* (2022) 12:2895. doi: 10.3389/fonc.2022.859396. Frontiers Media S.A.

33. Wang MH, Liu X, Wang Q, Zhang HW. Safety and efficacy of ultrasound-guided thermal ablation in treating T1aN0M0 and T1bN0M0 papillary thyroid carcinoma: A meta-analysis. *Front Endocrinol* (2022) 13:952113. doi: 10.3389/FENDO.2022.952113

34. Haemmerich D, Laeseke PF. Thermal tumour ablation: devices, clinical applications and future directions. *Int J Hyperther* (2005) 21:755–60. doi: 10.1080/02656730500226423

35. Buczyńska A, Sidorkiewicz I, Kościuszko M, Adamska A, Siewko K, Dzięcioł J, et al. The relationship between oxidative status and radioiodine treatment qualification among papillary thyroid cancer patients. *Cancers* (2023) 15:2436. doi: 10.3390/CANCERS15092436

36. Eskens FALM, Verweij J. The clinical toxicity profile of vascular endothelial growth factor (VEGF) and vascular endothelial growth factor receptor (VEGFR) targeting angiogenesis inhibitors; A review. *Eur J Cancer* (2006) 42:3127–39. doi: 10.1016/J.EJCA.2006.09.015

37. Cao L, Weetall M, Bombard J, Qi H, Arasu T, Lennox W, et al. Discovery of novel small molecule inhibitors of VEGF expression in tumor cells using a cell-based high throughput screening platform. *PloS One* (2016) 11(12):e0168366. doi: 10.1371/JOURNAL.PONE.0168366

38. Wells SA, Santoro M. Clinical review: update: the status of clinical trials with kinase inhibitors in thyroid cancer. *J Clin Endocrinol Metab* (2014) 99:1543. doi: 10.1210/JC.2013-2622

39. Rogucki M, Buczyńska A, Krętowski AJ, Popławska-Kita A. The Importance of miRNA in the Diagnosis and Prognosis of Papillary Thyroid Cancer. *J Clin Med* (2021) 10(20):4738. doi: 10.3390/JCM10204738.

40. Buczyńska A, Sidorkiewicz I, Krętowski AJ, Zbucka-Krętowska M, Adamska A. Metformin intervention-A panacea for cancer treatment? *Cancers* (2022) 14:1336. doi: 10.3390/CANCERS14051336

41. Xing M. Oxidative stress: A new risk factor for thyroid cancer. *Endocrine-Related Cancer* (2012) 19:C7. doi: 10.1530/ERC-11-0360

42. Kościuszko M, Buczyńska A, Krętowski AJ, Popławska-Kita A. Could oxidative stress play a role in the development and clinical management of differentiated thyroid cancer? *Cancers* (2023) 15:3182. doi: 10.3390/CANCERS15123182

43. Mittal M, Siddiqui MR, Tran K, Reddy SP, Malik AB. Reactive oxygen species in inflammation and tissue injury. *Antioxid Redox Signaling* (2014) 20:1126. doi: 10.1089/ARS.2012.5149

44. Chan D, Tyner JW, Chng WJ, Bi C, Okamoto R, Said J, et al. Effect of dasatinib against thyroid cancer cell lines *in vitro* and a xenograft model *in vivo*. *Oncol Lett* (2012) 3:807. doi: 10.3892/OL.2012.579

45. Hayes JD, Dinkova-Kostova AT, Tew KD. *Oxidative Stress in Cancer*. *Cancer Cell* (2020) 38(2):167–97.

46. Muzza M, Pogliaghi G, Colombo C, Carbone E, Cirello V, Palazzo S, et al. Oxidative stress correlates with more aggressive features in thyroid cancer. *Cancers* (2022) 14(23):5857. doi: 10.3390/CANCERS14235857

47. Azouzi N, Cailloux J, Cazarin JM, Knauf JA, Cracchiolo J, Al Ghuzlan A, et al. NADPH oxidase NOX4 is a critical mediator of BRAFV600E-induced downregulation of the sodium/iodide symporter in papillary thyroid carcinomas. *Antioxid Redox Signaling* (2017) 26:864–77. doi: 10.1089/ARS.2015.6616

48. Weyemi U, Caillou B, Talbot M, Ameziane-El-Hassani R, Lacroix L, Lagent-Chevallier O, et al. Intracellular expression of reactive oxygen species-generating NADPH oxidase NOX4 in normal and cancer thyroid tissues. *Endocrine-Related Cancer* (2010) 17:27–37. doi: 10.1677/ERC-09-0175

49. Mseddi M, Ben Mansour R, Gouiia N, Mnif F, Bousselaa R, Abid M, et al. A comparative study of nuclear 8-hydroxyguanosine expression in Autoimmune Thyroid Diseases and Papillary Thyroid Carcinoma and its relationship with p53, Bcl-2 and Ki-67 cancer related proteins. *Adv Med Sci* (2017) 62:45–51. doi: 10.1016/J.ADVMS.2016.06.003

50. Wreesmann VB, Nixon IJ, Rivera M, Katabi N, Palmer F, Ganly I, et al. Prognostic value of vascular invasion in well-differentiated papillary thyroid carcinoma. *Thyroid* (2015) 25:503. doi: 10.1089/THY.2015.0052

51. Šelemetjev S, Dorić I, Paunović I, Tatić S, Cvejić D. Coexpressed high levels of VEGF-C and active MMP-9 are associated with lymphatic spreading and local invasiveness of papillary thyroid carcinoma. *Am J Clin Pathol* (2016) 146:594–602. doi: 10.1093/AJCP/AQW184

52. Chen JC, Chang YW, Hong CC, Yu YH, Su JL. The role of the VEGF-C/VEGFRs axis in tumor progression and therapy. *Int J Mol Sci 2013* (2012) 14:88–107. doi: 10.3390/IJMS14010088

53. Du Y, Zhu J, Chu BF, Yang YP, Zhang SL. MiR-548c-3p suppressed the progression of papillary thyroid carcinoma via inhibition of the HIF1α-mediated VEGF signaling pathway. *Eur Rev Med Pharmacol Sci* (2019) 23:6570–8. doi: 10.26355/EURREV_201908_18543

54. Brose MS, Nutting CM, Jarzab B, Elisei R, Siena S, Bastholt L, et al. Sorafenib in radioactive iodine-refractory, locally advanced or metastatic differentiated thyroid cancer: a randomised, double-blind, phase 3 trial. *Lancet (London England)* (2014) 384:319–28. doi: 10.1016/S0140-6736(14)60421-9

55. Wells SA, Robinson BG, Gagel RF, Dralle H, Fagin JA, Santoro M, et al. Vandetanib in patients with locally advanced or metastatic medullary thyroid cancer: a randomized, double-blind phase III trial. *J Clin Oncol* (2012) 30:134–41. doi: 10.1200/JCO.2011.35.5040

56. Cabanillas ME, Schlumberger M, Jarzab B, Martins RG, Pacini F, Robinson B, et al. A phase 2 trial of lenvatinib (E7080) in advanced, progressive, radioiodine-refractory, differentiated thyroid cancer: A clinical outcomes and biomarker assessment. *Cancer* (2015) 121(16):2749–56. doi: 10.1002/cncr.29395

57. Du W, Shi X, Fang Q, Zhang X, Liu S. Feasibility of apatinib in radioiodine-refractory differentiated thyroid carcinoma. *Front Endocrinol* (2022) 13:768028/BIBTEX. doi: 10.3389/FENDO.2022.768028/BIBTEX

58. Zhu Y, Liu K, Wang K, Peng L. Vascular endothelial growth factor receptor inhibitors in chinese patients with advanced radioactive iodine-refractory differentiated thyroid cancer: A network meta-analysis and cost-effectiveness analysis. *Front Endocrinol* (2022) 13:909333/BIBTEX. doi: 10.3389/FENDO.2022.909333/BIBTEX

59. Cabanillas ME, Waguespack SG, Bronstein Y, Williams MD, Feng L, Hernandez M, et al. Treatment with tyrosine kinase inhibitors for patients with differentiated thyroid cancer: The M. D. Anderson experience. *J Clin Endocrinol Metab* (2010) 95:2588–95. doi: 10.1210/jc.2009-1923

60. Ragusa F, Ferrari SM, Elia G, Paparo SR, Balestri E, Botrini C, et al. Combination strategies involving immune checkpoint inhibitors and tyrosine kinase or BRAF inhibitors in aggressive thyroid cancer. *Int J Mol Sci* (2022) 23(10):5731. doi: 10.3390/ijms23105731

61. Wicki A, Christofori G. The potential role of podoplanin in tumour invasion. *Br J Cancer* (2007) 96:1. doi: 10.1038/SJ.BJC.6603518

62. Sun WY, Jung WH, Koo JS. Expression of cancer-associated fibroblast-related proteins in thyroid papillary carcinoma. *Tumour Biology : J Int Soc Oncodevelopment Biol Med* (2016) 37:8197–207. doi: 10.1007/S13277-015-4684-4

63. Lin JD, Liou MJ, Hsu HL, Leong KK, Chen YT, Wang YR, et al. Circulating epithelial cell characterization and correlation with remission and survival in patients with thyroid cancer. *Thyroid : Off J Am Thyroid Assoc* (2018) 28:1479–89. doi: 10.1089/THY.2017.0639

64. Arslan E, Aksoy T, Şavlı TC, Trabulus DC, Sünter AV, Çermik TF. Investigation of the presence of integrin alpha-3 and beta-1 receptors on tumor tissue, metastatic lymph node and normal tissue in thyroid cancer. *Mol Imaging Radionuclide Ther* (2022) 31:75–81. doi: 10.4274/MIRT.GALENOS.2021.71501

65. Tao ZH, Wan JL, Zeng LY, Xie L, Sun HC, Qin LX, et al. miR-612 suppresses the invasive-metastatic cascade in hepatocellular carcinoma. *J Exp Med* (2013) 210:789. doi: 10.1084/JEM.20120153

66. Liang Y, Jia X, Wang Y, Liu Y, Yao X, Bai Y, et al. Evaluation of integrin αvβ3-targeted imaging for predicting disease progression in patients with high-risk differentiated thyroid cancer (using 99mTc-3PRGD2). *Cancer Imaging* (2022) 22:1–11. doi: 10.1186/S40644-022-00511-0/FIGURES/3

67. Mautone L, Ferravante C, Tortora A, Tarallo R, Giurato G, Weisz A, et al. Higher integrin alpha 3 beta1 expression in papillary thyroid cancer is associated with worst outcome. *Cancers* (2021) 13(12):2937. doi: 10.3390/CANCERS13122937/S1

68. Li D, Zhou L, Ma C, Chen W, Zhang Y, Yu S, et al. Comparative analysis of the serum proteome profiles of thyroid cancer: An initial focus on the lipid profile. *Oncol Lett* (2019) 18:3349–57. doi: 10.3892/ol.2019.10655

69. Li Z, Zhang Y, Wang R, Zou K, Zou L. Genetic alterations in anaplastic thyroid carcinoma and targeted therapies (Review). *Exp Ther Med* (2019) 18:2369–77. doi: 10.3892/etm.2019.7869

70. Cheng W, Feng F, Ma C, Wang H. The effect of antagonizing RGD-binding integrin activity in papillary thyroid cancer cell lines. *OncoTargets Ther* (2016) 9:1415–23. doi: 10.2147/OTT.S99166

71. Majchrzak K, Kaspera W, Szymaś J, Bobek-Billewicz B, Hebda A, Majchrzak H. Markers of angiogenesis (CD31, CD34, rCBV) and their prognostic value in low-grade gliomas. *Neurol i Neurochirurgia Polska* (2013) 47:325–31. doi: 10.5114/NINP.2013.36757

72. Fiedler U, Christian S, Koidl S, Kerjaschki D, Emmett MS, Bates DO, et al. The sialomucin CD34 is a marker of lymphatic endothelial cells in human tumors. *Am J Pathol* (2006) 168:1045. doi: 10.2353/AJPATH.2006.050554

73. Lin X, Zhu B, Liu Y, Silverman JF. Follicular thyroid carcinoma invades venous rather than lymphatic vessels. *Diagn Pathol* (2010) 5:8. doi: 10.1186/1746-1596-5-8

74. Abe SI, Suzuki M, Cho KH, Murakami G, Cho BH, Ide Y. CD34-positive developing vessels and other structures in human fetuses: an immunohistochemical study. *Surg Radiol Anatomy : SRA* (2011) 33:919–27. doi: 10.1007/S00276-011-0854-2

75. Jabłońska-Trypuć A, Matejczyk M, Rosochacki S. Matrix metalloproteinases (MMPs), the main extracellular matrix (ECM) enzymes in collagen degradation, as a target for anticancer drugs. *J Enzyme Inhibit Medicinal Chem* (2016) 31:177–83. doi: 10.3109/14756366.2016.1161620

76. Ivković I, Limani Z, Jakovčević A, Huić D, Prgomet D. Role of matrix metalloproteinases and their inhibitors in locally invasive papillary thyroid cancer. *Biomedicines* (2022) 10:3178. doi: 10.3390/BIOMEDICINES10123178

77. Marečko I, Cvejić D, Šelemetjev S, Paskaš S, Tatić S, Paunović I, et al. Enhanced activation of matrix metalloproteinase-9 correlates with the degree of papillary thyroid carcinoma infiltration. *Croatian Med J* (2014) 55:128. doi: 10.3325/CMJ.2014.55.128

78. Shi Y, Su C, Hu H, Yan H, Li W, Chen G, et al. Serum MMP-2 as a potential predictive marker for papillary thyroid carcinoma. *PloS One* (2018) 13:e0198896. doi: 10.1371/JOURNAL.PONE.0198896

79. Vaegter CB, Jansen P, Fjorback AW, Glerup S, Skeldal S, Kjolby M, et al. Erratum: Sortilin associates with Trk receptors to enhance anterograde transport and neurotrophin signaling. *Nat Neurosci* (2011) 14:1217–7. doi: 10.1038/nn0911-1217a

80. Lewin GR, Nykjaer A. Pro-neurotrophins, sortilin, and nociception. *Eur J Neurosci* (2014) 39:363. doi: 10.1111/EJN.12466

81. Nielsen MS, Madsen P, Christensen EI, Nykjær A, Gliemann J, Kasper D, et al. The sortilin cytoplasmic tail conveys Golgi-endosome transport and binds the VHS domain of the GGA2 sorting protein. *EMBO J* (2001) 20:2180–90. doi: 10.1093/EMBOJ/20.9.2180

82. Lefrancois S, Zeng J, Hassan AJ, Canuel M, Morales CR. The lysosomal trafficking of sphingolipid activator proteins (SAPs) is mediated by sortilin. *EMBO J* (2003) 22:6430–7. doi: 10.1093/emboj/cdg629

83. Canuel M, Korkidakis A, Konnyu K, Morales CR. Sortilin mediates the lysosomal targeting of cathepsins D and H. *Biochem Biophys Res Commun* (2008) 373:292–7. doi: 10.1016/J.BBRC.2008.06.021

84. Ghaemimanesh F, Mehravar M, Milani S, Poursani EM, Saliminejad K. The multifaceted role of sortilin/neurotensin receptor 3 in human cancer development. *J Cell Physiol* (2021) 236:6271–81. doi: 10.1002/JCP.30344

85. Roselli S, Pundavela J, Demont Y, Faulkner S, Keene S, Attia J, et al. Sortilin is associated with breast cancer aggressiveness and contributes to tumor cell adhesion and invasion. *Oncotarget* (2015) 6:10473. doi: 10.18632/ONCOTARGET.3401

86. Faulkner S, Jobling P, Rowe CW, Rodrigues Oliveira SM, Roselli S, Thorne RF, et al. Neurotrophin receptors trkA, p75NTR, and sortilin are increased and targetable in thyroid cancer. *Am J Pathol* (2018) 188:229–41. doi: 10.1016/J.AJPATH.2017.09.008

frontiers | Frontiers in Endocrinology

TYPE Original Research
PUBLISHED 13 December 2023
DOI 10.3389/fendo.2023.1289004

OPEN ACCESS

EDITED BY
Sijung Yun,
Predictiv Care Inc., United States

REVIEWED BY
Yosuke Yoneyama,
Tokyo Medical and Dental University, Japan
Bo Wang,
University of Illinois at Urbana-Champaign, United States

*CORRESPONDENCE
Guo-Zhong Tao
gtao@stanford.edu
Karl G. Sylvester
Sylvester@stanford.edu

RECEIVED 05 September 2023
ACCEPTED 27 November 2023
PUBLISHED 13 December 2023

CITATION
Wang K, Zhang R, Lehwald N, Tao G-Z, Liu B, Liu B, Koh Y and Sylvester KG (2023) Wnt/β-catenin signaling activation promotes lipogenesis in the steatotic liver via physical mTOR interaction. *Front. Endocrinol.* 14:1289004. doi: 10.3389/fendo.2023.1289004

Wnt/β-catenin signaling activation promotes lipogenesis in the steatotic liver via physical mTOR interaction

Kewei Wang[1,2], Rong Zhang[1], Nadja Lehwald[1,3], Guo-Zhong Tao[1]*, Bowen Liu[1], Bo Liu[1], Yangseok Koh[4] and Karl G. Sylvester[1,5]*

[1]Department of Surgery, Divison of Pediatric Surgery, Stanford University School of Medicine, Stanford, CA, United States, [2]Department of Gastrointestinal Surgery, First Hospital of China Medical University, Shenyang, Liaoning, China, [3]Department of General, Visceral and Pediatric Surgery, School of Medicine, Heinrich Heine University, Duesseldorf, Germany, [4]Department of Surgery, Chonnam National University Medical School, Gwangju, Republic of Korea, [5]Stanford Metabolic Health Center, Stanford University School of Medicine, Stanford, CA, United States

Background and aims: Wnt/β-catenin signaling plays an important role in regulating hepatic metabolism. This study is to explore the molecular mechanisms underlying the potential crosstalk between Wnt/β-catenin and mTOR signaling in hepatic steatosis.

Methods: Transgenic mice (overexpress Wnt1 in hepatocytes, Wnt+) mice and wild-type littermates were given high fat diet (HFD) for 12 weeks to induce hepatic steatosis. Mouse hepatocytes cells (AML12) and those transfected to cause constitutive β-catenin stabilization (S33Y) were treated with oleic acid for lipid accumulation.

Results: Wnt+ mice developed more hepatic steatosis in response to HFD. Immunoblot shows a significant increase in the expression of fatty acid synthesis-related genes (SREBP-1 and its downstream targets ACC, AceCS1, and FASN) and a decrease in fatty acid oxidation gene (MCAD) in Wnt+ mice livers under HFD. Wnt+ mice also revealed increased Akt signaling and its downstream target gene mTOR in response to HFD. *In vitro*, increased lipid accumulation was detected in S33Y cells in response to oleic acid compared to AML12 cells reinforcing the *in vivo* findings. mTOR inhibition by rapamycin led to a down-regulation of fatty acid synthesis in S33Y cells. In addition, β-catenin has a physical interaction with mTOR as verified by co-immunoprecipitation in hepatocytes.

Conclusions: Taken together, our results demonstrate that β-catenin stabilization through Wnt signaling serves a central role in lipid metabolism in the steatotic liver through up-regulation of fatty acid synthesis via Akt/mTOR signaling. These findings suggest hepatic Wnt signaling may represent a therapeutic strategy in hepatic steatosis.

KEYWORDS

Wnt signaling, hepatic steatosis, fatty acid synthesis, high fat diet, beta-catenin (B-catenin)

1 Introduction

Fatty acid synthesis and oxidation in the liver are critical components of lipid homeostasis. Dysregulation of the balance between fatty acid synthesis and oxidation can lead to the accumulation of lipids within hepatocytes. Non-alcoholic fatty liver disease (NAFLD) is a series of progressive diseases caused by the accumulation of fat in the liver, characterized by increased hepatic triglyceride content in the absence of excessive alcohol consumption (1). In recent years, the prevalence of NAFLD is increasing globally, affecting nearly a quarter of the world's population, and has become the leading cause of chronic liver disease worldwide (2, 3).

Wnt signaling plays multiple functions in liver development, physiology, pathology and especially liver zonation, the abnormities of which has been indicated in the pathogenesis of diet-induced fatty liver and obesity, potentially via regulation of endoplasmic reticulum stress and enzymes involving lipid metabolism (4–6). The canonical Wnt signaling cascade polymerizes on the transcriptional regulator β-catenin, with the end result being nuclear translocation of β-catenin (7). Research in the MacDougald lab was the first to report that Wnt signaling functions as an adipogenesis switch *in vitro*. Specifically, they suggest that Wnt-10b is an endogenous regulator of adipogenesis, and overexpression of Wnt1 in 3T3-L1 preadipocytes can inhibit adipogenesis (8). Wnt1-overexpressing mice was constructed by our team, and we found that Wnt1 overexpression confers significant hepatic protection against ischemia-reperfusion injury (9). Previous studies have shown that persistent activation of the canonical Wnt signaling pathway in preadipocytes *in vivo* can also inhibit adipocyte differentiation, resulting in complete fibrosis of subcutaneous adipose tissue (10). However, recent studies have found that persistent activation of the canonical Wnt pathway leads to the accumulation of fat (4, 6, 11). These researches suggest that the activation of canonical Wnt signaling has regional differences in different adipose tissues, but the exact mechanism remains unclear.

Mammalian target of rapamycin (mTOR) is a serine/threonine protein kinase which downstream of phosphatidylinositol 3-kinase (PI3K)/protein kinase B (Akt) that acts as a central regulator of metabolism and can integrate a variety of nutritional and hormonal signals to control anabolic processes. The two major catalytic subunits of mTOR kinase, mTOR complex 1 (mTORC1) and mTOR complex 2 (mTORC2), provide NADPH necessary for lipid synthesis through regulation of pentose phosphate pathway. Activation of mTOR was associated with increased lipid synthesis and lipid droplets, whereas inhibition of mTOR resulted in higher rates of oxidation (12). Evidence has shown that KIF2C is a direct target of the Wnt/β-catenin pathway, and acts as a key factor in mediating the crosstalk between Wnt/β-catenin and mTORC1 signaling in hepatocellular carcinoma (13). These observations indicate that mTOR signaling may interact with the Wnt/β-catenin pathway in some way. However, no prior studies have explored the molecular mechanisms underlying the potential crosstalk between Wnt/β-catenin and mTOR signaling given a chronic metabolic exposure and injury like high fat diet (HFD). Since both Wnt/β-catenin and mTOR signaling have established roles in regulating hepatic metabolism, the present study was designed to elucidate the relevance and molecular mechanisms governing possible β-catenin/mTOR interactions in the clinical setting of hepatic steatosis in a Wnt/β-catenin activated murine *in vivo* and *in vitro* model under homeostatic conditions and in response to HFD.

2 Materials and methods

2.1 Transgenic mice model

Wnt1+ double transgenic mice were generated to overexpress Wnt1 in hepatocytes (Lap-tta-tetO-Wnt1) under the control of a tetracycline analog (doxycycline) as previously reported (9). Doxycycline water was given in all breeding cages and removed when the mice were 8 to 10 weeks old. After doxycycline withdrawal for 4 weeks, mice were used for experiments. To investigate the effects of Wnt/β-catenin signaling on hepatic steatosis, adult male Wnt1 overexpression transgenic mice (Wnt+) and wild-type (WT) mice were fed a HFD for 12 weeks. All experiments were conducted under a protocol approved by Stanford University School of Medicine Institutional Animal Care and in accordance with NIH guidelines.

2.2 Dietary treatments

To induce hepatic steatosis, mice at age of two months were fed free access to a HFD (BIO-SERV, F3282, Flemington, NJ) for 12 weeks before sacrifice for experiments (14, 15). Control mice were fed a standard control chow diet. Liver/body weight ratio was determined after sacrifice.

2.3 Hepatocellular function

To assess hepatocellular function, blood was obtained by cardiac puncture and serum was collected. Glucose, cholesterol, and triglyceride levels were determined using a standard clinical automatic analyzer.

2.4 Hematoxylin-eosin and oil red O staining

Liver tissues were fixed in 10% formalin, embedded in paraffin and sections were stained with hematoxylin-eosin (H&E). For oil red O (ORO) staining, cells were stained by incubation with 0.3% of filtered ORO solution in 60% isopropanol for 30 minutes at 37°C. The nuclei were counterstained with hematoxylin for 1 minute at room temperature. The cells were then photographed using phase-

contrast microscopy. For quantification of intracellular lipids, cells were scraped by PBS and pelleted by spin down at 13000 rpm for 10 minutes after ORO staining. ORO stain was extracted by adding 0.5 ml of isopropanol for 30 minutes at room temperature. The absorbance of the ORO-containing solution was read at 520 nm using a microplate reader (SpectraMax i3x, Molecular Devices, San Jose, CA) (16). Experiments were performed in triplicate for data summary and statistical analysis.

2.5 Cell culture

The differentiated non-transformed mouse hepatocyte cell lines AML12 cells (American Type Culture Collection, Manassas, VA) and mutant AML12 hepatocytes carrying an amino terminus phosphorylation-resistant point mutation (β-catenin stabilized cells) (S33Y) were derived as previously reported (9) and cultured in DMEM/F12 medium (HyClone Thermal Fisher Scientific, Pittsburgh, PA) supplemented with 10% fetal calf serum at 37°C with 5% CO_2. For induction of steatosis, cells were treated with 150 nM oleic acid (OA) for 24 hours followed by growth with normal medium overnight before being harvested for analysis. For mTOR inhibition, cells were treated with mTOR inhibitor rapamycin at a final concentration of 20 nM for one hour before being harvested for analysis. IWR-1-endo (IWR) was used as a Wnt/β-catenin inhibitor at a final concentration of 20 μM for pre-treatment of cells for 16 hours, and then continue to treat for additional 24 hours with or without 150 nM of OA. For activation of Wnt/β-catenin signaling, Wnt3a (50 ng/ml) and lithium chloride (LiCl, at 10 mM) were pre-incubated with AML12 cells for 16 hours respectively, then continue to treat the cells with or without 150 nM of OA for 24 hours.

2.6 Western blot analysis

Harvested cells after induction with or without OA for 24 hours or mouse liver samples were lysed in RIPA buffer containing protease inhibitor cocktails and sonicated for 10 seconds with the sonicator (Microson). 20μg of samples were added into each lane. Lysates were separated on SDS-polyacrylamide gels followed by immunoblotting with indicated primary antibodies at 4°C overnight according to standard protocol. The antibody Ab-α-tubulin served as a loading control. Reactive protein was visualized with the ECL kit (Amersham Pharmacia Biotech Inc, Piscataway, NJ) according to the manufacturer's protocol. Signals were semi-quantified with Image J software (NIH.gov.USA).

2.7 Co-immunoprecipitation assay

For co-immunoprecipitation (co-IP) assays, cells were lysed in Nonidet P-40 extraction buffer and incubated with 1μg anti-mTOR antibody and protein A/G sepharose beads (Invitrogen, Camarillo, CA) at 4°C overnight. Bead-bound proteins were eluted by incubating in SDS-sample buffer at 95°C for 10 minutes and detected by immunoblotting using β-catenin antibody. Normal rabbit immunoglobulin G was used as a negative control.

2.8 Reagents

The following chemicals and reagents were used: DMEM/F12 medium (Hyclone, UT), fetal bovine serum (FBA), penicillin-streptomycin, trypsin/EDTA, protease inhibitor cocktails (Sigma, ST Louis, MO). ECL kit was from Amersham Bioscience. Other reagents used in this study were analytical grade and obtained from Sigma Chemical. The following antibodies were used in this study: β-catenin, sterol regulatory element binding protein 1(SREBP-1), medium chain acetyl coenzyme A dehydrogenase (MCAD) (Santa Cruz Biotechnology Inc, Santa Cruz, CA), Cyclin D1, phospho-SREBP-1c (Ser372), fatty acid synthase (FASN), acetyl coenzyme A carboxylase (ACC), phospho- acetyl coenzyme A carboxylase (p-ACC), acetyl coenzyme A synthetase (AceCS1), peroxisome proliferator-activated receptor γ (PPAR-γ), Akt, phospho-Akt (Ser437), phospho-Akt (Thr308), S6K, phospho-S6K (p-S6K), mTOR and α-tubulin (Cell Signalling Technology Inc, Danvers, MA), peroxisome proliferator-activated receptor α (PPAR-α) (Abcam, Cambridge, MA).

2.9 Statistics

Each group consisted of at least five animals unless otherwise indicated. Data are expressed as mean ± standard deviation and evaluated by Student's t test (SPSS Statistics, version 19.0, Chicago). The data graphs were made with GraphPad Prism 5.0 software (Graph-Pad Software, CA). Significance was defined as $p<0.05$; "n.s." indicates not significant.

3 Results

3.1 Hepatocyte-specific Wnt1 overexpression induces hepatic steatosis and obesity in HFD-fed mice

Western blot (WB) analysis of proteins from liver tissue confirmed increased β-catenin and Cyclin D1 expression in Wnt+ mice compared to WT controls as a result of activated Wnt signaling (Figure 1A). By abdominal inspection, there was a grossly visible difference in adipose tissue deposits in the Wnt+ mice in response to HFD when compared to WT controls (Figure 1B). To assess the degree of steatosis induced by HFD, we performed H&E and ORO staining. In response to HFD, Wnt+ mice demonstrated increased steatosis with large vacuoles and lipid droplets consistent with macrovascular fatty changes (Figure 1C). In line with these findings, a significantly increased liver/body weight ratio in Wnt+ mice after HFD compared to WT controls ($p=0.0037$) (Figure 1D). Together these findings demonstrate that Wnt signaling activation in hepatocytes leads to hepatic steatosis under HFD.

10.3389/fendo.2023.1289004

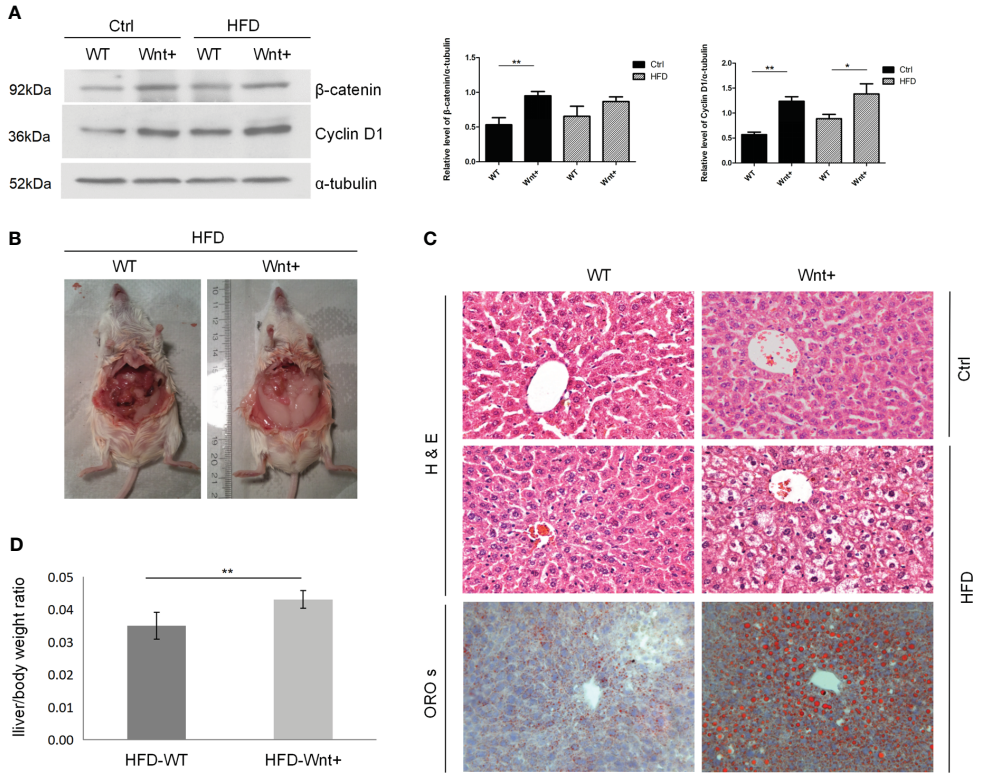

FIGURE 1
Wnt+ mice are more susceptible to liver steatosis under high fat diet. Wild-type and Wnt1 overexpressing (Wnt+) mice were fed with HFD or normal control diet for 12 weeks. **(A)** Immunoblot shows a significant increase in β-catenin and Cyclin D1 protein in Wnt+ livers. α-tubulin served as a loading control. Signals were semi-quantified with Image J software. **(B)** By abdominal inspection, Wnt+ mice demonstrated severe abdominal obesity. **(C)** Representative liver histology of untreated or HFD-treated livers. Severe hepatic steatosis is detected in Wnt+ mice after HFD. H&E staining reveals increased liver steatosis in β-catenin-stabilized livers with lipid accumulation and hepatocytes ballooning. Lipid droplets are detected by ORO staining. **(D)** The liver/body weight ratio was measured after HFD in WT and Wnt+ mice. A significantly increased liver/body weight ratio was observed in Wnt+ mice after HFD compared to WT controls. Data are expressed as means ± SD of three separate experiments. Ctrl control group, HFD high fat diet, WT Wild-type, Wnt+ Wnt1 overexpressing, H&E hematoxylin-eosin, ORO s oil red O staining. *p value<0.05, **p value<0.01.

3.2 Wnt signaling activation in hepatocytes increases fatty acid synthesis in HFD-fed mice liver

Since Wnt-activated livers demonstrated severe steatosis, we questioned whether Wnt signaling might also regulate fatty acid synthesis in the liver. WB analysis was used to compare the expression of various genes involved in adipogenesis in Wnt+ and WT mice. Our results demonstrated that Wnt+ mice showed increased expression of SREBP-1 and its downstream targets ACC, AceCS1, and FASN after 12 weeks of HFD (Figure 2A, lane 4 vs. 3). Interestingly, Wnt+ mice demonstrated significantly impaired medium chain acyl-CoA dehydrogenase (MCAD) expression in both Ctrl and HFD groups (Figure 2A, lane 2 vs. 1 and lane 4 vs. 3) suggesting a failed beta-oxidation of medium-chain triglycerides. Taken together, these findings indicate that mice with activated Wnt signaling demonstrate increased lipogenesis and disrupted β-oxidation.

3.3 The Akt/mTOR pathway is up-regulated in Wnt+ HFD-fed mice

Wnt+ mice demonstrated increased expression of p-Akt at these two residues (Figure 2A, lane 2 vs. 1 and lane 4 vs. 3). mTOR, a target of Akt, was significantly increased in Wnt+ mice in response to HFD (Figure 2A, lane 4 vs. 3). Phospho-S6K, a downstream gene of mTOR, was also increased in Wnt+ mice in response to HFD (Figure 2A, lane 4 vs. 3). All these results indicate mTOR is an important modulator for steatosis in Wnt+ mice. To determine the effect of nutrient stress on Wnt-activated livers, we measured serum cholesterol and triglycerides in Wnt+ and WT mice. As a sign of increased fatty acid synthesis, cholesterol and triglyceride levels were significantly higher in the Wnt+ mice in response to HFD (p=0.015 and p=0.001, respectively.) (Figures 2B, C). Wnt+ mice also exhibited markedly elevated serum glucose levels in response to HFD (p=0.004) (Figure 2D).

10.3389/fendo.2023.1289004

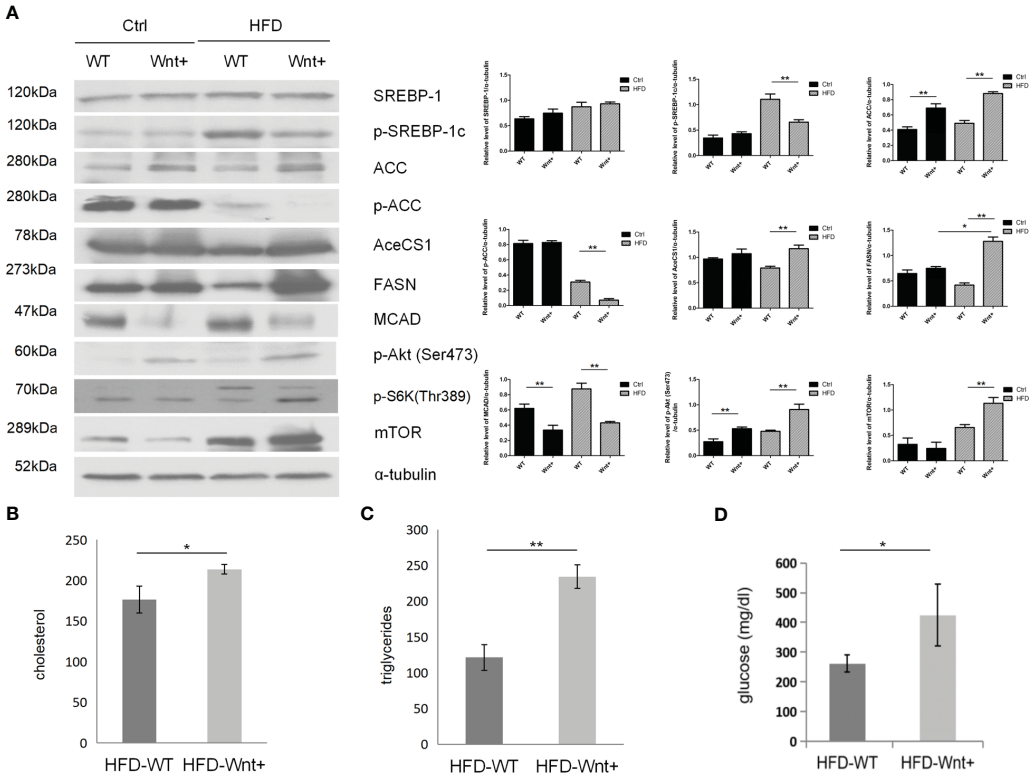

FIGURE 2
Increased fatty acid synthesis in Wnt+ mice under high fat diet. **(A)** Immunoblot shows a significant increase in the expression of fatty acid synthesis-related genes (SREBP-1 and its downstream targets ACC, AceCS1, and FASN) and a decrease in fatty acid oxidation gene (MCAD) in Wnt+ livers under HFD. mTOR and its downstream gene Phospho-S6K were significantly increased in Wnt+ mice in response to HFD. α-tubulin served as a loading control. Increased serum cholesterol **(B)**, triglycerides **(C)**, and glucose **(D)** levels were found in HFD-treated Wnt+ mice when compared to wildtype. WT Wild-type, HFD high fat diet. *p value<0.05, **p value<0.01.

3.4 β-catenin stabilization *in vitro* leads to increased lipid accumulation in hepatocytes with OA via mTOR signaling

S33Y cells demonstrated increased lipid accumulation with 150nM OA treatment as measured by ORO staining (Figure 3A) consistent with the steatotic phenotype seen in the *in vivo* model. The ORO dye was extracted from cells and quantified by absorbance reading which revealed a significant increase of lipid accumulation in the OA-treated S33Y cells compared to AML12 cells (0.19 ± 0.03 vs. 0.08 ± 0.02, p=0.0049) (Figure 3B). WB analysis demonstrates significantly increased expression of the fatty acid synthesis genes PPAR-γ and FASN in S33Y cells after OA treatment (Figure 3C, lane 4 vs. 2). However, this change was less pronounced in wildtype AML12 hepatocytes. (Figure 3C, lane 3 vs. 1).

To test whether increased fatty acid synthesis in S33Y cells is mediated through mTOR signaling, the mTOR inhibitor rapamycin (20nM) was added to interrogate its function as an upstream regulator. Inhibition of mTOR resulted in decreased expression of p-S6K, PPAR-γ, and FASN (Figure 3D, lane 3 vs. 4). Moreover, this similar trend is also shown in human huh7(hepatic cancer) cells (Figure 3D, lane 5 vs. 6).

3.5 β-catenin acts as an upstream regulator of mTOR in fatty acid synthesis.

In order to test whether the effect of β-catenin stabilization on mTOR and fatty acid synthesis can be reproduced through Wnt signaling activation to mimic the *in vivo* findings, the Wnt signaling agonists, Wnt3a and LiCl were added to AML12 cells. In the control (Ctrl) group, even administration of OA did not affect the changes in the expression of lipid synthesis-related gene (mTOR, p-S6K, FASN, and PPAR-γ) (Figure 4A, lane 1 vs. 2). In contrast, in the Wnt3a and LiCl groups, the expression level of lipid synthesis-related genes under the effect of OA was higher than that of levels without OA (Figure 4A, lane 4 vs. 3 and 6 vs. 5). In addition, under the same condition of OA, the expression level of lipid synthesis-related genes in Wnt3a and LiCl groups was higher than that in Ctrl group (Figure 4A, lane 4 vs.2 and 6 vs.2).

After adding IWR (IWR-1-endo, an inhibitor of Wnt-signaling) to AML12 cells, the expression of β-catenin and mTOR was down-regulated (Figure 4B, lane 2 vs. 1 and 4 vs. 3). In addition, after Wnt signaling was inhibited, even under the effect of OA, the expression level of mTOR and FASN did not increase (Figure 4B, lane 4 vs. 2). To further investigate if the activation of mTOR is a result of binding to β-

10.3389/fendo.2023.1289004

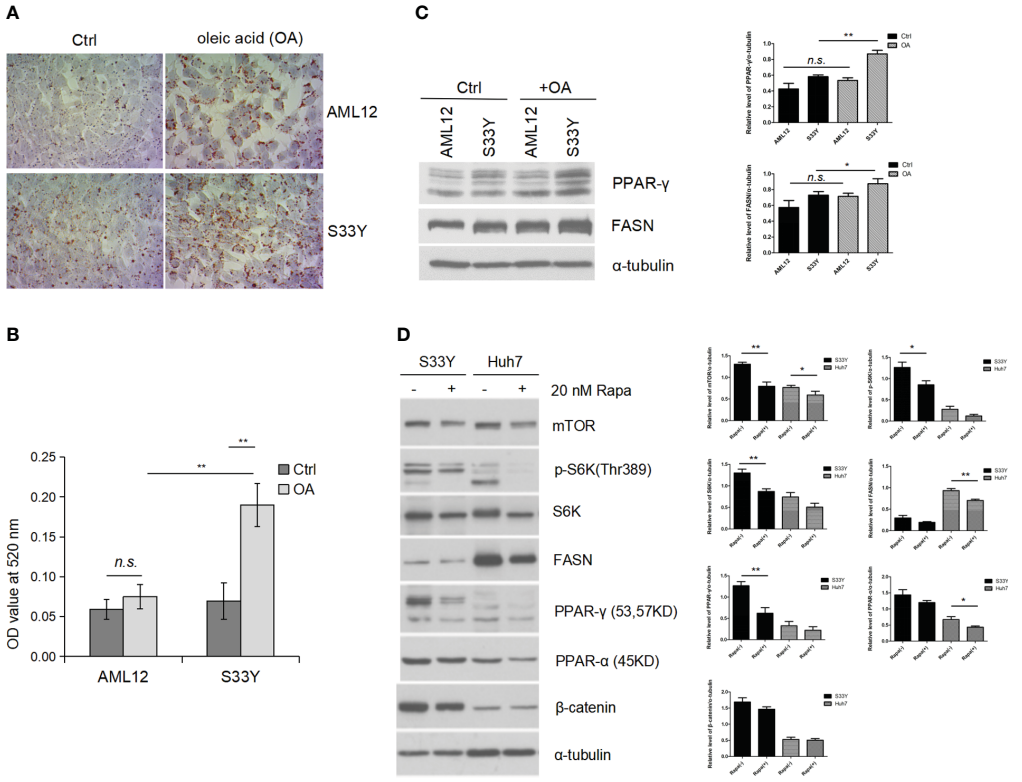

FIGURE 3
Activated Wnt/β-catenin signaling promotes steatosis *in vitro* under oleic acid. AML12 hepatocytes and β-catenin stabilized AML12 (S33Y) cells were treated with 150 nM OA for 24 hours for steatosis induction. **(A)** Increased lipid accumulation was detected in S33Y cells in response to OA treatment compared to AML12 cells as detected by ORO staining. **(B)** For quantification of intracellular lipids, ORO absorbance was measured by spectrophotometer. A significant increase of lipid accumulation in the OA-treated S33Y cells was observed compared to AML12 cells. **(C)** Increased fatty acid synthesis-related genes (PPRA γ, FASN) were up-regulated in S33Y hepatocytes after OA incubation for 24 hours. α-tubulin served as a loading control. **(D)** Cells were treated with the mTOR inhibitor rapamycin at 20 nM for one hour. Inhibition of mTOR led to decreased expression of p-S6K, PPAR-γ, and FASN as detected by immunoblot analysis. OA oleic acid. *p value<0.05, **p value<0.01, n.s., not significant.

catenin, co-IP assays were performed. The results reveal that β-catenin has a physical interaction with mTOR (Figure 4C). These findings suggest that fatty acids can induce and promote formation of β-catenin/mTOR complex.

Taken together these data support a model in which Wnt/β-catenin regulate lipid metabolism in the steatotic liver and function as a molecular regulator for fatty acid synthesis via Akt/mTOR signaling (Figure 5).

4 Discussion

NAFLD, characterized by fat accumulation in the liver, is a wide spectrum of liver diseases ranging from simple fatty liver to non-alcoholic steatohepatitis (NASH), which may progress further to end-stage liver diseases like cirrhosis and hepatocellular carcinoma (17). Behari J, et al. reported that HFD-fed hepatocyte-specific β-catenin transgenic mice rapidly developed diet-induced obesity. Canonical Wnt signaling in hepatocytes is essential for the development of diet-induced fatty liver and obesity (4). On the contrary, reducing β-catenin expression decreases the expression of enzymes involved in hepatic fatty acid esterification, and ameliorates hepatic steatosis (5). In recent years, activation of the Wnt/β-catenin pathway was found to increase lipogenesis in HepG2 cells via regulation of endoplasmic reticulum stress (6). In the present study, we found hepatocyte-specific Wnt1 overexpression induces hepatic steatosis and obesity in HFD-fed mice. However, in a previous study, β-Catenin was considered to act as an anti-adipogenic factor to inhibit the expression of PPAR-γ (18). Therefore, the effects of the Wnt/b-catenin signaling pathway on lipid metabolism are complicated.

Our results demonstrated a significant increase in the expression of fatty acid synthesis-related genes (SREBP-1 and its downstream targets ACC, AceCS1, and FASN) and a decrease in fatty acid oxidation gene (MCAD) in Wnt+ HFD-fed mice livers. SREBP-1 is a master regulator of lipid metabolism and activates a wide range of lipid genes including ACC, acetyl AceCS1, and FASN by binding promoter sites termed sterol regulatory elements (19). MCAD is one of the significant enzymes involved in the β-oxidation of mitochondrial fatty acids. The previous study found that the MCAD levels in the liver were significantly reduced in NASH patients compared to patients without NASH. Moreover, upregulation of MCAD expression also reduced lipid deposition and improved NASH *in vivo* and *in vitro* (20). Therefore, based on the above results, it is concluded that hepatic fat accumulation in Wnt+ HFD-fed mice may be due to increased lipid synthesis and

10.3389/fendo.2023.1289004

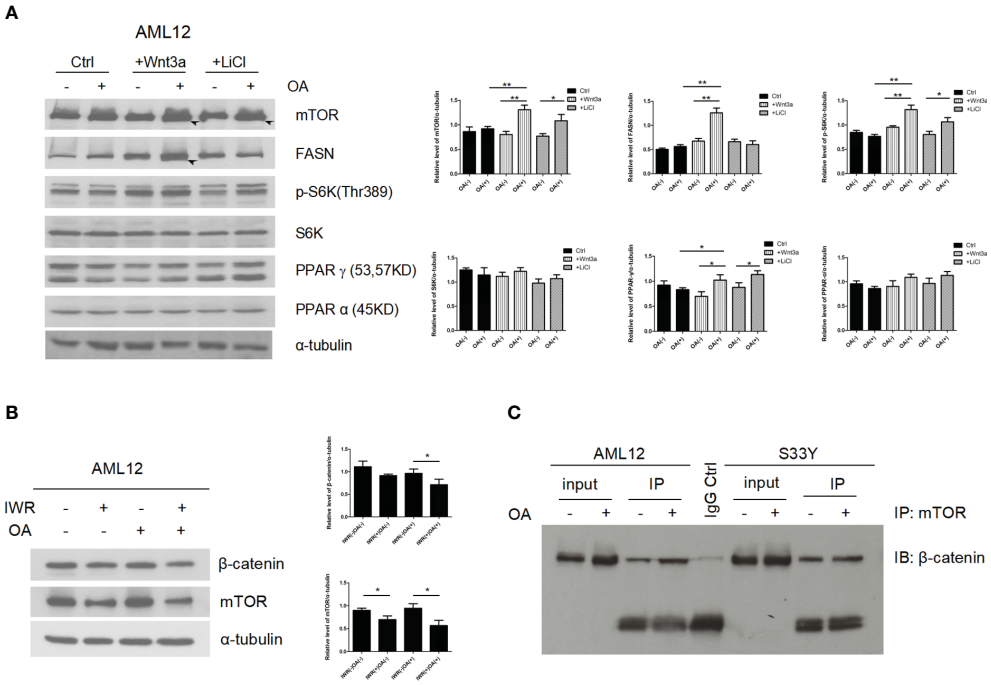

FIGURE 4
β-catenin directly interacts with mTOR signaling to induce lipogenesis. **(A)** Increased expression of lipid synthesis-related genes (mTOR, p-S6K, FASN, and PPAR-γ) were detected by immunoblotting in response to OA when Wnt/β-catenin signaling was activated via Wnt3a or LiCl application (lane 4 vs. 3 and 6 vs. 5). **(B)** After adding IWR (IWR-1-endo, an inhibitor of Wnt-signaling) to AML12 cells, the expression of β-catenin and mTOR was down-regulated (lane 2 vs. 1 and 4 vs. 3). In addition, after Wnt signaling was inhibited, even under the effect of OA, the expression level of mTOR did not increase (lane 4 vs. 2). **(C)** β-catenin has a physical interaction with mTOR, which was verified by co-immunoprecipitation in hepatocytes using anti-mTOR antibody followed by β-catenin immunoblotting. LiCl lithium chloride. Data were shown as mean ± SD of three separate experiments. *P < 0.05, **P < 0.01, based on a Student's t-test.

decreased oxidative catabolism caused by Wnt/β-catenin signaling activation. In addition, we also found that Wnt+ mice demonstrated increased expression of p-Akt (both Ser473 and Thr308). mTOR, a target of Akt, was also significantly increased in Wnt+ mice in response to HFD. These results indicate that the Akt/mTOR pathway is up-regulated in Wnt+ mice with HFD.

To further explore the role and specific mechanisms of Wnt/β-catenin signaling in hepatic steatosis, we selected S33Y and AML12 cells for *in vitro* assays. The results of oil-red O staining demonstrated that there were more lipid droplets in the S33Y cells treated with OA. Moreover, Our result showed that the expression of PPAR-γ and FASN was significantly increased in OA-treated S33Y cells compared to AML12. PPAR-γ is a key regulator of adipogenesis (21). It is well known that PPAR-γ is a key regulator of insulin sensitivity and adipocyte differentiation (22). Previous studies have also shown increased PPAR-γ expression in mice that are fed a high-fat diet to induce hepatic steatosis (23).FASN is an essential enzyme that catalyzes the *de novo* synthesis of long-chain fatty acids (24). Thus, we have again demonstrated *in vitro* that Wnt/β-catenin signaling activation promotes lipogenesis in hepatocytes.

Deregulated mTOR signaling is implicated in the progression of cancer and diabetes, as well as the aging process (25). Moreover, activation of mTOR is associated with increased lipid synthesis and lipid droplets (12). This function is similar to the activation of Wnt/β-catenin signaling found in our study, so we speculate that mTOR signaling may interact with the Wnt/β-catenin pathway in some way. In the present study, our results showed that the expression of both mTOR and its downstream lipid metabolism-related target genes was elevated when Wnt/β-catenin signaling agonists were used. In contrast, mTOR expression was downregulated with the use of Wnt/β-catenin signaling inhibitors. In addition, β-catenin has a physical interaction with mTOR, which was verified by co-immunoprecipitation in hepatocytes. With this study, we extend previous findings and present that β-catenin specifically is important for mTOR signal activation in the liver.

We provide the first evidence of β-catenin directly binding to mTOR to increase fatty acid synthesis in the setting of HFD. However, mTOR complex 1 (mTORC1) signaling has been reported to suppress canonical Wnt/β-catenin signaling to influence stem cell maintenance (26). This indicates that we have not fully discovered its specific mechanism. In addition, we only found that β-catenin and mTOR are linked in terms of physical binding, but the specific mechanism is not fully understood, and more experiments are still needed to confirm it in the future.

5 Conclusion

In summary, we demonstrate that hepatocyte-specific Wnt1 overexpressing mice fed by HFD develop hepatic steatosis and obesity accompanied by increased lipogenesis and disrupted

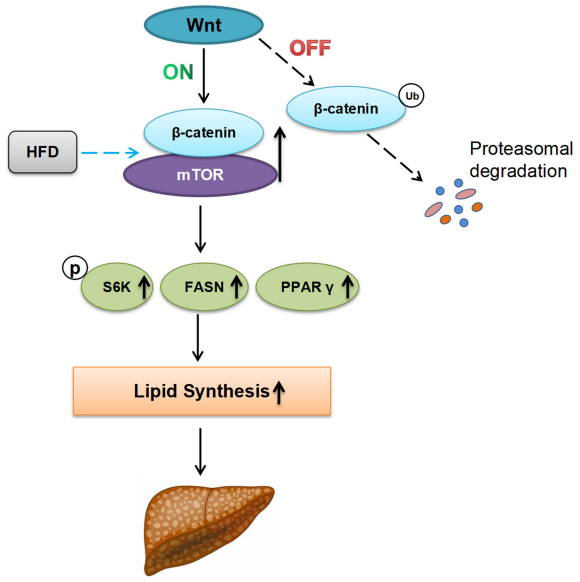

FIGURE 5
Proposed working model describing the possible role of Wnt/β-catenin signaling for hepatosteatosis. In the absence of Wnt-signal (Off-state), ubiquitination and proteasome degradation of β-catenin will occur. Under this condition, the effect of HFD on hepatic fat synthesis is minimal. In the presence of Wnt ligand (On-state), HFD can induce and promote the formation of β-catenin/mTOR complex in the liver, leading to the upregulation of lipid synthesis-related genes (p-S6K, FASN, and PPAR-γ), increasing the lipid synthesis, and the developing of hepatic steatosis finally. Ub ubiquitination, HFD high fat diet, P phosphorylation.

β-oxidation as well as augmented Akt/mTOR signaling. β-catenin stabilization *in vitro* leads to increased lipid accumulation in hepatocytes via mTOR crosstalk. Taken together, β-catenin stabilization through Wnt signaling serves a central role in lipid metabolism in the steatotic liver through up-regulation of fatty acid synthesis via Akt/mTOR signaling. These findings suggest hepatic Wnt signaling may represent a therapeutic strategy in metabolic liver disease.

Data availability statement

The original contributions presented in the study are included in the article/supplementary material. Further inquiries can be directed to the corresponding author.

Ethics statement

Ethical approval was not required for the studies on humans in accordance with the local legislation and institutional requirements because only commercially available established cell lines were used. The animal study was approved by Stanford University School of Medicine Institutional Animal Care. The study was conducted in accordance with the local legislation and institutional requirements.

Author contributions

KW: Writing – original draft. RZ: Writing – review & editing. NL: Writing – original draft. G-ZT: Writing – review & editing. BWL: Writing – review & editing. BL: Writing – review & editing. YK: Writing – review & editing. KS: Writing – review & editing.

Funding

The author(s) declare that no financial support was received for the research, authorship, and/or publication of this article.

Conflict of interest

The authors declare that the research was conducted in the absence of any commercial or financial relationships that could be construed as a potential conflict of interest.

Publisher's note

All claims expressed in this article are solely those of the authors and do not necessarily represent those of their affiliated organizations, or those of the publisher, the editors and the reviewers. Any product that may be evaluated in this article, or claim that may be made by its manufacturer, is not guaranteed or endorsed by the publisher.

References

1. Sarin SK, Kumar M, Eslam M, George J, Al Mahtab M, Akbar S, et al. Liver diseases in the Asia-Pacific region: a Lancet Gastroenterology & Hepatology Commission. *Lancet Gastroenterol Hepatol* (2020) 5:167–228. doi: 10.1016/S2468-1253(19)30342-5

2. Younossi Z, Tacke F, Arrese M, Chander Sharma B, Mostafa I, Bugianesi E, et al. Global perspectives on nonalcoholic fatty liver disease and nonalcoholic steatohepatitis. *Hepatology* (2019) 69:2672–82. doi: 10.1002/hep.30251

3. Wong WK, Chan WK. Nonalcoholic fatty liver disease: A global perspective. *Clin Ther* (2021) 43:473–99. doi: 10.1016/j.clinthera.2021.01.007

4. Behari J, Li H, Liu S, Stefanovic-Racic M, Alonso L, O'Donnell CP, et al. β-catenin links hepatic metabolic zonation with lipid metabolism and diet-induced obesity in mice. *Am J Pathol* (2014) 184:3284–98. doi: 10.1016/j.ajpath.2014.08.022

5. Popov VB, Jornayvaz FR, Akgul EO, Kanda S, Jurczak MJ, Zhang D, et al. Second-generation antisense oligonucleotides against β-catenin protect mice against diet-induced hepatic steatosis and hepatic and peripheral insulin resistance. *FASEB J* (2016) 30:1207–17. doi: 10.1096/fj.15-271999

6. Lei Z, Yang L, Yang Y, Yang J, Niu Z, Zhang X, et al. Activation of Wnt/β-catenin pathway causes insulin resistance and increases lipogenesis in HepG2 cells via

regulation of endoplasmic reticulum stress. *Biochem Biophys Res Commun* (2020) 526:764–71. doi: 10.1016/j.bbrc.2020.03.147

7. Albrecht LV, Tejeda-Muñoz N, De Robertis EM. Cell biology of canonical wnt signaling. *Annu Rev Cell Dev Biol* (2021) 37:369–89. doi: 10.1146/annurev-cellbio-120319-023657

8. Ross SE, Hemati N, Longo KA, Bennett CN, Lucas PC, Erickson RL, et al. Inhibition of adipogenesis by Wnt signaling. *Science* (2000) 289:950–3. doi: 10.1126/science.289.5481.950

9. Lehwald N, Tao GZ, Jang KY, Sorkin M, Knoefel WT, Sylvester KG. Wnt-β-catenin signaling protects against hepatic ischemia and reperfusion injury in mice. *Gastroenterology* (2011) 141:707–18. doi: 10.1053/j.gastro.2011.04.051

10. Zeve D, Seo J, Suh JM, Stenesen D, Tang W, Berglund ED, et al. Wnt signaling activation in adipose progenitors promotes insulin-independent muscle glucose uptake. *Cell Metab* (2012) 15:492–504. doi: 10.1016/j.cmet.2012.03.010

11. Chen M, Lu P, Ma Q, Cao Y, Chen N, Li W. CTNNB1/β-catenin dysfunction contributes to adiposity by regulating the cross-talk of mature adipocytes and preadipocytes. *Sci Adv* (2020) 6:eaax9605. doi: 10.1126/sciadv.aax9605

12. Simcox J, Lamming DW. The central moTOR of metabolism. *Dev Cell* (2022) 57:691–706. doi: 10.1016/j.devcel.2022.02.024

13. Wei S, Dai M, Zhang C, Teng K, Wang F, Li H, et al. KIF2C: a novel link between Wnt/β-catenin and mTORC1 signaling in the pathogenesis of hepatocellular carcinoma. *Protein Cell* (2021) 12:788–809. doi: 10.1007/s13238-020-00766-y

14. Guo J, Jou W, Gavrilova O, Hall KD. Persistent diet-induced obesity in male C57BL/6 mice resulting from temporary obesigenic diets. *PloS One* (2009) 4:e5370. doi: 10.1371/journal.pone.0005370

15. Wall CE, Whyte J, Suh JM, Fan W, Collins B, Liddle C, et al. High-fat diet and FGF21 cooperatively promote aerobic thermogenesis in mtDNA mutator mice. *Proc Natl Acad Sci U S A.* (2015) 112:8714–9. doi: 10.1073/pnas.1509930112

16. Varinli H, Osmond-McLeod MJ, Molloy PL, Vallotton P. LipiD-QuanT: a novel method to quantify lipid accumulation in live cells. *J Lipid Res* (2015) 56:2206–16. doi: 10.1194/jlr.D059758

17. Bhala N, Angulo P, van der Poorten D, Lee E, Hui JM, Saracco G, et al. The natural history of nonalcoholic fatty liver disease with advanced fibrosis or cirrhosis: an international collaborative study. *Hepatology* (2011) 54:1208–16. doi: 10.1002/hep.24491

18. Xu H, Wang J, Chang Y, Xu J, Wang Y, Long T, et al. Fucoidan from the sea cucumber Acaudina molpadioides exhibits anti-adipogenic activity by modulating the Wnt/β-catenin pathway and down-regulating the SREBP-1c expression. *Food Funct* (2014) 5:1547–55. doi: 10.1039/c3fo60716j

19. Shimano H. Sterol regulatory element-binding proteins (SREBPs): transcriptional regulators of lipid synthetic genes. *Prog Lipid Res* (2001) 40:439–52. doi: 10.1016/s0163-7827(01)00010-8

20. Wang Y, Shen QL, Xin Q, Sun B, Zhang S, Fang QH, et al. MCAD activation by empagliflozin promotes fatty acid oxidation and reduces lipid deposition in NASH. *J Mol Endocrinol* (2022) 69:415–30. doi: 10.1530/JME-22-0022

21. Xue P, Hou Y, Zuo Z, Wang Z, Ren S, Dong J, et al. Long isoforms of NRF1 negatively regulate adipogenesis via suppression of PPARγ expression. *Redox Biol* (2020) 30:101414. doi: 10.1016/j.redox.2019.101414

22. Kallwitz ER, McLachlan A, Cotler SJ. Role of peroxisome proliferators-activated receptors in the pathogenesis and treatment of nonalcoholic fatty liver disease. *World J Gastroenterol* (2008) 14:22–8. doi: 10.3748/wjg.14.22

23. Inoue M, Ohtake T, Motomura W, Takahashi N, Hosoki Y, Miyoshi S, et al. Increased expression of PPARgamma in high fat diet-induced liver steatosis in mice. *Biochem Biophys Res Commun* (2005) 336:215–22. doi: 10.1016/j.bbrc.2005.08.070

24. Jiang H, Gan T, Zhang J, Ma Q, Liang Y, Zhao Y. The structures and bioactivities of fatty acid synthase inhibitors. *Curr Med Chem* (2019) 26:7081–101. doi: 10.2174/0929867326666190507105022

25. Saxton RA, Sabatini DM. mTOR signaling in growth, metabolism, and disease. *Cell* (2017) 168:960–76. doi: 10.1016/j.cell.2017.02.004

26. Zeng H, Lu B, Zamponi R, Yang Z, Wetzel K, Loureiro J, et al. mTORC1 signaling suppresses Wnt/β-catenin signaling through DVL-dependent regulation of Wnt receptor FZD level. *Proc Natl Acad Sci U S A.* (2018) 115:E10362–10362E10369. doi: 10.1073/pnas.1808575115

frontiers | Frontiers in Endocrinology

TYPE Original Research
PUBLISHED 08 January 2024
DOI 10.3389/fendo.2023.1280221

OPEN ACCESS

EDITED BY
Sijung Yun,
Predictiv Care, Inc., United States

REVIEWED BY
Cesar Miguel Momesso Santos,
Faculty Enau, Brazil
Hojat Dehghanbanadaki,
Tehran University of Medical Sciences, Iran

*CORRESPONDENCE
Hengqing An
38518412@xjmu.edu.cn
Ning Tao
38518412@qq.com

†These authors share first authorship

RECEIVED 19 August 2023
ACCEPTED 15 December 2023
PUBLISHED 08 January 2024

CITATION
Zhou Y, Li T, Muheiyati G, Duan Y, Xiao S, Gao Y, Tao N and An H (2024) Triglyceride-glucose index is a predictor of the risk of prostate cancer: a retrospective study based on a transprostatic aspiration biopsy population.
Front. Endocrinol. 14:1280221.
doi: 10.3389/fendo.2023.1280221

Triglyceride-glucose index is a predictor of the risk of prostate cancer: a retrospective study based on a transprostatic aspiration biopsy population

Yijie Zhou[1†], Tianqi Li[1†], Guliman Muheiyati[1†], Yajun Duan[1], Songtao Xiao[1], Yi Gao[2], Ning Tao[1,3*] and Hengqing An[4*]

[1]School of Public Health, Xinjiang Medical University, Urumqi, Xinjiang, China, [2]School of Traditional Chinese Medicine, Xinjiang Medical University, Urumqi, Xinjiang, China, [3]Department of Epidemiological Statistics, School of Public Health, Xinjiang Medical University, Urumqi, Xinjiang, China, [4]Department of Urology, The First Affiliated Hospital of Xinjiang Medical University, Urumqi, Xinjiang, China

Background: Current research suggests that prostate cancer (PCa), one of the most common cancers in men, may be linked to insulin resistance (IR).Triglyceride-glucose index (TyG index) was made for a marker of insulin resistance. We investigated the relationship between the TyG index and the risk of PCa.

Objective: To assess the correlation and dose-response relationship between TyG index and prostate cancer.

Method: Retrospectively, 316 patients who required prostate biopsy puncture in the First Affiliated Hospital of Xinjiang Medical University from March 2017 to July 2021 were collected, and the relationship between factors such as the TyG index and prostate cancer was analyzed by Logistic regression model combined with a restricted cubic spline.

Results: (1) The differences in age, initial PSA and TyG index between the two groups were statistically significant; (2) Logistic regression results showed that the risk of prostate cancer in the highest quartile of the TyG index (Q4) was 3.387 times higher than that in the lowest quartile (Q1) (OR=3.387,95% CI [1.511,7.593], P=0.003); (3) The interaction results showed a significant interaction between the TyG index Q4 group and age with the risk of developing prostate cancer (P for interaction<0.001). (4) The results of the restricted cubic spline showed a linear dose-response relationship between the TyG index and the risk of prostate cancer; (5) The Receiver operating characteristic (ROC) curve results showed that the area under the curve (AUC) of the TyG index combined with initial PSA and age was 0.840, with a sensitivity and specificity of 62.5% and 93.3%, respectively.

Conclusion: TyG index and age are risk factors for prostate cancer, and the interaction between the TyG index and different risk factors may increase the risk of prostate cancer. TyG index has some predictive value for the risk of prostate cancer, and the risk of prostate cancer can be reduced by controlling the levels of blood lipids and blood glucose.

KEYWORDS

prostate cancer, triglyceride-glucose index, insulin resistance, endocrinology, urology

1 Introduction

According to GLOBOCAN, in 2020 there will be approximately 1.4 million new cases and 375,000 deaths worldwide from prostate cancer (PCa), the second most common cancer in men and the fifth leading cause of cancer death worldwide (1). And in China, the problem of an ageing population is becoming increasingly serious (2, 3), Prostate cancer incidence and mortality rates are on a significant rise (4–9). Prostate cancer has become a common urological tumor in men, posing a serious risk to human health (1–12). Current factors that may influence prostate cancer are age, family history of tumors, genetic mutations, African ancestry, metabolic syndrome, and others (13–16). Metabolic syndrome is characterized by obesity, insulin resistance (IR), hypertension, and hyperlipidemia (17), and several current studies have demonstrated that insulin resistance is associated with prostate cancer, which can affect the development and progression of Pca through a variety of mechanisms, including the inflammatory pathway (Nuclear Factor Kappa B) (NF-κB) and cytokines, and increase the risk of developing prostate cancer (18–22). The current gold standard for the diagnosis of insulin resistance is Euglycemic-Hyperinsulinemic Clamp (23), but it is slightly cumbersome and expensive to use in practice (24). Studies have demonstrated the high sensitivity of the triglyceride-glucose index (TyG index) for identifying IR (25), the TyG index combines triglycerides (TG) and fasting plasma glucose (FPG), which are important in the diagnosis of IR, so the TyG index can be a reliable proxy for the diagnosis of insulin resistance (26, 27). Elevated TG and FPG have been shown to increase the risk of prostate cancer by Arthur R et al (28–30). And many recent studies have demonstrated that the TyG index is closely associated with the occurrence and development of cancer (31), TyG index can be used as a predictor of breast, colorectal, gastric,thyroid and non-small cell lung cancers (32–42). However, no study has been conducted to illustrate the relationship between TyG index and prostate cancer. Therefore, this study aims to illustrate the relationship between TyG index and prostate cancer, to investigate the dose-response relationship between TyG index and prostate cancer and the predictive value of TyG index in prostate cancer.

Abbreviations: PCa, Prostate cancer; BPH, Benign prostatic hyperplasia; TyG index, Triglyceride-glucose index; PSA, Prostate-specific antigen; FPG, Fasting plasma glucose; TG, Triglyceride; TC, Total cholesterol; ALP, Alkaline phosphatase; LDL, Low-density lipoprotein; BMI, Body mass index; ROC, Receiver operating characteristic; AUC, Area under the curve; CI, Confidence interval; IGF, Insulin-likegrowth factors; IR, Insulin resistance; PI3K, Phosphatidylinositol 3-kinase; Akt, Protein kinase B; NF-κB, Nuclear Factor Kappa B; ERK, Extracellular signal-regulated kinase.

2 Materials and methods

2.1 Study subjects

The examination results of 316 patients who underwent prostate biopsy punctures from March 2017 to July 2021 in the First Affiliated Hospital of Xinjiang Medical University were retrospectively collected and patients were used as study subjects. Patients diagnosed with benign prostatic hyperplasia (BPH) according to histopathology and immunohistochemistry in the Department of Pathology of the First Affiliated Hospital of Xinjiang Medical University were used as the control group, and patients diagnosed with prostate cancer were used as the case group.

2.1.1 Inclusion criteria for the control group

① Those diagnosed with BPH between April 2017 and July 2021 based on histopathology and immunohistochemistry; ② Patients who meet the indications for prostate biopsy punctures; ③ First time prostate biopsy puncture performers; ④ People who are able to read, understand and provide consent.

2.1.2 Exclusion criteria for the control group

① Patients with any type of cancer or previous history of cancer; ② Patients with a history of diabetes mellitus, use of glucose-lowering drugs, use of fenofibrate triglyceride-lowering drugs, and a history of hepatic, renal, or other diseases associated with disorders of lipid metabolism; ③ The data examined are incomplete.

2.1.3 Inclusion criteria for the case group

① Patients diagnosed with prostate cancer based on histopathology and immunohistochemistry between April 2017

and July 2021; ② Patients who meet the indications for prostate biopsy punctures; ③ Patients undergoing their first prostate biopsy puncture with a first diagnosis of prostate cancer; ④ Patients with prostate cancer who were able to read, understand, and provide consent forms and complete medical records.

2.1.4 Exclusion criteria for the case group

① Patients with a history of other types of cancer; ② Patients with a history of diabetes mellitus, use of glucose-lowering drugs, use of fenofibrate triglyceride-lowering drugs, and a history of hepatic, renal, or other diseases associated with disorders of lipid metabolism; ③ The data examined are incomplete.

2.1.5 Indications for performing prostate biopsy punctures

① Patients with persistently elevated prostate-specific antigen (PSA) or greater than 4 ng/ml; ② A hard nodule of the patient's prostate gland was found on physical examination of the prostate gland; ③ Transrectal prostate ultrasound hypoechoic nodules, prostate magnetic resonance abnormal signal nodules; ④ If the patient's first puncture is negative, but with high-grade PIN, etc., and if the patient's prostate-specific antigen is persistently elevated, another prostate puncture biopsy may be performed.

2.2 Study methods

The study was a case-control study in which demographic data such as age, ethnicity, and education level of the study subjects were obtained based on hospital medical record information, and their family history of cancer was also asked; fasting vena cava blood was drawn from the study subjects to determine their initial serum PSA, fasting TG, FPG, blood calcium, testosterone, blood potassium, total cholesterol(TC), low-density lipoprotein (LDL), etc.

In both groups, blood specimens were collected from 8:00 to 9:00 am on the next day of admission in a fasting state, and were immediately sent for examination, and the results were kept. Patients who met the criteria for prostate biopsy were scheduled for transrectal prostate biopsy the day after the examination. Biopsies were performed by a number of senior urologists using the US BARD biopsy needles using the 12+X puncture method, in which 1-2 needles were punctured as the X-needle for suspicious areas suggested on nuclear magnetic resonance imaging or ultrasound, and the rest of the area was punctured by the systematic 12-needle puncture method (43, 44). Each needle of tissue was individually placed into a fixation vial containing 10% methanol aqueous solution, marked with the hospitalization number and date of puncture, and uniformly sent to the Department of Pathology of the First Affiliated Hospital of Xinjiang Medical University for examination, where the histopathological results were recorded and diagnosed by a senior pathologist.

2.2.1 Diagnostic criteria and index definitions

TyG index was calculated from the formula: TyG = LN (fasting TG [mg/gl] * FPG [mg/gl]/2) (45). Body mass index (BMI) = weight (kg)/[height (m)]^2 (46). According to the World Health Organization's criteria for smoking, divided into smokers and non-smokers. Alcohol consumption was also divided into drinkers and non-drinkers according to WHO criteria.

2.2.2 Statistical analysis

The data were analyzed using SPSS 26.0 and R 4.0.5 software. Use nonparametric tests, t-test, and restricted cubic spline plots to test the distribution of continuous data.

Normally distributed data are presented as means (standard deviations), while nonparametric data are expressed as median, minimum and maximum values. Categorical data were expressed as percentages, and the chi-square test was used for comparison between groups. The TyG index was divided into four quartiles according to the interquartile spacing method ('Q1' is<8.389, 'Q2' is 8.389-8.805, 'Q3' is 8.805-9.241, 'Q4' is>9.241), and the odds ratio (OR) of each quartile was calculated using the first quartile as a reference, and logistic regression was used to calculate the OR of the TyG index and prostate cancer. Logistic regression was used to develop correlation models to test the correlation between prostate cancer and the respective variables; model 1 was unadjusted, model 2 was adjusted for age and initial PSA, and model 3 was adjusted for age, initial PSA, smoking history, alcohol consumption, family history of cancer, BMI, TC, and LDL. Logistic regression was used to analyze the interaction between the TyG index and age and initial PSA. The test level $\alpha = 0.05$. The linearity of the dose-response curves was assessed using restricted cubic spline plots and logistic regression models. The Receiver operating characteristic (ROC) curve were applied to assess the predictive value of the TyG index for prostate cancer.

3 Results

3.1 Baseline characteristics

A total of 316 individuals were included. Among them, 136 were in the case group with an age of (70.73 ± 9.80) years. The control group consisted of 180 individuals aged (65.10 ± 8.51) years. The differences in age, initial PSA and TyG index between the two groups were statistically significant (P<0.05) Table 1.

3.2 Logistic regression analysis of factors affecting prostate cancer

The results showed that in model 1, the OR (95% CI) for prostate cancer was 1.000,1.292 (0.679-2.460),1.238 (0.652-2.351), and 2.403 (1.266-4.564) with increasing quartiles of TyG index (P for trend=0.012). In model 2, factors associated with the risk of developing prostate cancer included age (OR=1.056,95% CI [1.020,1.094], P=0.002), initial PSA (OR=1.059,95% CI [1.031,1.088], P<0.001), and TyG index (P for trend=0.001), the risk of prostate cancer in the highest quartile of the TyG index (Q4) was 3.387 times higher than that in the lowest quartile (Q1) (OR=3.387,95% CI [1.511,7.593], P=0.003). In model 3, the OR (95% CI) for prostate cancer was 1.000,0.886 (0.350-2.241),2.065

10.3389/fendo.2023.1280221

TABLE 1 Baseline characteristics of study participants in general.

Variable	Prostate cancer patients (n=136)	People with benign prostatic hyperplasia (n=180)	χ^2/t/w ratio	*P*
Age/[$\overline{x} \pm s$,years]	70.73 ± 9.80	65.10 ± 8.51	-5.345	<0.001
Education level/case (%)			2.989	0.224
Elementary school and below	29(21.30)	26(14.40)		
Middle school including technical secondary school	68(50.00)	104(57.80)		
College and above	39(28.70)	50(27.80)		
Domicile/case (%)			0.001	0.976
City	112(82.40)	148(82.20)		
Countryside	24(17.60)	32(17.80)		
Marital Status/case (%)			<0.001	>0.999
Married	132(97.10)	174(96.70)		
Other	4(2.90)	3(3.30)		
Nationality/case (%)			1.363	0.243
Han	98(72.10)	140(77.80)		
Other	38(27.90)	40(22.20)		
Family history of cancer/case (%)			0.430	0.512
Yes	8(5.90)	14(7.80)		
No	128(94.10)	166(92.20)		
Smoking history/case (%)			1.241	0.265
Yes	36(26.50)	38(21.10)		
No	100(73.50)	142(78.90)		
History of alcohol consumption/case (%)			0.088	0.767
Yes	15(11.00)	18(10.00)		
No	121(89.00)	162(90.00)		
Testosterone/[$M(P_{75},P_{25})$,nmol/L]	15.06(21.08,9.04)	15.68 (21.18,10.18)	0.952	0.342
LDL/[$M(P_{75},P_{25})$,mmol/L]	2.34 (3.10,1.58)	2.44 (3.33,1.55)	1.112	0.267
Blood potassium/[$M(P_{75},P_{25})$,mmol/L]	3.71 (4.16,3.26)	3.67 (4.07,3.27)	-0.820	0.413
TyG Index[$\overline{x} \pm s$]	8.93 ± 0.69	8.74 ± 0.58	-2.751	0.006
TyG Index grouping			8.228	0.042
Q1(<8.389)	28 (20.60)	52 (28.90)		
Q2(8.389-8.805)	32 (23.50)	46 (25.60)		
Q3(8.805-9.241)	32 (23.50)	48 (26.70)		
Q4(>9.241)	44 (32.40)	34 (18.90)		
Initial PSA/ [$M(P_{75},P_{25})$,ng/mL]	25.60(147.33,11.31)	8.10(12.58,6.27)	-9.160	<0.001
BMI/[$M(P_{75},P_{25})$,kg/m^2]	24.00(26.00,21.00)	24.00(26.00,21.00)	-0.403	0.687
ALP/[IU/L]	71.12(98.29,59.48)	71.35 (84.50,61.35)	-0.385	0.700
Blood Calcium/[$M(P_{75},P_{25})$,mmol/L]	2.27(2.33,2.19)	2.29(2.37,2.19)	-0.600	0.549
TC[$M(P_{75},P_{25})$,mmol/L]	4.01(4.68,3.48)	4.26(4.78,3.33)	-0.570	0.569

TyG, index triglyceride-glucose index; Initial PSA, initial prostate-specific antigen; TC, total cholesterol; LDL, low-density lipoprotein; BMI, body mass index; ALP, alkaline phosphatase.

(0.874-4.878), and 2.854 (1.200-6.790) as increasing quartiles of the TyG index (*P* for trend=0.002) Table 2.

3.3 Effect of TyG index interacting with different risk factors on prostate cancer

The interaction results showed a significant interaction between the TyG index Q4 group and age with the risk of developing prostate cancer (*P* for interaction<0.001). Tests for the interaction between TyG index Q2 group (*P* for interaction=0.079), Q3 group (*P* for interaction=0.077), and age and risk of prostate cancer, as well as TyG index Q3 group (*P* for interaction=0.100) and initial PSA and risk of prostate cancer, were not significant Table 3.

3.4 Dose-response relationship between TyG index and prostate cancer

After using restrictive cubic splines and adjusting for relevant confounders, there was a linear dose-response relationship between the TyG index and risk of prostate cancer prevalence (*P* overall<0.05, *P* non-linearity=0.412) Figure 1.

3.5 Predictive value of TyG index, initial PSA, and age on the risk of prostate cancer development

ROC curves for predicting prostate cancer were plotted based on the TyG index, initial PSA, and age. The results showed that the area under the curve (AUC) of TyG index, initial PSA, and age were 0.539, 0.801, and 0.680, respectively, while the AUC of TyG index combined with initial PSA and age was improved to 0.840, with a sensitivity and specificity of 62.5% and 93.3%, respectively. The accuracy of the TyG index combined with initial PSA and age in predicting the risk of prostate cancer was high. See Table 4 and Figure 2.

4 Discussion

In this retrospective study, we investigated the effect of the TyG index on the risk of developing PCa and found for the first time that the TyG index predicts the risk of developing PCa. A meta-analysis showed a strong association between TyG index and cancer development (31),Panigoro S S's study proved that there was a nonlinear dose-response relationship between TyG index and breast cancer (42), but so far no study has illustrated the dose-response relationship between TyG index and the risk of prostate cancer, and the restricted cubic spline model can intuitively describe the relationship between the independent variable and the dependent variable, therefore, the present study applies the restricted cubic spline model to analyze the relationship between the TyG index and the risk of prostate cancer. The results showed that there was a linear dose-response relationship between the TyG index and the risk of prostate cancer, and Logistic regression analysis showed that the risk of prostate cancer in the TyG index Q4 group was 3.387 times higher than that in the Q1 group, suggesting that the TyG index has an important effect on the occurrence and development of prostate cancer. We also used Logistic regression model to analyze the effect of interaction

TABLE 2 Logistic regression analysis of factors affecting prostate cancer.

Variable	Model 1		Model 2		Model 3	
	OR (95%CI)	*P* Value	OR (95%CI)	*P* Value	OR (95%CI)	*P* Value
TyG Index (mmol/L)		0.012[a]		0.001[a]		0.002[a]
Q1(<8.389)	1.000	0.045	1.000	0.006	1.000	0.012
Q2(8.389-8.805)	1.292(0.679-2.460)	0.436	1.041(0.437-2.479)	0.927	0.886(0.350-2.241)	0.737
Q3(8.805-9.241)	1.238(0.652-2.351)	0.514	2.064(0.919-4.636)	0.079	2.065(0.874-4.878	0.112
Q4(>9.241)	2.403(1.266-4.564)	0.007	3.387(1.511-7.593)	0.003	2.854(1.200-6.790)	0.011
Age (years)			1.056 (1.020-1.094)	0.002	1.071 (1.031-1.113)	<0.001
Initial PSA(ng/mL)			1.059(1.031-1.088)	<0.001	1.070(1.039-1.102)	<0.001
Smoking history					1.635(0.779-3.429)	0.194
alcohol consumption					0.527(0.169-1.649)	0.271
Family history of cancer					1.095(0.344-3.482)	0.878
BMI(kg/m2)					1.128(1.023-1.243)	0.016
TC(mmol/L)					0.857(0.706-1.039)	0.116
LDL(mmol/L)					1.058(0.709-1.578)	0.783

TyG, index triglyceride-glucose index; Initial PSA, initial prostate-specific antigen; TC, total cholesterol; LDL, low-density lipoprotein; BMI, body mass index.
Model 1 was unadjusted. Model 2 was adjusted for age and initial PSA. Model 3 adjusted for age, initial PSA, smoking history, alcohol consumption, family history of cancer, BMI, TC, LDL.
[a]P for trend.

10.3389/fendo.2023.1280221

TABLE 3 Effect of interaction between age, initial PSA and TyG index on prostate cancer.

		Initial PSA(ng/mL)	*P* for interaction	Age (years)	*P* for interaction
TyG Index, mmol/L (in quartile)	Q1(n=80)(<8.389)	1.000	0.079	1.000	0.005
	Q2(n=78)(8.389-8.805)	1.106(1.019-1.200)	0.016	1.008(0.999-1.018)	0.079
	Q3(n=80)(8.805-9.241)	1.076(0.986-1.174)	0.100	1.009(0.999-1.018)	0.077
	Q4(n=78)(>9.241)	1.118(1.016-1.231)	0.022	1.018(1.008-1.027)	<0.001

TyG, index triglyceride-glucose index; Initial PSA, initial prostate-specific antigen.

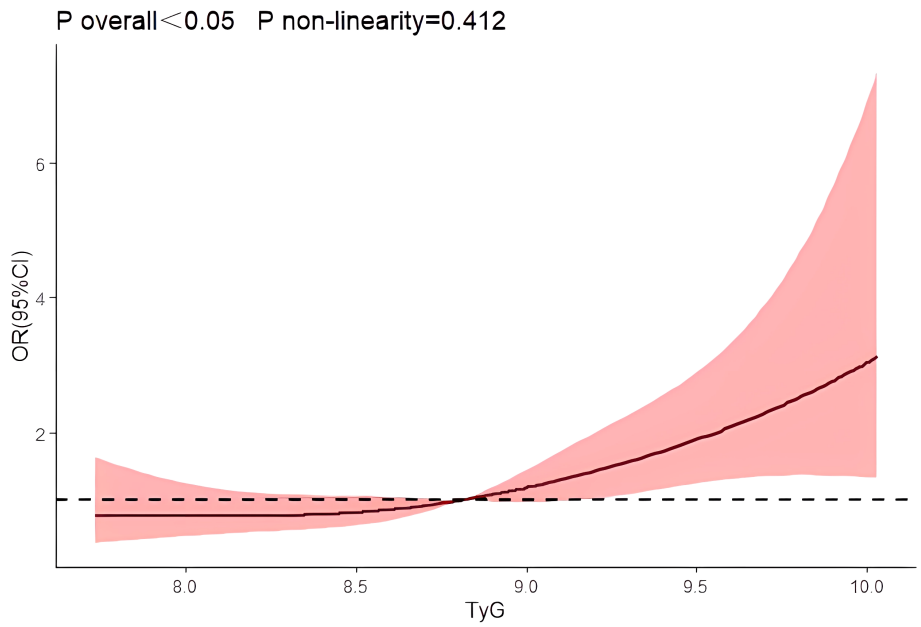

FIGURE 1
Dose-response relationship between TyG index and prostate cancer.

between age, initial PSA and TyG index groups on prostate cancer, and the results showed that there was an interaction between TyG index Q4 group and age and initial PSA, and the interaction between TyG index and different risk factors may increase the risk of prostate cancer. Therefore, we further analyzed the predictive value of TyG index and age on the risk of prostate cancer using ROC curves, and found that the AUCs of TyG index, initial PSA, and age were 0.539, 0.801, and 0.680, respectively. Whereas the AUC of TyG index combined with initial PSA and age was improved to 0.840, with a sensitivity and specificity of 62.5% and 93.3 percent. It indicates that TyG index combined with initial PSA and age has better accuracy than age, initial PSA and TyG index alone in predicting the risk of prostate cancer.

Studies by Albanes D et al. demonstrated that insulin resistance is associated with prostate cancer (20, 47), while Lebovitz HE et al. demonstrated that insulin resistance is associated with such as hyperinsulinemia (48), IGF levels (19, 20), and Phosphatidylinositol 3-kinase (PI3K)/protein kinase B (Akt) signaling pathways (49), which may play an important role in the development of prostate cancer. In patients with insulin resistance, insulin sensitivity is

TABLE 4 ROC curve analysis of TyG index, age, initial PSA, and all three in combination with prostate cancer.

Variables	AUC	95% CI	*P*	Sensitivity	Specificity	Youden's index	Truncation value
TyG Index	0.593	0.530-0.657	0.005	0.434	0.744	0.178	9.091
Initial PSA	0.801	0.750-0.852	<0.001	0.559	0.944	0.503	21.310
Age	0.680	0.620-0.740	<0.001	0.485	0.811	0.296	71.500
TyG Index+Initial PSA+Age	0.840	0.795-0.886	<0.001	0.625	0.933	0.588	0.456

TyG, index triglyceride-glucose index; Initial PSA, initial prostate-specific antigen.

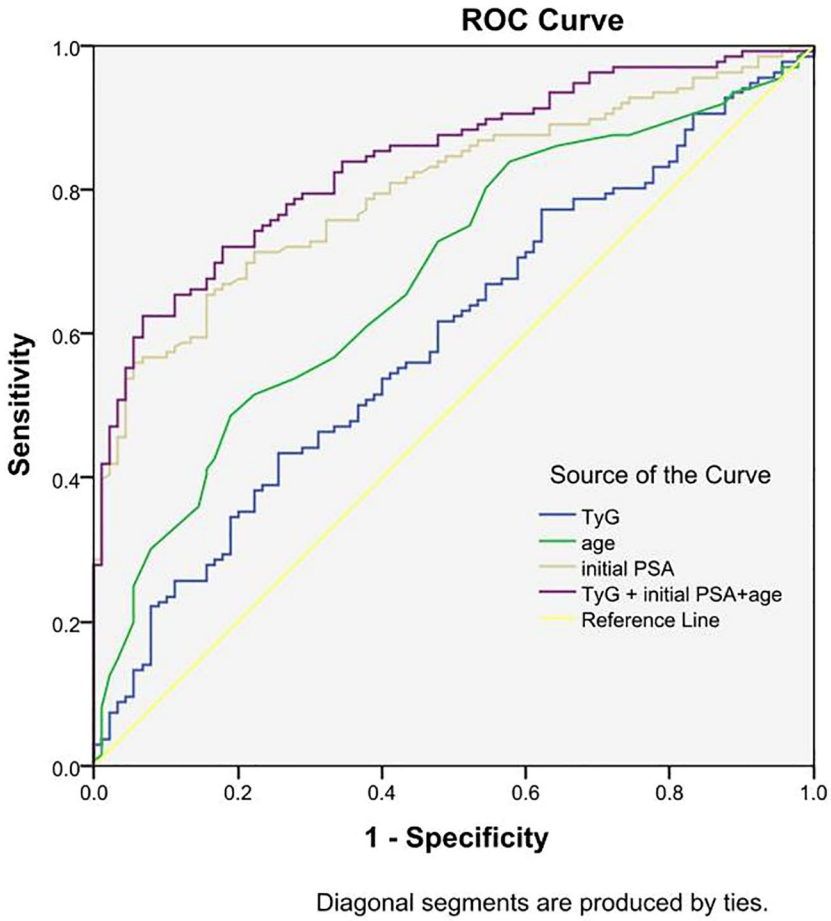

FIGURE 2
Predictive value of TyG index, initial PSA, and age on the risk of prostate cancer.

reduced, the efficiency of glucose uptake and utilization decreases, and the body compensatorily secretes excess insulin, inducing the development of hyperinsulinemia (50). Hyperinsulinemia has been shown to have a direct effect on the liver, inhibiting the production of insulin-like growth factor-binding proteins 1 and 2 (IGFBP-1,-2), while stimulating the production of insulin-like growth factor-1 (IGF-1) and increasing the bioavailability of IGF-1 (51–53). Whereas binding of IGF-1 to the IGF receptor activates the p21 ras/mitogen-activated protein kinase (MAPK) pathway and PI3K/Akt pathway (54). Activation of the MAPK pathway causes activated extracellular signal-regulated kinase (ERK) to translocate to the nucleus, reverse transcription activates transcription factors, alters gene expression, promotes cell growth, differentiation and mitosis, and facilitates PCa cell proliferation (55). Activation of the PI3K/Akt pathway promotes the phosphorylation of BAD that a pro-apoptotic Bcl2 family member in cells, phosphorylation of BAD inhibits the ability of BAD to bind and constrain the anti-apoptotic Bcl2 family members that BclxL and Bcl2, leading to apoptosis resistance in PCa cells, which in turn causes prostate cancer (54, 56). Increased bioavailability of IGF-1, increased binding of IGF-1 and IGF receptors, and increased intensity of IGF-1 action predispose to the induction of prostate cancer.

The TyG index, calculated from fasting triglycerides and blood glucose, was initially proposed as a biomarker of insulin resistance (25, 45), and subsequent studies by Tutunchi H and Lv L et al. have shown it to be associated with diabetes mellitus (57), hepatic fibrosis (58), cardiovascular disease (59), and erectile dysfunction (60). Blood glucose and lipids are important components of the TyG index, and some studies have reported a strong association between them and the development of prostate cancer (61–63). Aljada A et al. showed that hyperglycemia leads to an increase in intranuclear NF-κB in human subjects, that two of the target genes of NF-κB, such as cell cycle protein D1 and cMyc, play important roles in cell growth and proliferation, and that NF-κB itself regulates many genes involved in the process of cell proliferation, tumor formation, and metastasis, thereby influencing cancer development (61, 62). Elevation of body lipids causes enhanced lipid metabolism, which in turn causes enhanced adipocyte metabolism (63). Adipocytes produce inflammatory cytokines and form a protumorigenic environment (64), and periprostatic adipocytes also promote the

extracapsular expansion of prostate cancer through chemokines, which affect the development of prostate cancer (65). In addition, increased fat cell metabolism also increases leptin production, a hormone secreted from fat cells that suppresses appetite and increases basal metabolism through metabolic signaling. It has been suggested that high leptin levels are associated with prostate, colon, breast, and endometrial cancers and that leptin may play a role in this through cell proliferation via MAPK signaling. On the other hand, it has also been suggested that leptin may stimulate angiogenesis, increase matrix metalloproteinase-2 expression, and lead to cancer metastasis (66). In conclusion, elevated blood glucose and lipids can affect the development of prostate cancer through a variety of mechanisms, and there is a correlation between TyG index and prostate cancer.

There are certain limitations in this study: First, this study is a single-center case-control study, there are some limitations in the selection of samples, only some of the influencing factors have been collected, and there is a lack of data on patients from different geographical regions, pending the expansion of the sample size at a later stage and the collection of more comprehensive factors for a multicenter study. Secondly, this study is a cross-sectional survey, only investigated a certain point in time indicators, did not take into account the influence of the trend of the indicators on the results, and the TyG index will be affected by diet-related factors, later we will use this study as a baseline, and carry out a cohort study to further observe the impact of changes in the TyG index on the risk of prostate cancer.

In conclusion, the TyG index is an important influencing factor for prostate cancer and has some predictive value for the risk of prostate cancer, which needs to be further determined in future prospective studies.

5 Conclusions

This study found that the TyG index is a risk factor for prostate cancer, and the interaction between the TyG index and different risk factors may increase the risk of prostate cancer. There is a linear dose-response relationship between the TyG index and the risk of prostate cancer, and the TyG index has a certain predictive value of the risk of prostate cancer, and the risk of prostate cancer can be reduced by controlling the levels of blood lipids and blood glucose. By controlling blood lipid and blood glucose levels, the risk of prostate cancer can be reduced.

Ethics approval and consent to participate

The study involving human participants. The human data used in this study were obtained and applied in accordance with the Declaration of Helsinki. The study was reviewed and approved by the Ethics Committee of First Affiliated Hospital of Xinjiang Medical University (approval number: 20220308-166). Subjects provided written informed consent for participation in this study.

Data availability statement

The original contributions presented in the study are included in the article/Supplementary Material. Further inquiries can be directed to the corresponding authors.

Ethics statement

The studies involving humans were approved by Ethics committee of First Affiliated Hospital of Xinjiang Medical University. The studies were conducted in accordance with the local legislation and institutional requirements. The participants provided their written informed consent to participate in this study. Written informed consent was obtained from the individual(s) for the publication of any potentially identifiable images or data included in this article.

Author contributions

YZ: Methodology, Software, Writing – original draft, Writing – review & editing. TL: Formal analysis, Methodology, Project administration, Validation, Writing – review & editing. GM: Conceptualization, Data curation, Investigation, Writing – review & editing. YD: Investigation, Methodology, Software, Validation, Visualization, Writing – review & editing. SX: Formal analysis, Methodology, Supervision, Visualization, Writing – review & editing. YG: Conceptualization, Project administration, Resources, Writing – review & editing. NT: Data curation, Formal analysis, Methodology, Project administration, Resources, Supervision, Validation, Visualization, Writing – review & editing. HA: Conceptualization, Funding acquisition, Investigation, Resources, Software, Visualization, Writing – review & editing.

Funding

The author(s) declare financial support was received for the research, authorship, and/or publication of this article. This work was supported by Xinjiang Uygur Autonomous Region Natural Science Outstanding Youth Programme (Number: 2023D01E05), the Key Project of Natural Science Foundation of Xinjiang Uygur Autonomous Region (Number: 2022D01D39), Xinjiang Uygur Autonomous Region Tianshan Talent Youth Top-notch Project (Number: 2022TSYCCX0026), National Science and Nature Fund (Number: 82360476) and Xinjiang Medical University's 17th College Students' Innovative Training Program Project (Number: S202210760061).

Acknowledgments

The authors thank all participants and investigators.

Conflict of interest

The authors declare that the research was conducted in the absence of any commercial or financial relationships that could be construed as a potential conflict of interest.

Publisher's note

All claims expressed in this article are solely those of the authors and do not necessarily represent those of their affiliated organizations, or those of the publisher, the editors and the reviewers. Any product that may be evaluated in this article, or claim that may be made by its manufacturer, is not guaranteed or endorsed by the publisher.

Supplementary material

The Supplementary Material for this article can be found online at: https://www.frontiersin.org/articles/10.3389/fendo.2023.1280221/full#supplementary-material

References

1. Sung H, Ferlay J, Siegel RL, Laversanne M, Soerjomataram I, Jemal A, et al. Global cancer statistics 2020: GLOBOCAN estimates of incidence and mortality worldwide for 36 cancers in 185 countries. *Ca-a Cancer J Clin* (2021) 71:209–49. doi: 10.3322/caac.21660

2. Jiang QB, Feng QS. Aging and health in China. *Front Public Health* (2022) 10:998769. doi: 10.3389/fpubh.2022.998769

3. Zhang WL, Liu SF, Du JL, Liu LY, Guo XJ, Xu ZR. A framework of grey prediction models on China's population aging under the perspective of regional differences. *J Grey System* (2022) 34:1–14.

4. He J, Chen WQ, Li N, Cao W, Ye DW, Ma JH, et al. China guideline for the screening and early detection of prostate cancer (2022, Beijing). *Chin J Oncol* (2022) 44:29–53. doi: 10.3760/cma.j.cn112152-20211226-00975

5. Gu XY, Zheng RS, Zhang SW, Zeng HM, Sun KX, Zou XN, et al. Analysis of the incidence trend and age change of prostate cancer in China's tumor registration areas from 2000 to 2014. *Chin J Prev Med* (2018) 52:586–92. doi: 10.3760/cma.j.issn.0253-9624.2018.06.006

6. Liu JZ, Dong L, Zhu YJ, Dong BJ, Sha JJ, Zhu HH, et al. Prostate cancer treatment-China's perspective. *Cancer Lett* (2022) 550. doi: 10.1016/j.canlet.2022.215927

7. He J, Chen WQ, Li N, et al. Guidelines for screening and early diagnosis and treatment of prostate cancer in China (2022 Beijing). *Chin Tumor* (2022) 31:1–30. doi: 10.3760/cma.j.cn112152-20211226-00975

8. Li X, Zeng XY. Advances in epidemiology of prostate cancer in China. *Cancer Prev Res* (2021) 48:98–102. doi: 10.3971/j.issn.1000-8578.2021.20.0370

9. Chinese expert consensus on prostate cancer screening (2021 edition). *Chin J Cancer* (2021) 31:435–40. doi: 10.19401/j.cnki.1007-3639.2021.05.010

10. Nguyen-Nielsen M, Borre M. Diagnostic and therapeutic strategies for prostate cancer. *Semin Nucl Med* (2016) 46:484–90. doi: 10.1053/j.semnuclmed.2016.07.002

11. Groeben C, Wirth MP. Prostate cancer: Basics on clinical appearance, diagnostics and treatment. *Med Monatsschr Pharm* (2017) 40:192–201.

12. Vietri MT, D'Elia G, Caliendo G, Resse M, Casamassimi A, Passariello L, et al. Hereditary prostate cancer: genes related, target therapy and prevention. *Int J Mol Sci* (2021) 22. doi: 10.3390/ijms22073753

13. Pagadala M, Lui A, Lynch J, Panizzon M, Carter H, Hauger R, et al. Healthy lifestyle and Agent Orange exposure modulate inherited prostate cancer risk: An analysis of the Million Veteran Program. (2022). doi: 10.1101/2022.07.09.22277437

14. Fragkoulis C, Glykas I, Tzelves L, Stasinopoulos K, Lazarou L, Kaoukis A, et al. Association of metabolic syndrome with prostate cancer diagnosis and aggressiveness in patients undergoing transrectal prostate biopsy. *Arch Ital Urol Androl* (2021) 93:291–5. doi: 10.4081/aiua.2021.3.291

15. Gomez-Gomez E, Carrasco-Valiente J, Campos-Hernandez JP, Blanca-Pedregosa AM, Jimenez-Vacas JM, Ruiz-Garcia J, et al. Clinical association of metabolic syndrome, C-reactive protein and testosterone levels with clinically significant prostate cancer. *J Cell Mol Med* (2019) 23:934–42. doi: 10.1111/jcmm.13994

16. Zhang JQ, Geng H, Ma M, Nan XY, Sheng BW. Metabolic syndrome components are associated with increased prostate cancer risk. *Med Sci Monitor* (2015) 21:2387–96. doi: 10.12659/msm.893442

17. Lifshitz K, Ber Y, Margel D. Role of metabolic syndrome in prostate cancer development. *Eur Urol Focus* (2021) 7:508–12. doi: 10.1016/j.euf.2021.04.022

18. Li Q, Kuriyama S, Kakizaki M, et al. History of diabetes mellitus and the risk of prostate cancer: the Ohsaki Cohort Study. *Cancer Causes Control* (2010) 21:1025–32. doi: 10.1007/s10552-010-9530-9

19. Burton AJ, Tilling KM, Holly JM, Hamdy FC, Rowlands M-AE, Donovan JL, et al. Metabolic imbalance and prostate cancer progression. *Int J Mol Epidemiol Genet* (2010) 1:248–71.

20. Hsing AW, Gao Y-T, Chua S Jr., Deng J, Stanczyk FZ. Insulin resistance and prostate cancer risk. *J Natl Cancer Institute* (2003) 95:67–71. doi: 10.1093/jnci/95.1.67

21. Mendonça FM, de Sousa FR, Barbosa AL, et al. Metabolic syndrome and risk of cancer: which link? *Metabolism* (2015) 64:182–9. doi: 10.1016/j.metabol.2014.10.008

22. Hotamisligil GS, Shargill NS, Spiegelman BM. Adipose expression of tumor necrosis factor-alpha: direct role in obesity-linked insulin resistance. *Science* (1993) 259:87–91. doi: 10.1126/science.7678183

23. Tam CS, Xie VT, Johnson WD, Cefalu WT, Redman LM. Ravussin E.Defining insulin resistance from hyperinsulinemic-euglycemic clamps. *Diabetes Care* (2012) 35:1605–10. doi: 10.2337/dc11-2339

24. Pranata R, Huang IA, Irvan, Lim MA, Vania R. The association between triglyceride-glucose index and the incidence of type 2 diabetes mellitus-a systematic review and dose-response meta-analysis of cohort studies. *Endocrine* (2021) 74:254–62. doi: 10.1007/s12020-021-02780-4

25. Simental-Mendía LE, Rodríguez-Morán M. Guerrero-Romero F.The product of fasting glucose and triglycerides as surrogate for identifying insulin resistance in apparently healthy subjects. *Metab Syndr Relat Disord* (2008) 6:299–304. doi: 10.1089/met.2008.0034

26. Guerrero-Romero F, Simental-Mendia LE, Gonzalez-Ortiz M, Martinez-Abundis E, Ramos-Zavala MG, Hernandez-Gonzalez SO, et al. The product of triglycerides and glucose, a simple measure of insulin sensitivity. Comparison with the euglycemic-hyperinsulinemic clamp. *J Clin Endocrinol Metab* (2010) 95:3347–51. doi: 10.1210/jc.2010-0288

27. Sanchez-Garcia A, Rodriguez-Gutierrez R, Mancillas-Adame L, Gonzalez-Nava V, Gonzalez-Colmenero AD, Solis RC, et al. Diagnostic accuracy of the triglyceride and glucose index for insulin resistance: A systematic review. *Int J Endocrinol* (2020):4678526. doi: 10.1155/2020/4678526

28. Arthur R, Moller H, Garmo H, Holmberg L, Stattin P, Malmstrom H, et al. Association between baseline serum glucose, triglycerides and total cholesterol, and prostate cancer risk categories. *Cancer Med* (2016) 5:1307–18. doi: 10.1002/cam4.665

29. Murtola TJ, Salli SM, Talala K, Taari K, TammelaL TLJ, Auvinen A. Blood glucose, glucose balance, and disease-specific survival after prostate cancer diagnosis in the Finnish Randomized Study of Screening for Prostate Cancer. *Prostate Cancer Prostatic Dis* (2019) 22:453–60. doi: 10.1038/s41391-018-0123-0

30. Van Hemelrijck M, Garmo H, Holmberg L, Walldius G, Jungner I, Hammar N, et al. Prostate cancer risk in the swedish AMORIS study the interplay among triglycerides, total cholesterol, and glucose. *Cancer* (2011) 117:2086–95. doi: 10.1002/cncr.25758

31. Wang H, Yan FF, Cui YN, Chen FN, Wang GX, Cui WW. Association between triglyceride glucose index and risk of cancer: A meta-analysis. *Front Endocrinol* (2023) 13:1098492. doi: 10.3389/fendo.2022.1098492

32. Okamura T, Hashimoto Y, Hamaguchi M, Obora A, Kojima T, Fukui M. Triglyceride-glucose index (TyG index) is a predictor of incident colorectal cancer: a population-based longitudinal study. *BMC Endocrine Disord* (2020) 20. doi: 10.1186/s12902-020-00581-w

33. Liu T, Zhang QS, Wang YM, Ma XM, Zhang Q, Song MM, et al. Association between the TyG index and TG/HDL-C ratio as insulin resistance markers and the risk of colorectal cancer. *BMC Cancer* (2022) 22. doi: 10.1186/s12885-022-10100-w

34. Shi H, Zhou L, Yang S, Zhou H. The relationship between Triglyceride and glycose (TyG) index and the risk of gynaecologic and breast cancers. *Clin Nutr ESPEN* (2022) 51:345–52. doi: 10.1016/j.clnesp.2022.08.004

35. Karadag I, Karakaya S, Akkan T, Demir B, Alkurt EG, Dogan M. The potential prognostic marker tyG index predicts time to brain metastasis at HER2 positive breast cancer. *Cancer Manage Res* (2023) 15:311–7. doi: 10.2147/cmar.S403445

36. Alkurt EG, Ozkan MB, Turhan VB. Predictive value of triglyceride/glucose index (TyG) in predicting breast cancer in patients with breast mass. *Eur Rev Med Pharmacol Sci* (2022) 26:4671–6.

37. Jung MH, Yi SW, An SJ, Yi JJ, Ihm SH, Han S, et al. Associations between the triglyceride-glucose index and cardiovascular disease in over 150,000 cancer survivors: a population-based cohort study. *Cardiovasc Diabetol* (2022) 21. doi: 10.1186/s12933-022-01490-z

38. Yan X, Gao YJ, Tong JZ, Tian M, Dai JH, Zhuang Y. Association between triglyceride glucose index and non-small cell lung cancer risk in Chinese population. *Front Oncol* (2021) 11:585388. doi: 10.3389/fonc.2021.585388

39. Kim YM, Kim JH, Park JS, Baik SJ, Chun J, Youn YH, et al. Association between triglyceride-glucose index and gastric carcinogenesis: a health checkup cohort study. *Gastric Cancer* (2022) 25:33–41. doi: 10.1007/s10120-021-01222-4

40. Alkurt EG, Sahin F, Tutan B, Canal K, Turhan VB. The relationship between papillary thyroid cancer and triglyceride/glucose index, which is an indicator of insulin resistance. *Eur Rev Med Pharmacol Sci* (2022) 26:6114–20.

41. Jiang J, Teng L. Comment on: "Association between triglyceride-glucose index and gastric carcinogenesis: a health checkup cohort study. *Gastric Cancer* (2021) 24:1370–1. doi: 10.1007/s10120-021-01232-2

42. Panigoro SS, Sutandyo N, Witjaksono F, Siregar NC, Ramli R, Hariani R, et al. The association between triglyceride-glucose index as a marker of insulin resistance and the risk of breast cancer. *Front Endocrinol* (2021) 12:745236. doi: 10.3389/fendo.2021.745236

43. van der Leest M, Cornel E, Israel B, Hendriks R, Padhani AR, Hoogenboom M, et al. Head-to-head comparison of transrectal ultrasound-guided prostate biopsy versus multiparametric prostate resonance imaging with subsequent magnetic resonance-guided biopsy in biopsy-naive men with elevated prostate-specific antigen: A large prospective multicenter clinical study. *Eur Urol* (2019) 75:570–8. doi: 10.1016/j.eururo.2018.11.023

44. Huang C, Huang YH, Pu JX, Xi QL, Wei XD, Qiu F, et al. Comparison of MRI/US fusion targeted biopsy and systematic biopsy in biopsy-naive prostate patients with elevated prostate-specific antigen: A diagnostic study. *Cancer Manage Res* (2022) 14:1395–407. doi: 10.2147/cmar.S350701

45. Du T, Yuan G, Zhang MX, Zhou XR, Sun XX, Yu XF. Clinical usefulness of lipid ratios, visceral adiposity indicators, and the triglycerides and glucose index as risk markers of insulin resistance. *Cardiovasc Diabetol* (2014) 13. doi: 10.1186/s12933-014-0146-3

46. Robinson K, Muir S, Newbury A, Santos-Merx L, Appleton KM. Perceptions of body weight that vary by body mass index:Clear associations with perceptions based on personal control and responsibility. *J Health Psychol* (2022) 27:147–65. doi: 10.1177/1359105320916540

47. Albanes D, Weinstein SJ, Wright ME, Mannisto S, Limburg PJ, Snyder K, et al. Serum insulin, glucose, indices of insulin resistance, and risk of prostate cancer. *J Natl Cancer Institute* (2009) 101:1272–9. doi: 10.1093/jnci/djp260

48. Lebovitz HE. Insulin resistance: definition and consequences. *Exp Clin Endocrinol Diabetes* (2001) 109 Suppl 2:S135–48. doi: 10.1055/s-2001-18576

49. Ramasubbu K, Devi Rajeswari V. Impairment of insulin signaling pathway PI3K/Akt/mTOR and insulin resistance induced AGEs on diabetes mellitus and neurodegenerative diseases: a perspective review. *Mol Cell Biochem* (2023) 478:1307–24. doi: 10.1007/s11010-022-04587-x

50. Kolb H, Kempf K, Röhling M, Martin S. Insulin: too much of a good thing is bad. *BMC Med* (2020) 18:224. doi: 10.1186/s12916-020-01688-6

51. Uzunlulu M, Telci Caklili O, Oguz A. Association between metabolic syndrome and cancer. *Ann Nutr Metab* (2016) 68:173–9. doi: 10.1159/000443743

52. Barnard RJ, Aronson WJ, Tymchuk CN, Ngo TH. Prostate cancer: another aspect of the insulin-resistance syndrome? *Obes Rev* (2002) 3:303–8. doi: 10.1046/j.1467-789x.2002.00081.x

53. Calle EE, Kaaks R. Overweight, obesity and cancer: epidemiological evidence and proposed mechanisms. *Nat Rev Cancer* (2004) 4:579–91. doi: 10.1038/nrc1408

54. Ibrahim YH, Yee D. Insulin-like growth factor-I and cancer risk. *Growth Horm IGF Res* (2004) 14:261–9. doi: 10.1016/j.ghir.2004.01.005

55. Zhang W, Liu HT. MAPK signal pathways in the regulation of cell proliferation in mammalian cells. *Cell Res* (2002) 12:9–18. doi: 10.1038/sj.cr.7290105

56. Chen H, Zhou L, Wu X, et al. The PI3K/AKT pathway in the pathogenesis of prostate cancer. *Front Biosci* (2016) 21:1084–91. doi: 10.2741/4443

57. Selvi NMK, Nandhini S, Sakthivadivel V, Lokesh S, Srinivasan AR, Sumathi S. Association of triglyceride-glucose index (TyG index) with hbA1c and insulin resistance in type 2 diabetes mellitus. *Maedica (Bucur)* (2021) 16:375–81. doi: 10.26574/maedica.2021.16.3.375

58. Tutunchi H, Naeini F, Mobasseri M, Ostadrahimi A. Triglyceride glucose (TyG) index and the progression of liver fibrosis: A cross-sectional study. *Clin Nutr ESPEN* (2021) 44:483–7. doi: 10.1016/j.clnesp.2021.04.025

59. Tao LC, Xu JN, Wang TT, Hua F, Li JJ. Triglyceride-glucose index as a marker in cardiovascular diseases: landscape and limitations. *Cardiovasc Diabetol* (2022) 21:68. doi: 10.1186/s12933-022-01511-x

60. Yilmaz M, Karaaslan M, Tonyali S, Celik M, Toprak T, Odabas O. Triglyceride-Glucose Index (TyG) is associated with erectile dysfunction: A cross-sectional study. *Andrology* (2021) 9:238–44. doi: 10.1111/andr.12904

61. Aljada A, Friedman J, Ghanim H, et al. Glucose ingestion induces an increase in intranuclear nuclear factor kappaB, a fall in cellular inhibitor kappaB, and an increase in tumor necrosis factor alpha messenger RNA by mononuclear cells in healthy human subjects. *Metabolism* (2006) 55:1177–85. doi: 10.1016/j.metabol.2006.04.016

62. Chen C, Edelstein LC, Gélinas C. The Rel/NF-kappaB family directly activates expression of the apoptosis inhibitor Bcl-x(L). *Mol Cell Biol* (2000) 20:2687–95. doi: 10.1128/MCB.20.8.2687-2695.2000

63. Zhou C, Yao L. *Biochemistry and Molecular Biology. Ninth*. Beijing: People's Health Publishing House (2018) p. 152–7.

64. Esposito K, Chiodini P, Colao A, Lenzi A, Giugliano D. Metabolic syndrome and risk of cancer: a systematic review and meta-analysis. *Diabetes Care* (2012) 35:2402–11. doi: 10.2337/dc12-0336

65. Kaiser A, Haskins C, Siddiqui MM, Hussain A, D'Adamo C. The evolving role of diet in prostate cancer risk and progression. *Curr Opin Oncol* (2019) 31:222–9. doi: 10.1097/CCO.0000000000000519

66. Braun S, Bitton-Worms K, LeRoith D. The link between the metabolic syndrome and cancer. *Int J Biol Sci* (2011) 7:1003–15. doi: 10.7150/ijbs.7.1003

frontiers | Frontiers in Endocrinology

TYPE Systematic Review
PUBLISHED 11 January 2024
DOI 10.3389/fendo.2023.1275132

OPEN ACCESS

EDITED BY
Princy Francis,
Mayo Clinic, United States

REVIEWED BY
Jesus M. Martin-Campos,
Institut de Recerca de l'Hospital de la Santa Creu i Sant Pau, Spain
Robert Kiss,
McGill University, Canada

*CORRESPONDENCE
Yongqiang Deng
york6332@163.com

†These authors have contributed equally to this work

RECEIVED 09 August 2023
ACCEPTED 19 December 2023
PUBLISHED 11 January 2024

CITATION
Zeng L, Tang H, Chen J, Deng Y, Zhao Y, Lei H, Wan Y, Pan Y and Deng Y (2024) Causal association of lipoprotein-associated phospholipids on the risk of sepsis: a Mendelian randomization study.
Front. Endocrinol. 14:1275132.
doi: 10.3389/fendo.2023.1275132

Causal association of lipoprotein-associated phospholipids on the risk of sepsis: a Mendelian randomization study

Liying Zeng[1†], Haoxuan Tang[1†], Jiehai Chen[2†], Yijian Deng[3], Yunfeng Zhao[1], Hang Lei[1], Yufei Wan[1], Ying Pan[1] and Yongqiang Deng[1*]

[1]Guangdong Provincial Key Laboratory of Proteomics, State Key Laboratory of Organ Failure Research, Department of Pathophysiology, School of Basic Medical Sciences, Southern Medical University, Guangzhou, China, [2]Department of Anesthesiology, Nanfang Hospital, Southern Medical University, Guangdong Provincial Key Laboratory of Precision Anaesthesia and Perioperative Organ Protection, Guangzhou, Guangdong, China, [3]School of Traditional Chinese Medicine, Southern Medical University, Guangzhou, Guangdong, China

Background: Many previous studies have revealed a close relationship between lipoprotein metabolism and sepsis, but their causal relationship has, until now, remained unclear. Therefore, we performed a two-sample Mendelian randomization analysis to estimate the causal relationship of lipoprotein-associated phospholipids with the risk of sepsis.

Materials and methods: A two-sample Mendelian randomization (MR) analysis was performed to investigate the causal relationship between lipoprotein-associated phospholipids and sepsis based on large-scale genome-wide association study (GWAS) summary statistics. MR analysis was performed using a variety of methods, including inverse variance weighted as the primary method, MR Egger, weighted median, simple mode, and weighted mode as complementary methods. Further sensitivity analyses were used to test the robustness of the data.

Results: After Bonferroni correction, the results of the MR analysis showed that phospholipids in medium high-density lipoprotein (HDL; OR_{IVW} = 0.82, 95% CI 0.71-0.95, P = 0.0075), large HDL (OR_{IVW} = 0.92, 95% CI 0.85-0.98, P = 0.0148), and very large HDL ($OR_{MR\ Egger}$ = 0.83, 95% CI 0.72-0.95, P = 0.0134) had suggestive causal relationship associations with sepsis. Sensitivity testing confirmed the accuracy of these findings. There was no clear association between other lipoprotein-associated phospholipids and sepsis risk.

Conclusions: Our MR analysis data suggestively showed a correlation between higher levels of HDL-associated phospholipids and reduced risk of sepsis. Further studies are required to determine the underlying mechanisms behind this relationship.

KEYWORDS

lipoprotein-associated phospholipids, sepsis, Mendelian randomization, causal relationship, genetics

Introduction

In 2016, the Third International Consensus Definition for Sepsis and Septic Shock (Sepsis-3) defined sepsis as a life-threatening organ dysfunction resulting from dysregulated host responses to infection, and emphasized the primacy of the non-homeostatic host response to infection (1). Sepsis is a life -threatening disease with a high incidence and it remains one of the main causes of death globally. In 2017, an estimated 48.9 million incident cases of sepsis and 11 million sepsis-related deaths were reported worldwide, representing 19.7% of all global deaths (2). Sepsis is therefore significant public health problem with considerable economic consequences.

Based on differences in density, size, lipid and apolipoprotein composition, lipoproteins can be divided into five main subcategories: chylomicrons, very low-density lipoprotein (VLDL), low-density lipoprotein (LDL), intermediate-density lipoprotein (IDL) and high-density lipoprotein (HDL) (3). The lipids found in HDL are mainly surface phospholipids, internal cholesterol esters, and triglycerides. Phospholipids are mainly phosphatidylcholine, lysophosphatidylcholine, and sphingomyelin, each accounting for 32 – 35 mol%, 1.4 – 8.1 mol%, and 5.6 – 6.6 mol % of total lipids in HDL, respectively (4). At present, various activities of HDL have been reported, mainly including anti-inflammatory, anti-oxidative, immunomodulatory, anti-apoptotic, endothelial, and anti-thrombotic functions (5–8). Studies have shown that serum and HDL phospholipids are significantly reduced after a single intravenous dose of endotoxin (9). Phospholipids have also been suggested to play a specific role in HDL's protective capacity against the pro-inflammatory effects of C-reactive protein (CRP). A study has shown that HDL blocks the upregulation of CRP-induced inflammatory adhesion molecules through its phospholipid components (10). In addition, when recombinant HDL made with HDL apolipoprotein and phosphatidylcholine (PC) instead of saline was administered intravenously 3.5 hours before a single intravenous dose of endotoxin, healthy volunteers showed fewer flu-like symptoms and lower plasma inflammatory cytokines (11). These data suggest that the anti-inflammatory and immunomodulatory effects of HDL are closely related to its phospholipids. Although Mendelian randomization (MR) analysis has shown a causal relationship between high levels of high-density lipoprotein cholesterol and a reduced risk of infectious hospitalizations (12). However, the causal relationship between HDL-related phospholipids and infectious diseases or sepsis is unclear.

One observational study identified a reduction in LDL, HDL, and HDL-associated apolipoproteins in non-survivors of sepsis compared with survivors (13). LDL can reduce sepsis-associated lipopolysaccharide (LPS) damage by binding to LPS (14). In mouse models, the lethal effects of LPS were prevented by removing LDL receptor-induced high endogenous LDL levels (15). Thus, LDL can partially reduce the degree of LPS-induced post-inflammatory acute phase response. Other studies have shown that triglyceride-rich lipoproteins, such as chylomicrons and VLDL, also can inactivate LPS and prevent endotoxin-induced rodent deaths (16–18). IDL is a residual lipoprotein produced by VLDL hydrolysis. In a large study of more than 7,000 participants, endotoxemia was found to be associated with high concentrations of VLDL, IDL, and LDL particles, as well as low concentrations of HDL particles (19). Although the surface of all lipoproteins is composed of phospholipids, mainly PC and sphingomyelins (SM), there are significant differences in phospholipid species for different lipoproteins. Therefore, various lipoproteins and their phospholipids have different functions, and this study aims to explore the causal relationship between lipoprotein- associated phospholipids and sepsis.

Mendelian randomization (MR) refers to a statistical method based on genome-wide association studies (GWAS) that use genetic variation as instrumental variables (IVs) to assess the causality of observed associations between modifiable exposures or risk factors and clinically relevant outcomes (20). MR minimizes traditional confounding and reverses causation because genetic variants are randomly distributed during meiosis and are independent of environment, disease onset, and progression (21). Therefore, MR is not affected by the confounding

Abbreviations: MR, Mendelian randomization; GWAS, Genome-wide association study; IVW, Inverse variance weighted; MR-Egger, Mendelian randomization-Egger; OR, Odds ratio; CI, Confidence interval; SNP, Single nucleotide polymorphism; IV, Instrumental variable; HDL, High-density lipoprotein; LDL, Low-density lipoprotein; IDL, Intermediate-density lipoprotein; VLDL, Very low-density lipoprotein; LPS, Lipopolysaccharide; CRP, C-reactive protein; PC, Phosphatidylcholine; SM, Sphingomyelin; MAF, Minor allele frequency; LD, Linkage disequilibrium; S1P, Sphingosine 1-phosphate; PLTP, Phospholipid transfer active protein; EL, Endothelial lipase.

biases found in traditional observational studies. Based on this knowledge, we applied a two-sample MR analysis to comprehensively investigate the genetic association of lipoprotein-associated phospholipids with sepsis. The results of this study may offer novel strategies for personalized treatments for sepsis.

Materials and methods

MR analysis

MR uses genetic variation as a tool variable to assess non-confounding causal relationships between exposure and outcome and it must satisfy the following three assumptions (22): (1) There is a strong correlation between instrumental variables and exposure factors, (2) there is no connection between instrumental variables and confounding factors, and they are independent of each other, (3) the instrumental variables are associated with outcomes only by exposure, and there is no direct correlation. A flowchart of causal reasoning for lipoprotein-associated phospholipids and sepsis is depicted in Figure 1. In short, lipoprotein-associated phospholipids were classed as the exposure and sepsis was the result. Single nucleotide polymorphisms (SNPs) significantly associated with lipoprotein-associated phospholipids were selected as IVs based on strict inclusion and exclusion criteria. A series of heterogeneity and sensitivity analyses were performed to identify significant associations.

Data sources

This study used publicly available databases. Up to 24,925 individuals were tested in 14 genotype datasets from 10 European studies using additive genetic models. A genome-wide single nucleotide polymorphism (SNP) panel of 39 million genetic markers was tested for univariate associations with the concentrations of lipids and metabolites in 123 humans quantified by high-throughput NMR spectroscopy metabolomics. Individual lipoprotein phospholipids were analyzed using a high-throughput serum Nuclear Magnetic Resonance (NMR) metabolomics platform. The method provided serum measurement information, including lipoprotein subclass distribution and lipoprotein particle concentration, as well as detailed molecular information of serum lipids, including free and esterified cholesterol, sphingomyelin, and fatty acid saturation. (23). Individuals on lipid-lowering medications or pregnant individuals were excluded from the analyses. Genetic statistics for sepsis were derived from the UK Biobank, and we identified 11,643 cases of sepsis, with 474,841 controls of European ancestry. All cases were adjusted for age, sex, chip, and the first 10 principal component analysis.

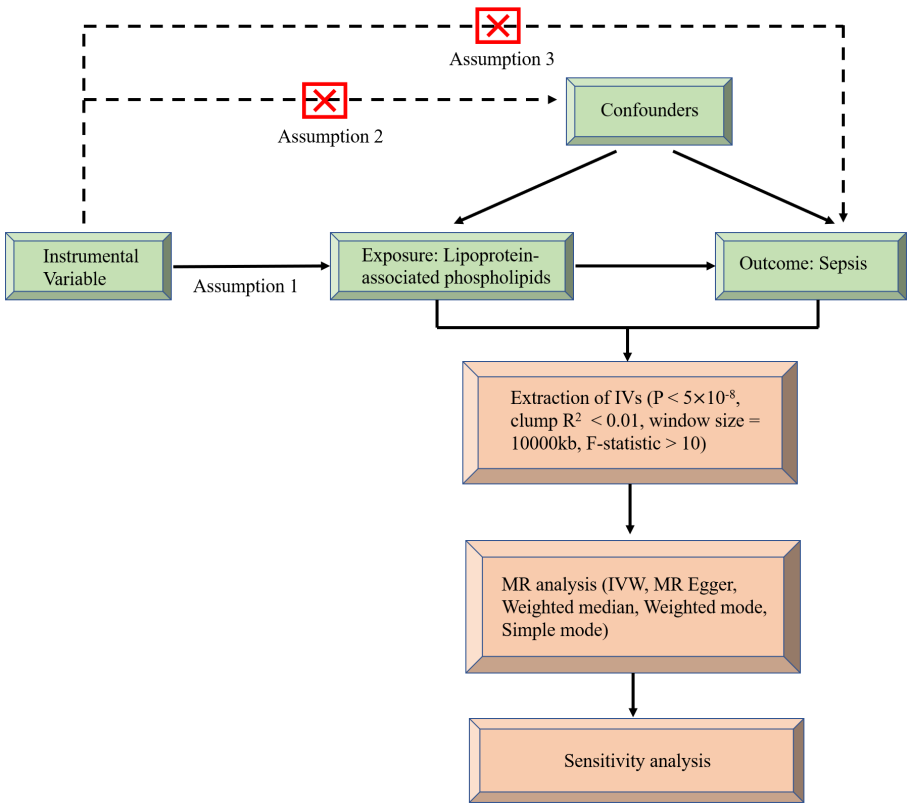

FIGURE 1
Flow chart of causal inference between lipoprotein-associated phospholipids and sepsis.

10.3389/fendo.2023.1275132

Selection of IVs

We extracted qualified IVs according to strict selection criteria. First, we selected independent SNPs closely related to various lipoprotein-associated phospholipids and $P < 5\times10^{-8}$ as potential IVs, respectively. Second, the European-based 1,000 Genome Projects reference panel was used to calculate the linkage disequilibrium (LD) and the threshold for clumping was set to $R^2 < 0.01$, while the clumping window size was set to 10,000 kb. Third, SNPs with palindromic and a minor allele frequency (MAF) of less than 0.3 were also eliminated. Finally, IV strength was assessed using the F-statistic to further extract SNPs that were closely related to the exposure. If F > 10, the results should not suffer from weak instrument bias (24).

Statistical analysis

R version 4.3.0 (R Foundation for Statistical Computing, Vienna, Austria) and the Two-Sample MR package were used for statistical analyses (25). *P* values < 0.05 were to be statistically significant. We performed MR analysis in five different ways: inverse variance weighted (IVW) as the primary method, MR Egger, weighted median, simple mode, and weighted mode as complementary methods (26–28).

We used Cochran's Q statistic to detect heterogeneity in MR analyses, with *P* values > 0.05 indicating no heterogeneity (25). If heterogeneity was present, the random-effects model of the IVW method was used. If heterogeneity was absent, then a random-effects analysis was equivalent to a fixed-effect analysis. (29, 30). MR Egger regression was used to examine the effect of horizontal pleiotropy, and *P* values > 0.05 were indicative of no horizontal pleiotropy (31). Therefore, in the absence of pleiotropy, the IVW analysis method was preferred, and in the presence of pleiotropy, the MR Egger regression method was used (32). MR Egger regression can detect pleiotropy. To test the effect of each SNP on the results, we used leave-one-out analysis to determine whether the estimates were biased or driven by outliers (30). We corrected multiple comparisons using the Bonferroni method and set the statistical significance to P < 0.0042 (0.05/12) based on the number of exposures. If the P value was between 0.0042 and 0.05, we considered suggestive evidence of the potential causal associations (33).

Results

Using the above method, SNPs were screened for this study and details of the selected SNPs are shown in Table S1. Further, the causal effects of each SNP on sepsis are shown in the forest plot (Figure S1).

In the MR analysis, we used a variety of methods to assess the causal relationship between lipoprotein-associated phospholipids and

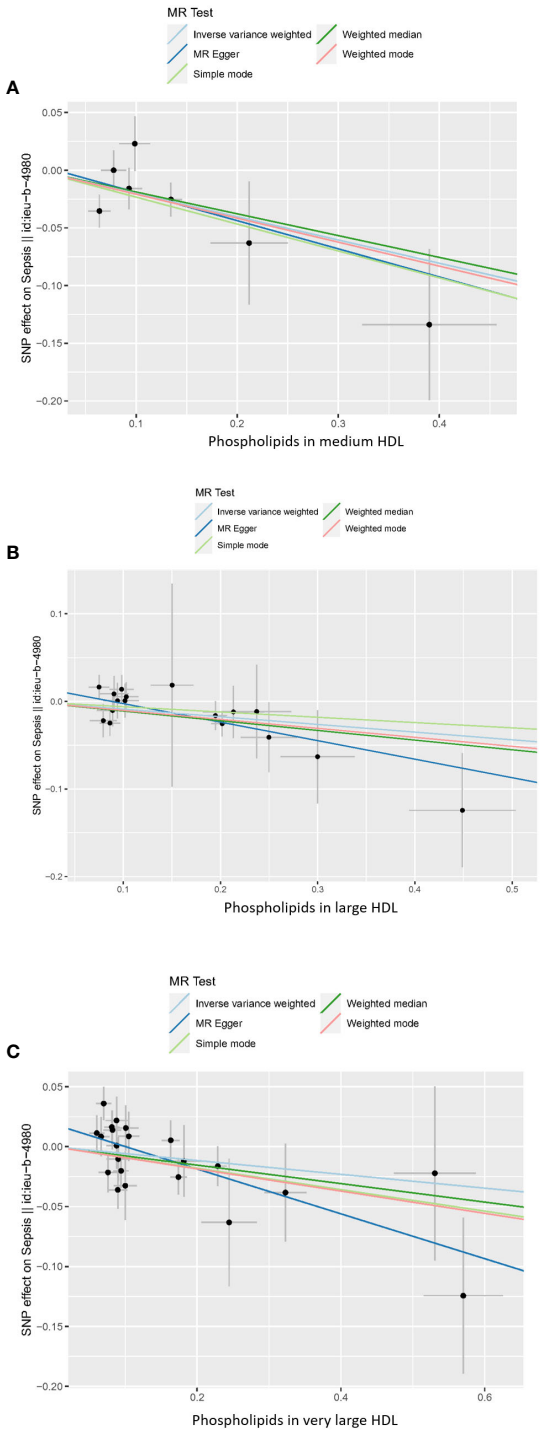

FIGURE 2
Scatter plot of the causal relationship between HDL-associated phospholipids and sepsis. **(A)** Phospholipids in medium HDL. **(B)** Phospholipids in large HDL. **(C)** Phospholipids in very large HDL. Analyses were conducted using IVW, weighted median, weighted mode, simple mode, and MR Egger methods. The slope of the line indicates the magnitude of the causal relationship. Error bars indicate 95% CI. MR, mendelian randomization; SNP, single nucleotide polymorphism.

10.3389/fendo.2023.1275132

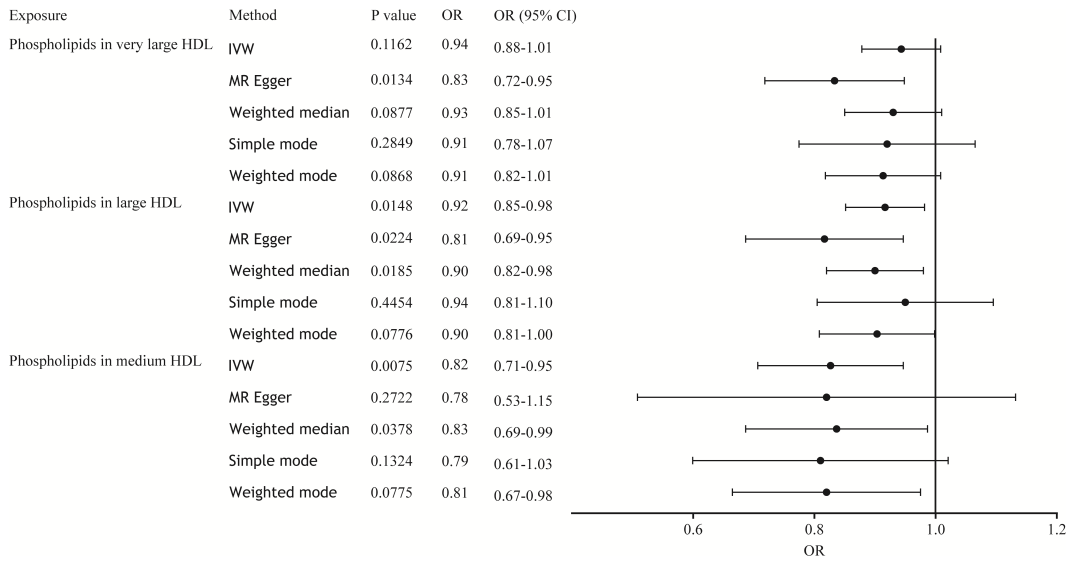

FIGURE 3
Forest plot of the causal relationship between HDL-associated phospholipids and sepsis. The black dots represent the OR value obtained by each method and the solid line represents the 95% CI. IVW, inverse variance weighted; MR, Mendelian randomization; OR, odds ratio; CI, confidence interval.

sepsis. The results of the MR analysis suggestively showed that HDL-associated phospholipids are causally related to sepsis (Figure 2). Phospholipids in medium HDL (OR_{IVW} = 0.82, 95% CI 0.71-0.95, P = 0.0075) and phospholipids in large HDL (OR_{IVW} = 0.92, 95% CI 0.85-0.98, P = 0.0148) were negatively associated with sepsis. Due to the pleiotropy of phospholipids in very large HDL, the MR Egger regression method was used ($OR_{MR\ Egger}$ = 0.83, 95% CI 0.72-0.95, P = 0.0134). However, phospholipids in LDL, IDL, VLDL, and chylomicrons were not causally associated with sepsis (Figure S2; Table S2). Thus, only three HDL-associated phospholipids (phospholipids in medium HDL, phospholipids in large HDL, and phospholipids in very large HDL) suggestively showed significant causal relationship associations with sepsis (Figure 3).

In sensitivity analysis, we performed heterogeneity, pleiotropy, and leave-one-out analysis to assess the reliability and robustness of the results (Table 1). Cochran's Q test showed no heterogeneity between IVs (phospholipids in medium HDL, P_{IVW} = 0.277, $P_{MR\ Egger}$ = 0.1914; phospholipids in large HDL, P_{IVW} = 0.7786, $P_{MR\ Egger}$ = 0.8902; phospholipids in very large HDL, P_{IVW} = 0.1084, $P_{MR\ Egger}$ = 0.2545). The symmetry of the funnel plot also confirmed the absence of heterogeneity, suggesting that causal associations were less likely to be affected by potential bias (Figure S3). Therefore, the random-effects model of the IVW method was used. To reduce bias due to horizontal pleiotropy, we performed MR Egger intercept testing, which showed that overall horizontal pleiotropism was absent in all IVs (phospholipids in medium HDL, P = 0.8224; phospholipids in large HDL, P = 0.1190). When horizontal pleiotropy is present, the MR Egger regression method can be used in MR analysis (phospholipids in very large HDL, P = 0.0435). The leave-one-out analysis (Figure S4) showed no substantial difference in the estimated causal effect when

TABLE 1 Heterogeneity and pleiotropy analysis of MR.

Exposure	Analysis	Methods	Effect size	*P* value
Phospholipids in medium HDL	Heterogeneity	Cochran's Q test	7.501 (Q_{IVW})	0.277
			7.418($Q_{MR\ Egger}$)	0.1914
	Pleiotropy	MR Egger regression	0.0051 (egger_intercept)	0.8224
Phospholipids in large HDL	Heterogeneity	Cochran's Q test	11.4849 (Q_{IVW})	0.7786
			8.7506 ($Q_{MR\ Egger}$)	0.8902
	Pleiotropy	MR Egger regression	0.0186 (egger_intercept)	0.119
Phospholipids in very large HDL	Heterogeneity	Cochran's Q test	29.2373 (Q_{IVW})	0.1084
			23.7268($Q_{MR\ Egger}$)	0.2545
	Pleiotropy	MR Egger regression	0.0188(egger_intercept)	0.0435

individual SNPs were systematically removed and the MR analysis was repeated. This showed a strong association between exposure and outcomes, thereby validating the reliability of the results of this study.

Discussion

The inference of causality in genetics was usually made by MR analysis. MR analysis was a form of instrumental variable analysis in which genetic marker SNPs were often used as tools to infer the causal effects of exposure variables on outcome variables. SNPs were the basis of genetic polymorphisms and lead to most of the genetic differences between individuals. It was well known that SNPs had a close relationship with disease, and this relationship was the basis for understanding the etiology, medical prevention, and diagnosis of disease. Studies had found that various genetic and environmental factors could lead to abnormalities in blood lipids and lipoproteins, and it could be seen that plasma lipid and lipoprotein concentrations were highly heritable. In addition, in the field of lipid and lipoprotein metabolism, almost 30 different genes encoding key proteins had been implicated, and more than 200 different SNPs had been identified in these genes (34). The genetic variability involved could affect the final plasma lipid levels. The two-sample MR analysis used in this study showed that HDL-associated phospholipids had a suggestive causal relationship with sepsis. There were no clear associations between other lipoprotein-associated phospholipids and sepsis risk, including LDL, IDL, VLDL-associated phospholipids, and phospholipids in chylomicrons.

Sepsis remains the leading cause of morbidity and mortality worldwide, and its pathogenesis is complex and involves multiple interactions between infecting microorganisms and the host. Studies have found a rapid and significant decrease in serum cholesterol, phospholipids, apoB, and apoA-I carried in LDL and HDL during acute phase reactions to endotoxemia and various inflammatory in humans (35, 36). Among them, HDL phospholipids have been shown to selectively decrease, while the number of HDL particles remains unchanged. Phospholipids showed a greater decline of approximately 20%, and a highly statistically significant linear relationship between the percentage reduction in phospholipids and the peak CRP (R^2 = 0.97, P = 0.001) (9). Although all lipoproteins bind endotoxins, HDL is the most protective because it is rich in surface phospholipids (37). HDL is the main carrier of phospholipids in lipoproteins and has significant endotoxin neutralization ability. Infusion of HDL prevented the fatal consequences of LPS administration in mice (38) and prevented LPS-induced cytokine production in rabbits (39) and human volunteers (40). Sphingosine 1-phosphate (S1P) is a lipid-signaling molecule and approximately 55% and 35% of plasma S1P is partitioned into HDL and albumin, respectively (41). As an extracellular and intracellular messenger, S1P regulates the pathophysiological processes involved in sepsis progression. In patients with sepsis, serum S1P levels were significantly reduced, leading to sepsis capillary leakage, impaired tissue perfusion, and organ failure, which are all inversely correlated with disease severity (42). Other HDL-associated sphingolipids, such as sphingosinephosphorylcholine and lysosulfatide may also enhance endothelial cell migration, survival, and the cytoprotective effects of HDL (43). It could be seen that the serum HDL-associated sphingolipids level can predict the prognosis of sepsis, which provides ideas for the clinical treatment of sepsis patients.

One study found that phospholipid transfer active protein (PLTP) and endothelial lipase (EL) were significantly higher than in patients with non-sepsis (44). This lipase plays a major role in hydrolyzing the phospholipids in HDL (45). Studies have also shown that increased PLTP activity might promote phospholipid transfer from HDL to tissues (46). Increased transfer of HDL phospholipids to tissues might contribute to the regeneration of damaged cell membranes and lung surfactants, and endotoxins bound to HDL phospholipids might be excreted into the bile (47). Thus, increased PLTP activity during inflammation may be a protective mechanism that can attenuate the LPS response by modulating HDL phospholipids. This study revealed the potential causal role of HDL-associated phospholipids in sepsis, suggesting that therapeutic strategies to increase serum levels of HDL-associated phospholipids might be beneficial in patients with sepsis. However, further studies are required to improve our understanding of the mechanisms by which HDL-associated phospholipids affect various aspects of sepsis pathology.

Our MR analysis showed a correlation between elevated HDL-associated phospholipid levels and a reduced risk of sepsis. HDL was the main carrier of phospholipids in lipoproteins and had a significant endotoxin neutralizing ability. The core functions of HDL were considered to be antioxidant and anti-inflammatory (48). In addition, studies had shown that the antioxidant activity of HDL could be significantly affected by the modulation of HDL surface lipids. The surface phospholipid composition of HDL also influenced the anti-inflammatory, anti-apoptotic and anti-infective effects of HDL (49). In conclusion, not only did the content of HDL-associated phospholipids and their ability to neutralize endotoxins contributed to the prevention of sepsis, but their antioxidant, anti-inflammatory, anti-apoptosis, and anti-infective effects were also beneficial for sepsis. Further research is needed to identify the underlying mechanisms behind this relationship.

This study had several strengths, including resistance to confounding factors in traditional epidemiology. We used a variety of MR analysis methods to obtain more reliable data. This study was more efficient and less costly than RCTs. In addition, instrumental variables with larger sample sizes were selected from recent GWAS studies to ensure adequate statistical power. However, it is important to note the limitations of this study. As our study only included European populations, the data do not apply to extrapolations from other non-European populations. Further research on more diverse populations is required.

Conclusion

Herein, we identified suggestive causal relationship associations between HDL-associated phospholipids levels and the risk of sepsis. These data could aid the development of novel strategies for the diagnosis and treatment of sepsis. However, more research is needed to further explore this question.

Data availability statement

Publicly available datasets were analyzed in this study. This data can be found here: Summary statistics were publicly available in the GWAS catalog (https://www.ebi.ac.uk).

Author contributions

LZ: Data curation, Writing – original draft, Writing – review & editing. HT: Methodology, Writing – review & editing. JC: Investigation, Methodology, Writing – review & editing. YiD: Validation, Writing – review & editing. YZ: Validation, Writing – review & editing. HL: Software, Writing – review & editing. YW: Investigation, Writing – review & editing. YP: Investigation, Writing – review & editing. YoD: Conceptualization, Funding acquisition, Project administration, Writing – original draft, Writing – review & editing.

Funding

The author(s) declare financial support was received for the research, authorship, and/or publication of this article. This study was supported by the National Natural Science Foundation of China (32170693).

Conflict of interest

The authors declare that the research was conducted in the absence of any commercial or financial relationships that could be construed as a potential conflict of interest.

Publisher's note

Supplementary material

The Supplementary Material for this article can be found online at: https://www.frontiersin.org/articles/10.3389/fendo.2023.1275132/full#supplementary-material

References

1. Singer M, Deutschman CS, Seymour CW, Shankar-Hari M, Annane D, Bauer M, et al. The third international consensus definitions for sepsis and septic shock (Sepsis-3). *JAMA* (2016) 315:801–10. doi: 10.1001/jama.2016.0287

2. Rudd KE, Johnson SC, Agesa KM, Shackelford KA, Tsoi D, Kievlan DR, et al. Global, regional, and national sepsis incidence and mortality 1990-2017: analysis for the global burden of disease study. *Lancet* (2020) 395:200–11. doi: 10.1016/S0140-6736(19)32989-7

3. Ding WY, Protty MB, Davies IG, Lip G. Relationship between lipoproteins, thrombosis, and atrial fibrillation. *Cardiovasc Res* (2022) 118:716–31. doi: 10.1093/cvr/cvab017

4. Qin S. LDL and HDL oxidative modification and atherosclerosis. *Adv Exp Med Biol* (2020) 1276:157–69. doi: 10.1007/978-981-15-6082-8_10

5. Mackness MI, Durrington PN, Mackness B. How high-density lipoprotein protects against the effects of lipid peroxidation. *Curr Opin Lipidol* (2000) 11:383–8. doi: 10.1097/00041433-200008000-00007

6. Barter PJ, Nicholls S, Rye KA, Anantharamaiah GM, Navab M, Fogelman AM. Antiinflammatory properties of HDL. *Circ Res* (2004) 95:764–72. doi: 10.1161/01.RES.0000146094.59640.13

7. Mineo C, Deguchi H, Griffin JH, Shaul PW. Endothelial and antithrombotic actions of HDL. *Circ Res* (2006) 98:1352–64. doi: 10.1161/01.RES.0000225982.01988.93

8. Marsche G, Saemann MD, Heinemann A, Holzer M. Inflammation alters HDL composition and function: implications for HDL-raising therapies. *Pharmacol Ther* (2013) 137:341–51. doi: 10.1016/j.pharmthera.2012.12.001

9. Hudgins LC, Parker TS, Levine DM, Gordon BR, Saal SD, Jiang XC, et al. A single intravenous dose of endotoxin rapidly alters serum lipoproteins and lipid transfer proteins in normal volunteers. *J Lipid Res* (2003) 44:1489–98. doi: 10.1194/jlr.M200440-JLR200

10. Wadham C, Albanese N, Roberts J, Wang L, Bagley CJ, Gamble JR, et al. High-density lipoproteins neutralize C-reactive protein proinflammatory activity. *Circulation* (2004) 109:2116–22. doi: 10.1161/01.CIR.0000127419.45975.26

11. Pajkrt D, Doran JE, Koster F, Lerch PG, Arnet B, van der Poll T, et al. Antiinflammatory effects of reconstituted high-density lipoprotein during human endotoxemia. *J Exp Med* (1996) 184:1601–8. doi: 10.1084/jem.184.5.1601

12. Trinder M, Walley KR, Boyd JH, Brunham LR. Causal inference for genetically determined levels of high-density lipoprotein cholesterol and risk of infectious disease. *Arterioscler Thromb Vasc Biol* (2020) 40:267–78. doi: 10.1161/ATVBAHA.119.313381

13. Barlage S, Gnewuch C, Liebisch G, Wolf Z, Audebert FX, Gluck T, et al. Changes in HDL-associated apolipoproteins relate to mortality in human sepsis and correlate to monocyte and platelet activation. *Intensive Care Med* (2009) 35:1877–85. doi: 10.1007/s00134-009-1609-y

14. Shor R, Wainstein J, Oz D, Boaz M, Matas Z, Fux A, et al. Low serum LDL cholesterol levels and the risk of fever, sepsis, and Malignancy. *Ann Clin Lab Sci* (2007) 37:343–8.

15. Netea MG, Demacker PN, Kullberg BJ, Boerman OC, Verschueren I, Stalenhoef AF, et al. Low-density lipoprotein receptor-deficient mice are protected against lethal endotoxemia and severe gram-negative infections. *J Clin Invest* (1996) 97:1366–72. doi: 10.1172/JCI118556

16. Harris HW, Grunfeld C, Feingold KR, Rapp JH. Human very low density lipoproteins and chylomicrons can protect against endotoxin-induced death in mice. *J Clin Invest* (1990) 86:696–702. doi: 10.1172/JCI114765

17. Harris HW, Grunfeld C, Feingold KR, Read TE, Kane JP, Jones AL, et al. Chylomicrons alter the fate of endotoxin, decreasing tumor necrosis factor release and preventing death. *J Clin Invest* (1993) 91:1028–34. doi: 10.1172/JCI116259

18. Read TE, Grunfeld C, Kumwenda ZL, Calhoun MC, Kane JP, Feingold KR, et al. Triglyceride-rich lipoproteins prevent septic death in rats. *J Exp Med* (1995) 182:267–72. doi: 10.1084/jem.182.1.267

19. Maatta AM, Salminen A, Pietiainen M, Leskela J, Palviainen T, Sattler W, et al. Endotoxemia is associated with an adverse metabolic profile. *Innate Immun* (2021) 27:3–14. doi: 10.1177/1753425920971702

20. Sekula P, Del GMF, Pattaro C, Kottgen A. Mendelian randomization as an approach to assess causality using observational data. *J Am Soc Nephrol* (2016) 27:3253–65. doi: 10.1681/ASN.2016010098

21. Lawlor DA, Harbord RM, Sterne JA, Timpson N, Davey SG. Mendelian randomization: using genes as instruments for making causal inferences in epidemiology. *Stat Med* (2008) 27:1133–63. doi: 10.1002/sim.3034

22. Smith GD, Ebrahim S. 'Mendelian randomization': can genetic epidemiology contribute to understanding environmental determinants of disease? *Int J Epidemiol* (2003) 32:1–22. doi: 10.1093/ije/dyg070

23. Kettunen J, Demirkan A, Wurtz P, Draisma HH, Haller T, Rawal R, et al. Genome-wide study for circulating metabolites identifies 62 loci and reveals novel systemic effects of LPA. *Nat Commun* (2016) 7:11122. doi: 10.1038/ncomms11122

24. Pierce BL, Burgess S. Efficient design for Mendelian randomization studies: subsample and 2-sample instrumental variable estimators. *Am J Epidemiol* (2013) 178:1177–84. doi: 10.1093/aje/kwt084

25. Hemani G, Zheng J, Elsworth B, Wade KH, Haberland V, Baird D, et al. The MR-Base platform supports systematic causal inference across the human phenome. *eLife* (2018) 7:e34408. doi: 10.7554/eLife.34408

26. Bowden J, Davey SG, Burgess S. Mendelian randomization with invalid instruments: effect estimation and bias detection through Egger regression. *Int J Epidemiol* (2015) 44:512–25. doi: 10.1093/ije/dyv080

27. Burgess S, Scott RA, Timpson NJ, Davey SG, Thompson SG. Using published data in Mendelian randomization: a blueprint for efficient identification of causal risk factors. *Eur J Epidemiol* (2015) 30:543–52. doi: 10.1007/s10654-015-0011-z

28. Bowden J, Davey SG, Haycock PC, Burgess S. Consistent estimation in Mendelian randomization with some invalid instruments using a weighted median estimator. *Genet Epidemiol* (2016) 40:304–14. doi: 10.1002/gepi.21965

29. Burgess S, Thompson SG. Interpreting findings from Mendelian randomization using the MR-Egger method. *Eur J Epidemiol* (2017) 32:377–89. doi: 10.1007/s10654-017-0255-x

30. Burgess S, Bowden J, Fall T, Ingelsson E, Thompson SG. Sensitivity analyses for robust causal inference from Mendelian randomization analyses with multiple genetic variants. *Epidemiology* (2017) 28:30–42. doi: 10.1097/EDE.0000000000000559

31. Bowden J, Del GMF, Minelli C, Davey SG, Sheehan NA, Thompson JR. Assessing the suitability of summary data for two-sample Mendelian randomization analyses using MR-Egger regression: the role of the I2 statistic. *Int J Epidemiol* (2016) 45:1961–74. doi: 10.1093/ije/dyw220

32. Sproviero W, Winchester L, Newby D, Fernandes M, Shi L, Goodday SM, et al. High blood pressure and risk of dementia: A two-sample mendelian randomization study in the UK biobank. *Biol Psychiatry* (2021) 89:817–24. doi: 10.1016/j.biopsych.2020.12.015

33. Larsson SC, Traylor M, Malik R, Dichgans M, Burgess S, Markus HS. Modifiable pathways in Alzheimer's disease: Mendelian randomization analysis. *BMJ* (2017) 359: j5375. doi: 10.1136/bmj.j5375

34. Garcia-Rios A, Perez-Martinez P, Delgado-Lista J, Lopez-Miranda J, Perez-Jimenez F. Nutrigenetics of the lipoprotein metabolism. *Mol Nutr Food Res* (2012) 56:171–83. doi: 10.1002/mnfr.201100513

35. Sammalkorpi K, Valtonen V, Kerttula Y, Nikkila E, Taskinen MR. Changes in serum lipoprotein pattern induced by acute infections. *Metabolism* (1988) 37:859–65. doi: 10.1016/0026-0495(88)90120-5

36. Barlage S, Frohlich D, Bottcher A, Jauhiainen M, Muller HP, Noetzel F, et al. ApoE-containing high density lipoproteins and phospholipid transfer protein activity increase in patients with a systemic inflammatory response. *J Lipid Res* (2001) 42:281–90. doi: 10.1016/S0022-2275(20)31690-4

37. Parker TS, Levine DM, Chang JC, Laxer J, Coffin CC, Rubin AL. Reconstituted high-density lipoprotein neutralizes gram-negative bacterial lipopolysaccharides in human whole blood. *Infect Immun* (1995) 63:253–8. doi: 10.1128/iai.63.1.253-258.1995

38. Levine DM, Parker TS, Donnelly TM, Walsh A, Rubin AL. *In vivo* protection against endotoxin by plasma high density lipoprotein. *Proc Natl Acad Sci USA* (1993) 90:12040–4. doi: 10.1073/pnas.90.24.12040

39. Hubsch AP, Powell FS, Lerch PG, Doran JE. A reconstituted, apolipoprotein A-I containing lipoprotein reduces tumor necrosis factor release and attenuates shock in endotoxemic rabbits. *Circ Shock* (1993) 40:14–23.

40. Pajkrt D, Lerch PG, van der Poll T, Levi M, Illi M, Doran JE, et al. Differential effects of reconstituted high-density lipoprotein on coagulation, fibrinolysis and platelet activation during human endotoxemia. *Thromb Haemost* (1997) 77:303–7. doi: 10.1055/s-0038-1655958

41. Murata N, Sato K, Kon J, Tomura H, Yanagita M, Kuwabara A, et al. Interaction of sphingosine 1-phosphate with plasma components, including lipoproteins, regulates the lipid receptor-mediated actions. *Biochem J* (2000) 352 Pt 3:809–15. doi: 10.1042/bj3520809

42. Winkler MS, Nierhaus A, Holzmann M, Mudersbach E, Bauer A, Robbe L, et al. Decreased serum concentrations of sphingosine-1-phosphate in sepsis. *Crit Care* (2015) 19:372. doi: 10.1186/s13054-015-1089-0

43. Kimura T, Sato K, Malchinkhuu E, Tomura H, Tamama K, Kuwabara A, et al. High-density lipoprotein stimulates endothelial cell migration and survival through sphingosine 1-phosphate and its receptors. *Arterioscler Thromb Vasc Biol* (2003) 23:1283–8. doi: 10.1161/01.ATV.0000079011.67194.5A

44. Reisinger AC, Schuller M, Sourij H, Stadler JT, Hackl G, Eller P, et al. Impact of sepsis on high-density lipoprotein metabolism. *Front Cell Dev Biol* (2021) 9:795460. doi: 10.3389/fcell.2021.795460

45. Yasuda T, Ishida T, Rader DJ. Update on the role of endothelial lipase in high-density lipoprotein metabolism, reverse cholesterol transport, and atherosclerosis. *Circ J* (2010) 74:2263–70. doi: 10.1253/circj.CJ-10-0934

46. Pownall HJ, Hickson-Bick D, Massey JB. Effects of hydrophobicity on turnover of plasma high density lipoproteins labeled with phosphatidylcholine ethers in the rat. *J Lipid Res* (1991) 32:793–800. doi: 10.1016/S0022-2275(20)42031-0

47. Mimura Y, Sakisaka S, Harada M, Sata M, Tanikawa K. Role of hepatocytes in direct clearance of lipopolysaccharide in rats. *Gastroenterology* (1995) 109:1969–76. doi: 10.1016/0016-5085(95)90765-3

48. Fazio S, Pamir N. HDL particle size and functional heterogeneity. *Circ Res* (2016) 119:704–7. doi: 10.1161/CIRCRESAHA.116.309506

49. Kontush A, Lhomme M, Chapman MJ. Unraveling the complexities of the HDL lipidome. *J Lipid Res* (2013) 54:2950–63. doi: 10.1194/jlr.R036095

frontiers | Frontiers in Endocrinology

TYPE Original Research
PUBLISHED 05 February 2024
DOI 10.3389/fendo.2024.1293850

OPEN ACCESS

EDITED BY
Sijung Yun,
Predictiv Care, Inc., United States

REVIEWED BY
Carol Johnston,
Arizona State University, United States
Miguel Rebollo-Hernanz,
Autonomous University of Madrid, Spain

*CORRESPONDENCE
Xiangliang Liu
ds9291@qq.com
Xiao Chen
chenxiao@jlu.edu.cn
Jiuwei Cui
cuijw@jlu.edu.cn

†These authors have contributed equally to this work and share first authorship

RECEIVED 13 September 2023
ACCEPTED 16 January 2024
PUBLISHED 05 February 2024

CITATION
Yuguang L, Chang Y, Li H, Li F, Zou Q, Liu X, Chen X and Cui J (2024) Inflammation mediates the relationship between diet quality assessed by healthy eating index-2015 and metabolic syndrome. *Front. Endocrinol.* 15:1293850. doi: 10.3389/fendo.2024.1293850

Inflammation mediates the relationship between diet quality assessed by healthy eating index-2015 and metabolic syndrome

Li Yuguang[1†], Yu Chang[2†], Hongwei Li[1†], Fangqi Li[1], Qing Zou[2], Xiangliang Liu[1*], Xiao Chen[1*] and Jiuwei Cui[1*]

[1]Cancer Center, The First Hospital of Jilin University, Changchun, China, [2]Department of Anesthesiology, The First Hospital of Jilin University, Changchun, China

Background: Metabolic syndrome is a cluster of metabolic disorders, including obesity, hypertension, hyperglycemia, and abnormal lipid levels. However, researches on the association between overall dietary quality measured by the Healthy Eating Index-2015 (HEI-2015) and the risk of metabolic syndrome is still lacking.

Methods: This study utilized data from four cycles (2011-2018) of the National Health and Nutrition Examination Survey (NHANES) database, including 17,582 participants. Logistic regression analysis was employed to explore the correlation between HEI and the risk of metabolic syndrome. Additionally, mediation analysis was conducted to examine the effects of Systemic Immune-Inflammation Index (SII) and serum uric acid as potential mediators between HEI and metabolic syndrome risk. Weighted quantile sum (WQS) regression evaluated the composite exposure impact of the 13 components of the HEI on metabolic syndrome, as well as the proportion of their weights.

Results: Higher dietary quality measured by HEI-2015 (at the 75th percentile) was negatively correlated with the risk of metabolic syndrome (OR=0.80, 95% CI=0.72-0.89, P=0.003). Higher SII and serum uric acid levels were identified as risk factors for metabolic syndrome (P for trend<0.001). Approximately 37.5% of the effect of HEI on metabolic syndrome occurrence was mediated by SII (Indirect effect=-0.002, 95%CI (-0.003,-0.001), Direct effect=-0.022, 95%CI (-0.0273,-0.015)). Additionally, 25% of the effect of HEI on metabolic syndrome occurrence was mediated by serum uric acid levels (Indirect effect=-0.006, 95%CI (-0.010,-0.012), Direct effect=-0.024, 95%CI (-0.041,-0.009)). WQS regression analysis revealed the highest weighted proportions for seafood and plant proteins (25.20%) and sodium (17.79%), while the weight for whole fruit was the lowest (0.25%).

Conclusion: Better dietary quality measured by HEI-2015 was associated with a lower likelihood of metabolic syndrome. Higher SII and serum uric acid levels were identified as risk factors for metabolic syndrome and potential mediators.

KEYWORDS

healthy eating index, metabolic syndrome, mediation effect, NHANES, chronic inflammation

1 Introduction

The metabolic syndrome (MetS) refers to a cluster of metabolic abnormalities that increase the risk of cardiovascular disease and type 2 diabetes mellitus (1). The key components of MetS include central obesity, hypertension, dyslipidemia and hyperglycemia (2). With the global epidemic of obesity, the prevalence of MetS has increased substantially over the past few decades. It is estimated that 20-30% of the adult population worldwide has MetS (3). The underlying mechanisms are complex and not yet fully understood, but diet and nutrition have been identified as modifiable factors that may help prevent MetS (4).

The Healthy Eating Index (HEI) developed by the United States Department of Agriculture (USDA) is a measure of diet quality and adherence to the Dietary Guidelines for Americans. The index categorizes food components or nutrients into 13 elements, comprising 9 adequacy components and 4 moderation components, emphasizing a high intake of total vegetables, vegetables and legumes, whole grains, total fruits, whole fruits, total protein foods, plant-based proteins, seafood, and fatty acids and limiting the intake of saturated fatty acids, refined grains, sodium, and added sugars (5). Higher HEI scores indicate closer alignment with key recommendations and better diet quality. Previous studies have shown that higher HEI scores are associated with lower risks of obesity, hypertension, dyslipidemia and diabetes (6–9). However, there is limited research on the association between overall diet quality measured by HEI and risk of MetS, especially in the US population.

Systemic inflammation has been implicated in the pathogenesis of MetS. Chronic, sustained, low-grade inflammation promotes the release of a multitude of inflammatory mediators and cytokines, predisposing the organism to insulin resistance, dyslipidemia, and other metabolic dysregulations (10). Systemic immune-inflammation index (SII), based on peripheral neutrophil, lymphocyte and platelet counts, is a novel composite inflammatory biomarker. Recent evidence suggests that higher SII is associated with increased risks of diabetes, hypertension and metabolic disorders (11–13). Serum uric acid is also linked to systemic inflammation, and hyperuricemia predicts MetS risk (14). Uric acid may mediate the effects of diet on MetS, but few studies have examined its potential mediating role.

In this study, we aimed to investigate the association between HEI and risk of MetS and examine whether SII and serum uric acid levels mediate the association in US adults based on the National Health and Nutrition Examination Survey (NHANES) 2011-2018. The findings will provide novel evidence on the link between diet quality, inflammation and MetS among Americans.

2 Methods

2.1 Study population

In this study, our data was obtained from the publicly available National Health and Nutrition Examination Survey (NHANES) database (https://www.cdc.gov/nchs/nhanes/index.htm). NHANES is a nationally representative cross-sectional survey conducted by the National Institutes of Health and the Centers for Disease Control and Prevention, which aims to comprehensively investigate the health and dietary status of the U.S. population. The database includes modules on demographics, questionnaires, physical examinations, and laboratory tests (including blood and urine samples). For this study, we downloaded four consecutive datasets (2011-2012, 2013-2014, 2015-2016, and 2017-2018) from the website to accurately assess the relationship between a healthy diet index and metabolic syndrome. A total of 39,156 participants' information was extracted.The following criteria were applied for inclusion and exclusion of participants: Inclusion criteria (1): All participants from 2011 to 2018; (2) Participants who cooperated with the follow-up and provided informed consent. Exclusion criteria: (1) Age< 18 years (n=15,331); (2) Participants with indeterminate MetS status (n=252), including individuals with missing data on blood pressure, total cholesterol, fasting blood glucose, glycated hemoglobin, and body mass index (BMI); (3) Individuals with incomplete or unreasonable dietary data that prevented the calculation of the healthy diet index (n=5,722). After applying these criteria, a total of 17,528 participants were included in this study. The specific details can be shown in Figure 1. This NHANES study was approved by the NCHS (National Center for Health Statistics) Ethics Review Board, and informed consent was obtained from all participants.

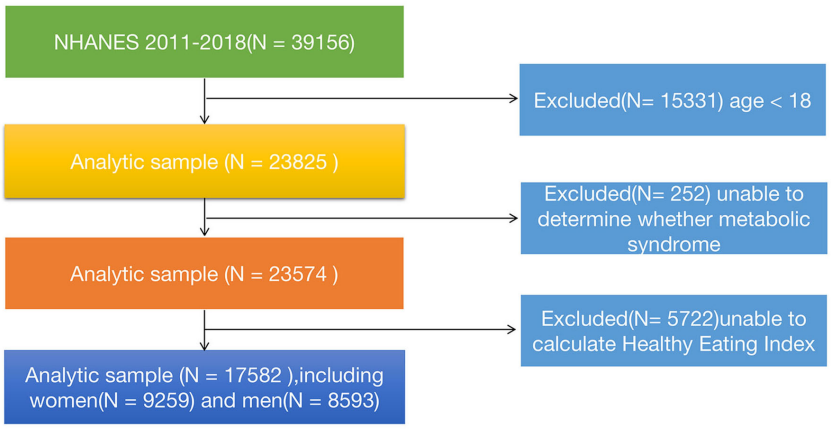

FIGURE 1
Flowchart of the study design and participants excluded from the study.

2.2 Data collection

The dietary data for this study was obtained from two 24-hour dietary recall surveys using the Automated Multiple-Pass Method (AMPM) standardized by the USDA (15). In the NHANES survey, trained interviewers conducted face-to-face interviews with participants to collect information on the nutrient composition and intake of various foods and beverages consumed in the past 24 hours. Based on the data from two 24-hour dietary recall surveys, equivalent data grouping transformations and relevant calculations were performed using the USDA Food and Nutrient Database.

The Healthy Eating Index-2015 (HEI-2015) utilizes the population ratio method based on dietary intake data from the entire polulation to assess the reasonableness of the population's average dietary quality, as well as the adherence to healthy dietary patterns by researchers. This index was jointly developed by the USDA and the Department of Health and Human Services (HHS) in the United States and consists of 13 components including total fruit, whole fruit, total vegetables, greens and beans, dairy, whole grains, protein foods, fats, added sugars, seafood and plant proteins, saturated fats and unsaturated fats, refined grains, and added sugars. These indicators evaluate the diet quality and health of individuals or populations in terms of whole grains, vegetables and fruits, dairy, fats, and sugars, among others. Each component is scored according to specific criteria, and an overall score out of 100 can be calculated. A higher total score indicates greater adherence to the Dietary Guidelines for Americans (DGA) and better overall diet quality (16). The index was calculated and constructed using dietary intake data collected from participants' two 24-hour dietary recalls, which were combined with USDA Food Patterns equivalent data. We utilized SAS code provided by the National Cancer Institute, and calculated the HEI-2015 score using the HEI scoring algorithm provided by the NHANES database. Detailed components, algorithms, and scoring criteria of HEI-2015 are available in the provided Supplementary Table 1.

In this study, participants diagnosed with MetS needed to meet three or more of the following conditions: 1) hypertriglyceridemia: serum triglyceride levels ≥150 mg/dL (1.7 mmol/L), or the use of lipid-lowering medication; 2) low high-density lipoprotein cholesterol levels: HDL<40 mg/dL (1.03 mmol/L) for men, HDL<50 mg/dL (1.29 mmol/L) for women; 3) high blood glucose levels: fasting blood glucose ≥100 mg/dL (5.6 mmol/L), or the use of glucose-lowering medication; 4) hypertension: systolic blood pressure ≥130 mmHg or diastolic blood pressure ≥85 mmHg, or the use of antihypertensive medication; 5) central obesity: waist circumference ≥102 cm for men, ≥88 cm for women (1).

The data for blood samples were measured and recorded by professional researchers utilizing automated hematological analyzers, including platelet count, neutrophil count, lymphocyte count, and uric acid levels. We calculated the Systemic Immune-Inflammation Index (SII), defined as (platelet count × neutrophil count)/lymphocyte count (17). Additionally, we gathered data on gender (female and male), age, race (Mexican American, Non-Hispanic Black, Non-Hispanic White, and other), poverty income ratio (≤1, 1–3, >3), education level (low high school, high school, college or above), smoking status, and alcohol consumption. Current smoker was defined as 'more than 100 cigarettes in lifetime and currently smoking all or some days', former smoker as 'more than 100 cigarettes in lifetime but not currently smoking', and never smoker as 'fewer than 100 cigarettes in lifetime'. In terms of alcohol consumption, heavy drinker was defined as 'weekly alcohol intake exceeding 14 standard drinks for women and 21 standard drinks for men', moderate drinker as 'weekly alcohol intake between 8-14 standard drinks for women and between 8-21 standard drinks for men', and mild drinker as 'weekly alcohol intake between 1-7 standard drinks', with one standard drink equivalent to 14 grams of pure alcohol. The HEI-2015 was categorized based on quartiles, Quartile 1 (Q1): <25th percentile, Quartile 2 (Q2): ≥25 to 50th percentile, Quartile 3 (Q3): ≥50 to 75th percentile, and Quartile 4 (Q4): ≥75th percentile. Additionally, both SII and uric acid levels were categorized into quartiles (Q1, Q2, Q3, Q4) using the same approach.

2.3 Statistical analysis

Given the complex, multi-stage, stratified sampling design of the NHANES database, we conducted a weighted analysis in

accordance with the database's weighting recommendations. The analysis was weighted. Weighting factors included two-year examination weights (WTMEC2YR) and two-day dietary interview weights (WTDR2D), strata (SDMVSTRA), and primary sampling units (SDMVPSU) were considered to account for the complex survey design. Besides,we employed the data processing method of deleting missing values and accurately documented the number of cases where missing variables were removed. In this study, continuous variables were described using the weighted mean ± standard deviation (Mean ± SD) or the median and interquartile range (M, IQR), statistical differences were assessed using the weighted Student's t-test or the Kruskal-Wallis rank sum test. Categorical variables were described by the number of samples (weighted percentage), with statistical differences evaluated using Pearson's Chi-squared test.

For non-normally distributed continuous variables like HEI-2015, SII, and uric acid levels, they were transformed into categorical variables (quartiles) and three multivariable logistic regression models were established to preliminarily assess the relationship between HEI and MetS.These models included: Crude model - not adjusting for any variables; Model 1 - adjusting for gender, age, and race; Model 2 - adjusting for gender, age, race, education level, poverty income ratio, smoking status, and drinking status. Additionally, a second multivariable logistic regression model was used to evaluate the relationship between SII, uric acid levels, and the outcome variable metabolic syndrome. Furthermore, we employed mediation analysis, a method used to determine whether the association between variables can be partially explained by the influence of a third or mediating variable. In this study, the method was conducted to determine whether SII and uric acid levels mediated the relationship between a healthy eating index and MetS. The total effect (TE) represents the direct relationship between HEI-2015 and MetS, unaffected by the mediating factors. The indirect effect (IE) refers to the influence of SII and uric acid levels on MetS through HEI-2015. The direct effect (DE) represents the effect of HEI-2015 on MetS after controlling for SII and uric acid levels. A significant IE indicates the presence of a mediating effect. Besides, We employed sub-group analysis to investigate the relationship between HEI-2015 and MetS across different age groups, genders, races, educational levels, poverty-income ratios and smoking status, and assessed the significance of interaction effects by using p-values of the product terms between HEI-2015 components and stratification factors.

The relationship between mixed exposure of the 13 components constituting HEI and MetS, along with the weight proportion of each component, was analyzed using the WQS regression model.The basic weighted index model is as follows:

$$g(\mu) = \beta_o + \beta_1 \left(\sum_{i=0}^{c} \omega_i \varphi_i\right) + z'\Phi$$

$$WQS = \sum_{i=1}^{c} \bar{\omega}_i \varphi_i$$

$g(\mu)$ denotes any differentiable link function, β_o represents the intercept, β_1 represents the regression coefficient, c denotes the count of HEI components included in the analysis, z' denotes the matrix of covariates, Φ represents the coefficients for these covariates, $(\sum_{i=0}^{c} \omega_i \varphi_i)$ denotes the sum of weighted quantiles for (c) components. ω_i represents the weighted index, where each index ranges from 0 to 1 ($0 \leq \omega_i \leq 1$), and the total sum of the weighted indices equals 1. φ_i represents the quartiles of the concentration for each chemical compound, where (i = 0,1,2,3) corresponds to the 1st, 2nd, 3rd, or 4th quartile, respectively (18).

All data analyses in this study were performed using R 4.2.2. All statistical tests were two-sided, and significance was set at P<0.05.

3 Results

3.1 Baseline characteristics

Participants were grouped based on the presence or absence of MetS, and detailed study characteristics are shown in Table 1. A total of 17,528 participants aged over 18 years were included, with 8,269 male participants (47.18%) and 9,259 female participants (52.82%). Among them, approximately 5,901 participants had MetS, while 11,951 participants did not. Compared to the group without metabolic syndrome, individuals with MetS were more likely to be in the age range of 18-65 years, female, non-Hispanic White, with a poverty income ratio (PIR) less than 3, college-educated or higher, non-smokers, drinkers, lower HEI and had higher SII and uric acid levels (p<0.050). For more specific details, please refer to Table 1.

3.2 Association between HEI and metabolic syndrome

Three multivariable logistic regression models were established to further investigate the impact of HEI on MetS. Compared to the Q1 group, the Q4 group showed a negative correlation with the occurrence of metabolic syndrome. In Model 1, compared to the Q1 quartile, the risk of developing MetS in the Q4 quartile was reduced by 22% (OR 0.78, 95% CI 0.66-0.92, p=0.003). In Model 2, compared to the Q1 quartile, the risk of developing MetS in the Q4 quartile was reduced by 23% (OR 0.77, 95% CI 0.66-0.91, p=0.003). Further details can be seen in Table 2.

3.3 The relationship between SII, uric acid levels, and metabolic syndrome

In order to further investigate the relationship between SII, uric acid levels, and MetS, and the role of covariates in the model, we categorized SII and uric acid levels into quartiles. We adjusted for gender, age, race, education level, poverty-income ratio, smoking status, and alcohol consumption in logistic regression models. Compared to the Q1 quartile for SII, the risk of developing MetS in the Q2, Q3, and Q4 quartiles increased by 21% (OR 1.21, 95% CI 1.06-1.38, p=0.010), 35% (OR 1.35, 95% CI 1.16-1.57, p<0.001), and 66% (OR 1.66, 95% CI 1.44-1.91, p<0.001), respectively. Compared to the Q1 quartile for uric acid levels, the risk of developing MetS in the Q2, Q3, and Q4 quartiles increased by 92% (OR 1.92, 95% CI

TABLE 1 Weighted characteristics of the study population by Metabolic syndrome.

Variable	Level	No Metabolic syndrome	Metabolic syndrome	*P*-value
N		11951	5901	
Sex (%)				0.08
	Female	50.01(0.68)	52.38(1.07)	
	Male	49.99(0.68)	47.62(1.07)	
Age				<0.0001
	[18, 65)	87.17(0.64)	74.66(0.91)	
	≥65	12.83(0.64)	25.34(0.91)	
Race/ethnicity (%)				<0.0001
	Mexican American	8.21(0.85)	9.40(1.10)	
	Non-Hispanic Black	11.33(1.00)	9.18(0.93)	
	Non-Hispanic White	65.71(1.77)	68.79(1.85)	
	Other Hispanic	5.65(0.59)	5.48(0.69)	
	Other Race - Including Multi-Racial	9.10(0.59)	7.14(0.71)	
Poverty (%)				0.003
	<1	14.83(0.90)	13.95(0.87)	
	[1, 3)	34.11(1.18)	38.39(1.15	
	≥3	51.06(1.54)	47.66(1.60)	
Education (%)				<0.0001
	low high school	11.46(0.76)	14.40(0.97)	
	High school	21.25(0.86)	26.46(1.30)	
	College or above	67.29(1.32)	59.14(1.52)	
Smokers(%)				<0.0001
	former smoker	21.21(0.81)	30.29(1.07)	
	Never smoker	60.69(0.97)	52.54(1.08)	
	Current smoker	18.09(0.80)	17.18(0.85)	
Alcohol drinkers(%)				<0.0001
	Former drinker	8.89(0.43)	15.72(0.77)	
	Heavy drinker	22.25(0.82)	17.79(0.97)	
	Mild drinker	37.72(1.08)	38.96(1.54)	
	Moderate drinker	19.97(0.68)	15.41(0.88)	
	Never drinker	11.17(0.83)	12.12(0.93)	
HEI(mean (SD))		51.94(0.35)	51.01(0.34)	0.01
SII (mean (SD))		497.62 (332.28)	539.48 (325.84)	<0.0001
Uric acid(mean (SD))		506.25(5.48)	553.29(5.90)	<0.0001

Mean ± SE for continuous variables: P-value was calculated by the weighted T test. % (SE) for categorical variables: P-value was calculated by the weighted chi-square test.

1.64-2.25, p<0.001), 184% (OR 2.84, 95% CI 2.37-3.40, p<0.001), and 404% (OR 5.04, 95% CI 4.25-5.98, p<0.001), respectively. Therefore, both SII and uric acid levels can be considered important risk factors for the occurrence of MetS. More details can be observed by referring to Table 3.

3.4 Mediation analysis

To explore whether SII and uric acid mediate the relationship between HEI and MetS, we conducted a mediation analysis. In this mediation model, HEI was treated as the independent variable,

TABLE 2 The associations between HEI and metabolic syndrome.

	Crude model[a]		Model 1[b]		Model 1[c]	
	OR(95% CI)	*P*-value	OR(95% CI)	*P*-value	OR(95% CI)	*P*-value
HEI						
Q1	Reference		Reference		Reference	
Q2	1.02(0.86,1.21)	0.80	0.97(0.82,1.16)	0.73	0.98(0.82,1.16)	0.80
Q3	1.00(0.85,1.17))	0.95	0.91(0.77,1.08)	0.27	0.92(0.77,1.10)	0.35
Q4	0.87(0.74,1.02)	0.08	0.78(0.66,0.92)	0.003	0.77(0.66,0.91)	0.003

Q, quartiles; Q1 represents the unhealthiest diet quality, Q4 represents the healthiest diet quality. OR, odds ratio; CI, confidence intervals. Crude model[a]: no covariates were adjusted. Model 1[b]: sex,age and race/ethnicity were adjusted. Model 2[c]: sex,age, race/ethnicity, education attainment, poverty income ratio, smoking status, and alcohol drinking status were adjusted.

MetS as the dependent variable, and SII and uric acid levels as the mediating variables. The results are shown in Figure 2: HEI has a significant indirect effect on the occurrence of MetS through serum uric acid levels, with an indirect effect of -0.006 (95%CI: -0.010, -0.012). This suggests that serum uric acid levels partially mediate the relationship between HEI and MetS. After controlling for serum uric acid levels, HEI still exerts a significant inhibitory effect on the occurrence of MetS, with a direct effect of -0.024 (95%CI: -0.041, -0.009). This indicates that there are both direct and indirect effects of HEI on the occurrence of MetS. Approximately 25% of the impact of HEI on the occurrence of MetS is mediated by serum uric acid levels.

Similarly, HEI also has a significant indirect effect on the occurrence of MetS through SII, with an indirect effect of -0.002 (95%CI: -0.003, -0.001), suggesting a partial mediating effect of SII. After controlling for SII, HEI still shows a significant inhibitory effect on the occurrence of MetS, with a direct effect of -0.022 (95% CI: -0.0273, -0.015). This further indicates the presence of both direct and indirect effects of HEI on the occurrence of MetS, with approximately 37.5% of the impact of HEI on MetS occurrence being mediated by SII. More details can be shown in Figure 3. Therefore, both SII and serum uric acid levels can be considered important mediating factors in the relationship between HEI and the occurrence of MetS.

TABLE 3 The correlation between SII, uric acid levels, and metabolic syndrome.

	OR	95% CI	*P*-value
SII			
Q1	Reference		
Q2	1.17	(1.06,1.30)	0.003
Q3	1.25	(1.13,1.39)	<0.001
Q4	1.44	(1.30.1.60)	<0.001
Uric acid			
Q1	Reference		
Q2	1.76	(1.58,197)	<0.001
Q3	2.62	(2.23,2.93)	<0.001
Q4	4.46	(3.96,5.02)	<0.001

Adjusted for sex,age, race/ethnicity, education attainment, poverty income ratio, smoking status, and alcohol drinking statuss. Q, quartiles; Q1 represents the unhealthiest diet quality, Q4 represents the healthiest diet quality. OR, odds ratio; CI, confidence intervals.

3.5 Subgroup analysis and interaction

The subgroup analysis revealed a significant interaction between HEI-2015 and age, gender, education level, PIR, and smoking status ($p<0.05$). The negative correlation between HEI-2015 and MetS was observed in older participants (aged > 65 years, OR 0.99, 95%CI (0.90,1.00)), female participants (OR 0.99, 95%CI (0.99,1.00)), non-Hispanic White participants (OR 0.99, 95%CI (0.99,0.99)), participants with a university or higher education level (OR 0.99, 95%CI (0.99,0.99)), and participants with a PIR≥3 (OR 0.99, 95%CI (0.99,0.99)). For more specific details, please refer to Figure 4.

3.6 Weighted quantile sum regression

The WQS regression model was employed to construct a weighted index for investigating the cumulative impact and proportional weights of the 13 components of the HEI on the risk of MetS. The findings illustrated a statistically significant inverse association between the overall HEI score and the prevalence of MetS (OR = -0.47, P< 0.001). Among the 13 components of the HEI, seafood and plant proteins (25.20%) along with sodium (17.79%) had the highest weights, whereas whole fruit had the lowest (0.25%). More detailed information can be obtained in Figure 5.

4 Discussion

In this large, nationally representative sample of US adults, we found that better diet quality measured by HEI-2015 was associated with lower odds of having MetS. The association remained significant after adjusting for demographics, socioeconomics, smoking and alcohol use. In addition, higher SII and serum uric acid levels were identified as risk factors for MetS. Mediation analysis further revealed that SII and uric acid partially mediated the association between HEI and MetS. The WQS regression model

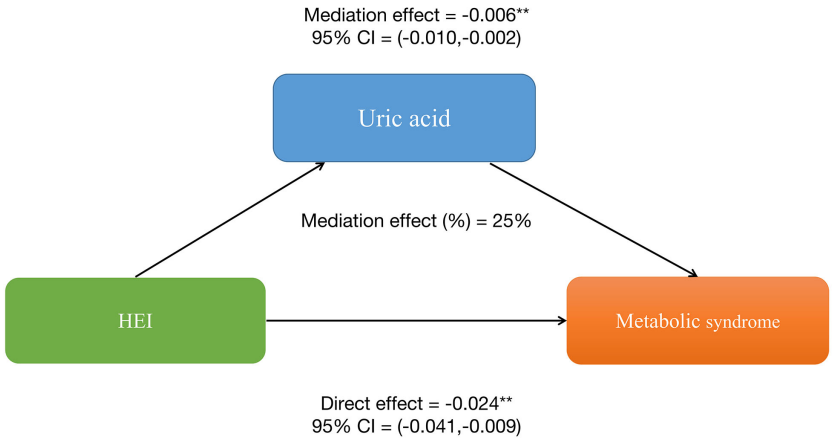

FIGURE 2
Serum uric acid levels partially mediates the relationship between healthy eating index-2015 and metabolic syndrome. *P<0.05, **P<0.01.

assessed the cumulative effects and weights of the 13 HEI components on MetS, with substantial consumption of seafood and plant proteins and moderate intake of sodium being most significantly associated with a reduced risk of MetS.

Our study provides new evidence that better adherence to the Dietary Guidelines for Americans and higher diet quality are associated with reduced Mets risk. The HEI-2015 assesses conformity to key dietary recommendations on fruits, vegetables, whole grains, dairy, protein, fatty acids, refined grains, sodium and empty calories (5). Meeting these targets may help prevent development of individual MetS components including central obesity, hypertension, dyslipidemia and hyperglycemia. In alignment with our findings, previous studies have linked higher HEI scores to lower prevalence of obesity, diabetes, hypertension and dyslipidemia (6–9). Two separate studies, one focusing on Korean adults and the other on Iranian adults, have also reported the associations between HEI scores and MetS risk (19, 20). Our research further confirmed the beneficial effects of diet quality in MetS among Americans. Interventions to improve diet quality should be a public health priority.

Chronic low-grade inflammation is involved in MetS pathogenesis (4). SII and uric acid are two emerging inflammatory markers associated with obesity, insulin resistance, diabetes and cardiovascular disease (11–14). Our study newly identified higher SII and uric acid as independent predictors of MetS after adjusting for confounders. Inflammation may be a key mechanism linking diet quality to MetS. Mediation analysis showed that the associations between HEI and MetS were partially mediated by SII and uric acid, suggesting both direct and indirect effects. A high-quality diet may help decrease systemic inflammation, thereby lowering MetS risk. The mediating roles of novel inflammatory markers warrant further investigation in diet and MetS research.

Compared to other diet quality indices, the HEI-2015 is unique as it quantifies conformance to federal dietary guidelines. However, associations between diet quality and inflammation/MetS likely reflect commonalities across indices like higher intakes of plant

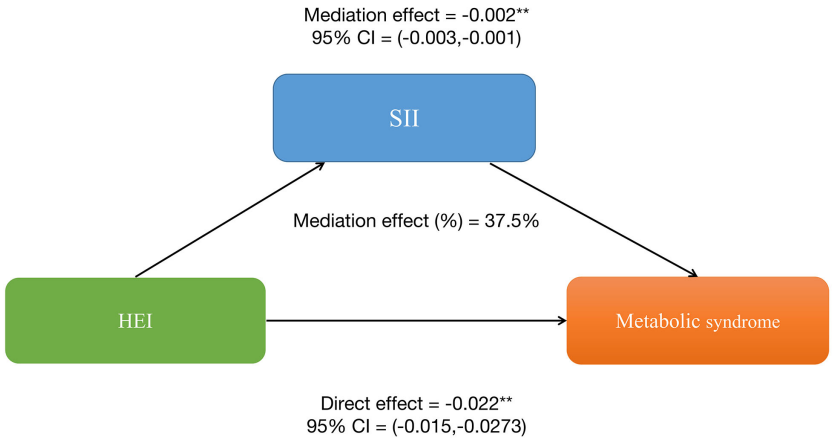

FIGURE 3
Systemic Immune-Inflammation Index (SII) partially mediates the relationship between healthy eating index-2015 and metabolic syndrome. *P<0.05, **P<0.01.

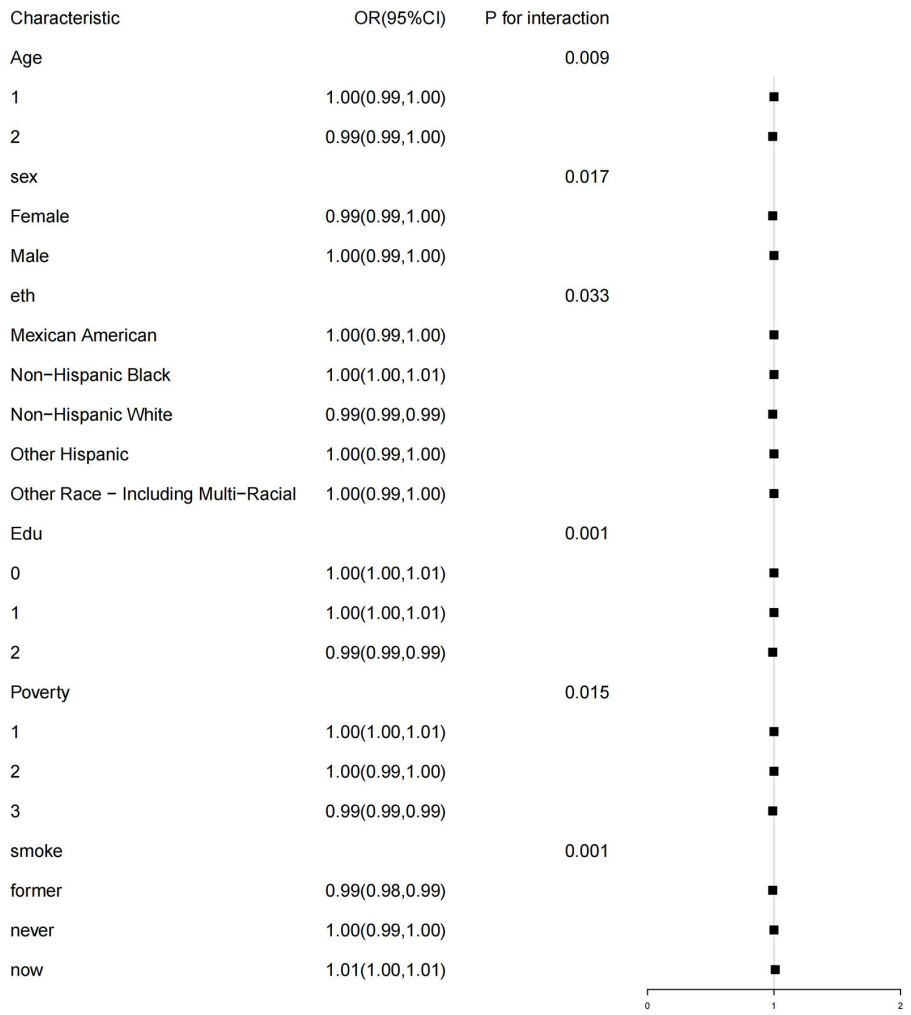

FIGURE 4
WQS model regression index weights for the metabolic syndrome (MetS), adjusted for sex,age, race/ethnicity, education attainment, poverty income ratio, smoking status, and alcohol drinking status.

foods and unsaturated fats versus processed foods and saturated fats. For instance, the Mediterranean diet characterized by high intakes of fruits, vegetables, legumes, cereals, fish, and monounsaturated fatty acids has been linked to lower systemic inflammation and MetS prevalence (21, 22). The DASH diet targeting high intake of fruits, vegetables, low-fat dairy, whole grains, chicken, fish, nuts and low intake of red meats, sweets, and sugar-sweetened beverages also reduces CRP and other inflammatory markers (23). Overall diet quality appears more influential than individual components. Further research can continue examining how different diet quality indices relate to inflammation, MetS risks, and cardiometabolic health. Our study utilized the HEI to evaluate diet quality in relation to MetS risk among Americans, providing dietary strategies for MetS prevention.

Our research found that SII and uric acid partially mediated the relationship between HEI and MetS. The potential beneficial effects of diet quality on mitigating inflammation and MetS risk likely accumulate over time. Long-term adherence to high-quality diets emphases fruits, vegetables, fiber, plant proteins, and unsaturated fats while limiting red meats, saturated fats, processed foods, and sugars. These healthy dietary patterns characterized by high HEI scores have been associated with lower systemic inflammation marked by CRP, interleukin-6, E-selectin and other biomarkers in both cross-sectional and prospective studies (24–26). The compounding anti-inflammatory effects could alleviate insulin resistance, endothelial dysfunction, and dyslipidemia central to MetS pathogenesis (27). For example, the phytochemicals and antioxidants in plant foods may improve insulin signaling and glucose metabolism through regulating oxidative stress and inflammatory pathways (28). Omega-3 fatty acids can inhibit nuclear factor kappa B activation, suppressing production of inflammatory cytokines like tumor necrosis factor alpha and interleukin-6 (29). The high fiber content in whole grains, fruits and vegetables may also contribute by producing short-chain fatty acids upon fermentation, which hold immunomodulatory activities (30), lower levels of purines, thus reducing the production of uric acid. These plant-based foods are abundant in vitamins C and E, and marine foods are rich in polyphenols and flavonoids. The rich content of these bioactive compounds exerts potent anti-inflammatory

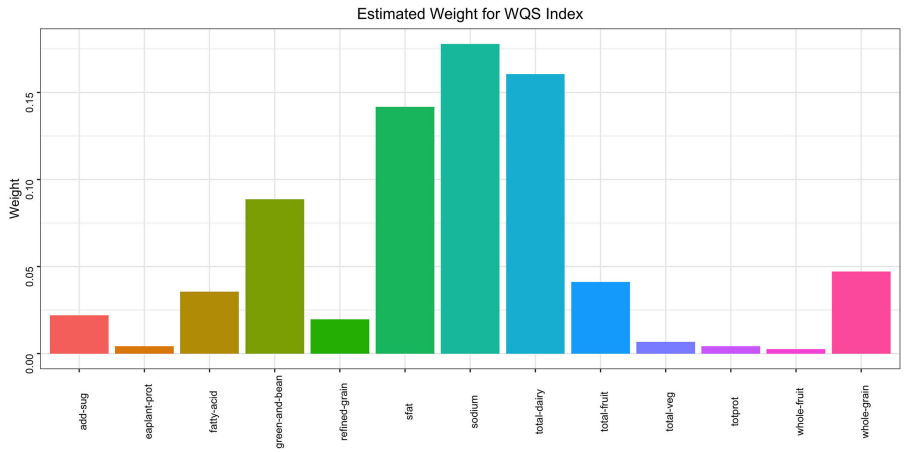

FIGURE 5
Subgroup analysis of the association of the HEI-2015 and the presence of metabolic syndrome (MetS). Each stratifcation was adjusted for age, sex, race/ethnicity, education attainment, poverty income ratio, smoking status. Age (1 aged 18-65 years; 2 ≥65years), Edu Education level (0 low high school; 1 high school; 2 College or above), Poverty (1<1; 2 [1, 3); 3 ≥3).

and antioxidant effects, mitigating systemic immune-inflammatory responses, thereby lowering the SII (31, 32). Chronic inflammation can interfere with the normal function of insulin, leading to insulin resistance; the release of inflammatory cells and mediators contributes to dysregulated lipid metabolism, increasing the risk of MetS (11). Elevated uric acid levels may promote oxidative stress and cellular apoptosis, heightening the incidence of hypertension, gout, and cardiovascular diseases (33).In addition, higher HEI signifies more balanced nutrition intake, which can improve insulin sensitivity and reduce inflammatory cytokine production (21, 34). Future research is warranted to investigate the anti-inflammatory effects of high-quality diets and their impacts on MetS.

Our study boasts several innovative advantages, firstly, it is based on a large national NHANES sample, ensuring ample sample size and validity of the research outcomes. We constructed several weighted multivariate logistic regression models, adjusting for multiple variables to robustly assess the impact of HEI on the risk of incident MetS. Moreover, we utilized mediation analysis to further elucidate the potential mediating roles of SII and uric acid in the association between HEI and MetS. We employed the weighted quantile sum regression approach to test the cumulative effects of the 13 components of HEI on MetS and quantified the significant contributions of each component, substantially advancing the reliability and robustness of dietary characteristics associated with MetS.

This study has important public health implications regarding the role of diet quality in metabolic health. Our findings that better adherence to federal dietary guidelines assessed by HEI-2015 is associated with lower likelihood of MetS in Americans further highlights the value of the HEI as a diet quality monitoring tool. The index could help shape dietary recommendations and policies aimed at curbing the growing prevalence of obesity, diabetes, hypertension and related metabolic disorders. Specifically, the HEI-2015 components with the greatest weights in relation to MetS risk in our analysis—including seafood/plant proteins, sodium and empty calories—can inform targeted efforts to improve these aspects of diet quality at the population level. Future revisions to federal dietary guidelines and educational campaigns can also emphasize overall diet patterns aligned with HEI-2015 targets rather than individual nutrients or foods.

However, our study has some limitations. The cross-sectional analysis prevents causal determination of the relationship between diet quality and MetS. While the NHANES dataset is nationally representative, the self-reported dietary data may be subject to recall biases. We identified certain novel inflammatory biomarkers as mediators but did not measure an exhaustive profile. Future longitudinal cohorts could track participants' diets using validated methods alongside periodic assessment of clinical parameters, MetS incidence and detailed inflammatory markers to elucidate long-term relationships. Examining how diet quality interacts with genetics, microbiome and other factors influencing MetS risks would also advance scientific understanding. Overall, our findings highlight diet quality as a modifiable factor and the utility of HEI-2015 to assess adherence to healthy dietary patterns for lowering metabolic disease burden.

5 Conclusion

In conclusion, we found that better diet quality assessed by HEI-2015 was associated with lower likelihood of having MetS in a nationally representative sample of US adults. Higher SII and serum uric acid levels were identified as risk factors for MetS and partial mediators. Our results highlight the importance of a high-quality diet and controlling inflammation in MetS prevention. The HEI-2015 index may be a useful tool to monitor diet quality at the population level. Our findings need to be confirmed by longitudinal

studies elucidating the interrelationships between diet, inflammation and metabolic disorders. Nutrition strategies to improve diet quality, reduce inflammation and alleviate the growing burden of MetS warrant further investigation.

Data availability statement

The raw data supporting the conclusions of this article will be made available by the authors, without undue reservation.

Ethics statement

The studies involving humans were approved by the National Center for Health Statistics Research Ethics Review Board, duly approved by the ethical review committee (protocol #2011-17, #2018-01). The patients/participants provided their written informed consent to participate in this study.

Author contributions

LY: Data curation, Formal analysis, Visualization, Writing – original draft. YC: Data curation, Formal analysis, Visualization, Writing – original draft. HL: Data curation, Formal analysis, Writing – original draft. FL: Methodology, Project administration, Writing – original draft. QZ: Methodology, Project administration, Writing – original draft. XL: Conceptualization, Methodology, Supervision, Writing – original draft, Writing – review & editing. XC: Conceptualization, Supervision, Writing – review & editing. JC: Conceptualization, Methodology, Supervision, Writing – review & editing.

Funding

The author(s) declare that no financial support was received for the research, authorship, and/or publication of this article.

Acknowledgments

The authors express their gratitude to the NHANES project members for their extensive work in data collection and follow-up.

Conflict of interest

The authors declare that the research was conducted in the absence of any commercial or financial relationships that could be construed as a potential conflict of interest.

Publisher's note

All claims expressed in this article are solely those of the authors and do not necessarily represent those of their affiliated organizations, or those of the publisher, the editors and the reviewers. Any product that may be evaluated in this article, or claim that may be made by its manufacturer, is not guaranteed or endorsed by the publisher.

Supplementary material

The Supplementary Material for this article can be found online at: https://www.frontiersin.org/articles/10.3389/fendo.2024.1293850/full#supplementary-material

References

1. Alberti KG, Eckel RH, Grundy SM, Zimmet PZ, Cleeman JI, Donato KA, et al. Harmonizing the metabolic syndrome: A joint interim statement of the international diabetes federation task force on epidemiology and prevention; National heart, lung, and blood institute; American Heart Association; World Heart Federation; international atherosclerosis society; and International association for the study of obesity. *Circulation.* (2009) 120:1640–5. doi: 10.1161/circulationaha.109.192644

2. Scott MG, Daniel B, Luther TC, Richard SC, Margo AD, Donald BH, et al. Executive summary of the third report of the national cholesterol education program (NCEP) expert panel on detection, evaluation, and treatment of high blood cholesterol in adults (Adult treatment panel III). *Jama* (2001) 285:2486–97. doi: 10.1001/jama.285.19.2486

3. O'Neill S, O'Driscoll L. Metabolic syndrome: A closer look at the growing epidemic and its associated pathologies. *Obes Rev an Off J Int Assoc Study Obes* (2015) 16:1–12. doi: 10.1111/obr.12229

4. Gustafson B. Adipose tissue, inflammation and atherosclerosis. *J Atheroscl thrombosis.* (2010) 17:332–41. doi: 10.5551/jat.3939

5. Krebs-Smith SM, Pannucci TE, Subar AF, Kirkpatrick SI, Lerman JL, Tooze JA, et al. Update of the healthy eating index: HEI-2015. *J Acad Nutr Dietetics.* (2018) 118:1591–602. doi: 10.1016/j.jand.2018.05.021

6. Zhang X, Guo Y, Yao N, Wang L, Sun M, Xu X, et al. Association between dietary inflammatory index and metabolic syndrome: Analysis of the NHANES 2005-2016. *Front Nutr* (2022) 9:991907. doi: 10.3389/fnut.2022.991907

7. Hiza HA, Casavale KO, Guenther PM, Davis CA. Diet quality of Americans differs by age, sex, race/ethnicity, income, and education level. *J Acad Nutr Dietetics.* (2013) 113:297–306. doi: 10.1016/j.jand.2012.08.011

8. Nicklas TA, O'Neil CE, Fulgoni VL 3rd. Diet quality is inversely related to cardiovascular risk factors in adults. *J Nutr* (2012) 142:2112–8. doi: 10.3945/jn.112.164889

9. Huffman FG, Maurcio DLC, Vaccaro JA, Zarini GG, Joel E, Deva G, et al. Healthy eating index and alternate healthy eating index among Haitian Americans and African Americans with and without type 2 diabetes. *J Nutr Metab* (2011) 2011:398324. doi: 10.1155/2011/398324

10. Grundy SM. Adipose tissue and metabolic syndrome: too much, too little or neither. *Eur J Clin Invest* (2015) 45:1209–17. doi: 10.1111/eci.12519

11. Chen JH, Zhai ET, Yuan YJ, Wu KM, Xu JB, Peng JJ, et al. Systemic immune-inflammation index for predicting prognosis of colorectal cancer. *World J gastroenterology.* (2017) 23:6261–72. doi: 10.3748/wjg.v23.i34.6261

12. Wang X, Bao W, Liu J, Ouyang YY, Wang D, Rong S, et al. Inflammatory markers and risk of type 2 diabetes: A systematic review and meta-analysis. *Diabetes Care* (2013) 36:166–75. doi: 10.2337/dc12-0702

13. Fu Y, Luo N, Klein RL, Garvey WT. Adiponectin promotes adipocyte differentiation, insulin sensitivity, and lipid accumulation. *J Lipid Res* (2005) 46:1369–79. doi: 10.1194/jlr.M400373-JLR200

14. Li Y, Xu C, Yu C, Xu L, Miao M. Association of serum uric acid level with non-alcoholic fatty liver disease: A cross-sectional study. *J hepatology.* (2009) 50:1029–34. doi: 10.1016/j.jhep.2008.11.021

15. Moshfegh AJ, Rhodes DG, Baer DJ, Murayi T, Clemens JC, Rumpler WV, et al. The US department of agriculture automated multiple-pass method reduces bias in the collection of energy intakes. *Am J Clin Nutr* (2008) 88:324–32. doi: 10.1093/ajcn/88.2.324

16. Reedy J, Lerman JL, Krebs-Smith SM, Kirkpatrick SI, Pannucci TE, Wilson MM, et al. Evaluation of the healthy eating index-2015. *J Acad Nutr Dietetics.* (2018) 118:1622–33. doi: 10.1016/j.jand.2018.05.019

17. Nøst TH, Alcala K, Urbarova I, Byrne KS, Guida F, Sandanger TM, et al. Systemic inflammation markers and cancer incidence in the UK Biobank. *Eur J Epidemiol* (2021) 36:841–8. doi: 10.1007/s10654-021-00752-6

18. Yorita Christensen KL, Carrico CK, Sanyal AJ, Gennings C. Multiple classes of environmental chemicals are associated with liver disease: NHANES 2003-2004. *Int J hygiene Environ Health* (2013) 216:703–9. doi: 10.1016/j.ijheh.2013.01.005

19. Park S, Kim K, Lee BK, Ahn J. A healthy diet rich in calcium and vitamin C Is inversely associated with metabolic syndrome risk in Korean adults from the KNHANES 2013-2017. *Nutrients.* (2021) 13:1300–12. doi: 10.3390/nu13041312

20. Saraf-Bank S, Haghighatdoost F, Esmaillzadeh A, Larijani B, Azadbakht L. Adherence to healthy eating index-2010 is inversely associated with metabolic syndrome and its features among Iranian adult women. *Eur J Clin Nutr* (2017) 71:425–30. doi: 10.1038/ejcn.2016.173

21. Esposito K, Marfella R, Ciotola M, Di Palo C, Giugliano F, Giugliano G, et al. Effect of a mediterranean-style diet on endothelial dysfunction and markers of vascular inflammation in the metabolic syndrome: A randomized trial. *Jama.* (2004) 292:1440–6. doi: 10.1001/jama.292.12.1440

22. Kastorini CM, Milionis HJ, Esposito K, Giugliano D, Goudevenos JA, Panagiotakos DB. The effect of Mediterranean diet on metabolic syndrome and its components: a meta-analysis of 50 studies and 534,906 individuals. *J Am Coll Cardiol* (2011) 57:1299–313. doi: 10.1016/j.jacc.2010.09.073

23. Saneei P, Salehi-Abargouei A, Esmaillzadeh A, Azadbakht L. Influence of Dietary Approaches to Stop Hypertension (DASH) diet on blood pressure: A systematic review and meta-analysis on randomized controlled trials. *Nutrition metabolism Cardiovasc Dis NMCD.* (2014) 24:1253–61. doi: 10.1016/j.numecd.2014.06.008

24. Ma Y, Hébert JR, Li W, Bertone-Johnson ER, Olendzki B, Pagoto SL, et al. Association between dietary fiber and markers of systemic inflammation in the Women's health initiative observational study. *Nutr (Burbank Los Angeles County Calif).* (2008) 24:941–9. doi: 10.1016/j.nut.2008.04.005

25. Lefevre M, Jonnalagadda S. Effect of whole grains on markers of subclinical inflammation. *Nutr Rev* (2012) 70:387–96. doi: 10.1111/j.1753-4887.2012.00487.x

26. Soltani S, Chitsazi MJ, Salehi-Abargouei A. The effect of dietary approaches to stop hypertension (DASH) on serum inflammatory markers: A systematic review and meta-analysis of randomized trials. *Clin Nutr (Edinburgh Scotland).* (2018) 37:542–50. doi: 10.1016/j.clnu.2017.02.018

27. Monteiro R, Azevedo I. Chronic inflammation in obesity and the metabolic syndrome. *Mediators inflammation.* (2010) 2010:1–10. doi: 10.1155/2010/289645

28. Wang Q, Yuan J, Yu Z, Lin L, Jiang Y, Cao Z, et al. FGF21 Attenuates High-Fat Diet-Induced cognitive impairment *via* metabolic regulation and Anti-inflammation of Obese Mice. *Mol neurobiology.* (2018) 55:4702–17. doi: 10.1007/s12035-017-0663-7

29. Li K, Huang T, Zheng J, Wu K, Li D. Effect of marine-derived n-3 polyunsaturated fatty acids on C-reactive protein, interleukin 6 and tumor necrosis factor α: A meta-analysis. *PloS One* (2014) 9:e88103. doi: 10.1371/journal.pone.0088103

30. Trompette A, Gollwitzer ES, Yadava K, Sichelstiel AK, Sprenger N, Ngom-Bru C, et al. Gut microbiota metabolism of dietary fiber influences allergic airway disease and hematopoiesis. *Nat Med* (2014) 20:159–66. doi: 10.1038/nm.3444

31. Casas R, Sacanella E, Estruch R. The immune protective effect of the Mediterranean diet against chronic low-grade inflammatory diseases. *Endocrine Metab Immune Disord Drug targets.* (2014) 14:245–54. doi: 10.2174/1871530314666140922153350

32. Ahmed MH, Byrne CD. Modulation of sterol regulatory element binding proteins (SREBPs) as potential treatments for non-alcoholic fatty liver disease (NAFLD). *Drug Discovery Today* (2007) 12:740–7. doi: 10.1016/j.drudis.2007.07.009

33. Copur S, Demiray A, Kanbay M. Uric acid in metabolic syndrome: Does uric acid have a definitive role? *Eur J Internal Med* (2022) 103:4–12. doi: 10.1016/j.ejim.2022.04.022

34. Giugliano D, Ceriello A, Esposito K. The effects of diet on inflammation: Emphasis on the metabolic syndrome. *J Am Coll Cardiol* (2006) 48:677–85. doi: 10.1016/j.jacc.2006.03.052

frontiers | Frontiers in Endocrinology

TYPE Original Research
PUBLISHED 14 February 2024
DOI 10.3389/fendo.2024.1291895

OPEN ACCESS

EDITED BY
Sijung Yun,
Predictiv Care, Inc., United States

REVIEWED BY
Cemil Oğlak,
Diyarbakır Gazi Yaşargil Training and Research Hospital, Türkiye
Maulana Yusuf Alkandahri,
Universitas Buana Perjuangan Karawang, Indonesia

*CORRESPONDENCE
Hongqing Wang
wanghongqing@bjfu.edu.cn

†These authors share first authorship

RECEIVED 10 September 2023
ACCEPTED 24 January 2024
PUBLISHED 14 February 2024

CITATION
Liu C, Yang H, Yang J and Wang H (2024) Correlation analysis of diabetes based on Copula.
Front. Endocrinol. 15:1291895.
doi: 10.3389/fendo.2024.1291895

Correlation analysis of diabetes based on Copula

Chang Liu[1†], Hu Yang[1†], Junjie Yang[2†] and Hongqing Wang[1*]

[1]College of Science, Beijing Forestry University, Beijing, China, [2]State Key Laboratory of Vegetation and Environmental Change, Institute of Botany, Chinese Academy of Sciences, Beijing, China

Introduction: The ratio of Triglyceride (TG) to high-density lipoprotein cholesterol (HDL-C) is a crucial indicator for diabetes diagnosis.

Methods: This study utilizes the Copula function to model and fit the non-linear correlation among fasting blood glucose (Glu), glycosylated hemoglobin (HbA1C), and TG/HDL-C in patients with diabetes. The Copula function chosen for this study includes the two-dimensional Archimedes and Elliptical distribution family, as well as the multidimensional Vine Copula function, for fitting the data. The evaluation of the fitting effect is performed using the mean absolute error (MAE) and mean square error (MSE).

Results: The results indicate that the Clayton Copula exhibits the highest effectiveness in fitting the pairwise relationship between Glu and TG/HDL-C, as well as HbA1C and TG/HDL-C, displaying the smallest fitting error. Additionally, the Vine Copula function produces a satisfactory fit for the relationship among all three indicators. Compared to linear analysis methods, the Copula function more accurately depicts the correlation among these three types of indicators.

Discussion: Moreover, our findings indicate a stronger correlation in the lower tail between Glu and HbA1C, as well as TG/HDL-C, suggesting that the Copula function provides greater accuracy and applicability in depicting the relationship among these indicators. As a result, it can offer a more precise auxiliary diagnosis and serve as a valuable reference in clinical judgment.

KEYWORDS

fasting blood glucose, glycosylated hemoglobin, triglyceride, high-density lipoprotein cholesterol, nonlinear correlation

1 Introduction

Diabetes is a metabolic disease characterized by hyperglycemia resulting from defective insulin secretion or damage to the pancreatic islets (1). A recent report indicates that the global population with diabetes reached approximately 537 million in 2021, and this number is continuously increasing at a rapid pace (2, 3). Due to the complex nature of the

disease, there is currently no medical cure for diabetes. Instead, treatment focuses on regulating blood glucose levels through various methods of control and management. Diabetes is prominently listed among the top 10 causes of death globally, according to the World Health Organization's 2019 report. Given the prevalence and treatment challenges associated with diabetes, it is crucial to explore its underlying causes and indicators, detect early signs, and intervene to mitigate its progression.

Chronically elevated blood glucose level in diabetic patients often leads to abnormal lipid metabolism, typically marked by increased Triglyceride (TG) concentration and decreased high-density lipoprotein cholesterol (HDL-C) concentration (2, 4). He et al. were the first to propose that TG/HDL-C is a more effective predictor of diabetes compared to individual TG or HDL-C levels, representing an independent risk factor for diabetes (5). Researchers typically employ one-way or multi-factorial analysis of variance, Pearson correlation analysis, linear analysis methods, and Cox proportional risk models to test the validity of their hypotheses and determine significant differences between factors, aiming to establish independent predictors of a given condition (4, 6–9). For example, in a study involving a test-control group, patient information such as age, gender, and Body Mass Index (BMI) is recorded. Logistic analysis modeling is then employed to analyze fasting blood glucose (Glu), 2-hour postprandial blood glucose (2hPG), glycosylated hemoglobin (HbA1C), TG, total cholesterol (TC), and HDL-C concentrations. Multifactorial analysis reveals a significant positive correlation between TG/HDL-C and Glu as well as HbA1C, highlighting the former as an important predictor of diabetes (2, 5, 10). Furthermore, some researchers have discovered nonlinear relationships among different indicators that cannot be adequately explored using linear analysis methods alone. For example, Chen noted the complex relationship between TG/HDL-C, Glu, and HbA1C and employed a generalized additive model to investigate this relationship further; however, the nonlinear correlation has yet to be thoroughly explored (2).

Copula function, a tool commonly used in probability theory and statistics, is primarily utilized for describing and modeling the joint probability distribution function of multi-dimensional random variables. It combines each marginal distribution with a function called Copula to represent the joint distribution of multi-dimensional random variables, which has the characteristics of flexible structure, simple solution, wide applicability, etc. It can fit the joint distribution of a variety of different distribution variables. At present, it is widely used in nonlinear relationships in finance, wind power, water conservancy, and other fields, but is still poorly used in the medical field (11–13). Espasandín-Domínguez et al. proposed the use of a generalized nonlinear additive model and Copula function to establish the dual response variable of glycosylated hemoglobin and fructosamine to investigate their relationship with blood glucose, providing valuable clinical insights (14). Robinson Dettoni et al. employed a semi-parametric recursive copula to model the relationship between obesity and related conditions such as hypertension, hyperlipidemia, and diabetes using the theory of health production. The results indicate that reducing obesity rates could help decrease morbidity and mortality rates associated with these diseases (15). In current clinical trials, it has been found that TG/HDL-C has a certain correlation with various indicators in patients, and the ratio can reflect the changes in blood glucose concentration to a certain extent (5, 9, 16). However, general linear methods struggle to accurately represent the complex nonlinear relationship among TG/HDL-C, Glu, and HbA1C. Consequently, there have been no studies exploring the nonlinear correlation between these three variables utilizing Copula functions. Thus, this paper aims to further investigate the nonlinear relationship between TG/HDL-C, Glu, and HbA1C in patients using Copula functions. We hypothesize that when TG/HDL-C levels are elevated, the correlations between these three variables strengthen, offering new perspectives for the auxiliary diagnosis of diabetes.

2 Materials and methods

2.1 Description of data

The data used in this study is obtained from the National Data Center for Population Health Sciences Data warehouse PHDA 2022, (https://www.ncmi.cn//phda/dataDetails.do?id=CSTR:A0006.11.A0005.201905.000282), a diabetes complication early warning dataset uploaded by the General Hospital of the Chinese People's Liberation Army. This dataset includes de-identified information for three thousand patients, encompassing personal details such as age, gender, ethnicity, and marital status. Additionally, it comprises measurements of Glu, HbA1C, TC, TG, HDL-C, and low-density lipoprotein cholesterol (LDL-C), all of which were appropriately processed and standardized.

2.2 Application of copula function in this paper

Sklar's definition of the Copula function highlights its critical role in one-dimensional and multidimensional joint distributions (17). In short, a joint distribution function H with marginal distribution functions F and G must have a unique Copula function such that:

$$H(x, y) = C(F(x, y), G(x, y)).$$

Different Copula functions serve different purposes, depending on the characteristics of the variables' distribution. For instance, the Clayton Copula function's asymmetric tail characteristics capture the asymmetric tail correlation between random variables and are more responsive to distribution changes in the lower tail. If the Clayton Copula function portrays the correlation structure between two variables, the lower tail of the distribution has a strong correlation. For joint distributions with three or more dimensions, the Vine Copula function describes many

correlations between variables, and the number of correlations it describes increases as the dimension of the joint distribution grows, making its advantages more pronounced.

This study primarily uses Copula functions from the two-dimensional Archimedes and Elliptical families for modeling the relationship between TG/HDL-C and Glu and between TG/HDL-C and HbA1C. To examine the nonlinear relationship among TG/HDL-C, Glu, and HbA1C, we utilize the Vine Copula function for multidimensional data.

If the Copula function effectively models the nonlinear correlation between TG/HDL-C, Glu, and HbA1C, it suggests a robust nonlinear correlation among the three. Thus, TG/HDL-C can serve as an auxiliary diagnostic indicator of diabetes, aiding in clinical prevention and diagnosis of diabetes.

2.3 Box-Cox transform

Box-Cox transform is a widely used method for data transformation, primarily employed to convert non-normally distributed datasets into approximately normally distributed ones (18). By adjusting the power parameters, the data is transformed as follows:

$$y(\lambda) = \begin{cases} \frac{(y+\varepsilon)^{\lambda}+1}{\lambda}, \lambda \neq 0 \\ \log\ (y), \lambda = 0 \end{cases},$$

where y denotes the original data, λ is the idempotent parameter and ε is a constant to ensure that the data are all positive. If $\lambda = 0$, it is a logarithmic transformation. In this paper, we utilize the method of minimizing the difference between skewness and kurtosis to determine the optimal λ value.

The Box-Cox transformation enhances the likelihood of the data conforming to normal distribution characteristics. Additionally, it aids in reducing unobservable errors in the data, thereby mitigating potential errors arising from manually recorded patient information. This process facilitates subsequent analysis in this paper.

3 Results

According to international standards, Glu and HbA1C are currently used as important indicators for the diagnosis of diabetes mellitus (19–21). Therefore, in this paper, Glu and HbA1C are considered as the dependent variables, and TG/HDL-C is analyzed as the independent variable (2, 3, 10). After addressing missing values by either removing or filling them, and eliminating outliers using the 3σ principle, a total of 2,901 valid data points are obtained. The present study then extracts and calculates the patients' Glu, HbA1C, and TG/HDL-C levels. Given that the internal indicators of patient data generally exhibit nonlinear relationships, the Spearman correlation coefficient is more representative of such relationships. Consequently, this paper conducts a Spearman correlation analysis among these three variables, and the results are depicted in Figure 1.

The correlation analysis plots indicate a positive correlation between TG/HDL-C and both Glu and HbA1C, with correlation coefficients of 0.18 and 0.067, respectively. However, these correlation coefficients are relatively low, suggesting that the positive correlation between TG/HDL-C and Glu or HbA1C is not very strong. Therefore, it can be speculated that the positive correlation between TG/HDL-C and both Glu and HbA1C is not completely independent of each other. To test the hypothesis of independence, the following hypotheses are considered:

the original hypothesis H_0: TG/HDL-C is independent of both Glu and HbA1C;

the alternative hypothesis H_1: TG/HDL-C is not independent of either Glu or HbA1C.

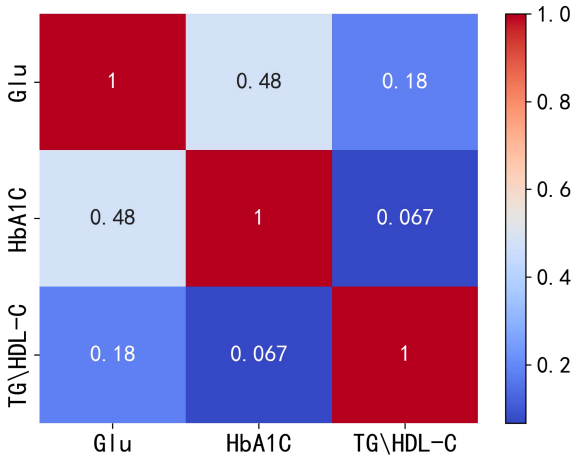

FIGURE 1
Heat map of correlation between Glu, HbA1C and TG/HDL-C. Glu, fasting blood glucose; HbA1C, glycosylated hemoglobin; TG/HDL-C, the ratio of Triglyceride(TG) to high-density lipoprotein cholesterol(HDL-C).

The results reveal a P value of 7.6362*e-13(***), which leads to the rejection of the original hypothesis and acceptance of the alternative hypothesis. This indicates that TG/HDL-C is indeed not independent of both Glu and HbA1C.

Considering the presence of correlation among the three variables, albeit with low correlation coefficients, and the lack of independence between TG/HDL-C and Glu or HbA1C, this study suggests the existence of a nonlinear relationship. To further analyze the correlation among these indicators in diabetic patients, the Copula function is introduced, which is known for its effectiveness in handling nonlinear relationships (17).

3.1 Marginal distribution of the fitted variables

In the paper, the Box-Cox transform is applied to normalize the data. Following the transformation, scatter plots, density distribution histograms, and Q-Q plots are utilized to assess the distribution of the variables. The closer the density distribution histogram resembles a normal curve and the more the data points in the Q-Q plots align with a straight line, the more indicative it is of the variables conforming to a normal distribution. Figures 2 and 3 present scatter plots, density distribution histograms, and Q-Q plots for TG/HDL-C, Glu, and HbA1C. These visualizations provide a rough evaluation of the distribution characteristics of the variables after the Box-Cox transform.

Based on Figures 2 and 3, it can be preliminarily observed that the density distribution histogram of Glu, HbA1C, and TG/HDL-C approximately conforms to a normal distribution curve, and the data points in the Q-Q plots mostly align with a straight line. This suggests that these variables may follow a normal distribution. To confirm the normality of these variables, a normality test is performed. Table 1 presents the results of the normality test for Glu, HbA1C, and TG/HDL-C.

Table 1 indicates that the p-values from the K-S test and normality test for Glu, HbA1C, and TG/HDL-C variables are greater than 0.05, which suggests that there is no significant evidence to reject the hypothesis of conformity to a normal distribution for these variables. Therefore, based on the test results, it can be concluded that all three variables conform to a normal distribution.

3.2 Fitting the edge distribution of the variables

According to the previous section, the study establishes that all three variables can be fitted with normal distribution, so in this section, this paper is going to select the appropriate copula function for fitting the joint distribution function of TG/HDL-C and Glu, as well as TG/HDL-C and HbA1C, and use the appropriate indexes to assess the goodness of fit.

3.2.1 Copula fitting of TG/HDL-C variables to Glu variables

Based on the different characteristics of the two types of index data, TG/HDL-C and Glu, in the dataset, a total of six copulas are selected for fitting, including Clayton Copula, Gumbel Copula, Frank Copula, Ali–Mikhail–Haq Copula in Archimedes Copula, Gauss Copula and Student(t) Copula in Elliptical Copulas. Copula function's density distribution and joint distribution images are produced. We use MAE and MSE to evaluate the fitting effect of each type of copula function and the smaller these indicators, the better the fit. The images of the joint distribution function and the probability distribution function obtained after fitting using the six copula functions mentioned above are depicted in Figures 4 and 5, respectively.

Table 2 presents the goodness of fit results for Clayton Copula, Gumbel Copula, Frank Copula, Ali–Mikhail–Haq Copula, Gauss Copula, and t Copula. The table includes the MAE and MSE values.

From the fitted images and the comparison of simulation fitting errors among the six copula functions, it is evident that copula functions are effective in fitting the correlation between TG/HDL-C and Glu. Among these, Clayton Copula produces the smallest error in both categories and exhibits the best-fitting effect for TG/HDL-C and Glu.

3.2.2 Copula fitting of TG/HDL-C variables to HbA1C variables

The dataset's distinct characteristics of the two types of data, TG/HDL-C and HbA1C, lead to the selection of six copulas for fitting: Clayton Copula, Gumbel Copula, Frank Copula, Ali–Mikhail–Haq Copula in Archimedes Copula, Gauss Copula, and t Copula in Elliptical Copulas. Subsequently, the density distribution

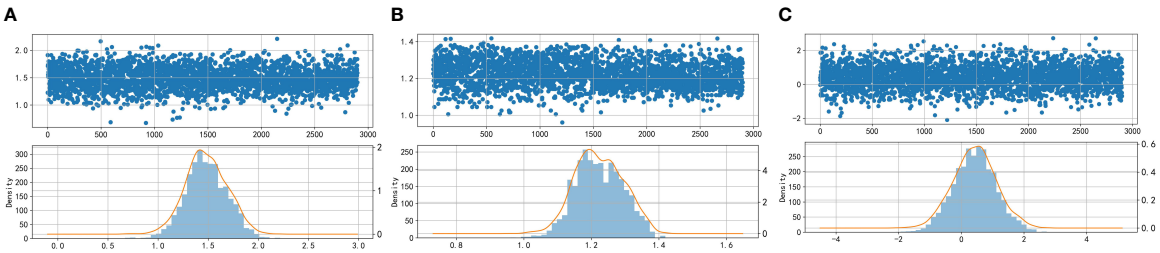

FIGURE 2
Scatter plots and histograms of density distributions of Glu **(A)**, HbA1C **(B)**, and TG/HDL-C **(C)**. Glu, fasting blood glucose; HbA1C, glycosylated hemoglobin; TG/HDL-C, the ratio of Triglyceride(TG) to high-density lipoprotein cholesterol(HDL-C). When the curves are approximately normally distributed, the data can be considered to be approximately fitted with a normal distribution.

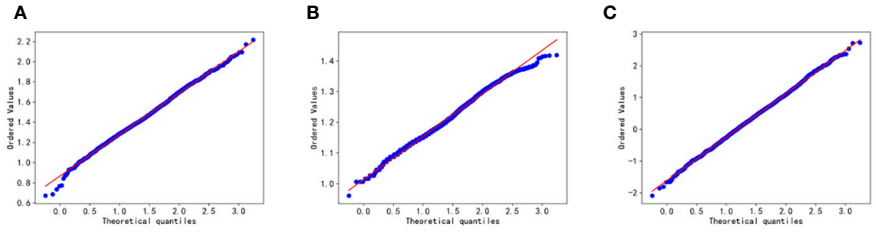

FIGURE 3
Q-Q plot test for Glu **(A)**, HbA1C **(B)**, and TG/HDL-C **(C)**. Glu, fasting blood glucose; HbA1C, glycosylated hemoglobin; TG/HDL-C, the ratio of Triglyceride(TG) to high-density lipoprotein cholesterol(HDL-C). Data are considered to pass the Q-Q plot normality test when the data points fall approximately on a straight line.

of each copula function is generated after fitting, resulting in the production of the density distribution function and joint distribution function images. Evaluation of the fitting effect for each type of copula function is conducted using MAE and MSE, with smaller values indicating better fitting. The graphical representation of the fit and effect of the six copula functions is depicted in Figures 6 and 7, showing the images of the joint distribution function and the probability distribution function obtained after fitting using the selected copula functions.

Table 3 presents the goodness of fit results for Clayton Copula, Gumbel Copula, Frank Copula, Ali–Mikhail–Haq Copula, Gauss Copula, and t Copula. The table includes the MAE and MSE values.

After fitting the images of the six copula functions and comparing the simulated fitting errors for the different copula functions, it can be concluded that copula functions effectively fit the correlation between TG/HDL-C and HbA1C. Clayton Copula produced the smallest error in both categories and exhibited the best fit for TG/HDL-C and HbA1C.

3.2.3 Fitting between TG/HDL-C, Glu and HbA1C

For modeling the function with both Glu and HbA1C variables as dependent variables and TG/HDL-C as an independent variable, a multidimensional Copula function can be utilized to achieve a good fit. In this paper, Vine Copula is selected for fitting based on data characteristics. However, due to the high dimensionality of the data, the joint distribution function and probability distribution function of the data could not be displayed graphically. To overcome this challenge, we employ the fitted three-dimensional Vine Copula to generate random numbers, which are then plotted against the dataset of this study for comparison. Figure 8 depicts the scatter plot of this dataset with the generated random data from the fitted Copula function.

By comparing the two scatter plots, it can be observed that there is no significant difference between the left and right plots. This finding suggests that Vine Copula provides a better fit for Glu, HbA1C, and TG/HDL-C variables.

TABLE 1 Tests for normal distribution of Glu, HbA1C and TG/HDL-C variables.

Variable	K-S test		Normality test	
	pass or fail	p-value	pass or fail	p-value
Glu	pass	0.1967	pass	0.7598
HbA1C	pass	0.2771	pass	0.9008
TG/HDL-C	pass	0.8942	pass	0.8205

Glu, fasting blood glucose; HbA1C, glycosylated hemoglobin; TG/HDL-C, the ratio of Triglyceride(TG) to high-density lipoprotein cholesterol(HDL-C).

3.3 Analysis of results

The six selected copula functions fit TG/HDL-C to Glu, TG/HDL-C to HbA1C, and the joint distribution of the three relatively well, with both types of errors (MAE and MSE) remaining within acceptable limits. Among them, the best fit is the Clayton Copula, which exhibits the lowest errors among the six copula functions. The parameters in the Clayton Copula function obtained by modeling TG/HDL-C and Glu, and TG/HDL-C and HbA1C are as follows, respectively:

$$\theta_{Glu} = 0.2146;$$
$$\theta_{HbA1C} = 0.0525.$$

This results in two Clayton Copula modeling function formulas, one obtained by modeling TG/HDL-C and Glu, and the other obtained by modeling TG/HDL-C and HbA1C:

$$C_1(u_{Glu}, u_{TG/HDL-C}; \theta_{Glu}) = \max\left\{\left(u_{Glu}^{-\theta_{Glu}} + u_{TG/HDL-C}^{-\theta_{Glu}} - 1\right)^{-\frac{1}{\theta_{Glu}}}, 0\right\};$$

$$C_2(u_{HbA1C}, u_{TG/HDL-C}; \theta_{HbA1C}) = \max\left\{\left(u_{HbA1C}^{-\theta_{HbA1C}} + u_{TG/HDL-C}^{-\theta_{HbA1C}} - 1\right)^{-\frac{1}{\theta_{HbA1C}}}, 0\right\}.$$

In Section 2, we discussed that the Clayton Copula is particularly sensitive to changes in the lower tail of variable distribution, and can more accurately reflect changes in the lower tail between variables (22). In our study, the lower tail portion of the variables is evident by an increase in TG/HDL-C accompanied by an increase in Glu or HbA1C. As the values of TG/HDL-C, Glu, or HbA1C increase, the nonlinear correlation between the three becomes stronger, indicating a significant correlation. Therefore, it can be concluded that TG/HDL-C is an important predictor of diabetes.

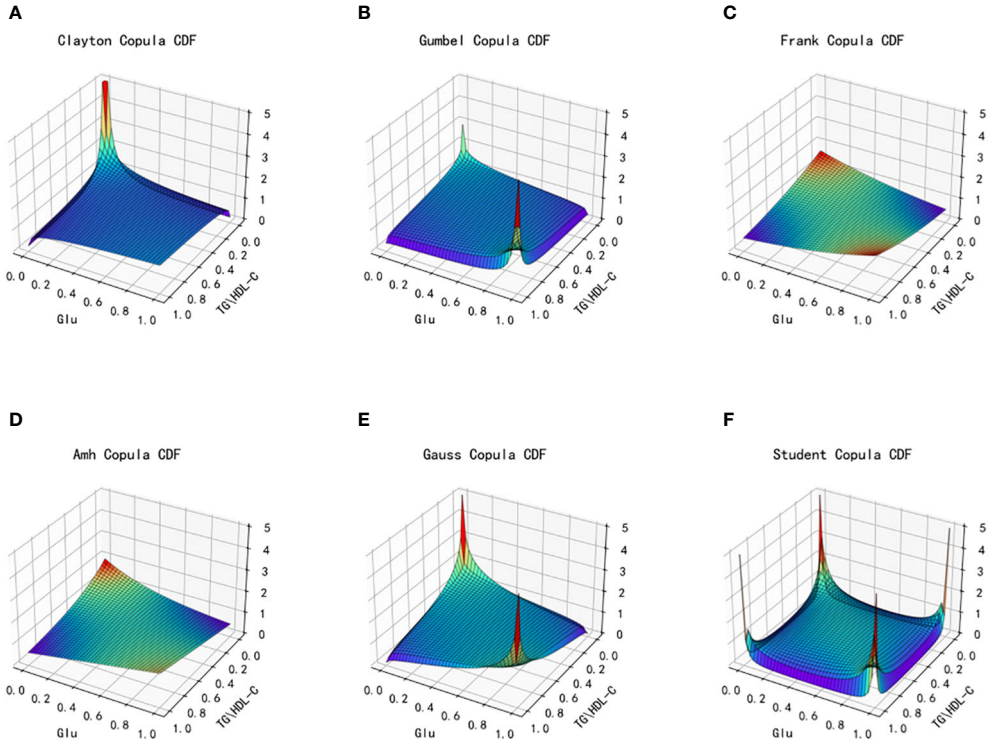

FIGURE 4
Joint distribution function images of six copulas fitting for TG/HDL-C and Glu. **(A)** Clayton Copula, **(B)** Gumbel Copula, **(C)** Frank Copula, **(D)** Ali–Mikhail–Haq Copula, **(E)** Gauss Copula, **(F)** student Copula. TG/HDL-C, the ratio of Triglyceride(TG) to high-density lipoprotein cholesterol(HDL-C); Glu, fasting blood glucose.

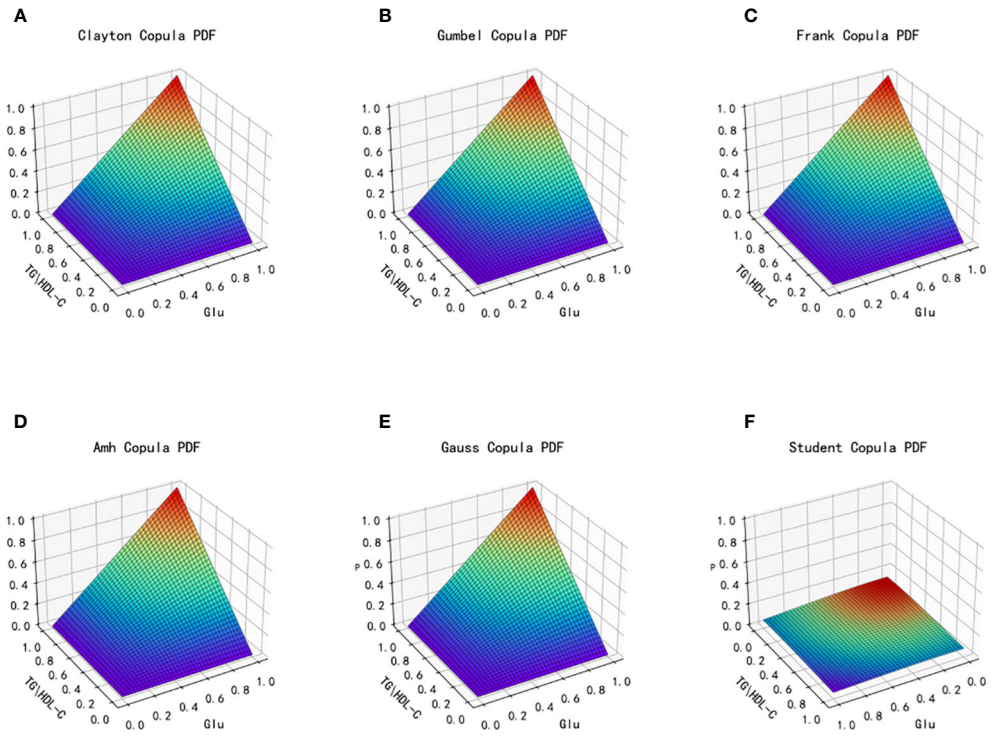

FIGURE 5
Probability distribution function images of six copulas fitting for TG/HDL-C and Glu. **(A)** Clayton Copula, **(B)** Gumbel Copula, **(C)** Frank Copula, **(D)** Ali–Mikhail–Haq Copula, **(E)** Gauss Copula, **(F)** student Copula. TG/HDL-C, the ratio of Triglyceride(TG) to high-density lipoprotein cholesterol(HDL-C); Glu, fasting blood glucose.

TABLE 2 Effect of copula function fitting for TG/HDL-C and Glu.

Types of copula functions	Copula function name	MAE	MSE
Archimedes Copula	Clayton Copula	0.6613	0.5880
	Gumbel Copula	0.7915	0.8308
	Frank Copula	0.7827	0.8152
	Ali–Mikhail–Haq Copula	0.7881	0.8188
Elliptical Copula	Gauss Copula	0.7880	0.8273
	Student(t) Copula	0.7819	0.8109

TG/HDL-C, the ratio of Triglyceride(TG) to high-density lipoprotein cholesterol(HDL-C); Glu, fasting blood glucose.

3.4 The linear analysis method fitting

Commonly used statistical methods in the medical field include one-way and multivariate analysis of variance, as well as simulations utilizing logistic analysis methods to obtain variable predictors and variability in trial data (23, 24). However, these methods fail to fully consider the complex nonlinear correlations between variables, often leading to overlooked factors or disregarded complex relationships, resulting in a poor fit and imprecise responses to variable changes. For the characteristics of this dataset, we opt for the linear analysis method to construct a simulation fit and compare it with the Copula functions used in this study.

TG/HDL-C is modeled as the independent variable, while Glu and HbA1C are modeled as dependent variables, respectively. Subsequently, we obtain the following linear analysis model equations:

$$\hat{y}_{Glu} = 0.2355x + 7.9132;$$

$$\hat{y}_{HbA1C} = 0.0699x + 7.6585.$$

For the established models, the same two metrics, MAE and MSE, are used to assess the fit of the models, and Table 4 shows a table of the effect of the linear analysis methods fitting TG/HDL-C to Glu and TG/HDL-C to HbA1C.

By examining the fitting errors of the linear analysis method, it is determined that the model's fitting errors for TG/HDL-C to Glu and TG/HDL-C to HbA1C both exceed 1, indicating substantial errors and an acceptable fit. Conversely, the six copula functions discussed in the previous section exhibit fitting errors all below 1. Among them, the best-fitting Clayton Copula function yields errors of 0.6613 (MAE), 0.5880 (MSE) for TG/HDL-C to Glu, and 0.4190 (MAE), 0.3794 (MSE) for TG/HDL-C to HbA1C. These results unequivocally demonstrate that the fitting effect of Copula functions surpasses that of the linear analysis method commonly employed in medical research.

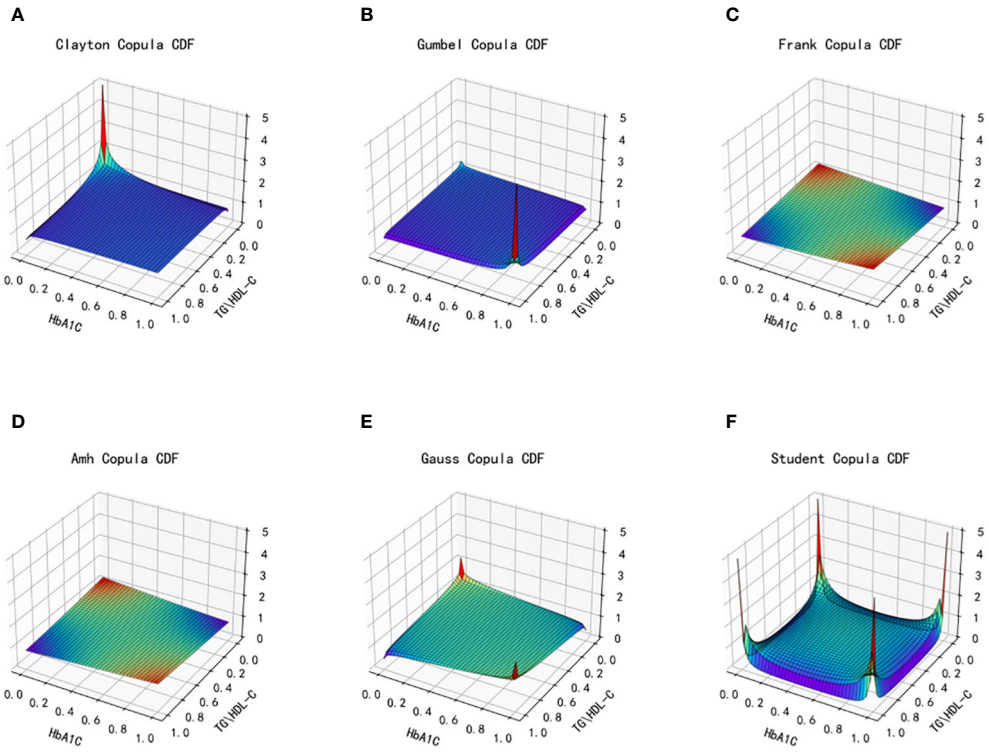

FIGURE 6
Joint distribution function images of six copulas fitting for TG/HDL-C and HbA1C. **(A)** Clayton Copula, **(B)** Gumbel Copula, **(C)** Frank Copula, **(D)** Ali–Mikhail–Haq Copula, **(E)** Gauss Copula, **(F)** student Copula. TG/HDL-C, the ratio of Triglyceride(TG) to high-density lipoprotein cholesterol(HDL-C); HbA1C, glycosylated hemoglobin.

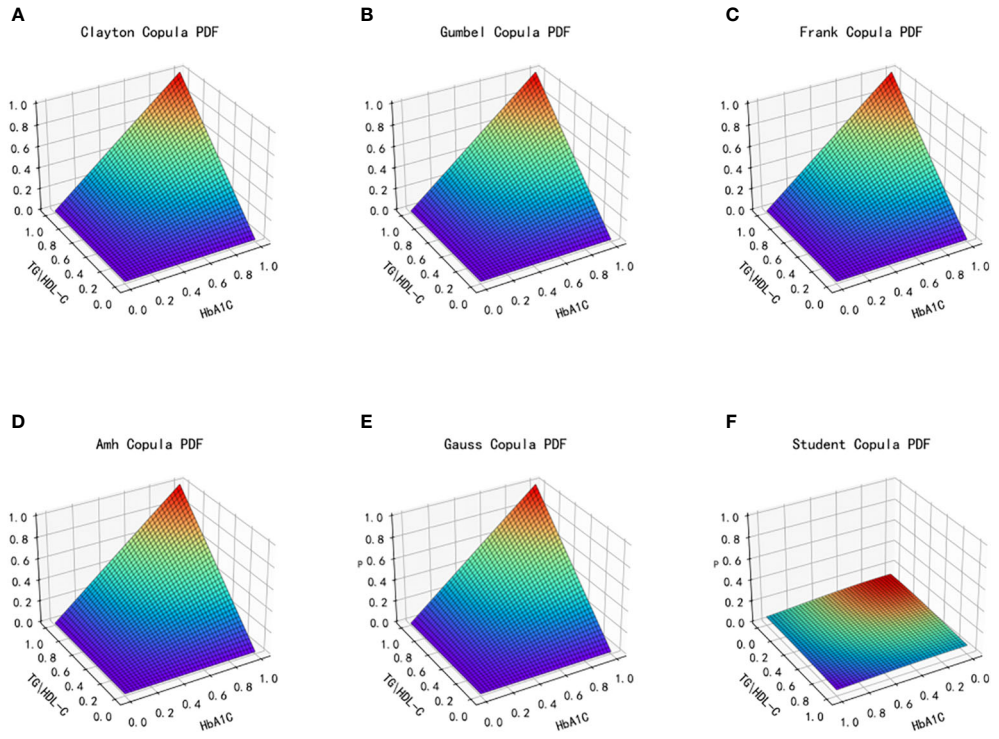

FIGURE 7
Probability distribution function images of six copulas fitting for TG/HDL-C and HbA1C. **(A)** Clayton Copula, **(B)** Gumbel Copula, **(C)** Frank Copula, **(D)** Ali–Mikhail–Haq Copula, **(E)** Gauss Copula, **(F)** student Copula. TG/HDL-C, the ratio of Triglyceride(TG) to high-density lipoprotein cholesterol (HDL-C); HbA1C, glycosylated hemoglobin.

3.5 Construct the linear analysis models and Copula function methods

Table 5 presents the simulation error tables constructed for the Copula function and the linear analysis method, demonstrating their application to TG/HDL-C to Glu and TG/HDL-C to HbA1C in this paper.

The error data obtained from fitting the linear analysis method in the aforementioned table indicates an inadequate correlation between TG/HDL-C and Glu, as well as TG/HDL-C and HbA1C. This suggests that the linear analysis method fails to adequately capture the intricate relationship between these indicators. A comparison with the previous error table for the copula function's fitting reveals that the Copula function is more accurate in depicting the nonlinear correlations among Glu, HbA1C, and TG/HDL-C indicators in diabetic patients. This is attributed to the Copula function's capability to capture intricate nonlinear relationships and tail correlations. In this study, the Copula function effectively demonstrates its capacity to identify intricate nonlinear relationships among TG/HDL-C, Glu, and HbA1C indicators. Particularly in the lower tail section, when the TG to HDL-C ratio is higher, the Copula function accurately represents the changes in Glu and HbA1C indicators, which exhibit stronger nonlinear correlations with it. Consequently, the Copula function proves to be more precise in the analysis of nonlinear correlations among TG/HDL-C, Glu, and HbA1C indicators. Consequently, the implementation of the Copula function in exploring the patient's internal index data yields more significant results. It enables the analysis and identification of nonlinear relationships in the patient's data through a closer fitting effect, consequently offering more precise predictions and diagnostic references in clinical judgment.

TABLE 3 Effect of copula function fitting for TG/HDL-C and HbA1C.

Types of copula functions	Copula function name	MAE	MSE
Gumbel Copula	Clayton Copula	0.4190	0.3794
	Archimedes Copula	0.5932	0.4975
	Frank Copula	0.5916	0.4929
	Ali–Mikhail–Haq Copula	0.4962	0.4064
Elliptical Copula	Gauss Copula	0.5954	0.4941
	t Copula	0.5890	0.4857

TG/HDL-C, the ratio of Triglyceride(TG) to high-density lipoprotein cholesterol(HDL-C); HbA1C, glycosylated hemoglobin.

4 Discussion

This study utilizes Copula functions to investigate the nonlinear relationships among three key indicators in diabetic patients: Glu, HbA1C, and TG/HDL-C. A comprehensive data analysis reveals that the Clayton Copula demonstrates particular sensitivity to the lower tail dependence of these indicators, effectively reflecting their variations. Remarkably, an elevated TG/HDL-C exhibits a

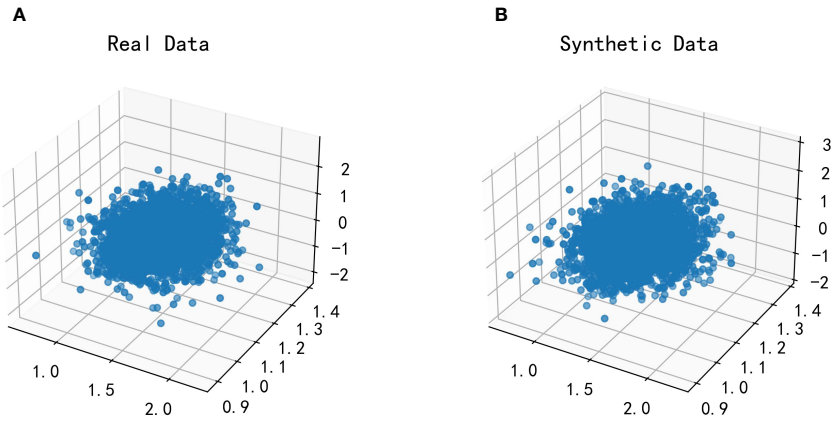

FIGURE 8
Plot of the effect of fitting the Vine Copula function for TG/HDL-C, Glu and HbA1C. Glu, fasting blood glucose; HbA1C, glycosylated hemoglobin; TG/HDL-C, the ratio of Triglyceride(TG) to high-density lipoprotein cholesterol(HDL-C). **(A)** is the scatter plot of the real dataset in this paper; **(B)** is the scatter plot of the randomized data generated after fitting by the Vine Copula function.

significant correlation with both Glu and HbA1C, highlighting the predictive significance of TG/HDL-C for diabetes. In comparison to traditional linear analysis methods, Copula functions excel at capturing the intricate nonlinear interrelationships among these indicators, particularly about extreme values.

From a biological standpoint, the relationships among these indicators signify prevalent biochemical alterations in metabolic syndrome, encompassing insulin resistance, dysregulated blood sugar control, and abnormalities in lipid metabolism. Diabetic patients with a high TG to HDL-C ratio exhibit a close association with elevated levels of Glu and HbA1C, unveiling intricate physiological interactions among these markers (2, 5, 6, 9, 10, 25, 26–28). This imparts vital information for clinicians, fostering a more comprehensive comprehension of the mechanisms underpinning diabetes and its complications, and enabling more precise diagnoses and personalized treatment plans for patients (29–32).

One of the most significant findings in this study is that employing Copula functions has facilitated a comprehensive comprehension of the intricate interactions among these pivotal indicators in diabetic patients. Nevertheless, our research possesses limitations, encompassing a limited scope of data and inadequate consideration of other pertinent biochemical markers. Subsequent studies ought to augment the sample size, incorporate a greater number of relevant indicators, and employ longitudinal data to further corroborate our findings. Furthermore, implementing these findings in clinical practice for wider validation and assessment also signifies a crucial avenue for future research.

In summary, by conducting a comprehensive analysis of the Glu, HbA1C, and TG/HDL-C indicators in diabetic patients and capitalizing on the strengths of Copula functions, this article offers a fresh standpoint for comprehending and forecasting the advancement of diabetes. These findings are not only groundbreaking in theory but also possess substantial practical applicability in clinical practice.

TABLE 4 Table of the linear analysis method fitting effects of TG/HDL-C with Glu and TG/HDL-C with HbA1C.

Class of equations	MAE	MSE
TG/HDL-C to Glu	2.7700	15.5800
TG/HDL-C to HbA1C	1.4553	7.4578

TG/HDL-C, the ratio of Triglyceride(TG) to high-density lipoprotein cholesterol(HDL-C); Glu, fasting blood glucose; HbA1C, glycosylated hemoglobin.

TABLE 5 Table of fitting effects of seven types of functions.

Function type	TG/HDL-C to Glu		TG/HDL-C to HbA1C	
	MAE	MSE	MAE	MSE
Clayton Copula	0.6613	0.5880	0.4190	0.3794
Gumbel Copula	0.7915	0.8308	0.5932	0.4975
Frank Copula	0.7827	0.8152	0.5916	0.4929
Ali–Mikhail–Haq Copula	0.7881	0.8188	0.4962	0.4064
Gauss Copula	0.7880	0.8273	0.5954	0.4941
t Copula	0.7819	0.8109	0.5890	0.4857
the linear analysis method	2.7700	15.5800	1.4553	7.4578

TG/HDL-C: the ratio of Triglyceride(TG) to high-density lipoprotein cholesterol(HDL-C); Glu:fasting blood glucose; HbA1C:glycosylated hemoglobin.

Data availability statement

The original contributions presented in the study are included in the article/supplementary material. Further inquiries can be directed to the corresponding author.

Ethics statement

The National Population Health Sciences Data Center belongs to public databases. The patients involved in the database have

obtained ethical approval. Users can download relevant data for free for research and publish relevant articles. Our study is based on open source data, so there are no ethical issues and other conflicts of interest.

Author contributions

CL: Conceptualization, Data curation, Formal analysis, Methodology, Software, Validation, Visualization, Writing – original draft. HY: Conceptualization, Writing – original draft. JY: Conceptualization, Formal analysis, Investigation, Resources, Writing – review & editing. HW: Funding acquisition, Investigation, Resources, Validation, Writing – review & editing.

Funding

The author(s) declare financial support was received for the research, authorship, and/or publication of this article. This work was supported by the National Natural Science Foundation of China (No. 41773092) and the National Natural Science Foundation of China (No. 11501032).

Acknowledgments

We would like to thank the National Population Health Sciences Data Center to provide the open datasets platform, and the People's Liberation Army General Hospital for the datasets they provide in this paper.

Conflict of interest

The authors declare that the research was conducted in the absence of any commercial or financial relationships that could be construed as a potential conflict of interest.

Publisher's note

References

1. Moin ASM, Butler AE. Alterations in beta cell identity in type 1 and type 2 diabetes. *Curr Diabetes Rep* (2019) 19:1–12. doi: 10.1007/s11892-019-1194-6

2. Chen Z, Hu H, Chen M, Luo X, Yao W, Liang Q, et al. Association of triglyceride to high-density lipoprotein cholesterol ratio and incident of diabetes mellitus: a secondary retrospective analysis based on a chinese cohort study. *Lipids Health Dis* (2020) 19:1–11. doi: 10.1186/s12944-020-01213-x

3. Zheng D, Li H, Ai F, Sun F, Singh M, Cao X, et al. Association between the triglyceride to high-density lipoprotein cholesterol ratio and the risk of type 2 diabetes mellitus among chinese elderly: the beijing longitudinal study of aging. *BMJ Open Diabetes Res Care* (2020) 8:e000811. doi: 10.1136/bmjdrc-2019-000811

4. Lee M-Y, Hsu W-H, Lai C-W, Chen S-C, Liang C-C. The association between glycated albumin, glycohemoglobin, and glycated albumin to glycohemoglobin ratio in diabetic retinopathy of prediabetes. *Kaohsiung J Med Sci* (2019) 35:695–701. doi: 10.1002/kjm2.12125

5. He S, Wang S, Chen X, Jiang L, Peng Y, Li L, et al. Higher ratio of triglyceride to high-density lipoprotein cholesterol may predispose to diabetes mellitus: 15-year prospective study in a general population. *Metabolism* (2012) 61:30–6. doi: 10.1016/j.metabol.2011.05.007

6. Wang Y-L, Koh W-P, Talaei M, Yuan J-M, Pan A. Association between the ratio of triglyceride to high-density lipoprotein cholesterol and incident type 2 diabetes in Singapore chinese men and women. *J Diabetes* (2017) 9:689–98. doi: 10.1111/1753-0407.12477

7. Johanna GPS, Antonio L-A, Andrés G-S. Correlation between type 2 diabetes, dry eye and meibomian glands dysfunction. *J optometry* (2019) 12:256–62. doi: 10.1016/j.optom.2019.02.003

8. Xie Z, Nikolayeva O, Luo J, Li D. Peer reviewed: building risk prediction models for type 2 diabetes using machine learning techniques. *Preventing chronic Dis* (2019) 16:E130. doi: 10.5888/pcd16.190109

9. Huang Y, Zhu Y, Peng Y, Xia W, Chen L, Yu H, et al. Triglycerides to high-density lipoprotein cholesterol (TG/HDL-C) ratio is an independent predictor of the severity of hyperlipidaemic acute pancreatitis. *J Hepatobiliary Pancreat Sci* (2023) 30(6):784–91. doi: 10.1002/jhbp.1281

10. Mirshafiei H, Darroudi S, Ghayour-Mobarhan M, Esmaeili H, AkbariRad M, Mouhebati M, et al. Altered triglyceride glucose index and fasted serum triglyceride high-density lipoprotein cholesterol ratio predict incidence of cardiovascular disease in the mashhad cohort study. *BioFactors* (2022) 48:643–50. doi: 10.1002/biof.1816

11. Li R, Cheng Y. Flexible association modelling and prediction with semi-competing risks data. *Can J Stat* (2016) 44:361–74. doi: 10.1002/cjs.11289

12. Black JE, Kueper JK, Terry AL, Lizotte DJ. Development of a prognostic prediction model to estimate the risk of multiple chronic diseases: constructing a copula-based model using Canadian primary care electronic medical record data. *Int J Popul Data Sci* (2021) 6(1):1395. doi: 10.23889/ijpds.v6i1.1395

13. Shewa F, Endale S, Nugussu G, Abdisa J, Zerihun K, Banbeta A. Time to kidneys failure modeling in the patients at adama hospital medical college: Application of copula model. *J Res Health Sci* (2022) 22(2):e00549. doi: 10.34172/jrhs.2022.84

14. Espasandín-Domínguez J, Cadarso-Suárez C, Kneib T, Marra G, Klein N, Radice R, et al. Assessing the relationship between markers of glycemic control through flexible copula regression models. *Stat Med* (2019) 38:5161–81. doi: 10.1002/sim.8358

15. Dettoni R, Bahamondes C, Yevenes C, Cespedes C, Espinosa J. The effect of obesity on chronic diseases in usa: a flexible copula approach. *Sci Rep* (2023) 13:1831. doi: 10.1038/s41598-023-28920-6

16. Che B, Zhong C, Zhang R, Pu L, Zhao T, Zhang Y, et al. Triglyceride-glucose index and triglyceride to high-density lipoprotein cholesterol ratio as potential cardiovascular disease risk factors: an analysis of uk biobank data. *Cardiovasc Diabetol* (2023) 22:1–11. doi: 10.1186/s12933-023-01762-2

17. Nelsen RB. *An introduction to copulas*. Springer (2006).

18. Box GE, Cox DR. An analysis of transformations. *J R Stat Soc Ser B: Stat Method* (1964) 26:211–43. doi: 10.1111/j.2517-6161.1964.tb00553.x

19. Kilpatrick ES, Bloomgarden ZT, Zimmet PZ.). International expert committee report on the role of the a1c assay in the diagnosis of diabetes: response to the international expert committee. *Diabetes Care* (2009) 32:e159–9. doi: 10.2337/dc09-1231

20. Association, A D. Diagnosis and classification of diabetes mellitus. *Diabetes Care* (2014) 37:S81–90. doi: 10.2337/dc14-S081

21. Lau C, Aw T. Hba1c in the diagnosis and management of diabetes mellitus: an update. *Diabetes* (2020) 6:1–4. doi: 10.15761/DU.1000137

22. Manstavičius M, Leipus R. Bounds for the clayton copula. *Nonlinear analysis: Model control* (2017) 22:248–60. doi: 10.15388/NA.2017.2.7

23. Ahlqvist E, Storm P, Käräjämäki A, Martinell M, Dorkhan M, Carlsson A, et al. Novel subgroups of adult-onset diabetes and their association with outcomes: a data-driven cluster analysis of six variables. *Lancet Diabetes Endocrinol* (2018) 6:361–9. doi: 10.1016/S2213-8587(18)30051-2

24. Kööts K, Pilt K, Sepa M, Pikta M, Fridolin I, Meigas K, et al. (2021). Assessment of Associations Between Arterial Mechanical Properties and Biochemical Blood Markers for Early Detection of Atherosclerosis, In: Jarm T., Cvetkoska A., Mahnič-

Kalamiza S., Miklavcic D. (eds) *8th European Medical and Biological Engineering Conference. EMBEC 2020*, IFMBE Proceedings. pp. 80. Springer, Cham. doi: 10.1007/978-3-030-64610-3_15

25. McLaughlin T, Reaven G, Abbasi F, Lamendola C, Saad M, Waters D, et al. Is there a simple way to identify insulin-resistant individuals at increased risk of cardiovascular disease? *Am J Cardiol* (2005) 96:399–404. doi: 10.1016/j.amjcard.2005.03.085

26. Kannel WB, Vasan RS, Keyes MJ, Sullivan LM, Robins SJ. Usefulness of the triglyceride–high-density lipoprotein versus the cholesterol–high-density lipoprotein ratio for predicting insulin resistance and cardiometabolic risk (from the framingham offspring cohort). *Am J Cardiol* (2008) 101:497–501. doi: 10.1016/j.amjcard.2007.09.109

27. Drew BG, Rye K-A, Duffy SJ, Barter P, Kingwell BA. The emerging role of hdl in glucose metabolism. *Nat Rev Endocrinol* (2012) 8:237–45. doi: 10.1038/nrendo.2011.235

28. Ikonen E. Cellular cholesterol trafficking and compartmentalization. *Nat Rev Mol Cell Biol* (2008) 9:125–38. doi: 10.1038/nrm2336

29. Kraegen EW, Cooney GJ, Turner N. Muscle insulin resistance: a case of fat overconsumption, not mitochondrial dysfunction. *Proc Natl Acad Sci* (2008) 105:7627–8. doi: 10.1073/pnas.0803901105

30. Li N, Fu J, Koonen DP, Kuivenhoven JA, Snieder H, Hofker MH. Are hypertriglyceridemia and low hdl causal factors in the development of insulin resistance? *Atherosclerosis* (2014) 233:130–8. doi: 10.1016/j.atherosclerosis.2013.12.013

31. Tenenbaum A, Motro M, Fisman EZ, Schwammenthal E, Adler Y, Goldenberg I, et al. Peroxisome proliferator–activated receptor ligand bezafibrate for prevention of type 2 diabetes mellitus in patients with coronary artery disease. *Circulation* (2004) 109:2197–202. doi: 10.1161/01.CIR.0000126824.12785.B6

32. Unger RH. Lipotoxic diseases. *Annu Rev Med* (2002) 53:319–36. doi: 10.1146/annurev.med.53.082901.104057

frontiers | Frontiers in Endocrinology

TYPE Original Research
PUBLISHED 04 March 2024
DOI 10.3389/fendo.2024.1295927

OPEN ACCESS

EDITED BY
Darko Stefanovski,
University of Pennsylvania, United States

REVIEWED BY
Khashayar Sakhaee,
University of Texas, United States
Claire Joanne Stocker,
Aston University, United Kingdom

*CORRESPONDENCE
Wei Song
songwei726@jlu.edu.cn
Jin Lu
lujin001@jlu.edu.cn
Xiangliang Liu
ds9291@qq.com

†These authors have contributed equally to this work and share first authorship

RECEIVED 17 September 2023
ACCEPTED 23 February 2024
PUBLISHED 04 March 2024

CITATION
Yuguang L, Chang Y, Chen N, Zhao Y, Zhang X, Song W, Lu J and Liu X (2024) Serum klotho as a novel biomarker for metabolic syndrome: findings from a large national cohort. *Front. Endocrinol.* 15:1295927. doi: 10.3389/fendo.2024.1295927

Serum klotho as a novel biomarker for metabolic syndrome: findings from a large national cohort

Li Yuguang[1†], Yu Chang[2†], Naifei Chen[1†], Yixin Zhao[1], Xinwei Zhang[1], Wei Song[1*], Jin Lu[1*] and Xiangliang Liu[1*]

[1]Cancer Center, The First Hospital of Jilin University, Changchun, China, [2]Department of Gastroenterology,The First Hospital of Jilin University, Changchun, China

Background: Metabolic syndrome is a cluster of metabolic abnormalities that significantly increase the risk of cardiovascular disease and mortality. The identification of novel biomarkers associated with mortality in patients with metabolic syndrome could facilitate early risk stratification and targeted interventions.

Methods: We conducted a large prospective cohort study using data from five cycles (2009-2016) of the National Health and Nutrition Examination Survey (NHANES) database, including a total of 40,439 participants. Logistic regression analysis was used to assess the association between serum klotho protein levels and metabolic syndrome, while Cox regression analysis was employed to examine the correlation between serum klotho levels and all-cause mortality. Mortality data were updated until December 31, 2019.

Results: After adjusting for demographic and socioeconomic confounders, the logistic regression model demonstrated that higher serum klotho levels were significantly associated with a decreased prevalence of metabolic syndrome (OR [95% CI] Highest vs. lowest quartile: 0.84 [0.70-0.99], P=0.038). In the Cox regression model, elevated klotho levels were found to significantly reduce the risk of all-cause mortality among individuals with metabolic syndrome (HR [95% CI] Highest vs. lowest quartile: 0.68 [0.51-0.90], P=0.006).

Conclusion: Serum klotho levels were found to be inversely associated with the prevalence of metabolic syndrome, independent of potential confounding factors such as demographics, socioeconomic status, and lifestyle factors. Furthermore, higher klotho levels strongly indicated a lower risk of all-cause mortality in individuals with metabolic syndrome.

KEYWORDS

metabolic syndrome, klotho, mortality, biomarkers, NHANES

1 Introduction

Metabolic syndrome refers to a cluster of metabolic abnormalities and cardiovascular risk factors, including abdominal obesity, dyslipidemia, hypertension, and hyperglycemia (1). The prevalence of metabolic syndrome has increased substantially worldwide over the past few decades, imposing a huge burden on public health (2). Epidemiological studies have consistently shown that metabolic syndrome significantly increases the risk of developing cardiovascular disease, type 2 diabetes, chronic kidney disease, and other metabolic disorders (3–5). Moreover, metabolic syndrome is associated with elevated risks of all-cause and cardiovascular mortality (6, 7). Given the high prevalence and detrimental health consequences of metabolic syndrome, identifying novel risk factors and prognostic biomarkers is of great importance to facilitate early prevention and treatment.

Klotho is an anti-aging protein predominantly produced in the kidney, brain, and endothelial cells (8). A growing body of evidence suggests that Klotho is involved in the regulation of various physiological processes, including oxidative stress, inflammation, insulin sensitivity, glucose homeostasis, etc (3). Animal studies demonstrate that Klotho deficiency results in vascular calcification, accelerated atherosclerosis, and hypertension (9). In humans, higher Klotho levels are associated with reduced risks of chronic kidney diseases (CKD), cardiovascular diseases (CVD), and mortality (7, 10, 11). Preventing the reduction of Klotho levels and enhancing its production can reduce renal fibrosis, slow down the progression of CKD, and improve mineral metabolism in CKD patients. In light of the potential role of Klotho in metabolism-related diseases, recent studies begin to investigate the relationship between Klotho and metabolic syndrome, but the results remain inconsistent, especially regarding the prognostic value of Klotho (12–14).

In the present study, we aim to systematically assess the associations of serum Klotho levels with the prevalence and mortality of metabolic syndrome using a large nationally representative cohort. Our findings may provide novel insights into the pathogenic role of Klotho in metabolic syndrome and support Klotho as an independent prognostic biomarker.

2 Methods

2.1 Study population

The NHANES (National Health and Nutrition Examination Survey) database is a cross-sectional study approved by the Centers for Disease Control and Prevention (CDC) and the Institutional Review Board (IRB), aiming to assess the nutritional status and health of the US population. It utilizes a probability and stratified, multi-stage random sampling method. Participants undergo a series of questionnaire surveys, physical examinations, as well as blood and urine sample collection. For more specific details about the database, please refer to the official website (https://www.cdc.gov/nchs/NHANES/index.htm). We downloaded four consecutive cycles of NHANES data (2009-2010, 2011-2012, 2013-2014, 2015-2016) from the website. A total of 40,439 participants were initially included. We excluded participants aged <60 years (n=32,833), those with missing klotho data (n=2,758), those with missing covariate data or inability to determine the presence of metabolic syndrome (n=446). Finally, 4,402 participants (2,205 females and 2,197 males) were included in the analysis. More specific details can be seen in Figure 1.

2.2 Acquisition of klotho samples

The blood samples of individuals aged 60 and above from four cycles (2009-2016) were collected by the personnel of the NHANES study. The samples were stored in dry ice at approximately -80°C and sent to the Northwest Lipid Metabolism and Diabetes Research Laboratory at the University of Washington for analysis. Serum levels of Klotho were determined for fresh frozen samples using the principle of enzyme-linked immunosorbent assay (ELISA) with the human α-Klotho test kit (intra-assay coefficient of variation <3.6%, inter-assay coefficient of variation <11.4%, detection sensitivity: 6pg/mL). Each sample was analyzed in duplicate by trained analysts, and the average of the two values was calculated as the final result. Each sample was analyzed twice, and the analysis results were automatically transferred to the laboratory's Oracle management system for evaluation by professional supervisors. If the repeated results exceeded 10%, the analysis was deemed invalid and a repeat sample analysis was required. For more detailed information on the Klotho measurement method, please refer to the NHANES website (15).

2.3 Diagnosis of metabolic syndrome

We screened participants diagnosed with metabolic syndrome based on guidelines provided by organizations such as the International Diabetes Federation (IDF) and the American Heart Association (AHA). The diagnosed individuals were required to meet three or more of the following criteria: 1) Male waist circumference ≥ 40 inches (102 cm), female waist circumference ≥ 35 inches (88 cm); 2) Elevated blood pressure: systolic pressure ≥ 130 mmHg or diastolic pressure ≥ 85 mmHg, or currently taking antihypertensive medication; 3) Abnormal blood lipid levels: triglycerides ≥ 150 mg/dL (1.7 mmol/L) or HDL < 40 mg/dL (1.03 mmol/L), or currently taking lipid-lowering medication; 4) Impaired glucose metabolism: fasting blood glucose ≥ 100 mg/dL

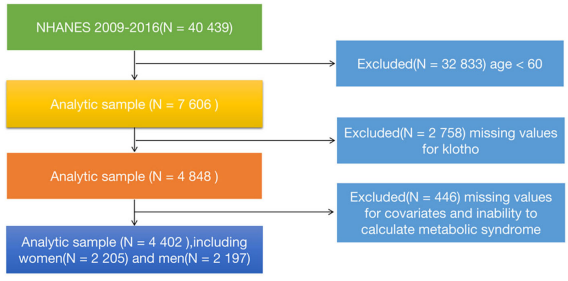

FIGURE 1
The flowchart of study and excluded participants.

(5.6 mmol/L) or currently using antidiabetic medication for blood sugar control (16).

2.4 Covariates

Covariates such as gender, poverty-income ratio (PIR), race, educational level, and smoking status were included in the analysis. PIR was categorized into three levels: ≤1, 1–3, and >3. Race was classified as Mexican American, Non-Hispanic Black, Non-Hispanic White, Other Hispanic, and other races (including multi-racial). Educational level was divided into three categories: below high school, high school, and college or above. Smoking status was grouped into three categories: former (having smoked more than 100 cigarettes in a lifetime but currently not smoking), never (having smoked fewer than 100 cigarettes in a lifetime), and now (having smoked more than 100 cigarettes in a lifetime and currently smoking all or some days).

2.5 Mortality

We linked the NHANES database with the National Death Index (NDI) database, which includes follow-up mortality statistics for participants in the NHANES survey through December 31, 2019. The NDI utilizes the International Classification of Diseases, 10th Edition (ICD-10), to determine the cause of death. Causes of death were categorized into six major groups: cardiovascular disease, Alzheimer's disease, cerebrovascular disease, malignant neoplasms (cancer), chronic lower respiratory diseases, and other causes of death.

2.6 Statistical analysis

Continuous variables following a normal distribution were described using the mean (standard deviation, SD), and statistical differences were assessed using t-tests or analysis of variance (ANOVA). Non-normally distributed continuous variables were described using the median (interquartile range, IQR), and non-parametric tests were used to assess statistical differences. Categorical variables were described using frequencies (percentages), and chi-square tests were employed to determine statistical differences.

In this study, due to the skewed distribution of klotho data, we performed a log2 transformation to present the analysis results more accurately. Subsequently, we classified the concentration of klotho based on quartiles, with the first quartile set as the reference group. We established a multivariable logistic regression model to explore the correlation between serum klotho levels and metabolic syndrome, adjusted for confounding factors including gender, race, education level, PIR, and smoking status, presenting the results as odds ratios (ORs) with 95% confidence intervals (CIs).

We also plotted restricted cubic spline (RCS) graphs and employed ten-fold cross-validation to examine whether there was a nonlinear relationship between log2-transformed serum klotho levels and metabolic syndrome. Additionally, we constructed a multivariable Cox regression model and generated Kaplan-Meier survival curves to investigate the association between log2-transformed serum klotho levels in patients with metabolic syndrome and all-cause mortality. Restricted cubic splines were used, and likelihood ratio tests were conducted to assess the nonlinear relationship between log2-transformed serum klotho levels and all-cause mortality. To ensure robustness of the research findings, sensitivity analyses were performed by excluding patients with a death time <30 months to eliminate potential causal associations. All statistical analyses and data visualizations were performed by R 4.2.2.

3 Results

3.1 Baseline features

According to the presence of metabolic syndrome, a total of 4,402 participants aged 60 and above were included in this analysis. Among them, there were 2,197 male participants (49.9%) and 2,205 female participants (50.1%). Among these participants, 2,185 participants (49.6%) had metabolic syndrome, and this group was more likely to be female, have an income-to-poverty ratio ≥1, be non-Hispanic white, have a high school or higher education level, and be never smokers. For more detailed baseline information, please refer to Table 1.

3.2 The association between klotho and metabolic syndrome

To further investigate the association between serum klotho levels and the occurrence of metabolic syndrome, we constructed a logistic regression model adjusting for above confounding factors. The serum klotho data was log2-transformed, and the logarithmically transformed concentrations were categorized according to quartiles (Q1, Q2, Q3, Q4). Compared to the first quartile of klotho, the Q2 group showed 16% decrease in metabolic syndrome risk (OR=0.84,95% CI = 0.71-1.00, P = 0.048), and the Q3 group showed 16% decrease in metabolic syndrome risk (OR=0.84,95% CI = 0.70-0.99, P = 0.038). Please refer to Figure 2 for specific details.

In the logistic regression model, with adjustment for above confounding factors, Figure 3 depicts a RCS plot describing the dose-response relationship between log2-transformed serum klotho levels and the risk of metabolic syndrome. Using the first quartile of klotho as the reference value, a significant nonlinear correlation was observed between serum klotho levels and the risk of metabolic syndrome (the P value for non-linearity was 0.0152).

3.3 Association between serum klotho levels and risk of mortality in patients with metabolic syndrome

We selected a total of 2185 participants with metabolic syndrome for our study. Serum klotho levels were transformed logarithmically and divided into quartiles. To investigate the relationship between serum klotho levels and the risk of mortality

10.3389/fendo.2024.1295927

TABLE 1 Baseline characteristic of the study population by Metabolic syndrome.

	Level	No metabolic syndrome	Metabolic syndrome	P-value
N (%)		2217 (50.36)	2185 (49.64)	
Klotho (%)				0.0934
	Q1	519 (23.41)	582 (26.64)	
	Q2	571 (25.76)	530 (24.26)	
	Q3	568 (25.62)	531 (24.30)	
	Q4	559 (25.21)	542 (24.81)	
Sex (%)				<0.0001
	Female	1026 (46.28)	1179 (53.96)	
	Male	1191 (53.72)	1006 (46.04)	
Poverty-income ratio (%)				<0.0001
	<1	378 (17.05)	481 (22.01)	
	[1, 3)	935 (42.17)	983 (44.99)	
	≥3	904 (40.78)	721 (33.00)	
Ethnicity (%)				<0.0001
	Mexican American	269 (12.13)	362 (16.57)	
	Non-Hispanic Black	491 (22.15)	400 (18.31)	
	Non-Hispanic White	989 (44.61)	975 (44.62)	
	Other Hispanic	237 (10.69)	270 (12.36)	
	Other Race - Including Multi-Racial	231 (10.42)	178 (8.15)	
Education (%)				<0.0001
	Low high school	583 (26.30)	699 (31.99)	
	High school	465 (20.97)	518 (23.71)	
	College or above	1169 (52.73)	968 (44.30)	
Smoke (%)				0.0313
	Former	792 (35.72)	864 (39.54)	
	Never	1090 (49.17)	1004 (45.95)	
	Now	335 (15.11)	317 (14.51)	
Calcium (mean (SD))		2.357 (0.093)	2.361 (0.099)	0.1812
Phosphorus (mean (SD))		1.200 (0.093)	1.198 (0.186)	0.7715

in patients with metabolic syndrome, we employed a multivariate Cox proportional hazards model, adjusting for above confounding factors. Figure 4 illustrates the results of this analysis.

After adjusting for these factors, compared to the first quartile (Q1) of log2-transformed serum klotho, the second quartile (Q2) showed a 41% decrease in all-cause mortality risk (HR=0.59, 95% CI=0.45-0.79, P<0.001), the third quartile (Q3) showed a 33% decrease in all-cause mortality risk (HR=0.67, 95% CI=0.50-0.88, P=0.004), and the fourth quartile (Q4) showed a 32% decrease in all-cause mortality risk (HR=0.68, 95% CI=0.51-0.90, P=0.006). These results indicate a significant association between lower all-cause mortality risk in patients with metabolic syndrome and higher log2-transformed serum klotho levels in the Q2, Q3, and Q4 groups compared to the Q1 group. More details can be seen in Figure 5.

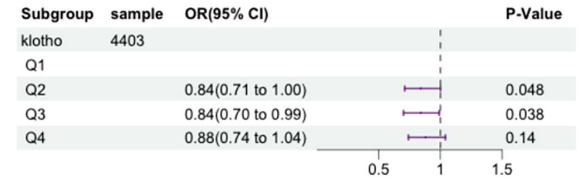

FIGURE 2
The forest plot displaying the associations between the levels of klotho and metabolic syndrome.

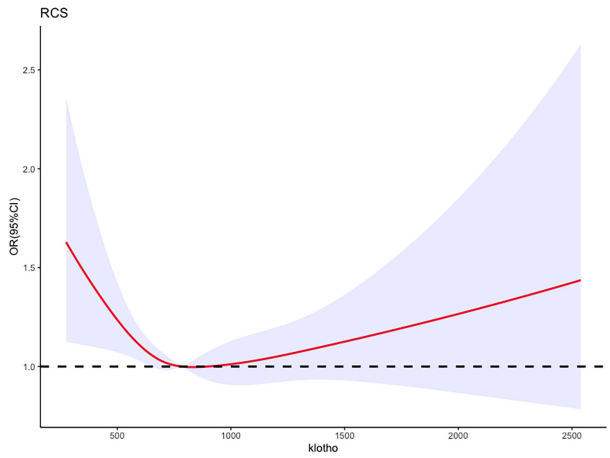

FIGURE 3
Adjusted restricted cubic spline curve between the levels of klotho and metabolic syndrome.

Additionally, the RCS analysis confirmed a significant non-linear relationship between serum klotho levels and all-cause mortality risk in patients with metabolic syndrome (P value for non-linearity <0.0001, total P value <0.0001). Kaplan-Meier survival curves were also plotted to demonstrate the all-cause mortality rates for the four quartiles of log2-transformed serum klotho, showing statistically significant differences (p<0.001) as shown in Figure 6. These findings support the notion that serum klotho levels play a significant role in the overall mortality risk among patients with metabolic syndrome.

3.4 Sensitivity analysis

As shown in Table 2, in the sensitivity analysis, participants with a death time of less than 30 months were excluded, and the

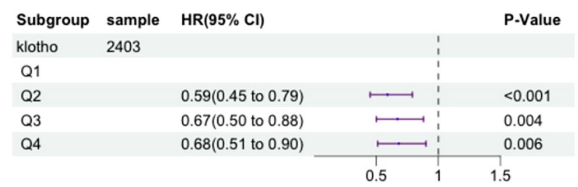

FIGURE 4
The forest plot displaying Hazard Ratios of klotho levels and all-cause mortality in patients with metabolic syndrome.

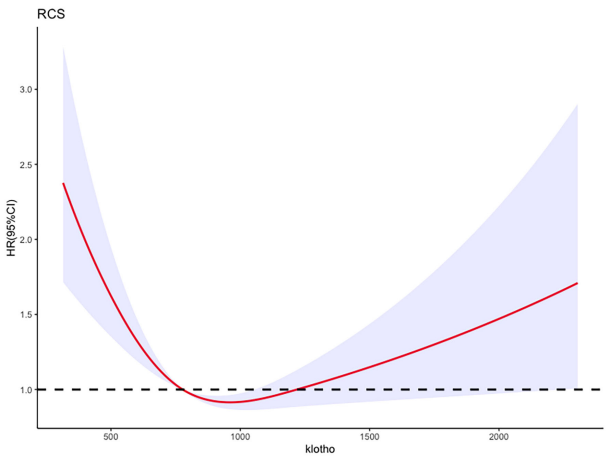

FIGURE 5
Adjusted restricted cubic spline curve between the levels of klotho and all-cause mortality in patients with metabolic syndrome.

results did not show significant changes. Compared to the Q1 group, the overall risk of death in the Q2, Q3, and Q4 groups decreased by 46% (HR=0.54, 95% CI=0.39-0.75, P<0.001), 46% (HR=0.54, 95% CI=0.38-0.75, P=0.004), and 32% (HR=0.68, 95% CI=0.49-0.93, P=0.016), respectively. Sensitivity analysis results indicated that serum klotho levels, transformed by log2, remained significantly associated with a decrease in overall risk of death.

4 Discussion

In this large nationally representative cohort of U.S. adults, we found a graded inverse association between serum Klotho levels and the prevalence of metabolic syndrome, independent of potential confounders including demographics, socioeconomics, and lifestyle factors. Moreover, higher Klotho levels strongly predicted lower risks of all-cause mortality among individuals with metabolic syndrome. Our study provides compelling evidence supporting Klotho as a novel protective factor against metabolic syndrome and an independent prognostic predictor. The prospective cohort design and linkage to longitudinal mortality data add to the significance of the findings. The population-based sample enhances generalizability to diverse real-world settings. Extensive adjustment for possible confounders including age, gender, race/ethnicity, smoking, PIR, and education level also represent major strengths.

Metabolic syndrome represents a cluster of metabolic abnormalities and cardiovascular risk factors, with central obesity, hypertension, dyslipidemia, and hyperglycemia as its principal components (1). The prevalence of metabolic syndrome has increased dramatically worldwide over recent decades. It now affects approximately 20-30% of the adult population globally, and up to 50% among older adults (2, 4). Metabolic syndrome significantly elevates the risks of developing type 2 diabetes, cardiovascular disease, chronic kidney disease, nonalcoholic fatty liver disease, and other metabolic disorders (3, 5–8). Moreover, numerous studies have demonstrated a 1.5- to 2.0-fold increase in cardiovascular mortality and a 1.5-fold elevation in all-cause mortality associated with metabolic syndrome (3, 7, 9). Therefore, metabolic syndrome confers a substantial health and economic burden both at the individual and societal levels. Identifying novel biomarkers and therapeutic targets is imperative to curb this growing public health threat.

Klotho is a transmembrane protein predominantly expressed in renal tubular cells that functions as an aging suppressor (10). Animal studies have revealed that Klotho-deficient mice exhibit multiple accelerated aging phenotypes, including shortened lifespan, arteriosclerosis, skin atrophy, osteoporosis, and cognitive impairment (11, 13). In humans, klotho deficiency is involved in the pathogenesis of various aging-related disorders, including cardiovascular disease, stroke, and chronic kidney disease (12, 14, 17).

Emerging evidence suggests that Klotho plays a vital role in metabolic regulation. Klotho activates insulin and insulin-like growth factor-1 (IGF-1) signaling by increasing the phosphorylation and glycosylation of their receptors (18, 19). This enhances insulin and IGF-1 receptor affinity and sensitivity. Klotho-overexpressing mice exhibit increased insulin sensitivity and resistance to diet-induced obesity (20). Conversely, Klotho loss-of-function mutant mice display impaired glucose tolerance and insulin resistance (21). In humans, lower Klotho levels are associated with increased fasting glucose, insulin resistance, increased glycated hemoglobin, and diabetes prevalence (22–24).

Regarding lipid metabolism, Klotho suppresses intracellular cholesterol biosynthesis by inhibiting HMG-CoA reductase (25). Klotho overexpression reduces triglyceride accumulation in the liver and circulation (26). Moreover, Klotho preserves endothelial function and prevents atherosclerosis by inhibiting vascular inflammation and oxidative stress (27). The pleiotropic metabolic benefits make Klotho an attractive candidate biomarker and therapeutic target for metabolic syndrome.

Klotho likely ameliorates metabolic syndrome through diverse mechanisms. As mentioned, Klotho enhances insulin sensitivity and improves lipid metabolism via modulating insulin/IGF-1 and HMG-CoA reductase signaling (18, 19, 21, 25, 26). Furthermore, Klotho activates the TRPV5 calcium channel in kidney tubules to increase calcium reabsorption (28). Elevated calcium can induce pancreatic β-cell dysfunction and peripheral insulin resistance (29, 30). Therefore, Klotho effectively ameliorates metabolic syndrome by increasing serum calcium. Previous studies have suggested a close association between Klotho levels and mineral metabolism as well as phosphate balance (10, 17).We further investigated the relationship between Klotho levels and blood calcium and phosphate concentrations, but did not find any underlying

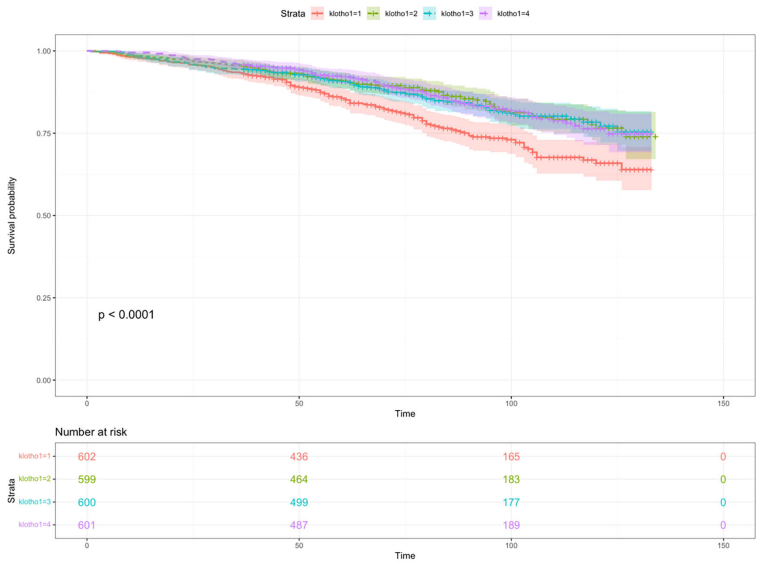

FIGURE 6
The Kaplan-Meier survival curve describing the relationship between klotho levels and all-cause mortality in patients with metabolic syndrome.

relationship between them, which may be closely related to the specific distribution of the metabolic syndrome population. Additionally, Klotho lowers serum phosphate by suppressing tubular phosphate reabsorption (31). Hyperphosphatemia promotes vascular smooth muscle cell transformation into osteoblast-like cells that calcify the vessel wall (32). Aberrant vascular calcification leads to increased arterial stiffness, impaired vasodilation, hypertension, and greater cardiac afterload (33, 34). Klotho prevents ectopic soft tissue calcification to ameliorate metabolic syndrome complications. Further research is warranted to elucidate the precise molecular pathways involved.

Our findings add to the emerging evidence supporting Klotho as a key regulator of metabolic homeostasis and a potential therapeutic target for metabolic syndrome. Recombinant Klotho protein administration could be a novel treatment approach. In mouse models, exogenous Klotho ameliorates vascular calcification, renal fibrosis, and cardiac hypertrophy (35–37). Phase 2 trials of Klotho protein therapy in chronic kidney disease patients are ongoing, showing acceptable safety and bioactivity profiles thus far (38). Developing targeted Klotho-based therapies may provide innovative management strategies to stem the rising tide of metabolic syndrome worldwide.

Several evident limitations of this study need to be acknowledged. First, the cross-sectional design of the study limited causal inference between Klotho and metabolic syndrome. Furthermore, while the sample size from the NHNAES database is nationally representative, its relative smallness might limit its power to detect minor effect sizes. Therefore, it is necessary to establish longitudinal cohort studies of Klotho biomarkers in the future. Clarifying how Klotho protein interacts with the genome, microbiota, and other factors influencing metabolic syndrome will have substantial research implications.

TABLE 2 The relationship between Klotho levels in patients with metabolic syndrome and all-cause mortality rate was assessed after excluding patients who died within 30 months of follow-up.

	HR[1]	95% CI[2]	*P*-value
Klotho			
Q1	Reference		
Q2	0.54	0.39 - 0.75	<0.001
Q3	0.54	0.38 - 0.75	<0.001
Q4	0.68	0.49 - 0.93	0.016

[1]HR, Hazard Ratios.
[2]CI, Confidence Intervals.

5 Conclusion

In summary, our study reveals a robust inverse association between circulating Klotho levels and metabolic syndrome prevalence and mortality. The results highlight the potential role of Klotho as a novel biomarker for early risk stratification and prognostication, as well as a promising therapeutic target for metabolic syndrome prevention and treatment. Further research is warranted to advance the translational potential of harnessing Klotho biology against this major global public health threat.

Data availability statement

The raw data supporting the conclusions of this article will be made available by the authors, without undue reservation.

Ethics statement

The studies involving humans were approved by National Center for Health Statistics Research Ethics Review Board. The

studies were conducted in accordance with the local legislation and institutional requirements. Written informed consent for participation in this study was provided by the participants' legal guardians/next of kin.

Author contributions

LY: Data curation, Formal analysis, Visualization, Writing – original draft. YC: Data curation, Formal analysis, Visualization, Writing – original draft. NC: Investigation, Methodology, Writing – original draft. YZ: Investigation, Methodology, Writing – original draft. XZ: Investigation, Methodology, Writing – original draft. WS: Conceptualization, Methodology, Supervision, Writing – review & editing. JL: Conceptualization, Methodology, Writing – review & editing. XL: Conceptualization, Methodology, Supervision, Writing – original draft, Writing – review & editing.

Funding

The author(s) declare that no financial support was received for the research, authorship, and/or publication of this article.

Acknowledgments

The authors would like to express their sincere gratitude to the entire research team at NHANES for their invaluable assistance in collecting, managing, and providing access to the data.

Conflict of interest

The authors declare that the research was conducted in the absence of any commercial or financial relationships that could be construed as a potential conflict of interest.

Publisher's note

References

1. Kassi E, Pervanidou P, Kaltsas G, Chrousos G. Metabolic syndrome: definitions and controversies. *BMC Med*. (2011) 9:48. doi: 10.1186/1741-7015-9-48

2. Park YW, Zhu S, Palaniappan L, Heshka S, Carnethon MR, Heymsfield SB. The metabolic syndrome: prevalence and associated risk factor findings in the US population from the Third National Health and Nutrition Examination Survey, 1988-1994. *Arch Internal Med*. (2003) 163:427–36. doi: 10.1001/archinte.163.4.427

3. Mottillo S, Filion KB, Genest J, Joseph L, Pilote L, Poirier P, et al. The metabolic syndrome and cardiovascular risk a systematic review and meta-analysis. *J Am Coll Cardiol*. (2010) 56:1113–32. doi: 10.1016/j.jacc.2010.05.034

4. Ford ES, Giles WH, Dietz WH. Prevalence of the metabolic syndrome among US adults: findings from the third National Health and Nutrition Examination Survey. *Jama*. (2002) 287:356–9. doi: 10.1001/jama.287.3.356

5. Anstee QM, Targher G, Day CP. Progression of NAFLD to diabetes mellitus, cardiovascular disease or cirrhosis. *Nat Rev Gastroenterol hepatol*. (2013) 10:330–44. doi: 10.1038/nrgastro.2013.41

6. Thomas G, Sehgal AR, Kashyap SR, Srinivas TR, Kirwan JP, Navaneethan SD. Metabolic syndrome and kidney disease: a systematic review and meta-analysis. *Clin J Am Soc Nephrol: CJASN*. (2011) 6:2364–73. doi: 10.2215/cjn.02180311

7. Gami AS, Witt BJ, Howard DE, Erwin PJ, Gami LA, Somers VK, et al. Metabolic syndrome and risk of incident cardiovascular events and death: a systematic review and meta-analysis of longitudinal studies. *J Am Coll Cardiol*. (2007) 49:403–14. doi: 10.1016/j.jacc.2006.09.032

8. Cooney LG, Lee I, Sammel MD, Dokras A. High prevalence of moderate and severe depressive and anxiety symptoms in polycystic ovary syndrome: a systematic review and meta-analysis. *Hum Reprod (Oxford England)*. (2017) 32:1075–91. doi: 10.1093/humrep/dex044

9. Malik S, Wong ND, Franklin SS, Kamath TV, L'Italien GJ, Pio JR, et al. Impact of the metabolic syndrome on mortality from coronary heart disease, cardiovascular disease, and all causes in United States adults. *Circulation*. (2004) 110:1245–50. doi: 10.1161/01.CIR.0000140677.20606.0E

10. Hu MC, Moe OW. Klotho as a potential biomarker and therapy for acute kidney injury. *Nat Rev Nephrol*. (2012) 8:423–9. doi: 10.1038/nrneph.2012.92

11. Kuro-o M, Matsumura Y, Aizawa H, Kawaguchi H, Suga T, Utsugi T, et al. Mutation of the mouse klotho gene leads to a syndrome resembling ageing. *Nature*. (1997) 390:45–51. doi: 10.1038/36285

12. Brandenburg VM, Kleber ME, Vervloet MG, Tomaschitz A, Pilz S, Stojakovic T, et al. Fibroblast growth factor 23 (FGF23) and mortality: the Ludwigshafen Risk and Cardiovascular Health Study. *Atherosclerosis*. (2014) 237:53–9. doi: 10.1016/j.atherosclerosis.2014.08.037

13. Dubal DB, Yokoyama JS, Zhu L, Broestl L, Worden K, Wang D, et al. Life extension factor klotho enhances cognition. *Cell Rep*. (2014) 7:1065–76. doi: 10.1016/j.celrep.2014.03.076

14. Xie J, Yoon J, An SW, Kuro-o M, Huang CL. Soluble klotho protects against uremic cardiomyopathy independently of fibroblast growth factor 23 and phosphate. *J Am Soc Nephrol: JASN*. (2015) 26:1150–60. doi: 10.1681/asn.2014040325

15. Yamazaki Y, Imura A, Urakawa I, Shimada T, Murakami J, Aono Y, et al. Establishment of sandwich ELISA for soluble alpha-Klotho measurement: Age-dependent change of soluble alpha-Klotho levels in healthy subjects. *Biochem Biophys Res Commun*. (2010) 398:513–8. doi: 10.1016/j.bbrc.2010.06.110

16. Alberti KG, Eckel RH, Grundy SM, Zimmet PZ, Cleeman JI, Donato KA, et al. Harmonizing the metabolic syndrome: a joint interim statement of the International Diabetes Federation Task Force on Epidemiology and Prevention; National Heart, Lung, and Blood Institute; American Heart Association; World Heart Federation; International Atherosclerosis Society; and International Association for the Study of Obesity. *Circulation*. (2009) 120:1640–5. doi: 10.1161/circulationaha.109.192644

17. Gołembiewska E, Stępniewska J, Kabat-Koperska J, Kędzierska K, Domański M, Ciechanowski K. The role of klotho protein in chronic kidney disease: studies in animals and humans. *Curr Protein Pept sci*. (2016) 17:821–6. doi: 10.2174/1389203717666160526123646

18. Chang Q, Hoefs S, van der Kemp AW, Topala CN, Bindels RJ, Hoenderop JG. The beta-glucuronidase klotho hydrolyzes and activates the TRPV5 channel. *Sci (New York NY)*. (2005) 310:490–3. doi: 10.1126/science.1114245

19. Kurosu H, Ogawa Y, Miyoshi M, Yamamoto M, Nandi A, Rosenblatt KP, et al. Regulation of fibroblast growth factor-23 signaling by klotho. *J Biol Chem*. (2006) 281:6120–3. doi: 10.1074/jbc.C500457200

20. Yamamoto M, Clark JD, Pastor JV, Gurnani P, Nandi A, Kurosu H, et al. Regulation of oxidative stress by the anti-aging hormone klotho. *J Biol Chem*. (2005) 280:38029–34. doi: 10.1074/jbc.M509039200

21. Tsujikawa H, Kurotaki Y, Fujimori T, Fukuda K, Nabeshima Y. Klotho, a gene related to a syndrome resembling human premature aging, functions in a negative regulatory circuit of vitamin D endocrine system. *Mol Endocrinol (Baltimore Md)*. (2003) 17:2393–403. doi: 10.1210/me.2003-0048

22. Milovanova LY, Mukhin NA, Kozlovskaya LV, Milovanov YS, Kiyakbaev GG, Rogova IV, et al. [Decreased serum levels of klotho protein in chronic kidney disease patients: clinical imortance]. *Vestnik Rossiiskoi akademii meditsinskikh nauk*. (2016) 71:288–96. doi: 10.15690/vramn581

23. Donate-Correa J, Martín-Núñez E, Delgado NP, de Fuentes MM, Arduan AO, Mora-Fernández C, et al. Implications of Fibroblast growth factor/Klotho system in

glucose metabolism and diabetes. *Cytokine Growth factor Rev*. (2016) 28:71–7. doi: 10.1016/j.cytogfr.2015.12.003

24. Semba RD, Cappola AR, Sun K, Bandinelli S, Dalal M, Crasto C, et al. Plasma klotho and mortality risk in older community-dwelling adults. *journals gerontol Ser A Biol Sci Med Sci*. (2011) 66:794–800. doi: 10.1093/gerona/glr058

25. Hu MC, Shi M, Zhang J, Quiñones H, Griffith C, Kuro-o M, et al. Klotho deficiency causes vascular calcification in chronic kidney disease. *J Am Soc Nephrol: JASN*. (2011) 22:124–36. doi: 10.1681/asn.2009121311

26. Lee J, Kim D, Lee HJ, Choi JY, Min JY, Min KB. Association between serum klotho levels and cardiovascular disease risk factors in older adults. *BMC Cardiovasc Disord*. (2022) 22:442. doi: 10.1186/s12872-022-02885-2

27. Maekawa Y, Ishikawa K, Yasuda O, Oguro R, Hanasaki H, Kida I, et al. Klotho suppresses TNF-alpha-induced expression of adhesion molecules in the endothelium and attenuates NF-kappaB activation. *Endocrine*. (2009) 35:341–6. doi: 10.1007/s12020-009-9181-3

28. Nabeshima Y, Imura H. alpha-Klotho: a regulator that integrates calcium homeostasis. *Am J nephrol*. (2008) 28:455–64. doi: 10.1159/000112824

29. Draznin B. Molecular mechanisms of insulin resistance: serine phosphorylation of insulin receptor substrate-1 and increased expression of p85alpha: the two sides of a coin. *Diabetes*. (2006) 55:2392–7. doi: 10.2337/db06-0391

30. Byon CH, Javed A, Dai Q, Kappes JC, Clemens TL, Darley-Usmar VM, et al. Oxidative stress induces vascular calcification through modulation of the osteogenic transcription factor Runx2 by AKT signaling. *J Biol Chem*. (2008) 283:15319–27. doi: 10.1074/jbc.M800021200

31. Hu MC, Shiizaki K, Kuro-o M, Moe OW. Fibroblast growth factor 23 and Klotho: physiology and pathophysiology of an endocrine network of mineral metabolism. *Annu Rev Physiol*. (2013) 75:503–33. doi: 10.1146/annurev-physiol-030212-183727

32. Boström K, Demer LL. Regulatory mechanisms in vascular calcification. *Crit Rev eukaryotic Gene expression*. (2000) 10:151–8. doi: 10.1615/CritRevEukarGeneExpr.v10.i2

33. London GM, Marchais SJ, Guerin AP, Pannier B. Arterial stiffness: pathophysiology and clinical impact. *Clin Exp hypertension (New York NY: 1993)*. (2004) 26:689–99. doi: 10.1081/ceh-200031982

34. Covic A, Mardare N, Gusbeth-Tatomir P, Prisada O, Sascau R, Goldsmith DJ. Arterial wave reflections and mortality in haemodialysis patients–only relevant in elderly, cardiovascularly compromised? *Nephrol dialysis Transplant*. (2006) 21:2859–66. doi: 10.1093/ndt/gfl307

35. Xie J, Cha SK, An SW, Kuro OM, Birnbaumer L, Huang CL. Cardioprotection by Klotho through downregulation of TRPC6 channels in the mouse heart. *Nat Commun*. (2012) 3:1238. doi: 10.1038/ncomms2240

36. Zhou L, Mo H, Miao J, Zhou D, Tan RJ, Hou FF, et al. Klotho ameliorates kidney injury and fibrosis and normalizes blood pressure by targeting the renin-angiotensin system. *Am J pathol*. (2015) 185:3211–23. doi: 10.1016/j.ajpath.2015.08.004

37. Hu MC, Shi M, Cho HJ, Adams-Huet B, Paek J, Hill K, et al. Klotho and phosphate are modulators of pathologic uremic cardiac remodeling. *J Am Soc Nephrol: JASN*. (2015) 26:1290–302. doi: 10.1681/asn.2014050465

38. Chen CD, Podvin S, Gillespie E, Leeman SE, Abraham CR. Insulin stimulates the cleavage and release of the extracellular domain of Klotho by ADAM10 and ADAM17. *Proc Natl Acad Sci United States America*. (2007) 104:19796–801. doi: 10.1073/pnas.0709805104

frontiers | Frontiers in Endocrinology

TYPE Original Research
PUBLISHED 04 March 2024
DOI 10.3389/fendo.2024.1284152

OPEN ACCESS

EDITED BY
Princy Francis,
Mayo Clinic, United States

REVIEWED BY
Jesus Rico-Feijoo,
Hospital Universitario Río Hortega, Spain
Meng Zhou,
Wenzhou Medical University, China
Chuanfu Li,
East Tennessee State University, United States
Guochang Hu,
University of Illinois Chicago, United States

*CORRESPONDENCE
Rui-tao Wang
ruitaowang@126.com
Guang-yu Wang
guangyuwang@hrbmu.edu.cn

†These authors have contributed equally to this work and share first authorship

RECEIVED 28 August 2023
ACCEPTED 06 February 2024
PUBLISHED 04 March 2024

CITATION
Liu L, Zhang B-b, Li Y-z, Huang W-j, Niu Y, Jia Q-c, Wang W, Yuan J-r, Miao S-d, Wang R-t and Wang G-y (2024) Preoperative glucose-to-lymphocyte ratio predicts survival in cancer. *Front. Endocrinol.* 15:1284152. doi: 10.3389/fendo.2024.1284152

Preoperative glucose-to-lymphocyte ratio predicts survival in cancer

Le Liu[1†], Bei-bei Zhang[1†], Yuan-zhou Li[2†], Wen-juan Huang[1], Ye Niu[1], Qing-chun Jia[1], Wen Wang[1], Jia-rui Yuan[1], Shi-di Miao[3], Rui-tao Wang[1*] and Guang-yu Wang[4*]

[1]Department of Internal Medicine, Harbin Medical University Cancer Hospital, Harbin Medical University, Harbin, Heilongjiang, China, [2]Department of Radiology, Harbin Medical University Cancer Hospital, Harbin Medical University, Harbin, Heilongjiang, China, [3]Department of Science and Education, School of Computer Science and Technology, Harbin University of Science and Technology, Harbin, Heilongjiang, China, [4]Department of Gastrointestinal Medical Oncology, Harbin Medical University Cancer Hospital, Harbin Medical University, Harbin, Heilongjiang, China

Background: Systemic inflammation and glucose metabolism have been closely related to the survival of cancer patients. Therefore, we aimed to evaluate whether preoperative glucose-to-lymphocyte ratio (GLR) can be used to predict the survival of cancer patients.

Methods: We retrospectively examined 2172 cancer patients who underwent surgery from January 1, 2014, to December 31, 2016. There were 240 patients with non-small cell lung cancer (NSCLC), 378 patients with colorectal cancer (CRC), 221 patients with breast cancer (BC), 335 patients with gastric cancer (GC), 270 patients with liver cancer, 233 patients with esophageal cancer (EC), 295 patients with renal cancer, and 200 patients with melanoma. The formula for preoperative GLR calculation was as follows: GLR=glucose/lymphocyte count. The overall survival (OS) was estimated using the Kaplan-Meier method. The predictive factors for OS were determined using multivariate analysis.

Results: The Kaplan-Meier analysis showed that the median survival time in the high-GLR group was much shorter than that of those in the low-GLR group for different cancers. Cox multivariate regression analysis reveals that preoperative GLR was an independent factor for predicting overall survival in different tumor types.

Conclusion: Elevated preoperative GLR was remarkably associated with a poorer prognosis in patients with NSCLC, CRC, breast cancer, gastric cancer, kidney cancer, liver cancer, esophageal cancer, and melanoma. Preoperative GLR promises to be an essential predictor of survival for cancer patients.

KEYWORDS

cancer, survival, prognosis, glucose to lymphocyte ratio, lung cancer

Introduction

As the morbidity rate continues to climb, cancer is not only a major public health problem but also one of the leading contributors to death in the world (1). Up to date, surgery resection is still the mainstay of curative treatment options for most tumors (2). However, despite efforts to develop new surgical strategies, overall survival is still unsatisfactory. Therefore, a more accurate evaluation index to predict the long-term survival of patients has high clinical value.

Diabetes mellitus (DM) and cancer are two prevalent disorders that coexist, and the incidence and prevalence of both are rising (3). DM and hyperglycemia have been demonstrated to have significant impacts on the incidence and prognosis of cancer (4–6). Moreover, the metabolic abnormalities in hyperglycemia and diabetes substantially contribute to the development and progression of cancer (7). A meta-analysis revealed that metformin is an independent protective factor for cancer risk in DM patients (8). In addition, large bodies of accumulated research have also confirmed that the development and progression of cancer increase the risk of diabetes (9).

At the same time, lymphocytes, being one of the crucial components of the systemic inflammatory response, are engaged in cell-mediated antitumor responses (10). Furthermore, its profound role in immune surveillance that protects the host from tumor development has also been observed in mice and humans (11).

The available literature demonstrated the potential association of glucose-to-lymphocyte ratio (GLR) with prognosis in gallbladder, colorectal cancer (CRC), and pancreatic cancer (12). However, there are relatively few studies on the prognostic association of GLR with other tumors. The objective of our study is to evaluate the prognostic role of preoperative GLR in patients with gastric cancer (GC), renal carcinoma, colorectal cancer, non-small cell lung cancer, breast cancer (BC), liver cancer, esophageal cancer (EC), and melanoma.

Patients and methods

Study population

We reviewed the clinical information of 2172 cancer patients who underwent curative resection at the Harbin Medical University Cancer Hospital between January 1, 2014, and December 31, 2016. There were 240 patients with non-small cell lung cancer, 378 patients with colorectal cancer, 221 patients with breast cancer, 335 patients with gastric cancer, 270 patients with liver cancer, 233 patients with esophageal cancer, 295 patients with renal cell cancer, and 200 patients with melanoma. Patients were included according to the following criteria: (1) pathologically confirmed evidence of each cancer, (2) completed preoperative blood tests involving fasting glucose and lymphocyte counts, and (3) followed for more than 60 months. Exclusion criteria for patients were as follows: (1) they had received antitumor therapy before surgery; (2) they had a history of other primary malignancies; (3) they had acute inflammatory disease; and (4) they failed to follow up.

Overall survival (OS) was defined from the date of surgery to the date of death or the date of the last follow-up. All patients were followed up by telephone once every 3-6 months. The cut-off date for follow-up evaluations is December 31, 2021. The survival data was derived from medical records and telephone follow-ups. And the work has been reported in line with the REMARK criteria (13). Patients' demographic characteristics and laboratory parameters were extracted from their electronic medical records. All laboratory parameters were assayed within a week before the operation. The formula for preoperative GLR calculation was as follows: GLR=fasting blood glucose (mmol/L)/lymphocyte count ($\times 10^9$/L).

This research was in strict compliance with the Helsinki Declaration. This study was approved by our Institutional Review Board (approval number KY2022-10). Since it was a retrospective study, we waived informed consent.

Statistical analysis

Statistical tests were performed with SPSS version 25.0 software (SPSS Inc., Chicago, IL, USA). Receiver operating characteristic (ROC) curves were constructed using MedCalc version 15.0 software to assign cut-off values for GLR levels as well as sensitivities and specificities. The Kolmogorov-Smirnov test was used to determine if the data were normally distributed. T-tests were utilized for the comparison of normally distributed continuous variables, while categorical variables were compared with chi-square tests. The Kaplan-Meier method was used to derive OS, and the results were compared with the log-rank test. Multivariate analysis was conducted using the Cox proportional hazards regression model to estimate the independent predictors of OS. The proportional-hazards assumption was examined before Cox regression analysis. Univariate and multivariate Cox regression analyses were carried out to determine the hazard ratio (HR) and the corresponding 95% confidence interval (CI). Variables with a p value of < 0.10 in the univariate analysis were subjected to multivariate analysis. All reported p values were two-sided, and p values < 0.05 were regarded as statistically significant.

Results

Among the 2172 patients collected, the mean age was 55.72 years (range 10-87), 1265 (58.2%) were men, and 907 (41.8%) were women.

The patient's clinical characteristics based on preoperative GLR levels are summarized in Table 1. In gastric cancer, colorectal cancer, liver cancer, esophageal cancer, and renal cancer, lower hemoglobin and platelet count were likely to appear in the high-GLR group. In non-small cell lung cancer, colorectal cancer, and renal cancer, age in the two groups showed a significant difference. Moreover, high GLR levels were correlated with white blood cell in melanoma, breast cancer, liver cancer, esophageal cancer, renal cancer, and non-small cell lung cancer.

10.3389/fendo.2024.1284152

TABLE 1 Patient characteristics according to glucose-to-lymphocyte ratio status.

Variables	Total n (%)	Low GLR	High GLR	P value
Non-small-cell Lung Cancer				
Age (years)				0.022
≤ 60	159 (66.3)	119 (70.8)	40 (55.6)	
> 60	81 (33.8)	49 (29.2)	32 (44.4)	
Gender				0.502
Female	89 (37.1)	60 (35.7)	29 (40.3)	
Male	151 (62.9)	108 (64.3)	43 (59.7)	
Tumor size (cm)				0.586
< 4	164 (68.3)	113 (67.3)	51 (70.8)	
≥ 4	76 (31.7)	55 (32.7)	21 (29.2)	
Smoking history				0.308
No	132 (55.0)	96 (57.1)	36 (50.0)	
Yes	108 (45.0)	72 (42.9)	36 (50.0)	
Hypertension				0.374
No	198 (82.5)	141 (83.9)	57 (79.2)	
Yes	42 (17.5)	27 (16.1)	15 (20.8)	
Diabetes mellitus				0.111
No	223 (92.9)	159 (94.6)	64 (88.9)	
Yes	17 (7.1)	9 (5.4)	8 (11.1)	
Adjuvant chemotherapy				0.775
No	100 (41.7)	71 (42.3)	29 (40.3)	
Yes	140 (58.3)	97 (57.7)	43 (59.7)	
Histology				0.734
Adenocarcinoma	134 (55.8)	95 (56.5)	39 (54.2)	
Others	106 (44.2)	73 (43.5)	33 (45.8)	
T classification				0.154
T1/T2	29 (12.1)	17 (10.1)	12 (16.7)	
T3/T4	211 (87.9)	151 (89.9)	60 (83.3)	
Lymph node status				0.421
Absent	159 (66.3)	114 (67.9)	45 (62.5)	
Present	81 (33.8)	54 (32.1)	27 (37.5)	
Clinical stage				0.126
I/II	176 (73.3)	128 (76.2)	48 (66.7)	
III	64 (26.7)	40 (23.8)	24 (33.3)	
BMI (kg/m^2)	23.28 ± 3.06	23.31 ± 3.10	23.22 ± 3.20	0.838
WBC ($\times10^9$/L)	6.92 ± 2.41	7.12 ± 2.36	6.45 ± 2.48	0.048
Hemoglobin (g/L)	137.75 ± 18.24	139.13 ± 18.70	134.51 ± 16.82	0.072
Platelet count ($\times10^9$/L)	243.95 ± 70.69	243.32 ± 67.23	245.42 ± 78.66	0.834
Colorectal Cancer				
Age (years)				0.002
≤ 65	305 (80.7)	285 (82.6)	20 (60.6)	
> 65	73 (19.3)	60 (17.4)	13 (39.4)	
Gender				0.079
Female	133 (35.2)	126 (36.5)	7 (21.2)	
Male	245 (64.8)	219 (63.5)	26 (78.8)	
Hypertension				0.853
No	280 (74.1)	256 (74.2)	24 (72.7)	
Yes	98 (25.9)	89 (25.8)	9 (27.3)	
Diabetes mellitus				< 0.001
No	328 (86.8)	309 (89.6)	19 (57.6)	
Yes	50 (13.2)	36 (10.4)	14 (42.4)	
T classification				0.248
T1/T2	68 (18.0)	65 (18.8)	3 (9.1)	
T3/T4	310 (82.0)	280 (81.2)	30 (90.9)	
Lymph node status				0.073
Absent	205 (54.2)	192 (55.7)	13 (39.4)	
Present	173 (45.8)	153 (44.3)	20 (60.6)	
Clinical stage				0.108
I/II	188 (49.7)	176 (51.0)	12 (36.4)	
III/IV	190 (50.3)	169 (49.0)	21 (63.6)	
BMI (kg/m^2)	23.20 ± 3.13	23.34 ± 3.13	21.81 ± 2.75	0.007
WBC ($\times10^9$/L)	6.47 ± 2.24	6.44 ± 2.17	6.77 ± 2.96	0.425
Hemoglobin (g/L)	129.69 ± 24.43	130.17 ± 23.73	124.66 ± 30.81	0.324
Platelet count ($\times10^9$/L)	271.62 ± 94.76	275.05 ± 95.10	235.79 ± 84.36	0.023
Breast Cancer				
Age (years)				0.586
≤ 50	112 (50.7)	69 (49.3)	43 (53.1)	
> 50	109 (49.3)	71 (50.7)	38 (46.9)	
Tumor size (cm)				0.727
< 2.5	172 (77.8)	110 (78.6)	62 (76.5)	
≥ 2.5	49 (22.2)	30 (21.4)	19 (23.5)	

(Continued)

(Continued)

TABLE 1 Continued

Variables	Total n (%)	Low GLR	High GLR	P value
Breast Cancer				
Menopausal status				0.882
Pre	86 (38.9)	55 (39.3)	31 (38.3)	
Post	135 (61.1)	85 (60.7)	50 (61.7)	
Hypertension				0.999
No	191 (86.4)	121 (86.4)	70 (86.4)	
Yes	30 (13.6)	19 (13.6)	11 (13.6)	
Diabetes mellitus				0.002
No	214 (96.8)	140 (100.0)	74 (91.4)	
Yes	7 (3.2)	0 (0.0)	7 (8.6)	
ER				0.569
Negative	79 (35.7)	52 (37.1)	27 (33.3)	
Positive	142 (64.3)	88 (62.9)	54 (66.7)	
PR				0.285
Negative	81 (36.7)	55 (39.3)	26 (32.1)	
Positive	140 (63.3)	85 (60.7)	55 (67.9)	
HER2				0.348
Negative	121 (54.8)	80 (57.1)	41 (50.6)	
Positive	100 (45.2)	60 (42.9)	40 (49.4)	
Ki-67				0.196
< 20	135 (61.1)	81 (57.9)	54 (66.7)	
≥ 20	86 (38.9)	59 (42.1)	27 (33.3)	
T classification				0.764
T1/T2	210 (95.0)	134 (95.7)	76 (93.8)	
T3/T4	11 (5.0)	6 (4.3)	5 (6.2)	
Lymph node status				0.559
Absent	184 (83.3)	115 (82.1)	69 (85.2)	
Present	37 (16.7)	25 (17.9)	12 (14.8)	
Clinical stage				0.340
I/II	196 (88.7)	122 (87.1)	74 (91.4)	
III	25 (11.3)	18 (12.9)	7 (8.6)	
BMI (kg/m^2)	23.69 ± 3.57	23.79 ± 3.75	23.52 ± 3.25	0.583
WBC (×10^9/L)	6.13 ± 1.71	6.56 ± 1.74	5.38 ± 1.38	< 0.001
Hemoglobin (g/L)	135.36 ± 11.83	135.70 ± 11.72	134.77 ± 12.08	0.577
Platelet count (×10^9/L)	236.66 ± 50.61	241.16 ± 48.57	228.89 ± 53.39	0.082
Gastric Cancer				
Age (years)				0.906

(Continued)

TABLE 1 Continued

Variables	Total n (%)	Low GLR	High GLR	P value
Gastric Cancer				
≤ 65	252 (75.2)	205 (75.1)	47 (75.8)	
> 65	83 (24.8)	68 (24.9)	15 (24.2)	
Gender				0.046
Female	100 (29.9)	75 (27.5)	25 (40.3)	
Male	235 (70.1)	198 (72.5)	37 (59.7)	
Hypertension				0.281
No	276 (82.4)	222(81.3)	54 (87.1)	
Yes	59 (17.6)	51 (18.7)	8 (12.9)	
Diabetes mellitus				0.273
No	313 (93.4)	257 (94.1)	56 (90.3)	
Yes	22 (6.6)	16 (5.9)	6 (9.7)	
Tumor size (cm)				0.386
≤ 5.0	222 (66.3)	178 (65.2)	44 (71.0)	
> 5.0	113 (33.7)	95 (34.8)	18 (29.0)	
Histology				0.022
Well/Moderate	61 (18.2)	56 (20.5)	5 (8.1)	
Poor	274 (81.8)	217 (79.5)	57 (91.9)	
CEA (ng/mL)				0.176
≤ 5 ng/mL	274 (81.8)	227 (83.2)	47 (75.8)	
> 5 ng/mL	61 (18.2)	46 (16.8)	15 (24.2)	
T classification				0.236
T1/T2	83 (24.8)	64 (23.4)	19 (30.6)	
T3/T4	252 (75.2)	209 (76.6)	43 (69.4)	
Lymph node status				0.695
Absent	71 (21.2)	59 (21.6)	12 (19.4)	
Present	264 (78.8)	214 (78.4)	50 (80.6)	
Clinical stage				0.588
I/II	129 (38.5)	107 (39.2)	22 (35.5)	
III/IV	206 (61.5)	166 (60.8)	40 (64.5)	
BMI (kg/m^2)	22.84 ± 3.51	22.83 ± 3.55	22.89 ± 3.34	0.900
WBC (×10^9/L)	6.47 ± 2.16	6.57 ± 2.14	6.02 ± 2.19	0.069
Hemoglobin (g/L)	128.28 ± 26.64	129.97 ± 25.41	120.83 ± 30.60	0.032
Platelet count (×10^9/L)	271.28 ± 94.95	276.40 ± 96.32	248.76 ± 85.76	0.038
Liver Cancer				
Age (years)				0.360
≤ 55	161 (59.6)	119 (61.3)	42 (55.3)	

(Continued)

10.3389/fendo.2024.1284152

TABLE 1 Continued

Variables	Total n (%)	Low GLR	High GLR	P value
Liver Cancer				
> 55	109 (40.4)	75 (38.7)	34 (44.7)	
Gender				0.370
Female	141 (52.2)	98 (50.5)	43 (56.6)	
Male	129 (47.8)	96 (49.5)	33 (43.4)	
Hypertension				0.322
No	236 (87.4)	172 (88.7)	644 (84.2)	
Yes	34 (12.6)	22 (11.3)	12 (15.8)	
Diabetes mellitus				1.000
No	270 (100.0)	194 (100.0)	76 (100.0)	
Yes	0 (0.0)	0 (0.0)	0 (0.0)	
Smoking history				0.064
No	172 (63.7)	117 (60.3)	55 (72.4)	
Yes	98 (36.3)	77 (39.7)	21 (27.6)	
Drinking history				0.985
No	224 (83.0)	161 (83.0)	63 (82.9)	
Yes	46 (17.0)	33 (17.0)	13 (17.1)	
Tumor size (cm)				0.722
< 5	129 (47.8)	94 (48.5)	35 (46.1)	
≥ 5	141 (52.2)	100 (51.5)	41 (53.9)	
Hepatitis B				0.662
Absent	58 (21.5)	43 (22.2)	15 (19.7)	
Present	212 (78.5)	151 (77.8)	61 (80.3)	
Liver Cirrhosis				0.002
Absent	100 (37.0)	83 (42.8)	17 (22.4)	
Present	170 (63.0)	111 (57.2)	59 (77.6)	
T classification				0.321
T1/T2	155 (57.4)	115 (59.3)	40 (52.6)	
T3/T4	115 (42.6)	79 (40.7)	36 (47.4)	
Lymph node status				0.971
Absent	252 (93.3)	181 (93.3)	71 (93.4)	
Present	18 (6.7)	13 (6.7)	5 (6.6)	
Clinical stage				0.518
I/II	147 (54.4)	108 (55.7)	39 (51.3)	
III/IV	123 (45.6)	86 (44.3)	37 (48.7)	
BMI (kg/m^2)	24.00 ± 2.98	23.96 ± 3.11	24.10 ± 2.65	0.724
WBC (×10^9/L)	5.33 ± 1.85	5.73 ± 1.71	4.33 ± 1.81	< 0.001
Hemoglobin (g/L)	137.47 ± 17.81	139.23 ± 15.74	132.98 ± 21.73	0.024
Platelet count (×10^9/L)	155.71 ± 73.82	173.75 ± 71.63	109.66 ± 57.88	< 0.001
Esophageal Cancer				
Age (years)				0.667
≤ 65	169 (72.5)	133 (71.9)	36 (75.0)	
> 65	64 (27.5)	52 (28.1)	12 (25.0)	
Gender				0.734
Female	13 (5.6)	10 (5.4)	3 (6.3)	
Male	220 (94.4)	175 (94.6)	45 (93.8)	
Hypertension				0.325
No	201 (86.3)	157 (84.9)	44 (91.7)	
Yes	32 (13.7)	28 (15.1)	4 (8.3)	
Diabetes mellitus				0.177
No	222 (95.3)	174 (94.1)	48 (100.0)	
Yes	11 (4.7)	11 (5.9)	0 (0.0)	
Smoking history				0.152
No	46 (19.7)	33 (17.8)	13 (27.1)	
Yes	187 (80.3)	152 (82.2)	35 (72.9)	
Drinking history				0.854
No	31 (13.3)	25 (13.5)	6 (12.5)	
Yes	202 (86.7)	160 (86.5)	42 (87.5)	
Tumor size (cm)				0.164
< 3.5	40 (17.2)	35 (18.9)	5 (10.4)	
≥ 3.5	193 (82.8)	150 (81.1)	43 (89.6)	
Histology				0.371
Squamous carcinoma	226 (97.0)	178 (96.2)	48 (100.0)	
Others	7 (3.0)	7 (3.8)	0 (0.0)	
T classification				0.050
T1/T2	107 (45.9)	91 (49.2)	16 (33.3)	
T3/T4	126 (54.1)	94 (50.8)	32 (66.7)	
Lymph node status				0.678
Absent	120 (51.5)	94 (50.8)	26 (54.2)	
Present	113 (48.5)	91 (49.2)	22 (45.8)	
Clinical stage				0.132
I/II	100 (42.9)	84 (45.4)	16 (33.3)	
III/IV	133 (57.1)	101 (54.6)	32 (66.7)	
BMI (kg/m^2)	22.08 ± 2.96	22.06 ± 2.90	22.15 ± 3.19	0.846

(Continued)

10.3389/fendo.2024.1284152

TABLE 1 Continued

Variables	Total n (%)	Low GLR	High GLR	P value
Esophageal Cancer				
WBC ($\times10^9$/L)	6.90 ± 1.99	7.07 ± 1.82	6.26 ± 2.48	0.039
Hemoglobin (g/L)	142.20 ± 14.09	143.39 ± 13.66	137.60 ± 14.91	0.011
Platelet count ($\times10^9$/L)	239.18 ± 70.51	241.81 ± 69.95	229.04 ± 72.48	0.265
Renal Cancer				
Age (years)				0.042
≤ 65	235 (79.7)	92 (86.0)	143 (76.1)	
> 65	60 (20.3)	15 (14.0)	45 (23.9)	
Gender				0.278
Female	104 (35.3)	42 (39.3)	62 (33.0)	
Male	191 (64.7)	65 (60.7)	126 (67.0)	
Hypertension				0.037
No	244 (82.7)	95 (88.8)	149 (79.3)	
Yes	51 (17.3)	12 (11.2)	39 (20.7)	
Diabetes mellitus				0.004
No	266 (90.2)	104 (97.2)	162 (86.2)	
Yes	29 (9.8)	3 (2.8)	26 (13.8)	
Smoking history				0.472
No	259 (87.8)	92 (86.0)	167 (88.8)	
Yes	36 (12.2)	15 (14.0)	21 (11.2)	
Drinking history				0.087
No	279 (94.6)	98 (91.6)	181 (96.3)	
Yes	16 (5.4)	9 (8.4)	7 (3.7)	
Tumor size (cm)				0.132
≤ 4.0	121 (41.0)	50 (46.7)	71 (37.8)	
> 4.0	174(59.0)	57 (53.3)	117 (62.2)	
Histology				0.612
Others	27 (9.2)	11 (10.3)	16 (8.5)	
Clear cell	268 (90.8)	96 (89.7)	172 (91.5)	
T classification				0.278
T1/T2	275 (93.2)	102 (95.3)	173 (92.0)	
T3/T4	20 (6.8)	5 (4.7)	15 (8.0)	
Lymph node status				0.451
Absent	285 (96.6)	105 (98.1)	180 (95.7)	
Present	10 (3.4)	2 (1.9)	8 (4.3)	
Clinical stage				0.111
I/II	255 (86.4)	97 (90.7)	158 (84.0)	

(Continued)

TABLE 1 Continued

Variables	Total n (%)	Low GLR	High GLR	P value
Renal Cancer				
III/IV	40 (13.6)	10 (9.3)	30 (16.0)	
BMI (kg/m^2)	24.21 ± 3.67	24.00 ± 2.85	24.33 ± 4.07	0.450
WBC ($\times10^9$/L)	6.49 ± 2.03	6.96 ± 1.34	6.22 ± 2.30	0.001
Hemoglobin (g/L)	133.59 ± 20.00	134.60 ± 20.05	133.02 ± 20.00	0.515
Platelet count ($\times10^9$/L)	242.44 ± 91.19	256.74 ± 90.73	234.30 ± 90.69	0.042
Melanoma				
Age (years)				0.209
≤ 60	126 (63.0)	97 (65.5)	29 (55.8)	
> 60	74 (37.0)	51 (34.5)	23 (44.2)	
Gender				0.250
Female	94 (47.0)	66 (44.6)	28 (53.8)	
Male	106 (53.0)	82 (55.4)	24 (46.2)	
Hypertension				0.643
No	161 (80.5)	118 (79.7)	43 (82.7)	
Yes	39 (19.5)	30 (20.3)	9 (17.3)	
Diabetes mellitus				0.713
No	185 (92.5)	138 (93.2)	47 (90.4)	
Yes	15 (7.5)	10 (6.8)	5 (9.6)	
Tumor location				0.361
Sun-exposed (head and neck)	20 (10.0)	17 (11.5)	3 (5.8)	
Sun-protected (others)	180 (90.0)	131 (88.5)	49 (94.2)	
Ulceration				0.617
Negative	125 (62.5)	91 (61.5)	34 (65.4)	
Positive	75 (37.5)	57 (38.5)	18 (34.6)	
Histology				0.201
SSM/NM	104 (52.0)	73 (49.3)	31 (59.6)	
ALM/LMM/others	96 (48.0)	75 (50.7)	21 (40.4)	
T classification				0.293
T1/T2	167 (83.5)	126 (85.1)	41 (78.8)	
T3/T4	33 (16.5)	22 (14.9)	11 (21.2)	
Lymph node status				0.656
Absent	147 (73.5)	110 (74.3)	37 (71.2)	
Present	53 (26.5)	38 (25.7)	15 (28.8)	
Clinical stage				0.315
I/II	138 (69.0)	105 (70.9)	33 (63.5)	

(Continued)

10.3389/fendo.2024.1284152

TABLE 1 Continued

Variables	Total n (%)	Low GLR	High GLR	P value
Melanoma				
III/IV	62 (31.0)	43 (29.1)	19 (36.5)	
BMI (kg/m^2)	24.42 ± 3.41	24.46 ± 3.51	24.29 ± 3.14	0.757
WBC (×10^9/L)	6.25 ± 2.06	6.47 ± 1.89	5.63 ± 2.41	0.011
Hemoglobin (g/L)	138.49 ± 27.72	139.24 ± 30.21	136.36 ± 19.01	0.520
Platelet count (×10^9/L)	234.63 ± 66.98	237.76 ± 61.10	225.71 ± 81.47	0.266

Supplement: SSM, superficial spreading melanoma; NM, nodular melanoma; ALM, acromacular melanoma; LMM, lentigo maligna melanoma.

A ROC curve analysis was constructed to determine the optimal cutoff value for GLR in different tumor types (Figure 1). Based on the analysis of receiver operating characteristic curves, the optimal GLR cut-off values for gastric, renal, colorectal, non-small cell lung, breast, liver, esophageal, and melanoma cancers were 4.1, 2.53, 6.17, 3.27, 3.2, 4.08, 3.46, and 3.5, respectively. And the corresponding sensitivity and specificity are shown in Figure 1. Patients were classified as having high or low preoperative GLR according to cut-off values. We found that elevated GLR significantly predicted overall survival (Figure 2). Among patients with non-small cell lung cancer, 72 (30%) had higher preoperative GLR levels. With a median follow-up of 60 months, 43 (17.9%) patients had death events. 22 patients with GLR > 3.27 and 21 patients with GLR ≤ 3.27 had death events. Overall survival was significantly shorter in patients with high GLR (n=72) versus those with low GLR (n=168) ($p < 0.001$). The mean survival time was 45.5 months for patients with GLR > 3.27 and 53.4 months for patients with GLR ≤ 3.27, respectively. Kaplan-Meier OS curves for normal versus increased GLR showed a notable separation (Figure 2A). In patients with colorectal cancer, there were 212 (56.1%) patients who had death events. Compared to those with low GLR levels, the patients with high GLR levels had significantly shorter overall survival (survival rates of 21.2% and 46.1%, respectively, $p < 0.001$; Figure 2B). In breast cancer, OS was lower in high-GLR subjects than in low-GLR counterparts (mean survival time, 54.1 months vs 55.9 months, $p < 0.001$; Figure 2C). In gastric cancer, the OS rate was markedly worse in the high-GLR group than that in the low-GLR group (5-year survival rates of 32.3% and 53.1%, respectively, $p < 0.001$; Figure 2D). In liver cancer, OS was lower in high-GLR subjects than that in low-GLR counterparts (mean survival time, 27.3 months vs 30.6 months, $p = 0.027$; Figure 2E). Among patients with renal cancer, the high GLR grade group had a worse OS than the low GLR grade group (mean survival time, 46.1 months vs 54.3 months, $p < 0.001$; Figure 2G). Similarly, in melanoma, subjects with a high GLR have a shorter OS compared to patients with a lower GLR (mean survival time, 44.9 months vs 52.8 months, $p = 0.005$; Figure 2H). And in esophageal cancer, OS was lower in high-GLR subjects than in low-GLR subjects (mean survival time, 34.7 months vs 43.9 months, $p = 0.017$; Figure 2F).

The univariate and multivariate analyses were performed to evaluate the preoperative predictors for OS (Table 2). According to the univariate analysis, GLR, gender, adjuvant chemotherapy, histology, clinical stage, and white blood cell were significantly correlated with OS in patients with NSCLC. In colorectal cancer, GLR, age, T classification, lymph node status, clinical stage, hemoglobin, and white blood cell were related to OS. In gastric cancer, GLR, age, tumor size, histology, T classification, lymph node status, clinical stage, carcinoma embryonic antigen (CEA), BMI, and white blood cell were in correlation with OS. In patients with renal cancer, GLR, age, hypertension, diabetes mellitus, tumor size, T classification, lymph node status, clinical stage, hemoglobin, and platelet count were significantly related to OS. In melanoma, GLR, lymph node status, and clinical stage were prognostic-related risk factors for OS. In patients with liver cancer, GLR, hypertension, tumor size, T classification, lymph node status, clinical stage, and white blood cell were related to OS. In esophageal cancer, GLR, T classification, lymph node status, and clinical stage were significantly related to OS. And, in breast cancer, GLR, progesterone receptor (PR), human epidermal growth factor receptor-2 (HER-2), Ki-67, T classification, lymph node status, clinical stage, hypertension, BMI, and platelet count were significantly related to OS. Next, the variables showing statistical significance in the univariate analysis ($p < 0.10$) were included in the multivariate analysis. In multivariate analysis, GLR was identified as an independent prognostic factor for OS in different tumor types.

Discussion

In this study, we retrospectively analyzed the predictive value of preoperative GLR in patients with CRC, NSCLC, GC, EC, BC, renal cancer, liver cancer, and melanoma. It was found that increased GLR was markedly associated with shorter OS.

Previous studies have proven that GLR is a prognostic marker for some tumors, such as CRC (14), pancreatic carcinoma (12) and PT2 gallbladder carcinoma (15). Our study was consistent with the above results. In addition, our results showed the prognostic value of preoperative GLR in other cancers. Consistent with previous studies (16–19), our findings confirmed that age, BMI, WBC, and platelet count were independently associated with OS in the multivariate analysis in some cancers.

GLR is derived from the ratio of blood glucose to lymphocyte count (20). Altered glucose metabolism is a marked trait of cancer. Therefore, it is worth considering that tumor cell glycolytic activity increases when blood glucose is elevated, and then cancer cells transport extracellular glucose through the cytoplasm, leading to an increase in intracellular glucose, whose fermentation into lactic acid generates energy that activates cellular signaling pathways, thereby mediating the spread, invasion, and metastasis of cancer cells (21). It has been confirmed that the diabetes caused by hyperglycemia gives

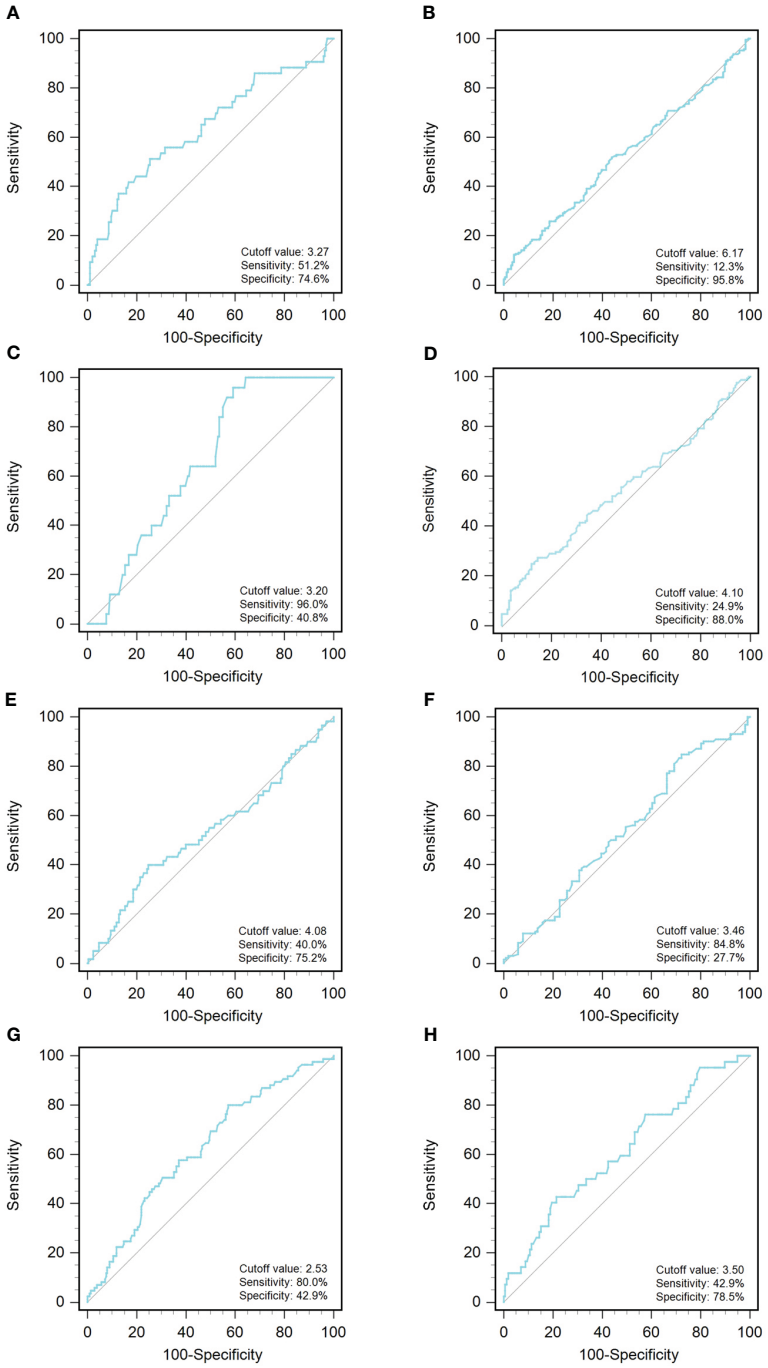

FIGURE 1
An optimized cut-off value was determined for preoperative GLR using ROC curve analysis. The ROC curve identified the optimal cutoff value of GLR with sensitivity and specificity. **(A)** non-small-cell lung cancer; **(B)** colorectal cancer; **(C)** breast cancer; **(D)** gastric cancer; **(E)** liver cancer; **(F)** esophageal cancer; **(G)** renal cancer; and **(H)** melanoma. ROC curve, receiver operating characteristic curve; GLR, glucose to lymphocyte ratio.

rise to hyperinsulinemia and insulin resistance, which may lead to changes in the tumor microenvironment by producing irreversible glycation end products or by affecting the expression of angiogenic factors and the acidity of the microenvironment, promoting tumor development, and even increasing tumor metastasis and resistance to chemotherapy (22–24). Also, the abysmal outcome of hyperglycemia is associated with chronic subclinical inflammation, referred to as "meta-inflammation". Chronic subclinical inflammation exacerbates hyperglycemia by modulating insulin resistance, leading to a series of diabetic complications, while hyperglycemia promotes the production of free radicals, leading to inflammation and metabolic disorders, thus creating a vicious cycle

10.3389/fendo.2024.1284152

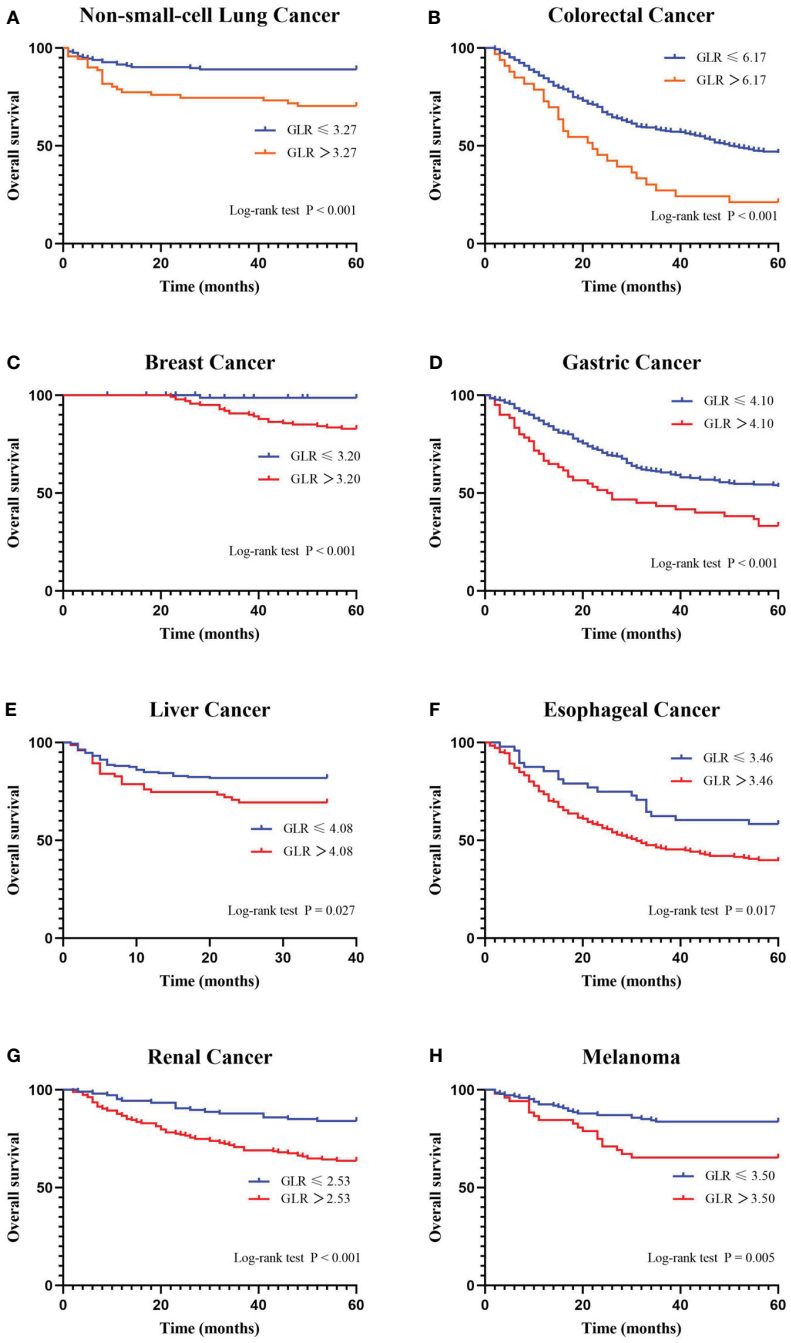

FIGURE 2
Kaplan-Meier curves for overall survival stratifed by preoperative GLR. Overall survival Kaplan-Meier survival curves according to GLR levels for patients who underwent radical surgery. The 5-year overall survival in patients with high GLR or low GLR is plotted. Kaplan-Meier analysis demonstrated that high GLR was significantly associated with the shorter overall survival. **(A)** non-small-cell lung cancer; **(B)** colorectal cancer; **(C)** breast cancer; **(D)** gastric cancer; **(E)** liver cancer; **(F)** esophageal cancer; **(G)** renal cancer; and **(H)** melanoma. GLR, glucose to lymphocyte ratio.

that exacerbates disease progression (25, 26). These form the basis of a poorer prognosis for tumor patients. Moreover, lymphocytes have an essential role in immune regulation and the prevention of tumor development. On the one hand, lymphocytes suppress cancer progression by inhibiting cell proliferation and promoting cell death (24). Several reports have revealed that lymphocytes can activate a cell-mediated immune response and stimulate the release of cytokines such as interferon and TNF-α to exert organismal protective effects, even leading to the lysis of tumor cells (27–29). On the other hand, cumulative evidence demonstrated that lymphocytes could indicate the nutritional status of patients (30). In brief, elevated GLR, that is, high glucose and low lymphocyte count, is strongly associated with cancer progression and worse OS, which is in accordance with our findings.

10.3389/fendo.2024.1284152

TABLE 2 Univariate analysis and Multivariate analysis of overall survival in cancer patients.

Variables	Univariate Analysis		Multivariate Analysis	
	Hazard ratio (95% CI)	*P*	Hazard ratio (95% CI)	*P*
Non-small-cell Lung Cancer				
GLR	1.477 (1.164 - 1.875)	0.001	1.602 (1.245 - 2.061)	**< 0.001**
Age (years)	1.025 (0.995 - 1.057)	0.109		
Gender (Male vs Female)	2.365 (1.134 - 4.931)	0.022	2.883 (1.280 - 6.491)	**0.011**
Hypertension (Yes vs No)	1.061 (0.472 - 2.385)	0.885		
Diabetes mellitus (Yes vs No)	1.013 (0.313 - 3.276)	0.982		
Tumor size (≥ 4cm vs < 4cm)	1.084 (0.573 - 2.051)	0.805		
Smoking history (Yes vs No)	1.473 (0.809 - 2.682)	0.206		
Adjuvant chemotherapy (Yes vs No)	0.287 (0.133 - 0.618)	0.001	0.454 (0.183 - 1.126)	0.088
Histology (Others vs Adenocarcinoma)	1.834 (1.001 - 3.362)	0.050	1.246 (0.659 - 2.357)	0.499
T classification (T3/T4 vs T1/T2)	1.092 (0.430 - 2.774)	0.853		
Lymph node status (Present vs Absent)	1.065 (0.569 - 1.994)	0.843		
Clinical Stage (III vs I/II)	2.778 (1.525 - 5.060)	0.001	1.502 (0.984 - 2.292)	0.059
BMI (kg/m^2)	1.025 (0.930 - 1.129)	0.623		
WBC ($\times10^9/L$)	1.161 (1.069 - 1.262)	< 0.001	1.170 (1.068 - 1.281)	**0.001**
Hemoglobin (g/dl)	0.994 (0.980 - 1.009)	0.461		
Platelet count ($\times10^9/L$)	1.003 (0.999 - 1.007)	0.156		
Colorectal Cancer				
GLR	1.073 (1.029 - 1.120)	0.001	1.051 (1.005 - 1.100)	**0.030**
Age (years)	1.019 (1.003 - 1.034)	0.016	1.021 (1.006 - 1.037)	**0.006**
Gender (Male vs Female)	1.062 (0.801 - 1.408)	0.675		
Hypertension (Yes vs No)	0.775 (0.562 - 1.069)	0.121		
Diabetes mellitus (Yes vs No)	1.146 (0.775 - 1.696)	0.495		
T classification (T3/T4 vs T1/T2)	2.884 (1.799 - 4.625)	< 0.001	1.840 (1.124 - 3.012)	**0.015**
Lymph node status (Present vs Absent)	2.591 (1.963 - 3.418)	< 0.001	0.719 (0.420 - 1.230)	0.228
Clinical Stage (III/IV vs I/II)	3.129 (2.342 - 4.181)	< 0.001	3.764 (2.125 - 6.667)	**< 0.001**
BMI/m (kg^2)	0.983 (0.941 - 1.027)	0.446		
WBC ($\times10^9/L$)	1.097 (1.037 - 1.161)	0.001	1.090 (1.031 - 1.152)	**0.002**
Hemoglobin (g/dl)	0.994 (0.989 - 0.999)	0.032	0.995 (0.990 - 1.001)	0.082
Platelet count ($\times10^9/L$)	1.000 (0.998 - 1.001)	0.722		
Breast Cancer				
GLR	14.693 (1.988 - 108.615)	0.008	13.015 (1.683 - 100.676)	**0.014**
Age (years)	1.027 (0.988 - 1.068)	0.176		
Hypertension (Yes vs No)	2.710 (1.132 - 6.489)	0.025	0.578 (0.187 - 1.787)	0.341
Diabetes mellitus (Yes vs No)	0.047 (0.000 - 711.277)	0.534		
Menopausal status (Post vs Pre)	0.800 (0.363 - 1.762)	0.579		
ER (Positive vs Negative)	0.663 (0.301 - 1.459)	0.307		
PR (Positive vs Negative)	2.362 (0.886 - 6.293)	0.086	1.578 (0.531 - 4.684)	0.412

(Continued)

10.3389/fendo.2024.1284152

TABLE 2 Continued

Variables	Univariate Analysis		Multivariate Analysis	
	Hazard ratio (95% CI)	*P*	Hazard ratio (95% CI)	*P*
Breast Cancer				
HER2 status (Positive vs Negative)	3.527 (1.323 - 9.399)	0.012	1.879 (0.637 - 5.547)	0.253
Ki-67 (≥ 20% vs < 20%)	4.656 (1.944 - 11.152)	0.001	2.118 (0.697 - 6.436)	0.186
Tumor size (≥ 2.5cm vs < 2.5cm)	1.827 (0.788 - 4.235)	0.160		
T classification (T3/T4 vs T1/T2)	4.306 (1.285 - 14.437)	0.018	1.041 (0.213 - 5.086)	0.961
Lymph node status (Present vs Absent)	42.730 (14.571 - 125.306)	< 0.001	24.641 (5.956 - 101.939)	**< 0.001**
Clinical stage(III vs I/II)	21.082 (9.358 - 47.496)	< 0.001	1.401 (0.482 - 4.066)	0.536
BMI (kg/m^2)	1.094 (1.000 - 1.196)	0.050	1.041 (0.906 - 1.195)	0.570
WBC ($\times10^9/L$)	1.069 (0.874 - 1.308)	0.516		
Hemoglobin (g/dl)	1.007 (0.974 - 1.041)	0.665		
Platelet count ($\times10^9/L$)	1.009 (1.002 - 1.016)	0.015	1.005 (0.995 - 1.014)	0.331
Gastric Cancer				
GLR	1.201 (1.082 - 1.334)	0.001	1.169 (1.055 - 1.295)	**0.003**
Age (years)	1.024 (1.008 - 1.040)	0.002	1.025 (1.009 - 1.041)	**0.003**
Gender (Male vs Female)	1.012 (0.728 - 1.408)	0.942		
Hypertension (Yes vs No)	1.037 (0.699 - 1.538)	0.858		
Diabetes mellitus (Yes vs No)	1.211 (0.688 - 2.133)	0.506		
Tumor size (> 5cm vs ≤ 5cm)	1.390 (1.022 - 1.892)	0.036	1.055 (0.764 - 1.456)	0.745
Histology (Poor vs Well/Moderate)	1.681 (1.083 - 2.609)	0.021	1.673 (1.051 - 2.662)	**0.030**
T classification (T3/T4 vs T1/T2)	1.824 (1.215 - 2.737)	0.004	1.409 (0.888 - 2.236)	0.145
Lymph node status (Present vs Absent)	2.904 (1.781 - 4.736)	< 0.001	1.767 (0.980 - 3.188)	0.058
Clinical Stage (III/IV vs I/II)	2.265 (1.601 - 3.204)	< 0.001	1.326 (0.839 - 2.095)	0.227
CEA (> 5 ng/mL vs ≤ 5 ng/mL)	1.791 (1.260 - 2.547)	0.001	1.315 (0.898 - 1.925)	0.159
BMI (kg/m^2)	0.938 (0.896 - 0.982)	0.007	0.922 (0.878 - 0.969)	**0.001**
WBC ($\times10^9/L$)	1.140 (1.066 - 1.219)	< 0.001	1.136 (1.060 - 1.216)	**< 0.001**
Hemoglobin (g/dl)	0.998 (0.992 - 1.003)	0.390		
Platelet count ($\times10^9/L$)	1.001 (0.999 - 1.002)	0.200		
Liver Cancer				
GLR	1.809 (1.079 - 3.033)	0.024	2.233 (1.277 - 3.904)	**0.005**
Age (years)	1.014 (0.986 - 1.043)	0.321		
Gender (Male vs Female)	0.861 (0.518 - 1.432)	0.564		
Tumor size (≥ 5 cm vs< 5 cm)	2.811 (1.586 - 4.984)	< 0.001	1.924 (0.945 - 3.916)	0.071
Smoker (Yes vs No)	1.085 (0.645 - 1.826)	0.758		
Drinking (Yes vs No)	0.844 (0.415 - 1.714)	0.639		
Hypertension (Yes vs No)	2.211 (1.196 - 4.088)	0.011	1.723 (0.909 - 3.267)	0.095
Hepatitis B (Present vs Absent)	0.692 (0.391 - 1.227)	0.207		
Liver Cirrhosis (Present vs Absent)	0.728 (0.437 - 1.213)	0.222		
T classification (T3/T4 vs T1/T2)	2.244 (1.338 - 3.762)	0.002	0.703 (0.187 - 2.641)	0.601

(Continued)

10.3389/fendo.2024.1284152

TABLE 2 Continued

Variables	Univariate Analysis		Multivariate Analysis	
	Hazard ratio (95% CI)	*P*	Hazard ratio (95% CI)	*P*
Liver Cancer				
Lymph node status (Present vs Absent)	3.843 (1.945 - 7.595)	< 0.001	2.087 (0.832 - 5.234)	0.117
Clinical Stage (III/IV vs I/II)	2.725 (1.592 - 4.663)	< 0.001	1.984 (0.486 - 8.105)	0.340
BMI (kg/m^2)	1.021 (0.939 - 1.110)	0.629		
WBC (×10^9/L)	1.182 (1.045 - 1.337)	0.008	1.153 (1.007 - 1.320)	**0.040**
Hemoglobin (g/dl)	1.003 (0.989 - 1.018)	0.661		
Platelet count (×10^9/L)	1.002 (0.998 - 1.005)	0.323		
Esophageal Cancer				
GLR	1.771 (1.100 - 2.852)	0.019	1.925 (1.190 - 3.114)	**0.008**
Age (years)	1.006 (0.983 - 1.029)	0.624		
Gender (Male vs Female)	0.673 (0.353 - 1.284)	0.230		
Tumor size (≥ 3.5 cm vs < 3.5 cm)	1.266 (0.794 - 2.019)	0.321		
Smoker (Yes vs No)	0.774 (0.513 - 1.169)	0.224		
Drinking (Yes vs No)	0.705 (0.442 - 1.125)	0.143		
Hypertension (Yes vs No)	0.647 (0.371 - 1.126)	0.123		
Diabetes mellitus (Yes vs No)	1.437 (0.671 - 3.079)	0.351		
Histology (Others vs Squamous carcinoma)	1.564 (0.639 - 3.824)	0.327		
T classification (T3/T4 vs T1/T2)	1.707 (1.202 - 2.424)	0.003	1.418 (0.567 - 3.545)	0.455
Lymph node status (Present vs Absent)	1.980 (1.399 - 2.802)	< 0.001	1.778 (1.238 - 2.553)	**0.002**
Clinical Stage (III/IV vs I/II)	1.794 (1.253 - 2.568)	0.001	1.184 (0.459 - 3.058)	0.727
BMI (kg/m^2)	0.981 (0.927 - 1.039)	0.512		
WBC (×10^9/L)	1.022 (0.940 - 1.111)	0.608		
Hemoglobin (g/dl)	0.995 (0.983 - 1.007)	0.408		
Platelet count (×10^9/L)	1.001 (0.999 - 1.004)	0.273		
Renal Cancer				
GLR	1.153 (1.068 - 1.245)	< 0.001	1.139 (1.054 - 1.232)	**0.001**
Age (years)	1.017 (0.997 - 1.037)	0.098	1.006 (0.984 - 1.028)	0.620
Gender (Male vs Female)	1.430 (0.891 - 2.293)	0.138		
Smoker (Yes vs No)	1.363 (0.755 - 2.460)	0.304		
Hypertension (Yes vs No)	1.728 (1.055 - 2.829)	0.030	1.262 (0.730 - 2.180)	0.405
Diabetes mellitus (Yes vs No)	2.373 (1.358 - 4.148)	0.002	1.518 (0.773 - 2.980)	0.226
Drinking (Yes vs No)	0.813 (0.298 - 2.219)	0.686		
Tumor size (> 4 cm vs ≤ 4 cm)	2.360 (1.441 - 3.866)	0.001	1.779 (1.054 - 3.003)	**0.031**
Histology (Clear cell vs Others)	2.226 (0.816 - 6.074)	0.118		
T classification (T3/T4 vs T1/T2)	4.606 (2.622 - 8.093)	< 0.001	0.811 (0.364 - 1.807)	0.608
Lymph node status (Present vs Absent)	4.738 (2.771 - 8.100)	< 0.001	2.018 (1.010 - 4.034)	**0.047**
Clinical Stage (III/IV vs I/II)	5.169 (3.287 - 8.130)	< 0.001	3.463 (1.815 - 6.606)	**< 0.001**
BMI (kg/m^2)	0.963 (0.902 - 1.029)	0.265		

(Continued)

TABLE 2 Continued

Variables	Univariate Analysis		Multivariate Analysis	
	Hazard ratio (95% CI)	*P*	Hazard ratio (95% CI)	*P*
Renal Cancer				
WBC ($\times10^9$/L)	1.058 (0.966 - 1.158)	0.226		
Hemoglobin (g/dl)	0.977 (0.968 - 0.987)	< 0.001	0.998 (0.984 - 1.012)	0.761
Platelet count ($\times10^9$/L)	1.005 (1.003 - 1.007)	< 0.001	1.005 (1.002 - 1.007)	**0.001**
Melanoma				
GLR	1.519 (1.172 - 1.968)	0.002	1.486 (1.120 - 1.972)	**0.006**
Age (years)	0.990 (0.967 - 1.013)	0.388		
Gender (Male vs Female)	0.787 (0.430 - 1.443)	0.439		
Hypertension (Yes vs No)	1.538 (0.648 - 3.651)	0.329		
Diabetes mellitus (Yes vs No)	1.342 (0.324 - 5.553)	0.685		
Tumor location (Sun-exposed vs Sun-protected)	1.245 (0.489 - 3.169)	0.645		
Ulceration (Yes vs No)	1.413 (0.735 - 2.718)	0.300		
Histology (SSM/NM vs ALM/LMM/others)	0.653 (0.354 - 1.203)	0.172		
T classification (T3/T4 vs T1/T2)	1.236 (0.572 - 2.670)	0.590		
Lymph node status (Present vs Absent)	2.957 (1.613 - 5.421)	< 0.001	1.054 (0.347 - 3.196)	0.926
Clinical stage (III/IV vs I/II)	3.582 (1.943 - 6.604)	< 0.001	3.228 (1.057 - 9.859)	**0.040**
BMI (kg/m^2)	0.933 (0.850 - 1.023)	0.140		
WBC ($\times10^9$/L)	0.868 (0.725 - 1.040)	0.125		
Hemoglobin (g/dl)	0.996 (0.983 - 1.010)	0.574		
Platelet count ($\times10^9$/L)	1.001 (0.996 - 1.005)	0.719		

Supplement: SSM, superficial spreading melanoma; NM, nodular melanoma; ALM, acromacular melanoma; LMM, lentigo maligna melanoma.
Bold values mean P < 0.05.

Compared with the existing studies, this research involved a wide range of diseases, and the results were more comprehensive. However, our research had some limitations. Firstly, the study has a retrospective design and the sample size was not large enough. Secondly, the potential confounders that may exist (e.g., drug administration, patient selection, and surgical procedures) may have caused the sampling error. Thirdly, the cut-off values for specific cancer types are required for further evaluation in the future. Finally, further investigation is needed regarding the mechanisms at the molecular level. Moreover, serum lactate and inflammatory cytokines, such as TNFα or IL-10, should be detected in future studies.

GLR is a simple, cost-effective, and noninvasive parameter in clinical practice. Our study revealed the prognostic value of preoperative GLR in some resectable tumors. Future prospective studies are required to confirm the findings. Moreover, it would be interesting to investigate whether adding GLR to other prognosis scores could improve their performance.

In conclusion, elevated preoperative GLR was remarkably associated with a poorer prognosis in patients with NSCLC, CRC, breast cancer, gastric cancer, kidney cancer, liver cancer, esophageal cancer, and melanoma. Preoperative GLR promises to be an essential predictor of survival for cancer patients.

Data availability statement

The raw data supporting the conclusions of this article will be made available by the authors, without undue reservation.

Ethics statement

This research was in strict compliance with the Helsinki Declaration. This study was approved by our Institutional Review Board (approval number KY2022-10). As the study was retrospective, written informed consent was waived.

Author contributions

LL: Data curation, Writing – original draft. BZ: Investigation, Writing – original draft, Data analysis. RW: Formal analysis, Methodology, Writing – review & editing. WH: Data curation, Investigation, Software, Writing – review & editing. YN: Conceptualization, Supervision, Validation, Writing – review & editing. WW: Investigation, Validation, Visualization, Writing –

review & editing. QJ: Data curation, Methodology, Supervision, Writing – original draft. JY: Formal analysis, Validation, Visualization, Writing – review & editing. GW: Conceptualization, Methodology, Writing – review & editing. SM: Software, Supervision, Validation, Writing – review & editing. YL: Formal analysis, Investigation, Visualization, Writing – review & editing.

Funding

The author(s) declare that no financial support was received for the research, authorship, and/or publication of this article. This study did not receive any specific funding from public, commercial or non-profit sector funding agencies. None of the authors have any financial and relevant financial and personal relationships with other people or organisations to disclosure in this paper.

Conflict of interest

The authors declare that the research was conducted in the absence of any commercial or financial relationships that could be construed as a potential conflict of interest.

Publisher's note

References

1. Siegel RL, Miller KD, Fuchs HE, Jemal A. Cancer statistics, 2022. *CA Cancer J Clin*. (2022) 7:33. doi: 10.3322/caac.21708.

2. Wyld L, Audisio RA, Poston GJ. The evolution of cancer surgery and future perspectives. *Nat Rev Clin Oncol*. (2015) 115:124. doi: 10.1038/nrclinonc.2014.191.

3. Magliano DJ, Sacre JW, Harding JL, Gregg EW, Zimmet PZ, Shaw JE. Young-onset type 2 diabetes mellitus - implications for morbidity and mortality. *Nat Rev Endocrinol*. (2020) 321:331. doi: 10.1038/s41574-020-0334-z.

4. Barone BB, Yeh HC, Snyder CF, Peairs KS, Stein KB, Derr RL, et al. Long-term all-cause mortality in cancer patients with preexisting diabetes mellitus: a systematic review and meta-analysis. *JAMA*. (2008) 2754:2764. doi: 10.1001/jama.2008.824.

5. Suh S, Kim KW. Diabetes and cancer: cancer should be screened in routine diabetes assessment. *Diabetes Metab J*. (2019) 733:743. doi: 10.4093/dmj.2019.0177.

6. Tsilidis KK, Kasimis JC, Lopez DS, Ntzani EE, Ioannidis JP. Type 2 diabetes and cancer: umbrella review of meta-analyses of observational studies. *BMJ*. (2015) 350: g7607. doi: 10.1136/bmj.g7607.

7. Bánhegyi RJ, Gazdag A, Rácz B, Beke S, Fülöp N, Onkodiabetológia I. Metabolikus és molekuláris összefüggések a rosszindulatú daganatok és a cukorbetegség között [Oncodiabetology I. Metabolic and molecular relationships between cancer and diabetes]. *Orv Hetil*. (2022) 163(39):1535–43. doi: 10.1556/650.2022.32564

8. Zhang K, Bai P, Dai H, Deng Z. Metformin and risk of cancer among patients with type 2 diabetes mellitus: A systematic review and meta-analysis. *Prim Care Diabetes*. (2021) 52:58. doi: 10.1016/j.pcd.2020.06.001.

9. Hwangbo Y, Kang D, Kang M, Kim S, Lee EK, Kim YA, et al. Incidence of diabetes after cancer development: A korean national cohort study. *JAMA Oncol*. (2018) 1099:1105. doi: 10.1001/jamaoncol.2018.1684.

10. Paijens ST, Vledder A, De Bruyn M, Nijman HW. Tumor-infiltrating lymphocytes in the immunotherapy era. *Cell Mol Immunol*. (2021) 842:859. doi: 10.1038/s41423-020-00565-9.

11. Wu SY, Fu T, Jiang YZ, Shao ZW. Natural killer cells in cancer biology and therapy. *Mol Cancer*. (2020) 19(1):120. doi: 10.1186/s12943-020-01238-x.

12. Zhong A, Cheng CS, Kai J, Lu R, Guo L. Clinical significance of glucose to lymphocyte ratio (GLR) as a prognostic marker for patients with pancreatic cancer. *Front Oncol*. (2020) 520330. doi: 10.3389/fonc.2020.520330.

13. McShane LM, Altman DG, Sauerbrei W, Taube SE, Gion M, Clark GM, et al. Reporting recommendations for tumor marker prognostic studies (REMARK). *J Natl Cancer Inst*. (2005) 1180:1184. doi: 10.1093/jnci/dji237.

14. Yang M, Zhang Q, Ge Y, Tang M, Zhang X, Song M, et al. Glucose to lymphocyte ratio predicts prognoses in patients with colorectal cancer [published online ahead of print, 2022 Dec 7]. *Asia Pac J Clin Oncol*. (2022) 19(4):542–8. doi: 10.1111/ajco.13904.

15. Navarro J, Kang I, Hwang HK, Yoon DS, Lee WJ, Kang CW. Glucose to lymphocyte ratio as a prognostic marker in patients with resected pT2 gallbladder cancer. *J Surg Res*. (2019) 17:29. doi: 10.1016/j.jss.2019.02.043.

16. Laconi E, Marongiu F, Degregori J. Cancer as a disease of old age: changing mutational and microenvironmental landscapes. *Br J Cancer*. (2020) 943:52. doi: 10.1038/s41416-019-0721-1.

17. Schwartz SS, Grant S FA, Herman ME. Intersections and clinical translations of diabetes mellitus with cancer promotion, progression and prognosis. *Postgrad Med*. (2019) 597:606. doi: 10.1080/00325481.2019.1657358.

18. Smeda M, Przyborowski K, Stojak M, Chlopicki S. The endothelial barrier and cancer metastasis: Does the protective facet of platelet function matter? *Biochem Pharmacol*. (2020) 176:113886. doi: 10.1016/j.bcp.2020.113886.

19. Xu H, Zheng X, Ai J, Yang L. Hemoglobin, albumin, lymphocyte, and platelet (HALP) score and cancer prognosis: A systematic review and meta-analysis of 13,110 patients. *Int Immunopharmacol*. (2023) 114:109496. doi: 10.1016/j.intimp.2022.109496.

20. Li L, Zou G, Liu J. Preoperative glucose-to-lymphocyte ratio is an independent predictor for acute kidney injury after cardiac surgery in patients in intensive care unit. *Int J Gen Med*. (2021) 6529:6537. doi: 10.2147/IJGM.S335896.

21. Wahdan-Alaswad R, Fan Z, Edgerton SM, Liu B, Deng XS, Arnadottir SS, et al. Glucose promotes breast cancer aggression and reduces metformin efficacy. *Cell Cycle*. (2013) 3759:3769. doi: 10.4161/cc.26641.

22. Chott A, Sun Z, Morganstern D, Pan J, Li T, Susani M, et al. Tyrosine kinases expressed *in vivo* by human prostate cancer bone marrow metastases and loss of the type 1 insulin-like growth factor receptor. *Am J Pathol*. (1999) 1271:1279. doi: 10.1016/S0002-9440(10)65229-7.

23. Li W, Zhang X, Sang H, Zhou Y, Shang C, Wang Y, et al. Effects of hyperglycemia on the progression of tumor diseases. *J Exp Clin Cancer Res*. (2019) 38(1):327. doi: 10.1186/s13046-019-1309-6.

24. Siska PJ, Rathmell JC. T cell metabolic fitness in antitumor immunity. *Trends Immunol*. (2015) 257:264. doi: 10.1016/j.it.2015.02.007.

25. Berbudi A, Rahmadika N, Tjahjadi AI, Ruslami R. Type 2 diabetes and its impact on the immune system. *Curr Diabetes Rev*. (2020) 442:449. doi: 10.2174/1573399815666191024085838.

26. De Heredia FP, Gómez-Martínez S, Marcos A. Obesity, inflammation and the immune system. *Proc Nutr Soc*. (2012) 332:338. doi: 10.1017/S0029665112000092.

27. Greten FP, Grivennikov SI. Inflammation and cancer: triggers, mechanisms, and consequences. *Immunity*. (2019) 27:41. doi: 10.1016/j.immuni.2019.06.025.

28. Koliaraki V, Prados A, Armaka M, Kollias G. The mesenchymal context in inflammation, immunity and cancer. *Nat Immunol*. (2020) 974:982. doi: 10.1038/s41590-020-0741-2.

29. Lin DZ, Qu N, Shi RL, Lu ZW, Ji QH, Wu WL. Risk prediction and clinical model building for lymph node metastasis in papillary thyroid microcarcinoma. *Onco Targets Ther*. (2016) 5307:5316. doi: 10.2147/OTT.

30. Reljic D, Herrmann HJ, Neurath MF, Zopf Y. Iron Beats Electricity: Resistance Training but Not Whole-Body Electromyostimulation Improves Cardiometabolic Health in Obese Metabolic Syndrome Patients during Caloric Restriction-A Randomized-Controlled Study. *Nutrients*. (2021) 13(5):1604. doi: 10.3390/nu13051640.

Frontiers in Endocrinology

Explores the endocrine system to find new therapies for key health issues

The second most-cited endocrinology and metabolism journal, which advances our understanding of the endocrine system. It uncovers new therapies for prevalent health issues such as obesity, diabetes, reproduction, and aging.

Discover the latest Research Topics

See more →

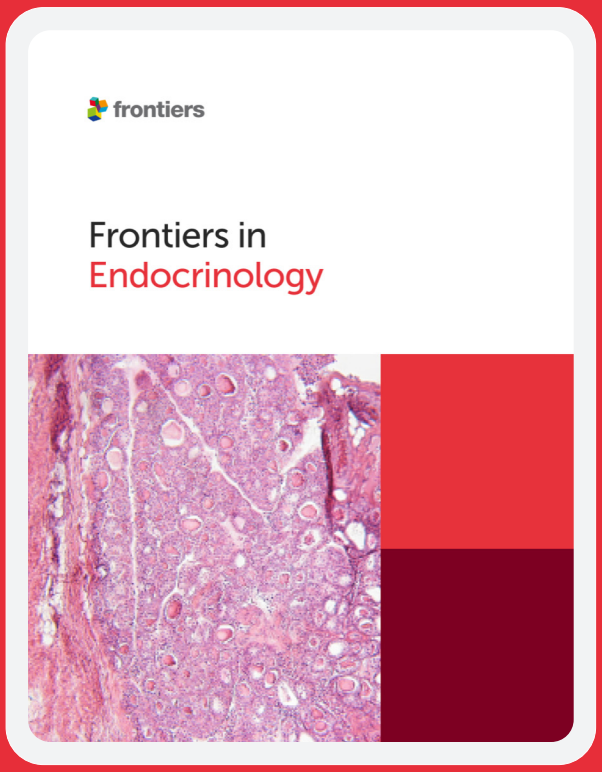

Frontiers

Avenue du Tribunal-Fédéral 34
1005 Lausanne, Switzerland
frontiersin.org

Contact us

+41 (0)21 510 17 00
frontiersin.org/about/contact